ELECTRICALLY CONDUCTIVE MEMBRANES FOR WATER AND WASTEWATER TREATMENT

ELECTRICALLY CONDUCTIVE MEMBRANES FOR WATER AND WASTEWATER TREATMENT: THEIR SURFACE PROPERTIES, ANTIFOULING MECHANISMS, AND APPLICATIONS

By

MOHAMAD AMIN HALALI, M. Sc.

A Thesis Submitted to the School of Graduate Studies in Partial Fulfillment of the Requirements for the Degree Doctor of Philosophy

McMaster University Ph.D. of Engineering (2021) Hamilton, Ontario (Chemical Engineering)

DOCTOR OF PHILOSOPHY (2021) McMaster University

(Chemical Engineering) Hamilton, Ontario

TITLE: ELECTRICALLY CONDUCTIVE MEMBRANES FOR WATER AND WASTEWATER TREATMENT: THEIR SURFACE PROPERTIES, ANTIFOULING MECHANISMS, AND APPLICATIONS

AUTHOR: Mohamad Amin Halali, B. Sc. (Petroleum University of Technology)

M.Sc. (Sharif University of Technology)

SUPERVISOR: Dr. Charles-François de Lannoy

NUMBER OF PAGES: xxxiii, 318

Abstract

Climate change, water stress, and rapid population growth have increased the need to manage water resources through innovative sustainable technologies. Decentralized systems such as membrane treatment trains have become increasingly important to provide high volumes of potable water to millions of people. Pressure-driven membrane systems have dominated separation processes due to their low cost, small footprint, ease of operation, and high permeate quality. Conventionally, pressure-driven membranes are classified into microfiltration (MF), ultrafiltration (UF), nanofiltration (NF), and reverse osmosis (RO). MF and UF membranes operate under low pressure (< 7 bar, <~100 psi). They can separate a variety of large particles such as bacteria, natural organic matter, suspended solids, and colloids. In contrast, NF and RO membranes are more energy-intense due to operating at high pressures (7 – 80 bar, ~100 – 1200 psi) and can remove small molecules such as ions, pharmaceuticals, and heavy metals. Fouling is a primary challenge with membranes that compromises the membrane performance, increases energy consumption, and reduces the membrane lifetime. Many strategies are used to address fouling, such as pre-treatment (pH adjustment, screening, coagulation), membrane modification (chemical and morphological properties), and membrane cleaning (physical, chemical). However, such strategies increase operational expenditures, produce waste products that can impact the environment, and negatively impact membrane lifetimes.

Recently, electrically conductive membranes (ECMs) have been introduced to address the challenges with traditional membranes. They contain conductive surfaces that offer self-cleaning and antifouling properties across the surface in response to electrical

potential externally applied to them. ECMs are advantageous as compared to traditional membranes because (a) they are more effective in treating foulants as they target foulants at the membrane/solvent interface, (b) they are more economical and environmentally friendly as they reduce the need for chemical consumption, and (c) they can be responsive to fouling conditions as their antifouling mechanisms can be easily manipulated by changing the applied current type (positive, negative, direct current, alternating current) to match the foulant.

ECMs have been formed from all categories of membranes (MF, UF, NF, MD, FO, and RO) with a range of applications. Despite the remarkable progress in demonstrating their excellent antifouling performance, there are many hurdles to overcome before they can be commercialized. Two of these are (a) a fundamental understanding of their underlying mechanisms, (b) surface materials that can withstand extreme chemical and electrical conditions. In this work, we have comprehensively discussed antifouling mechanisms with respect to surface polarization and elaborated on the impact of electrically-induced mechanisms on four major fouling categories. i.e., biofouling, organic fouling, mineral scaling, and oil wetting. In addition, we characterized surface properties of a common electrically conductive composite membrane composed of carbon nanotubes (CNTs) and polyvinyl alcohol (PVA). We then investigated the impact of cross-linkers in CNT/PVA network on transmembrane flux, electrical conductivity, hydrophilicity, and surface roughness. In addition, we proposed standard, practical, and straightforward methodologies to detect and quantify the electrochemical, physical, and mechanical stability of ECMs, using chronoamperometry and cyclic voltammetry, an evaluation of

polymer leaching from membranes, and micro mechanical scratch testing, respectively. Our methods can readily be extended to all membrane-based separation processes and different membrane materials (carbonaceous materials, ceramics, metal-based, and polymers).

To demonstrate the antifouling properties of ECMs, we challenged ECMs with mixed-bacterial cultures in a flow-through system. Although ECMs showed high rejection, comparable flux, and excellent self-cleaning performance under application of electrical potential, understanding the relationship between applied electrical currents and antifouling mechanisms demands a well-controlled investigation. To this end, we quantified the impact of electrochemically-induced acidic conditions, alkaline conditions, and H_2O_2 concentration on model bacteria, *Escherichia Coli*. We first quantified the electrochemical potential of CNT-based ECMs in generating stressors such as protons, hydroxyl ions, and H_2O_2, under a range of applied electrical currents (± 0-150 mA). Next, these individual stressors with identical magnitude were imposed on *E. Coli* cells and biofilms in batch and flow-through systems, respectively. This thesis guides researchers to understand the underlying antifouling mechanisms associated with ECMs, how to match the mechanisms to the application of ECMs, and offers benchmarks for making practical ECMs.

Acknowledgments

I would first like to thank my supervisor, Dr. Charles de Lannoy for his continuous support, guidance, and encouragement throughout my Ph.D. This work could not have been completed without your much-needed wisdom, insight, and supervision. Thank you for trusting me to be the first student in your lab, giving me the confidence to run projects from developing initial ideas all the way to delivering the outcomes to the scientific community. I feel privileged to have received your mentorship and support within and beyond my academic life. Your curiosity, passion for research, and critical thinking have left a great imprint on my life which I am always going to be grateful for.

I would also like to sincerely thank my committee members, Dr. Carlos Filipe and Dr. David Latulippe from The Chemical Engineering Department and Dr. Alex Adronov from The Chemistry Department for their invaluable insight, advice, and suggestions throughout my research and for providing valuable feedback all along the way. Their clever interpretations, insightful recommendations, and out-of-the-box questions helped me to become a better researcher and allowed me to explore my project from different angles. Many thanks to Dr. Li Xi, Dr. Dwight Houweling, and Dr. Charles de Lannoy for their help during my TAship.

I want to acknowledge the help from all the staff in the Department of Chemical Engineering, Kristina Trollip, Michelle Whalen, Linda Ellis, Doug Keller. A big thank you to Paul Gatt and Mike Clarke, who have helped me with their generous technical insight and manufacturing expertise. You are absolute gems! Many thanks to Tim Stephens for his

tremendous efforts to run issue-free labs during my TAship for 3rd- and 4th-year chemical engineering laboratory courses and for helping to provide students with a pleasant laboratory experience.

I have been very lucky to work with a number of amazing people in the lab (former and current members), thank you for making my graduate studies such a pleasant journey full of love and laughter. Special thanks to Maria, Alex, Mohamed, Melissa, Nan, Cassandra, Daniel, Yichen, and Scott for all the support and company anytime, even at nights or during the weekends. Special thanks to my undergraduate students Alex, Ace, and Thomas. I would also like to thank all my friends in the Club JHE 296. You have made the office environment much happier and more friendly with your presence.

Many thanks to all my friends at McMaster University who have made this journey much more enjoyable and such a great experience.

Something that I admire the most about McMaster University is its tight-knit community and collaborative environment. I have always felt being part of a big family at McMaster University and enjoyed the intimate and collaborative environment. Thank you to all PIs who generously allowed me to use the facilities in their lab, Dr. Latulippe, Dr. Filipe, Dr. Hosseini Doust, Dr. Pelton, Dr. Zhu, Dr. Sheardown, Dr. Cranston, Dr. Hoare from The Chemical Engineering Department and Dr. Adronov from The Chemistry Department. I would also like to thank the Biointerfaces Institute (BI) at McMaster for providing access to the contact angle measurement instrument, X-Ray photoelectron spectroscopy, and Fourier-transform infrared spectroscopy, Canadian Center for Electron

Microscopy (CCEM) for allowing to use scanning electron microscopy, and transmission electron microscopy, Centre for Emerging Device Technologies (CEDT) for giving me the access to four point probe conductivity meter, the McMaster Manufacturing Research Institute (MMRI) for the permit to use micro-scratch tester, and Natural Sciences and Engineering Research Council of Canada (NSERC) for their financial support. I would like to acknowledge the assistance from research associates at McMaster University: Marta Princz, Chris Butcher, Shahram Ghanad-Tavakoli, and Heera Marway.

Thank you to my industrial collaborators Trojan Technologies and Pall Water. I would like to especially thank Siva Sarathy, Arndt Nottrott, and Erick Cornfoot for their valuable feedback on my project during our meetings.

Last but not least, I want to thank my family, my mother, my father, and my two sisters who have always been my biggest support. I am extremely lucky to have you in my life, and words cannot describe how much your unconditional and endless love means to me! Thank you for believing in me and constantly shaping me into a better person. A special thank you to my girlfriend, who has always been there for me and supported me through ups and downs.

Finally, I would like to dedicate this thesis to the memory of the victims of the flight PS752, especially my friends Iman Aghabali and Mehdi Eshagian. You may not be longer with us but you live eternally in our hearts and minds. God bless your souls and may you rest in peace.

Table of Contents

1. Introduction and Literature Review 1
1.1. Water stress 2
1.2. Membrane technology 3
1.2.1. Membrane classification and application 4
Microfiltration membranes 4
Ultrafiltration membranes 5
Reverse osmosis membranes 5
Nanofiltration membranes 6
1.2.2. Membrane materials 6
1.2.3. Membrane geometry and module configurations 8
1.3. Membrane fouling and conventional control strategies 9
1.3.1. Biofouling 12
1.3.2. Organic fouling 14
1.3.3. Scaling 14
1.3.4. Colloidal fouling 15
1.4. Application of electrically conductive membranes to mitigate fouling 15
1.5. CNT-based electrically conductive membranes 17
1.6. Motivations, objective, and thesis structure 18
1.7. References 21
2. Electrically Conductive Membranes – A Review of their Anti-Fouling Mechanisms – Part I. 30
2.1. Abstract 31
2.2. Introduction 32
2.3. Antifouling mechanisms 35
2.4. Cathodic current 37
2.4.1. Electrostatic repulsion 38
2.4.2. Hydrogen gas generation 40
2.4.3. Indirect oxidation 42
Hydrogen peroxide 43
Radicals 44
2.4.4. High local pH 45

2.4.5. Electroporation 46
2.4.6. Electrical field-induced mobility 47
2.4.7. Electro-wetting 48
2.4.8. Direct reduction 49
2.4.9. Temperature 49
2.5. Anodic current 49
2.5.1. Electrostatic repulsion 50
2.5.2. Oxidation 50
Direct oxidation 50
Radicals 52
2.5.3. Gas generation 54
2.5.4. Low local pH 55
2.5.5. Electric field-induced mobility 56
2.5.6. Electroporation 57
2.5.7. Electro-wetting 57
2.6. AC-variable potential 57
2.6.1. Combination of mechanisms 57
2.6.2. Ion rearrangement 58
2.6.3. Temperature 58
Direct temperature effect 58
Rayleigh-Bernard convection 59
2.6.4. Volume changes of biofilm 60
2.6.5. Coupling reduction-oxidation reactions 60
2.6.6. Less detrimental to membrane materials 60
2.6.7. Disadvantages 61
2.7. Challenges and perspectives 61
2.8. References 65
3. Electrically Conductive Membranes – A Review of their Anti Fouling Applications – Part II 83
3.1. Abstract 84
3.2. Introduction 85
3.3. Antifouling applications 88
3.3.1. Biofouling 88

Anodic potential 90
Cathodic potential 96
Alternating potential 101
3.3.2. Organic fouling 107
Anodic potential 109
Cathodic potential 117
Alternating potential 123
3.3.3. Oil wetting 124
Anodic potential 125
Cathodic potential 125
3.3.4. Scaling and ion separation 128
Anodic potential 130
Cathodic potential 133
Alternating potential 140
3.4. Challenges and perspectives 140
3.5. References 142
4. The Effect of Cross-Linkers on the Permeability of Electrically Conductive Membrane 150
4.1. Abstract 151
4.2. Introduction 152
4.3. Materials and methods 156
4.3.1. Materials 156
4.3.2. Membrane fabrication 157
4.3.3. Surface analysis 159
4.3.4. Pure water flux 160
4.3.5. Selectivity test 160
4.4. Results and discussion 161
4.4.1. Selectivity 161
4.4.2. Chemical structure 162
4.4.3. Thin film morphology 162
4.4.4. Pure water permeance 165
4.4.5. Conductivity 168
4.4.6. Surface hydrophilicity 172

4.4.7. Surface roughness 174
4.5. Conclusions 176
4.6. Acknowledgments 177
4.7. References 177
4.8. Supporting Information 182
5. Investigating the Stability of Electrically Conductive Membranes 191
5.1. Abstract 192
5.2. Introduction 193
5.3. Materials and methods 195
5.3.1. Materials 195
5.3.2. Electrically conductive membrane preparation 195
5.3.3. Biosolution preparation and characterization 197
5.3.4. Biofouling experiment 197
5.3.5. Surface analysis 198
5.3.6. Electrochemical cell 199
5.3.7. Flux and rejection tests 199
5.4. Results and discussion 200
5.4.1. Anti-biofouling performance of ECMs 200
5.4.2. ECM stability 205
Electrochemical stability 205
Physical stability 211
Mechanical stability 216
5.4.3. Surface hydrophilicity and surface conductivity of ECMs 217
5.5. Conclusion 219
5.6. References 220
5.7. Supplementary Information 226
5.8. Supplementary Information II 241
Abstract 242
Method details 243
Materials and procedures 245
Electrochemical stability 245
Fixed potential chronoamperometry 246

Cyclic voltammetry 246
Four-point conductivity meter 247
Total organic carbon analyzer 247
Fourier-transform infrared spectroscopy (FTIR) 248
Micro scratch tester 248
Model foulant separation test 250
Method validation 252
Anodic oxidation 252
Scratch test 254
Rejection test 255
Acknowledgments 256
References 257
Supplementary Information 259
6. Quantifying the impact of Electrically Conductive Membrane Generated Hydrogen Peroxide and Extreme pH on the viability of Escherichia Coli Biofilms 260
6.1. Abstract 261
6.2. Introduction 262
6.3. Materials and methods 263
6.3.1. Chemical and solutions 263
6.3.2. CNT characterization 264
6.3.3. Membrane fabrication 264
6.3.4. Electrochemical cell 264
6.3.5. Hydrogen peroxide measurement 266
6.3.6. pH and zeta potential measurements 266
6.3.7. *E. Coli* suspension, treatment, and characterization 266
6.3.8. Biofilm formation and treatment in a flow cell 267
6.3.9. Biofilm characterization 267
6.4. Results and discussion 268
6.4.1. Electrochemical characteristics of the CNT-based electrode 268
Surface hydrogen peroxide production 268
Surface pH change 271
Other surface properties of CNT-based ECM 271

6.4.2. *E. Coli* cell viability in batch 272
Cell culturability using plate counting method 272
Cell viability using LIVE/DEAD staining method 274
6.4.3. *E. Coli* cell and biofilm integrity on flow-through membranes 275
Viability of biofilm under no stimuli 275
Impact of H_2O_2 on biofilm viability 276
Impact of high pH on biofilm viability 276
Impact of low pH on biofilm viability 277
6.5. Outlook 280
6.6. Acknowledgements 282
6.7. References 282
6.8. Supplementary Information 287
7. Conclusions and Recommendations 311
7.1. Key findings and contributions 312
7.2. Future work and recommendations 315
7.3. References 318

List of Figures

Figure 1.1. Membrane-based separation processes, pore sizes, molecular weight cut-off (MWCO) and examples of sizes of particles. Reprinted from [13], Copyright 2009, with permission from Elsevier. 4
Figure 1.2. Layers of typical thin film composite (TFC) flat sheet RO membrane. The chemical structure of the polyamide active layer (skin layer) creates selectivity. Reprinted from [30], Copyright 2015, with permission from Elsevier. 8
Figure 1.3. SEM of four fouling types on membrane surfaces: (a) Biofouling, (b) Organic fouling, (c) Inorganic scaling, and (d) Colloidal fouling. Reprinted from [37], Copyright 2017, with permission from Elsevier…….10
Figure 1.4. Membrane fouling process in MBRs: (a) pore blocking and (b) cake layer. Reprinted from [37], Copyright 2017, with permission from Elsevier……..11
Figure 1.5 Factors affecting bacteria attachment to membrane surface. Reprinted from [37], Copyright 2017, with permission from Elsevier……....12
Figure 1.6. Schematic of (a) EPS structure and (b) cell structure. Reprinted from [47], Copyright 2014, with permission from Elsevier……13
Figure 1.7. Sequence of events leading to the formation of a Biofilm. Reprinted from [46], Copyright 2011, with permission from Elsevier……14
Figure 1.8. Common studies on inorganic fouling for RO membranes between 2007 to 2017. Reprinted from [37], Copyright 2017, with permission from Elsevier……15
Figure 2.1. ECM review papers from 2015 to 2021 [9–11,27–33].....35
Figure 2.2. Examples of different electric current configurations applied to ECMs, (a), (c), and (e): Direct current. (b), (d), and (f): Alternating current. (e) and (f) are sometimes referred to as block current. 36
Figure 2.3. The range of electrical potentials commonly applied to ECMs, and the resulting electrical and electrochemical phenomena that could be used to prevent fouling. *: activation at low voltages requires high frequencies. §: depends on the foulant type (the range is for organic contaminates). †: depends on the gas evolution potential of the electrode (ranges are for carbon-based membranes). ‡: requires the presence of Cl and S in the solution.....37
Figure 3.1. SEM images supporting electroporation of *E. Coli* after filtration under (a) No current, (b) 20 V, (c) 20 V, higher magnification. Adapted with permission from [39]. Copyright 2013 American Chemical Society. 95
Figure 3.2. Normalized flux versus time during filtration of yeast, (Left): 2-3 min electrolysis (2 V cathodic potential, 2-3 min) every hour on CNT/PVDF membrane, black and green lines represent no electrolysis, and with electrolysis, respectively. Reprinted from [42], Copyright 2015, with permission from Elsevier. (Right): 30 s electrolysis (2 V cathodic potential) after biofiltration intervals of 30 min (green), 40 min (purple), and 60 min (blue) on MWCNT/PVDF membrane coated with Silver lines. Red line represents

the control experiment (absence of electrical potential). Reprinted from [43], Copyright 2014, with permission from Elsevier. 100
Figure 3.3. Normalized flux versus time during *Pseudomonas aeruginosa* filtration with and without application of electrical current on electrically conductive membranes (ECMs). Green, orange, and blue lines represent using electrochemical cleaning on ECMs, using electrochemical cleaning on non-conductive membranes, and absence of electrical field on ECMs, respectively. Red circles represent flush treatments. Reprinted with permission from [46]. Copyright 2013 American Chemical Society. 102
Figure 3.4. Permeate flux recovery by 30 min electrolysis using positive potential (1 V), negative potential (1 V), or alternating potential (1 V, 16.7 mHz) after 24-hour biofiltration of *Pseudomonas aeruginosa* using Ti as conductive feed spacer in a RO process. Reprinted with permission from [31]. Copyright 2014 American Chemical Society.....103
Figure 3.5. (Left): bacterial attachment versus block current exchange time intervals of 1 s, 1 min, 5 min, and 10 min (equivalent frequencies of 1 Hz, 16.7 mHz, 3.30 mHz, and 1.67 mHz) during 40 min of *Pseudomonas aeruginosa* filtration. In the control experiment, no current was applied. (Right): Dead/live staining images after 40 min of biofiltration (a) No current, (b) cathodic current (15 $\mu A/cm2 \approx 0.5 - 2.4$ V) (c) anodic current (15 $\mu A/cm2 \approx 0.5 - 2.4$ V), (d) alternating block current (15 $\mu A/cm2 \approx 0.5 - 2.4$ V, 1 min interval (equivalent frequency of 16.7 mHz). Damaged cells were detected by red color in propidium iodide (PI)/SYTO 9 ^{TM} assay kit and were assumed dead. Intact cells were detected by green color and assumed live. Reproduced with permission from [33]. 104
Figure 3.6. Removal efficiency of *E. Coli* under 10 V versus different frequencies. Adapted with permission from [39]. Copyright 2013 American Chemical Society.....107
Figure 3.7. (a) Schematic of apparatus for electrochemical filtration of 0.2 mM tetracycline (TC) using a CNT filter as the anode; (b) TC oxidative flux as a function of total cell potential and cathode potential. Reproduced from. Reprinted with permission from [76]. Copyright 2015 American Chemical Society. 112
Figure 3.8. Scheme of electrooxidation mechanisms of organic contaminants in the reactive electrochemical membrane (sub-stoichiometric titanium oxide) as a function of the depth of the membrane. Reprinted from [78], Copyright 2018, with permission from Elsevier. 113
Figure 3.9. Organic removal using ECMs. Schematic of electrochemical membrane filtration showing the effects of direct and indirect oxidation of tetracyline at an electrically conductive membrane used as an anode. Reprinted from [80], Copyright 2017, with permission from Elsevier. 114
Figure 3.10. Representative schemes of an electro-filtration system. The antifouling effect is produced by an applied external electrical field which produces a negative surface charges to repel NOM. Reprinted from [90], Copyright 2014, with permission from Elsevier. 119

Figure 3.11. TMP as a function of time for pristine PVDF and CNT/PVDF membranes in filtration of with a synthetic wastewater: (A) No electrical field; (B) 2V DC; (C) 0 V/2 V DC pulsed with 5 s intervals. Reprinted from [93], Copyright 2015, with permission from Elsevier. 121
Figure 3.12. (a) Normalized flux of CNTs/ceramic membrane during NOM filtration under different polarizations, (b) TOC removal efficiency on electropolarized CNTs/ceramic membranes. Conditions: [HA]in= 10 ppm, [pulse time] = 60 s, and [pressure] = 0.1 bar, cathodic, anodic, and alternating potentials applied were +1 V, -1 V, ± 1 V with a frequency of 16.7 mHz, respectively. Reprinted from [75], Copyright 2016, with permission from Elsevier. 124
Figure 3.13. On the left: Specific permeate flux versus time for treatment of 200 mg/L emulsified oily water with CTAB as surfactant [88]. Orange, purple, blue, and green represent uncoated membrane, Al_2O_3/ Ti_4O_7 ECM under no potential, Al_2O_3/ Ti_4O_7 ECM under anodic 30 V, and Al_2O_3/ Ti_4O_7 ECM under anodic 40 V, respectively. On the right: (a) flux decline over time for filtration of produced water from oil sands using graphene-based ECM. Red, brown, blue, and green represent no potential, 3 V cathodic potential, 6 V cathodic potential, and 9 V cathodic potential, respectively (b) optical images of feed and permeate solutions collected under different applied potentials, and (c) TOC removal performance of ECMs. Reprinted from [97], Copyright 2020, with permission from Elsevier. 128
Figure 3.14. Effect of applied anodic potential on silica and latex filtration using CNT/Al_2O_3 ECM: (a) silica removal efficiency, (b) normalized permeate flux for the filtration of silica solutions, and (c) latex removal efficiency. Black, red, green, and blue bars represent no potential, 0.5 V, 1 V, and 1.5 V, respectively. Reprinted with permission from [77]. Copyright 2015 American Chemical Society. 132
Figure 3.15. Iodine oxidation as a function of time at different anodic potentials in filtration of aqueous iodide and chloride solutions on MWCNT-ECMs. Application of 2 V and 3 V anodic potential resulted in significant iodine oxidation (green and blue lines, respectively), whereas application of 1 V and no potential cause no significant oxidation (red and black lines, respectively). Adapted with permission from [102]. Copyright 2011 American Chemical Society.....133
Figure 3.16. Effect of electrochemical cleaning (three consecutive cycles of 20 mA (3.6 V) cathodic DC for 50 min) on the permeate flux when filtering synthetic silicate solution CNTs/PVA coated polypropylene membrane. Using electrical field, permeate flux was rapidly recovered (red and black line), while in the absence of electrical potential, membrane was continuously fouled (blue and purple lines). Reprinted with permission from [103]. Copyright 2017 American Chemical Society. 134
Figure 3.17. Effect of cathodic applied potentials on the permeate flux by filtering synthetic wastewater solution on polypyrrole coated ECM working in an MBR. (a) under application of 1 V (0.2 V/cm potential drop, red line) and no potential (black line). Reprinted from [105], Copyright 2012, with permission from Elsevier. (b) under

application of 1 V (0.2 V/cm, red line), 2 V (0.4 V/cm, blue line), and no potential (black line). Reprinted from [104], Copyright 2013, with permission from Elsevier. 136
Figure 3.18. Effect of applying periodic electric current on the normalized permeate flux when filtering $CaCO_3$ solution through MWCNTs coated PVDF membrane. Periodic electric field (cathodic 2 V) was applied between filtration cycles of 60 min (blue line), 40 min (purple line), 30 min (green line), while control experiment (no electrochemical cleaning) is presented by red line. Reprinted from [43], Copyright 2014, with permission from Elsevier. 137
Figure 3.19. Schematic illustration of ammonia recovery from nitrogen-rich wastewater using electrically conductive membrane cathode. ECMs produced high local concentrations of OH^- under application of negative potential (0.8 V), that promotes transformation of ammonium to ammonia gas. Reprinted with permission from [108]. Copyright 2018 American Chemical Society. 140
Figure 4.1. (a) the CNT network contains cross-linkers which help control the porosity of the network. (b) dicarboxylic acids of different lengths are used as cross-linkers. 156
Figure 4.2. (a) Pristine PES membrane (on the left) and electrically conductive membrane (on the right), (b) Four-point conductivity probe.....160
Figure 4.3. Rejection properties of pristine PES as well as 1 mg and 3 mg CNT UF membranes using 250 ppm PEO filtration test. 162
Figure 4.4. SEM images of MF membranes with CNT thin film made with 1 mg (left column) and 3 mg (right column). Top row (A), (B): control CNT thin films, Middle row (C), (D): succinic acid cross-linked CNT thin films (20% CL), Bottom row (E), (D): suberic acid cross-linked CNT thin films (20% CL). 164
Figure 4.5. SEM images of UF membranes with CNT thin film made with 1 mg (left column) and 3 mg (right column). Top row (A), (B): control CNT thin films, Middle row (C), (D): succinic acid cross-linked CNT thin films (20% CL), Bottom row (E), (D): suberic acid cross-linked CNT thin films (20% CL). 165
Figure 4.6. Pure water permeance of (a) MF and (b) UF membranes having different cross-linkers. 168
Figure 4.7. Effect of CNT mass, cross-linkers, and degree of functionalization on the surface conductance of the (a) MF and (b) UF thin film. 171
Figure 4.8. Effect of CNT mass, cross-linkers, and degree of functionalization on the bulk conductivity of the (a) MF and (b) UF thin film. 172
Figure 4.9. Contact angle test for (a) MF and (b) UF membranes with different CNT mass, cross-linkers, and degree of functionalization. 174
Figure 4.10. AFM images for MF membranes (A) Control 1mg, (B) Control 3mg, (C) Suberic acid 1mg, (D) Suberic acid 3 mg. 175
Figure 4.11. AFM images for UF membranes (A) Control 1mg, (B) Control 3mg, (C) Suberic acid 1mg, (D) Suberic acid 3 mg. 176
Figure 4.S1. Top view SEM images of A) MF 3 mg CNT, succinic acid, B) MF 3mg CNT, suberic. 182

Figure 4.S2. TOC results of water and 250 ppm 2MDa PEO filtration.....184
Figure 4.S3. (Top) Four-point conductivity probe, (bottom) Result sheet of Hall software. 186
Figure 4.S4. Sequence of contact angle images from dispense time to steady state (Control 1mg CNT).....187
Figure 4.S5. AFM images for MF membranes where 2D images are on the left column and height mode is on the right column. (A) Control 1mg, (B) Control 3mg, (C) Suberic acid 1mg, (D) Suberic acid 3 mg. 189
Figure 4.S6. AFM images for UF membranes where 2D images are on the left column and height mode is on the right column. (A) Control 1mg, (B) Control 3mg, (C) Suberic acid 1mg, (D) Suberic acid 3 mg. 190
Figure 5.1. a) Schematic of the custom-designed cross-flow cell to assess ECM anti-biofouling performance b) Schematic of the batch electrochemical cell to check ECM anodic stability. 198
Figure 5.2. Membrane flux during a 4 h cross-flow filtration of the bacterial suspension. Gray: Control PES membrane with no applied potential, Black: Control CNT membrane (1 mg CNT) with no applied potential, Red: CNT membrane (1 mg CNT) used as an anode with an applied total cell potential of 2 V, Blue: CNT membrane (1 mg CNT) used as a cathode with an applied total cell potential of 2 V (a) rejection and actual measured flux, and (b) relative flux values. Error bars represent standard deviation for two membranes. 203
Figure 5.3. SEM images of the pristine PES membranes (first row), biofouled PES after 4 h (second row), biofouled ECM without applied potential after 4 h (third row), biofouled ECM after 4 h under an applied anodic potential of 2 V (fourth row), and biofouled ECM after 4 h under an applied cathodic potential of 2 V (fifth row). Left column: low magnification, middle column: medium magnification, and right column: high magnification of the membrane surfaces. 204
Figure 5.4. Electrochemical batch test for ECMs containing glutaraldehyde (GA), and a blend of polyvinyl alcohol (PVA) and either GA or succinic acid (SA). The ECM, graphite sheet, and an Ag/AgCl electrode were used as the working electrode (anode), counter electrode, and reference electrode, respectively. (a) Fixed potential chronoamperometry was applied to the conductive membrane with a total cell potential of 4 V (vs. Ag/AgCl reference electrode) for 20 min. (b) Normalized conductivity before and after a constant linear potential of 4V (vs. Ag/AgCl electrode) was applied to ECMs. (c) Fixed potential chronoamperometry was applied to the conductive membrane with a total cell potential of 2 V (vs. Ag/AgCl reference electrode) for 240 min. Error bars represent standard deviation for two membranes. All ECMs contained 1 mg CNT. "xPVA" shows the mass ratio of PVA to CNT. [PBS]= 137 mM sodium chloride, 2.7 mM potassium chloride, and 10 mM phosphate buffer. 211
Figure 5.5. SEM images of UF electrically conductive membrane composed of CNT and PVA with a mass ratio of 1:10. Left: low magnification, right: high magnification. 212

Figure 5.6. Carbon content in the collected permeate in the PEO (2 MDa) separation tests measured by a TOC analyzer. ECMs contained 1 mg CNT in the nanolayer. "N× PVA" shows the mass ratio of PVA to CNT where N is the multiplicative factor for mass. (a) Values were measured at PEO concentrations of either 50 or 250 ppm in water and at pressures of 10 psi or 100 psi (0.69 bar or 6.90 bar). PVA to CNT mass ratio was kept at 10:1. (b) CNT: PVA ratio was varied from 1:0.5 to 1:10 and the resultant leaching of PVA was measured. Concentration of GA solution was 2.12w% in all cases. GA and SA stand for glutaraldehyde and succinic acid used in the network. Error bars represent standard deviation for three membranes. Tests were conducted at 10 psi (0.69 bar). 213
Figure 5.7. (a) The impact of CNT mass in the nanolayer on permeate carbon content. 1 mg or 3 mg CNT mass loadings were used in ECMs. PVA to CNT mass ratio was 10:1 in both cases. PEO (2 MDa) was used as the model foulant with a concentration of 250 ppm in water. Error bars represent standard deviation for three membranes. (b) Mechanistic diagram of the correlation between CNT thickness and concentration polarization. I) The thin nanolayer induces a more significant CP effect and subsequent local pressure increases, which causes PVA leaching. II) An increase in the nanolayer thickness reduces the effect of CP on surface pressure, which leads to less PVA leaching. 216
Figure 5.8. The Mechanical stability of ECMs containing different polymer binders, polyvinyl alcohol (PVA), succinic acid (SA), and glutaraldehyde (GA) measured in the micro-scratch tester. Nanolayer consists of (a) CNT, (b) CNT/PVA/SA, and (c) CNT/PVA/GA. The tip applied a normal force of 0.5 N with a scratch length of 5 mm and a scratch speed of 5 mm/min. All ECMs contained 1 mg CNT in the nanolayer. PVA to CNT mass ratio was kept at 10:1. 217
Figure 5.9. (a) Contact angle, and (b) Surface conductance of ECMs containing different polymer binders, polyvinyl alcohol (PVA), glutaraldehyde (GA), succinic acid (SA) and a blend of PVA and GA. All ECMs contained 1 mg CNT in the nanolayer. "xPVA" shows the mass ratio of PVA to CNT. The PVA: CNT mass ratio was changed from 0:1 to 10:1. Error bars represent the standard deviation of nine measurements (three samples each measured three times). 219
Figure 5.S1. Custom-made cross-flow cell for biofouling experiments. 228
Figure 5.S2. Electrochemical Cell. ECM, Ag/AgCl electrode, and graphite were used as anode, reference electrode, and cathode, respectively. The electrolyte used was 10 mM PBS. 229
Figure 5.S3. Crystal violet-stained membranes after filter bacteria for 4 h. (a) Relative bacteria concentrations on the surface of membranes as measured by crystal violet staining Red: control PES membrane with no applied potential, Black: Control CNT membrane (1 mg CNT mass loading) with no applied potential, Gray: CNT membrane (1 mg CNT) used as a cathode with 2V applied potential. Error bars represent the standard deviation for two membranes. Images under (b) ambient light, and (c) UV light at a wavelength of 365 nm. 229

Figure 5.S4. Potential of the cathode in response to a 150 mA current (vs. Ag/AgCl reference electrode) applied to the electrode composed of CNT/PVA/SA for 3 hr. 230
Figure 5.S5. Electrochemical batch test for ECMs containing glutaraldehyde (GA), and a blend of polyvinyl alcohol (PVA) and either GA or succinic acid (SA). The ECM, graphite sheet, and an Ag/AgCl electrode were used as the working electrode (anode), counter electrode, and reference electrode, respectively. Fixed potential chronoamperometry was applied to the conductive membrane (a) with a total cell potential of 4 V (vs. Ag/AgCl reference electrode) for 20 min. (b) with a total cell potential of 2 V (vs. Ag/AgCl reference electrode) for 240 min. All ECMs contained 1 mg CNT. "xPVA" shows the mass ratio of PVA to CNT. [PBS]= 137 mM sodium chloride, 2.7 mM potassium chloride, and 10 mM phosphate buffer. 232
Figure 5.S6. Fourier-transform infrared (FTIR) spectroscopy reflecting the presence of carbonyl bonds. 232
Figure 5.S7. Fixed potential chronoamperometry for membranes with different chemistries. Trials were conducted for each network as follows: (a) Control CNT, (b) CNT/GA, (c) CNT /10x PVA /SA (1:10), (d)-(e) CNT/PVA/GA. ECM, graphite sheet, and an Ag/AgCl electrode were used as the working electrode (anode), counter electrode, and reference electrode, respectively. The total cell potential was 2 V. All ECMs contain 1 mg CNT. 233
Figure 1.S8. Cyclic voltammetry for conductive membranes with different chemistries. ECMs contain 1 mg CNT mass loading. The conductive ECM, graphite sheet, and an Ag/AgCl electrode were used as the working electrode (anode), counter electrode, and reference electrode, respectively. The scan range was 0-3 V at a scan rate of 0.1 mVs^{-1}……..……...234
Figure 5.S9. Measurements of carbon content in the 200 mL electrochemical cell electrolyte after a constant linear potential of 4V (vs. Ag/AgCl electrode) was applied to ECMs containing different polymer binders, polyvinyl alcohol (PVA), glutaraldehyde (GA), and succinic acid (SA) for 20 min. The ECM, graphite sheet, and an Ag/AgCl electrode were used as the working electrode (anode), counter electrode, and reference electrode, respectively.....235
Figure 5.S10. The carbon content for the collected permeate in the PEO separation tests, measured by a TOC analyzer. PEO (2 MDa) was used as the model foulant at a feed concentration of 250 ppm in water. ECMs contained 1 mg CNT in the nanolayer.....236
Figure 5.S11. High degree of carbon content found in the permeate during the PEO rejection test can be solely ascribed to PVA leaching. 237
Figure 5.S12. The impact of CNT incorporation in the nanolayer on TOC results. 1 mg or 3 mg CNT mass loadings were used in ECMs. PEO (2 MDa) was used as the model foulant with a concentration of 250 ppm in water. Error bars represent the standard deviation for three membranes.....237
Figure 5.S13. The mechanical stability of membranes with different chemistries measured by micro-scratch testing. Two trials for each nanolayer network were conducted as

follows: (I) CNT, (II) CNT/PVA/SA, (III) CNT/GA, and (IV) Pristine PES. The tip applied a normal force of 0.5 N and the scratch length and scratch speed were 1 mm and 5 mm/min, respectively.....239
Figure 5.S14. Surface images of membranes after the micro-scratch test. Trials for each nanolayer network were conducted as follows: (I) CNT, (II) CNT/PVA/SA, (III) CNT/GA, and (IV) Pristine PES. The tip applied a normal force of 0.5 N and the scratch length and scratch speed were 5 mm and 5 mm/min, respectively.....240
Figure 1. Cyclic voltammetry. ECM contains 1 mg CNT mass loading. The conductive ECM, graphite sheet, and an Ag/AgCl electrode were used as the working electrode (anode), counter electrode, and reference electrode, respectively. The scan range was 0-3 V at a scan rate of 0.1 mVs^{-1}.....253
Figure 2. Fixed potential chronoamperometry for membranes with different chemistries containing CNT, PVA, and cross-linkers. Trials were conducted for each network as follows. ECM, graphite sheet, and an Ag/AgCl electrode were used as the working electrode (anode), counter electrode, and reference electrode, respectively. The total cell potential was 4 V. All ECMs contain 1 mg CNT. 254
Figure 3. The mechanical stability of an ECM measured in the micro-scratch test with different input settings. The settings are as follows: (A) The tip of radius 200 μm applied a normal force of 0.5 N and the scratch length and scratch speed were 1 mm and 5 mm/min, and (B) The tip of radius 100 μm applied a normal force of 15 N and the scratch length and scratch speed were 5 mm and 5 mm/min. 255
Figure S1. The mechanical stability of an ECM measured in the micro-scratch test with different input settings. The settings are as follows: (A) The tip of radius 100 μm applied a normal force of 0.5 N and the scratch length and scratch speed were 5 mm and 5 mm/min, and (B) The tip of radius 200 μm applied a normal force of 0.5 N and the scratch length and scratch speed were 5 mm and 5 mm/min, respectively. 259
Figure 6.1. (a) Schematic of the electrochemical batch cell. Electrochemical flow-through cell: (b) Schematic, (c) Picture; green, orange, and blue colors represent feed, retentate, and permeate lines.....266
Figure 6.2. (a) Cyclic voltammetry for CNT-ECM. The conductive ECM, graphite sheet, and an Ag/AgCl electrode were used as the working electrode, counter electrode, and reference electrode, respectively. The scan range was -3 V to +3 V at a scan rate of 0.1 mVs-1. Red arrows show applied current direction and the star indicates the onset of hydrogen peroxide generation , (b) Steady state H2O2 measured at the bulk of the electrochemical cell under different applied negative currents (20 – 150 mA, 1.66 – 2.69 V) over 180 min, Blue, red, black, and green colors represent 20 mA, 50 mA, 100 mA, and 150 mA, respectively, (c) Steady state pH measured at the surface of the CNT-ECM under different applied electrical currents (± 20 – 100 mA, 1.66 – 2.45 V), (d) pH measured at the bulk of the electrochemical cell under different applied negative currents (20 – 100 mA, 1.66 – 2.45 V) over 180 min, (e) Dissolved oxygen measured in the bulk

of the electrochemical cell under different applied negative currents (20 – 150 mA, 1.66 – 2.69 V) over 180 min, (f) CNT-ECM before and after electrolysis working as a cathode under 150 mA (2.69 V) for 180 min. ECMs contain 1 mg CNT. Error bars represent the standard deviation for three data points. 270
Figure 6.3. (Top row) Cell culturability of E. Coli after exposure to different pH values (3, 5, 10, and 12) and different H2O2concentrations (0, 33.2, and 188 μM). Error bars represent the standard deviation for four data points. (Bottom row) Cell viability of E. Coli using LIVE/DEAD staining method after exposure to different pH values (3, 5, 10, and 12) and different H2O2 concentrations (0, 33.2 and 188 μM). Error bars represent standard deviation for six data points. 274
Figure 6.4. (a) Confocal laser scanning microscopy images, and (b) Quantitative cell count analysis of Treated E. Coli biofilms under different stimuli including the following conditions: control, H2O2 (188 μM), NaOH (pH 11), HCl (pH 3.5), cathodic potential (2 V), and anodic potential (2 V). Error bars represent the standard deviation for four samples.....280
Figure 6.5. Scanning electron microscopy images of treated E. Coli biofilm under different stimuli including control condition, H2O2 (188 μM), low pH (3.5), high pH (11), anodic potential (2 V), and cathodic potential (2 V). Yellow ovals highlight representative bacteria at the surface. 280
Figure 6.S1. Picture of the electrochemical batch cell.....288
Figure 6.S2. Detection of H_2O_2 using the Amplex® Red Hydrogen Peroxide/Peroxidase Assay Kit. The inset shows the sensitivity of the assay at very low levels of H_2O_2. Background fluorescence, determined for a no-H_2O_2 control reaction, has been subtracted from each value. The best linear model fit on data is Y=2059 X with an R^2 value of 0.9966, where Y is fluorescence and X is hydrogen peroxide concentration (μM). Error bars represent the standard deviation for three data points. 290
Figure 6.S3. The zeta potential of *E. Coli* suspension at different pH values (4, 7, and 11). Error bars represent the standard deviation for three data points. 291
Figure 6.S4. Relative viability of *Escherichia Coli* in fluorescence microplate reader. Live and Dead suspensions were mixed with ratios of 100:0, 90:10, 50:50, 10:90, and 0:100. Green fluorescence was acquired by cell excitation and emission of 485 ± 20 nm and 535 ± 25 nm, respectively. Red fluorescence was acquired by cell excitation and emission 485 ± 20 nm and 635 ± 35 nm, respectively. Green/Red fluorescence ratio was calculated for each proportion of live:dead *Escherichia Coli* suspension. The best linear model fit on data is Y=1.32 X + 0.28 with an R^2 value of 0.9884, where Y is Green/Red fluorescence ratio and X is live percentage of *Escherichia Coli* suspension. Error bars represent the standard deviation for six data points. 292
Figure 6.S5. Picture of the low-pressure flow-through system. 1: Reservoir, 2: Pump, 3: Flow cell, 4: Air regulator, 5: Pressure sensor, 6: Flow sensor, 7: DC power generator. Green, orange, and blue colors represent feed, retentate, and permeate lines. 294

Figure 6.S6. Absorbance values of bacterial enriched suspension at different dilution ratios with PBS buffer. Biosuspension had initial concentration of 7×108 CFU/mL and mixtures were prepared with biosuspension: PBS ratios of 1:0, 0.8:0.2, 0.6:0.4, 0.4:0.6, 0.3:0.7, 0.2:0.8, 0.1:0.9, 0.075:0.925, 0.05:0.95, 0.025:0.975, and 0:1. The best linear model fit on data is Y=0.1729 X + 0.046 with an R^2 value of 0.9928, where Y is absorbance at OD_{600} and X is percentage of bacterial enriched suspension. Error bars represent the standard deviation for three data points. 295
Figure 6.S7. Picture of the biofouled membrane after 18 h filtration of *E. Coli* suspension with a concentration of 1×107 CFU/mL. 295
Figure 6.S8. (a) Transmission electron microscopy (TEM) of carbon nanotubes, (b) Scanning electron microscopy (SEM) of CNT-ECM. 297
Figure 6.S9. XPS scans of carboxylated CNTs. (a) Survey spectrum (0.0-1100.0 eV), (b) C1s (284.8-291.3 eV) and O1s (531.3-535.7 eV) scans. 298
Figure 6.S10. EDS analysis on carbon nanotubes. (Top) Map sum spectrum, (bottom) Electron image, carbon map, and oxygen map. 299
Figure 6.S11. Thermal analysis curve of carboxylated CNTs. 300
Figure 6.S12. Measured hydrogen peroxide concentration at the bulk of the electrochemical cell under different applied currents (20-150 mA) over 180 min. Error bars represent the standard deviation for three data points. 301
Figure 6.S13. Measured and theoretical molar mass of generated hydrogen peroxide at the bulk of the electrochemical cell under applied electrical current equal to 50 mA over time. 303
Figure 6.S14. The measured hydrogen peroxide concentration at the bulk of the electrochemical cell at 50 mA over 180 min. Red and black lines represent hydrogen peroxide concentration for CNT and graphite electrodes, respectively. 305
Figure 6.S15. pH measured at the bulk of the electrochemical cell under different applied current equal to -150 mA over 180 min. 306
Figure 6.S16. Measured electrical potential of the working electrode (CNT-ECM) under different applied currents (20-150 mA) over 180 min, and (c) CNT-ECM before and after electrolysis working as a cathode under 150 mA for 180 min. Blue, red, black, and green colors represent 20 mA, 50 mA, 100 mA, and 150 mA, respectively. 307
Figure 6.S17. CNT membrane before and after electrolysis acting as a working electrode (anode) under 150 mA for 180 min. 307
Figure 6.S18. Top row: Cell culturability of *E. Coli* after exposure to different pH values (4, 11) and different H_2O_2 concentrations (0, 33.2, and 188 μM). Error bars represent the standard deviation for four data points. Bottom row: Cell viability of *E. Coli* using LIVE/DEAD staining method after exposure to different pH values (4, 11) and different H_2O_2 concentrations (0, 33.2 and 188 μM). Error bars represent standard deviation for six data points. 308
Figure 6.S19. CNT-ECM rejection over 21 h filtration of *E. Coli* suspension in flow-through cell. Biosuspension had initial concentration of 1×107 CFU/mL. 309

Figure 6.S20. (a) Scanning electron microscopy images of treated *E. Coli* biofilm with the magnification of x3000. In the top row, biofilms are treated with no stimulus, anodic potential (2 V), and low pH (4), respectively, and in the bottom row, the biofilms are treated with hydrogen peroxide (188 μM), cathodic potential (2 V), and high pH (11), respectively, (b) advanced stage of cellular deformation induced by anodic oxidation. .310

List of Tables

Table 3.1. Summary of research on biofouling control and biofouling inactivation on conductive membranes by applying different current types and magnitudes. 89
Table 3.2. Summary of published ECM studies targeting organic matter. 108
Table 3.3. Summary of ECM studies targeting oil separation. 124
Table 3.4. Summary of published studies regarding scale removal and ion rejection on conductive membranes. 129
Table 4.1. Thickness of the membranes obtained from SEM images 169
Table 1. Specifications of the micro scratch tester (Anton Paar) 249
Table 2. Micro scratch settings used 249
Table 3. Operating conditions of the separation test 252
Table 6.S1. Information on materials, their properties, and suppliers. 287
Table 6.S2. The proportions of elements in XPS spectra of CNTs. 298
Table 6.S3. Information of UF membrane process for calculating specific energy consumptions. 310

List of Acronyms and Abbreviations

aSBR	anaerobic sequencing batch reactors
AA	alginic acid
AC	alternating current
AFM	atomic force microscopy
AOP	advanced oxidation processes
BDD	boron-doped diamond
BI	Biointerfaces Institute
BPA	Bisphenol A
BSA	bovine serum albumin
BTO	bismuth-doped tin oxide
CA	cellulose acetate
CCEM	Canadian Centre for Electron Microscopy
CE	counter electrode
CFU	colony forming units
CLSM	confocal laser scanning microscopy
CM	coal-based carbon membrane
CN	cellulose nitrate
CNF	carbon nanofiber
CNS	carbon nanostructures
CNT	carbon nanotube

CoA	coenzyme A
COD	chemical oxygen demand
CP	concentration polarization
CV	cyclic voltammetry
DC	direct current
DI	Deionized
DLVO	Derjaguin, Landau, Verwey, and Overbeek
DWCNT	double-walled carbon nanotube
EAOP	electrochemical advanced oxidation process
ECM	electrically conductive membrane
ECMR	electrochemical ceramic membrane reactor
EDL	electric double layer
EIS	electrochemical impedance spectroscopy
EPS	extracellular polymeric substances
FO	forward osmosis
FS	flat sheet
FTIR	Fourier-transform infrared spectroscopy
GA	glutaraldehyde
GO	graphene oxide
HA	humic acid
HEP	hydrogen evolution potential
HF	hollow fiber

ITO	indium tin oxide
LIG	laser-induced graphene
MBR	membrane bioreactor
MD	membrane distillation
MEC	microbial electrolysis cell
MF	microfiltration
MO	metal oxide
MW	molecular weight
MWCNT	multi-walled carbon nanotube
MWCO	molecular weight cut-off
NF	nanofiltration
NOM	natural organic matter
NSERC	Natural Sciences and Engineering Research Council of Canada
OA	oxalic acid
OCP	open circuit potential
OEP	oxygen evolution potentials
OER	oxygen evolution reactions
ORR	oxygen reduction reactions
PA	polyamide
PAN	polyacrylonitrile
PANI	polyaniline

PB	Poisson-Boltzmann
PBS	phosphate buffered saline
PCT	paracetamol
PE	polyethylene
PEO	poly(ethylene oxide)
PES	polyether sulfone
PI	propidium iodide
PP	polypropylene
PPSU	polyphenylsulfone
PPy	polypyrrole
PS	polysulfone
PTFE	polytetrafluoroethylene
PVA	polyvinyl alcohol
PVDF	polyvinylidene fluoride
PVP	polyvinylpyrrolidone
RE	reference electrode
REM	reactive electrochemical membranes
RO	reverse osmosis
ROS	reactive oxygen species
SA	succinic acid
SDS	sodium dodecyl sulfate

SEC specific energy consumption

SEM scanning electron microscopy

SMP soluble microbial products

SP spiral wound

TC tetracycline

TFC think film composite

TMP transmembrane pressure

TOC total organic content

UF ultrafiltration

WE working electrode

WHO World Health Organization

Preface – **Declaration of Academic Achievement**

This Ph.D. dissertation is organized in a "sandwich style" based on published, submitted, and prepared for submission articles described below:

- Chapter 2: Halali, M. A.; de Lannoy, C.-F. Electrically Conductive Membranes – A Review of their Anti-Fouling Mechanisms. Pending submission to Elsevier Water Research: June 2021.
- Chapter 3: Halali, M. A.; Zhang, N.; Ganzoury, M.; de Lannoy, C.-F. Electrically Conductive Membranes – Electrically Conductive Membranes – A Review of their Anti Fouling Applications. Pending submission to Elsevier Water Research: June 2021.
- Chapter 4: Halali, M. A.; de Lannoy, C.-F. The Effect of Cross-Linkers on the Permeability of Electrically Conductive Membranes. Ind. Eng. Chem. Res. 2019, 58 (9), 3832–3844. https://doi.org/10.1021/acs.iecr.8b05691.
- Chapter 5: Halali, M. A.; Larocque, M.; de Lannoy, C. F. Investigating the Stability of Electrically Conductive Membranes. J. Memb. Sci. 2021, 627, 119181. https://doi.org/10.1016/j.memsci.2021.119181.
- Chapter 5-Supplemtary Information: Halali, M. A.; de Lannoy, C.-F. Stability assessment of electrically conductive membranes. Submitted to Elsevier MethodsX: June 2021.
- Chapter 6: Halali, M. A.; de Lannoy, C.-F. Quantifying the impact of Electrically Conductive Membrane Generated Hydrogen Peroxide and

Extreme pH on the viability of Escherichia Coli Biofilms. Submitted to ACS Environmental Science and Technology: June 2021.

All the papers listed above were prepared, conducted, analyzed, and written by Mohamad Amin Halali between Jan 2017 to May 2021 under direct supervision of Dr. Charles-François de Lannoy, who also contributed to project planning as well as writing and revising the articles. In Chapter 3, Nan Zhang and Mohamed Ganzoury helped with writing some subsections of the paper. In Chapter 4, undergraduate students Alexander Sutherland and Al-Asel Maizer helped perform a part of flux experiments, and Dr. Heera Marway helped with conducting the AFM test. In Chapter 5, Melissa Larocque helped with final proofreading. Dr. Carlos Filipe kindly donated bacterial samples and Dr. David Latulippe generously offered bench space in Biosafety Lab JHE 221 to conduct the experiments described in section 6.

Chapter 1

Introduction and Literature Review

1.1. Water stress

Water stress has become a global concern as millions of people lack access to potable water more particularly over the last decade. While water covers 97% of our "blue earth", only 2.5% of water resources is considered as fresh water. Fresh water is mostly stored as glaciers in the poles (70%), while less than 30% is accessible to us as fresh surface water and groundwater [1]. In addition to limited available water resources, unequal distribution of freshwater resources across the globe has signified the water stress. Water scarcity has primarily occurred in countries with high population density or intense irrigated agriculture (India, China) as well as countries with low natural resources regardless of their population or agricultural activities (Arabian Desert, Sahara, Gobi, and Central Australia deserts) [2]. In addition, the availability of fresh water has been seriously threatened by rapid population growth, climate change, and environmental contamination [3]. Rapid Population growth, constant improvements in living standards, and expansion of irrigated agriculture have dramatically enhanced the demand for fresh water, leading to depletion of ground water resources. Global warming has led to drastic changes in the weather, such as drought, while environmental contamination has compromised our ecosystem by lowering fresh water quality.

A study conducted in 2016 has shown that 66% of the global population (4 billion) live under severe water scarcity [2]. The severity of water scarcity has raised concerns at local and global levels. Local authorities have sought to manage water resources to better allocate fresh water to populated areas and communities of need [4], while on a global level, the United Nations has acknowledged the importance of equitable access to clean and safe water as a human right [5]. Recognition of water scarcity as a high-level global concern and inadequacy of the current infrastructures to purify water necessitates fostering newer strategies for innovative water resource management and development of advanced sustainable technologies. Water resource management has recently aimed to expand water

supply beyond the traditional hydrological cycle, unlocking the full potential of lesser-used unlimited water supplies such as seawater and wastewater. Desalination is considered a viable unban water source, particularly in areas affected by climate change, limited freshwater resources, or frequent flooding. In addition, desalination has found applications for agriculture, food processing units, power plants, and oil refineries.

The reuse of wastewater is another viable strategy, playing a pivotal role in expanding urban water supplies. Wastewater is an unlimited water source with predicted effluent quality and quantity, turning it into an exciting option for water reuse applications [6]. Recycling wastewater is challenging due to presence of recalcitrant contaminants, the possibility of waterborne bacterial and viral diseases, cost of transportation via pipes, strict regulations, and low public acceptance. Recently, decentralized systems such as membranes have been adopted in many wastewater treatment plants across Europe and North America to enhance the quality of effluent and comply with strict regulations [5]. The main advantage of decentralized facilities is their flexibility, low energy consumption, and lower cost of technology replacement. Membranes have shown promise among decentralized technologies due to their high reliability, small size, and high permeate quality. Membranes are well-compatible with the existing infrastructure in treatment plants. In fact, membranes have shown great promise to replace conventional upstream treatment operations such as flocculation, settling, and granular media filtration. In addition, membranes have been presented as rapid solutions to wastewater treatment challenges in developing countries owing to their ease of transportation and installation, flexibility, and wide range of selectivity.

Fouling is the major problem plaguing membranes' performance regardless of their application. However, advantages with their quality, flexibility and versatility have made them popular and reliable options for water treatment, wastewater treatment, and water reuse applications, while advances in their energy-efficiency and antifouling properties have been constantly sought by researchers across academia and industry.

1.2.Membrane technology

1.2.1. Membrane classification and application

Since the development of the first commercial membrane in 1963 by Loeb-Sourirajan [7] (although the first recorded membrane dates back to 1867 [8]), membrane technology has proved to be a rapidly growing technology and has found an important role in several applications [9–12]. Pressure-driven membranes are classified with respect to their pore size and separation mechanisms. Commercially available membranes include microfiltration (MF), ultrafiltration (UF), nanofiltration (NF), and reverse osmosis (RO). In pressure-driven membranes, the solvents and solutes are forced to permeate through the membrane while other particles and solutes are separated with respect to membrane structure. For example, MF membranes separate a wide range of particles with respect to their pore size, while RO membranes are nonporous, and their selectivity results from the solution-diffusion mechanism. There is no sharp cut-off between selectivity of pressure-driven membranes; however, a breakdown of membranes and their properties is presented in Figure 1.1.

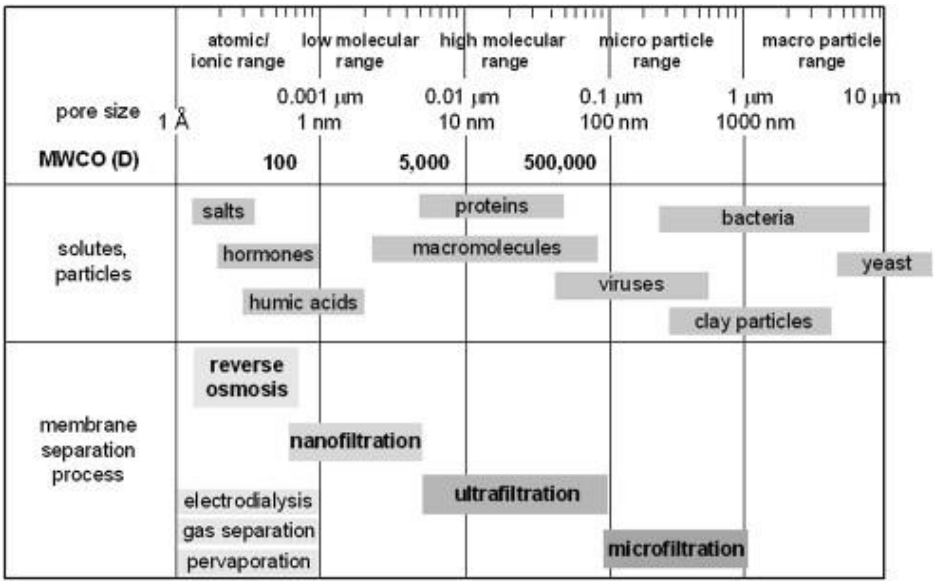

Figure 1.1. Membrane-based separation processes, pore sizes, molecular weight cut-off (MWCO) and examples of sizes of particles. Reprinted from [13], Copyright 2009, with permission from Elsevier.

Microfiltration membranes

The pore size of microfiltration (MF) membranes ranges from 0.1 to 10 µm. Molecular weight cut-off (MWCO) is an alternative method to classify membranes. MWCO of a membrane represents the lowest molecular weight (MW, often reported as Daltons (Da)) with the rejection efficiency equal to or higher than 90%. MF membranes can remove particles with MW larger than 1000 kDa, such as suspended solid, proteins, oil-water emulsions, bacteria, and viruses [14]. The application of MF membranes can be found in pharmaceutical industry (separation and purification of enzymes and antibiotics), electronic industry (ultra-pure water for semiconductors), cell harvesting and membrane bioreactors, analytical processes, and automobile industry [15,16]. In addition, MF membranes have received significant attention in water treatment and wastewater treatment to replace the clarification stage, where sand filtration had been traditionally used. MF membrane can be used in combination with downstream membrane processes (UF, NF, RO) to minimize fouling caused by large particles [17].

Ultrafiltration membranes

Ultrafiltration membranes are the closest class to MF membranes with a narrower pore size (0.01-0.1 µm) [15,16]. UF membranes can retain macromolecules, colloids, algae, bacteria, viruses, and turbidity. MF and UF membrane are both considered as low-pressure operating membranes as compared to NF and RO membrane where rejection is mainly controlled by their pore size and shape of the foulant. Application of UF membranes has been progressed to the pharmaceutical industry, food and dairy industry, textile industry, metallurgy, and paper industry [15,16]. In addition, UF membranes have become popular systems to replace traditional separation units such as coagulation, clarification, sedimentation, and sand filtration processes [18].

Reverse osmosis membranes

Reverse osmosis (RO) membranes are nonporous and allow for water passage while selectively removing monovalent ions and small charged organic compounds. RO membranes can reject NaCl with rejection efficiencies higher than 95% [19]. RO processes have been used for seawater desalination, brackish water desalination inland, and water

reuse applications [20,21]. The common RO membranes are made of polyamide (PA) and cellulose acetate (CA), with PA holding over 90% of the market share [19]. The major downfalls with RO membranes is susceptibility to chlorine and their low boron rejection efficiency [19].

Nanofiltration membranes

Nanofiltration (NF) membranes have small pore size (1-10 nm) [22]. NF membranes are mainly fabricated via interfacial polymerization (IP) like RO membranes but have significant differences with RO membrane, including being (a) more permeable, (b) less selective, and (c) less energy-intense. The main applications of NF membrane include water softening, removal of small organic particles and micro-pollutant, and removal of small-sized dyes in the textile industry [18,22].

1.2.2. Membrane materials

The selection of membrane materials depends on many parameters including their physicochemical properties (hydrophilicity, charge, roughness), cost, chemical and mechanical stability, ease of fabrication, scalability, and versatility to different operations. For example, many studies have shown that hydrophilic surfaces alleviate fouling intensity [23,24], as most particles in water are hydrophobic including organic substances, bacteria, and oil contaminants. Therefore, increases in surface hydrophilicity enhance the surface energy and decrease the affinity between hydrophobic contaminants and surface [23,24]. In addition, the chemical, physical, and thermal stability is another important factor in membrane fabrication due to the repetitive exposure of membranes to harsh chemical and thermal cleaning procedures depending on their application.

Membrane materials are classified into two main groups: inorganic and polymeric [25]. Inorganic materials mostly consist of ceramics, inorganic metals, glass, and zeolite [26]. Inorganic membranes have recently received growing attention due to their excellent thermal and chemical stability and long lifetime [26]. However, their high capital cost, low flexibility, and being less functionable have restricted their application in water and wastewater treatment processes [25]. Polymers dominate commercial membranes.

Commonly used polymers include polysulfone (PS), polyether sulfone (PES), polyvinylidene fluoride (PVDF), cellulose acetate (CA), cellulose nitrate (CN), polyvinylpyrrolidone (PVP), polyacrylonitrile (PAN), polytetrafluoroethylene (PTFE), polypropylene (PP), and polyethylene (PE). It should be noted that great scientific effort has been continuously carried out to develop membranes with advanced surface chemistries and antifouling properties. The details of advanced membranes are out of the scope of this section and can be found elsewhere [21,27,28]. The application of polymeric membranes is discussed further below.

MF membranes – MF membranes are typically fabricated by phase inversion, sintering, track-etching, or stretching [6,12]. The most common polymers in MF applications are PVDF, PTFE, PP, PS, PE, polycarbonate, polyester, polyether imide, and nylon 6. Water treatment and wastewater treatment applications demand membrane material with high hydrophilicity and chemical stability. Although cellulosic membranes are hydrophilic, their susceptibility to acid and alkaline hydrolysis, high temperature, and biodegradation has challenged their wide application. The most widely used MF membranes are PTFE, PVDF, and PE due to their excellent chemical stability [15]. These polymers are often blended with hydrophilic polymers to reduce the surface hydrophobicity [14].

UF membranes – UF membranes are commonly manufactured using phase inversion method [6,7,12]. The most common UF polymer is PS; however, other polymers have been also used, such as PVDF, cellulose, PES, PAN, and polyvinylpyrrolidone (PVP). Cellulosic polymers have demonstrated good antifouling properties and high flux with comparable rejection properties. Although, their application is restricted due to their low chemical stability [14].

RO/NF membranes – Asymmetric CA and PA membranes and thin film composites (TFC) have been used for RO processes over the past three decades. TFC PA membranes dominate the NF/RO market with the CA standing as a distant second. TFC PA has high intrinsic permeability due to extremely thin film (100 nm) and withstands a broader pH

range than CA [22]. The selectivity of TFC PA membrane is with respect to the free-volume hole (referred to as network holes) in PA structure which is reported in the range of 0.20 to 0.29 nm (Figure 1.2) [29]. PA membranes are negatively charged and slightly hydrophilic with the contact angle reported in the range of 50° to 60°. Less attention to CA membranes is likely due to their low stability under oxidizing agents such as chlorine and higher fouling intensity due to their rough surface [22].

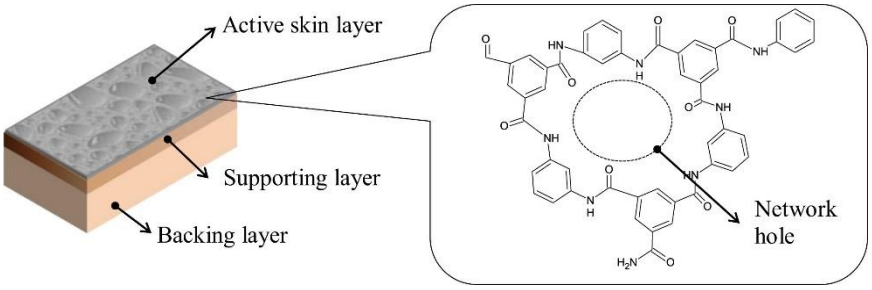

Figure 1.2. Layers of typical thin film composite (TFC) flat sheet RO membrane. The chemical structure of the polyamide active layer (skin layer) creates selectivity. Reprinted from [29], Copyright 2015, with permission from Elsevier.

1.2.3. Membrane geometry and module configurations

The most common membrane modules for water and wastewater treatment include hollow fibers, spiral wound, tubular, monolith, and plates [22] which are further discussed below.

Hollow fibers – Hollow fiber (HF) membranes are the most common configuration for MF/UF applications, while they have also been used in RO operations. The outer diameter, inner diameter (lumen), and the length of hollow fibers are usually 0.5-1.5 mm, 0.3-0.8 mm, and 1-2.5 m, respectively. HF membranes can be operated in two modes: inside-out or outside-in. In the former, influent is passed inside fibers, and permeate is collected from outside, while in outside-in mode the direction of flow is reversed. The advantages of hollow fibers include their high packing density with several thousands of fibers packed in a module and ease of cleaning.

Spiral wounds – Spiral wound (SP) modules are widely used for NF/RO membranes. SP modules cannot be back-washed, so they have been less used in MF/UF applications, although some UF applications have been reported for SPs in dairy processing.

Tubular – The design of tubular membrane is similar to HF modules but with a larger diameter (10-30 mm). The flow direction is inside-out, and they have been used in food and beverage industries and wastewater treatment. The primary advantage of tubular membranes is being able to process influents with high levels of suspended solids. Tubular modules are less prone to fouling as they operate in turbulent conditions (Re > 3000).

Monolith – Monolith module is typically used for ceramic membranes either in the configuration of a single tube or multi-channel honeycomb filter (up to 10 channels/cm^2). The filters are often manufactured via ZrO_2 or alumina with pore sizes ranging from 4 nm to 50 nm. Monolith modules have high stability due to their inorganic structure but are expensive and suffer from low effective surface area.

Plate and frame – Flat sheet (FS) membranes typically consisted of two membranes bound together with a spacer in between. The thickness of spacers is between 2 mm to 4 mm [92,146]. In conventional FS module configurations, a number of FS membranes (80 to 150) stack together in a module, and the flow is from outside to inside where the permeate is collected from the center. The complexity of cleaning procedures and high leakage possibility have limited the application of FS membranes to small wastewater treatment units with high turbidity.

1.3.Membrane fouling and conventional control strategies

Membranes are subjected to fouling as their biggest problem, which is also known as their “Achilles hill”. Consistent separation of compounds at the membrane/solvent interface can lead to clogging of membrane pores or forming a layer on the membrane surface that blocks the easy passage of solvent [30]. Fouling is detrimental to membrane performance; it negatively impacts the permeate flux, enhances energy consumption,

increases operational downtime, and reduces the membrane lifetime [31,32]. Depends on the foulant type, fouling can be classified into biofouling, organic fouling, inorganic scaling, and colloidal fouling [33]. Different fouling types on RO membranes is presented in Figure 1.3. In practice, membrane fouling usually originates from a combination of foulant types, and membrane autopsy is used to identify the type and distribution of foulants [34,35].

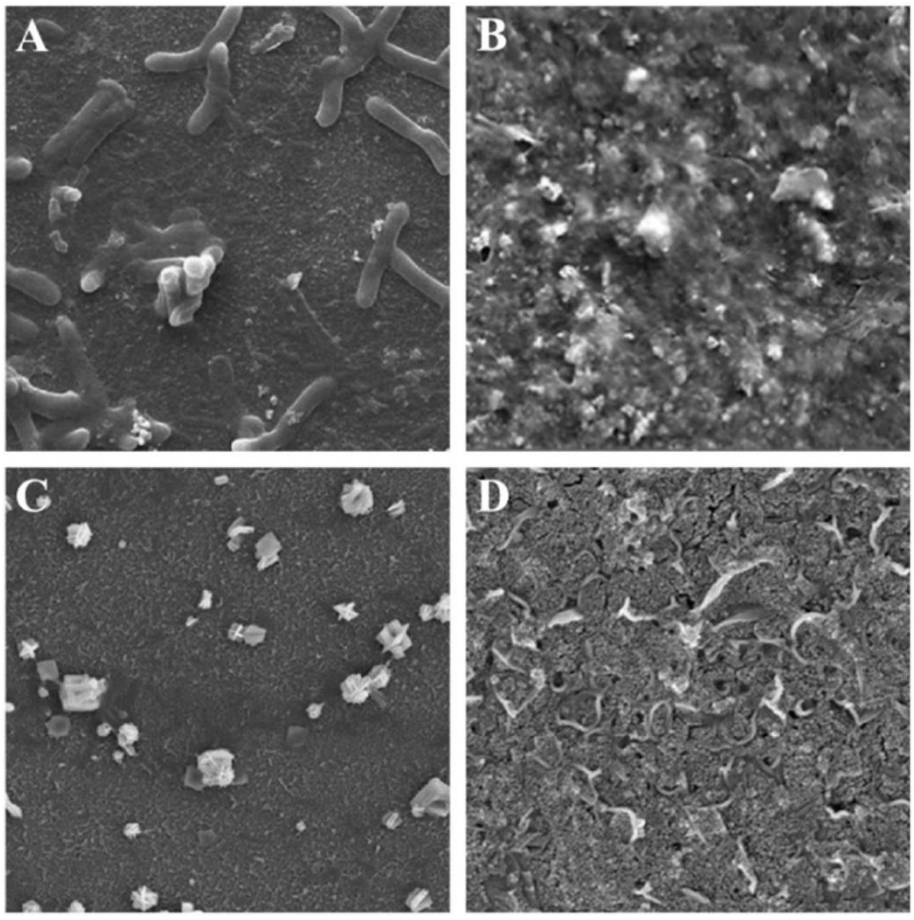

Figure 1.3. SEM of four fouling types on membrane surfaces: (a) Biofouling, (b) Organic fouling, (c) Inorganic scaling, and (d) Colloidal fouling. Reprinted from [36], Copyright 2017, with permission from Elsevier.

In a more general classification, fouling is categorized into internal fouling (pore blockage) and external fouling (surface fouling) [37,38]. If foulants are comparable or smaller with the membrane pores, they may permeate through the surface and adsorb on

pore wall, leading to pore blockage. Internal fouling often leads to irreversible fouling. Irreversible fouling cannot be removed by physical cleaning and is removable only by chemical cleaning. If foulants are much larger than pores, they form a layer on the membrane surface (often referred to as the cake layer). Surface fouling is often reversible with a few exceptions (such as biofouling) and can be removed using either physical or chemical cleaning [37,39]. The schematic of internal and external fouling is presented in Figure 1.4. It is worth noting that fouling behaviour is different in low-pressure membrane operations (i.e., MF/UF) than in high-pressure processes (i.e., NF/RO). In MF/UF membranes, the chance of internal fouling and pore blockages is higher, while in NF/RO processes surface fouling dominates due to the relatively tight and nonporous structure of NF/RO membranes [40,41].

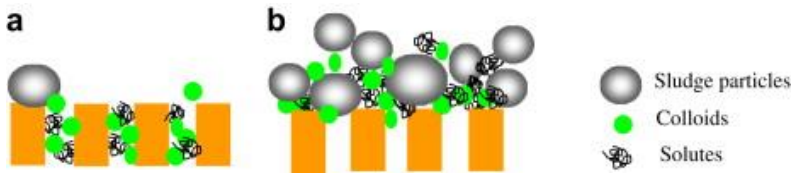

Figure 1.4. Membrane fouling process in MBRs: (a) pore blocking and (b) cake layer. Reprinted from [36], Copyright 2017, with permission from Elsevier.

Fouling is a complex process and intermolecular interactions among solvent, foulant, and membrane are strongly influenced by the physicochemical properties of membrane such as charge, hydrophilicity, roughness, and affinity. Many studies have sought to understand and advance antifouling strategies over the past three decades. The interplay between parameters co-influencing fouling mechanisms is further describes below. In addition, factors impacting bacterial attachment is illustrated in Figure 1.5.

- Physicochemical properties of the foulant including particles' shape and size distribution, charge, and hydrophobicity
- Feed characteristics such as pH and viscosity.
- Membrane and module properties including pore size and shape, surface characteristics (hydrophobicity, surface morphology, polarity, and porosity), and module geometry.

- Operating conditions including crossflow velocity, flow rate, and aeration rate (submerged membrane modules).

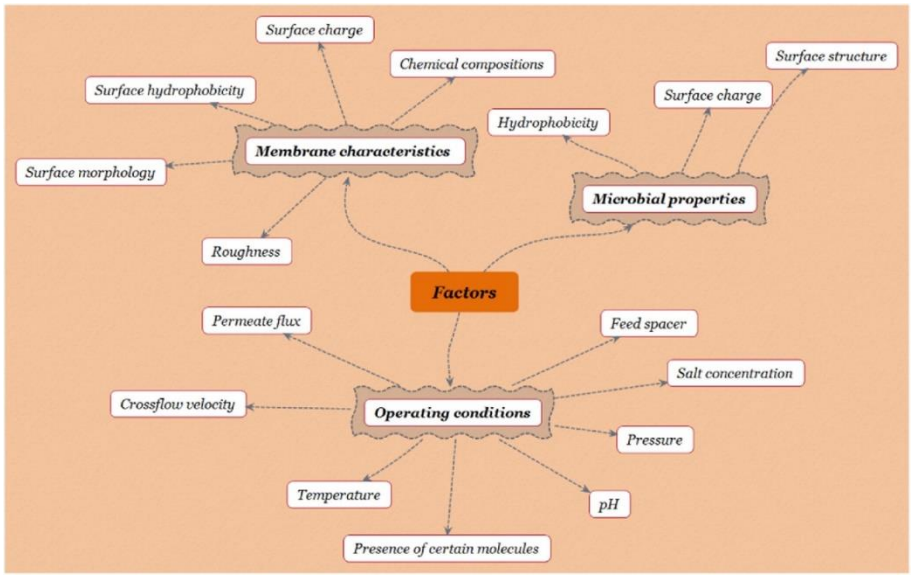

Figure 1.5. Factors affecting bacteria attachment to membrane surface. Reprinted from [36], Copyright 2017, with permission from Elsevier.

An overview of fouling categories and common cleaning procedures is provided as follows.

1.3.1. Biofouling

Biofouling is defined as the adhesion and proliferation of microorganisms on membrane surfaces [42]. Biofouling is the most complex process among fouling types and consists of two main components: bacteria and extracellular polymeric substances (EPS). Microorganisms excrete EPS during the metabolism cycle [43]. EPS are mainly composed of proteins, polysaccharides, lipoproteins, glycoproteins, nucleic acids, or lipids [37,44,45]. A schematic of EPS is shown in Figure 1.6.

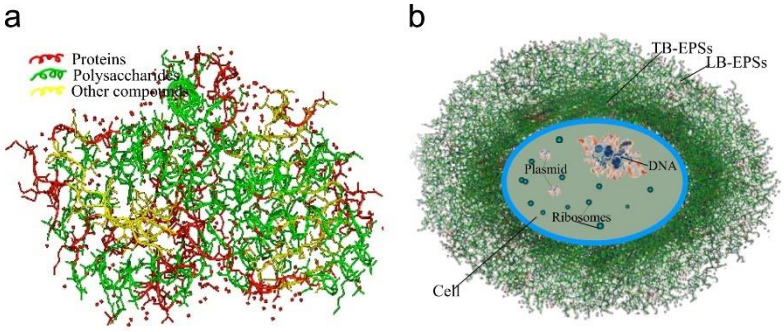

Figure 1.6. Schematic of (a) EPS structure and (b) cell structure. Reprinted from [46], Copyright 2014, with permission from Elsevier.

The development of biofilm includes three phases: bacteria attachment, reproduction, and detachment [47], as illustrated in Figure 1.7. Bacteria attachment is the most critical stage in biofouling, and a number of other factors can affect this process including microbial properties (hydrophobicity, surface charge, and surface structure) [48,49], membrane surface characteristics (surface hydrophobicity, surface charge, chemical compositions, roughness, surface morphology) [50,51], as well as operational conditions (permeate flux, crossflow velocity, temperature, pressure, pH, salt concentration, presence of certain molecules) [52]. In the reproduction stage, attached bacteria use nutrients in the media to proliferate and excrete EPS [43]. The excretion of EPS results in a more robust and resistant biofilm [53,54]. In addition, EPS can protect the biomass from shear forces and biocides [55]. Finally in the detachment stage, microorganisms leave the biomass due to lack of nutrients and migrate to new sites to grow a biofilm [56].

It is suggested to control the biofilm at the early stages of formation as mature biofilms are harder to remove. It is worthy to note that presence of other foulant types can impact the biofouling rate. Weinrich et al. [57] studied the relationship between membrane fouling rate and organic carbon content (bacteria nutrient) and found a strong correlation between membrane biofouling and influents' nutrient level.

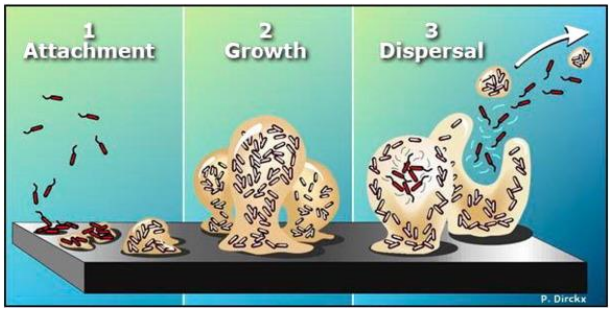

Figure 1.7. Sequence of events leading to the formation of a Biofilm. Reprinted from [45], Copyright 2011, with permission from Elsevier.

Biofouling can be developed on all membrane categories (MF, UF, NF, RO). The most common anti-biofouling strategy is the use of chemicals and biocides [47,58–60]. However, chemical cleaning forces operational downtime, demands high chemical consumption, and can be detrimental to membrane surface. For example, chlorine as an anti-biofouling agent is oxidative for polyamide RO membranes [59]. Many studies have been devoted to control and mitigate biofouling [61–63].

1.3.2. Organic fouling

Organic fouling is due to the accumulation of organic matters such as humic substances, polysaccharides, proteins, lipids, amino acids, and organic acids on the host membrane material [64,65]. Since organic compounds cover a wide range of substances, many studies that have investigated organic fouling used model foulants to represent organic fouling. The most common model foulants are bovine serum albumin (BSA), alginate, and humic acid. In organic fouling, co-interactions between water, foulant, and surface play a significant role in the intensity of fouling. The MW of organic compounds is another crucial factor [66]. Organic fouling is typically controlled by physical cleaning, chemical cleaning, or a combination [67].

1.3.3. Scaling

Mineral scaling is referred to the deposition of inorganic compounds on membranes or inside membrane pores [68,69]. Inorganic ion concentration substantially increases at the surface hydrodynamic boundary layer during filtration processes and forms a

supersaturated layer, known as the concentration polarization (CP) layer. When ions exceed the equilibrium solubility product in the boundary layer, they become prone to nucleation, deposition, and crystal growth, collectively called scaling process [70,71]. Scaling can be homogenous or inhomogeneous. Homogeneous nucleation occurs in the solvent bulk, while inhomogeneous nucleation occurs at the surface, following a much faster crystal growth. Common scalants include calcium sulfate, calcium carbonate, calcium phosphate, and barium sulfate, with calcium sulfate and calcium carbonate being the most common (Figure 1.8).

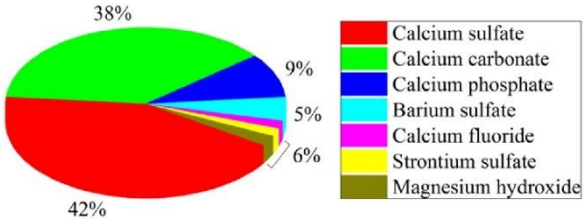

Figure 1.8. Common studies on inorganic fouling for RO membranes between 2007 to 2017. Reprinted from [36], Copyright 2017, with permission from Elsevier.

1.3.4. Colloidal fouling

Colloids are fine suspended particles ranging from a few nanometers to a few micrometers [71,72]. Colloidal fouling is caused by the deposition of colloids on membrane surfaces [69]. Two major colloidal foulants are inorganic compounds and organic macromolecules. In many published articles, colloidal fouling is integrated into inorganic scaling or/and organic fouling and discussed as a whole. The common inorganic foulants in marine environments include aluminum silicate, silica, iron oxides/hydroxides, while organic compounds in the water mainly consist of polysaccharides and proteins [73]. Similar to other fouling types, colloidal fouling could be heavily influenced by operating conditions, foulant characteristics (colloids size, charge, shape), and interactions with other foulants [74–78].

1.4.Application of electrically conductive membranes to mitigate fouling

Electrically conductive membranes (ECMs) can control and mitigate fouling by using electrical potential externally applied to their surfaces. ECMs, owing to their conductive surface, can distribute the charge across the surface that in turn induce antifouling and self-cleaning mechanisms at the membrane/solvent interface [79–83]. Electrical currents are either positive (referred to as anodic) or negative (referred to as cathodic) and can be applied in direct or alternative modes. ECMs can change the physicochemical properties of the surface (charge, hydrophilicity) with respect to the current type externally applied to them. In addition to antifouling properties, ECMs can also be deployed in water purification and disinfection applications owing to their advanced reduction-oxidation properties. Their enhanced removal efficiency is due to their unique electrochemical flow-through filtration configuration, confining degradation pathways to membrane's electroactive pores [84–87]. ECMs have effectively removed various contaminants such as pharmaceuticals [88], heavy metals [89], organic compounds [90], and pathogenic microorganisms [91,92].

Application of electrical field in membrane-based separation processes is often referred to as electrofiltration [93]. In electrofiltration processes, two electrodes are placed in the filtration cell, where ECM operates as the working electrode, and a conductive electrode acts as the counter electrode [72,94]. The application of ECMs have been extended to different membrane categories (MF, UF, NF, and RO) and they became available at different membrane configuration (flat sheets [79–83], hollow fibers [95–97]). The primary challenges associated with the commercialization of ECMs include stability of ECMs [98], additional energy consumption [99], and practical module configuration [100]. High electrical current can be destructive to conductive surfaces and induce electro-corrosion. Moreover, advanced antifouling properties of the membranes come at the cost of additional energy consumption. Finally, the commercially available membrane modules are not compatible with ECMs and cannot readily host counter electrodes.

ECMs have been made of different materials such as conductive polymers (e.g., polyaniline, polypyrrole) [101], carbonaceous materials (CNT, graphite, graphene, CNFs) [102–107], or inorganic materials (i.e. Ti_4O_7, lead, zirconate, titanate) [108,109]. The

application of conductive polymers is restricted due to their lower-range conductivity and susceptibility to harsh conditions of water treatment (exposure to chemicals). Although inorganic metals and ceramics have recently received significant attention, their application is limited due to their high cost and low processability. Carbonaceous materials are the most common class of ECMs due to their flexibility, processibility, and low cost. Carbon-based membranes are synthesized using various techniques such as vacuum filtration [105], interfacial polymerization [110], phase inversion [111], and electrospinning [112,113]. Most ECMs are fabricated as composites which consist of a conductive layer deposited on porous support [103,106,107,114].

Since the introduction of ECMs, great research effort has been carried out to demonstrate the application of ECMs, their advanced flux, and antifouling properties in water and wastewater treatment operations [80,115]. In addition to separation applications, ECMs have been used in several other applications such as electronic devices, fuel cells, sensors, catalysts, and biomimetic devices [116–120].

1.5.CNT-based electrically conductive membranes

Membranes made of carbon nanotubes (CNTs) were among the first generation of ECMs, and thus far have stimulated the most interest in electrically-assisted filtration processes [103,114,121]. CNTs have a 3D tube-like structure with aspect ratios greater than 1000 [122]. CNTs are available as single cylinders (refereed as single-walled CNT (SWCNT), or two or more coaxial cylinders (referred to as double-walled CNT (DWCNT) and multi-walled CNT (MWCNT)). CNTs possess high specific surface area, exceptional mechanical strength, and excellent electrical conductivity [123]. For example, SWCNTs have high electrical conductivity in the order of 10^4 S/cm at room temperature [124]. CNTs have been used in a wide range of applications [60,125]. Their 3D structure and high specific surface area allow them to form porous structures with facilitated mass transfer and convective flux [126]. In addition, on account of their high specific surface area (50-1000 m^2/gr) [127] and ease of functionality, they have been considered as adsorbents for organic compounds [47,128] or heavy metals [129].

The major obstacle associated with CNTs is their susceptibility to anodic oxidation. CNTs are unstable under high anodic currents due to degradation of the CNT structure [130–132]. CNT corrosion decreases the CNT conductivity (by damaging the surface sp^2 conjugation) critical for electrochemical applications [133]. The anodic stability of SWCNT, and MWCNT was reported as 1.0 V (vs. Ag/AgCl) and 1.7 V (vs. Ag/AgCl), respectively [98]. The commonly applied potentials to ECMs to promote electrochemical reactions are often beyond their anodic stability [98,134]. Therefore, research development for more stable material is critical to facilitate the broad application of ECMs.

1.6.Motivations, objective, and thesis structure

Electrically conductive membranes have received growing attention due to their advanced antifouling performance, electro-catalytic properties, and ease of operation. Since the introduction of ECMs, many studies have consistently attempted to advance ECMs. The significant body of studies was focused on the application of ECMs, innovating stable material, exploring their surface chemistry, and expanding their configuration. The application of ECMs has been mainly demonstrated for water treatment and wastewater treatment. Although most of the studies have been carried in the lab scale, they have demonstrated excellent antifouling properties of ECMs against biological substances, organic compounds, mineral ions, and colloids. Developing stable surfaces that can withstand long-term exposure to harsh chemical and electrical stress has been another research-intense scope of the ECM field. For example, application of conductive ceramic membranes [108,109], or methods such as doping the carbonaceous material with other elements to enhance their electrochemical stability [98] have been suggested. In addition, many studies have focused on improving the surface chemistry of ECMs. The majority of research work was directed to (a) Fabrication of more conductive membranes to enhance the rate of electron transfer and lower the energy consumption [101], (b) Increasing the porosity of conductive layer to make the membrane less hydraulic resistant. For example, some studies have suggested using metal spacers between graphene sheets to enhance permeability [135–137], and (c) Incorporation of functionalities and polymers in ECMs for applications beyond antifouling purposes such as electro-catalytic processes. For example,

it has been shown that decorating CNT with nano zerovalent iron successfully enhanced the reductive potential of ECMs for the removal of azo dyes under application of cathodic current [138]. The majority of these reports were for flat sheet membranes, however, a few reports have indicated the practicality of ECMs in hollow fiber modules.

Despite promising results disclosed by ECMs, their underlying mechanisms have never been comprehensively discussed. Antifouling mechanisms occur in response to the current pattern externally applied to the surface, including current type (positive, negative), configuration (direct, alternating), magnitude, and frequency. Therefore, taking full advantage of responsive surfaces demands a deep understanding of antifouling mechanisms with respect to surface polarization. In addition, since the application of ECMs in separation processes is still considered a relatively new field, the connection between the current pattern and application is of great importance for optimizing electrofiltration processes. In ECM applications, electrical current has often been applied without deep consideration of foulant's physicochemical properties. Foulants in water and wastewater treatment processes (biological, organic, ions, colloids) cover a wide range of properties and it is anticipated that they react differently to identical current patterns. Therefore, establishing a robust connection between ECM applications and the governing antifouling mechanisms is needed to guide researchers to more optimized ECM applications. Moreover, although the instability of conductive surfaces is well-recognized, there is still a lack of standard methodologies to detect and quantify such instabilities. Quantification of instabilities gauges the advances in this regard, helps setting benchmarks for surface stability, and discloses the actual properties of ECMs during operation.

The present work follows several goals as follows: understand and discuss antifouling mechanisms associated with ECM, systematically review the connection of mechanisms with ECM applications, explore the surface chemistry of ECMs for tunable properties using crosslinking chemistry, setting innovative methodologies to quantify physical, electrochemical, and mechanical stability of ECMs, and investigate the impact of different electrically-induced antifouling mechanisms on a model biofoulant. This thesis

consists of seven chapters including the current one. The scopes and goals of chapter 2 to 7 are presented as follows:

Chapter 2 summarizes how different electrode polarizations such as positive current, negative current, direct current (DC), or alternating current (AC) can induce various antifouling mechanisms in electrically-assisted separation processes. In addition, we analyzed the mechanistic behaviour of each mechanism across membrane applications by providing examples. Understanding the mechanisms, it is crucial to establish a connection between the current patterns commonly applied to ECMs and the ECM's applications in separation processes, which is presented in Chapter 3. In so doing, we critically reviewed antifouling applications of ECMs for four major fouling categories (i.e., biological, organic, oil wetting, and mineral scaling) with the focus on the relevant antifouling mechanisms and their interactions with the foulants discussed at the end of each subsection.

In chapter 4, we explored the surface chemistry of CNT-based ECMs. We fabricated a nanocomposite consisted of an electrically conductive layer on top and a PES membrane as support. We showed that integration of cross-linkers with different lengths in the network could change the compactness of the thin layer and impact the pure water flux and electrical conductivity of the membrane. We analyzed the impact of cross-linker lengths, mass of CNTs, and crosslinking degree on the thin film's electrical conductivity, pore size, surface hydrophilicity, and the resultant ECM permeate flux.

While the wide range of characterization tests carried out in Chapter 4 provides us with physicochemical properties of ECMs, it is important to understand such properties during the operation. Therefore, we investigated the stability of ECM from different aspects which is presented in Chapter 5. In more detail, we studied the 1) electrochemical, 2) physical, and 3) mechanical stability of microfiltration (MF) and ultrafiltration (UF) CNT/PVA-based ECMs, as commonly used membranes in the literature. We investigated 1) the anodic oxidation of the surface to quantify the electrochemical stability using chronoamperometry and cyclic voltammetry, 2) the physical stability of membranes

stabilized with common crosslinking agents under various operating conditions such as transmembrane pressure (TMP), temperature, and foulant concentration, and 3) the mechanical stability of ECMs with micro scratch testing. In addition, we showed the antifouling potential of fabricated ECMs towards a realistic mixed bacterial culture in an aqueous feed under application of electrical potential. As our aim in this work was to provide standard, innovative, and straightforward methodologies for researchers in the field, we disclosed the details on the design, operation, and proper data analysis of our proposed standardized methods, i.e., 1) electrochemical oxidation, 2) pressurized leaching, and 3) surface scratch testing in Chapter 5. The outcome of Chapter 5 can provide insight for making more practical ECMs.

The antibiofouling experiment carried out in Chapter 5 demonstrated the excellent anti-biofouling performance of ECMs, however, the impact of antifouling mechanisms involved was only hypothesized. Therefore, Chapter 6 is devoted to identifying the primary mechanisms responsible for advanced performance of ECMs against biofilms. To this end, we quantified the CNT-based ECM's (CNT-ECM) electrochemical anti-biofouling mechanisms (generation of protons, hydroxyl ions, and H_2O_2) at their surface, under wide range of applied electrical currents (± 0-150 mA). We grew *E. Coli* on the surface of ECMs and then investigated how each of these products electrochemically-generated from the ECM surface impacted *E. Coli's* viability in batch systems and when the membranes were operated in flow-through mode. This study provides guidance on matching antifouling mechanisms to the application of ECMs and on identifying the current pattern to maximize the efficiency of these mechanisms.

1.7.References

[1] H. Hoff, Global water resources and their management Introduction-globalization of water resources, Curr. Opin. Environ. Sustain. 1 (2009) 141–147. https://doi.org/10.1016/j.cosust.2009.10.001.

[2] M.M. Mekonnen, A.Y. Hoekstra, Four billion people facing severe water scarcity, (n.d.). https://doi.org/10.1126/sciadv.1500323.

[3] C.J. Vörösmarty, P. Green, J. Salisbury, R.B. Lammers, Global Water Resources: Vulnerability from Climate Change and Population Growth Downloaded from, 2000. http://science.sciencemag.org/ (accessed May 17, 2021).

[4] Emerging Membrane Technology for Sustainable Water Treatment | ScienceDirect, (n.d.). https://www.sciencedirect.com/book/9780444633125/emerging-membrane-technology-for-sustainable-water-treatment (accessed May 17, 2021).

[5] J.G. Hering, T.D. Waite, R.G. Luthy, J.E. Drewes, D.L. Sedlak, A changing framework for urban water systems, Environ. Sci. Technol. 47 (2013) 10721–10726. https://doi.org/10.1021/es4007096.
[6] K. Kümmerer, D.D. Dionysiou, D. Fatta-Kassinos, Scope of the Book Wastewater Reuse and Current Challenges, in: 2015: pp. 1–5. https://doi.org/10.1007/698_2015_448.
[7] S.. S. Loeb, Saline Water Conversion-II, Adv. Chem. Ser. Am. Chem. Soc. (1963).
[8] E.A. Mason, From pig bladders and cracked jars to polysulfones: An historical perspective on membrane transport, J. Memb. Sci. 60 (1991) 125–145. https://doi.org/10.1016/S0376-7388(00)81529-X.
[9] G.M. Geise, H.-S. Lee, D.J. Miller, B.D. Freeman, J.E. McGrath, D.R. Paul, Water purification by membranes: The role of polymer science, J. Polym. Sci. Part B Polym. Phys. 48 (2010) 1685–1718. https://doi.org/10.1002/polb.22037.
[10] P. Kumar, N. Sharma, R. Ranjan, S. Kumar, Z.F. Bhat, D.K. Jeong, Perspective of membrane technology in dairy industry: A review, Asian-Australasian J. Anim. Sci. 26 (2013) 1347–1358. https://doi.org/10.5713/ajas.2013.13082.
[11] M. Takht Ravanchi, T. Kaghazchi, A. Kargari, Application of membrane separation processes in petrochemical industry: a review, Desalination. 235 (2009) 199–244. https://doi.org/10.1016/j.desal.2007.10.042.
[12] A.S. Jönsson, R. Wimmerstedt, The application of membrane technology in the pulp and paper industry, Desalination. 53 (1985) 181–196. https://doi.org/10.1016/0011-9164(85)85060-8.
[13] M. Peter-Varbanets, C. Zurbrügg, C. Swartz, W. Pronk, Decentralized systems for potable water and the potential of membrane technology, Water Res. 43 (2009) 245–265. https://doi.org/10.1016/j.watres.2008.10.030.
[14] M.D. Kennedy, J. Kamanyi, S.G. Salinas Rodríguez, N.H. Lee, J.C. Schippers, G. Amy, Water Treatment by Microfiltration and Ultrafiltration, in: Adv. Membr. Technol. Appl., John Wiley & Sons, Inc., 2008: pp. 131–170. https://doi.org/10.1002/9780470276280.ch6.
[15] L.J. Zeman, A.L. Zydney, Microfiltration and ultrafiltration: Principles and applications, CRC Press, 2017. https://doi.org/10.1201/9780203747223.
[16] N. Kubota, T. Hashimoto, Y. Mori, Microfiltration and Ultrafiltration, in: Adv. Membr. Technol. Appl., John Wiley & Sons, Inc., 2008: pp. 101–129. https://doi.org/10.1002/9780470276280.ch5.
[17] H.J. Lee, M.A. Halali, T. Baker, S. Sarathy, C.F. de Lannoy, A comparative study of RO membrane scale inhibitors in wastewater reclamation: Antiscalants versus pH adjustment, Sep. Purif. Technol. 240 (2020). https://doi.org/10.1016/j.seppur.2020.116549.
[18] B. Van Der Bruggen, C. Vandecasteele, T. Van Gestel, W. Doyen, R. Leysen, A review of pressure-driven membrane processes in wastewater treatment and drinking water production, Environ. Prog. 22 (2003) 46–56. https://doi.org/10.1002/ep.670220116.
[19] T. Uemura, M. Henmi, Thin-Film Composite Membranes for Reverse Osmosis, in: Adv. Membr. Technol. Appl., John Wiley & Sons, Inc., 2008: pp. 1–19. https://doi.org/10.1002/9780470276280.ch1.
[20] S.S. Shenvi, A.M. Isloor, A.F. Ismail, A review on RO membrane technology: Developments and challenges, Desalination. 368 (2015) 10–26. https://doi.org/10.1016/j.desal.2014.12.042.
[21] R.H. Hailemariam, Y.C. Woo, M.M. Damtie, B.C. Kim, K.D. Park, J.S. Choi, Reverse osmosis membrane fabrication and modification technologies and future trends: A review, Adv. Colloid Interface Sci. 276 (2020) 102100. https://doi.org/10.1016/j.cis.2019.102100.
[22] R. Singh, N.P. Hankins, Introduction to Membrane Processes for Water Treatment, in: Emerg. Membr. Technol. Sustain. Water Treat., Elsevier Inc., 2016: pp. 15–52. https://doi.org/10.1016/B978-0-444-63312-5.00002-4.
[23] J. Wu, Z. Wang, W. Yan, Y. Wang, J. Wang, S. Wang, Improving the hydrophilicity and fouling resistance of RO membranes by surface immobilization of PVP based on a metal-polyphenol precursor layer, J. Memb. Sci. 496 (2015) 58–69. https://doi.org/10.1016/j.memsci.2015.08.044.
[24] Y.F. Zhao, L.P. Zhu, Z. Yi, B.K. Zhu, Y.Y. Xu, Improving the hydrophilicity and fouling-resistance of polysulfone ultrafiltration membranes via surface zwitterionicalization mediated by polysulfone-based triblock copolymer additive, J. Memb. Sci. 440 (2013) 40–47. https://doi.org/10.1016/j.memsci.2013.03.064.

[25] J. Kim, B. Van Der Bruggen, The use of nanoparticles in polymeric and ceramic membrane structures: Review of manufacturing procedures and performance improvement for water treatment, Environ. Pollut. 158 (2010) 2335–2349. https://doi.org/10.1016/j.envpol.2010.03.024.
[26] C. Li, W. Sun, Z. Lu, X. Ao, S. Li, Ceramic nanocomposite membranes and membrane fouling: A review, Water Res. 175 (2020) 115674. https://doi.org/10.1016/j.watres.2020.115674.
[27] C. Santhosh, V. Velmurugan, G. Jacob, S.K. Jeong, A.N. Grace, A. Bhatnagar, Role of nanomaterials in water treatment applications: A review, Chem. Eng. J. 306 (2016) 1116–1137. https://doi.org/10.1016/j.cej.2016.08.053.
[28] M.M. Pendergast, E.M.V. Hoek, A review of water treatment membrane nanotechnologies, Energy Environ. Sci. 4 (2011) 1946–1971. https://doi.org/10.1039/c0ee00541j.
[29] T. Fujioka, N. Oshima, R. Suzuki, W.E. Price, L.D. Nghiem, Probing the internal structure of reverse osmosis membranes by positron annihilation spectroscopy: Gaining more insight into the transport of water and small solutes, J. Memb. Sci. 486 (2015) 106–118. https://doi.org/10.1016/j.memsci.2015.02.007.
[30] L. Malaeb, G.M. Ayoub, Reverse osmosis technology for water treatment: State of the art review, Desalination. 267 (2011) 1–8. https://doi.org/10.1016/j.desal.2010.09.001.
[31] H. Lin, W. Peng, M. Zhang, J. Chen, H. Hong, Y. Zhang, A review on anaerobic membrane bioreactors: Applications, membrane fouling and future perspectives, Desalination. 314 (2013) 169–188. https://doi.org/10.1016/j.desal.2013.01.019.
[32] A. Ruiz-García, N. Melián-Martel, I. Nuez, Short Review on Predicting Fouling in RO Desalination, Membranes (Basel). 7 (2017) 62. https://doi.org/10.3390/membranes7040062.
[33] J.N. Hakizimana, B. Gourich, C. Vial, P. Drogui, A. Oumani, J. Naja, L. Hilali, Assessment of hardness, microorganism and organic matter removal from seawater by electrocoagulation as a pretreatment of desalination by reverse osmosis, Desalination. 393 (2016) 90–101. https://doi.org/10.1016/j.desal.2015.12.025.
[34] A.S. Gorzalski, O. Coronell, Fouling of nanofiltration membranes in full- and bench-scale systems treating groundwater containing silica, J. Memb. Sci. 468 (2014) 349–359. https://doi.org/10.1016/j.memsci.2014.06.013.
[35] S.J. Kim, B.S. Oh, H.W. Yu, L.H. Kim, C.M. Kim, E.T. Yang, M.S. Shin, A. Jang, M.H. Hwang, I.S. Kim, Foulant characterization and distribution in spiral wound reverse osmosis membranes from different pressure vessels, Desalination. 370 (2015) 44–52. https://doi.org/10.1016/j.desal.2015.05.013.
[36] S. Jiang, Y. Li, B.P. Ladewig, A review of reverse osmosis membrane fouling and control strategies, Sci. Total Environ. 595 (2017) 567–583. https://doi.org/10.1016/j.scitotenv.2017.03.235.
[37] Q. She, R. Wang, A.G. Fane, C.Y. Tang, Membrane fouling in osmotically driven membrane processes: A review, J. Memb. Sci. 499 (2016) 201–233. https://doi.org/10.1016/j.memsci.2015.10.040.
[38] W. Yu, N.J.D. Graham, Performance of an integrated granular media - Ultrafiltration membrane process for drinking water treatment, J. Memb. Sci. 492 (2015) 164–172. https://doi.org/10.1016/j.memsci.2015.05.032.
[39] E.M.V. Hoek, J. Allred, T. Knoell, B.H. Jeong, Modeling the effects of fouling on full-scale reverse osmosis processes, J. Memb. Sci. 314 (2008) 33–49. https://doi.org/10.1016/j.memsci.2008.01.025.
[40] L.F. Greenlee, D.F. Lawler, B.D. Freeman, B. Marrot, P. Moulin, Reverse osmosis desalination: Water sources, technology, and today's challenges, Water Res. 43 (2009) 2317–2348. https://doi.org/10.1016/j.watres.2009.03.010.
[41] W.S. Ang, M. Elimelech, Protein (BSA) fouling of reverse osmosis membranes: Implications for wastewater reclamation, J. Memb. Sci. 296 (2007) 83–92. https://doi.org/10.1016/j.memsci.2007.03.018.
[42] S.A. Creber, T.R.R. Pintelon, D.A.W. Graf Von Der Schulenburg, J.S. Vrouwenvelder, M.C.M. Van Loosdrecht, M.L. Johns, Magnetic resonance imaging and 3D simulation studies of biofilm accumulation and cleaning on reverse osmosis membranes, Food Bioprod. Process. 88 (2010) 401–408. https://doi.org/10.1016/j.fbp.2010.08.010.
[43] W. Yu, Y. Yang, N. Graham, Evaluation of ferrate as a coagulant aid/oxidant pretreatment for

mitigating submerged ultrafiltration membrane fouling in drinking water treatment, Chem. Eng. J. 298 (2016) 234–242. https://doi.org/10.1016/j.cej.2016.03.080.

[44] A. Drews, Membrane fouling in membrane bioreactors-Characterisation, contradictions, cause and cures, J. Memb. Sci. 363 (2010) 1–28. https://doi.org/10.1016/j.memsci.2010.06.046.

[45] A. Matin, Z. Khan, S.M.J. Zaidi, M.C. Boyce, Biofouling in reverse osmosis membranes for seawater desalination: Phenomena and prevention, Desalination. 281 (2011) 1–16. https://doi.org/10.1016/j.desal.2011.06.063.

[46] H. Lin, M. Zhang, F. Wang, F. Meng, B.Q. Liao, H. Hong, J. Chen, W. Gao, A critical review of extracellular polymeric substances (EPSs) in membrane bioreactors: Characteristics, roles in membrane fouling and control strategies, J. Memb. Sci. 460 (2014) 110–125. https://doi.org/10.1016/j.memsci.2014.02.034.

[47] H.C. Flemming, Reverse osmosis membrane biofouling, Exp. Therm. Fluid Sci. 14 (1997) 382–391. https://doi.org/10.1016/S0894-1777(96)00140-9.

[48] T.A. Camesano, B.E. Logan, Influence of fluid velocity and cell concentration on the transport of motile and nonmotile bacteria in porous media, Environ. Sci. Technol. 32 (1998) 1699–1708. https://doi.org/10.1021/es970996m.

[49] B. Tang, C. Yu, L. Bin, Y. Zhao, X. Feng, S. Huang, F. Fu, J. Ding, C. Chen, P. Li, Q. Chen, Essential factors of an integrated moving bed biofilm reactor-membrane bioreactor: Adhesion characteristics and microbial community of the biofilm, Bioresour. Technol. 211 (2016) 574–583. https://doi.org/10.1016/j.biortech.2016.03.136.

[50] V. Nguyen, E. Karunakaran, G. Collins, C.A. Biggs, Physicochemical analysis of initial adhesion and biofilm formation of Methanosarcina barkeri on polymer support material, Colloids Surfaces B Biointerfaces. 143 (2016) 518–525. https://doi.org/10.1016/j.colsurfb.2016.03.042.

[51] S.T. Kang, A. Subramani, E.M.V. Hoek, M.A. Deshusses, M.R. Matsumoto, Direct observation of biofouling in cross-flow microfiltration: Mechanisms of deposition and release, J. Memb. Sci. 244 (2004) 151–165. https://doi.org/10.1016/j.memsci.2004.07.011.

[52] O. Habimana, A.J.C. Semião, E. Casey, The role of cell-surface interactions in bacterial initial adhesion and consequent biofilm formation on nanofiltration/reverse osmosis membranes, J. Memb. Sci. 454 (2014) 82–96. https://doi.org/10.1016/j.memsci.2013.11.043.

[53] S.C. Leterme, C. Le Lan, D.A. Hemraj, A. V. Ellis, The impact of diatoms on the biofouling of seawater reverse osmosis membranes in a model cross-flow system, Desalination. 392 (2016) 8–13. https://doi.org/10.1016/j.desal.2016.04.019.

[54] E. Ben-Dov, E. Ben-David, R. Messalem, M. Herzberg, A. Kushmaro, Biofilm formation on RO membranes: the impact of seawater pretreatment, Desalin. Water Treat. 57 (2016) 4741–4748. https://doi.org/10.1080/19443994.2014.998294.

[55] A. Belila, J. El-Chakhtoura, N. Otaibi, G. Muyzer, G. Gonzalez-Gil, P.E. Saikaly, M.C.M. van Loosdrecht, J.S. Vrouwenvelder, Bacterial community structure and variation in a full-scale seawater desalination plant for drinking water production, Water Res. 94 (2016) 62–72. https://doi.org/10.1016/j.watres.2016.02.039.

[56] S.A. Creber, J.S. Vrouwenvelder, M.C.M. van Loosdrecht, M.L. Johns, Chemical cleaning of biofouling in reverse osmosis membranes evaluated using magnetic resonance imaging, J. Memb. Sci. 362 (2010) 202–210. https://doi.org/10.1016/j.memsci.2010.06.052.

[57] L. Weinrich, M. LeChevallier, C.N. Haas, Contribution of assimilable organic carbon to biological fouling in seawater reverse osmosis membrane treatment, Water Res. 101 (2016) 203–213. https://doi.org/10.1016/j.watres.2016.05.075.

[58] H.C. Flemming, Biofouling in water systems - Cases, causes and countermeasures, Appl. Microbiol. Biotechnol. 59 (2002) 629–640. https://doi.org/10.1007/s00253-002-1066-9.

[59] S.E. Coetser, T.E. Cloete, Biofouling and biocorrosion in industrial water systems, Crit. Rev. Microbiol. 31 (2005) 213–232. https://doi.org/10.1080/10408410500304074.

[60] J.S. Baker, L.Y. Dudley, Biofouling in membrane systems - a review, Desalination. 118 (1998) 81–89. https://doi.org/10.1016/S0011-9164(98)00091-5.

[61] R.A. Al-Juboori, T. Yusaf, Biofouling in RO system: Mechanisms, monitoring and controlling, Desalination. 302 (2012) 1–23. https://doi.org/10.1016/j.desal.2012.06.016.

[62] M.R. Hibbs, L.K. McGrath, S. Kang, A. Adout, S.J. Altman, M. Elimelech, C.J. Cornelius, Designing a biocidal reverse osmosis membrane coating: Synthesis and biofouling properties, Desalination. 380 (2016) 52–59. https://doi.org/10.1016/j.desal.2015.11.017.
[63] L. Ni, J. Meng, X. Li, Y. Zhang, Surface coating on the polyamide TFC RO membrane for chlorine resistance and antifouling performance improvement, J. Memb. Sci. 451 (2014) 205–215. https://doi.org/10.1016/j.memsci.2013.09.040.
[64] J. Cho, G. Amy, J. Pellegrino, Membrane filtration of natural organic matter: Initial comparison of rejection and flux decline characteristics with ultrafiltration and nanofiltration membranes, Water Res. 33 (1999) 2517–2526. https://doi.org/10.1016/S0043-1354(98)00498-9.
[65] S. Jeong, G. Naidu, R. Vollprecht, T.O. Leiknes, S. Vigneswaran, In-depth analyses of organic matters in a full-scale seawater desalination plant and an autopsy of reverse osmosis membrane, Sep. Purif. Technol. 162 (2016) 171–179. https://doi.org/10.1016/j.seppur.2016.02.029.
[66] M.R. Teixeira, V.S. Sousa, Fouling of nanofiltration membrane: Effects of NOM molecular weight and microcystins, Desalination. 315 (2013) 149–155. https://doi.org/10.1016/j.desal.2012.03.012.
[67] R. Fabris, C.W.K. Chow, M. Drikas, B. Eikebrokk, Comparison of NOM character in selected Australian and Norwegian drinking waters, Water Res. 42 (2008) 4188–4196. https://doi.org/10.1016/j.watres.2008.06.023.
[68] L. Henthorne, B. Boysen, State-of-the-art of reverse osmosis desalination pretreatment, Desalination. 356 (2015) 129–139. https://doi.org/10.1016/j.desal.2014.10.039.
[69] M. Khayet, Fouling and Scaling in Desalination, Desalination. 393 (2016) 1. https://doi.org/10.1016/j.desal.2016.05.005.
[70] S. Shirazi, C.J. Lin, D. Chen, Inorganic fouling of pressure-driven membrane processes - A critical review, Desalination. 250 (2010) 236–248. https://doi.org/10.1016/j.desal.2009.02.056.
[71] A. Al-Amoudi, R.W. Lovitt, Fouling strategies and the cleaning system of NF membranes and factors affecting cleaning efficiency, J. Memb. Sci. 303 (2007) 4–28. https://doi.org/10.1016/j.memsci.2007.06.002.
[72] X. Zhu, M. Elimelech, Colloidal fouling of reverse osmosis membranes: Measurements and fouling mechanisms, Environ. Sci. Technol. 31 (1997) 3654–3662. https://doi.org/10.1021/es970400v.
[73] C.Y. Tang, T.H. Chong, A.G. Fane, Colloidal interactions and fouling of NF and RO membranes: A review, Adv. Colloid Interface Sci. 164 (2011) 126–143. https://doi.org/10.1016/j.cis.2010.10.007.
[74] R.Y. Ning, T.L. Troyer, R.S. Tominello, Chemical control of colloidal fouling of reverse osmosis systems, Desalination. 172 (2005) 1–6. https://doi.org/10.1016/j.desal.2004.06.192.
[75] M.M. Motsa, B.B. Mamba, J.M. Thwala, A.R.D. Verliefde, Osmotic backwash of fouled FO membranes: Cleaning mechanisms and membrane surface properties after cleaning, Desalination. 402 (2017) 62–71. https://doi.org/10.1016/j.desal.2016.09.018.
[76] Y. Ju, S. Hong, Nano-colloidal fouling mechanisms in seawater reverse osmosis process evaluated by cake resistance simulator-modified fouling index nanofiltration, Desalination. 343 (2014) 88–96. https://doi.org/10.1016/j.desal.2014.03.012.
[77] J. Wang, Y. Mo, S. Mahendra, E.M.V. Hoek, Effects of water chemistry on structure and performance of polyamide composite membranes, J. Memb. Sci. 452 (2014) 415–425. https://doi.org/10.1016/j.memsci.2013.09.022.
[78] J. Buffle, K.J. Wilkinson, S. Stoll, M. Filella, J. Zhang, A generalized description of aquatic colloidal interactions: The three- culloidal component approach, Environ. Sci. Technol. 32 (1998) 2887–2899. https://doi.org/10.1021/es980217h.
[79] F. Ahmed, B.S. Lalia, V. Kochkodan, R. Hashaikeh, Electrically conductive polymeric membranes for fouling prevention and detection: A review, Desalination. 391 (2016) 1–15. https://doi.org/10.1016/J.DESAL.2016.01.030.
[80] A. Ronen, S.L. Walker, D. Jassby, Electroconductive and electroresponsive membranes for water treatment, Rev. Chem. Eng. 32 (2016) 533–550. https://doi.org/10.1515/revce-2015-0060.
[81] P. Formoso, E. Pantuso, G. De Filpo, F. Nicoletta, Electro-Conductive Membranes for Permeation Enhancement and Fouling Mitigation: A Short Review, Membranes (Basel). 7 (2017) 39. https://doi.org/10.3390/membranes7030039.
[82] I.-H. Loh, R.A. Moody, J.C. Huang, Electrically conductive membranes: Synthesis and applications,

J. Memb. Sci. 50 (1990) 31–49. https://doi.org/10.1016/S0376-7388(00)80884-4.

[83] W. Hu, S. Chen, Z. Yang, L. Liu, H. Wang, Flexible electrically conductive nanocomposite membrane based on bacterial cellulose and polyaniline, J. Phys. Chem. B. 115 (2011) 8453–8457. https://doi.org/10.1021/jp204422v.

[84] Q. Ji, D. Yu, G. Zhang, H. Lan, H. Liu, J. Qu, Microfluidic Flow through Polyaniline Supported by Lamellar-Structured Graphene for Mass-Transfer-Enhanced Electrocatalytic Reduction of Hexavalent Chromium, Environ. Sci. Technol. 49 (2015) 13534–13541. https://doi.org/10.1021/acs.est.5b03314.

[85] Q. Ji, G. Zhang, H. Liu, R. Liu, J. Qu, Field-Enhanced Nanoconvection Accelerated Electrocatalytic Conversion of Water Contaminants and Electricity Generation, Environ. Sci. Technol. 53 (2019) 2713–2719. https://doi.org/10.1021/acs.est.8b06620.

[86] Z. Yang, J. Qian, A. Yu, B. Pan, Singlet oxygen mediated iron-based Fenton-like catalysis under nanoconfinement, Proc. Natl. Acad. Sci. U. S. A. 116 (2019) 6659–6664. https://doi.org/10.1073/pnas.1819382116.

[87] S. Zhang, M. Sun, T. Hedtke, A. Deshmukh, X. Zhou, S. Weon, M. Elimelech, J.H. Kim, Mechanism of Heterogeneous Fenton Reaction Kinetics Enhancement under Nanoscale Spatial Confinement, Environ. Sci. Technol. 54 (2020) 10868–10875. https://doi.org/10.1021/acs.est.0c02192.

[88] J.E. Yanez H., Z. Wang, S. Lege, M. Obst, S. Roehler, C.J. Burkhardt, C. Zwiener, Application and characterization of electroactive membranes based on carbon nanotubes and zerovalent iron nanoparticles, Water Res. 108 (2017) 78–85. https://doi.org/10.1016/j.watres.2016.10.055.

[89] X. Wang, Z. Wang, H. Chen, Z. Wu, Removal of Cu(II) ions from contaminated waters using a conducting microfiltration membrane, J. Hazard. Mater. 339 (2017) 182–190. https://doi.org/10.1016/j.jhazmat.2017.06.038.

[90] J. Zheng, Z. Wang, J. Ma, S. Xu, Z. Wu, Development of an Electrochemical Ceramic Membrane Filtration System for Efficient Contaminant Removal from Waters, Environ. Sci. Technol. 52 (2018) 4117–4126. https://doi.org/10.1021/acs.est.7b06407.

[91] L. Guo, K. Ding, K. Rockne, M. Duran, B.P. Chaplin, Bacteria inactivation at a sub-stoichiometric titanium dioxide reactive electrochemical membrane, J. Hazard. Mater. 319 (2016) 137–146. https://doi.org/10.1016/j.jhazmat.2016.05.051.

[92] A. Ronen, W. Duan, I. Wheeldon, S. Walker, D. Jassby, Microbial Attachment Inhibition through Low-Voltage Electrochemical Reactions on Electrically Conducting Membranes, Environ. Sci. Technol. 49 (2015) 12741–12750. https://doi.org/10.1021/acs.est.5b01281.

[93] M. Öner, Ö. Doğan, G. Öner, The influence of polyelectrolytes architecture on calcium sulfate dihydrate growth retardation, J. Cryst. Growth. 186 (1998) 427–437. https://doi.org/10.1016/S0022-0248(97)00518-6.

[94] G. Amy, Fundamental understanding of organic matter fouling of membranes, Desalination. 231 (2008) 44–51. https://doi.org/10.1016/j.desal.2007.11.037.

[95] L. Du, X. Quan, X. Fan, G. Wei, S. Chen, Conductive CNT/nanofiber composite hollow fiber membranes with electrospun support layer for water purification, J. Memb. Sci. 596 (2020) 117613. https://doi.org/10.1016/j.memsci.2019.117613.

[96] M.J. Larocque, D.R. Latulippe, C.F. de Lannoy, Formation of electrically conductive hollow fiber membranes via crossflow deposition of carbon nanotubes – Addressing the conductivity/permeability trade-off, J. Memb. Sci. 620 (2021) 118859. https://doi.org/10.1016/j.memsci.2020.118859.

[97] K.P. Katuri, C.M. Werner, R.J. Jimenez-Sandoval, W. Chen, S. Jeon, B.E. Logan, Z. Lai, G.L. Amy, P.E. Saikaly, A novel anaerobic electrochemical membrane bioreactor (AnEMBR) with conductive hollow-fiber membrane for treatment of low-organic strength solutions, Environ. Sci. Technol. 48 (2014) 12833–12841. https://doi.org/10.1021/es504392n.

[98] H. Liu, A. Vajpayee, C.D. Vecitis, Bismuth-doped tin oxide-coated carbon nanotube network: Improved anode stability and efficiency for flow-through organic electrooxidation, ACS Appl. Mater. Interfaces. 5 (2013) 10054–10066. https://doi.org/10.1021/am402621v.

[99] N. Hilal, O.O. Ogunbiyi, N.J. Miles, R. Nigmatullin, Methods employed for control of fouling in MF and UF membranes: A comprehensive review, Sep. Sci. Technol. 40 (2005) 1957–2005. https://doi.org/10.1081/SS-200068409.

[100] X. Zhu, D. Jassby, Electroactive Membranes for Water Treatment: Enhanced Treatment Functionalities, Energy Considerations, and Future Challenges, Acc. Chem. Res. 52 (2019) 1177–1186. https://doi.org/10.1021/acs.accounts.8b00558.
[101] W. Duan, A. Ronen, S. Walker, D. Jassby, Polyaniline-Coated Carbon Nanotube Ultrafiltration Membranes: Enhanced Anodic Stability for *In Situ* Cleaning and Electro-Oxidation Processes, ACS Appl. Mater. Interfaces. 8 (2016) 22574–22584. https://doi.org/10.1021/acsami.6b07196.
[102] C. de Lannoy, D. Jassby, D.D. Davis, M.R. Wiesner, A highly electrically conductive polymer–multiwalled carbon nanotube nanocomposite membrane, J. Memb. Sci. 415–416 (2012) 718–724. https://doi.org/10.1016/J.MEMSCI.2012.05.061.
[103] M.S.P. Shaffer, A.H. Windle, Fabrication and Characterization of Carbon Nanotube/Poly(vinyl alcohol) Composites, Adv. Mater. 11 (1999) 937–941. https://doi.org/10.1002/(SICI)1521-4095(199908)11:11<937::AID-ADMA937>3.0.CO;2-9.
[104] F. Ahmed, B.S. Lalia, V. Kochkodan, N. Hilal, R. Hashaikeh, Electrically conductive polymeric membranes for fouling prevention and detection: A review, Desalination. 391 (2016) 1–15. https://doi.org/10.1016/j.desal.2016.01.030.
[105] M.A. Halali, C.-F. de Lannoy, The Effect of Cross-Linkers on the Permeability of Electrically Conductive Membranes, Ind. Eng. Chem. Res. 58 (2019) 3832–3844. https://doi.org/10.1021/acs.iecr.8b05691.
[106] H. Chen, M.B. Müller, K.J. Gilmore, G.G. Wallace, D. Li, Mechanically Strong, Electrically Conductive, and Biocompatible Graphene Paper, Adv. Mater. 20 (2008) 3557–3561. https://doi.org/10.1002/adma.200800757.
[107] H. Kim, Y. Miura, C.W. Macosko, Graphene/Polyurethane Nanocomposites for Improved Gas Barrier and Electrical Conductivity, Chem. Mater. 22 (2010) 3441–3450. https://doi.org/10.1021/cm100477v.
[108] W. Fu, X. Wang, J. Zheng, M. Liu, Z. Wang, Antifouling performance and mechanisms in an electrochemical ceramic membrane reactor for wastewater treatment, (2018). https://doi.org/10.1016/j.memsci.2018.10.077.
[109] P. Geng, G. Chen, Magnéli Ti4O7 modified ceramic membrane for electrically-assisted filtration with antifouling property, J. Memb. Sci. 498 (2016) 302–314. https://doi.org/10.1016/j.memsci.2015.07.055.
[110] C.F. De Lannoy, D. Jassby, K. Gloe, A.D. Gordon, M.R. Wiesner, Aquatic biofouling prevention by electrically charged nanocomposite polymer thin film membranes, Environ. Sci. Technol. 47 (2013) 2760–2768. https://doi.org/10.1021/es3045168.
[111] K.C. Ho, Y.H. Teow, A.W. Mohammad, W.L. Ang, P.H. Lee, Development of graphene oxide (GO)/multi-walled carbon nanotubes (MWCNTs) nanocomposite conductive membranes for electrically enhanced fouling mitigation, J. Memb. Sci. 552 (2018) 189–201. https://doi.org/10.1016/j.memsci.2018.02.001.
[112] D. Chen, Y.E. Miao, T. Liu, Electrically conductive polyaniline/polyimide nanofiber membranes prepared via a combination of electrospinning and subsequent in situ polymerization growth, ACS Appl. Mater. Interfaces. 5 (2013) 1206–1212. https://doi.org/10.1021/am303292y.
[113] M. Kang, H.J. Jin, Electrically conducting electrospun silk membranes fabricated by adsorption of carbon nanotubes, Colloid Polym. Sci. 285 (2007) 1163–1167. https://doi.org/10.1007/s00396-007-1668-y.
[114] C. de Lannoy, D. Jassby, D.D. Davis, M.R. Wiesner, A highly electrically conductive polymer–multiwalled carbon nanotube nanocomposite membrane, J. Memb. Sci. 415–416 (2012) 718–724. https://doi.org/10.1016/J.MEMSCI.2012.05.061.
[115] P. Formoso, E. Pantuso, G. De Filpo, F.P. Nicoletta, Electro-conductive membranes for permeation enhancement and fouling mitigation: A short review, Membranes (Basel). 7 (2017). https://doi.org/10.3390/membranes7030039.
[116] M. Ates, A review study of (bio)sensor systems based on conducting polymers, Mater. Sci. Eng. C. 33 (2013) 1853–1859. https://doi.org/10.1016/j.msec.2013.01.035.
[117] T.F. Otero, J.G. Martinez, J. Arias-Pardilla, Biomimetic electrochemistry from conducting polymers. A review: Artificial muscles, smart membranes, smart drug delivery and computer/neuron interfaces,

Electrochim. Acta. 84 (2012) 112–128. https://doi.org/10.1016/j.electacta.2012.03.097.
[118] S. Ma, J. Meng, J. Li, Y. Zhang, L. Ni, Synthesis of catalytic polypropylene membranes enabling visible-light-driven photocatalytic degradation of dyes in water, J. Memb. Sci. 453 (2014) 221–229. https://doi.org/10.1016/j.memsci.2013.11.021.
[119] B. Guo, L. Glavas, A.C. Albertsson, Biodegradable and electrically conducting polymers for biomedical applications, Prog. Polym. Sci. 38 (2013) 1263–1286. https://doi.org/10.1016/j.progpolymsci.2013.06.003.
[120] I.H. Loh, R.A. Moody, J.C. Huang, Electrically conductive membranes: Synthesis and applications, J. Memb. Sci. 50 (1990) 31–49. https://doi.org/10.1016/S0376-7388(00)80884-4.
[121] M.H.O. Rashid, S.F. Ralph, Carbon nanotube membranes: Synthesis, properties, and future filtration applications, Nanomaterials. 7 (2017). https://doi.org/10.3390/nano7050099.
[122] S. Iijima, Helical microtubules of graphitic carbon, Nature. 354 (1991) 56–58. https://doi.org/10.1038/354056a0.
[123] M.F.L. De Volder, S.H. Tawfick, R.H. Baughman, A.J. Hart, Carbon nanotubes: Present and future commercial applications, Science (80-.). 339 (2013) 535–539. https://doi.org/10.1126/science.1222453.
[124] M.S. Dresselhaus, P. Avouris, Introduction to Carbon Materials Research, in: Carbon Nanotub., Springer Berlin Heidelberg, 2007: pp. 1–9. https://doi.org/10.1007/3-540-39947-x_1.
[125] S.E. Coetser, T.E. Cloete, Biofouling and biocorrosion in industrial water systems, Crit. Rev. Microbiol. 31 (2005) 213–232. https://doi.org/10.1080/10408410500304074.
[126] J. Huang, Z. Wang, J. Zhang, X. Zhang, J. Ma, Z. Wu, A novel composite conductive microfiltration membrane and its anti-fouling performance with an external electric field in membrane bioreactors, Sci. Rep. 5 (2015) 1–8. https://doi.org/10.1038/srep09268.
[127] X.Y. Li, S.F. Yang, Influence of loosely bound extracellular polymeric substances (EPS) on the flocculation, sedimentation and dewaterability of activated sludge, Water Res. 41 (2007) 1022–1030. https://doi.org/10.1016/j.watres.2006.06.037.
[128] H.C. Flemming, Biofouling in water systems - Cases, causes and countermeasures, Appl. Microbiol. Biotechnol. 59 (2002) 629–640. https://doi.org/10.1007/s00253-002-1066-9.
[129] P. V. Zumbusch, W. Kulcke, G. Brunner, Use of alternating electrical fields as anti-fouling strategy in ultrafiltration of biological suspensions - Introduction of a new experimental procedure for crossflow filtration, J. Memb. Sci. 142 (1998) 75–86. https://doi.org/10.1016/S0376-7388(97)00310-4.
[130] C.D. Vecitis, M.H. Schnoor, M. Saifur Rahaman, J.D. Schiffman, M. Elimelech, Electrochemical Multiwalled Carbon Nanotube Filter for Viral and Bacterial Removal and Inactivation, Environ. Sci. Technol. 45 (2011) 3672–3679. https://doi.org/10.1021/es2000062.
[131] M. Tominaga, Y. Yatsugi, N. Watanabe, Oxidative corrosion potential vs. pH diagram for single-walled carbon nanotubes, RSC Adv. 4 (2014) 27224–27227. https://doi.org/10.1039/c4ra02875a.
[132] S. Ohmori, T. Saito, Electrochemical durability of single-wall carbon nanotube electrode against anodic oxidation in water, Carbon N. Y. 50 (2012) 4932–4938. https://doi.org/10.1016/j.carbon.2012.06.023.
[133] H. Liu, A. Vajpayee, C.D. Vecitis, Bismuth-Doped Tin Oxide-Coated Carbon Nanotube Network: Improved Anode Stability and Efficiency for Flow-Through Organic Electrooxidation, (2013). https://doi.org/10.1021/am402621v.
[134] Q. Zhuo, S. Deng, B. Yang, J. Huang, G. Yu, Efficient electrochemical oxidation of perfluorooctanoate using a Ti/SnO2-Sb-Bi anode, Environ. Sci. Technol. 45 (2011) 2973–2979. https://doi.org/10.1021/es1024542.
[135] D. Van Lam, T. Gong, S. Won, J.H. Kim, H.J. Lee, C. Lee, S.M. Lee, A robust and conductive metal-impregnated graphene oxide membrane selectively separating organic vapors, Chem. Commun. 51 (2015) 2671–2674. https://doi.org/10.1039/c4cc08896d.
[136] C. Xu, A. Cui, Y. Xu, X. Fu, Graphene oxide-TiO2 composite filtration membranes and their potential application for water purification, Carbon N. Y. 62 (2013) 465–471. https://doi.org/10.1016/j.carbon.2013.06.035.
[137] Z. yang Han, L. jun Huang, H. jiao Qu, Y. xin Wang, Z. jie Zhang, Q. lin Rong, Z. qi Sang, Y. Wang,

M.J. Kipper, J. guo Tang, A review of performance improvement strategies for graphene oxide-based and graphene-based membranes in water treatment, J. Mater. Sci. 56 (2021) 9545–9574. https://doi.org/10.1007/s10853-021-05873-7.

[138] A.J. Sutherland, M.X. Ruiz-Caldas, C.F. de Lannoy, Electro-catalytic microfiltration membranes electrochemically degrade azo dyes in solution, J. Memb. Sci. 611 (2020) 118335. https://doi.org/10.1016/j.memsci.2020.118335.

Chapter 2

Electrically Conductive Membranes – A Review of their Anti-Fouling Mechanisms – Part I

2.1.Abstract

The past decade has witnessed extensive research in developing and applying electrically conductive membranes (ECMs) to water and wastewater treatment. These membranes combine separations with electrochemical reactions and demonstrate anti-fouling and self-cleaning properties, in-situ degradation of contaminants, surface-meditate reactions, and sensing capabilities among other abilities. Most studies have focused on their promising anti-fouling properties, but discovering their full potential demands a deep understanding of underlying antifouling mechanisms. Activation of electrically-promoted antifouling mechanisms depends on the applied current pattern, which includes current type (anodic, cathodic), configuration (direct, alternating), magnitude (amplitude), and frequency. We summarized how different electrode polarizations can generate various antifouling mechanisms in membrane-based processes. We then analyzed the mechanistic behaviour of each mechanism across membrane applications. Finally, the future outlook of ECMs is reviewed to highlight challenges that need to be overcome and opportunities for researchers and industry alike.

2.2.Introduction

Membrane-based separations are the technology of choice for producing high quality potable water and will be increasingly important for providing millions of people with access to potable water across the globe. Pressure-driven membranes have dominated these separations due to their low cost, ease and versatility of operation, small footprint, energy efficiency, and high permeate quality [1]. Commercial pressure-driven membranes are categorized by their selectivity into four major groups: microfiltration (MF), ultrafiltration (UF), nanofiltration (NF), and reverse osmosis (RO). MF and UF membranes are commonly used to separate large pollutants such as bacteria, suspended solids, oil particles, and organic matter, while NF and RO membranes can separate smaller sized dissolved organic matter and ions, such as ions and heavy metals. Despite the widespread use of membranes, improvements have been steadily sought for higher membrane longevity, better energy efficiency, higher selectivity towards recalcitrant contaminants, and higher resistance against fouling, the so-called “Achilles heel” of membrane-based processes.

Fouling arises from the accumulation of contaminants at the separation interface and can be categorized into biofouling (e.g., bacteria, viruses), organic fouling (e.g., organic matter, hydrocarbons, oil particles), mineral scaling (e.g., salts), and colloidal fouling (e.g., silica, clay) [2,3]. Many strategies have been proposed to address fouling issues including feed pre-treatment (feed screening, using antiscalants, pH adjustment), physical cleaning (backflushing, cross-flushing), chemical cleaning (using detergents, acids/bases), and mechanical cleaning [4–8]. Although such strategies have evolved over the years, they are considered energy- and time-intensive due to operational downtime, environmentally detrimental due to the release of hazardous chemical waste, and uneconomical as they compromise membrane integrity, reduce membrane lifetime, and consume substantial quantities of chemicals. Thus, it is essential to develop membranes with advanced antifouling properties. In addition, it is desired to develop membranes with targeted selectivity to enhance their overall separation performance. Selective membranes

target contaminants with regard to their physicochemical properties such as hydrodynamic size, charge, hydrophobicity, and solubility.

Electrically conductive membranes (ECM) were invented to eliminate the challenges involved with traditional cleaning techniques by incorporating self-cleaning mechanisms to membranes [9–13]. ECMs contain a conductive surface that facilitates a current or electrical charge accumulation, in turn enabling many antifouling mechanisms at the membrane surface/water interface including a strong electrostatic repulsion between the membrane surface and like-charged contaminants, electrochemical reactions driven by electrical current, and enhanced electrophoretic mobility of particles at the surface. ECMs' active anti-fouling mechanisms are particularly beneficial because they a) are more effective than conventional treatment, b) reduce chemical usage, and c) can be specific to the foulants of concern. Specifically, electrically-induced antifouling mechanisms target foulants where they deposit, i.e. locally at the membrane/foulant interface, which makes ECMs more effective than traditional antifouling methods. The chemical-free in-situ generation of anti-foulants reduces the reliance on antifoulants and biocides, which reduces hazards associated with chemical handling and storage, chemical transportation and storage costs, the negative impact that chemicals have to membrane integrity, and the volume of chemical waste produced. Finally, a responsive, in-situ anti-fouling method can be tailored to a foulant type by applying the correct current configuration that most effectively removes or degrades that foulant.

Since the introduction of ECMs in the separation-based technologies, their application has been extended to different membrane categories including MF, UF, NF, and RO. For instance, incorporating ECMs in anaerobic MBRs has been suggested as a viable option for antifouling purposes as MBRs are highly susceptible to fouling and air-scouring is not possible in anaerobic conditions [14]. ECMs have been fabricated from a wide range of materials including carbon-based material (e.g. carbon nanotubes (CNTs), graphene, graphite, carbon nanofibers (CNFs)) [15–20], electrically conductive polymers (e.g. polyaniline) [21], and inorganic materials (e.g. ceramics, metals) [22,23]. Hybrid membranes are the most common type of ECMs. These are primarily composed of non-

conductive membranes (PES, PVDF, ceramic), which support a conductive coating layer. In addition to ECMs' antifouling properties, they can be coupled to electrochemical impedance spectroscopy (EIS) to detect and monitor fouling at the early stages of filtration [24]. Their self-cleaning abilities coupled to their foulant detection potential has found applications in sensors [25,26]. In addition, ECMs have shown promise for applications in other technologies including fuel cells, catalysts, and biomedical applications.

Over the past five years, many review papers have been devoted to ECMs [9–11,27–32]. A summary of the relevant work is presented in Figure 2.1.. Papers have offered a comprehensive review on ECMs, their material type, and their antifouling application; however, the underlying mechanisms have never been comprehensively discussed. The present review aims to explain the governing antifouling mechanisms to provide an understanding of published anti-fouling results and guide researchers to more effective materials and voltage application. Herein we provide a comprehensive and systematic discussion on electrically-induced antifouling mechanisms. Finally, this review discusses the outlook and limitations of ECMs and projects the opportunities that exist for academics, innovators, and industry within design, testing, operation, and optimization of ECMs for broad industrial adoption.

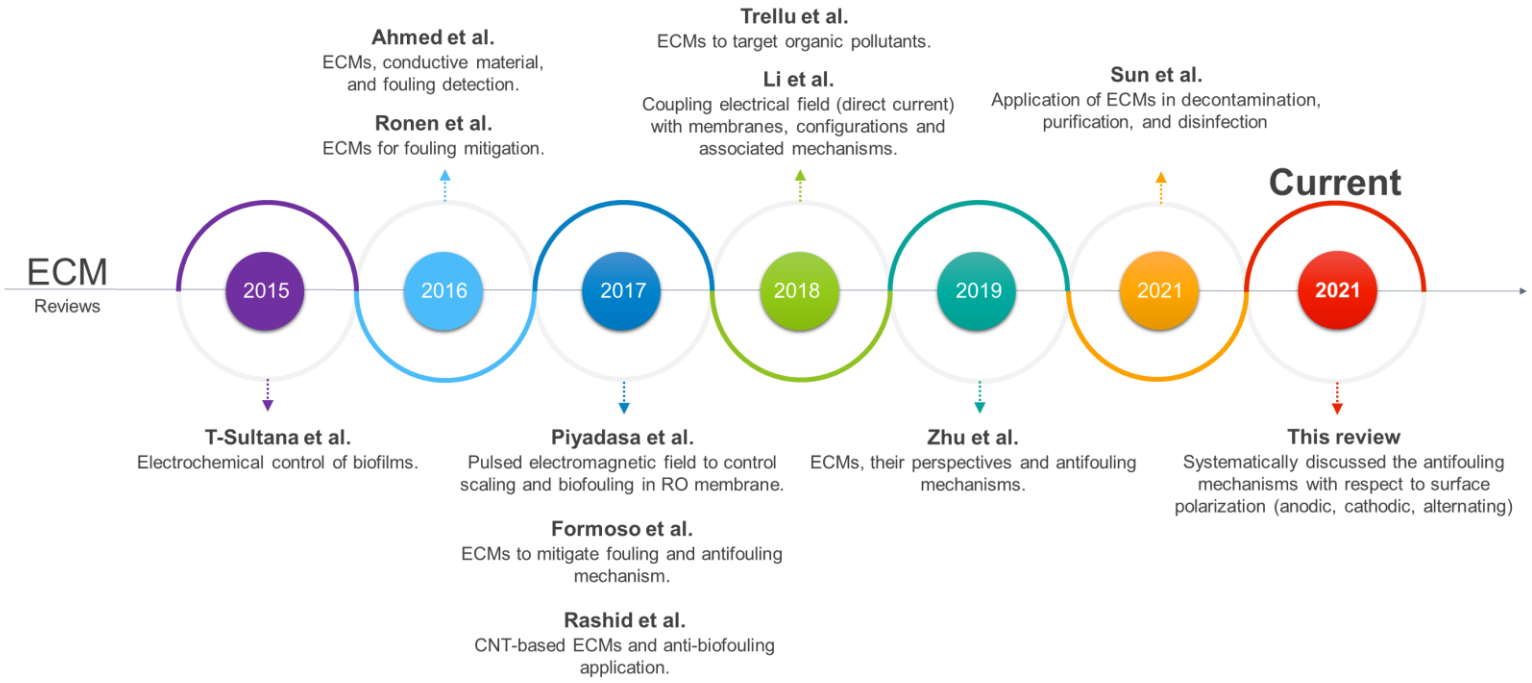

Figure 2.1. ECM review papers from 2015 to 2021 [9–11,27–33].

2.3.Antifouling mechanisms

Cathodic and anodic currents have been widely used in electrically conductive membranes (ECMs) for antifouling purposes. The conductive surfaces of these membranes are exposed to currents in the form of direct current (DC, electrical charge is applied in a single polarity) or alternating currents (AC, electrical charge is reversed polarity intermittently). DC can be applied with constant or changing current magnitudes, and AC can be applied with periodic or irregular intervals with changing amplitude as shown in Figure 2.2.

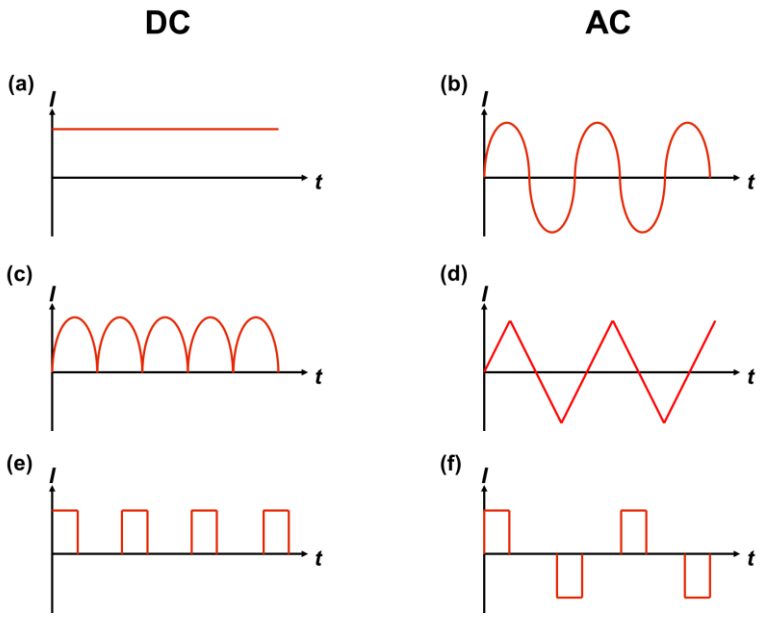

Figure 2.2. Examples of different electric current configurations applied to ECMs, (a), (c), and (e): Direct current. (b), (d), and (f): Alternating current. (e) and (f) are sometimes referred to as block current.

Cathodic and anodic currents activate different antifouling mechanisms at the interface of the ECM and the solute depending on the current range. Electrically-assisted antifouling mechanisms are exclusive to the current type as well as to the current configuration. The range of potentials commonly applied to ECMs to activate a specific type of antifouling mechanism is provided in Figure 2.3. ECM anti-fouling effectiveness is maximized when the antifouling mechanism is matched to the foulant type.

Investigations of ECM antifouling have thus far focused on the impact of electrical potential on specific types of fouling, i.e., biofouling, scaling, organic fouling, or colloidal fouling, however a fundamental understanding of the antifouling mechanisms and their interactions with the foulants of interest is not often considered. Energy-efficient and optimized ECM applications necessitate a deep understanding of underlying mechanisms and their impact on foulants. Therefore, it is important to identify the current type and the corresponding current range at which ECMs induce specific antifouling mechanisms. To this end, electrically-induced antifouling mechanisms are explained in detail in this review.

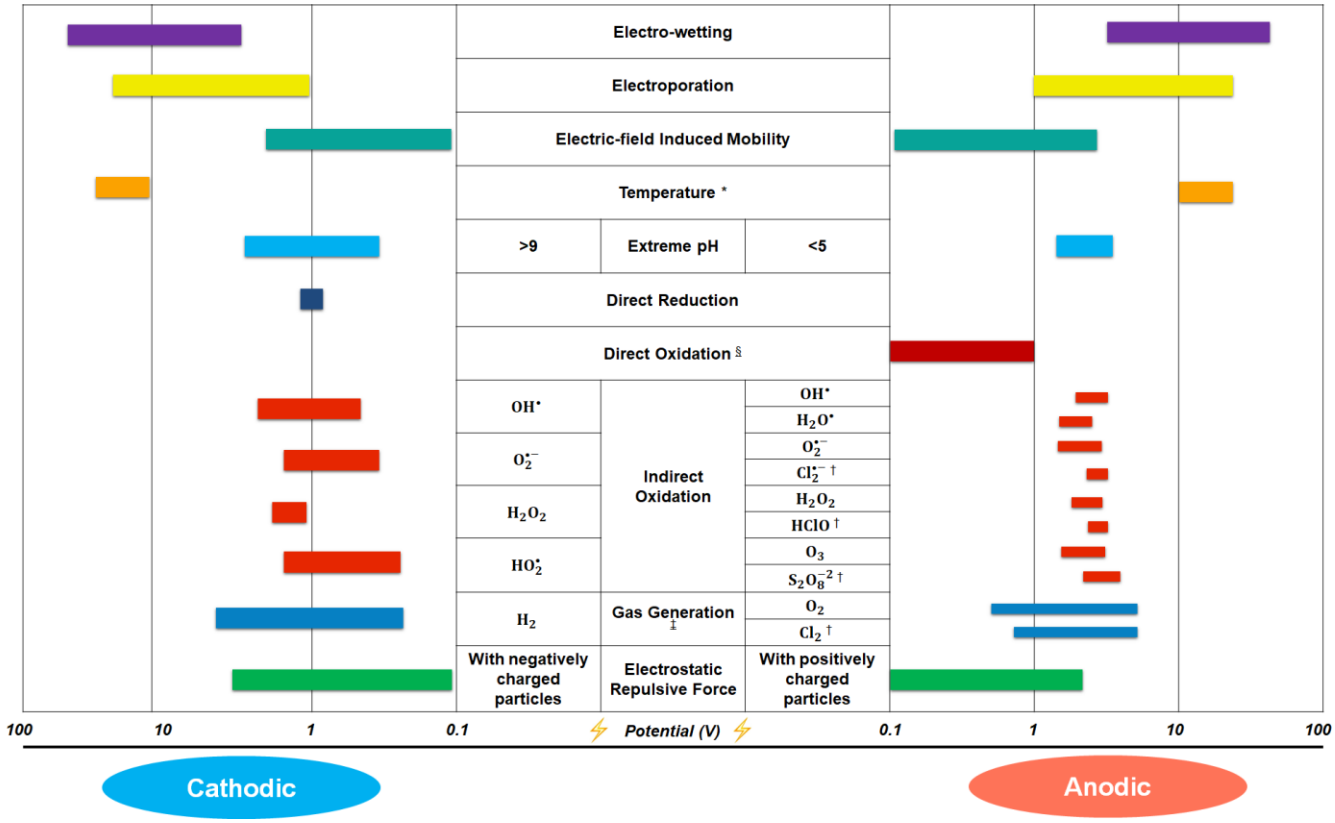

Figure 2.3. The range of electrical potentials commonly applied to ECMs, and the resulting electrical and electrochemical phenomena that could be used to prevent fouling. *: activation at low voltages requires high frequencies. §: depends on the foulant type (the range is for organic contaminates). †: depends on the gas evolution potential of the electrode (ranges are for carbon-based membranes). ‡: requires the presence of Cl and S in the solution.

2.4.Cathodic current

Cathodic current has been widely used on electrically conductive membranes (ECMs) either directly or in combination with anodic current in separation processes. Despite the critical role of cathodic current in antifouling performance of ECMs, few manuscripts have studied the antifouling mechanisms associated with cathodic current. In addition, there have been no systematic studies on the optimum current range to achieve the greatest antifouling performance. An understanding of the various mechanisms associated with different cathodic currents can guide future studies on the optimal applied current for membrane-based separation technology.

2.4.1. Electrostatic repulsion

Cathodic current provides a negative charge across the surface that induces a repulsive force to negatively charged particles. Many aqueous particles and molecules relevant to water treatment have negative surface charges, including bacteria, viruses, anionic organic particles, and anions. For instance, the majority of particles in the decanted effluent of sequencing batch reactors (SBRs) are negatively charged [34].

At the interface of the membrane surface, particles are influenced by the electrostatic force (F_{ES}), van der Walls forces (F_{vdW}), cross-flow lift (F_L), as well as permeation drag (F_D). The net force (F_T) applied on the particle is determined as follows:

$$F_T = F_D + F_L + F_{ES} + F_{vdW} \quad \text{Eq. (1)}$$

The electrically-generated repulsive force dominates at short-ranges within a few nanometers (<10 nm) [35–37]. The Derjaguin, Landau, Verwey, and Overbeek (DLVO) model incorporates the Poisson-Boltzmann (PB) equation to determine the electrostatic forces from regular surfaces and can be used to describe how charged surfaces influence foulants [36].

The DLVO model indicates that the magnitude and direction of net force from charged surfaces (e.g., ECMs) on particles varies with respect to the distance from the surface. At very short distances (<0.1 nm), the attractive Van der Walls force is dominant while at longer distances (>3 nm), the permeate drag force and the electrostatic force dominate particle-membrane surface interactions [38]. The drag force impacts the settling of particles towards membranes, and significantly impacts large particles (e.g. 0.22 nN and 0.40 nN for particles of size 1.16 μm and 2 μm, respectively) while it is negligible for small particles such as ions [36]. Thamaraiselvan et al. calculated interfacial forces for adhering bacteria in a flow cell at 3-6 nm away from a polarized surface under 2 V cathodic potential [36]. At such distances, they found that the net repulsive force from Van der Walls ($\sim 10^{-3}$ nN) and cross-flow lift (2.12×10^{-5} nN) was negligible compared to the electrostatic (0.85-1 nN) and permeation drag force (0.09 nN). At shorter distances (< 3

nm), the attractive Van der Walls forces were found to cause the attachment of negatively charged bacteria to the cathode electrode, despite their like polarity. An electric potential applied to the surface of an ECM impacts the distances over which electrostatic repulsive forces are felt by charged particles in solution. This distance is represented by the boundary layer from DLVO theory, which shifts away from the surface at higher potentials.

The maximum electrostatic repulsive force that can be achieved is not substantially enhanced beyond approximately 2 V [35]. The electrostatic force is directly related to ion hydrated size, ion valence number, and ions concentration accumulated on the surface [37]. Therefore, the maximum electrostatic repulsive force is restricted by the limited number of hydrated ions that can accumulate on the surface. It is worth noting that electrostatic force is sensitive to the ionic strength of the media. At a high ionic strength, electric fields may not have much impact on fouling because the ions in solution form a thin, dense electric double layer [37].

A few research investigations have discussed the role of electrostatic forces to prevent surface scaling [39–41]. Scaling occurs at the interface of surface and liquid where high concentrations of ions accumulate and develop concentration polarization. Scale is formed when ions and counterions co-exist in the same stochiometric ratio as a possible crystal structure and when those ions reach their solubility limit at a surface. When an electric current is applied to the surface, an electric double layer (EDL) is formed and like-charged ions are pushed away from the surface and replaced by unlike-charged ions. The migrations of ions can disrupt the stoichiometric ratios leading to an unbalanced concentration of either anions or cations on the surface. This imbalance can retard the formation of scale, while also disrupting the nucleation and growth rate of crystal structures [39–41]. Crystals formed under the influence of electrical fields have been suggested to be larger and more porous and thereby less resistant to water flux and more susceptible to cleaning procedures [41].

While the majority of cathodic-based experiments were carried out to take advantage of the repulsive force, their adsorption potential mediated by electrostatic

attraction has been also reported. Weidlich et al. [42] reported a significant decrease in the Ca concentration in the permeate due to the adsorption of Ca^{2+} ions on the negatively charged membrane cathode (under 0.8 V).

2.4.2. Hydrogen gas generation

Cathodic surfaces generate hydrogen gas following Reaction 1 and Reaction 2. Generated hydrogen gas forms micro- and nano-bubbles that subsequently induce several antifouling mechanisms at the liquid-membrane interface.

$$H^+ + e^- \rightarrow \frac{1}{2} H_2 \quad (1)$$

$$H_2O + 2e^- \rightarrow 2OH^- + H_2 \quad (2)$$

Once bubbles are formed and overcome the membrane surface tension, they leave the surface due to buoyancy and surface charge which can be described by their electrophoretic mobility [43]. Release of hydrogen bubbles across the surface can mitigate fouling in different ways, including by a) electro-steric repulsion, b) changing the feed flow behavior, and c) physically impacting the foulants upon bubble bursting.

Bubbles act as electro-steric barriers at the interface of the membrane, causing both steric repulsion from the generated bubble itself and electric repulsion from their surface charge, both of which increase the surface energy between the surface and the foulant. Bubbles have a surface zeta potential, which is strongly dependent on the pH of the solution. In neutral and basic pH, hydrogen microbubbles are negatively charged [44]. For example, it was reported that the average surface charge of hydrogen micro-bubbles is -35 mV at pH 5.8 and decreases with increasing pH until it reaches a plateau at pH 10 with a value of -110 mV. While in extremely acidic solutions (pH<4.5), the surface charge of bubbles is positive with an average of 20 mV [45]. As discussed later, cathodic and anodic surfaces have extremely high local basic and acidic pH values, respectively. As such, the zeta potential of the generated bubbles is expected to be negative at the cathode and positive at the anode. Therefore, cathodic and anodic surfaces enhance the movement of released

bubbles due to the repulsion with like-charged bubbles. The generation of many bubbles under the application of an electrical current at the surface can cause changes to the flow behaviour at the liquid membrane interface. Movement of bubbles increases the Reynold's number (Re) locally across the surface. The average rising velocity of bubbles with a diameter of 50 μm is reported to be 1000 μm/s [45]. Subsequently, the local turbulent flow attenuates fouling intensity. Generation of bubbles has been shown effective in fouling control by changing the hydrodynamic and mass transfer across flat sheet membranes [46–48].

Bubbles can be formed in different sizes within the micro (0.1-50 μm) and nano range (1-100 nm) [47,49] and burst at different rates. Bubble stability depends on the bubble size, gas-liquid interface permeability, Laplace pressure, type of fluid, fluid impurities, and flow behavior [50]. Unlike macro bubbles, which rise and expand inside water and burst at a liquid-gas interface such as the surface of a liquid, micro- and nano-bubbles shrink gradually due to dissolution of the gas into the water and burst once they become sufficiently small (sub-nano). The Young-Laplace equation describes the pressure difference and the radius of the bubble as follows:

$$\mathrm{P} = \mathrm{P_l} + 2\,{}^{\sigma}/_{\mathrm{r}} \qquad \text{Eq. (2)}$$

where P is the internal gas pressure required to maintain the bubble integrity, P_l is the liquid pressure, σ is the surface tension, and r is the bubble radius. Micro- and nano-bubbles contain high inner pressures that lead to the fast dissolution of gases into water. For instance, bubbles with diameters of 1 μm and 0.1 μm have inner pressures of 56.87 and 436.47 psi on average, respectively. Micro-bubbles are more stable than nano-bubbles due to their lower inner pressure, such that micro bubbles are stable within a few seconds (<10s), while nano-bubbles are only stable for a fraction of a second [43,51]. The mass transfer coefficient for small gas bubbles has been previously empirically modelled [52].

Micro- and nano-bubbles undergo self-bursting in aqueous solutions [53]. The burst generates free active radicals such as $OH^{\bullet}$. Radicals are important for fouling mitigation and control as discussed in section 2.4.3. The detailed mechanisms of radical generation

are beyond this review and can be found elsewhere [43]. In short, the concentration of ions (OH^- and H^+) at the interface of bubbles rapidly increases as micro- and nano-bubbles shrink. It has been suggested that the drastic increase in the density of ions triggers the generation of radicals. Takahashi et al. have reported the generation of free radicals from bubble bursting [43], although there is no direct evidence that the bubble bursting mechanisms mitigates fouling [54]. Further, the energy released from the micro and nano-bubbles bursting exerts shear forces and shock waves on surrounding particles. Together the high shear and free radicals formed likely contribute to bubble-induced antifouling, however there have not been any studies that have confirmed the impact of each mechanism on foulants.

2.4.3. Indirect oxidation

Indirect oxidation is responsible for the degradation of pollutants such as biofoulants and organic matter, which can help reduce surface fouling. Indirect oxidation occurs in the aqueous media through a series of reactions that are mediated by electrochemically generated oxidants. Cathodic surfaces can generate reactive oxygen species (ROS) such as hydroxyl radicals ($OH^\bullet$), hydrogen peroxide (H_2O_2), hydroperoxyl radicals ($HO_2^\bullet$) and superoxides ($O_2^{\bullet-}$), listed in order from most to least reactive. [55,56]. Surface-generated oxidants can attack foulants at their surface adhesion interface, representing a significant advantage over bulk-added oxidants. Biofoulants often produce a defensive layer or biofilm in solution, but lack significant protection at their adhesion interface. Therefore, biofoulants may be more susceptible to oxidants generated from the surface to which they are adhered as compared to oxidants added into the bulk [57,58]. Furthermore, biocides and antibiotics added in the bulk are further limited in their efficacy by diffusion limitations within the biofilm. As such, local concentrations of biocides might be ineffective despite high concentrations added to bulk feed solutions [27].

We surmise that the discrepancy in interpreting the impact of indirect oxidation within the literature stems from inaccurate measurement of oxidants' local concentration

at the surface of biofilms [38,59–63]. The antifouling mechanisms of specific cathodic-generated oxidants are discussed below.

Hydrogen peroxide

Hydrogen peroxide can limit both biofouling and organic fouling. Hydrogen peroxide has been shown to be moderately effective in mitigating biofouling [57,58,64–66]. Cathodic surfaces generate hydrogen peroxide as follows [58,59,67–72]:

$$O_2(g) + 2H^+ + 2e^- \rightarrow H_2O_2 \ (E° = 0.465 - 1.000 \text{ V vs. Ag/AgCl}) \quad (3)$$

It has been reported that hydrogen peroxide oxidizes polysaccharides and proteins leading to reduced soluble microbial products (SMP) and extracellular polymeric substances (EPS) across the membrane [73]. Biomolecules can sense ROS and hydrogen peroxide at deficient concentrations (<1 μM) [38]. Hydrogen peroxide imposes oxidative stress on biological cells, which weakens cell adhesion and can lead to detachment and dispersal [74–76]. Hydrogen peroxide can also decrease cell selectivity which can result in cells becoming vulnerable to surrounding chemicals and stimuli [77–82]. As such, hydrogen peroxide is often applied in combination with other biocides to enhance the biocidal impact. Similarly, hydrogen peroxide can also enhance organic oxidative degradation and thereby combat organic fouling when it is used in combination with other advanced oxidation processes (AOPs) such as UV, Fenton reactions, and ozonation [83–90]. For example, in the presence of UV, hydrogen peroxide can reduce natural organic matter (NOM) membrane fouling by transforming phenolic groups in aromatic moieties of NOM to quinone groups. These quinone groups readily form hydrogen bonds with water molecules, reduce the homo-interactions of NOM and thereby reduce the adsorption propensity of NOM on membrane surfaces [90]. In a Fenton-like reaction, hydrogen peroxide generates powerful hydroxyl radical species in the presence of Fe ion, which acts as a catalyst (reactions 4 and 5). These reactions have the potential to fully mineralize the NOM in the industrial and municipal waste streams [89].

$$H_2O_2 + Fe^{3+} \rightarrow HO_2^{\bullet} + H^+ + Fe^{2+} \quad (4)$$

$$H_2O_2 + Fe^{2+} \rightarrow + OH^{\bullet} + OH^{-} + Fe^{3+} \quad (5)$$

The major limitation of cathodic-induced peroxide generation is the limited availability of oxygen due to the low solubility of gaseous oxygen in water (8 mg/L in contact with air at ambient temperature and pressure) as well as the many competing oxygen reduction reactions [91]:

$$O_2(g) + 4H^+ + 4e^- \rightarrow 2H_2O \quad (6)$$

$$O_2(g) + 2H_2O + 4e^- \rightarrow 4OH^- \quad (7)$$

$$O_2(g) + 4H_2O + 4e^- \rightarrow 2H_2O^- + 4OH^- \quad (8)$$

$$H_2O_2 + 2H^+ + 2e^- \rightarrow 2H_2O \quad (9)$$

Radicals

Research findings suggest that cathodic processes are able to form ROS such as hydroxyl radicals ($OH^{\bullet}$) [92], superoxides ($O_2^{\bullet -}$) [93–95], and hydroperoxyl radicals ($HO_2^{\bullet}$) [96] as shown in Reaction 10-14. These reactions take place above surface over potential (1.27 V for carbonaceous material and 2.2 V for inorganic coatings). During cathode generated radical formation, superoxide is the dominant product [92].

$$O_2 + e^- \rightarrow O_2^{\bullet -} \quad (10)$$

$$O_2^{\bullet -} + AH \rightarrow HO_2^{\bullet} + A^- \quad (11)$$

$$H_2O_2 + H_2O^- \rightarrow OH^{\bullet} + O_2^{\bullet -} + H_2O \quad (12)$$

$$H_2O_2 + e^- \rightarrow OH^{\bullet} + OH^- \quad (13)$$

$$O_2 + 2H^+ + 3e^- \rightarrow OH^{\bullet} + OH^- \quad (14)$$

Such radicals are highly active and can attack and degrade pollutants including organic, inorganic, and biological compounds. The inactivation/degradation process follows the following stages: (a) generation of active radicals (formation time in the order of 10^{-10} s), (b) diffusion into the media (time in the order of 10^{-3} s), and (c) inducing the reaction

between the radical and the pollutant (high reaction rate in the range of 10^6 to 10^9 $M^{-1}s^{-1}$) [97]. Many studies have indicated the promising application of radicals in water and wastewater treatment processes to degrade organic compounds and, more particularly compounds that are resistant to biological degradation such as pharmaceuticals and personal care products [98–104]. Amongst ROS, the hydroxyl radical is the only compound that can readily react and degrade aromatic compounds. Hydroxyl radicals react with most aromatic and unsaturated compounds through hydrogen abstraction, oxidation, and addition [92], and near complete organic mineralization of aromatics is possible [105–107].

Many studies have elucidated the role of radicals to disinfect and inactivate bio-compounds as biocides [36,108–113]. Radicals react with biological molecules at diffusion-controlled rates [109,113]. Radicals make the cell vulnerable to external stress by disrupting or damaging the cell wall integrity leading to cell lysis [110,112].

2.4.4. High local pH

Electrochemical reactions result in changes in the local pH across the electrodes. Water electrolysis generates high concentrations of hydroxyl ions (Reaction 15) when the electrode is used as a cathode [41,114].

$$2H_2O + 2e^- \rightarrow 2OH^- + H_2 \quad (15)$$

Hydroxyl ions diffuse into the membrane-liquid interface and alter the pH. The pH profile across the surface depends on the potential distribution and solution ionic strength. Large local pH change can beneficially control scaling and biofouling, reducing the need for additions of pH-adjusting chemicals (NaOH) and reducing storage and handling costs and complications. Electrochemical modification of pH induces pH change within a few nanometers of the surface. The distance over which pH is changed depends on the current density and the pH of the bulk solution [114]. Tang et al. applied a current density of 5 A m^{-2} (3.6 V) to a CNT surface and calculated that a 30 μm diffusive layer with pH 13.5 was formed [114].

Scaling occurs at the surface of the membrane where the local concentration of sparingly soluble salts exceeds their solubility limit. The most common inorganic scales are calcium sulfate dihydrate (gypsum), calcium carbonate (calcite), barium sulfate (barite), and silica [115]. Bulk pH adjustment is a known strategy to minimize scaling, thus surface generated pH change has strong potential to be effective in scale reduction. Not all scale is pH sensitive, however precipitated silica can be redissolved and caused to rediffuse into the feed at high pH. The dissolution rate of silica is reported to be directly correlated to concentration of hydroxyl ions with a rate of $[OH^-]^{0.5}$ in the pH range of 10-13 [114,116]. The mechanism of silicate dissolution at a high pH is well documented [114,117–119]. In short, at a high pH (particularly above 12), silica becomes fully deprotonated and negatively charged, leading to detachment of Si from the polymeric chain scale (depolymerization) and scale resolubilization [116–118].

In addition, heavy metals such as As, Cu, and Zn are less stable and insoluble at higher pH values. pH adjustment has been used to enhance the separation efficiency of toxic semi-metallic elements in filtration processes [120–124]. Therefore, such practice can be promoted by ECMs working as a cathode, increasing the local pH at the surface.

2.4.5. Electroporation

A high electric field can induce a potential difference across bacterial cytoplasmic membranes which can damage their cell wall [125]. If the potential difference exceeds the membrane electroporation threshold, the pores of the cytoplasmic membrane expand leading to changes in cell permeability and conductivity [126]. As such, the cell undergoes ionic imbalance-induced metabolic stress, and the osmotic imbalance can cause cell lysis [127]. The electroporation threshold is assumed to be 1 V across a bacterium [128], and high electric fields (20 V) induce irreparable damages to cell membranes [129–131]. Electroporation has been demonstrated to inactive bacteria [132,133], protozoa [134], and viruses [133,135]. The inactivation efficiency due to electroporation relies on the intensity of electric field, frequency and magnitude of the pulses, size of microorganism, incubation time, and temperature [136,137]. The effective frequency of electric field pulses for

electroporation is in the range of kHz to GHz [138–140]. High frequencies are even able to damage microbial DNA. It has been suggested that while low frequencies (50 Hz) might not be sufficient to damage the cell membrane directly, low frequencies can alter microbial morphotypes which may suppress bacterial population growth [141,142].

2.4.6. Electrical field-induced mobility

Movement of a particle in an electro-flow cell can be described by extended Nernst-Plank (Eq. 3).

$$J_i = -D_i \frac{\partial_{C_i}}{\partial_x} - D_i c_i \frac{z_i F}{RT} \frac{\partial_\phi}{\partial_x} + c_i v(x) \qquad \text{Eq. (3)}$$

Where the first, second, and third terms are diffusive, electric field-induced, and convective fluxes. J_i represents the average flux of charged particles i. D_i and c_i are the diffusion coefficient and particle concentration, respectively. F and R are the Faraday constant and ideal gas constant, respectively. T is the absolute temperature, z_i is the valence number of charged particles i, $v(x)$ is the velocity of the fluid through media, and $\frac{\partial_\phi}{\partial_x}$ is the electrical field. According to Eq. 3, an externally applied electric field can be used to control the mobility of charged particles by counteracting the diffusive and convection fluxes. An applied electric field induces an electrophoretic force on the adhering particles which is proportional to electrophoretic mobility and electric field strength. The electrophoretic velocity of particles can be described by the Smoluchowski's equation as follows:

$$U = \left(\frac{\varepsilon \xi_p}{4\pi\eta}\right) E_\infty \qquad \text{Eq. (4)}$$

Where ξ_p is the zeta potential (electrostatic surface potential) of the adhering particles. ε and η represent the dielectric constant and viscosity of the fluid and E_∞ is the externally applied electrical field. The ratio $\frac{U}{E_\infty}$ describes the electrophoretic mobility of the particle [143].

Electrically-induced forces are either perpendicular to the surface (electrostatic and electrophoretic forces) or parallel to the surface (electroosmotic forces). The electrostatic force enhances the movement of particles perpendicular to the electrode surface, by attracting unlike-charged particles and repeling like-charged particles. Bacteria and other natural organic foulants are often negatively charged, thus the electrostatic force can repel them from surfaces under cathodic bias. Poortinga et al. reported the magnitude of the electrophoretic force for the bacterium, *Streptococcus oralis*, to be in the order of 10^{-4} nN under 1.9 V (0.8 mA) applied potential [144]. The strength of the electrophoretic force is insufficient to overcome the bacterial adhesion force which is reported to be two orders of magnitude larger [144]. However, the enhanced particle mobility due to the electric field, can weaken the surface binding energy sufficiently such that adhered particles can be detached by lateral shear forces induced by convective flow [145].

In contrast, the electroosmotic force is the motion of charges and the associated liquid within the electric double layer along a charged surface in the direction of an applied electric field. Poortinga et al. have estimated the electroosmotic force for bacterial cells positioned 1 μm away from the surface at a current of 0.8 mA to be on the order of 10^{-4} nN [144]. It has been shown that forces in the range of 10^{-3}-10^{-5} nN can induce lateral movements to bacteria [146].

2.4.7. Electro-wetting

Electric fields can change the wettability of carbon-based material (graphene and CNT) from hydrophobic to hydrophilic [147,148]. Many studies have shown that hydrophilization of membrane surfaces can reduce fouling intensity, thus electro-wetting effects could indirectly reduce surface fouling, in particular that associated with hydrophobic foulants [149–152]. Under high applied potentials to electrically conductive membrane surfaces, solvated ions are attracted to charges along the surface causing water droplets to spread and fill hydrophobic pores. This effect decreases the surface energy enhancing the surface hydrophilicity [148]. The electrical field-assisted transition from super-hydrophobicity to super-hydrophilicity can be explained by classical models, i.e.

Cassie-Baxter and Wenzel which are out of the scope of this study [153]. It has been shown that the application of electrical potentials (up to 20 V) on MWCNTs could decrease the surface contact angle by as much as 70% (from 140° to 40°) [148]. The threshold potential for the reduction of contact angle has been reported to be 3 V on CNT surfaces [148]. Beyond a certain voltage (20 V), little change in contact angle occurs due to surface saturation with water [148]. There is contradictory evidence for the polarity dependence of water wettability. Pu et al. [154] have reported the same degree of electro-wetting for anodic and cathodic potentials of the same magnitude for CNT and graphene films, while Wang et al. [155] have demonstrated significantly different threshold voltages for anodic and cathodic polarization (1.7 V vs. 60 V, respectively).

2.4.8. Direct reduction

Direct reduction has been suggested for partial degradation of environmentally recalcitrant contaminants in wastewater treatment [156–159]. In spite of some promising results of direct reduction of wastewater contaminants, less research has been conducted on direct reduction as compared to direct oxidation. In general, cathodic current can be applied for electrochemical dehalogenation of organochlorinated contaminants such as dechlorination of dyes, reduction of amino-derivative compounds such as antibiotic sulfonic acid, and reduction of nitroaromatic contaminants such as nitrobenzene [91,157,160–162]. The main research challenge is the selection of materials that prevent hydrogen evolution as a side reaction. Cathodic reduction is not suggested as an efficient antifouling mechanism, but it is an excellent option for removing recalcitrant contaminants that are resistant to conventional treatment processes.

2.4.9. Temperature

Local temperature rise generated by electrical current has been mostly observed during anodic polarization at either direct or alternating current modes, hence it is discussed in section 2.6.3.

2.5.Anodic current

Anodic current has been extensively applied in electrically conductive membranes to achieve antifouling performance. In the following sections, an in-depth discussion is provided for each mechanism associated with anodic current.

2.5.1. Electrostatic repulsion

The impact of electrostatic repulsive force on foulants was discussed in section 2.4.1. Anodic surfaces have demonstrated antifouling potential through electrostatic repulsive force with positively charged particles, ions, and metals (e.g., 1-2 V) [30,38,163,164] or through electro-kinetic rearrangement of ions, hence, unbalancing the stoichiometric concentration suitable for scaling (e.g., 1.5 V) [41].

2.5.2. Oxidation

The electrochemical advanced oxidation process (EAOP) has gained interest in the scientific community for the excellent potential in abatement of organic pollutants due to this process's inherent environmental compatibility, energy efficiency, amenability to automation, and low cost. Conventionally, configurations applied in reactors suffer from limited mass transfer critical for electrolysis. ECMs, however, have been recently introduced to EAOPs and have shown promise to transform the field by taking advantage of their flow-through configuration. When a contaminant containing medium is filtered through a membrane, the diffusion pathway between the contaminant and the electro-active surface shortens to the radius of the pore, leading to enhanced electrochemical activity including direct electrooxidation as well as indirect removal by mediators. For instance, low-pressure ECMs can be used to target a wide range of contaminants such as organic compounds, microorganisms, or poorly biodegradable compounds such as pharmaceuticals, antibiotics, pesticides, and personal care products [32,91]. Different types of anodically-induced oxidation are discussed below.

Direct oxidation

Direct anodic oxidation is a process where contaminants become oxidized upon adsorption on the anode electrode, without the involvement of any chemical or mediators

other than electrons, which have been called the “clean reagent”. Direct oxidation is a well-established method that has been demonstrated for the removal of organic pollutants and microorganisms [11,30,165–167]. For example, Liu et al. reported the rate of electron transfer to be 8.5×10^{15} and 1.3×10^{17} $e^{-}s^{-1}m^{-2}$ at anodic potentials of 0.35 and 1.50 V, respectively [163].

Due to direct contact of contaminants with the surface, often organic compounds experience electropolymerization through direct anodic oxidation, which subsequently causes surface fouling and poor electrocatalytic activity of the electrode, commonly called a “poisoning effect” [166,168–174]. The poisoning effect caused by direct oxidation of phenol results in electrode passivation and irreversible fouling, and has been described by many studies [175,176]. Electropolymerization reduces the flux and enhances the pressure drop across the membrane. Therefore, removal of organic compounds such as phenols solely through anodic oxidation has not been adapted as a sustainable approach due to pore blockage and irreversible fouling.

Theoretically, anodic oxidation of organic contaminants is effective at potentials above that needed for water electrolysis. High anode overpotentials (above the range of water electrolysis (1.2 V)) are suggested to minimize electropolymerization. High potentials favor aromatic ring-opening and complete oxidation, however, it may be at the cost of electrooxidizing the anode material, which is a particular issue for carbon-based electrodes [177]. Doping carbon-based materials with Bi and Sb can enhance the stability of electrodes and decrease the extent of electropolymerization by allowing enhanced electron transfer for phenol oxidation.

Direct electron transfer can also control biofouling by inactivating microbial cells. Inactivation of bacteria is likely due to the oxidation of intracellular coenzyme A (CoA) to dimeric CoA at approximately 0.7 V [108]. CoA exists in the walls of bacteria and takes part in the synthesis of pyruvate in the citric acid cycle, hence its oxidation halts cell respiration and cell viability [38]. Loss of respiration activity has been observed in *Bacillus subtilis* [178] and *E. coli* [38], *Vibrio alginolyticus* [179], and *P. aeruginosa* [145].

Radicals

Indirect oxidation is often the preferred method for pollutant degradation, as oxidation through radical mediators (e.g. reactive oxygen species, active chlorine, persulphate, and ozone) avoids the destructive impact of direct oxidation on anode materials.

Hydroxyl radicals are extremely active and known as the second most potent oxidant after fluorine [157]. Water electrolysis leads to the electrogeneration of either physisorbed hydroxyl radicals at the anode (as active $OH^{\bullet}$) or chemisorbed active oxygen (in the lattice of metal oxide anodes) [157]. Available hydroxyl radicals can readily react with organic compounds as well as with the anode, depending on materialist material composition. Anode materials are considered "active" or "non-active" based on their reactivity with hydroxyl radicals. Active materials (OER<0.3) that strongly react with hydroxyl radicals include Pt, RuO_2, and IrO_2, while non-active materials (OER>0.4) such as boron-doped diamond (BDD), PbO_2, TiO_x, and SnO_2 lead to preferential oxidation of organic compounds by electrochemically generated radicals [30,91,166,180]. Generated hydroxyl radicals desorb from the surface depending on the thermodynamic state of the anode. If the free energy of hydroxyl radicals is comparable at the surface and in the aqueous solution, it desorbs into the solution. Otherwise, if the free energy of physisorbed radicals is much lower than the aqueous solution, they readily react to form oxygen or hydrogen peroxide [181]. Hydroxyl radicals are limited to the interface layer (<1 μm) due to their high reactivity and short lifetime [182,183]. Hydroxyl radicals have been used to both degrade organic contaminants as well as combat biofouling. Free radical have been hypothesized to alter the charge of EPS that in turn weakens the biofilm stability [184]. Interestingly, cell signaling role of hydroxyl radicals might take part in increasing the genetic variants of the biocell [185], thereby increasing the versatility and adaptability of biofilms, which may be counter-productive to combatting long-term biofouling [186].

The chemical composition of the feed solution strongly influences the oxidation pathways and electrocatalytic mechanisms. In the presence of available chloride ions,

active chemical species such as Cl_2, hypochlorous acid (HOCl), and hypochlorous anions (OCl^-), collectively called active chlorine species, can be generated at the anode described by a series of reactions as follows:

$$2Cl^- \rightarrow Cl_2 + 2e^- \quad (E = 1.36\ V) \tag{16}$$

$$Cl_2 + H_2O \rightarrow HClO + H^+ + Cl^- \tag{17}$$

$$HClO \rightarrow ClO^- + H^+ \tag{18}$$

The in-situ generation of active chlorine has been suggested to degrade organic compounds [174,187,188]. The stable state of active chlorine species is pH dependent: Cl_2 is the predominant state at pH<3, hypochlorous acid (HOCl) becomes the stable form at 5<pH<6, and hypochlorous anions (OCl^-) are dominant at pH ≥6 [189]. Hypochlorous acid is the most potent oxidant among the chlorine species, hence, electrochemical processes derived by active chlorine oxidation are most optimally conducted in acidic media. Active chlorine production has been widely used to treat wastewaters due to the natural abundance of chloride ions [167]. Biological organisms are susceptible to electrochemically-generated active compounds such as active chlorine species, which target microbial cell components such as DNA, RNA, proteins, and lipids. In addition, electrochemistry coupled to reverse osmosis (RO) has been successfully used to remove COD in RO concentrate by direct oxidation and indirect oxidation via chlorine species [190]. However, the possibility of producing toxic byproducts such as chlorinated organic compounds has raised concerns for expanding the application of this method. For instance, it was reported that the toxicity due to chlorine compounds exceeded the regulated limits during oxidation of phenol in the presence of NaCl [191].

Other examples of strong anodically-promoted oxidants are persulfate [192], percarbonate [193], and perphosphate [194] generated by materials such as diamond and PbO_2-coatings and in the presence of sulfate, carbonate, or phosphate anions, respectively, which are described as follows:

$$2{SO_4}^{2-} \rightarrow {S_2O_8}^{2-} + 2e^- \tag{19}$$

$$2CO_3^{2-} \rightarrow C_2O_6^{2-} + 2e^- \quad (20)$$

$$2PO_4^{3-} \rightarrow P_2O_8^{4-} + 2e^- \quad (21)$$

The impact of anode material, their efficiency, selectivity, as well as the pollutant type, its concentration, and operating parameters on electrochemical processes have been considered in depth by many review papers in the electrochemical field [30,91,157,165–167,195–198].

Active chlorine species are known bacterial disinfectant and their biocidal activity at low concentrations (25-100 mg/L) has been shown on *S. epidermidis* [199–201] or *S. aureus* [202], and *P. aeruginosa* [201].

2.5.3. Gas generation

Anodic surfaces are able to generate oxygen and chlorine gas. The antifouling mechanisms associated with gas generation include steric repulsive force, enhanced convection, and bubble blast force that were discussed in section 2.4.2. Hence, here the side effects exclusively induced by each gas are discussed.

Water electrolysis at the anode leads to the oxygen-evolution reaction (OER, Reaction 22).

$$2H_2O \rightarrow O_2 + 4H^+ + 4e^- \quad (22)$$

OER competes with other oxidation reactions occurring at the anode/water interface. Anodic surfaces have different oxygen evolution potentials (OEP). CNTs for instance, have OEP of 1.2 V. Water as a solvent is more accessible to the anode electrode compared to contaminants, therefore, OER is the preferred reaction at the anode. OER substantially reduces the current efficiency for contaminant oxidation. Therefore, it is desired to incorporate materials with higher OEP to improve contaminant oxidation efficiency [177]. In addition, the continuous generation of oxygen gas bubbles is a steric barrier and reduces the direct contact of contaminates with anode's electro-active sites. Further, oxygen bubbles can block pores and reduce surface electrical conductivity. Hence, OER may

suppress the oxidation rate of contaminants. Several studies have attributed an observed reduced permeate flux to the pore blockage from electrolysis-generated oxygen bubbles [30,177,203,204].

As discussed in section 2.4.3, oxygen is in high demand at the cathode. Oxygen gas generated at the anode can enhance hydrogen peroxide production at the cathode, however oxygen solubility remains a limitation. Another side effect of OER is to support the metabolic activity of aerobic microorganisms by providing sufficient oxygen [205].

2.5.4. Low local pH

Anodic surfaces generate protons across the conductive surface following reaction 22. Excess protons shift the local pH at the surface to acidic which can be advantageous for controlling scaling or biological fouling.

Calcium carbonate (calcite) is the most common mineral scale and the main precipitant in reverse osmosis filtration [28]. Formation of calcite can be prevented in acidic environments [206]. By decreasing pH to below 7, solubility of calcium carbonate shifts to a soluble state (carbonate to bicarbonate), leading to mitigation of crystal nucleation and scale formation. Further, the addition of acid to the bulk can resolubilize calcium carbonate scale. Hydrochloric acid and/or sulphuric acid are commonly used to adjust feed water pH in drinking water and wastewater applications. This process is laborious and can corrode system piping. It was shown that aggressive acidic adjustment cause corrosion of system piping (by dissolution of Fe and Cu), in turn changing the water composition and negatively impacting scale formation [207]. Alternatively, electrically conductive membranes can electrochemically adjust the local pH without effecting the bulk pH. Further, this pH change can be targeted at the source of nucleation on the surface of the membrane. It was demonstrated that the application of anodic potential (1.8 V vs. Ag/AgCl) led to the successful removal of calcium carbonate and 98% permeate flux recovery. In addition, low pH (2.8-3) catalyzes electro-Fenton reactions in the presence of abundant Fe ions in the solution [197].

Extreme acidic conditions mitigate the growth of pH-sensitive microorganisms [82,208]. The role of pH in the inactivation of microorganisms is complex and involves developing proton imbalances across the cell wall, proton infiltration into the cell, and disruption of DNA, ATP, and various enzyme. [209,210]. Electric fields can further enhance the inactivation of microorganisms [209]. Electrical fields increase the pore size of the cell thereby increasing the proton influx [209,211,212]. More fundamental details about the relation between pH and inactivation mechanism can be found elsewhere [211–214]. Gram-positive bacteria such as *Listeria monocytogenes*, *Staphylococcus aureus* have been shown to be more resistive to low pH [82].

Electro-induced pH changes happen at the membrane surface and are often not detected in the bulk. Further, in undivided flowcells, high local pH of the cathode cancels out the low pH of the anode, and Ca ions or CO_2 generated from oxidation of carbon-based anode materials act as buffers in the solution [215]. As such, little research has demonstrated the impact of electrochemically generated extreme local pH produced at the surface of ECMs.

2.5.5. Electric field-induced mobility

The concept of electrophoretic mobility was discussed in section 2.4.6. In general, the movement of microorganisms is shown to be different under cathodic and anodic polarization. Under cathodic current, electrophoretic mobility of bacteria has been shown to be the dominant factor contributing to detachment of bacteria due to net negative surface charge of bacteria, while under anodic polarization the electroosmotic force has been predominantly studied. The electroosmotic force does not directly contribute to desorption of bacteria, however, desorption probability was observed to increase by 1000 fold compared to control experiments [216], which is thought to be due to the oscillating motion of bacteria accompanied by shear stress reducing the adhesion force. In different studies, the translation motion of a model bacteria, *P. aeruginosa* PAO1, was demonstrated via a quantitative particle tracking approach under anodic polarization and the trajectories of the bacterial cell showed a movement of 1.2-1.43 μm for 10 s [145,217] which was

approximately 20 times longer than movements on unpolarized surfaces. Under anodic current, the mobility of the negatively charged bacteria is governed by the trade-off between the lateral electroosmotic force and the attractive electrostatic force. The electrostatic attractive force becomes weaker at higher ionic strength (due to denser electric double layers) [217,218]. The combination of both forces induces a random movement to the bacteria until the electrostatic attractive force dominates at high ionic strength [217]. It should be noted that electric field-induced forces do not equally stimulate all the bacterial strains depends on how strongly they are bound to the surface. In addition, the binding energy is non-uniformly distributed across the surface, which leads to uneven adhesive force between the bacteria and the surface [145]. It justifies incomplete detachment (80%) of *Staphylococcus epidermidis* [218,219] and *Pseudomonas aeruginosa* (PAO1) [145] under the influence of electrical field.

2.5.6. Electroporation

Inactivation of microorganisms due to electrical field-assisted electroporation is independent of electrode polarization. The inactivation mechanisms were summarized in section 2.4.5.

2.5.7. Electro-wetting

Electro-wetting phenomenon and its impact on water contact angle were discussed in section 2.4.7.

2.6. AC-variable potential

In addition to DC (anodic, cathodic), alternating current (AC) has been suggested in electrically promoted filtration processes for its improved capabilities in controlling fouling. AC periodically changes the direction of the current and provides several advantages as compared to DC which are discussed next.

2.6.1. Combination of mechanisms

The combined effects of anodic and cathodic currents can be used for advanced antifouling performance by providing a variety of mechanisms in separation-based technologies. In the context of biofouling, anodic current has been proposed to inactivate bacteria through direct electron transfer while cathodic current has been suggested to cause bacterial detachment through electrostatic repulsive force. [144].Direct current has been mostly applied to synthetic and model wastewater, therefore, the results might be different in treating real wastewater. Real wastewater contains various foulant types with different physicochemical properties that makes the treatment much more complicated. Therefore, we surmise that application of AC current is more efficient in treating real wastewater. As such, a few studies have demonstrated a benefit from using AC to prevent or limit biofouling [36,145,220–224]. The frequency and magnitude of AC currents are of significant importance due to co-interactions between various foulants in the real wastewater. Hence, more research is demanded for tuning the current pattern to successfully employ ECMs for the treatment of complex wastewater.

2.6.2. Ion rearrangement

Rapid electro-kinetic rearrangement of ions at the surface of a membrane can be achieved by tuning the AC frequency which can result in a thinner electric double layer, slower nucleation rate, and ultimately reduced scaling. A few experimental studies have shown the application of AC in controlling/mitigating scaling [225]. As discussed, application of AC currents is considered new and has not been widely implemented in desalination processes. Therefore, future studies should be directed to understanding the impact of AC on movement of ions and investigating the viability of AC in real wastewater.

2.6.3. Temperature

Direct temperature effect

The application of an alternating current to a resistor produces thermal energy in a process known as Joule heating or Ohmic heating, which can increase the temperature of the surface and thereby locally heat the solution. [226]. It has been demonstrated that thermal energy required for membrane distillation can be substantially decreased by

electrons flow through conductive surfaces [226]. In the absence of electrolyte or in low saline solutions, electrons only travel through conductive surface that leads to a significant increase in temperature of conductive surfaces (up to 70 °C). In strong electrolytes, electron flow is through the conductive surface as well as the media which leads to surface charging and electrochemical reactions, respectively. Under commonly reported potentials suitable for joule heating (20 V), harsh electrochemical reactions are expected to occur that subsequently lead to electro-degradation of conductive surfaces. Hence, application of alternating current at sufficiently high frequencies (0.1-1 kHz) is recommended to avoid excessive electro-degradation [226].

The self-heating ability of conductive surfaces can be used to inactivate biofilms. Inactivation of microorganisms through Ohmic heating is directly proportional to strength of the electrical field. It has been shown that electric field with a magnitude higher than 20 V/cm could successfully inactivate microorganisms [227]. Timmermans et al. experimentally investigated inactivation of food pathogens such as *Escherichia coli*, *Salmonella Panama*, *Saccharomyces cerevisiae*, and *Listeria monocytogenes* under electric field with strength of 20 kV/cm where rises in temperature were suggested to make the bacterial cells more susceptible to electric pulses and inactivation [209]. It is important to note that Joule heating is reported to be minor under low voltages (<3 V) and in flowcell configurations, possibly due to efficient recirculation of flow dissipating the electrically-generated heat [36].

Rayleigh-Bernard convection

In filtration processes, the concentration of foulants is intensified at the surface (concentration polarization (CP)), leading to solidification or settlement of particles. One common approach to counteract this effect is to enhance the convection of the flow across the surface for a thinner CP layer. Hydrodynamic instabilities at the surface lead to local turbulence and subsequently enhanced convective mass transfer across the surface which is called Rayleigh-Bernard convection. Thermal gradients caused by electrically-assisted

self-heating (e.g., at 1.5 V [224]) promotes Rayleigh-Bernard convection at the interface of the membrane and solution which helps to limit surface fouling [228,229].

2.6.4. Volume changes of biofilm

Oscillating the polarity of electrodes can cause contraction and expansion of the biofilm [230]. Biofilms become more susceptible to electrical fields and biocides as a result of bioelectric-induced volume changes [230]. It has been shown that biofilms can be expanded (up to 4%) and compacted (up to 74%) under cathodic and anodic polarization, respectively [230]. This effect was ascribed to local pH changes induced by electrolysis under different polarization and has been seen in strains such as *Pseudomonas aeruginosa*, *Pseudomonas fluorescens*, and *Klebsiella pneumonia* [230]. Biofilms were tested at pH 10 and 3 to resemble the cathodic and anodic polarization, respectively, where the same structural impact was observed on biofilms.

2.6.5. Coupling reduction-oxidation reactions

Applying alternating currents to ECM surfaces produces both reductive and oxidative mechanisms. In Redox processes, complete mineralization of pollutants is not easily achieved due to the presence of electrogenerated byproducts. Hence, coupling anodic and cathodic reactions using AC, so-called “paired electrolysis”, have been proposed to obtain full mineralization of pollutants [91]. In electrolytic processes, anodic oxidation can be coupled either to direct reduction [231–235] or electro-generation of hydrogen peroxide [61,94,236–239]. An experimental study reported that direct cathodic reduction, anodic oxidation, and oxidation-reduction treatment each resulted in 10%, 75%, and 94% COD removal for reactive orange 4 [232]. In addition, coupled oxidation-reduction treatment was reported to decolorize the solution faster with fewer toxic aromatic byproducts as compared to direct reduction [232].

2.6.6. Less detrimental to membrane materials

Applying alternating current reduces the detrimental impact of electrooxidation and prolongs the anode’s lifetime, particularly for carbon-based materials [226]. It has been

shown that low frequencies (<10 Hz) still lead to the rapid destruction of CNTs but the degradation can be drastically reduced at moderate to high frequencies (> 100 Hz) [226].

2.6.7. Disadvantages

One of the major drawbacks with the application of AC is sub-optimal frequency usage, due to a lack of fundamental understandings of the anti-fouling mechanisms and the amount of time required at each polarity to maximize the anti-fouling effects. The frequency in alternating current or pulse duty ratio (ratio of pulsing time over one cycle) in pulsed direct current, impacts the antifouling mechanisms, biofilm behavior, and membrane performance. Antifouling mechanisms such as electrostatic repulsive force, gas generation, and reactive radical generation become less effective at higher frequencies, thus careful selection of the current pattern is necessary to maximize outcomes. Antifouling mechanisms such as electron transfer, ion diffusion, and electrochemical reactions can co-occur at the surface with different response times. Current cycles shorter than the targeted mechanism response-time will not produce the desire mechanism. For instance, water splitting, gas generation, or formation of active chlorine [240,241] readily occur in DC or low-frequency AC modes at potentials above 1 V. However, these effects become restricted at high frequencies (4-20 kHz for water dissociation, 50 kHz for chlorine formation) even at much higher applied potentials [242]. Similarly, oxidation pathways mediated by hydrogen peroxide or chlorine may not reach inhibitory concentrations at high frequencies. Perez-Roa et al. [223] studied the low-voltage (0.5-5 V) pulsed electric field to mitigate *Pseudomonas aeruginosa* biofilms and observed that voltage magnitude, frequency, and duty ratio play a significant role in antifouling. Similarly, Wang et al. [243] reported the dependence of biofilm viability to AC frequency and amplitude.

In addition, it has been shown that antifouling mechanisms such as electrostatic force and electroosmotic force under short exchange times (high frequency) cannot cause bacterial movement or detachment [145]. The impact of frequency in AC mode on fouling control has been discussed by several studies [219,244–247].

2.7.Challenges and perspectives

The excellent antifouling, self-cleaning, and electrically-reactive properties of ECMs have made them viable candidates to revolutionize separation-based technology. ECMs are environmentally friendly and use the electrical current transferred to the electrically-responsive surface to motivate antifouling mechanisms at the membrane/water interface. The antifouling mechanisms depend on the current type and configuration; thus, they should be chosen carefully to match the foulant type and maximize the efficiency of ECMs. In this review, we discussed the underlying mechanisms for cathodic and anodic surfaces separately. In a subsequent review (Part II), we elaborated on how different polarizations have been used to overcome major types of fouling (i.e., biological, organic, oil-based, or scaling). With regard to the detailed discussion provided in Part I and II, it is important to highlight a few key points:

i. Research must have a strong understanding of activation potentials for the mechanisms of interest when constructing ECMs from various materials or composites. ECMs are made of a wide range of conductive material, including carbon-based material (CNT, graphene, CNF) [15,16,19,20,248], electrically conductive polymers (polyaniline) [21], and inorganic material (ceramics) [22,23] with different electrochemical characteristics such as electrical conductivity, oxygen evolution potential (OEP), and hydrogen evolution potential (HEP). Therefore, the activation potential range for antifouling mechanisms such as gas generation, pH change, and indirect oxidation may differ depending on the surface material.

ii. Researchers should assess the electrochemical stability of their ECMs for the range of conditions under which they could be used [249]. For instance, CNT-based ECMs have been found to be unstable under high anodic currents which degrade ECM conductivity and thereby compromise their antifouling performance [250–252]. Conductive surfaces need to withstand harsh mechanical stimuli (abrasion [253], chemical cleaning [254]) to minimize delamination and the extreme release of nanomaterials in the environment. Further, changes to ECM surfaces as a result of material instability to operating

conditions are likely to reduce their anti-fouling abilities [255], or even generate undesired electrochemical effects. Therefore, future research should focus on developing materials with high conductivity and excellent mechanical and electrochemical stability.

iii. ECMs can be relied on to enhance the performance of filtration processes, however, their efficiency should not be overestimated for complex wastewater treatment. Membrane antifouling properties depend on physicochemical properties of the membrane such as pore size, surface roughness, and surface interfacial energy, as well as operating parameters such as flow rate, hydraulic residence time, and mass transfer. Also, the interplay between different fouling types may make the treatment process overly complicated. As such, the presence of competitive contaminants (ions, NOMs, bacteria) may lead to the occurrence of side reactions or generation of by-products, which results in a decrease in the electrochemical current efficiency due to competition between species/byproducts for available reactive sites.

iv. Electrochemical methods cannot be entirely relied upon for electrostatic repulsion. The adsorption of non-ionic contaminants (organic or biological macromolecules) to membranes is mostly governed by convective flow through and/or across the membrane.

v. Research on major foulant categories and single biological strains can be used to identify the optimal current pattern and to narrow down the design options in practice.

ECMs have offered fouling-resistant, environmentally friendly, and electrically-responsive surfaces with great promise to be incorporated into water treatment processes (water reuse, desalination, MBR) as well as separations in the chemical, oil and gas, biomedical, and electronics industries. However, they face challenges that must be tackled before they can be scaled for industrial application. For instance, development of techniques to mass-produce thin conductive porous surfaces with low hydraulic pressure resistance is still yet to be achieved. In addition, the incorporation of ECMs into standard

membrane modules has not been developed. For low-pressure applications (MF, UF), ECMs are desired in hollow fiber, flat-sheet, or spiral-wound configurations, while for high-pressure applications (NF, RO), flat sheet and spiral-wound may be favored. A significant challenge is identifying the electrochemical cell organization for hollow-fiber and spiral-wound configurations.

Excellent antifouling properties of ECMs come with the price of additional material and energy cost. A simple materials analysis for a typical CNT-based membrane indicates that coating a porous UF polymeric support (PES) with approximately 1 μm functionalized multi-walled CNTs layer would cost 2.88 $\$/m^2$ in materials cost. Thus, modifying PES membranes into an ECM would add 0.4% in total material cost, which is a marginal increase for substantial potential benefits. Approximately 0.42 gr of CNT is required for the fabrication of a 1 m^2 membrane. CNTs are readily available at in kilogram quantities on the market which would reduce the overall materials costs. Thus, conductive coating materials are not likely to be a bottleneck in production. However, there has not been any techno-economic analysis of ECMs that accounts for increased processing costs associated with the changes to polymer extrusion lines, modules and housings, and the OPEX associated with increased complexity during manufacture, as well as the increased operational costs associated with energy usage, and application OPEX. However, we would not anticipate a dramatic cost increase in membrane fabrication if existing standard manufacturing methods (spray coating, phase inversion) can be modified to accommodate ECM synthesis.

The additional energy consumption for a typical CNT-based UF ECM is equal to 0.01-0.0015 kWh/m^3. With regard to the average specific energy consumption of pressurized MF/UF membrane processes (0.1-0.2 kWh/m^3) [256], the additional energy consumption by the ECM over total energy demand is anticipated to be 0.75-10 %. ECMs offer higher permeate flux, better flux recovery, less downtime for membrane cleaning, low or no chemical and biocide usage for membrane/feed treatment, and lower associated chemical labor costs. Thus, it is expected that such outstanding advantages make ECMs an economically profitable option for membrane processes.

2.8.References

[1] C.A. Quist-Jensen, F. Macedonio, E. Drioli, Membrane technology for water production in agriculture: Desalination and wastewater reuse, Desalination. 364 (2015) 17–32. https://doi.org/10.1016/j.desal.2015.03.001.

[2] H. Lin, W. Peng, M. Zhang, J. Chen, H. Hong, Y. Zhang, A review on anaerobic membrane bioreactors: Applications, membrane fouling and future perspectives, Desalination. 314 (2013) 169–188. https://doi.org/10.1016/j.desal.2013.01.019.

[3] A. Ruiz-García, N. Melián-Martel, I. Nuez, Short Review on Predicting Fouling in RO Desalination, Membranes (Basel). 7 (2017) 62. https://doi.org/10.3390/membranes7040062.

[4] W. Gao, H. Liang, J. Ma, M. Han, Z. lin Chen, Z. shuang Han, G. bai Li, Membrane fouling control in ultrafiltration technology for drinking water production: A review, Desalination. 272 (2011) 1–8. https://doi.org/10.1016/j.desal.2011.01.051.

[5] B.X. Thanh, N.P. Dan, N.T. Binh, Fouling mitigation in a submerged membrane bioreactor treating dyeing and textile wastewater, Desalin. Water Treat. 47 (2012) 150–156. https://doi.org/10.1080/19443994.2012.696799.

[6] E. Celik, H. Park, H. Choi, H. Choi, Carbon nanotube blended polyethersulfone membranes for fouling control in water treatment, Water Res. 45 (2011) 274–282. https://doi.org/10.1016/j.watres.2010.07.060.

[7] C. Thamaraiselvan, M. Noel, Membrane Processes for Dye Wastewater Treatment: Recent Progress in Fouling Control, Crit. Rev. Environ. Sci. Technol. 45 (2015) 1007–1040. https://doi.org/10.1080/10643389.2014.900242.

[8] J. Park, N. Yamashita, H. Tanaka, Membrane fouling control and enhanced removal of pharmaceuticals and personal care products by coagulation-MBR, Chemosphere. 197 (2018) 467–476. https://doi.org/10.1016/j.chemosphere.2018.01.063.

[9] F. Ahmed, B.S. Lalia, V. Kochkodan, R. Hashaikeh, Electrically conductive polymeric membranes for fouling prevention and detection: A review, Desalination. 391 (2016) 1–15. https://doi.org/10.1016/J.DESAL.2016.01.030.

[10] A. Ronen, S.L. Walker, D. Jassby, Electroconductive and electroresponsive membranes for water treatment, Rev. Chem. Eng. 32 (2016) 533–550. https://doi.org/10.1515/revce-2015-0060.

[11] P. Formoso, E. Pantuso, G. De Filpo, F. Nicoletta, Electro-Conductive Membranes for Permeation Enhancement and Fouling Mitigation: A Short Review, Membranes (Basel). 7 (2017) 39. https://doi.org/10.3390/membranes7030039.

[12] I.-H. Loh, R.A. Moody, J.C. Huang, Electrically conductive membranes: Synthesis and applications, J. Memb. Sci. 50 (1990) 31–49. https://doi.org/10.1016/S0376-7388(00)80884-4.

[13] W. Hu, S. Chen, Z. Yang, L. Liu, H. Wang, Flexible electrically conductive nanocomposite membrane based on bacterial cellulose and polyaniline, J. Phys. Chem. B. 115 (2011) 8453–8457. https://doi.org/10.1021/jp204422v.

[14] W. Duan, A. Ronen, J.V. de Leon, A. Dudchenko, S. Yao, J. Corbala-Delgado, A. Yan, M. Matsumoto, D. Jassby, Treating anaerobic sequencing batch reactor effluent with electrically conducting ultrafiltration and nanofiltration membranes for fouling control, J. Memb. Sci. 504 (2016) 104–112. https://doi.org/10.1016/J.MEMSCI.2016.01.011.

[15] C. de Lannoy, D. Jassby, D.D. Davis, M.R. Wiesner, A highly electrically conductive polymer–

multiwalled carbon nanotube nanocomposite membrane, J. Memb. Sci. 415–416 (2012) 718–724. https://doi.org/10.1016/J.MEMSCI.2012.05.061.

[16] M.S.P. Shaffer, A.H. Windle, Fabrication and Characterization of Carbon Nanotube/Poly(vinyl alcohol) Composites, Adv. Mater. 11 (1999) 937–941. https://doi.org/10.1002/(SICI)1521-4095(199908)11:11<937::AID-ADMA937>3.0.CO;2-9.

[17] F. Ahmed, B.S. Lalia, V. Kochkodan, N. Hilal, R. Hashaikeh, Electrically conductive polymeric membranes for fouling prevention and detection: A review, Desalination. 391 (2016) 1–15. https://doi.org/10.1016/j.desal.2016.01.030.

[18] M.A. Halali, C.-F. de Lannoy, The Effect of Cross-Linkers on the Permeability of Electrically Conductive Membranes, Ind. Eng. Chem. Res. 58 (2019) 3832–3844. https://doi.org/10.1021/acs.iecr.8b05691.

[19] H. Chen, M.B. Müller, K.J. Gilmore, G.G. Wallace, D. Li, Mechanically Strong, Electrically Conductive, and Biocompatible Graphene Paper, Adv. Mater. 20 (2008) 3557–3561. https://doi.org/10.1002/adma.200800757.

[20] H. Kim, Y. Miura, C.W. Macosko, Graphene/Polyurethane Nanocomposites for Improved Gas Barrier and Electrical Conductivity, Chem. Mater. 22 (2010) 3441–3450. https://doi.org/10.1021/cm100477v.

[21] W. Duan, A. Ronen, S. Walker, D. Jassby, Polyaniline-Coated Carbon Nanotube Ultrafiltration Membranes: Enhanced Anodic Stability for *In Situ* Cleaning and Electro-Oxidation Processes, ACS Appl. Mater. Interfaces. 8 (2016) 22574–22584. https://doi.org/10.1021/acsami.6b07196.

[22] W. Fu, X. Wang, J. Zheng, M. Liu, Z. Wang, Antifouling performance and mechanisms in an electrochemical ceramic membrane reactor for wastewater treatment, (2018). https://doi.org/10.1016/j.memsci.2018.10.077.

[23] P. Geng, G. Chen, Magnéli Ti4O7 modified ceramic membrane for electrically-assisted filtration with antifouling property, J. Memb. Sci. 498 (2016) 302–314. https://doi.org/10.1016/j.memsci.2015.07.055.

[24] N. Zhang, M.A. Halali, C.F. de Lannoy, Detection of fouling on electrically conductive membranes by electrical impedance spectroscopy, Sep. Purif. Technol. 242 (2020) 116823. https://doi.org/10.1016/j.seppur.2020.116823.

[25] Y. Gao, W. Li, W.C.L. Lay, H.G.L. Coster, A.G. Fane, C.Y. Tang, Characterization of forward osmosis membranes by electrochemical impedance spectroscopy, Desalination. 312 (2013) 45–51. https://doi.org/10.1016/j.desal.2012.03.006.

[26] J.S. Ho, L.N. Sim, R.D. Webster, B. Viswanath, H.G.L. Coster, A.G. Fane, Monitoring fouling behavior of reverse osmosis membranes using electrical impedance spectroscopy: A field trial study, Desalination. 407 (2017) 75–84. https://doi.org/10.1016/j.desal.2016.12.012.

[27] S.T. Sultana, J.T. Babauta, H. Beyenal, Electrochemical biofilm control: A review, Biofouling. 31 (2015) 745–758. https://doi.org/10.1080/08927014.2015.1105222.

[28] C. Piyadasa, H.F. Ridgway, T.R. Yeager, M.B. Stewart, C. Pelekani, S.R. Gray, J.D. Orbell, The application of electromagnetic fields to the control of the scaling and biofouling of reverse osmosis membranes - A review, Desalination. 418 (2017) 19–34. https://doi.org/10.1016/j.desal.2017.05.017.

[29] M.H.O. Rashid, S.F. Ralph, Carbon nanotube membranes: Synthesis, properties, and future filtration applications, Nanomaterials. 7 (2017). https://doi.org/10.3390/nano7050099.

[30] C. Trellu, B.P. Chaplin, C. Coetsier, R. Esmilaire, S. Cerneaux, C. Causserand, M. Cretin, Electro-oxidation of organic pollutants by reactive electrochemical membranes, Chemosphere. 208 (2018) 159–175. https://doi.org/10.1016/j.chemosphere.2018.05.026.

[31] C. Li, X. Guo, X. Wang, S. Fan, Q. Zhou, H. Shao, W. Hu, C. Li, L. Tong, R.R. Kumar, J. Huang, Membrane fouling mitigation by coupling applied electric field in membrane system: Configuration, mechanism and performance, Electrochim. Acta. 287 (2018) 124–134. https://doi.org/10.1016/j.electacta.2018.06.150.

[32] X. Zhu, D. Jassby, Electroactive Membranes for Water Treatment: Enhanced Treatment Functionalities, Energy Considerations, and Future Challenges, Acc. Chem. Res. 52 (2019) 1177–1186. https://doi.org/10.1021/acs.accounts.8b00558.

[33] M. Sun, X. Wang, L.R. Winter, Y. Zhao, W. Ma, T. Hedtke, J.-H. Kim, M. Elimelech, Electrified Membranes for Water Treatment Applications, ACS ES&T Eng. 1 (2021) 725–752. https://doi.org/10.1021/acsestengg.1c00015.

[34] W. Duan, A. Ronen, J.V. de Leon, A. Dudchenko, S. Yao, J. Corbala-Delgado, A. Yan, M. Matsumoto, D. Jassby, Treating anaerobic sequencing batch reactor effluent with electrically conducting ultrafiltration and nanofiltration membranes for fouling control, J. Memb. Sci. 504 (2016) 104–112. https://doi.org/10.1016/j.memsci.2016.01.011.

[35] K. Wang, L. Xu, K. Li, L. Liu, Y. Zhang, J. Wang, Development of polyaniline conductive membrane for electrically enhanced membrane fouling mitigation, J. Memb. Sci. 570–571 (2019) 371–379. https://doi.org/10.1016/j.memsci.2018.10.050.

[36] C. Thamaraiselvan, A. Ronen, S. Lerman, M. Balaish, Y. Ein-Eli, C.G. Dosoretz, Low voltage electric potential as a driving force to hinder biofouling in self-supporting carbon nanotube membranes, Water Res. 129 (2018) 143–153. https://doi.org/10.1016/j.watres.2017.11.004.

[37] A. V Dudchenko, J. Rolf, K. Russell, W. Duan, D. Jassby, Organic fouling inhibition on electrically conducting carbon nanotube – polyvinyl alcohol composite ultra fi ltration membranes, J. Memb. Sci. 468 (2014) 1–10. https://doi.org/10.1016/j.memsci.2014.05.041.

[38] A. Ronen, W. Duan, I. Wheeldon, S. Walker, D. Jassby, Microbial Attachment Inhibition through Low-Voltage Electrochemical Reactions on Electrically Conducting Membranes, Environ. Sci. Technol. 49 (2015) 12741–12750. https://doi.org/10.1021/acs.est.5b01281.

[39] M.J. Lochhead, S.R. Letellier, V. Vogel, Assessing the role of interfacial electrostatics in oriented mineral nucleation at charged organic monolayers, J. Phys. Chem. B. 101 (1997) 10821–10827. https://doi.org/10.1021/jp972283w.

[40] F. Alimi, A. Gadri, Kinetics and morphology of formed gypsum, Desalination. 166 (2004) 427–434. https://doi.org/10.1016/j.desal.2004.06.097.

[41] W. Duan, A. Dudchenko, E. Mende, C. Flyer, X. Zhu, D. Jassby, Electrochemical mineral scale prevention and removal on electrically conducting carbon nanotube-polyamide reverse osmosis membranes † The electrochemical prevention and removal of CaSO 4 and CaCO 3 mineral scales on electrically, (2014). https://doi.org/10.1039/c3em00635b.

[42] C. Weidlich, K.M. Mangold, Electrochemically switchable polypyrrole coated membranes, in: Electrochim. Acta, 2011: pp. 3481–3484. https://doi.org/10.1016/j.electacta.2010.11.065.

[43] M. Takahashi, K. Chiba, P. Li, Free-Radical Generation from Collapsing Microbubbles in the Absence of a Dynamic Stimulus, (2007). https://doi.org/10.1021/jp0669254.

[44] H. Tsuge, Micro- and Nanobubbles, Jenny Stanford Publishing, 2014.

https://doi.org/10.1201/b17278.

[45] M. Takahashi, Potential of Microbubbles in Aqueous Solutions: Electrical Properties of the Gas-Water Interface, (2005). https://doi.org/10.1021/jp0445270.

[46] K. Zhang, Z. Cui, R.W. Field, Effect of bubble size and frequency on mass transfer in flat sheet MBR, J. Memb. Sci. 332 (2009) 30–37. https://doi.org/10.1016/j.memsci.2009.01.033.

[47] Z.H. Wu, H.B. Chen, Y.M. Dong, H.L. Mao, J.L. Sun, S.F. Chen, V.S.J. Craig, J. Hu, Cleaning using nanobubbles: Defouling by electrochemical generation of bubbles, J. Colloid Interface Sci. 328 (2008) 10–14. https://doi.org/10.1016/j.jcis.2008.08.064.

[48] B. Singh, F. Ejaz, T. Shah, N. Hilal, R. Hashaikeh, Electrically conductive membranes based on carbon nanostructures for self-cleaning of biofouling, DES. 360 (2015) 8–12. https://doi.org/10.1016/j.desal.2015.01.006.

[49] R. Hashaikeh, B.S. Lalia, V. Kochkodan, N. Hilal, A novel in situ membrane cleaning method using periodic electrolysis, J. Memb. Sci. 471 (2014) 149–154. https://doi.org/10.1016/J.MEMSCI.2014.08.017.

[50] J. Hanwright, J. Zhou, G.M. Evans, K.P. Galvin, Influence of surfactant on gas bubble stability, Langmuir. 21 (2005) 4912–4920. https://doi.org/10.1021/la0502894.

[51] F.Y. Ushikubo, T. Furukawa, R. Nakagawa, M. Enari, Y. Makino, Y. Kawagoe, T. Shiina, S. Oshita, Evidence of the existence and the stability of nano-bubbles in water, Colloids Surfaces A Physicochem. Eng. Asp. 361 (2010) 31–37. https://doi.org/10.1016/j.colsurfa.2010.03.005.

[52] P.H. Calderbank, M.B. Moo-Young, The continuous phase heat and mass-transfer properties of dispersions, Chem. Eng. Sci. 16 (1961) 39–54. https://doi.org/10.1016/0009-2509(61)87005-X.

[53] D. Lohse, Sonoluminescence: Cavitation hots up, Nature. 434 (2005) 33–34. https://doi.org/10.1038/434033a.

[54] A. Agarwal, W. Jern Ng, Y. Liu, Removal of biofilms by intermittent low-intensity ultrasonication triggered bursting of microbubbles, Biofouling. 30 (2014) 359–365. https://doi.org/10.1080/08927014.2013.876624.

[55] W.H. Koppenol, D.M. Stanbury, P.L. Bounds, Electrode potentials of partially reduced oxygen species, from dioxygen to water, Free Radic. Biol. Med. 49 (2010) 317–322. https://doi.org/10.1016/j.freeradbiomed.2010.04.011.

[56] J. Nordberg, E.S.J. Arnér, Reactive oxygen species, antioxidants, and the mammalian thioredoxin system, Free Radic. Biol. Med. 31 (2001) 1287–1312. https://doi.org/10.1016/S0891-5849(01)00724-9.

[57] Y.K. Wang, W.W. Li, G.P. Sheng, B.J. Shi, H.Q. Yu, In-situ utilization of generated electricity in an electrochemical membrane bioreactor to mitigate membrane fouling, Water Res. 47 (2013) 5794–5800. https://doi.org/10.1016/j.watres.2013.06.058.

[58] L. Fu, S.-J. You, F. Yang, M. Gao, X. Fang, G. Zhang, Synthesis of hydrogen peroxide in microbial fuel cell, J. Chem. Technol. Biotechnol. 85 (2010) 715–719. https://doi.org/10.1002/jctb.2367.

[59] J.T. Babauta, H.D. Nguyen, O. Istanbullu, H. Beyenal, Microscale gradients of oxygen, hydrogen peroxide, and pH in freshwater cathodic biofilms, ChemSusChem. 6 (2013) 1252–1261. https://doi.org/10.1002/cssc.201300019.

[60] O. Istanbullu, J. Babauta, H. Duc Nguyen, H. Beyenal, Biofouling The Journal of Bioadhesion and Biofilm Research Electrochemical biofilm control: mechanism of action Electrochemical biofilm

control: mechanism of action, (n.d.). https://doi.org/10.1080/08927014.2012.707651.

[61] C.T. Wang, W.L. Chou, Y.M. Kuo, F.L. Chang, Paired removal of color and COD from textile dyeing wastewater by simultaneous anodic and indirect cathodic oxidation, J. Hazard. Mater. 169 (2009) 16–22. https://doi.org/10.1016/j.jhazmat.2009.03.054.

[62] W. Fu, X. Wang, J. Zheng, M. Liu, Z. Wang, Antifouling performance and mechanisms in an electrochemical ceramic membrane reactor for wastewater treatment, J. Memb. Sci. 570–571 (2019) 355–361. https://doi.org/10.1016/j.memsci.2018.10.077.

[63] S. Shim, S. Hoon Hong, Y. Tak, J. Yoon, Biofouling The Journal of Bioadhesion and Biofilm Research Prevention of Pseudomonas aeruginosa adhesion by electric currents, (n.d.). https://doi.org/10.1080/08927014.2011.554831.

[64] J. Huang, Z. Wang, J. Zhang, X. Zhang, J. Ma, Z. Wu, A novel composite conductive microfiltration membrane and its anti-fouling performance with an external electric field in membrane bioreactors, Sci. Rep. 5 (2015) 1–8. https://doi.org/10.1038/srep09268.

[65] Z. Wang, J. Ma, C.Y. Tang, K. Kimura, Q. Wang, X. Han, Membrane cleaning in membrane bioreactors: A review, J. Memb. Sci. 468 (2014) 276–307. https://doi.org/10.1016/j.memsci.2014.05.060.

[66] R.A. Rozendal, E. Leone, J. Keller, K. Rabaey, Efficient hydrogen peroxide generation from organic matter in a bioelectrochemical system, Electrochem. Commun. 11 (2009) 1752–1755. https://doi.org/10.1016/j.elecom.2009.07.008.

[67] Y. Liu, ab Juen Hon Dustin Lee, Q. Xia, Y. Ma, Y. Yu, L. Yue Lanry Yung, J. Xie, C. Nam Ong, C.D. Vecitis, Z. Zhou, A graphene-based electrochemical filter for water purification †, (2014). https://doi.org/10.1039/c4ta04006f.

[68] Y. Yang, M. Kitajima, T.P.T. Pham, L. Yu, R. Ling, K.Y.H. Gin, M. Reinhard, Using *Pseudomonas aeruginosa* PAO1 to evaluate hydrogen peroxide as a biofouling control agent in membrane treatment systems, Lett. Appl. Microbiol. 63 (2016) 488–494. https://doi.org/10.1111/lam.12674.

[69] O. Istanbullu, J. Babauta, H. Duc Nguyen, H. Beyenal, Electrochemical biofilm control: mechanism of action, Biofouling. 28 (2012) 769–778. https://doi.org/10.1080/08927014.2012.707651.

[70] Z. Qiang, J.H. Chang, C.P. Huang, Electrochemical generation of hydrogen peroxide from dissolved oxygen in acidic solutions, Water Res. 36 (2002) 85–94. https://doi.org/10.1016/S0043-1354(01)00235-4.

[71] P. Ilea, S. Dorneanu, I.C. Popescu, Electrosynthesis of hydrogen peroxide by partial reduction of oxygen in alkaline media. Part II: Wall-jet ring disc electrode for electroreduction of dissolved oxygen on graphite and glassy carbon, J. Appl. Electrochem. 30 (2000) 187–192. https://doi.org/10.1023/A:1003830813424.

[72] G. Gao, Q. Zhang, Z. Hao, C.D. Vecitis, Carbon nanotube membrane stack for flow-through sequential regenerative electro-Fenton, Environ. Sci. Technol. 49 (2015) 2375–2383. https://doi.org/10.1021/es505679e.

[73] J. Huang, Z. Wang, J. Zhang, X. Zhang, J. Ma, Z. Wu, A novel composite conductive microfiltration membrane and its anti-fouling performance with an external electric field in membrane bioreactors, Sci. Rep. 5 (2015) 9268. https://doi.org/10.1038/srep09268.

[74] A. Hegde, G. Bhat, S. Mallya, Effect of exposure to hydrogen peroxide on the virulence of Escherichia coli, (2008).

[75] N. Barraud, D.J. Hassett, S.H. Hwang, S.A. Rice, S. Kjelleberg, J.S. Webb, Involvement of nitric oxide in biofilm dispersal of Pseudomonas aeruginosa, J. Bacteriol. 188 (2006) 7344–7353. https://doi.org/10.1128/JB.00779-06.

[76] A. Mai-Prochnow, P. Lucas-Elio, S. Egan, T. Thomas, J.S. Webb, A. Sanchez-Amat, S. Kjelleberg, Hydrogen peroxide linked to lysine oxidase activity facilitates biofilm differentiation and dispersal in several gram-negative bacteria, J. Bacteriol. 190 (2008) 5493–5501. https://doi.org/10.1128/JB.00549-08.

[77] G.E. Rhizobium, Complete Genome Sequence of the Sesbania Symbiont and Rice, Nucleic Acids Res. 1 (2013) 13–14. https://doi.org/10.1093/nar.

[78] N.R. Asad, L.M.B.O. Asad, C.E.B. de Almeida, I. Felzenszwalb, J.B. Cabral-Neto, A.C. Leitão, Several pathways of hydrogen peroxide action that damage the E. coli genome, Genet. Mol. Biol. 27 (2004) 291–303. https://doi.org/10.1590/S1415-47572004000200026.

[79] A. Thibessard, A. Fernandez, B. Gintz, N. Leblond-Bourget, B. Decaris, Hydrogen peroxide effects on Streptococcus thermophilus CNRZ368 cell viability, Res. Microbiol. 152 (2001) 593–596. https://doi.org/10.1016/S0923-2508(01)01234-7.

[80] J.A. Imlay, S. Linn, Mutagenesis and stress responses induced in Escherichia coli by hydrogen peroxide, J. Bacteriol. 169 (1987) 2967–2976. https://doi.org/10.1128/jb.169.7.2967-2976.1987.

[81] M.S. Munna, Influence of Exogenous Oxidative Stress on Escherichia Coli Cell Growth, Viability and Morphology, Am. J. Biosci. 1 (2013) 59. https://doi.org/10.11648/j.ajbio.20130104.12.

[82] R.S. Tanner, S.A. James, Rapid bactericidal effect of low pH against Pseudomonas aeruginosa, 1992. https://doi.org/10.1007/BF01569771.

[83] J. Koivunen, H. Heinonen-Tanski, Inactivation of enteric microorganisms with chemical disinfectants, UV irradiation and combined chemical/UV treatments, Water Res. 39 (2005) 1519–1526. https://doi.org/10.1016/j.watres.2005.01.021.

[84] M. Belosevic, G.R. Finch, Inactivation of Giardia muris Using Ozone and Ozone-Hvdrogen Peroxide, Ozone Sci. Eng. 16 (1994) 67–78. https://doi.org/10.1080/01919519408552381.

[85] J.I. Nieto-Juarez, K. Pierzchla, A. Sienkiewicz, T. Kohn, Inactivation of MS2 coliphage in Fenton and Fenton-like systems: Role of transition metals, hydrogen peroxide and sunlight, Environ. Sci. Technol. 44 (2010) 3351–3356. https://doi.org/10.1021/es903739f.

[86] E. Ortega-Gómez, B. Esteban García, M.M. Ballesteros Martín, P. Fernández Ibáñez, J.A. Sánchez Pérez, Inactivation of natural enteric bacteria in real municipal wastewater by solar photo-Fenton at neutral pH, Water Res. 63 (2014) 316–324. https://doi.org/10.1016/j.watres.2014.05.034.

[87] J. Rodríguez-Chueca, A. Mediano, M.P. Ormad, R. Mosteo, J.L. Ovelleiro, Disinfection of wastewater effluents with the Fenton-like process induced by electromagnetic fields, Water Res. 60 (2014) 250–258. https://doi.org/10.1016/j.watres.2014.04.040.

[88] M.N. Chong, B. Jin, C.W.K. Chow, C. Saint, Recent developments in photocatalytic water treatment technology: A review, Water Res. 44 (2010) 2997–3027. https://doi.org/10.1016/J.WATRES.2010.02.039.

[89] M. V. Morales, K. Góra-Marek, H. Musch, A. Pineda, B. Murray, S. Stefanidis, L. Falco, K. Tarach, E. Ponomareva, J.H. Marsman, I. Melián-Cabrera, Advanced oxidation process for coke removal: A systematic study of hydrogen peroxide and OH-derived-Fenton radicals of a fouled zeolite, Appl. Catal. A Gen. 562 (2018) 215–222. https://doi.org/10.1016/j.apcata.2018.06.008.

[90] W. Song, V. Ravindran, B.E. Koel, M. Pirbazari, Nanofiltration of natural organic matter with H2O2/UV pretreatment: Fouling mitigation and membrane surface characterization, J. Memb. Sci. 241 (2004) 143–160. https://doi.org/10.1016/j.memsci.2004.04.034.

[91] C.A. Martínez-Huitle, M.A. Rodrigo, I. Sirés, O. Scialdone, Single and Coupled Electrochemical Processes and Reactors for the Abatement of Organic Water Pollutants: A Critical Review, Chem. Rev. 115 (2015) 13362–13407. https://doi.org/10.1021/acs.chemrev.5b00361.

[92] J.M. Noël, A. Latus, C. Lagrost, E. Volanschi, P. Hapiot, Evidence for OH radical production during electrocatalysis of oxygen reduction on pt surfaces: Consequences and application, J. Am. Chem. Soc. 134 (2012) 2835–2841. https://doi.org/10.1021/ja211663t.

[93] J.M. Fang, R.C. Sun, D. Salisbury, P. Fowler, J. Tomkinson, Comparative study of hemicelluloses from wheat straw by alkali and hydrogen peroxide extractions, Polym. Degrad. Stab. 66 (1999) 423–432. https://doi.org/10.1016/S0141-3910(99)00095-6.

[94] H. Wang, J.L. Wang, The cooperative electrochemical oxidation of chlorophenols in anode-cathode compartments, J. Hazard. Mater. 154 (2008) 44–50. https://doi.org/10.1016/j.jhazmat.2007.09.102.

[95] K. Kinoshita, Electrochemical Oxygen Technology, 1992. https://www.wiley.com/en-gl/9780471570431 (accessed June 23, 2020).

[96] É. Mahé, P. Bornoz, E. Briot, J. Chevalet, C. Comninellis, D. Devilliers, A selective chemiluminescence detection method for reactive oxygen species involved in oxygen reduction reaction on electrocatalytic materials, Electrochim. Acta. 102 (2013) 259–273. https://doi.org/10.1016/j.electacta.2013.03.190.

[97] J. Rivera-Utrilla, M. Sánchez-Polo, M.Á. Ferro-García, G. Prados-Joya, R. Ocampo-Pérez, Pharmaceuticals as emerging contaminants and their removal from water. A review, Chemosphere. 93 (2013) 1268–1287. https://doi.org/10.1016/j.chemosphere.2013.07.059.

[98] M.M. Huber, S. Canonica, G.Y. Park, U. Von Gunten, Oxidation of pharmaceuticals during ozonation and advanced oxidation processes, Environ. Sci. Technol. 37 (2003) 1016–1024. https://doi.org/10.1021/es025896h.

[99] E. Brillas, E. Mur, R. Sauleda, L. Sànchez, J. Peral, X. Domènech, J. Casado, Aniline mineralization by AOP's: Anodic oxidation, photocatalysis, electro-Fenton and photoelectro-Fenton processes, Appl. Catal. B Environ. 16 (1998) 31–42. https://doi.org/10.1016/S0926-3373(97)00059-3.

[100] S. Esplugas, D.M. Bila, L.G.T. Krause, M. Dezotti, Ozonation and advanced oxidation technologies to remove endocrine disrupting chemicals (EDCs) and pharmaceuticals and personal care products (PPCPs) in water effluents, J. Hazard. Mater. 149 (2007) 631–642. https://doi.org/10.1016/j.jhazmat.2007.07.073.

[101] S. Baumgarten, H.F. Schröder, C. Charwath, M. Lange, S. Beier, J. Pinnekamp, Evaluation of advanced treatment technologies for the elimination of pharmaceutical compounds, in: Water Sci. Technol., IWA Publishing, 2007: pp. 1–8. https://doi.org/10.2166/wst.2007.550.

[102] C. Von Sonntag, Advanced oxidation processes: Mechanistic aspects, Water Sci. Technol. 58 (2008) 1015–1021. https://doi.org/10.2166/wst.2008.467.

[103] J.L. Wang, L.J. Xu, Advanced oxidation processes for wastewater treatment: Formation of hydroxyl radical and application, Crit. Rev. Environ. Sci. Technol. 42 (2012) 251–325. https://doi.org/10.1080/10643389.2010.507698.

[104] C. Trellu, B.P. Chaplin, C. Coetsier, R. Esmilaire, S. Cerneaux, C. Causserand, M. Cretin, Electro-oxidation of organic pollutants by reactive electrochemical membranes, Chemosphere. 208 (2018)

159–175. https://doi.org/10.1016/j.chemosphere.2018.05.026.

[105] M.R. Prairie, L.R. Evans, B.M. Stange, S.L. Martinez, An Investigation of Ti02 Photocatalysis for the Treatment of Water Contaminated with Metals and Organic Chemicals, 1993. https://pubs.acs.org/sharingguidelines (accessed June 25, 2020).

[106] D.F. Ollis, E. Pelizzetti, N. Serpone, Destruction of water contaminants, Environ. Sci. Technol. 25 (1991) 1522–1529. https://doi.org/10.1021/es00021a001.

[107] W.R. Haag, J. Hoigné, Photo-sensitized oxidation in natural water via .OH radicals, Chemosphere. 14 (1985) 1659–1671. https://doi.org/10.1016/0045-6535(85)90107-9.

[108] J. Jeong, J.Y. Kim, M. Cho, W. Choi, J. Yoon, Inactivation of Escherichia coli in the electrochemical disinfection process using a Pt anode, Chemosphere. 67 (2007) 652–659. https://doi.org/10.1016/j.chemosphere.2006.11.035.

[109] R.J. Watts, S. Kong, M.P. Orr, G.C. Miller, B.E. Henry, Photocatalytic inactivation of coliform bacteria and viruses in secondary wastewater effluent, Water Res. 29 (1995) 95–100. https://doi.org/10.1016/0043-1354(94)E0122-M.

[110] Y. Hou, X. Li, Q. Zhao, G. Chen, C.L. Raston, Role of Hydroxyl Radicals and Mechanism of Escherichia coli Inactivation on Ag/AgBr/TiO 2 Nanotube Array Electrode under Visible Light Irradiation, (2012). https://doi.org/10.1021/es204079d.

[111] N. Baram, D. Starosvetsky, J. Starosvetsky, M. Epshtein, R. Armon, Y. Ein-Eli, Enhanced inactivation of E. coli bacteria using immobilized porous TiO2 photoelectrocatalysis, Electrochim. Acta. 54 (2009) 3381–3386. https://doi.org/10.1016/j.electacta.2008.12.033.

[112] C. Hu, Y. Lan, J. Qu, X. Hu, A. Wang, Ag/AgBr/TiO2 visible light photocatalyst for destruction of azodyes and bacteria, J. Phys. Chem. B. 110 (2006) 4066–4072. https://doi.org/10.1021/jp0564400.

[113] C. Pablos, R. Van Grieken, J. Marugán, B. Moreno, Photocatalytic inactivation of bacteria in a fixed-bed reactor: Mechanistic insights by epifluorescence microscopy, Catal. Today. 161 (2011) 133–139. https://doi.org/10.1016/j.cattod.2010.10.051.

[114] L. Tang, A. Iddya, X. Zhu, A. V Dudchenko, W. Duan, C. Turchi, J. Vanneste, T.Y. Cath, D. Jassby, Enhanced Flux and Electrochemical Cleaning of Silicate Scaling on Carbon Nanotube-Coated Membrane Distillation Membranes Treating Geothermal Brines, (2017). https://doi.org/10.1021/acsami.7b12615.

[115] S.R. Pandey, V. Jegatheesan, K. Baskaran, L. Shu, Fouling in reverse osmosis (RO) membrane in water recovery from secondary effluent: A review, Rev. Environ. Sci. Biotechnol. 11 (2012) 125–145. https://doi.org/10.1007/s11157-012-9272-0.

[116] Y. Niibori, T. Chida, O. Tochiyama, Journal of Nuclear Science and Technology, Vol. 37, No. 4, 2000: Pp. 349–357, J. Nucl. Sci. Technol. 37 (2000) 349–357. https://doi.org/10.1080/18811248.2000.9714905.

[117] L.H. Allen, E. Matijevíc, L. Meites, Exchange of Na+ for the silanolic protons of silica, J. Inorg. Nucl. Chem. 33 (1971) 1293–1299. https://doi.org/10.1016/0022-1902(71)80423-2.

[118] P. V. Brady, J. V. Walther, Controls on silicate dissolution rates in neutral and basic pH solutions at 25°C, Geochim. Cosmochim. Acta. 53 (1989) 2823–2830. https://doi.org/10.1016/0016-7037(89)90160-9.

[119] Y. Niibori, T. Chida, O. Tochiyama, Journal of Nuclear Science and Technology, Vol. 37, No. 4, 2000: Pp. 349–357, J. Nucl. Sci. Technol. 37 (2000) 349–357.

https://doi.org/10.1080/18811248.2000.9714905.

[120] R.S. Harisha, K.M. Hosamani, R.S. Keri, S.K. Nataraj, T.M. Aminabhavi, Arsenic removal from drinking water using thin film composite nanofiltration membrane, Desalination. 252 (2010) 75–80. https://doi.org/10.1016/j.desal.2009.10.022.

[121] V.T. Nguyen, S. Vigneswaran, H.H. Ngo, H.K. Shon, J. Kandasamy, Arsenic removal by a membrane hybrid filtration system, Desalination. 236 (2009) 363–369. https://doi.org/10.1016/j.desal.2007.10.088.

[122] L. Cumbal, A.K. Sengupta, Arsenic removal using polymer-supported hydrated iron(III) oxide nanoparticles: Role of Donnan membrane effect, Environ. Sci. Technol. 39 (2005) 6508–6515. https://doi.org/10.1021/es050175e.

[123] L. Hao, N. Wang, C. Wang, G. Li, Arsenic removal from water and river water by the combined adsorption - UF membrane process, Chemosphere. 202 (2018) 768–776. https://doi.org/10.1016/j.chemosphere.2018.03.159.

[124] M.C. Shih, An overview of arsenic removal by pressure-driven membrane processes, Desalination. 172 (2005) 85–97. https://doi.org/10.1016/j.desal.2004.07.031.

[125] S. Jeyamkondan, D. Jayas, R.H.-N.C.A. Meeting, undefined Brookings, undefined 1998, Pasteurization of foods by pulsed electric fields at high voltages, (n.d.).

[126] J.R. Beveridge, S.J. MacGregor, L. Marsili, J.G. Anderson, N.J. Rowan, O. Farish, Comparison of the effectiveness of biphase and monophase rectangular pulses for the inactivation of micro-organisms using pulsed electric fields, IEEE Trans. Plasma Sci. 30 (2002) 1525–1531. https://doi.org/10.1109/TPS.2002.804204.

[127] H. Vega-Mercado, U.R. Pothakamury, F.J. Chang, G. V. Barbosa-Cánovas, B.G. Swanson, Inactivation of Escherichia coli by combining pH, ionic strength and pulsed electric fields hurdles, Food Res. Int. 29 (1996) 117–121. https://doi.org/10.1016/0963-9969(96)00015-4.

[128] T.F. Wu, S.Y. Tseng, J.C. Hung, Generation of pulsed electric fields for processing microbes, IEEE Trans. Plasma Sci. 32 (2004) 1551–1562. https://doi.org/10.1109/TPS.2004.831732.

[129] A. Goel, W. Foshee, H. Kirkici, Pulsed electric field studies of bio-dielectrics, in: Conf. Electr. Insul. Dielectr. Phenom. (CEIDP), Annu. Rep., 2003: pp. 56–59. https://doi.org/10.1109/ceidp.2003.1254793.

[130] D. García, N. Gómez, S. Condón, J. Raso, R. Pagán, Pulsed electric fields cause sublethal injury in Escherichia coli, Lett. Appl. Microbiol. 36 (2003) 140–144. https://doi.org/10.1046/j.1472-765X.2003.01282.x.

[131] K.H. Schoenbach, R.W. Alden, T.J. Fox, Biofouling prevention with pulsed electric fields, in: IEEE Conf. Rec. Power Modul. Symp., IEEE, 1996: pp. 75–78. https://doi.org/10.1109/modsym.1996.564454.

[132] W.J. Dower, J.F. Miller, C.W. Ragsdale, High efficiency transformation of E.coli by high voltage electroporation, n.d. https://academic.oup.com/nar/article-abstract/16/13/6127/1046461 (accessed July 2, 2020).

[133] C. Liu, X. Xie, W. Zhao, N. Liu, P.A. Maraccini, L.M. Sassoubre, A.B. Boehm, Y. Cui, Conducting Nanosponge Electroporation for Affordable and High-Efficiency Disinfection of Bacteria and Viruses in Water, (2013). https://doi.org/10.1021/nl402053z.

[134] R. Nickel, E. Tannich, Transfection and transient expression of chloramphenicol acetyltransferase

gene in the protozoan parasite Entamoeba histolytica, Proc. Natl. Acad. Sci. U. S. A. 91 (1994) 7095–7098. https://doi.org/10.1073/pnas.91.15.7095.

[135] R.M. Duenki, G. Schwarz, Electric field effects on the virus M13, detected by electro-optical measurements, Biochem. Biophys. Res. Commun. 151 (1988) 768–773. https://doi.org/10.1016/S0006-291X(88)80347-4.

[136] S. Ravishankar, H. Zhang, M.L. Kempkes, Pulsed Electric Fields, Food Sci. Technol. Int. 14 (2008) 429–432. https://doi.org/10.1177/1082013208100535.

[137] K.H. Schoenbach, S. Katsuki, R.H. Stark, E.S. Buescher, S.J. Beebe, Bioelectrics - New applications for pulsed power technology, in: IEEE Trans. Plasma Sci., 2002: pp. 293–300. https://doi.org/10.1109/TPS.2002.1003873.

[138] E. Di Campli, S. Di Bartolomeo, R. Grande, M. Di Giulio, L. Cellini, Effects of extremely low-frequency electromagnetic fields on helicobacter pylori biofilm, Curr. Microbiol. 60 (2010) 412–418. https://doi.org/10.1007/s00284-009-9558-9.

[139] K.H. Schoenbach, R.P. Joshi, J.F. Kolb, N. Chen, M. Stacey, P.F. Blackmore, E.S. Buescher, S.J. Beebe, Ultrashort electrical pulses open a new gateway into biological cells, in: Proc. IEEE, Institute of Electrical and Electronics Engineers Inc., 2004: pp. 1122–1136. https://doi.org/10.1109/JPROC.2004.829009.

[140] M. Lindgren, K. Aronsson, S. Galt, T. Ohlsson, Simulation of the temperature increase in pulsed electric field (PEF) continuous flow treatment chambers, Innov. Food Sci. Emerg. Technol. 3 (2002) 233–245. https://doi.org/10.1016/S1466-8564(02)00044-9.

[141] A.M. Wesche, J.B. Gurtler, B.P. Marks, E.T. Ryser, Stress, sublethal injury, resuscitation, and virulence of bacterial foodborne pathogens, J. Food Prot. 72 (2009) 1121–1138. https://doi.org/10.4315/0362-028X-72.5.1121.

[142] A. Ahlbom, M. Feychting, Electromagnetic radiation, Br. Med. Bull. 68 (2003) 157–165. https://doi.org/10.1093/bmb/ldg030.

[143] J.L. Erson, Boundary effects on electrophoretic motion of colloidal spheres, J. Fluid Mech. 153 (1985) 417–439. https://doi.org/10.1017/S002211208500132X.

[144] A.T. Poortinga, J. Smit, H.C. van der Mei, H.J. Busscher, Electric field induced desorption of bacteria from a conditioning film covered substratum, Biotechnol. Bioeng. 76 (2001) 395–399. https://doi.org/10.1002/bit.10129.

[145] S.H. Hong, J. Jeong, S. Shim, H. Kang, S. Kwon, K.H. Ahn, J. Yoon, Effect of electric currents on bacterial detachment and inactivation, Biotechnol. Bioeng. 100 (2008) 379–386. https://doi.org/10.1002/bit.21760.

[146] H. Morisaki, Measurement of the force necessary for removal of bacterial cells from a quartz plate, J. Gen. Microbiol. 137 (1991) 2649–2655. https://doi.org/10.1099/00221287-137-11-2649.

[147] D. Bratko, C.D. Daub, K. Leung, A. Luzar, Effect of field direction on electrowetting in a nanopore, J. Am. Chem. Soc. 129 (2007) 2504–2510. https://doi.org/10.1021/ja0659370.

[148] W. Cui, H. Ma, B. Tian, Y. Ji, F. Su, Electrowetting on a multi-walled carbon nanotube membrane with different droplet sizes in an electric field, J. Mater. Sci. 51 (2016) 4031–4036. https://doi.org/10.1007/s10853-016-9721-1.

[149] J. Wu, Z. Wang, W. Yan, Y. Wang, J. Wang, S. Wang, Improving the hydrophilicity and fouling resistance of RO membranes by surface immobilization of PVP based on a metal-polyphenol

precursor layer, J. Memb. Sci. 496 (2015) 58–69. https://doi.org/10.1016/j.memsci.2015.08.044.

[150] Y.F. Zhao, L.P. Zhu, Z. Yi, B.K. Zhu, Y.Y. Xu, Improving the hydrophilicity and fouling-resistance of polysulfone ultrafiltration membranes via surface zwitterionicalization mediated by polysulfone-based triblock copolymer additive, J. Memb. Sci. 440 (2013) 40–47. https://doi.org/10.1016/j.memsci.2013.03.064.

[151] X. Lu, Y. Peng, H. Qiu, X. Liu, L. Ge, Anti-fouling membranes by manipulating surface wettability and their anti-fouling mechanism, Desalination. 413 (2017) 127–135. https://doi.org/10.1016/j.desal.2017.02.022.

[152] L. Shen, X. Wang, R. Li, H. Yu, H. Hong, H. Lin, J. Chen, B.Q. Liao, Physicochemical correlations between membrane surface hydrophilicity and adhesive fouling in membrane bioreactors, J. Colloid Interface Sci. 505 (2017) 900–909. https://doi.org/10.1016/j.jcis.2017.06.090.

[153] B.A. Kakade, Chemical control of superhydrophobicity of carbon nanotube surfaces: Droplet pinning and electrowetting behavior, Nanoscale. 5 (2013) 7011–7016. https://doi.org/10.1039/c3nr01359f.

[154] J. Pu, S. Wan, Z. Lu, G.A. Zhang, L. Wang, X. Zhang, Q. Xue, Controlled water adhesion and electrowetting of conducting hydrophobic graphene/carbon nanotubes composite films on engineering materials, J. Mater. Chem. A. 1 (2013) 1254–1260. https://doi.org/10.1039/c2ta00344a.

[155] Z. Wang, L. Ci, L. Chen, S. Nayak, P.M. Ajayan, N. Koratkar, Polarity-dependent electrochemically controlled transport of water through carbon nanotube membranes, Nano Lett. 7 (2007) 697–702. https://doi.org/10.1021/nl062853g.

[156] R. Jain, M. Bhargava, N. Sharma, Electrochemical studies on a pharmaceutical azo dye: Tartrazine, Ind. Eng. Chem. Res. 42 (2003) 243–247. https://doi.org/10.1021/ie020228q.

[157] C.A. Martínez-Huitle, E. Brillas, Decontamination of wastewaters containing synthetic organic dyes by electrochemical methods: A general review, Appl. Catal. B Environ. 87 (2009) 105–145. https://doi.org/10.1016/j.apcatb.2008.09.017.

[158] R. Jain, S. Varshney, S. Sikarwar, Electrochemical techniques for the removal of Reactofix Golden Yellow 3 RFN from industrial wastes, J. Colloid Interface Sci. 313 (2007) 248–253. https://doi.org/10.1016/j.jcis.2007.04.035.

[159] A.J. Sutherland, M.X. Ruiz-Caldas, C.F. de Lannoy, Electro-catalytic microfiltration membranes electrochemically degrade azo dyes in solution, J. Memb. Sci. 611 (2020) 118335. https://doi.org/10.1016/j.memsci.2020.118335.

[160] A. El-Ghenymy, C. Arias, P.L. Cabot, F. Centellas, J.A. Garrido, R.M. Rodríguez, E. Brillas, Electrochemical incineration of sulfanilic acid at a boron-doped diamond anode, Chemosphere. 87 (2012) 1126–1133. https://doi.org/10.1016/j.chemosphere.2012.02.006.

[161] J.D. Rodgers, N.J. Bunce, Electrochemical treatment of 2,4,6-trinitrotoluene and related compounds, Environ. Sci. Technol. 35 (2001) 406–410. https://doi.org/10.1021/es001465s.

[162] S. Rondinini, A. Vertova, Electroreduction of halogenated organic compounds, in: Electrochem. Environ., Springer New York, 2010: pp. 279–306. https://doi.org/10.1007/978-0-387-68318-8_12.

[163] H. Liu, C.D. Vecitis, Reactive transport mechanism for organic oxidation during electrochemical filtration: Mass-transfer, physical adsorption, and electron-transfer, J. Phys. Chem. C. 116 (2012) 374–383. https://doi.org/10.1021/jp209390b.

[164] S. Wang, S. Liang, P. Liang, X. Zhang, J. Sun, S. Wu, X. Huang, In-situ combined dual-layer CNT/PVDF membrane for electrically-enhanced fouling resistance, J. Memb. Sci. 491 (2015) 37–44.

https://doi.org/10.1016/j.memsci.2015.05.014.

[165] H. Särkkä, A. Bhatnagar, M. Sillanpää, Recent developments of electro-oxidation in water treatment — A review, J. Electroanal. Chem. 754 (2015) 46–56. https://doi.org/10.1016/J.JELECHEM.2015.06.016.

[166] M. Panizza, G. Cerisola, Direct and mediated anodic oxidation of organic pollutants, Chem. Rev. 109 (2009) 6541–6569. https://doi.org/10.1021/cr9001319.

[167] Y. Feng, L. Yang, J. Liu, B.E. Logan, Electrochemical technologies for wastewater treatment and resource reclamation, Environ. Sci. Water Res. Technol. 2 (2016) 800–831. https://doi.org/10.1039/c5ew00289c.

[168] C. Trellu, C. Coetsier, J.C. Rouch, R. Esmilaire, M. Rivallin, M. Cretin, C. Causserand, Mineralization of organic pollutants by anodic oxidation using reactive electrochemical membrane synthesized from carbothermal reduction of TiO2, Water Res. 131 (2018) 310–319. https://doi.org/10.1016/j.watres.2017.12.070.

[169] A.M. Zaky, B.P. Chaplin, Mechanism of p-substituted phenol oxidation at a Ti4O 7 reactive electrochemical membrane, Environ. Sci. Technol. 48 (2014) 5857–5867. https://doi.org/10.1021/es5010472.

[170] A.M. Zaky, B.P. Chaplin, Porous substoichiometric TiO2 anodes as reactive electrochemical membranes for water treatment, Environ. Sci. Technol. 47 (2013) 6554–6563. https://doi.org/10.1021/es401287e.

[171] N. Belhadj Tahar, A. Savall, Electropolymerization of phenol on a vitreous carbon electrode in alkaline aqueous solution at different temperatures, Electrochim. Acta. 55 (2009) 465–469. https://doi.org/10.1016/j.electacta.2009.08.040.

[172] N. Belhadj Tahar, A. Savall, Electrochemical removal of phenol in alkaline solution. Contribution of the anodic polymerization on different electrode materials, Electrochim. Acta. 54 (2009) 4809–4816. https://doi.org/10.1016/j.electacta.2009.03.086.

[173] M.A. Rodrigo, P.A. Michaud, I. Duo, M. Panizza, G. Cerisola, C. Comninellis, Oxidation of 4-Chlorophenol at Boron-Doped Diamond Electrode for Wastewater Treatment, J. Electrochem. Soc. 148 (2001) D60. https://doi.org/10.1149/1.1362545.

[174] E. Chatzisymeon, A. Dimou, D. Mantzavinos, A. Katsaounis, Electrochemical oxidation of model compounds and olive mill wastewater over DSA electrodes: 1. The case of Ti/IrO2 anode, J. Hazard. Mater. 167 (2009) 268–274. https://doi.org/10.1016/j.jhazmat.2008.12.117.

[175] M. Gattrell, A Study of Electrode Passivation during Aqueous Phenol Electrolysis, J. Electrochem. Soc. 140 (1993) 903. https://doi.org/10.1149/1.2056225.

[176] G. Gao, C.D. Vecitis, Reactive depth and performance of an electrochemical carbon nanotube network as a function of mass transport, ACS Appl. Mater. Interfaces. 4 (2012) 6096–6103. https://doi.org/10.1021/am301724n.

[177] H. Liu, A. Vajpayee, C.D. Vecitis, Bismuth-doped tin oxide-coated carbon nanotube network: Improved anode stability and efficiency for flow-through organic electrooxidation, ACS Appl. Mater. Interfaces. 5 (2013) 10054–10066. https://doi.org/10.1021/am402621v.

[178] S. Pandit, S. Shanbhag, M. Mauter, Y. Oren, M. Herzberg, Influence of Electric Fields on Biofouling of Carbonaceous Electrodes, (2017). https://doi.org/10.1021/acs.est.6b06339.

[179] T. Nakayama, H. Wake, K. Ozawa, H. Kodama, N. Nakamura, T. Matsunaga, Use of a titanium

nitride for electrochemical inactivation of marine bacteria, Environ. Sci. Technol. 32 (1998) 798–801. https://doi.org/10.1021/es970578h.

[180] C. Comninellis, ELECTROCATALYSIS IN THE ELECTROCHEMICAL CONVERSION/COMBUSTION OF ORGANIC POLLUTANTS FOR WASTE WATER TREATMENT, 1994.

[181] S. Siahrostami, G.L. Li, V. Viswanathan, J.K. Nørskov, One- or Two-Electron Water Oxidation, Hydroxyl Radical, or H2O2 Evolution, J. Phys. Chem. Lett. 8 (2017) 1157–1160. https://doi.org/10.1021/acs.jpclett.6b02924.

[182] A. Donaghue, B.P. Chaplin, Effect of select organic compounds on perchlorate formation at boron-doped diamond film anodes, Environ. Sci. Technol. 47 (2013) 12391–12399. https://doi.org/10.1021/es4031672.

[183] A. Kapałka, A.E. György, F. Ae, C. Comninellis, Kinetic modelling of the electrochemical mineralization of organic pollutants for wastewater treatment, (n.d.). https://doi.org/10.1007/s10800-007-9365-6.

[184] C. Mayer, R. Moritz, C. Kirschner, W. Borchard, R. Maibaum, J. Wingender, H.C. Flemming, The role of intermolecular interactions: Studies on model systems for bacterial biofilms, Int. J. Biol. Macromol. 26 (1999) 3–16. https://doi.org/10.1016/S0141-8130(99)00057-4.

[185] M. Čáp, L. Váchová, Z. Palková, Reactive oxygen species in the signaling and adaptation of multicellular microbial communities, Oxid. Med. Cell. Longev. 2012 (2012). https://doi.org/10.1155/2012/976753.

[186] B.R. Boles, P.K. Singh, Endogenous oxidative stress produces diversity and adaptability in biofilm communities, Proc. Natl. Acad. Sci. U. S. A. 105 (2008) 12503–12508. https://doi.org/10.1073/pnas.0801499105.

[187] O. Scialdone, A. Galia, S. Randazzo, Oxidation of carboxylic acids in water at IrO2-Ta2O5 and boron doped diamond anodes, Chem. Eng. J. 174 (2011) 266–274. https://doi.org/10.1016/j.cej.2011.09.016.

[188] M.E.H. Bergmann, A.S. Koparal, Studies on electrochemical disinfectant production using anodes containing RuO 2, (n.d.). https://doi.org/10.1007/s10800-005-9064-0.

[189] K.C. Ho, Y.H. Teow, A.W. Mohammad, Optimization of nanocomposite conductive membrane formulation and operating parameters for electrically-enhanced palm oil mill effluent filtration using response surface methodology, Process Saf. Environ. Prot. 126 (2019) 297–308. https://doi.org/10.1016/j.psep.2019.03.019.

[190] M. Zhou, L. Liu, Y. Jiao, Q. Wang, Q. Tan, Treatment of high-salinity reverse osmosis concentrate by electrochemical oxidation on BDD and DSA electrodes, Desalination. 277 (2011) 201–206. https://doi.org/10.1016/j.desal.2011.04.030.

[191] C. Comninellis, A. Nerini, Anodic oxidation of phenol in the presence of NaCI for wastewater treatment, 1995.

[192] K. Serrano, P.A. Michaud, C. Comninellis, A. Savall, Electrochemical preparation of peroxodisulfuric acid using boron doped diamond thin film electrodes, Electrochim. Acta. 48 (2002) 431–436. https://doi.org/10.1016/S0013-4686(02)00688-6.

[193] E.J. Ruiz, R. Ortega-Borges, J.L. Jurado, T.W. Chapman, Y. Meas, Simultaneous anodic and cathodic production of Sodium percarbonate in aqueous solution, Electrochem. Solid-State Lett. 12 (2008) E1. https://doi.org/10.1149/1.3005555.

[194] P. Cañizares, F. Larrondo, J. Lobato, M.A. Rodrigo, C. Sáez, Electrochemical Synthesis of Peroxodiphosphate Using Boron-Doped Diamond Anodes, J. Electrochem. Soc. 152 (2005) D191. https://doi.org/10.1149/1.2039936.

[195] K. Rajeshwar, J.G. Ibanez, G.M. Swain, Electrochemistry and the environment, J. Appl. Electrochem. 24 (1994) 1077–1091. https://doi.org/10.1007/BF00241305.

[196] C.A. Martínez-Huitle, S. Ferro, Electrochemical oxidation of organic pollutants for the wastewater treatment: Direct and indirect processes, Chem. Soc. Rev. 35 (2006) 1324–1340. https://doi.org/10.1039/b517632h.

[197] I. Sirés, E. Brillas, M.A. Oturan, M.A. Rodrigo, M. Panizza, Electrochemical advanced oxidation processes: Today and tomorrow. A review, Environ. Sci. Pollut. Res. 21 (2014) 8336–8367. https://doi.org/10.1007/s11356-014-2783-1.

[198] F.C. Moreira, R.A.R. Boaventura, E. Brillas, V.J.P. Vilar, Electrochemical advanced oxidation processes: A review on their application to synthetic and real wastewaters, Appl. Catal. B Environ. 202 (2017) 217–261. https://doi.org/10.1016/j.apcatb.2016.08.037.

[199] W.M. Davison, B. Pitts, P.S. Stewart, Spatial and temporal patterns of biocide action against Staphylococcus epidermidis biofilms, Antimicrob. Agents Chemother. 54 (2010) 2920–2927. https://doi.org/10.1128/AAC.01734-09.

[200] K. Buckingham-Meyer, D.M. Goeres, M.A. Hamilton, Comparative evaluation of biofilm disinfectant efficacy tests, J. Microbiol. Methods. 70 (2007) 236–244. https://doi.org/10.1016/j.mimet.2007.04.010.

[201] E.L. Sandvik, B.R. Mcleod, A.E. Parker, P.S. Stewart, Direct Electric Current Treatment under Physiologic Saline Conditions Kills Staphylococcus epidermidis Biofilms via Electrolytic Generation of Hypochlorous Acid, PLoS One. 8 (2013) 55118. https://doi.org/10.1371/journal.pone.0055118.

[202] S. UEDA, Y. KUWABARA, Susceptibility of Biofilm Escherichia coli, Salmonella Enteritidis and Staphylococcus aureus to Detergents and Sanitizers, Biocontrol Sci. 12 (2007) 149–153. https://doi.org/10.4265/bio.12.149.

[203] C. Trellu, C. Coetsier, J.C. Rouch, R. Esmilaire, M. Rivallin, M. Cretin, C. Causserand, Mineralization of organic pollutants by anodic oxidation using reactive electrochemical membrane synthesized from carbothermal reduction of TiO2, Water Res. 131 (2018) 310–319. https://doi.org/10.1016/j.watres.2017.12.070.

[204] Y. Liu, H. Liu, Z. Zhou, T. Wang, ‖ Choon, N. Ong, C.D. Vecitis, Degradation of the Common Aqueous Antibiotic Tetracycline using a Carbon Nanotube Electrochemical Filter, (2015). https://doi.org/10.1021/acs.est.5b00870.

[205] D.M. Warsinger, J. Swaminathan, E. Guillen-Burrieza, H.A. Arafat, J.H. Lienhard V, Scaling and fouling in membrane distillation for desalination applications: A review, Desalination. 356 (2015) 294–313. https://doi.org/10.1016/j.desal.2014.06.031.

[206] M.M. Tlili, M. Benamor, C. Gabrielli, H. Perrot, B. Tribollet, Influence of the Interfacial pH on Electrochemical CaCO[sub 3] Precipitation, J. Electrochem. Soc. 150 (2003) C765. https://doi.org/10.1149/1.1613294.

[207] H.J. Lee, M.A. Halali, T. Baker, S. Sarathy, C.F. de Lannoy, A comparative study of RO membrane scale inhibitors in wastewater reclamation: Antiscalants versus pH adjustment, Sep. Purif. Technol. 240 (2020). https://doi.org/10.1016/j.seppur.2020.116549.

[208] J. Reid, The disinfectant action of certain organic acids, Am. J. Epidemiol. (n.d.).

http://www.panelamonitor.org/media/docrepo/document/files/the-desinfectant-action-of-certain-organic-acids.pdf (accessed June 30, 2020).

[209] R.A.H. Timmermans, M.N. Nierop Groot, A.L. Nederhoff, M.A.J.S. van Boekel, A.M. Matser, H.C. Mastwijk, Pulsed electric field processing of different fruit juices: Impact of pH and temperature on inactivation of spoilage and pathogenic micro-organisms, Int. J. Food Microbiol. 173 (2014) 105–111. https://doi.org/10.1016/j.ijfoodmicro.2013.12.022.

[210] H. Vega-Mercado, U.R. Pothakamury, F.J. Chang, G. V. Barbosa-Cánovas, B.G. Swanson, Inactivation of Escherichia coli by combining pH, ionic strength and pulsed electric fields hurdles, Food Res. Int. 29 (1996) 117–121. https://doi.org/10.1016/0963-9969(96)00015-4.

[211] D. García, N. Gómez, J. Raso, R. Pagán, Bacterial resistance after pulsed electric fields depending on the treatment medium pH, Innov. Food Sci. Emerg. Technol. 6 (2005) 388–395. https://doi.org/10.1016/j.ifset.2005.04.003.

[212] N. Gómez, D. García, I. Álvarez, S. Condón, J. Raso, Modelling inactivation of Listeria monocytogenes by pulsed electric fields in media of different pH, Int. J. Food Microbiol. 103 (2005) 199–206. https://doi.org/10.1016/j.ijfoodmicro.2004.11.033.

[213] P.D. Cotter, C. Hill, Surviving the Acid Test: Responses of Gram-Positive Bacteria to Low pH, Microbiol. Mol. Biol. Rev. 67 (2003) 429–453. https://doi.org/10.1128/mmbr.67.3.429-453.2003.

[214] G. Saldaña, E. Puértolas, S. Condón, I. Álvarez, J. Raso, Modeling inactivation kinetics and occurrence of sublethal injury of a pulsed electric field-resistant strain of Escherichia coli and Salmonella Typhimurium in media of different pH, Innov. Food Sci. Emerg. Technol. 11 (2010) 290–298. https://doi.org/10.1016/j.ifset.2010.01.003.

[215] M.R. Singh, Y. Kwon, Y. Lum, J.W. Ager, A.T. Bell, Hydrolysis of Electrolyte Cations Enhances the Electrochemical Reduction of CO2 over Ag and Cu, J. Am. Chem. Soc. 138 (2016) 13006–13012. https://doi.org/10.1021/jacs.6b07612.

[216] J.M. Meinders, H.C. van der Mei, H.J. Busscher, Deposition Efficiency and Reversibility of Bacterial Adhesion under Flow, J. Colloid Interface Sci. 176 (1995) 329–341. https://doi.org/10.1006/jcis.1995.9960.

[217] H. Kang, S. Shim, S.J. Lee, J. Yoon, K.H. Ahn, Bacterial Translational Motion on the Electrode Surface under Anodic Electric Field, Environ. Sci. Technol. 45 (2011) 5769–5774. https://doi.org/10.1021/es200752h.

[218] A.J. van der Borden, H.C. van der Mei, H.J. Busscher, Electric-current-induced detachment ofStaphylococcus epidermidis strains from surgical stainless steel, J. Biomed. Mater. Res. 68B (2004) 160–164. https://doi.org/10.1002/jbm.b.20015.

[219] A.J. Van Der Borden, H.C. Van Der Mei, H.J. Busscher, Electric block current induced detachment from surgical stainless steel and decreased viability of Staphylococcus epidermidis, Biomaterials. 26 (2005) 6731–6735. https://doi.org/10.1016/j.biomaterials.2004.04.052.

[220] C.F. De Lannoy, D. Jassby, K. Gloe, A.D. Gordon, M.R. Wiesner, Aquatic biofouling prevention by electrically charged nanocomposite polymer thin film membranes, Environ. Sci. Technol. 47 (2013) 2760–2768. https://doi.org/10.1021/es3045168.

[221] Y. Baek, H. Yoon, S. Shim, J. Choi, J. Yoon, Electroconductive Feed Spacer as a Tool for Biofouling Control in a Membrane System for Water Treatment, Environ. Sci. Technol. Lett. 1 (2014) 179–184. https://doi.org/10.1021/ez400206d.

[222] S. Shim, S.H. Hong, Y. Tak, J. Yoon, Prevention of Pseudomonas aeruginosa adhesion by electric

currents, Biofouling. 27 (2011) 217–224. https://doi.org/10.1080/08927014.2011.554831.

[223] R.E. Perez-Roa, D.T. Tompkins, M. Paulose, C.A. Grimes, M.A. Anderson, D.R. Noguera, Effects of localised, low-voltage pulsed electric fields on the development and inhibition of Pseudomonas aeruginosa biofilms., Biofouling. 22 (2006) 383–90. https://doi.org/10.1080/08927010601053541.

[224] C. Liu, X. Xie, W. Zhao, N. Liu, P.A. Maraccini, L.M. Sassoubre, A.B. Boehm, Y. Cui, Conducting Nanosponge Electroporation for Affordable and High-Efficiency Disinfection of Bacteria and Viruses in Water, (2013). https://doi.org/10.1021/nl402053z.

[225] A. V Dudchenko, C. Chen, A. Cardenas, J. Rolf, D. Jassby, Frequency-dependent stability of CNT Joule heaters in ionizable media and desalination processes, Nat. Nanotechnol. |. 12 (2017). https://doi.org/10.1038/NNANO.2017.102.

[226] A. V Dudchenko, C. Chen, A. Cardenas, J. Rolf, D. Jassby, Frequency-dependent stability of CNT Joule heaters in ionizable media and desalination processes, Nat. Nanotechnol. |. 12 (2017). https://doi.org/10.1038/NNANO.2017.102.

[227] C. Jiménez-Sánchez, J. Lozano-Sánchez, A. Segura-Carretero, A. Fernández-Gutiérrez, C. Jim Enez-S Anchez, J. Us Lozano-S Anchez, A. Fern Andez-Guti Errez, Critical Reviews in Food Science and Nutrition Alternatives to conventional thermal treatments in fruit-juice processing. Part 1: Techniques and applications Alternatives to conventional thermal treatments in fruit-juice processing. Part 1: Techniques and, (2017). https://doi.org/10.1080/10408398.2013.867828.

[228] D. Bell, R. Sengpiel, M. Wessling, Metallized hollow fiber membranes for electrochemical fouling control, J. Memb. Sci. 594 (2020) 117397. https://doi.org/10.1016/j.memsci.2019.117397.

[229] T. Lohaus, N. Herkenhoff, R. Shankar, M. Wessling, Feed flow patterns of combined Rayleigh-Bénard convection and membrane permeation, J. Memb. Sci. 549 (2018) 60–66. https://doi.org/10.1016/j.memsci.2017.11.061.

[230] P. Stoodley, D. Debeer, H.M. Lappin-Scott, Influence of Electric Fields and pH on Biofilm Structure as Related to the Bioelectric Effect, 1997.

[231] P. Jiang, J. Zhou, A. Zhang, Y. Zhong, Electrochemical degradation of p-nitrophenol with different processes, J. Environ. Sci. 22 (2010) 500–506. https://doi.org/10.1016/S1001-0742(09)60140-6.

[232] A.I. del Río, J. Molina, J. Bonastre, F. Cases, Influence of electrochemical reduction and oxidation processes on the decolourisation and degradation of C.I. Reactive Orange 4 solutions, Chemosphere. 75 (2009) 1329–1337. https://doi.org/10.1016/j.chemosphere.2009.02.063.

[233] A.J. Méndez-Martínez, M.M. Dávila-Jiménez, O. Ornelas-Dávila, M.P. Elizalde-González, U. Arroyo-Abad, I. Sirés, E. Brillas, Electrochemical reduction and oxidation pathways for Reactive Black 5 dye using nickel electrodes in divided and undivided cells, Electrochim. Acta. 59 (2012) 140–149. https://doi.org/10.1016/j.electacta.2011.10.047.

[234] J. Wei, Y. Feng, X. Sun, J. Liu, L. Zhu, Effectiveness and pathways of electrochemical degradation of pretilachlor herbicides, J. Hazard. Mater. 189 (2011) 84–91. https://doi.org/10.1016/j.jhazmat.2011.02.002.

[235] D.M. Gilbert, T.C. Sale, Sequential electrolytic oxidation and reduction of aqueous phase energetic compounds, Environ. Sci. Technol. 39 (2005) 9270–9277. https://doi.org/10.1021/es051452k.

[236] E. Brillas, B. Boye, I. Sirés, J.A. Garrido, R.M. Rodríguez, C. Arias, P.L. Cabot, C. Comninellis, Electrochemical destruction of chlorophenoxy herbicides by anodic oxidation and electro-Fenton using a boron-doped diamond electrode, Electrochim. Acta. 49 (2004) 4487–4496. https://doi.org/10.1016/j.electacta.2004.05.006.

[237] J.S. Do, W.C. Yeh, In situ paired electrooxidative degradation of formaldehyde with electrogenerated hydrogen peroxide and hypochlorite ion, J. Appl. Electrochem. 28 (1998) 703–710. https://doi.org/10.1023/A:1003294011228.

[238] C. Zhang, Y. Jiang, Y. Li, Z. Hu, L. Zhou, M. Zhou, Three-dimensional electrochemical process for wastewater treatment: A general review, Chem. Eng. J. 228 (2013) 455–467. https://doi.org/10.1016/j.cej.2013.05.033.

[239] H. Wang, Z. Bian, G. Lu, L. Pang, Z. Zeng, D. Sun, Preparation of multifunctional gas-diffusion electrode and its application to the degrading of chlorinated phenols by electrochemical reducing and oxidizing processes, Appl. Catal. B Environ. 125 (2012) 449–456. https://doi.org/10.1016/j.apcatb.2012.06.019.

[240] J. Speight, LANGE'S HANDBOOK OF CHEMISTRY, 2017. https://www.accessengineeringlibrary.com/binary/mheaeworks/ea71143cd46bc712/7b87106e446793264e4b0625f45999c830e326b570e3044d32e4dddd9cf9e781/book-summary.pdf (accessed May 5, 2021).

[241] W.K. Liu, M.R.W. Brown, T.S.J. Elliott, Mechanisms of the bactericidal activity of low amperage electric current (DC), J. Antimicrob. Chemother. 39 (1997) 687–695. https://doi.org/10.1093/jac/39.6.687.

[242] R.E. Perez-Roa, D.T. Tompkins, M. Paulose, C.A. Grimes, M.A. Anderson, D.R. Noguera, Effects of localised, low-voltage pulsed electric fields on the development and inhibition of Pseudomonas aeruginosa biofilms, Biofouling. 22 (2006) 383–390. https://doi.org/10.1080/08927010601053541.

[243] X. Wang, L. Zhou, L. Lu, F.L. Lobo, N. Li, H. Wang, J. Park, Z.J. Ren, Alternating current influences anaerobic electroactive biofilm activity, Environ. Sci. Technol. 50 (2016) 9169–9176. https://doi.org/10.1021/acs.est.6b00813.

[244] H. Wake, H. Takahashi, T. Takimoto, H. Takayanagi, K. Ozawa, H. Kadoi, M. Okochi, T. Matsunaga, Development of an electrochemical antifouling system for seawater cooling pipelines of power plants using titanium, Biotechnol. Bioeng. 95 (2006) 468–473. https://doi.org/10.1002/bit.21022.

[245] A.J. Van Der Borden, H. Van Der Werf, H.C. Van Der Mei, H.J. Busscher, Electric current-induced detachment of Staphylococcus epidermidis biofilms from surgical stainless steel, Appl. Environ. Microbiol. 70 (2004) 6871–6874. https://doi.org/10.1128/AEM.70.11.6871-6874.2004.

[246] T. Nakayama, H. Wake, K. Ozawa, N. Nakamura, T. Matsunaga, Electrochemical prevention of marine biofouling on a novel titanium- nitride-coated plate formed by radio-frequency arc spraying, Appl. Microbiol. Biotechnol. 50 (1998) 502–508. https://doi.org/10.1007/s002530051327.

[247] S.H. Hong, J. Jeong, S. Shim, H. Kang, S. Kwon, K.H. Ahn, J. Yoon, Effect of electric currents on bacterial detachment and inactivation, Biotechnol. Bioeng. 100 (2008) 379–386. https://doi.org/10.1002/bit.21760.

[248] B.C.H. Steele, A. Heinzel, Materials for fuel-cell technologies, in: Mater. Sustain. Energy, Co-Published with Macmillan Publishers Ltd, UK, 2010: pp. 224–231. https://doi.org/10.1142/9789814317665_0031.

[249] W. Duan, A. Ronen, S. Walker, D. Jassby, Polyaniline-Coated Carbon Nanotube Ultrafiltration Membranes: Enhanced Anodic Stability for In Situ Cleaning and Electro-Oxidation Processes, (2016). https://doi.org/10.1021/acsami.6b07196.

[250] C.D. Vecitis, M.H. Schnoor, M. Saifur Rahaman, J.D. Schiffman, M. Elimelech, Electrochemical Multiwalled Carbon Nanotube Filter for Viral and Bacterial Removal and Inactivation, Environ. Sci. Technol. 45 (2011) 3672–3679. https://doi.org/10.1021/es2000062.

[251] M. Tominaga, Y. Yatsugi, N. Watanabe, Oxidative corrosion potential vs. pH diagram for single-walled carbon nanotubes, RSC Adv. 4 (2014) 27224–27227. https://doi.org/10.1039/c4ra02875a.

[252] S. Ohmori, T. Saito, Electrochemical durability of single-wall carbon nanotube electrode against anodic oxidation in water, Carbon N. Y. 50 (2012) 4932–4938. https://doi.org/10.1016/j.carbon.2012.06.023.

[253] B. Siembida, P. Cornel, S. Krause, B. Zimmermann, Effect of mechanical cleaning with granular material on the permeability of submerged membranes in the MBR process, Water Res. 44 (2010) 4037–4046. https://doi.org/10.1016/j.watres.2010.05.016.

[254] J. Mansouri, S. Harrisson, V. Chen, Strategies for controlling biofouling in membrane filtration systems: Challenges and opportunities, J. Mater. Chem. 20 (2010) 4567–4586. https://doi.org/10.1039/b926440j.

[255] A.L. McGaughey, R.D. Gustafson, A.E. Childress, Effect of long-term operation on membrane surface characteristics and performance in membrane distillation, J. Memb. Sci. 543 (2017) 143–150. https://doi.org/10.1016/j.memsci.2017.08.040.

[256] R. Singh, Desalination and Water Treatment Analysis of energy usage at membrane water treatment plants, (2011). https://doi.org/10.5004/dwt.2011.1810.

Chapter 3

Electrically Conductive Membranes – A Review of their Anti Fouling Applications – Part II

3.1.Abstract

Electrically conductive membranes (ECM) have the promise to eliminate the challenges involved with traditional cleaning techniques owing to their electroactive and electro-responsive surface. ECMs have found applications across water and wastewater treatment sectors, including controlling membrane fouling or water disinfection/decontamination. Discovering the full potential of ECMs requires a deep understanding of the interplay between current patterns, antifouling mechanisms, and foulant's physicochemical properties. Current pattern includes current type (anodic, cathodic), configuration (direct, alternating), magnitude, and frequency. Herein, we aim to establish a robust connection between ECM applications and the governing antifouling mechanisms to provide an understanding of published anti-fouling results and guide researchers to more effective materials and voltage applications. In so doing, this review compiles antifouling applications of ECMs for four major fouling categories (i.e., biological, organic, oil wetting, and mineral scaling) with the focus on the relevant mechanisms. Finally, this review highlights the perspectives and limitations of ECMs and presents opportunities and considerations within the design, build, and operation of ECMs across academia and industry.

3.2.Introduction

Addressing water shortage and providing millions of people with access to high quality water demands technologies that are accessible, energy-efficient, versatile, safe, and scalable. Membrane processes are the technology of choice due to their versatility of operation, selectivity, energy efficiency, and high permeate quality [1], playing a critical role in desalination, wastewater treatment, water treatment and water reuse processes [1]. Pressure-driven membranes are categorized into microfiltration (MF), ultrafiltration (UF), nanofiltration (NF), and reverse osmosis (RO), which target foulants with respect to their pore size, selectivity, surface physicochemical properties. In separation processes, accumulation of particles (natural organic matter, biological compounds, ions) across the separation interface leads to formation of fouling that in turn compromises the efficiency of the membrane (operating at lower flux and higher energy), reduces the membrane lifetime, and raises environmental concerns by forcing chemical cleaning procedures (using detergents, biocides, acids/bases). Conventionally, fouling is categorized into biofouling (e.g., bacteria, viruses), organic fouling (e.g. organic matter, oil, hydrocarbons), colloidal fouling (e.g. silt, clay), and scaling (e.g. salts) [2,3]. Many strategies have been developed to control and mitigate fouling, such as pre-treatment, physical cleaning, chemical cleaning, and mechanical cleaning. However, these procedures are often considered time- and energy-intensive, environmentally-detrimental, and damage the membrane integrity. Thus, it is essential to develop membranes with targeted selectivity and advanced antifouling properties.

Many studies have sought to advance membrane surface antifouling properties by incorporating chemistries (e.g., modifying hydrophilicity, surface tension), functionalities (e.g., antimicrobial particles, charged molecules), or altered morphological structures (branch-like structure). Although surface modifications bring added value to membranes by enhancing flux and lowering fouling rate, they still get subjected to fouling and surface passivation over long-term operation. In addition, presence of foulants with a wide range of physicochemical properties next to significant fluctuations in the influent chemistry

make it difficult to treat the real wastewater. As such, it is not likely that a membrane surface chemistry maintains the advanced efficiency in treating complex solutions.

Electrically conductive membranes (ECM) were invented to eliminate the challenges involved with traditional membranes by offering a self-cleaning electrically-responsive surface [4–8]. ECMs contain a conductive surface that induces antifouling mechanisms in response to the externally-applied electrical potential. Conductive surfaces are exposed to currents in the formats of direct current (DC, electrical charge flows only in one direction) or alternating currents (AC, electrical current reverses direction). Cathodic and anodic currents promote different antifouling mechanisms at the interface of the ECM and the solute depending on the current range. Electrically-assisted antifouling mechanisms are exclusive to the current type as well as to the current configuration (Please see Part I). On account of their responsive surface, a conductive coating can retain different electrochemical properties, posing different mechanisms to match foulants with different properties. For example, tuning surface polarization controls the chemical and hydrodynamic properties at the surface during a filtration process including the surface charge (type, density), reductive and oxidative state, local pH (acidic, alkaline), or gas bubble formation. In addition to electro-responsive properties of ECMs, they are (a) more effective than conventional membranes by treating the foulants locally at the separation interface and (b) more environmentally friendly. The chemical-free generation of anti-foulants reduces the reliance on chemicals and biocides, which reduces hazards associated with chemical handling, storage, and waste, reduces chemical and storage costs, and reduces the negative impact of chemicals on membrane integrity.

Since the introduction of ECMs in the separation-based technologies, their application has been extended to different membrane categories (MF, UF, NF, and RO) and module configurations (flat sheet, hollow fibers). Hybrid membranes are the most common type of ECMs. These are primarily composed of non-conductive membranes (PES, PVDF, ceramic), which support an electrically active coating layer. ECM coatings have been fabricated from a wide range of materials including carbonaceous material (e.g., carbon nanotubes (CNTs), graphene, graphite, carbon nanofibers (CNFs)) [9–14],

inorganic materials (e.g., ceramics, metals) [15,16], and electrically conductive polymers (e.g., polyaniline, polypyrrole) [17]. Our meta-analysis indicates that carbonaceous material, inorganic material, conductive polymers consist 61%, 30%, and 9% of the ECMs. Carbonaceous ECMs have low surface overpotential (< 1.2 V) and are widely used due to their low cost, ease of fabrication, processibility, and high conductivity. Their low surface overpotential for oxygen evolution reactions (OER) has made them applicable to induce mechanisms such as electrostatic repulsion, gas generation, indirect oxidation, and direct oxidation (for contaminants with low oxidation potential). Application of inorganic coatings is restricted due to their high-cost, low flexibility, and low processibility. However, high surface over potential (> 2.2 V), high conductivity, and chemical stability have made them viable candidates for direct oxidation in long-term anodic applications. Conductive polymers have been also used in a few studies as ECMs, however, their low-conductivity and flux have limited their broad application in filtration processes. ECMs' self-cleaning properties, oxidation potential, and detection properties coupled to electrochemical impedance spectroscopy, have made them viable for applications beyond water treatment including in sensors [18–20], fuel cells, catalysts, and biomedical applications.

Over the last five years, many review papers have offered a comprehensive review on ECMs, their material type, and their antifouling application [4–6,21–27]; however, the underlying mechanisms have never been comprehensively discussed. Effective and energy-efficient ECM applications necessitate a deep understanding of underlying mechanisms and their impact on foulants. The comprehensive and systematic discussion on electrically-induced antifouling and removal mechanisms was presented in Part I of this review paper. The present review aims to establish a robust connection between ECM applications and the governing antifouling mechanisms to provide an understanding of published anti-fouling results and guide researchers to more optimized ECM applications. In so doing, this review compiles antifouling applications of ECMs for four major fouling categories (i.e., biological, organic, oil wetting, and mineral scaling) with the focus on the relevant antifouling mechanisms and their interactions with the foulants explained at the end of each

subsection. Finally, this review discusses the outlook and limitations of ECMs and projects the opportunities that exist for academics, innovators, and industry within design, testing, operation, and optimization of ECMs for broad industrial adoption.

3.3.Antifouling applications

This section reviews the experimental works using electrically conductive membranes (ECMs) to combat fouling. Depending on the membrane application, ECMs can be used to prevent or limit fouling, such as biofouling, organic fouling, mineral scaling, and oil wetting. A decade of research has shown how anodic and cathodic polarization were able to mitigate fouling in contrast to unpolarised surfaces. However, to date, optimal current parameters (current type and magnitude) have not been identified for each foulant type. In addition, the underlying mechanisms governing the antifouling performance have been mostly overlooked in favour of showcasing the promising antifouling results. Therefore, this section provides in-depth discussion of the main current types (anodic, catholic) used for each type of foulant in comparison to their corresponding outcome (maintaining flux, enhancing flux recovery, and/or reducing fouling). In addition, the main mechanisms identified as responsible for the improved performance are explained.

3.3.1. Biofouling

Membrane biofouling refers to the deposition, colonization, growth, and metabolism of biological cells or flocs, algae, and fungi on the surface of membranes. Biofouling is regarded as the most serious type of fouling due to the complexity of formation and the severity of the impact on the membrane performance as well as membrane lifetime. A mature biofilm is able to produce extracellular polymeric secretions (EPS) consisting of polysaccharides, proteins, carbohydrates, and other biomacromolecules which makes the biofilm stable and difficult to disrupt. Therefore, it is preferred to mitigate and control biofilms at the early stages of formation to prevent irreversible fouling [28]. Table 3.1 summarizes works on ECMs used in biofouling control as well as their hypothesized antifouling mechanisms. The many ways in which ECMs have been used to control biofouling are systematically discussed as follows:

Table 3.1. Summary of research on biofouling control and biofouling inactivation on conductive membranes by applying different current types and magnitudes.

Antifouling mechanisms	Materials	Foulants	Charge of Foulants	Concentration	Current Pattern and Reaction Time	Results	Reference
			Anodic potential				
Redox (Direct oxidation)	Gold electrodes	*Pseudomonas fluorescens*	Negative	10^8 cells/mL	0.5-0.7 V for 2 h	Anodic current caused cell lysis.	[29]
Redox (Direct oxidation/indirect oxidation)	Papyex graphite (PA), carbon aerogel (CA)	*Pseudomonas aeruginosa*		0.1 (OD_{600})	0.9 V for 12 or 36 h	Higher potential resulted in better biofilm control.	[30]
Redox (Direct oxidation)	Ti as conductive feed spacer RO	*Pseudomonas aeruginosa*	-20 mV	10^7 CFU/mL	1 V for 30 min after 24 h biofouling	Flux recovery was 91%. No significant destructive impact on RO membrane.	[31]
H2O2	CNT/PVA UF	*Escherichia coli* Micro particles	-0.74 mV 6.63 mV	$5x10^5$ cells/mL	0/0.5/1/1.5 V for 30 min	Percent of dead bacteria was 67 ± 3.6% post-electrolysis.	[32]
Redox (Direct oxidation)	Indium tin oxide (ITO)-coated glass	*Pseudomonas aeruginosa*	-20 mV	$1x10^8$ -$1.5x10^8$ CFU/mL	15µA/cm^2 (0.5-2.4 V) for 40 min	Anodic current resulted in cell lysis.	[33]
Direct oxidation (antimicrobial surface)	Laser Induced Graphene (LIG)/GO	BSA Mixed Bacteria	Negative	1000 ppm BSA in phosphate buffered saline (PBS)	1.5 - 3.0 V for 48 h	99.9 % bacteria removal. BSA rejection of 55 % after 2 h. 17 % flux loss.	[34]
Electrostatic attraction (direct oxidation)	MWCNT/ PTFE MF	Virus bacteriophage (MS2) Alginate NOM	Negative	Viral particles with the host *E. Coli* (10^6-10^7 PFU/mL) 1 ppm alginate 5 ppm NOM	2-3 V for 30 min	Full virus removal under application of 2 or 3 V; Good performance for ionic strength 1-100 mM NaCl and pH 3-9;	[35]
Redox (Direct oxidation/indirect oxidation)	MWCNT/ PTFE MF	*Escherichia coli*	Negative	$2.5x10^5$ CFU/mL	2V or 3 V during filtration. 2V or 3 V for 30 s post-filtration	Complete removal of bacteria; Inactivated >75% of the sieved bacteria	[36]
Redox (Direct oxidation/indirect oxidation)	MWCNT/ PTFE MF	Virus (MS2)	-	10^7 CFU/mL MS2 584 ppm NaCl	2V or 3 V during filtration. 2V or 3 V for 30 s post-filtration.	Multi-log removal of viruses in filtration. Inactivated >99.6% of the adsorbed viruses.	[36]
Direct oxidation (antimicrobial surface)	LIG/PVA	BSA Mixed Bacteria	Negative	1000 ppm BSA in PBS, 10^6 CFU/mL mixed bacteria from wastewater	2-3 V for 2-9 h	Up to 63 % BSA rejection. Complete disinfection at 2.5 V compared to 39 % with no voltage.	[37]
Indirect Oxidation (Hydrogen peroxide, active chlorine)	IrO_2/Ti	Mixed bacterial culture from textile wastewater	-	-	4.6-6.9 A/m^2 (5.6-10.8 V) for 40 h	4 bacterial log removal	[38]
Redox (Direct oxidation)	CNT/polyurethane/Ag	*Escherichia coli*		10^7 CFU/mL	0-20 V for 2 h	99.9999% removal of bacteria due to electroporation. Log-removal was 4 and 6 at 5 V and 10 V, respectively.	[39]
Redox (Direct oxidation)	CNT/polyurethane/Ag	*Salmonella enterica Typhimirium*		10^7 CFU/mL	0-20 V for 2 h	99.9999% removal of bacteria due to electroporation. Log-removal was 2 and 6 at 5 V and 10 V, respectively.	[39]
Redox (Direct oxidation)	CNT/polyurethane/Ag	*Enterococcus faecalis*		10^7 CFU/mL	0-20 V for 2 h	99.9999% removal of bacteria due to electroporation. Log-removal was 1 and 6 at 5 V and 10 V, respectively.	[39]
Redox (Direct oxidation)	CNT/polyurethane/Ag	*Bacillus subtilis*		10^7 CFU/mL	0-20 V for 2 h	99.9999% removal of bacteria due to electroporation. Log-removal was 4 and 6 at 5 V and 10 V, respectively.	[39]
Redox (Direct oxidation)	CNT/polyurethane/Ag	Bacteriophage MS2		10^7 CFU/mL	0-20 V for 2 h	99% removal of one model virus due to electroporation. Log-removal was 1. 1.5, and 2 at 5 V,10 V, and 15 V, respectively.	[39]
			Cathodic potential				
Hydrogen gas (electrostatic force)	Gold electrodes	*Pseudomonas fluorescens*	Negative	10^8 cells/mL	0.5-0.7 V for 2 h	Cathodic current resulted in cell detachment.	[29]

Hydrogen peroxide	Papyex graphite (PA), carbon aerogel (CA)	*Pseudomonas aeruginosa*		0.1 (OD_{600})	0.9 V for 12 or 36 h	Hydrogen peroxide concentration of ≈2.4μM (at ±0.9 V) caused biofouling inhibition.	[30]
Electrostatic repulsion	Ti as conductive feed spacer RO	*Pseudomonas aeruginosa*	-20 mV	10^7 CFU/mL	1 V for 30 min after 24 hr biofouling	Flux recovery was 89%.	[31]
Electrostatic repulsion	Graphene oxide/Ppy MF	Yeast suspension	-12.9 mV	5000 ppm (MLSS)	1 V in three cycles (1.5 h each)	1 V/cm increased the flux as high as 20%.	[40]
Hydrogen peroxide	CNT/PVA UF	*Escherichia coli* Micro particles	-0.74 mV 6.63 mV	$5x10^5$ cells/mL	0/0.5/1/1.5 V for 30 min	Percent of dead bacteria was 32 ± 2.1.	[32]
Electrostatic repulsion	Indium tin oxide (ITO)-coated glass	*Pseudomonas aeruginosa*	-20 mV	$1x10^8$ -$1.5x10^8$ CFU/mL	15μA/cm² (0.5-2.4 V) for 40 min	Cathodic current resulted in cell detachment.	[33]
Hydrogen peroxide (antimicrobial surface)	LIG/PES	*Pseudomonas aeruginosa*	-23.3 mV	10^6 CFU/mL	1.5 - 2.5 / 20 V for 2-9 h	6 log reduction in bacteria at 2.5 V. 20 V achieved total disinfection. Enhanced H_2O_2 production.	[41]
Hydrogen gas	CNS/PVDF NF	Yeast suspension	Negative	100 ppm	2 V at 60 min intervals with 2-3 min electrolysis	60% reduction in Flux w/o electrolysis after 4.6 hr. 25% reduction in flux with E-cleaning.	[42]
Electrostatic repulsion (hydrogen gas)	CNT/PVDF	Yeast suspension	Negative	50 ppm	2 V, 3 min every 30/40/60 min	80% reduction in flux was improved to 60% over 200 min with electrolysis (every 30 min).	[43]
Hydrogen gas (electrostatic force)	Ni/PES hollow fiber	Yeast suspension		1000 ppm	100 mA/cm² (2 V) for 3 s every 15 min	TMP recovery up to 60% and a TMP saving of 28%.	[44]
Hydrogen gas	PVA-networked cellulose-CNT	Yeast Humic acid		500 ppm	5 V for 20 min ~3.75 mA/cm²	Membrane was recovered from foulant after electrolysis.	[45]
			Alternating potential				
Electrostatic repulsion/Direct oxidation	CNT polyamide NF	*Pseudomonas aeruginosa*	Negative	10^8 CFU/mL	1.5 V square wave, 16.7 mHz for 150 h	Complete flux recovery with 1 min of cross-flow flushing.	[46]
Electrostatic repulsion/Direct oxidation	Ti as conductive feed spacer RO	*Pseudomonas aeruginosa*	-20 mV	10^7 CFU/mL	1 V for 30 min, 16.7 mHz after 24 h biofouling	Flux recovery was 80%.	[31]
Electrostatic repulsion/Direct oxidation	Indium tin oxide (ITO)-coated glass	*Pseudomonas aeruginosa*	-20 mV	$1x10^8$ -$1.5x10^8$ CFU/mL	15μA/cm² (0.5-2.4 V) for 40 min, 1.67-1000 mHz	70% less adhered bacteria under AC	[33]
Electrostatic repulsion	Indium tin oxide (ITO)-coated glass	*Pseudomonas aeruginosa*	-20 mV	10^8 CFU/mL	15 μA/cm² (2.7 V), 16.7 mHz for 90 min	58% inactivation under AC.	[47]
Electrostatic repulsion/Direct oxidation	CNT	*Pseudomonas putida*	Negative	10^4 CFU/mL	0.3-6.0 V, 10-10,000 Hz for 72 h	Under 1.5 V, 1 kHz caused 41.4% and 92.0% bacterial attachment inhibition and inactivation.	[48]
Redox (Direct oxidation)	Titanium coated glass	*Pseudomonas aeruginosa*	Negative	10^8 CFU/mL	0.5-5 V, 200-10000 Hz for 13 h	A pulse configuration of 1% duty ratio, 5 V, and 200 Hz frequency reduced the biofilm by 50%.	[49]
Electrostatic repulsion/Direct oxidation	CNT/polyurethane/Ag	*Escherichia coli*		10^7 CFU/mL	10 V, 0-10^8 Hz for 2 h	Low frequencies (<100 Hz) resulted in 2 log-removal higher disinfection.	[39]
Electrostatic repulsion/electrophoretic mobility	polyaniline-Ag-polysulfone	*Staphylococcus aureus*	Negative	10^3 CFU/mL	60 μA (5 MV/m), 60 Hz for 24 h	AC resulted in full bacterial inactivation.	[50]

Anodic potential

Many studies have used anodic potentials in direct current (DC) operation to mitigate and control biofouling. Anodic current has been hypothesized to be effective in inactivating biological organisms due to its biocidal and biostatic properties. Anodic potentials can destruct membrane surfaces, particularly carbonaceous materials, due to anodic oxidation. Therefore, low potentials (~ <2 V) are preferred to reduce the harmful effect of anodic oxidation and maintain the membrane surface conductivity. The primary anti-biofouling mechanisms associated with low anodic potentials include direct inactivation, enhanced electrophoretic mobility, and electrostatic repulsive force.

At potentials below the overpotential values, direct electron transfer dominates the inactivation of microorganisms. In an experimental work, low anodic direct potentials (< 1 V) were used to control the formation of *Pseudomonas aeruginosa* biofilm on carbon aerogel and Papyex graphite electrodes [30]. Briefly, bacteria generate reactive oxygen species as a defensive mechanism to regulate their metabolic activity in response to environmental stressors. Under intense or abrupt changes in temperature, dissolved oxygen, or electrical field, cells produce excessive ROS, which eventually leads to cell inactivation. They recorded the highest cellular ROS activity under extreme potentials (0.9 V) critical for inhibition of bacterial growth. They hypothesized that free radicals contributed to cell inactivation by hampering the cell's regular metabolic activity and respiration however no direct evidence was provided.

Hong et al. [33] carried out a study to investigate the impact of anodic current on indium tin oxide (ITO) biofouling with *Pseudomonas aeruginosa*. Over 60 min biofiltration, above 80% of bacterial particles adhered on ITO under either anodic current ($15\ \frac{\mu A}{cm^2} \approx 0.5 - 2.4$ V) or no current. They suggested that the pre-adsorbed bacterial strains act as adhesion sites for accelerated bacterial attachment and colonization over the filtration period. Bacterial viability study was performed with live/dead staining microscopy which revealed that anodic current could cause cell lysis under the range of current applied. It should be noted that the electrode in their study did not function as a membrane thereby, limiting the extension of these results to separation-based processes in which convective

flow through the membrane acts in opposition to the electrostatic and electrophoretic forces.

The deposition of large bacterial particles is governed by convective flow. However, many studies have claimed that the inactivation of microorganisms next to their enhanced translational mobility across the surface leads to a higher permeate recovery rate. Baek et al. [31] showcased the application of electroconductive feed spacers to control *Pseudomonas aeruginosa* biofouling in a RO module under anodic current. Their results indicated that 30 min application of anodic potential (1 V) after 24 h biofiltration could recover the permeate flux to 80%. In contrast, in the control experiment, the flux was dropped to 47%. They proposed that translational motion governed the advanced bacterial detachment rate under anodic polarization. They also claimed that indirect oxidation due to chlorine generation was unable to govern biofouling control due to low potentials applied in their study (<1.5 V).

Ronen et al. [32] used a UF CNT/PVA ECM and applied anodic potential (0.5-1.5 V) to study their impact on a model bacteria (*E. Coli*). They found the potentials of 1 V and below 1 V insufficient for bacterial inactivation (less than 10%) while external potential of 1.5 V resulted in 67 ± 3.6% inactivation. Also, a significant particle detachment (86 ± 0.21%) was observed under application of external electrical charge. They hypothesized that direct oxidation caused significant cellular detachment under anodic potentials. Bacterial cell integrity was examined with SEM images where the shape of remained bacteria on the surface was found irregular due to cellular inactivation under anodic stress. In addition, no visible bubbles during electrolysis were observed in their study.

Electrostatic repulsive force is not a dominant mechanism for deposition of large bacterial particles; however, it has been claimed that the application of anodic potential during filtration of negatively charged bacteria results in a loose biofilm across the membrane which is easier to disrupt. Gall et al. [29] used a quartz crystal microbalance with dissipation (QCM-D) to investigate the adhesion behavior of biomass under very low potentials (less than 1 V). In their setup, shifts in frequency and dissipation were used to

study the adhesion of negatively charged *Pseudomonas fluorescens* strain to the gold electrode as well as the biomass rigidity. Their findings counter-intuitively indicated that an anodic surface (positive polarity) resulted in formation of a loose biofilm. They theorized under anodic current (positive polarization), electrostatic repulsive force between electrode's negative EDL and negatively charged bacteria keeps the bacterial cells away from the surface, allowing them to have a larger hydrodynamic ratio and form a soft biofilm.

Indirect oxidation can contribute to inactivation of microorganisms at higher potentials (~ >2 V). Electrochemical reactions become activated once the electrical potential exceeds the overpotential of surface material leading to generation of oxygen gas, ROS, and chlorine in the presence of Cl^-. Rahaman et al. [35] used a MWCNT electrode with an applied anodic potential (2-3 V) for removal of MS2 viral particles where almost complete removal was achieved over 30 min. The high removal rate was ascribed to electrophoresis as well as direct oxidation across the MWCNT membrane. As MS2 particles are negatively charged, applied anodic current promoted the migration of viral particles into the vicinity of CNT active sites, where they were inactivated through oxidation. At potentials above 2 V, indirect inactivation through anodically-generated oxidants such as hydroxyl radicals and free chlorine was suggested [35]. They claimed that pH and ionic strength of the solution had a minor impact on viral removal under electrochemical treatment. Complete viral removal was attained at a wide range of pH (3-9) except pH 9 where the electrostatic repulsive force kept a portion of negatively charged viral capsids away from short-range anodic oxidation [35]. Full viral inactivation was achieved through direct oxidation over the entire range of ionic strength investigated (1-100 mM NaCl), suggesting that the thickness of the electric double layer (EDL) and its effect on adsorption had no impact on viral inactivation.

In a similar study [36], full removal of virus particles (MS2) and 75% removal of bacteria (*E. Coli*) were achieved with the application of 2-3 V anodic potential. The potential was applied on MWCNT/PTFE membrane only for 30 s after biofiltration. Direct oxidation was claimed as the primary inactivation mechanism as *E. Coli* experienced

morphological changes during the electrochemical treatment supported by SEM images [36]. The contribution of the indirect oxidation was reported insignificant even at high potentials (3 V).

Recently, laser-induced graphene (LIG) filters have been developed by the Arnusch group [34,37,41]. They have formed LIG on the active surfaces of polymer membranes (polysulfone (PSU), poly(ether sulfone) (PES), polyphenylsulfone (PPSU)) to fabricate electrically conductive low fouling membranes. They showed that PVA-LIG membranes achieved near complete bacterial elimination while maintaining high membrane performance [37]. Direct electron transfer, natural biocidal effect of LIG network, and generation of toxic species such as H_2O_2 were noted as the primary cause of antimicrobial performance. In another study, LIG was cross-linked with GO to fabricate hybrid membranes with advanced separation performance (over 95% bacteria removal) [34].

Mameda et al. [38] employed electrochemical filtration to treat secondary effluent of textile wastewater. In laboratory and pilot-scale systems, they applied anodic current (4.6-6.9 $A/m^2 \approx$ 5.6-10.8 V) to an IrO_2/Ti electrode which resulted in more than 4-log bacterial removal over 40 h. They evaluated the impact of indirect oxidation by separately dosing the secondary wastewater effluent with radicals/oxidants generated by the electrode including hydroxyl radicals, superoxide, ozone, chlorine/dichloride radicals, and hydrogen peroxide. It was revealed that reactive chlorine and hydrogen peroxide played a more significant part in bacterial decontamination. Finally, they compared the electrical-assisted antifouling with air sparging (1 L/min) and membrane relaxation (1 min every 20 min) where the impact of air sparging and membrane relaxation combined were found subinhibitory without electrochemical assistance.

High anodic potentials (~ >10 V) induce a different set of antifouling mechanisms such as electroporation and electrowetting. [51–55]. It has been reported that electrical pulses with an intensity of 55 kV/cm cause up to 2.56 log-cycle reductions in *E. Coli* over 8 pulses [56]. Another study reported over 98% inactivation of *E. coli* only after a few seconds of treatment under potentials of ± 20 V [55]. Liu et al. [39] employed a nano-

sponge filtration system made of polyurethane sponge coated with CNTs and silver nanowires to disinfect bacteria and viruses. At voltages above 10 V, complete disinfection (99.9999%) was achieved for different bacterial strains such as *Escherichia coli, Bacillus subtilis, Enterococcus faecalis, and Salmonella enterica Typhimirium,* as well as efficient removal (99%) for the model virus MS2. They reported electroporation as the primary mechanism for the advanced removal rate under the investigated potential range. They observed that Gram-positive bacteria (*Enterococcus faecalis*) required a greater electric field as their peptidoglycan layer could relax the physical stress caused by electroporation. The damaged bacteria with electroporation pores were evidenced by SEM images (Figure 3.1a-c).

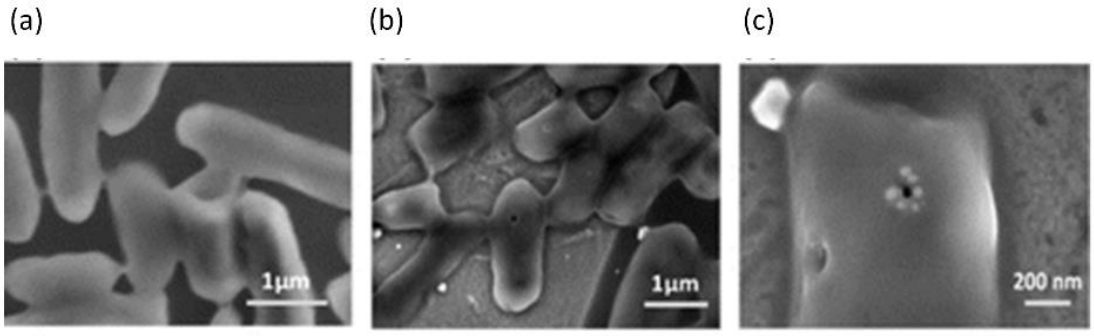

Figure 3.1. SEM images supporting electroporation of *E. Coli* after filtration under (a) No current, (b) 20 V, (c) 20 V, higher magnification. Adapted with permission from [39]. Copyright 2013 American Chemical Society.

The direct inactivation, enhanced electrophoretic mobility, and electrostatic repulsive force were often reported as the primary reasons for the membranes' advanced antifouling performance under anodic polarization. However, as discussed in Part I, there are other mechanisms induced by anodic polarization that can be accounted for advanced properties of anodic surfaces. For instance, it has been shown that anodic surfaces can promote extreme acidic conditions (pH < 5) that in turn inactivates microorganisms. In addition, generation of oxygen gas enhances the steric repulsion across the membrane surface, assisting with antifouling performance. We suspect that the lack of established

methodologies to detect and quantify electrically induced extreme pH and gas generation has led to little exploration of such mechanisms.

Cathodic potential

Many studies have used cathodic potential to control and prevent formation of biofilms. Cathodic potential has been suggested to be effective through electrostatic repulsion, hydrogen gas evolution, and hydrogen peroxide generation.

Biological compounds are typically negatively charged; therefore, electrostatic repulsive force can control and reduce the formation of biofilm across the surface. At low potentials (<1 V), electrostatic repulsion is the dominant mechanism as compared to gas generation or hydrogen peroxide evolution. Baek et al. [31] showed the application of electroconductive feed spacers to control *Pseudomonas aeruginosa* biofouling on a RO membrane under cathodic potential (1 V). Their results indicated that 30 min application of cathodic after 24 h biofiltration could recover the permeate flux to 89% as compared to 47% for the control experiment. In another study, low negative direct potentials (< 1 V) were applied on carbon aerogel and Papyex graphite electrodes to control the formation of *Pseudomonas aeruginosa* biofilm [30]. In both studies, they suggested that electrostatic repulsive force governed the advanced bacterial detachment rate and decreased biovolume on electrodes under cathodic polarization.

In a similar research study [40], a polypyrrole (PPy)/graphene oxide (GO) membrane was fouled with yeast suspension over 4 h. 1 V cathodic potential was applied and a 20% increase in flux was observed. No conclusive explanations were provided for the improved flux properties, however, based on our meta-analysis, we hypothesize that electrostatic repulsion could account for the observations.

The application of CNT-based hollow fiber membranes was demonstrated in an MBR plant composed of planktonic microorganisms, bacteria, and extracellular polymeric substances (EPS) [57]. They applied a cathodic potential (1.2 V) and obtained a slower TMP build-up, a better TMP recovery as well as over 95% COD removal using cathodic

potential (1.2 V) over 100 days of operation. They claimed that electrostatic repulsion reduced the EPS adhesion, in turn mitigating gel formation and pore blockage across the membrane.

As discussed in Part I, ECMs generate hydrogen peroxide as an antifouling mechanism under cathodic polarization. Using electrical surfaces to generate hydrogen peroxide is advantageous because it offers a) safe and economical process due to in-situ generation of hydrogen peroxide as compared to external dosing of the solution by reducing the cost of transportation, storage, and handling, b) an efficient inactivation because generation of hydrogen peroxide across the surface directly exposes the contaminant to concentrated hydrogen peroxide as compared to dosing the bulk solution. Istanbullu et al. [58] quantified the H_2O_2 generation of metallic surfaces (316L stainless steel) using microelectrodes under a cathodic current (0.6 V). They identified the active potential zone for generation of H_2O_2. The onset of H_2O_2 generation was found to be 0.4 V, and 0.8 V was reported as the end of active zone where further increase in the potential would cause reduction of available oxygen and accumulated H_2O_2 at the surface. They then fed the polarized and non-polarized surfaces with identical *Pseudomonas aeruginosa* biofilm over 40 h. Similar initial attachment (1.9 + 0.5%) was observed for both polarized and non-polarized surfaces, while after 40 h exposure, 99 + 0.6% cell coverage was found for non-polarized surfaces as compared to <4% cell coverage for polarized surfaces. They attributed the improved antifouling performance to H_2O_2 generation as well as the lack of sufficient oxygen near the electrode. The results were further supported by SEM images where they suggested electrically-generated H_2O_2 attacked thiol groups of enzymes on the cell wall leading to bacterial deformation. Dosing the bulk with 50 μM H_2O_2 under no current applied resulted in the same reduced bacterial coverage. It is worth noting that they were not able to measure any H_2O_2 in the bulk solution, which they explained due to a) the direction of convective flow and b) degradation of H_2O_2 by catalase enzymes in bacteria.

In a study, the impact of cathodic potentials (0.5-1.5 V) on *E. Coli* was studied using UF CNT/PVA ECM [32]. They found that external potential of 1.5 V resulted in 32 ± 2.1% inactivation under cathodic polarization. They noticed that bacterial deposition was

independent of surface potential or microbial viability and mainly controlled by the drag force regarding the size of particles (1.16 ± 0.31 μm). In contrast, significant particle detachment (86 ± 0.21%) was observed under cathodic polarization. They hypothesized that hydrogen peroxide generation caused significant cellular detachment under cathodic potentials. SEM images verified the damage to cell integrity where the shape of bacteria was found irregular after exposure to cathodic current. To confirm the indirect oxidation by hydrogen peroxide, they exposed bacterial particles to identical dosages generated electrochemically and observed the same inactivation percentage (decrease of 61 ± 1.51% and 58 ± 8% for electrochemistry and hydrogen peroxide, respectively). They suspected electrostatic repulsion force played an insignificant role as *E. Coli* particles were reported nearly neutral (−0.74 ± 4.42 mV). In the meantime, no visible bubbles during electrolysis were observed in their study.

Hong et al. [33] studied the impact of cathodic current ($15\ \mu A/cm^2 \approx 0.5 - 2.4$ V) on indium tin oxide (ITO) biofouling with *Pseudomonas aeruginosa*. Over 60 min biofiltration, cathodic current resulted in 20% adhered bacteria, while above 80% of bacterial particles adhered on ITO at control experiment (no current). They considered the electrostatic repulsive force to be the dominant mechanism for less adhered bacteria under cathodic current. Live/dead staining microscopy revealed no significant cell lysis under cathodic current suggesting the deficient biocidal impact of hydrogen peroxide on bacterial strains.

Based on our analysis, different studies have been carried out in support or opposed to the impact of hydrogen peroxide on bacterial inactivation. Many studies have defined a concentration or a potential at which hydrogen peroxide imposes biocidal impacts. For instance, it is shown that 20 μM is the concentration at which hydrogen peroxide begins to impact the biovolume and cell viability [60], or It is claimed that cathodic surfaces produce subinhibitory concentration at applied potential of 2.0 V or below [33]. However, such statements cannot be generalized due to lack to standard methodologies for evaluating the biocidal impact of hydrogen peroxide in filtration processes. We have identified a few points to explain the discrepancy in interpreting the impact of hydrogen peroxide on

biological compounds, (a) In electrochemically-assisted operations, accurate measurement of hydrogen peroxide concentration at the surface is critical for accurate evaluation of the hydrogen peroxide biocidal impact, however, hydrogen peroxide concentration is often reported at the bulk which might be significantly lower than the local concentration [32,59–65], (b) the concentrations of biocides in bulk cannot represent the real concentrations on the surface due to diffusion limitations in the biofilm [21]. For instance, it has been shown that externally dosing the biofilm with a 96 μM hydrogen peroxide resulted in 75% reduction of biomass while the local concentration at the surface might be lower [66], and (c) operating conditions (flow pattern, temperature, pressure), film condition (maturity and thickness), and bacterial type affect the biocidal concentration of hydrogen peroxide. For instance, some biofilms are resistant to low concentrations of hydrogen peroxide due to presence of catalase enzymes in their strain that disproportionate and neutralize hydrogen peroxide [67,68]. Also depends on the material type, competitor side reactions occurring at the surface including oxygen reduction reactions (ORR) limit the generation of hydrogen peroxide by decreasing the current efficiency (Part I, Reaction 4-10) [69,70].

Once the electrical potential exceeds the overpotential of the membrane material, occurrence of electrochemical reactions including water electrolysis promotes generation of gas bubbles which contributes to antifouling performance of the membrane. Lalia et al. [42] challenged a CNT/PVDF membrane with a yeast suspension for 4 h. They observed that with intervals of cathodic electrolysis (2V) for 2-3 min per hour, the permeate flux regained 35% of the original flux (Figure 3.2.a). They attributed the improved flux to hydrogen gas generation as it was theoretically activated at potentials above 0.5 V. Our meta-analysis indicate that the electrostatic repulsive force also contributed to the performance of the ECMs regarding the negative charge of yeast particles, however, foulant characterization data was not provided in the study [42].

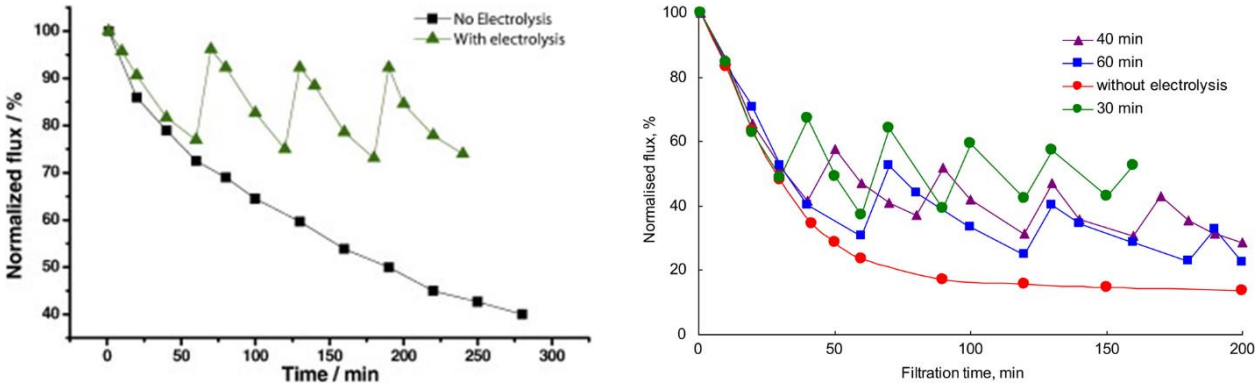

Figure 3.2. Normalized flux versus time during filtration of yeast, (Left): 2-3 min electrolysis (2 V cathodic potential, 2-3 min) every hour on CNT/PVDF membrane, black and green lines represent no electrolysis, and with electrolysis, respectively. Reprinted from [42], Copyright 2015, with permission from Elsevier. (Right): 30 s electrolysis (2 V cathodic potential) after biofiltration intervals of 30 min (green), 40 min (purple), and 60 min (blue) on MWCNT/PVDF membrane coated with Silver lines. Red line represents the control experiment (absence of electrical potential). Reprinted from [43], Copyright 2014, with permission from Elsevier.

Hashaikeh et al. [43] assessed the electrochemical cleaning performance of a CNT/PVA membrane with yeast and $CaCO_3$ suspension over 200 min. The membrane was cleaned by 3 min electrolysis with a 2 V cathodic potential at different time intervals (30, 40, or 60 min). Without electrochemical cleaning, the permeate flux dropped to 15% of the original flux. In contrast, with a cathodic potential applied every 30 min, the permeate flux regained 20% of its original flux after each cycle on average (Figure 3.2.b). The formation of hydrogen micro-bubbles at the cathode was assumed to explain the self-cleaning efficiency of ECMs.

More recently, a Ni metalized hollow fiber membrane was employed to challenge the formation of yeast biofilm under application of cathodic current ($100\ mA/cm^2 \approx 2\ V$) [44]. In their experiment, the membrane was fouled with yeast suspension over 15 min consecutive cycles with 3 s of electrochemical cleaning in between. Enhanced transmembrane pressure (TMP) recovery up to 60% was achieved by electrolysis compared to no electrochemical cleaning, and hydrogen gas evolution was assumed as the primary self-cleaning mechanism in their research.

In another study, using cathodic potential of 2.5 V across conductive PES-LIG membranes resulted in 6-log reduction of *Pseudomonas aeruginosa* [41]. The results indicated high H_2O_2 generation up to 2.8 mg/L under the cathodic potentials applied (1.5-2.5 V). They attributed the anti-biofouling performance of LIG surface to a combination of physical (wettability and surface charge), chemical (H_2O_2 generation), and biological (antimicrobial 3D texture) properties of LIG surfaces.

Ahmed et al. [45] synthesized a conductive RO membrane composed of PVA, networked cellulose, and CNTs and observed improved antifouling performance under the application of 5 V cathodic potential for 20 min. Electrolysis and hydrogen gas generation were suggested as governing antifouling mechanisms. Although it has not been suggested in their study, it is likely that electrostatic repulsive force between negatively charged yeast particles and the cathodic polarized electrode further contributed to antifouling performance.

Based on our metanalysis, other mechanisms such as high local pH (> 9) can be accounted for advanced anti-biofouling performance of cathodic surfaces next to electrostatic repulsion, hydrogen gas evolution, and hydrogen peroxide generation. It is worthy to note that often a combination of antifouling mechanisms lead to advanced membrane properties with a mechanism being more dominant at a certain potential range. Based on our meta-analysis, electrostatic repulsion is more dominant at low potentials (< 2 V), while high rates of gas generation are more potent at higher potentials (> 2 V).

Alternating potential

Many ECM studies targeting biofouling have used alternating current (AC) instead of direct current (DC), which takes advantage of both anodic and cathodic polarization antifouling mechanisms. In addition to the magnitude of the applied potential, the frequency of the applied current in AC mode also impacts the antifouling mechanisms, biofilm behavior, and membrane performance. Antifouling mechanisms involve interfacial phenomena such as electron transfer, ion diffusion, and electrochemical reactions. These phenomena co-occur at the surface with different response times. Therefore, frequencies

higher than the mechanism response time prevents the occurrence of the mechanism. For instance, potentials above 1 V can cause water splitting, gas generation, or formation of active chlorine [71,72]. These mechanisms readily occur in DC or low-frequency AC modes, while they become restricted in the KHz range (4-20 kHz) for water dissociation (gas generation, pH modification, ROS generation), and above 50 Hz for chlorine formation [73]. Some researchers have explored the impact of tunning parameters (frequency, duty ratio) to identify the optimal application of AC.

In so doing, many studies have induced low frequency AC (mHz-Hz) to a) allow for the electrochemically reactions to occur at the surface (water electrolysis, chlorine formation), and b) take advantage of a combination of mechanisms promoted by anodic and cathodic polarizations. In a study, AC current (1.5 V square wave, 16.7 mHz) was applied to control the irreversible biofouling of *Pseudomonas aeruginosa* on NF membranes [46]. ECMs under AC current experienced a 45% reduction in the flux over 150 h, while an 80% flux reduction was observed in the control experiment (ECM with no current applied) (Figure 3.3). In addition, 1 min cross-flow chemical-free flushing resulted in 92% to 100% flux recovery while the same flushing procedure on control ECMs led to no recovery. The authors hypothesized that pH instabilities and the changes in osmotic pressure at the biofilm resulting from varying EDL thickness were the primary reasons for findings under AC current.

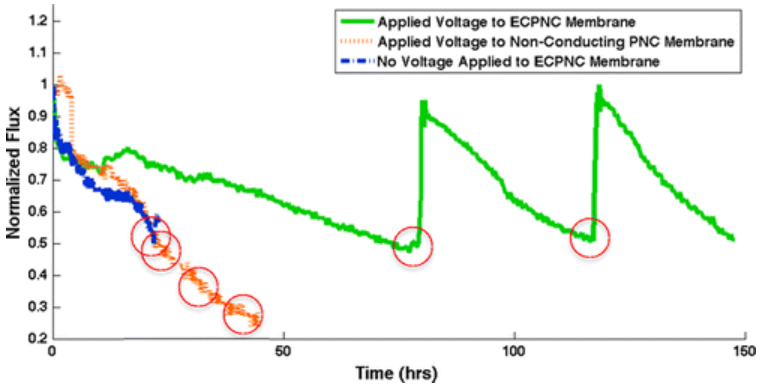

Figure 3.3. Normalized flux versus time during *Pseudomonas aeruginosa* filtration with and without application of electrical current on electrically conductive membranes (ECMs). Green, orange, and blue lines represent using electrochemical cleaning on ECMs, using

electrochemical cleaning on non-conductive membranes, and absence of electrical field on ECMs, respectively. Red circles represent flush treatments. Reprinted with permission from [46]. Copyright 2013 American Chemical Society.

Baek et al. [31] indicated that 30 min application of alternating potential (1 V, 16.7 mHz) after 24 h *Pseudomonas aeruginosa* filtration in a RO module could recover the permeate flux to 91%. In contrast, in the control experiment, the flux was dropped to 47% (Figure 3.4). They proposed that electrostatic repulsive force and translational motion governed the advanced bacterial detachment rate under cathodic and anodic polarization, respectively.

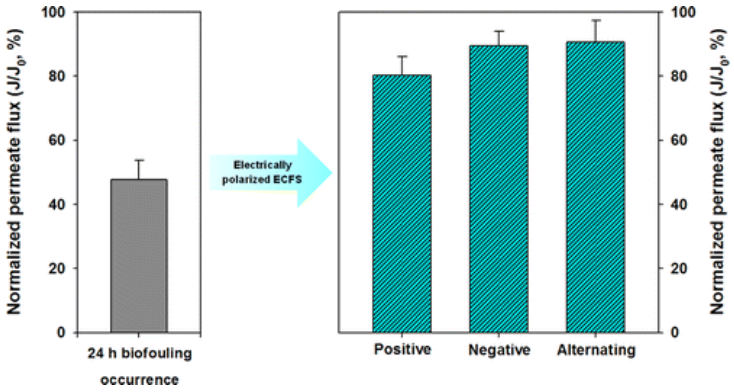

Figure 3.4. Permeate flux recovery by 30 min electrolysis using positive potential (1 V), negative potential (1 V), or alternating potential (1 V, 16.7 mHz) after 24-hour biofiltration of *Pseudomonas aeruginosa* using Ti as conductive feed spacer in a RO process. Reprinted with permission from [31]. Copyright 2014 American Chemical Society.

In one of the early studies in the field, Shim et al. [47] presented an indium tin oxide (ITO) film at which they applied cathodic and anodic DC mode (7.5-15.0 μA/cm^2 ≈ 2.0 – 2.7 V), as well as AC mode (15 μA/cm^2 ≈ 2.7 V, 16.7 mHz) to study the formation of *Pseudomonas aeruginosa* biofilm. They obtained 81%, 73%, and 19% bacterial detachment in response to cathodic, alternating, and anodic current over 90 min. They also noticed that cell detachment increased with increasing current intensity under cathodic current while no correlation was observed under anodic current. In the context of cell inactivation, surprisingly, only AC caused significant inactivation (58%) as compared to 4% cell inactivation for positive and negative currents. The impact of oxidants such as hydrogen peroxide and hydroxyl radical on the biofilm was studied separately and found

insufficient for bacterial inactivation. The low inactivation ratio under anodic current was not explained in their study. However, high detachment ratio under cathodic DC and AC was attributed to electrostatic repulsive force.

Hong et al. [33] investigated the impact of AC current on indium tin oxide (ITO) biofouling with *Pseudomonas aeruginosa*. AC current ($15\ \mu A/cm^2 \approx 0.5 - 2.4\ V$, 16.7 mHz) resulted in 10% adhered bacteria, while above 80% of bacterial particles adhered on ITO under no current. They considered the electrostatic and electrophoretic repulsive force to be the dominant mechanisms for less adhered bacteria. The adhesion rate under AC was examined at different exchange time intervals (1.67-1000 mHz), and it turned out that intervals of 16.7 mHz or smaller are necessary to promote antifouling mechanisms such as electrostatic and electroosmotic forces (Figure 3.5). Bacterial viability study was performed with live/dead staining microscopy which revealed that anodic current could cause cell lysis under the range of current applied while no significant cell lysis was observed under cathodic current (Figure 3.5).

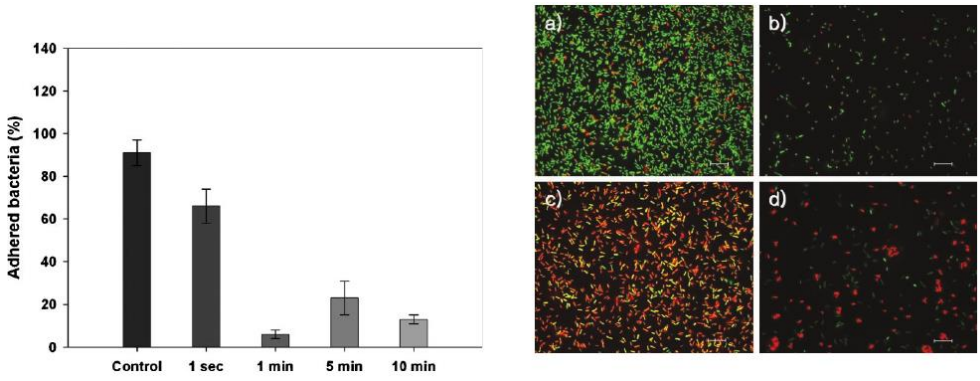

Figure 3.5. (Left): bacterial attachment versus block current exchange time intervals of 1 s, 1 min, 5 min, and 10 min (equivalent frequencies of 1 Hz, 16.7 mHz, 3.30 mHz, and 1.67 mHz) during 40 min of *Pseudomonas aeruginosa* filtration. In the control experiment, no current was applied. (Right): Dead/live staining images after 40 min of biofiltration (a) No current, (b) cathodic current ($15\ \mu A/cm^2 \approx 0.5 - 2.4\ V$) (c) anodic current ($15\ \mu A/cm^2 \approx 0.5 - 2.4\ V$), (d) alternating block current ($15\ \mu A/cm^2 \approx 0.5 - 2.4\ V$, 1 min interval (equivalent frequency of 16.7 mHz). Damaged cells were detected by red color in propidium iodide (PI)/SYTO 9 ™ assay kit and were assumed dead. Intact cells were detected by green color and assumed live. Reproduced with permission from [33].

Zhou et al. [50] applied cathodic DC (60 μA ≈ 25 MV/m) and AC (60 μA ≈ 5 MV/m , 60 Hz) modes to investigate colonization of Staphylococcus aureus on polyaniline-silver nanoparticles-polysulfone membrane over 24 h biofiltration. In their study, they studied the effect of cathodic and alternating current, demonstrating that AC was more effective (6 log removal) than cathodic current (4 log removal) in preventing bacterial colonization. They hypothesized that cathodic current kept the bacteria away from the membrane through electrostatic repulsive force. In AC mode, they suggested AC-induced particle vibration in the gel layer and periodic ion oscillation produced an unstable zone for bacterial attachment.

From our meta-analysis, it seems that low-frequency AC currents are preferred over DC and high-frequency AC for anti-biofouling applications. AC current provides the ECM with a combination of anodic- and cathodic-induced mechanisms as compared to DC. In addition, low frequencies allow for indirect oxidation, pH change, and gas generation as compared to high frequencies. Low frequencies also allow the microorganisms to react to the electrostatic and electroosmosis forces. A few studies have applied a wide range of frequencies (Hz-MHz) to compare the anti-biofouling performance of AC on ECMs.

Thamaraiselvan and his colleagues investigated the effect of the direct and alternating current on *Pseudomonas putida* biofilm inhibition [48]. Cathodic and anodic potentials (0.6-3.0 V) and alternating potential (0.3-6.0 V, 10-10,000 Hz) were applied on a self-supporting CNT membrane over 72 h. They realized that AC could outperform both anodic and cathodic currents in terms of bacterial detachment and inactivation. The bacterial detachment and inactivation rate had an inverse relationship with the current frequency with the highest rates observed at 10-100 Hz. Increasing the magnitude of the electrical field in AC mode from 1.0 V to 6.0 V led to significant bacterial inactivation, i.e., 6% to 82%. Although the DC mode followed the same trend in higher potentials applied, the detachment and inactivation rates were lower as compared to AC mode. The superior performance of AC mode was due to the synergy between electrostatic repulsion and electrical oxidation. For instance, AC mode under 1.5 V, 1 kHz caused more than 98.5% and 95% bacterial attachment inhibition and inactivation, respectively. They suggested

electroporation and direct oxidation as the primary mechanisms responsible for inactivation. They ruled out a major contribution of indirect oxidation (hydroxyl radical, active chlorine) as AC disfavored hydroxyl radical and active chlorine generation in kHz range and >50 Hz frequencies, respectively. They calculated the interface forces including electrostatic force, cross-flow lift force, permeation drag force, and van der Waals force. They reported that under negative potential (0.5-3.0 V), net repulsive forces (0.85-1 nN) dominate the net attractive force (~10^{-3} nN).

Perez-Roa et al. investigated the impact of frequency (200 Hz, 10,000 Hz), magnitude (0.5 V, 5.0 V), and duty ratio, defined as the fraction of one period in which the potential is applied (1%, 50%), of the voltage on the development and inhibition of *Pseudomonas aeruginosa* biofilms on interdigitated electrodes [49]. Their results revealed that a combination of 5.0 V, 200 Hz, and 1% duty ratio led to the least biofilm coverage over the period of filtration (13 h). They claimed that 0.5 V was not able to induce electrolysis or radical generation as water dissociation occurs at 1.229 V and chlorine gas generation happens at potentials above 1.358 V. In addition, water dissociation readily occurs under DC and low-frequency AC. In their study, bubble formation was only observed at 200 Hz as proof of electrolysis. It has been demonstrated that higher AC frequencies between 4,000 and 20,000 Hz reduce the chance of water dissociation and electrolysis. They also suggested that local instabilities such as pH variation under AC disrupt the cell adhesion process. Under 1% duty ratio, no correlation was observed between cell viability and surface coverage, while the 50% duty ratio caused cell lysis for adsorbed bacteria.

Liu et al. [39] employed a nano-sponge filtration system made of polyurethane sponge coated with CNTs and silver nanowires to disinfect bacteria and viruses. Their setup applied external AC in a range of 0-20 V. Antifouling mechanisms showed different response times with respect to the external potential. Electrochemical reactions for instance, became less likely to happen at high frequencies. Under the application of 10 V, the removal efficiency of *E. Coli* was investigated by varying the frequency from 10 mHz to 100 MHz. The maximum removal efficiency was observed at 10 mHz to 100 Hz

(99.9999%), while the removal rate was maintained at 99.99% in the range of 100 Hz to 100 MHz, ruling out a major contribution of electrochemical reactions (Figure 3.6). They cultivated the already electroporated bacteria in agar plates and noticed that damaged *Enterococcus faecalis* under had the ability to partially repair the wall pores and reproduce under a nutrient-rich environment suggesting reversible electroporation. They also suggested that silver nanoparticles contribute to removal efficiency of bacteria due to their inherent biocidal activity and enhanced chemical uptake potential of electroporated bacteria.

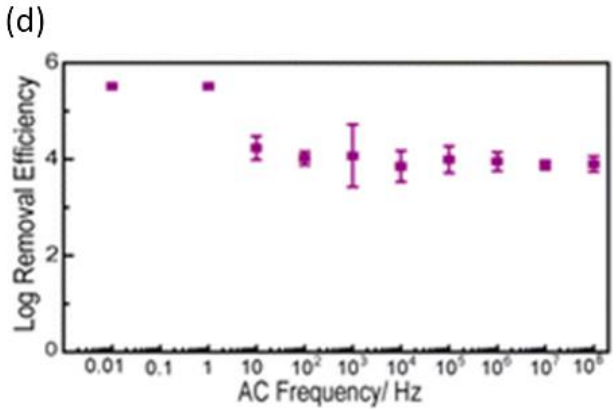

Figure 3.6. Removal efficiency of *E. Coli* under 10 V versus different frequencies. Adapted with permission from [39]. Copyright 2013 American Chemical Society.

As discussed, our analysis has shown that low frequencies are preferred in biofouling applications, however, other important factors should be considered in optimizing the frequency in AC mode for other applications. For instance, we expect that the response time to electrostatic and electroosmosis forces is much shorter for lower-sized particles such as ions as compared to larger-sized bacteria, therefore, higher range of frequencies can be used for antiscaling applications. In addition, it has been shown that AC current can minimize the destructive impact of anodic current on electrode material, more particularly on carbonaceous material. Therefore, the membrane life should also be considered when designing the current pattern for ECM applications.

3.3.2. Organic fouling

Organic matter that causes fouling is the sticky foulants that deposit on membrane surfaces during pressurized filtration. The degree of organic fouling on the ECMs may be impacted by membrane surface energy, the feed solution characteristics, and operating conditions. In this section, the discussion focuses on the fouling prevention and control performance of ECMs by applying various current patterns. A summary of research on ECMs focused on organic matter fouling is presented in Table 3.2.

Table 3.2. Summary of published ECM studies targeting organic matter.

Antifouling Mechanisms	Materials	Foulants	Charge of Foulants	Concentration (ppm)	Current or Voltage Patterns & Application Time	Results	Reference
				Anodic potential			
Direct oxidation	Bismuth-doped tin oxide-coated CNT	Oxalate Formaldehyde Formate MeOH EtOH	/	100 11 20 5 7	1-60 mA (0.1-6.3 V) for 20 min	TOC removals were 2-8 times greater, current efficiencies were 1.5-3.5 times greater, and energy consumption 4-5 times less than the uncoated CNT.	[74]
Direct oxidation	CNTs/Ceramic	Humic Acid	/	10	1 V 60 min	Flux was 1.1 times higher. The TOC removal efficiency was 71%.	[75]
Direct oxidation (antimicrobial activity)	CNT/PTFE	Tetracycline (TC)	/	89	0-3 V	TC oxidative flux increased with increasing total cell potential to a maximum at 2.5 V.	[76]
Direct oxidation	CNT/Al_2O_3	Phenol	/	5	0.5-1.5 V 30 min	Phenol removal was <20% (0 V), 38% (0.5 V), 100% (1-1.5 V).	[77]
Direct oxidation	CNT/Al_2O_3	Humic Acid	/	10	0.5-1.5 V 60 min	1.6-fold enhancement in flux and 3-fold improvement in HA removal at 1.5 V.	[77]
Direct oxidation	Ti_5O_9/Ti_4O_7	Paracetamol (PCT)	/	15 – 347	4 - 6.5 V (6 – 30 mA/cm^2) 90 min	6.7 g m^{-2} h^{-1} TOC removal rate and 47% mineralization with a single passage.	[78]
Direct oxidation /indirect oxidation	Ti_5O_9/Ti_4O_7	Oxalic acid (OA)	/	94.5 – 4536	4 - 6.5 V (6 – 30 mA/cm^2) 120 min	47 g m^{-2} h^{-1} TOC removal rate and 72% mineralization with a single passage.	[78]
Direct oxidation /indirect oxidation	CNT/PTFE	Ibuprofen	/	20	0-3 V	Near complete removal of ibuprofen was achieved at 2-3 V.	[79]
Direct oxidation /indirect oxidation	Sb-doped SnO_2-coated coal-based carbon	Tetracycline (TC)	/	50	3 V 6 h	The TC removal rate of Sb-SnO_2/CM was 96.5% after 6 h.	[80]
Direct oxidation /indirect oxidation	CNT/PTFE	Methyl orange (MO)	/	98	0-1.4 V (vs SCE)	Direct oxidation was the predominant mechanism. Indirect oxidation contributed at >1.0 V.	[81]
Direct oxidation /indirect oxidation	MWCNT - PTFE Boron-doped MWCNT-PTFE	Bisphenol A (BPA)	/	1	0-3 V	Complete removal at 2 and 3 V. Increasing residence time (2 to 14.9 s) increased the removal by 7.4-fold. Bisphenol A has no fouling effects.	[82]
Indirect oxidation	TiO_2-coated carbon	Tetracycline (TC)	/	50	0.5 – 2.5 mA/cm^2 10 h (residence time of 0.22-8.8 min)	TC removal (100%) and COD removal (75%) at 0.5 mA/cm^2. COD removal rate was 91% at 2 mA/cm^2.	[83]
Indirect oxidation	CNT/PTFE	Phenol	/	94	0.2-3.5 V 6 h	≥2.1V prevented phenol polymerization.	[84]
Indirect oxidation	CNF/forward osmosis PES	Phenol	/	470	0-3 V 24 h	>92% phenol removal at 2.5 V.	[85]
Indirect oxidation	Undoped B-doped N-doped CNT/PTFE	Phenol	/	19 or 94	0.5-3 V 270 min	Similar phenol removal with all CNT networks at 1.6 V. B-CNT more resistant toward anodic passivation.	[86]

Indirect oxidation	CNT-EO-PTFE CNT-HNO_3-PTFE Fresh-CNT-PTFE	Phenol Oxalate	/	94 128	1.6 V 3 h	Phenol and oxalate mineralization were 4-fold and 2-fold greater for CNT–EO, and unmodified CNT as compared to CNT–HNO_3, respectively.	[87]
Electrophoretic mobility	Al_2O_3 modified with Magnéli Ti_4O_7 inner layer	Humic acid (HA)	-44.4 mV	200	30-40 V (10 mA) for 60 min	Flux maintenance was 97% and 66% under 30 V and 0 V, respectively. HA removal was increased from 2% to 96% under 0 V and 30 V, respectively.	[88]
Electrophoretic mobility	Al_2O_3 modified with Magnéli Ti_4O_7 inner layer	Bovine serum albumin (BSA)	-17.9 mV	200	30-40 V (10 mA) for 60 min	Flux maintenance was increased from 41% (0 V) to 87% (30 V). HA removal was increased from 2% (0 V) to 96% (30 V).	[88]
			Cathodic potential				
Electrostatic repulsion	DBSA doped polyaniline (PANI)	BSA	-	1000	0 ~ 1 V	Increasing the potential from 0 V to 1 V lead to enhanced fouling mitigation with 40% reduction in flux after 30 mL filtration.	[89]
Electrostatic repulsion	CNTs/Ceramic	Humic Acid	/	10	1 V 60 min	Flux was 1.4 times higher. The TOC removal efficiency was 62%.	[75]
Electrostatic repulsion	CNT-PVDF/PES UF	Fulvic acid Sodium alginate Polyacrylic acid PEG	-7.1 meq g/C -13.9 meq g/C -7.50 meq g/C Neutral	10	2 V 1-9 hr	High rejection for PAA (97%) and SRFA (73%) and low rejection for PEG (18%).	[90]
Electrostatic repulsion	CNT/PVA	Decanted reactor effluent	/	/	0, 3, 5 V 5 h 1.5 V anode during backflush	The pressure was increased from 1.5 psi to 3.1 psi (0 V), 2.4 psi (3 V), and 2.2 psi (5 V). Anodic current during the backflushing contributes to fouling formation.	[91]
Electrostatic repulsion	CNT/PVA NF	Post-UF effluent	/	/	0, 5 V 5 h +1.5 V anode during backflush	Applied potential has no obvious impact on NF fouling.	[91]
Electrostatic repulsion	PVA-CNT/PS (polysulfone)	Alginic acid	-68.1 mV for AA	5000	3V or 5 V 100 min	The pressure was decreased by 33% (3V) and 51% (5 V).	[92]
Electrostatic repulsion (hydrogen gas)	CNT/PVDF	Sodium alginate BSA Humic acid	/	15 4 8	0-2 V Filtration/cleaning:1 h/5 min	Lower increase in TMP with electrolysis. Pulsed 0 V/2 V led to the best antifouling performance.	[93]
Hydrogen gas	Pyrolytic graphite	Bovine serum albumin (BSA)	/	10-20	1.5 V 20 to 50 s	20 s electrolysis decreased protein coverage by 26-34%. BSA removal was 82-100% after 50 s electrolysis.	[94]
Hydrogen gas	SWCNT embedded epoxy	Bovine serum albumin (BSA)	/	2000	2 V 10 min	Defouling efficiency was 85% (first cycle) and 60% (second cycle) at 2 V.	[95]
Hydrogen gas	PVA-NC (networked cellulose)-CNS	Humic acid	/	500	5 V (~3.75 mA/cm^2) 20 min	Fouled membrane was recovered via electrolytic self-cleaning.	[45]
Indirect oxidation	Ceramic with build-in Ti mesh	Sodium alginate	/	50	1, 2, 3 V 2 min	Lowest membrane fouling at 3 V.	[64]
			Alternating potential				
Electrostatic repulsion (direct oxidation)	CNTs/Ceramic	Humic Acid	/	10	± 1 V with pulse width of 60 s 60 min	Flux was 1.5 times higher. The TOC removal efficiency was 76%.	[75]
Electrostatic repulsion (hydrogen gas)	CNT/PVDF	Sodium alginate BSA Humic acid	/	15 4 8	Pulsed 0 V/1-2 V with 5 s interval Filtration/cleaning:1 h/5 min	Lower increase in TMP with electrolysis.	[93]

Anodic potential

The integration of membrane filtration with the electrochemical oxidation process creates a hybrid technology known as electrochemical filtration, which has shown great

potential to treat organic contaminants in effluents. The electrochemical filtration membrane serves as both a separation membrane and an active anode that can effectively degrade contaminants by electrochemical oxidation. Most of the ECM research that used anodic potentials targeted oxidation of organic molecules rather than fouling prevention. Fouling degradation is a possible pathway to serve organic fouling mitigation in ECMs. A full discussion of electrochemical oxidation of organics is outside the scope of this review. Instead, this section will review only those papers that investigated fouling recovery by the application of anodic potentials, which may have also contributed to organic molecule oxidation.

Direct electron transfer or reactive oxygen species-mediated indirect degradation are the main mechanisms used for removal of organic compounds under anodic polarization. At potential below surface over potential, direct oxidation by electrons is the dominant mechanism, while above surface over potential, electrochemical reactions become the primary contributor to organic removal. Higher anodic potential typically leads to higher removal rate (due to faster electron transfer and contribution of electrochemical reactions), however, it is at the cost of surface material deterioration that in turn reduces the current efficacy and organic removal over long filtration periods. Furthermore, a few studies have pointed out that gas generation, promoted by electrochemical reactions, hinders the permeate flux and challenges easy contacts of organic compounds with the surface. Many studies have quantified the removal efficiency of organics under anodic potentials and discussed the primary mechanisms.

Quan et al. [77] achieved 38.2% removal at a potential of +0.5 V, and complete removal at a potential of either + 1.0 V or +1.5 V using the CNTs/Al_2O_3 membrane for phenol remediation. Because of the overpotential of +0.6 V for phenol oxidation on the CNTs/Al_2O_3 membrane, electrooxidation and adsorption were responsible for high removal efficiency at +1.0 V or +1.5 V. They revealed that phenol was converted to benzoquinone at +1.0 V and the complete mineralization of phenol to CO_2 was achieved at + 1.5 V. Additionally, 87.7% of humic acid (HA) removal efficiency and a 92.6% increase in permeate flux for the CNTs/Al_2O_3 membrane were attained at an anodic potential of +1.5

V. The removal of HA was mainly dominated by electrochemical oxidation due to the overpotential of +0.5 V for HA oxidation on the CNTs/Al_2O_3 membrane.

Vecitis et al. [74] fabricated a bismuth-doped tin oxide (BTO)-coated CNT anode for oxalate oxidation. Compared to an uncoated CNT anode with an oxygen evolution potential (OEP) of +1.27 V and the corrosion potential of +1.4 V, BTO-CNT anode possesses a higher OEP of +1.71 V and anodic stability up to a potential of +2.2 V. Due to increased conductivity, OEP and electrochemical stability for the BTO-CNT anode, they achieved 98% oxalate oxidation with a residence time of 1.2 s under application of +3 V. The advanced investigation of electro-oxidative removal of ethanol, methanol, formaldehyde, and formate was further carried out on BTO-CNT anode and it demonstrated to have TOC removals 2 to 8 times greater, mineralization current efficiencies 1.5 to 3.5 times greater, and energy consumption 4 to 5 times less than the uncoated CNT anode.

In another study, Vecitis et al. [76] investigated the efficacy of CNT filters for Tetracycline (TC) oxidation as a function of total cell potentials and cathode materials in an electrochemical filtration system. The feed solution passed through either a perforated Ti cathode or a CNT network cathode, followed by a PTEF membrane to separate the electrodes, and finally a CNT network anode (Figure 3.7a). Figure 3.7b showed that the TC oxidative flux increased with increasing total cell potential up to 2.5 V, regardless of cathode materials. As the cell potential was positive than 2.5 V, oxygen generation led to the blockage of CNT pores and even CNT filter oxidation, deteriorating the performance of the electroactive CNT filter. Additionally, the oxidation flux for a CNT cathode was 2.3 times higher than that for a Ti cathode at an anodic potential of 1.0 V. They attributed the improved performance to electrocatalysis of CNT (water reduction), facilitating the fraction of the total cell potential towards the TC oxidation, and larger surface area of CNT with lower charge transfer resistance in the cathode, in turn increasing the anode potential and the extent of electrooxidation.

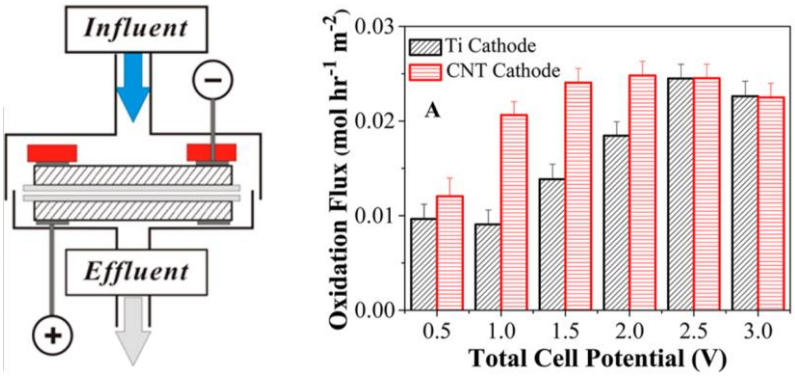

Figure 3.7. (a) Schematic of apparatus for electrochemical filtration of 0.2 mM tetracycline (TC) using a CNT filter as the anode; (b) TC oxidative flux as a function of total cell potential and cathode potential. Reproduced from. Reprinted with permission from [76]. Copyright 2015 American Chemical Society.

Trellu et al. [78] used anodic oxidation to mineralize paracetamol (PCT) and oxalic acid (OA) using sub-stoichiometric titanium oxide (TiO_x) reactive electrochemical membranes (REM). PCT mineralization was caused by OH• mediated oxidation in the top layer of the REM. Deeper into the membrane (at a depth of 23 nm), potential dramatically dropped in a cylindrical pore and reached a value below the overpotential to produce OH•, where direct electron transfer dominates. The electropolymerization of PCT and the presence of organic compounds refractory to direct electron transfer led to the accumulation of insoluble polymers (membrane fouling) and pore blockage. To decrease the membrane passivation, PCT was first exposed to ring cleavage mediated by OH• to form short-chain carboxylic acids highly reactive to electron transfer (Figure 3.8). Then, carboxylic acid experienced full mineralization under direct electron transfer. Similarly, the mechanism for OA (short-chain carboxylic acid) mineralization is direct electron transfer.

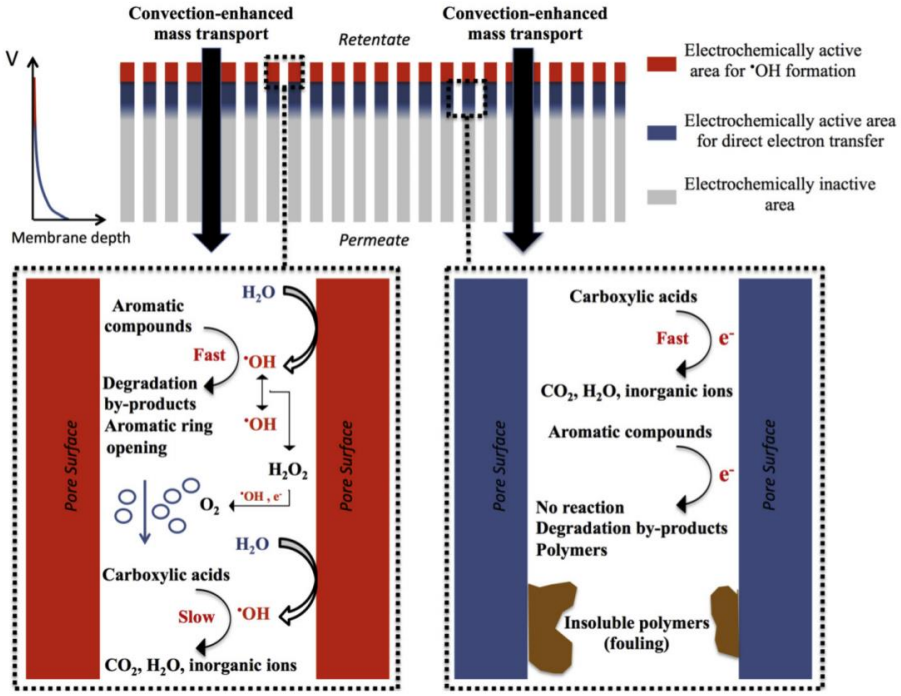

Figure 3.8. Scheme of electrooxidation mechanisms of organic contaminants in the reactive electrochemical membrane (sub-stoichiometric titanium oxide) as a function of the depth of the membrane. Reprinted from [78], Copyright 2018, with permission from Elsevier.

Ibuprofen and tetracycline (TC) are the typical antibiotics in wastewater treatment plant effluents that have adverse effects on natural water bodies and the potential to increase pathogen resistance. Anodic oxidation has been extensively studied for removal and inactivation of antibiotics using an electrochemical filter. Rahaman et al. [79] achieved efficient removal of ibuprofen using carboxylated CNT modified membranes (MWNTs-COOH) through physical adsorption by surface interaction between carboxyl groups of prepared membranes and ibuprofen, as well as electrooxidation by production of electroactive species. In a dead-end electrochemical cell, at an applied DC potential of +2 V (corresponding to an anodic potential of +0.9 V), 82.4% removal of ibuprofen was achieved. With the direct oxidation potential for ibuprofen (1.13 V vs. Ag/AgCl), it is impossible to initiate the direct electron transfer on the MWNTs-COOH anode at +2 V of applied potential. Instead, the formation of superoxide anion contributed to an indirect degradation reaction of ibuprofen. When the applied potential was risen to 3 V (corresponding to an anodic potential of +1.72 V), near 100% removal of the target

molecule was achieved under the same conditions. The higher reaction kinetic for ibuprofen oxidation at 3 V was attributed to synergistic effects of direct oxidation and indirect oxidation, i.e. the increased formation of reactive species (superoxide and hypochlorous acid).

Zhu et al. [80] prepared a novel membrane anode by coating nano antimony-doped tin dioxide (Sb-SnO_2) on a porous coal-based carbon membrane (CM). Compared to the oxygen evolution potential (OEP) of 1.31 V (vs. Ag/AgCl) for CM, a higher oxygen evolution potential (OEP) of 1.58 V (vs. Ag/AgCl) for Sb-SnO_2/CM reduced the competition between oxygen generation and the target molecule (TC) oxidation. Thus, Sb-SnO_2/CM exhibited excellent electrocatalytic activity and improved tetracycline (TC) degradation efficiency. They achieved 96.5% and 72.8% of TC removal rate for Sb-SnO_2/CM and CM, respectively, over 6 h operation at an anodic potential of 3 V. Complete degradation of TC to carbon dioxide was caused by synergistic effects of direct electron transfer and production of OH• radicals, as illustrated in Figure 3.9.

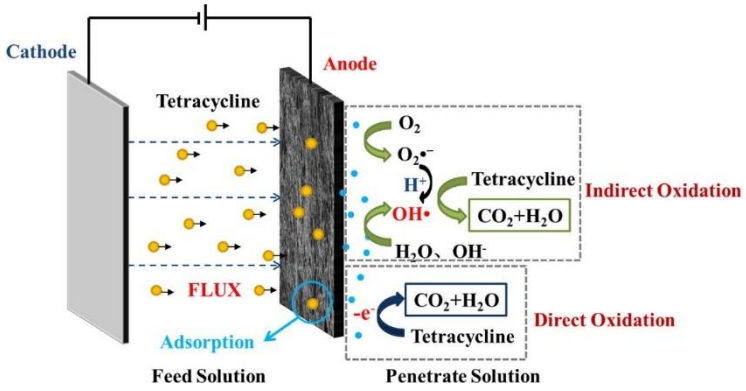

Figure 3.9. Organic removal using ECMs. Schematic of electrochemical membrane filtration showing the effects of direct and indirect oxidation of tetracyline at an electrically conductive membrane used as an anode. Reprinted from [80], Copyright 2017, with permission from Elsevier.

The mechanism for MO oxidation using a CNT filter anode was illustrated by Vecitis et al. [81]. The initial oxidation of MO at an anodic potential up to 1.0 V (vs. SCE) is due to direct electron transfer, Reaction 1. Once the anode potential increases to >1.0 V, oxygen produced from water electrolysis, Reaction 2, immediately reacts with carbon

radicals to form ROS (i.e., peroxy radicals) that indirectly oxidizes MO. In this case, both indirect and direct oxidation accounts for MO removal. Another indirect pathway may occur when Cl^- is oxidized to Cl_2 at an anode potential >1.2 V.

$$MO^- + nh^+ - CNT \rightarrow MO_{OX}(-nh^+) + CNT \quad (1)$$

$$H_2O \rightarrow 4H^+ + O_2 + 4e^- \quad (2)$$

Bisphenol A (BPA) is used for manufacturing chemical products including adhesives, plastic, powder paints, paper coating, and epoxy resin. Human exposure to such a harmful chemical is likely to cause hazardous health effects. Rahaman and his colleagues [82] explored the removal efficacy of bisphenol A using boron-doped CNT (BMWNTs) filters and provided insight into the possible degradation pathways. The anode potentials corresponding to applied anodic potential of 2 V and 3 V were measured to be 0.79 V and 1.57 V (vs. Ag/AgCl), respectively for BMWNTs. The fast degradation rate of BPA was achieved at applied potentials due to low BPA oxidation potential (0.5 V- 0.9 V) on electrochemical BMWNTs filters. The primary mechanism for BPA degradation is direct oxidation through electron transfer at moderately applied potentials (< 2 V) as compared to the dominant participation of superoxide anions ($O_2^{\bullet}$) at a higher anodic potential of 3 V. BPA is initially oxidized through an attack by superoxides on the aromatic rings and isopropyledene bridge cleavage, generating one-ring hydroxylated phenolic derivatives. The complete mineralization of BPA is achieved by the further degradation of the phenolic intermediates to non-toxic aliphatic products due to aromatic ring cleavage. The absence of polymeric passivation effect of BPA on BMWNTs was observed, suggesting the unstable of polymeric intermediates and the fast reaction kinetics during the electro-filtration process. Additionally, residence time is a dominant parameter to improve the participation of direct electron transfer due to its slower kinetics than indirect oxidation pathway. As a result, increasing residence time (from 2 to 14.9 s) by 7.4-fold led to ~100% degradation of BPA and significant removal of its aliphatic by-products at an anodic potential of 3 V.

Zhu et al. [83] prepared a novel nano-TiO_2/carbon electrocatalytic membrane for TC removal. TiO_2 could be excited to generate reactive intermediates such as $OH^{\bullet}$, $O_2^{\bullet-}$ and $HO_2\bullet$, which can decompose the organics located on the membrane and exhibit high stability for TC degradation. 100% removal of TC and 75% removal of COD were achieved in the permeate stream with the anodic current density of 0.5 mA/cm^2. As current density rose to 2 mA/cm^2, the maximum COD removal rate (91%) was reached, where abundant superoxides were beneficial for complete TC mineralization. However, the decline in COD removal rate at a current density of 2.5 mA/cm^2 resulted from water hydrolysis that hindered an easy contact of organics with the electrocatalytic membrane.

A simple aromatic pollutant, phenol, is commonly present in effluent released from chemical and biological water treatment plants. Vecitis et al. [84] revealed the CNT anode was susceptible to oxidative polymerization and electrode passivation for phenol removal in the electrochemical flow-through filtration. To avoid phenol polymerization and maintain electrode lifetimes, the application of an anode potential ≥2.1V for complete phenol mineralization was required.

Xie et al. [85] achieved >92% removal of phenolic compounds on the CNF-embedded FO membrane at an anodic potential of 2.5 V. The higher voltage led to a greater removal efficiency. However, the removal of phenol slightly decreased beyond 3 V due to water electrolysis. The generation of gas bubbles blocked the electroactive sites on the CNT-FO membrane, leading to adverse effects on phenol oxidation and membrane water flux.

Vecitis et al. [86] investigated the impacts of CNT doping on the electrochemical oxidative performance to remediate phenol. Boron-doped (B-CNT), and nitrogen-doped (N-CNT) carbon nanotube networks were reported to possess higher conductivity and thus improve the electrochemical activity of CNT anodes compared to the undoped CNT. All three doping CNT networks removed a similar amount of phenol at an anodic potential of 1.6 V. However, B-CNT anode was more desirable as it showed the most resistance to electrode passivation and electrolyte participation. The absence of passivation for B-CNT

could be attributed to its relatively higher work function (corresponds to the Fermi level redox potential) leading to a greater extent of phenol oxidation.

Gao et al. [87] produced CNT filters with specific surface oxy-functional groups to investigate how the CNT groups affected the inner electrooxidation kinetics for phenol and oxalate mineralization. As compared to unmodified CNT anode (fresh-CNT), the oxidative performance of CNT synthesized via anodic oxidation (CNT-EO, enriched -COH) was increased by 2-fold and the CNT synthesized via nitric acid (CNT-HNO_3, enriched -COOH) was decreased by 2-fold for phenol mineralization over 180 min of continued single-pass filtration at an anodic potential of +1.6 V (vs. Ag/AgCl). A similar trend was observed for oxalate mineralization. CNT-EO contains more -COH and thus electroactive sites since -COH can produce twice as many defect sites as -COOH under a similar O/C ratio. CNT-EO is more hydrophilic than CNT-HNO_3 as -COH tends to form H-bond with H_2O rather than -COOH. More defect sites and hydrophilic nature of CNT-EO account for more surface H_2O, indicating greater potential to generate more hydroxyl radicals for indirect oxidation. This hypothesis was consistent with lower charge transfer resistance and greater extent of oxidation for CNT-EO.

Electrophoretic mobility has been suggested as a mechanism promoted by anodic potential for advanced antifouling performance in organic separation processes. High anodic potentials (30-40 V) were applied on a tubular ceramic (Al_2O_3) membrane coated with a modified Magnéli (Ti_4O_7) for 60 min to separate humic acid (HA) and bovine serum albumin (BSA) [88]. High potentials resulted in small currents (less than 10 mA) due to low ionic strength of the feed led to low energy consumption by the ECM. Application of 30 V and 40 V, ECM maintained over 90% of the initial values, while the flux for uncoated membranes was reported lower after 60 min, 62.7% for HA, and 41.6% for BSA. They suggested that enhanced electrophoretic mobility for negatively charged HA ($-3.5\ (\mu m S^{-1})(V cm^{-1})^{-1}$), and BSA ($-1.4\ (\mu m S^{-1})(V cm^{-1})^{-1}$) led to a lower membrane fouling and higher flux maintenance.

Cathodic potential

Natural organic matter (NOM) is commonly found in water bodies, consisting of complex macromolecular degradation products of plant and animal residuals. Many studies have reported that significant migration of NOM fouling on ECMs can be inhibited by applying cathodic potentials. The main antifouling mechanisms associated with cathodic potential are electrostatic repulsion and gas generation. Electrostatic repulsion between negatively charged NOM and negative surface is more dominant at low potentials. As discussed in Part I, electrostatic repulsive force is effective in short range and is restricted by the ionic strength. At potentials higher than hydrogen evolution potential (HEP), electrochemically generated gas bubbles enhance the antifouling performance through steric repulsion at the water/membrane interface.

Xu et al. [89] reported the preparation of DBSA doped polyaniline (PANI) membranes for improved membrane antifouling in the presence of negative potentials. After 30 mL filtration of BSA solution, the permeate flux was dropped by 40% under cathodic potential (1 V), while the permeate flux drop was 76% under no potential applied. The lower potential of BSA adsorption on the PANI membrane under cathodic polarization was attributed to increased electrostatic forces to repel the foulants from the membrane surface.

Vecitis et al. [90] studied the use of a carbon nanotube-polyvinylidene fluoride (CNT-PVDF) porous cathode on top of a UF membrane to reduce NOM fouling via the application of -2 V. They suggested an optimal electrode-membrane configuration for the electro-filtration system where the feed stream flowed through the porous anode, the CNT-PVDF cathode, and finally the UF membrane in sequence, as shown in Figure 3.10. Further, the presence of the spacers between electrodes not only prevented short circuit but also produced the near-surface turbulence for fouling reduction. The extent of NOM fouling in the optimal configuration was evaluated under different conditions of anode material, ionic strength and cathode potential. The predominant mechanism for NOM mitigation was the potential-induced negative surface charges to repel the negatively charged NOM fouling, consistent with the theories that the application of cathodic current increased the DLVO

energy barrier and reduced collision efficiency between organic colloids and the cathode surface.

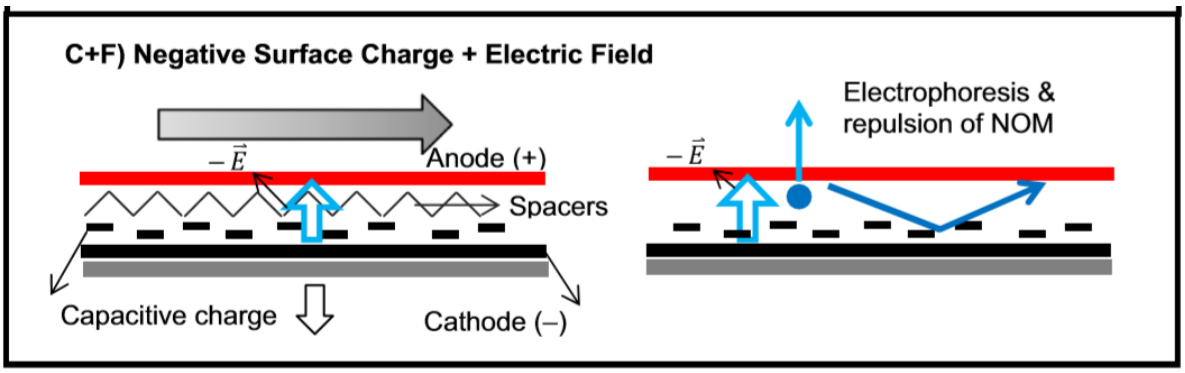

Figure 3.10. Representative schemes of an electro-filtration system. The antifouling effect is produced by an applied external electrical field which produces a negative surface charges to repel NOM. Reprinted from [90], Copyright 2014, with permission from Elsevier.

As discussed, the impact hydrogen bubble evolution as an antifouling mechanism becomes significant when cathodic potential exceeds surface over potential. Mid-to-high potentials are more commonly applied in cathodic polarization due to little destructive impact of cathodic polarization on membrane surfaces as compared to anodic potentials [96]. Wu and Craig et al. [94] studied the ability of electrochemically generated nanobubbles to limit BSA fouling, and to clean BSA-fouled conductive pyrolytic graphite surfaces. To limit BSA fouling, a cathodic potential of 1.5 V applied for 20 s before exposure to BSA was found to decrease protein coverage by up to 34%, which was explained by nanobubbles acting as a physical barrier against adsorption. To clean fouled surfaces, a cathodic potential of 1.5 V was applied for 50 s to pyrolytic graphite fouled with pre-adsorbed BSA. Under these conditions, 100% to 82% of the BSA was removed. It was hypothesized that nanobubbles forming on the conductive substrate could actively remove protein at the liquid-vapor interface by a low-shear water stream, although a small portion of protein at the solid-liquid interface remained. Similarly, defouling of BSA on SWCNT embedded epoxy membrane was explored by Hinds et al. [95]. Bubble generation at a cathodic potential of 2 V resulted in 85% removal efficiency for the first defouling cycle and 60% for the second defouling cycle.

Liang and Huang et al. [93] challenged a dual-layer CNT-PVDF membrane with a synthetic wastewater solution containing sodium alginate (SA), HA, BSA as well as inorganic compounds. As shown in Figure 3.11, compared to the pristine PVDF membrane, the lower surface energy of the CNT layer with poor affinity towards foulants could maintain constant flux at a lower TMP. The application of -2 V DC and 0 V/-2 V DC on the CNT/PVDF membrane generated large amounts of gas bubbles which reduced the adsorption of foulants further lower the required TMP to maintain flux, as compared to 0 V condition. Further, they attributed the most effective antifouling performance achieved at 0 V/-2 V DC to the intermittent charging mode. The negatively charged foulants were repelled from the membrane cathode, whereas cations in bulk moved toward the membrane. Neutralization by cations was expected to dissipate the strength of applied electric fields. Thus, a temporary pause in applied potential allowed the release of cations, recovering the receded repulsive force and contributing to an increase in ionic strength.

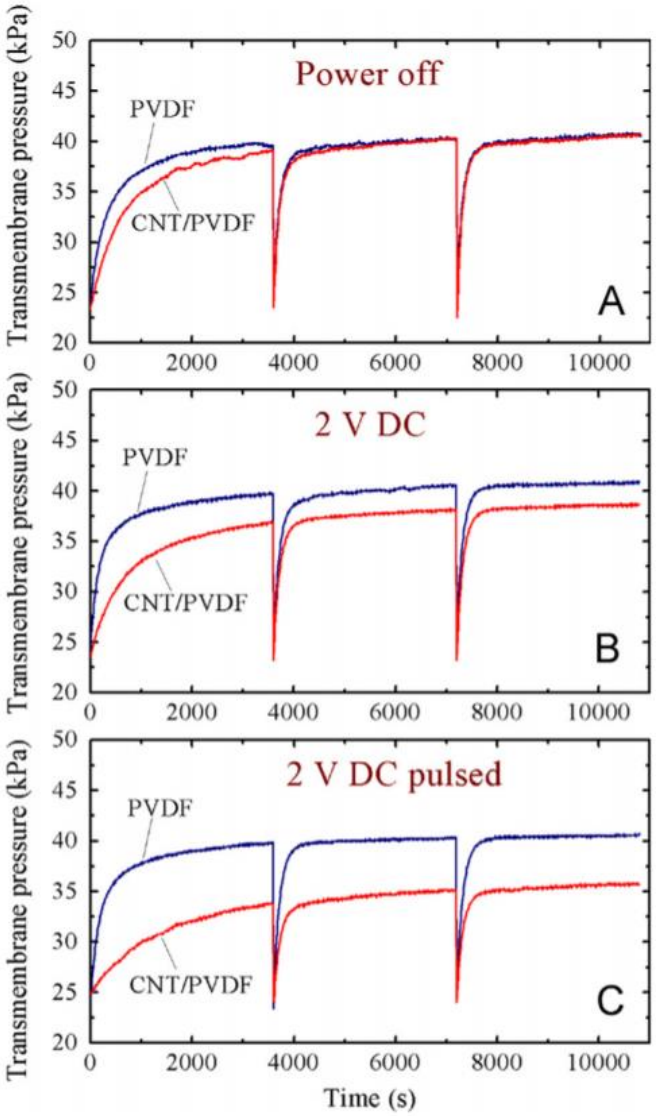

Figure 3.11. TMP as a function of time for pristine PVDF and CNT/PVDF membranes in filtration of with a synthetic wastewater: (A) No electrical field; (B) 2V DC; (C) 0 V/2 V DC pulsed with 5 s intervals. Reprinted from [93], Copyright 2015, with permission from Elsevier.

Nidal et al. [45] fabricated electrolytic self-cleaning membranes by incorporating carbon nanostructures (CNS) into networked cellulose composites for mitigating humic acid (HA). The addition of CNS both enhanced the water flux by disrupting the compression of polymer chains and provided the ability for self-cleaning through applied potentials. Modified membranes showed a 93% increase in flux compared to control

(PVA-NC membranes) and fouled membrane was recovered via the evolution of hydrogen with a cathodic potential of -5 V (equivalent to 3.75 mA/cm^2) for 20 min.

The use of electrical UF/NF in series to treat anaerobic reactor effluent containing benzyl alcohol and its degradation products was investigated in Jassby lab [91]. UF and NF membrane modules in series were utilized for remediation of the SBR effluent. The application of -3 V and -5 V on the CNT-UF membrane over 5 h electrofiltration led to decrease of required pressure by 22.6% and 29.0%, respectively, compared to membranes without an applied potential. We hypothesize that generation of hydrogen bubbles as well as electrostatic repulsion led to the lower increase rate in TMP during filtration. During backflushing of the membranes, fouling formation was enhanced at an anodic potential of +1.5 V, attributed to the attraction between positively charged CNT membrane and negatively charged HA, as well as the irreversible fouling caused by electro-polymerization. Interestingly, fouling was not inhibited on CNT-NF membrane at either a cathodic potential of -5 V or an anodic potential of +1.5 V likely due to abundant neutral particles in the NF feed produced from the UF module.

Jassby et al. [92] investigated the prevention of high concentration (5 g/L) of alginic acid (AA) on PVA-CNT-COOH modified membranes by applying negative potentials for electro-filtration. The application of -3 V and -5 V on the PVA-CNT-COOH membranes repelled the negatively charged humic acid, resulting in 33% and 51% reduction in pressure under the constant flux of 20 LMH, respectively, compared to 0 V condition. From our metanalysis, the improved performance of ECMs can be attributed to generation of hydrogen gas bubbles at the potential range applied (3-5 V).

Recently, the application of hybrid systems for enhanced antifouling performance has received attention, where electrochemical interactions at the anode and cathode are combined to maximize the efficiency of the system. In a study, Fu et al. [64] developed an electrochemical ceramic membrane reactor (ECMR) by using the Ti-mesh embedded ceramic membrane as a cathode and Ti/SnO_2-Sb-Ce as anodes for mitigating membrane fouling during sodium alginate filtration. They evaluated the antifouling performance by

monitoring the TMP over filtration period (120 h). Their results revealed that application of 3 V led to lowest increase rate in TMP as compared to application of 1 V, 2 V, and control experiment (no electrical filed), likely due to activation of electrochemical reactions at 3 V. They suggested the generation of oxidants including ROS ($HO^{\bullet}$, $O_2^{\bullet-}$, H_2O_2), and active chlorine under cell potential of 3 V. High rates of electrochemical reactions at 3 V were confirmed with the average current of ECMR under application of 3 V (4.32 mA) as compared to 1 V (0.037 mA), and 2 V (0.73 mA).

Alternating potential

Quan et al. [75] explored the mitigation of humic acid (HA) fouling on a ceramic hollow fiber membrane coated with interconnected carbon nanotubes under different polarizations, including anodic, cathodic and alternating polarization. As shown in Figure 3.12, they found that under the conditions of anodic polarization at +1 V, cathodic polarization at -1 V, and alternating polarization at ± 1 V with a frequency of 16.7 mHz (pulse width value of 60 s), the permeate flux of CNTs/ceramic membrane was 1.1, 1.4, and 1.5 times as high as that without electropolarization (1060 LMH/bar) after 60 min operation. The TOC removal efficiencies of electropolarized membrane were 71%, 62%, and 76% under anodic, cathodic, and alternating polarization, respectively. At an anodic potential of +1.0 V, HA was oxidized on the CNT/ceramic membrane; however, the small portion of HA that remained adsorbed caused flux decline. At a cathodic potential of -1.0 V, electrostatic repulsion between the negatively charged membrane and negatively charged HA contributed to significant decrease in HA fouling. The least flux loss and the most TOC removal efficiency on the CNT/ceramic membrane were achieved by alternating polarization. Under cathodic polarization, adhesion of HA on the membrane surface was greatly reduced, and while some HA remained adsorbed onto the surface of the membrane, it could be immediately degraded by electrooxidation when the applied potential switched from negative to positive. Further, HA migration caused by either electroosmosis or electrophoresis could reduce the adhesion forces between HA molecules and the anodically polarized membrane.

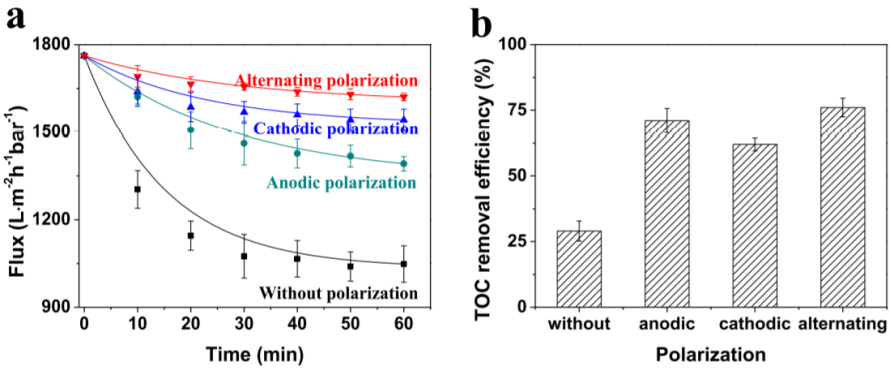

Figure 3.12. (a) Normalized flux of CNTs/ceramic membrane during NOM filtration under different polarizations, (b) TOC removal efficiency on electropolarized CNTs/ceramic membranes. Conditions: [HA]in= 10 ppm, [pulse time] = 60 s, and [pressure] = 0.1 bar, cathodic, anodic, and alternating potentials applied were +1 V, -1 V, ± 1 V with a frequency of 16.7 mHz, respectively. Reprinted from [75], Copyright 2016, with permission from Elsevier.

3.3.3. Oil wetting

Many industries deal with oily wastewater that requires purification before these waters can be returned safely to the environment. In some cases, the application of ECMs has been proposed to assist with improving flux and separation properties of typical membranes. With a few exceptions, appropriate polarity was chosen with respect to the charge of oil particles. Electrophoretic mobility, electrostatic interactions, gas generation, and oxidation (direct, indirect) are the likely mechanisms that can account for the antifouling behavior of ECMs used for oil-water separations. Some of these mechanisms have been overlooked in the literature and are discussed below. Table 3.3 summarizes the published articles focused on oil separation using ECMs.

Table 3.3. Summary of ECM studies targeting oil separation.

Antifouling Mechanisms	Materials	Foulants	Charge of Foulants	Concentration (ppm)	Current or Voltage Patterns & Reaction Time	Results	Reference
				Anodic potential			
Electrophoretic mobility	Al_2O_3 modified with Magnéli Ti_4O_7 inner layer	Peanut oil	+41.4 mV	200	30-40 V (10 mA) for 60 min	Flux was maintained at 91% and 42% of the initial flux under 30 V and 0 V, respectively. ECM also increased the separation efficiency from 95% to 99%.	[88]
Electrophoretic mobility (gas bubbling, redox)	PANI-reduced graphene oxide (rGO)	Real oil sands produced water	Negative	300 (TOC) 470 (Na^+) 6 (Mg^{2+})	2-3 V for 100 min	Total fouling ratio was decreased by 25% under 2 V. Severe pore blockage under 3 V.	[97]
				Cathodic potential			

Electrophoretic mobility	Carbon fibre-carbon composite	Vegetable oil-based emulsion	-67±5 mV	150-1000	0-30 V for 5 h	Electrical field enhanced the flux (by 100%) and separation efficiency (by 13%).	[98]
Electrostatic forces (gas bubbling, redox)	PANI-reduced graphene oxide (rGO)	Real oil sands produced water	Negative	300 (TOC) 470 (Na^+) 6 (Mg^{2+})	2-9 V for 100 min	Enhanced the flux by 31.9%.	[97]
Electrostatic forces	GO/MWCNT/PVDF	Palm oil mill effluent filtration	Negative	/	221 V/cm for 300 min of direct or pulsed potential (6 min on/54 min off)	Cathodic current maintained the flux by up to 90%. Intermittent mode resulted in the same flux performance (2% higher).	[99]

Anodic potential

Electrophoretic mobility has been mentioned as the primary mechanism promoted by anodic potential for advanced performance of ECMs in oil separation applications. A tubular ceramic (Al_2O_3) membrane coated with a modified Magnéli (Ti_4O_7) was used to separate positively charged (41.4 ± 3 mV) peanut oil [88]. Positive potentials (30-40 V) were applied on the ECM during a 60 min separation of oily wastewater. It is worthy to note that a very low-conductive electrolyte was used as feed as high ionic strength suppresses the electrophoretic mobility of particles via electrostatic shielding. With no current applied, the permeate flux dropped by more than 50%, while application of 30 V and 40 V maintained 83.2% and 91.8% of the initial flux, respectively (Figure 3.13). The range of electrical potential applied was close to the theoretical critical value (35.2 V). High potentials (30-40 V) resulted in small currents (less than 10 mA) due to low ionic strength of the feed which demonstrated low energy consumption by the ECM. They suggested that electrophoretic mobility between the anodic membrane and the stainless-steel cathodic electrode drags the oil particles away from the membrane surface enabling higher permeate flux and consequently a higher purity permeate.

It should be noted that anodic potential can cause mineralization and electropolymerization of organic particles. Drastic electropolymerization can lead to blockage the membrane pores which is known as ““poisoning effect”. Karkooti et al. [97] employed a graphene-based ECM for the treatment of wastewater from oil sands, where they observed immediate stoppage of the permeate flow under application of anodic potential (3 V) due to pore blockage likely as a result of drastic electropolymerization.

Cathodic potential

There are three primary mechanisms for oil separation associated with cathodic potentials: electrophoretic mobility, electrostatic force, and gas generation. The individual mechanisms are discussed below in more detail.

In one of the earliest studies in this area, application of cathodic potential (0-30 V) was shown to effectively separate oily wastewater [98]. In this work, permeate flux was increased by nearly 5-fold with the application of a cathodic current. The authors suggested that the enhancement in permeate flux was a result of electrical field-induced electrophoretic mobility of oil particles. Without an applied electric field, the membrane underwent irreversible fouling while with an electrical field, the cake layer was mitigated. To drive the critical electrical potential, they coupled the electrophoretic mobility term to Stoke's law as follows:

$$E_{critical} = \frac{J}{u_e} \qquad \text{Eq. (1)}$$

where, $E_{critical}$ represents critical field strength (Vcm^{-1}), J and u_e denote the corresponding pure water flux (LMH) and electrophoretic mobility of the particle ($m.s^{-1}/V.cm^{-1}$), respectively. The applied electrical field was proposed to be close to critical electrical potential to avoid excessive energy consumption.

Continuous and intermittent cathodic currents have been used to treat palm oil mill effluent [99]. They carried out a response surface methodology to optimize the performance of the membrane during continuous and intermittent modes separately. In continuous mode, carbon concentration (3.96-11.04 wt%) and electrical field strength (18.93-231.07 V/cm) and in intermittent mode, filtration interval (23.79-66.21 min) and electrical treatment application time (1.38-5.62 min) were investigated. Under continuous mode, the highest normalized flux was observed for 5 wt% carbon concentration, and electrical field strength of 221 V/cm with 23 % drop in the permeate flux. Under intermittent mode, filtration intervals of 30 min with 5 min electrolysis (using electrical field strength of 221 V/cm) resulted in the highest permeate flux with 21% drop in the permeate flux. While in the control experiment (no electrical field), the permeate flux was 2.79-287 times lower as

compared to optimized continuous or intermittent modes. They justified the improved flux to the enhancement of electrostatic repulsion between foulants and the membrane surface. However, intermitted current resulted in a slightly better flux as compared to continuous mode. They theorized that prolonged application of cathodic current forces intense accumulation of positively charged cations on the surface that shields the electrical field. An intermittent electric field allows for the desorption of cations from the cathode and thereby a recovery of the electrical field. They suggested that higher carbon content (up to 5 wt%) increases the surface conductivity, a better distribution of electrical charge across the surface and eventually greater electrostatic repulsive force. Further increase in carbon content causes nanomaterial agglomeration and increases in surface roughness that favors fouling propensity.

In a more recent study, Karkooti et al. [97] employed cathodic potentials (2-9 V) for the improved treatment of wastewater from oil sands using a graphene-based ECM. Cathodic potential resulted in 82.75%, 72.20%, and 67.18% flux decline under 3, 6, and 9 V potentials while under no electrical current the permeate flux decline was 89.19% (Figure 3.13). Cathodic current also significantly enhanced the TOC removal up to 85.52% as compared to the reported 33.29% under no current (Figure 3.13). The authors suggested electrostatic forces, electrophoretic mobility, gas bubbling, and electrochemical reactions to justify the observations. The cathodic potential range applied in this study exceeds the surface overpotential. Therefore, it is likely that electrostatic repulsion, and electrophoretic mobility were responsible for higher permeate flux, while indirect oxidation of oil particles promoted by electrochemical reactions could account for low TOC values reported in the permeate.

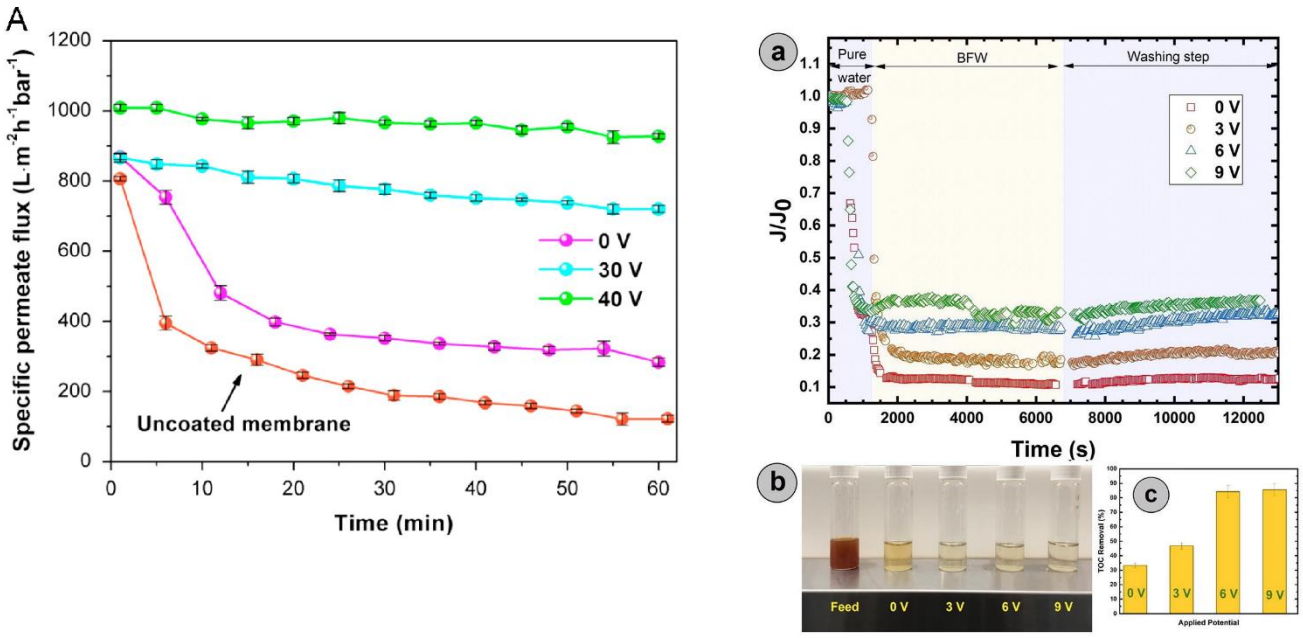

Figure 3.13. On the left: Specific permeate flux versus time for treatment of 200 mg/L emulsified oily water with CTAB as surfactant [88]. Orange, purple, blue, and green represent uncoated membrane, Al_2O_3/ Ti_4O_7 ECM under no potential, Al_2O_3/ Ti_4O_7 ECM under anodic 30 V, and Al_2O_3/ Ti_4O_7 ECM under anodic 40 V, respectively. On the right: (a) flux decline over time for filtration of produced water from oil sands using graphene-based ECM. Red, brown, blue, and green represent no potential, 3 V cathodic potential, 6 V cathodic potential, and 9 V cathodic potential, respectively (b) optical images of feed and permeate solutions collected under different applied potentials, and (c) TOC removal performance of ECMs. Reprinted from [97], Copyright 2020, with permission from Elsevier.

3.3.4. Scaling and ion separation

Scale removal from ECMs was carried out in some cases by applying anodic potential to ECMs and in another situation by cathodic potential. As previously mentioned in Part I, the choice of applying anodic or cathodic potential depends on the type of scale required to be removed from the membrane surface. Scale formation can be inhibited electrostatic repulsion, direct redox reactions, bubble formation, and pH-change induced dissolution. Scale formation inhibition can occur by electrostatic interaction, in which either cathodic (negative) potential can be applied to the ECM to repel anions from the ECM surface, or anodic potential can be applied to repel cations. Scale can also be removed and scale formation can be limited through redox reactions. Cathodic potential can be

applied to cause direct reduction of scalants, while anodic potential can be applied to cause direct oxidation of scalants. Scale formation can also be limited through gas bubbles generation at either the anode or cathode: cathodic potential is usually applied to produce micro hydrogen bubbles at the ECM by water electrolysis, oxygen bubbles at the anode could also impede scale formation. Finally, some types of scales are pH-sensitive (they dissolve at high or low pH), which enables scale removal by raising or lowering the local pH at the ECM through the application of a cathodic or anodic potential, respectively. Table 3.4 presents research articles focused on scale removal and ion rejection using ECMs.

Table 3.4. Summary of published studies regarding scale removal and ion rejection on conductive membranes.

Antifouling Mechanisms	Materials	Foulants	Charge of Foulants	Concentration (ppm)	Current Patterns & Reaction Time	Results	Reference
				Anodic potential			
Low pH	CNT/ polyamide	Na_2SO_4 $MgSO_4$ $CaCl_2$	Positive	1420 1685 1776	2.5 V for 30 min (5 min on/5 min off)	Dissolved $CaCO_3$ lead to 98% recovery	[100]
Electrostatic repulsion	CNT/ polyamide	Na_2CO_3 KCl $CaCl_2$ $MgCl_2$	Positive	996 797 800 447	1.5 V for 140 min	Repelled Ca^{2+} ions lead to 30% enhancement in flux maintenance.	[100]
Electrostatic repulsion	CNT/Al_2O_3	Silica particles	+7.6 mV	100	0.5, 1, 1.5 V for 30 min	Increased silica rejection from 87.2% (0 V) to 99% (1.5 V).	[77]
Electrostatic attraction	CNT/Al_2O_3	Latex particles	-8.4 mV	500	0.5, 1, 1.5 V for 30 min	Increased latex log removal from 2.24 (0 V) to 6.59 (1.5 V).	[77]
Electrostatic repulsion	Polypyrrole/ PVDF	$CaCl_2$	Positive (Ca^{2+})	555	0.8 V for 20 min	Desorption leads to higher Ca^{2+} (1%) in the filtrate.	[101]
Oxidation	MWCNT	NaI NaCl	Negative (I^-)	1500 584	1, 2, 3 V for 90 min	1-2% oxidation of I^- was achieved under 2-3 V.	[102]
				Cathodic potential			
High pH	Polypropylene coated with CNT/PVA	Silicate scale	Neutral	1906 ($NaSiO_3 \cdot 5H_2O$)	20 mA (3.6 V) for 50 min	Electrochemical cleaning nearly restored the permeate flux to its initial value for three consecutive cycles.	[103]
Electrostatic attraction	Polypyrrole/ PVDF	$CaCl_2$	Positive (Ca^{2+})	555	0.8 V for 20 min	Adsorption leads to lower Ca^{2+} (1%) in the filtrate.	[101]
Electrostatic repulsion	Polypyrrole coated terylene	NH_4Cl KH_2PO_4 $CaCl_2$ $FeSO_4$ Sucrose	Neutral	100 30 2 10 500	0, 0.2, 0.4 V/cm in three consecutive cycles of 90 min each	Flux decline was 5% (0.2 V/cm) as compared to 25% (0 V).	[104]
Electrostatic repulsion	Polypyrrole	NH_4Cl KH_2PO_4 $CaCl_2$ $FeSO_4$ Sucrose	Neutral	100 30 2 10 500	0.2 V/cm in three consecutive cycles of 4 h each	Electric field enhanced the flux by two times.	[105]
Reduction	CNT/ PVA/polysulfone	Hexavalent chromium (Cr(VI))	Negative ($CrO4^-$)	1	3, 5, 7 V for 6 h	Highest removal rate (95%) was achieved at 7 V.	[106]
Reduction	Pd-Cu and Pd-In coated TiO_2	$NaNO_3$	Negative (NO_3^-)	85	3.6 V (cathode-anode flow mode) for 2 h 2.5 V (anode-cathode flow mode) for 2 h	Nitrate reduction in the anode-cathode flow mode was higher (43-65 %) than the cathode-anode flow mode (20 %).	[107]
Reduction	Ni/polypropylene	NH_4Cl	Positive (NH_4^+)	4000	0.8 V in three consecutive cycles of 96 h each	40% increase in NH_3-N recovery rate.	[108]

Hydrogen gas	MWCNT/PVDF	$CaCO_3$ NaCl	Positive (Ca^{2+})	100 10000	2V periodically for 3 min after cycles of 30-60 min	Electric field enhanced the permeate flux by 40%.	[43]
				Alternating potential			
Self-heating	CNT	NaCl	Neural	10^4-10^5	20 V AC (0.3-10000 Hz) for 100 min	Single pass recovery of ~100%	[109]

Anodic potential

There are three main mechanisms for ion removal associated with anodic potentials: dissolution under low pH, electrostatic repulsion/attraction, and direct oxidation. The individual mechanisms are discussed below for different scalants and ions.

Duan et al. [100] studied the effect of electric current on the prevention of $CaCO_3$ scaling on polyamide RO membranes coated with carbon nanotubes (CNTs). $CaCO_3$ solution of saturation index of 4.38 was filtered through the RO membranes at crossflow velocity of 4.5 cm/s. After 460 min, the permeate flux decreased to 82% of the initial flux. However, the intermittent application of 2.5 V anodic potential on the membrane surface/counter electrode for 30 min (5 min on/5 min off) recovered the flux to 98% of its initial value. This flux enhancement resulted from the dissolution of the deposited $CaCO_3$ on the membrane surface. $CaCO_3$ crystals are very sensitive to pH and dissolve rapidly at low pH, thus the produced protons from water oxidation at this applied potential (2.5 V) dissolved the $CaCO_3$ crystals at the RO membranes, see Part I. From our meta-analysis, we suspect that electrostatic repulsion between positively charged Ca and surface as well as oxygen gas evolution further contributed to improved performance of CNT-ECMs. In the same study [100], they also examined the effect of electric current on $CaSO_4$ (gypsum) scale prevention on the CNTs coated RO membranes. $CaSO_4$ solution of saturation index of 1.01 was filtered through the RO membranes at the same crossflow velocity (4.5 cm/s). The application of 1.5 V while filtering the $CaSO_4$ solution delayed the $CaSO_4$ scale on the RO membrane, slightly enhancing the permeate flux. Moreover, when an inline microfilter was used on the retentate line to remove $CaSO_4$ particles formed during the experiment (to prevent secondary deposition on the RO membrane), the application of anodic potential (1.5 V) on the membrane caused 30% enhancement in the flux decline after 140 min. While it is well known that $CaSO_4$ is pH insensitive, two reasons are believed to cause the

enhancement in the permeate flux. Firstly, the application of anodic electric potential changed the morphology of the deposited $CaSO_4$ from tightly packed needle morphology to larger, less packed structure which enhanced the permeate flux. Secondly, the application of positive potential on the membrane surface pushed the positive Ca ions away from the membrane which created nucleation free zone away from the membrane which also caused enhancement in permeate flux, see Part I. However, we suspect that the contribution of oxygen gas generation at the reported potential (1.5 V) cannot be ruled out.

Fan et al. [77] studied the effect of electrochemistry on enhancing the performance of CNTs/Al_2O_3 membrane while filtering solution containing silica spheres (140 nm) having a comparable size to the membrane pore size (142 nm). In the absence of electrical field, 87% of silica particles were retained on the membrane surface in a cross-flow filtration setup. While, applying positive potential of 0.5 V, 1 V, and 1.5 V on the CNTs/Al_2O_3 membrane increased silica rejection to 90%, 94%, and 99%, respectively, as shown in Figure 3.14a. Interestingly, the permeate flux also increased with applying electrical potential (1.5 times when applying 1.5 V), as shown in Figure 3.14b. It was hypothesized that silica spheres with positive charge (+7.6 mv zeta potential) in the feed solution (neutral pH) were repelled from the membrane under applying positive potential by electrostatic interactions and then removed by the crossflow. In the same study, the separation of latex particles that have smaller size (57.7 nm) than the membrane pore size (142 nm) was also investigated. In the absence of electrical field, only 15% of the latex particles were removed from the solution. On applying positive 0.5 V anodic potential, the latex removal efficiency was doubled, and it further increased with applying 1V, and it reached 4 times the initial value when applying 1.5 V, as shown in Figure 3.14c.

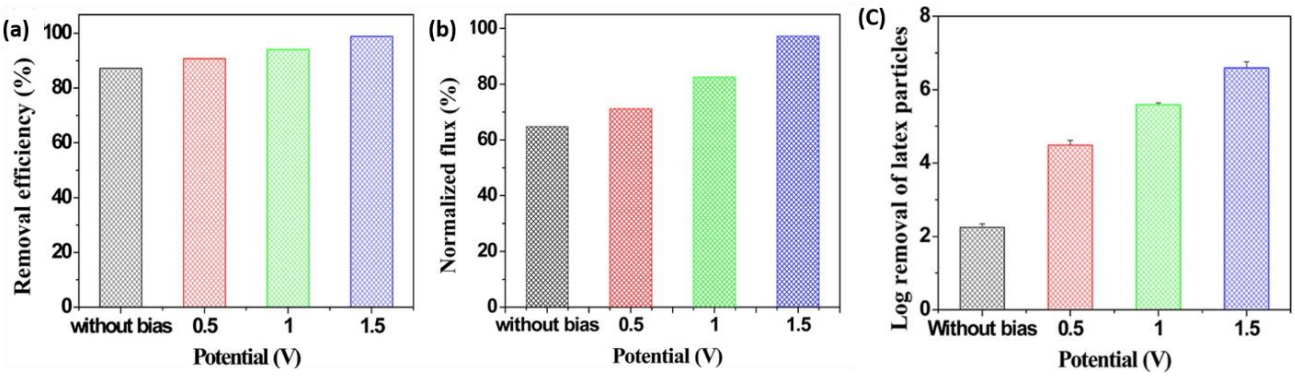

Figure 3.14. Effect of applied anodic potential on silica and latex filtration using CNT/Al_2O_3 ECM: (a) silica removal efficiency, (b) normalized permeate flux for the filtration of silica solutions, and (c) latex removal efficiency. Black, red, green, and blue bars represent no potential, 0.5 V, 1 V, and 1.5 V, respectively. Reprinted with permission from [77]. Copyright 2015 American Chemical Society.

Vecitis et al. [102] studied iodine (I^-) oxidation during the electrochemical filtration of aqueous iodide and chloride solutions on a multi-wall carbon nanotubes (MWCNTs) microfilter in a dead-end filtration system. The MWCNT membrane was used as an anode in an electrochemical filtration device, and stainless-steel electrode was used as a cathode. A solution containing 10 mM NaCl and 10 mM NaI was filtered at a flow rate of 1.5 mL/min. When no potential was applied, I^- ions showed 0% oxidation. However, increasing the applied potential to 1 V resulted in a gradual increase of I^- oxidation until it reached a plateau of 0.3% after 1 h, as shown in Figure 3.15. I^- oxidation occurs by two reactions; a two-electrons oxidation reaction (yielding iodine) occurring at 0.55 V standard potential (Reaction 3), and one-electron oxidation reaction (yielding I atom) occurring at 1.5 V (Reaction 4). At 1 V applied potential, only the two-electron transfer reactions occur, which explains the long reaction times (1 h) taken to reach the maximum I^- oxidation (0.3%) as two I^- ions are required to be close to each other at the MWCNT filter for the oxidation to occur. On the other hand, applying 2 V or 3 V resulted in (1) a steady state I^- oxidation and (2) a higher value of I^- oxidation (1-2%) because both the one-electron and two-electrons oxidation reactions (Reaction 3 and Reaction 4) are occurring at such applied potentials (2V or 3V), see Figure 3.15.

$$2\,I^- + 2\,h^+ \rightarrow I_2 \quad (E_0 = 0.55\,V) \tag{3}$$

$$I^- + h^+ \rightarrow I \ (E_0 = 1.5\ V) \quad (4)$$

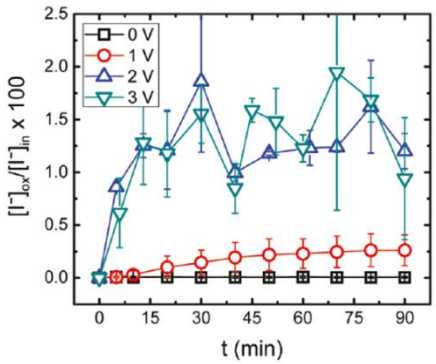

Figure 3.15. Iodine oxidation as a function of time at different anodic potentials in filtration of aqueous iodide and chloride solutions on MWCNT-ECMs. Application of 2 V and 3 V anodic potential resulted in significant iodine oxidation (green and blue lines, respectively), whereas application of 1 V and no potential cause no significant oxidation (red and black lines, respectively). Adapted with permission from [102]. Copyright 2011 American Chemical Society.

Cathodic potential

There are four main mechanisms for ion removal associated with cathodic potentials: dissolution under high pH, electrostatic repulsion/attraction, direct reduction, and H_2 bubble formation. While some of these effects occur simultaneously, the individual mechanisms are discussed sequentially.

Tang et al. [103] studied electrochemical cleaning of silicate scale on membrane distillation (MD) membranes. In their study, polypropylene membrane coated with CNT/PVA was used in membrane distillation process treating synthetic silicate brine solution in a crossflow cell. The distillation process was carried out without applying electric current until the permeate flux was decreased to 40% of its initial value. Afterward, the brine solution was replaced by deionized water and 20 mA (3.6 V) DC current was applied between the membrane cathode and titanium anode for 50 min. The electrochemical cleaning nearly restored the permeate flux to its initial value for three consecutive cycles, as shown in Figure 3.16. The increase in flux with electrochemical cleaning was attributed to hydroxide ions generation via water electrolysis which raised the pH near the membrane

dissolving silicate scale on the membrane. We suspect that the generation of hydrogen bubbles as well as the electrostatic repulsion between surface and deprotonated -Si-O^- species further assisted with advanced electrochemical cleaning performance. Interestingly, the flux declined rapidly after electrochemical cleaning, see Figure 3.16. This was suggested to be caused by scale crystals remaining on the membrane after the electrochemical cleaning, which acted as nucleation sites for the new silicate monomers decreasing the scale crystallization induction time.

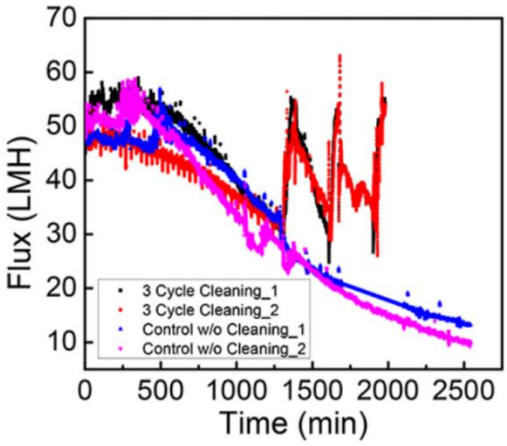

Figure 3.16. Effect of electrochemical cleaning (three consecutive cycles of 20 mA (3.6 V) cathodic DC for 50 min) on the permeate flux when filtering synthetic silicate solution CNTs/PVA coated polypropylene membrane. Using electrical field, permeate flux was rapidly recovered (red and black line), while in the absence of electrical potential, membrane was continuously fouled (blue and purple lines). Reprinted with permission from [103]. Copyright 2017 American Chemical Society.

Weidlich et al. [101] studied the electrochemical rejection of calcium on PVDF microfiltration membranes coated with electrically conductive polypyrole with polystyrene sulfonate (PSS). The electrochemical rejection behavior of the membranes to 0.005 M $CaCl_2$ solution was illustrated at flow rates of 2-3 mL/min. Applying 0.8 V cathodic potential caused a significant decrease in the Ca concentration in the permeate due to the adsorption of Ca^{2+} ions on the negatively charged membrane cathode. On the other hand, applying 0.8 V anodic potential failed to separate Ca ions due to significant convective flow through large pores [101].

In more complex media including primarily Ca and Fe foulants, Liu et al. [105] studied fouling reduction in a membrane bioreactor (MBR) when applying electrical field on terylene cloth membrane coated with electrically conductive polypyrrole. The MBR influent was a synthetic wastewater solution of NH_4Cl (100 ppm), KH_2PO_4 (30 ppm), $CaCl_2$ (2 ppm), $FeSO_4$ (10 ppm), and sucrose (500 ppm). The polypyrrole coated membrane was utilized as cathode in an electrochemical cell, and two stainless meshes placed 5 cm away from either sides of the membrane were used as anodes. Applying 1 V (0.2 V/cm potential drop) showed a significant enhancement in permeate flux where the permeate flux was approximately two times higher than the flux in the absence of electrical field after 4 h filtration in a consecutive three cycles, as shown in Figure 3.17a. This enhancement in flux was attributed to the electrophoresis of the negatively charged foulants away from the membrane, which decreased the scale deposited on the membrane. Along the same line, Liu et al. [104] in another study, used the same system to investigate fouling prevention on the polypyrrole coated terylene membrane when subjected to the same feed solution but at higher applied potential (2 V (0.4 V/cm potential drop)). Figure 3.17b showed that during the first two cycles, applying 2 V showed the most significant enhancement in the flux in comparison with applying 1 V as the higher potential provides a greater repulsive force between the membrane and foulant anions. In addition, we suspect that application of 2 V promotes generation of gas bubbles which assist with antifouling performance. However, electrostatic repulsive force seems to be the dominant mechanism due to insignificant increase in flux from 1 V to 2 V. In the third cycle, the permeate flux under 1 V applied potential was higher than 2 V applied potential. They suggested that the higher potential disturbed the formation of the dynamic cake layer beneficial for protecting large pores from blockage.

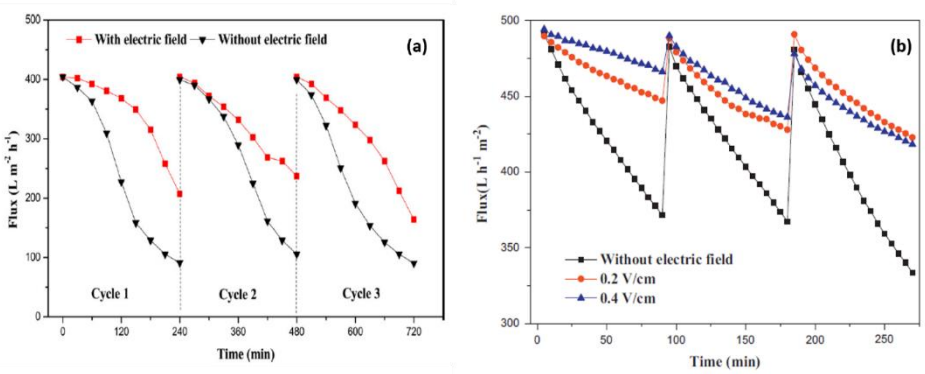

Figure 3.17. Effect of cathodic applied potentials on the permeate flux by filtering synthetic wastewater solution on polypyrrole coated ECM working in an MBR. (a) under application of 1 V (0.2 V/cm potential drop, red line) and no potential (black line). Reprinted from [105], Copyright 2012, with permission from Elsevier. (b) under application of 1 V (0.2 V/cm, red line), 2 V (0.4 V/cm, blue line), and no potential (black line). Reprinted from [104], Copyright 2013, with permission from Elsevier.

Hashaikeh et al. [43] studied the periodic electrochemical cleaning of multiwalled carbon nanotubes (MWCNT)-coated PVDF MF membranes during the filtration of aqueous $CaCO_3$ suspension in a cross-flow filtration cell at operating pressure of 1 bar. An electric field was applied on the MWCNT-coated membrane for 3 min after each filtration cycle where the membrane was used as the cathode in an electrochemical cell, stainless-steel electrode was used as the anode, and an electrical potential of 2 V was applied. Figure 3.18 shows that applying a periodic electric field between the filtration cycles significantly enhanced the permeate flux in comparison with the absence of electrical field. Figure 3.18 also shows that decreasing the filtration cycle duration (from 60 min to 40 min to 30 min) between the electrolysis process enhanced the overall flux significantly at the end of a total 2.5 h filtration duration. The enhancement in permeate flux with applying cathodic current on the membrane was hypothesized to be due to the production of hydrogen microbubbles via water electrolysis at the membrane which removed the $CaCO_3$ scale through shear effect.

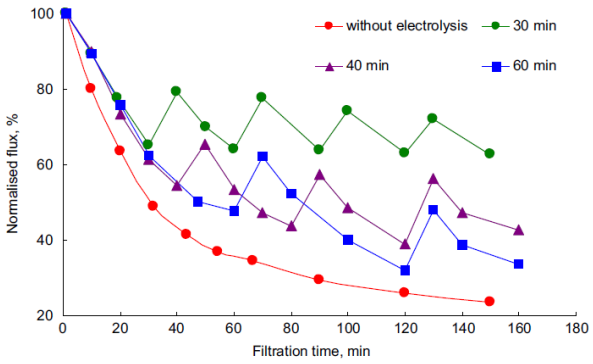

Figure 3.18. Effect of applying periodic electric current on the normalized permeate flux when filtering $CaCO_3$ solution through MWCNTs coated PVDF membrane. Periodic electric field (cathodic 2 V) was applied between filtration cycles of 60 min (blue line), 40 min (purple line), 30 min (green line), while control experiment (no electrochemical cleaning) is presented by red line. Reprinted from [43], Copyright 2014, with permission from Elsevier.

Although electrostatic repulsion and hydrogen gas generation seem to be the dominant mechanisms for antiscaling applications, reduction of ions can lead to rapid precipitation and advanced separation of ions. Reduction of ions promoted by electrochemical reactions occurs at high ionic concentrations and potentials higher than the surface overpotentials. A few studies have investigated the impact of reductive reaction in filtration processes. Duan et al. [106] studied the electrochemical removal of hexavalent chromium (Cr(VI)) using polysulfone UF membranes coated with CNT/polyvinyl alcohol (PVA) composite in a crossflow filtration cell. They demonstrated that the application of cathodic potential on the CNT/PVA coated UF membrane can efficiently remove Cr(VI) from the permeate stream. In a low ionic strength solution (1 ppm Cr(VI) in DI water, pH= 6.5), the coated UF membrane showed 44% rejection of the Cr(VI) in the solution without applying electric field due to the electrostatic repulsion between the negatively charged carboxylic groups attached to CNTs and the CrO_4^- species formed at neutral pH. However, upon applying 3V, 5V, and 7V between the UF membrane cathode and a titanium anode, the rejection of Cr(VI) by the UF membrane increased to 64.4%, 83.4%, and 86.5%, respectively. The enhanced rejection upon application of cathodic potential is explained by the enhanced electrostatic repulsion between the negatively charged membrane and CrO_4^-

species in the solution (see Part I). Cr(VI) was not found to be electrochemically reduced due to the very low electric conductivity of the low ionic strength solution [106].

When performing experiments in a high ionic strength solution, the ions shielded the electrostatic repulsion between the negative carboxylic groups on the CNT-coated membrane and the CrO_4^- species in the solution, where increasing the concentration of background electrolyte (Na_2SO_4) from 0 mM to 100 mM, decreased the Cr(VI) rejection from 44% to nearly 0% in the absence of applied electric fields. Using 5 V between the membrane and counter electrode at high ionic strength showed no enhancement in the Cr(VI) rejection by UF membrane (0% rejection). However, increasing the applied potential to 7V increased the rejection to 53%. It is worth mentioning that there was a huge voltage drop between the membrane cathode and the titanium anode during these experiments due to corrosion of the titanium anode by the oxidizing current. Therefore, the relative potentials on the UF membrane cathode when applying 5 V and 7 V between the anode and cathode are equal to -0.27 V and -0.37 V vs. Ag/AgCl, respectively. The reduction potential of Cr(VI) is equal to -0.37 V, thus at 7 V the Cr(VI) can be reduced to Cr(III) forming solid precipitate on the membrane which enhanced Cr(VI) rejection (see Part I). To further enhance the Cr(VI) rejection on the CNT/PVA UF membrane at 7V applied potential, the thickness of CNTs on the membrane was increased from 2 µm to 6 µm which increased the Cr(VI) rejection on the UF membrane from 53 % to 94% due to the increase in contact time between Cr(VI) ions and the membrane cathode [106].

Gayen et al. [107] studied the electrocatalytic reduction of nitrate on substoichiometric Ti_nO_{2n-1} electrochemically reactive membranes (REM) doped with Pd-Cu or Pd-In catalysts. Electrochemical reduction experiments were done in a flow-through reactor with two flow modes, (1) anode-cathode flow mode (solution flowed from boron-doped diamond (BDD) anode to REM cathode) and (2) cathode-anode flow mode (solution flowed from REM cathode to the BDD anode). 1 mM $NaNO_3$ solution was filtered through the MF membranes at 600 LMH permeate flux while applying negative potential on the membrane surface to reduce the nitrate. REM membranes doped with Pd-Cu showed a better selectivity than that doped with Pd-In or the bare REM membranes. Interestingly, the

nitrate reduction in the anode-cathode flow mode was observed at lower potentials (-0.2 V) than that of the cathode-anode flow mode (-1.2 V). Moreover, the nitrate conversion was higher in case of the anode-cathode flow mode than the cathode-anode flow mode. These results were attributed to (1) the significant hydrogen production that occurred in the cathode-anode flow mode which competed with the nitrate reduction reaction, and (2) the lower local pH in case of the anode-cathode flow mode which could lower mineral scaling on the cathode pH [107].

Hou. et al. [108] developed a hydrophobic polypropylene membrane coated with hydrophilic thin nickel layer to enable ammonia recovery from wastewater in a microbial electrolysis cell (MEC). A negative potential (0.8 V) applied on the super hydrophilic nickel layer supported by the gas permeable hydrophobic PP membrane drove water reduction to produce hydrogen gas and OH^-. The accumulation of OH^- induces transformation from ammonium ions to ammonia where ammonia gas was separated quickly by the PP membrane. The consumption of OH^- and the spontaneous separation of NH_3 reduced the overpotential, resulting in a high recovery rate and low energy consumption. Further, cathodic potential reduced the degree of fouling due to electrostatic repulsion. The process is shown in Figure 3.19.

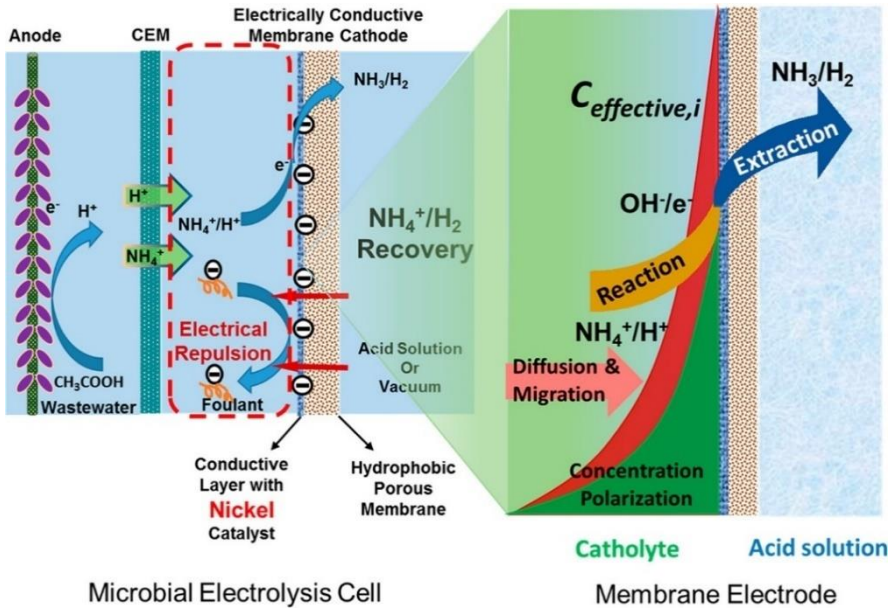

Figure 3.19. Schematic illustration of ammonia recovery from nitrogen-rich wastewater using electrically conductive membrane cathode. ECMs produced high local concentrations of OH^- under application of negative potential (0.8 V), that promotes transformation of ammonium to ammonia gas. Reprinted with permission from [108]. Copyright 2018 American Chemical Society.

Alternating potential

Recently, application ECMs has been suggested for membrane distillation processes due to their self-heating (Joule heating) properties under application of current, discussed in Part I. Briefly, application of high potentials (> 10 V) leads to conversion of electron's kinetic energy to thermal energy across the ECM surface, in turn resulting in high recovery rate in distillation processes. In highly saline solutions, anodic potentials higher than 1.2 V are destructive to membranes surfaces, therefore, alternating current was suggested because: (a) prevent surface degradation in high-saline solutions, and (b) minimize scaling through enhanced electrophoretic mobility. Dudchenko et al. [109] applied AC potential (20 V, 1-10000 Hz) to CNT-based ECMs for recovering high-saline brine. They have demonstrated that frequencies higher than 100 Hz did not cause CNT degradation. In their study, application of 10 kHz increased the surface temperature by up to 30 °C, in turn achieving high single-pass recovery of up to 100%.

3.4.Challenges and perspectives

ECMs have offered self-cleaning properties on account of their electrically-responsive surface. The antifouling properties of ECMs depend on the current pattern externally-applied to their surfaces. In part I, we identified and discussed the antifouling mechanisms with respect to surface polarization. Understanding the interplay between current pattern, antifouling mechanism, and foulant characteristics is critical for energy-efficient and optimized ECM applications. In this review, we offered a systematic discussion on the impact of electrically-induced antifouling mechanisms on major fouling categories, i.e., biological, organic, oil wetting, or scaling with respect to surface polarization (positive direct current, negative direct current, alternating current). Despite

the promising results of ECMs, practical application of ECMs necessitates highlighting a few points:

i. Despite the intense devotion of studies and articles into ECMs, utmost care should be paid before extending the application of electrochemical process to full-scale wastewater. Many studies examined synthetic and model wastewater under well-controlled laboratory conditions, where intermediate pathways, competing foulants, and surface passivation in real wastewater filtration process can be easily overlooked [70,110]. In addition, bridging the gas between experimental studies and practical applications is heavily influenced by design and development of filtration modules to accommodate ECMs in an effective and economical way.

ii. Co-occurrence of biofouling and organic fouling is complex and warrants more research. Adsorption of organic foulants promotes biofilm formation by providing a conditioned nutrient-enriched surface for bacterial adhesion and growth [22]. In addition, biofilm formation relies on the surface of the electrode, heterogeneity, and metabolic pathways of bacteria [111,112]. Therefore, developing optimal antifouling strategies using electrified membranes for real wastewater has not been realized and requires continued research for broad categories of fouling conditions due to the complexity of simultaneously occurring surface interactions.

iii. The application of ECMs for oil removal has often been conducted under low saline concentrations and high potentials. It is worthy to note that application of high potentials under higher ionic concentrations dramatically enhances the electrochemical reactions detrimental to membrane surfaces. Therefore, development of more electrochemically stable surfaces is critical for anti-oil-wetting applications.

iv. ECMs offer advanced antifouling performance at the cost of additional energy consumption. Economically, the application of ECMs can be most promising for desalination, distillation, and water-reuse processes where the energy-

related operating cost is significantly high [113]. In addition, ECMs lower the reliance on harsh chemical and mechanical cleaning, extending the membrane lifetime. However, the current module design for NF and RO membranes is not compatible with ECMs. ECMs need a counter electrode to complete the electrochemical cycle, which is hard to accommodate in the current spiral wound modules. It is expected that innovation of ECM-accommodating RO modules revolutionizes the energy-intense desalination processes.

3.5.References

[1] C.A. Quist-Jensen, F. Macedonio, E. Drioli, Membrane technology for water production in agriculture: Desalination and wastewater reuse, Desalination. 364 (2015) 17–32. https://doi.org/10.1016/j.desal.2015.03.001.

[2] H. Lin, W. Peng, M. Zhang, J. Chen, H. Hong, Y. Zhang, A review on anaerobic membrane bioreactors: Applications, membrane fouling and future perspectives, Desalination. 314 (2013) 169–188. https://doi.org/10.1016/j.desal.2013.01.019.

[3] A. Ruiz-García, N. Melián-Martel, I. Nuez, Short Review on Predicting Fouling in RO Desalination, Membranes (Basel). 7 (2017) 62. https://doi.org/10.3390/membranes7040062.

[4] F. Ahmed, B.S. Lalia, V. Kochkodan, R. Hashaikeh, Electrically conductive polymeric membranes for fouling prevention and detection: A review, Desalination. 391 (2016) 1–15. https://doi.org/10.1016/J.DESAL.2016.01.030.

[5] A. Ronen, S.L. Walker, D. Jassby, Electroconductive and electroresponsive membranes for water treatment, Rev. Chem. Eng. 32 (2016) 533–550. https://doi.org/10.1515/revce-2015-0060.

[6] P. Formoso, E. Pantuso, G. De Filpo, F. Nicoletta, Electro-Conductive Membranes for Permeation Enhancement and Fouling Mitigation: A Short Review, Membranes (Basel). 7 (2017) 39. https://doi.org/10.3390/membranes7030039.

[7] I.-H. Loh, R.A. Moody, J.C. Huang, Electrically conductive membranes: Synthesis and applications, J. Memb. Sci. 50 (1990) 31–49. https://doi.org/10.1016/S0376-7388(00)80884-4.

[8] W. Hu, S. Chen, Z. Yang, L. Liu, H. Wang, Flexible electrically conductive nanocomposite membrane based on bacterial cellulose and polyaniline, J. Phys. Chem. B. 115 (2011) 8453–8457. https://doi.org/10.1021/jp204422v.

[9] C. de Lannoy, D. Jassby, D.D. Davis, M.R. Wiesner, A highly electrically conductive polymer–multiwalled carbon nanotube nanocomposite membrane, J. Memb. Sci. 415–416 (2012) 718–724. https://doi.org/10.1016/J.MEMSCI.2012.05.061.

[10] M.S.P. Shaffer, A.H. Windle, Fabrication and Characterization of Carbon Nanotube/Poly(vinyl alcohol) Composites, Adv. Mater. 11 (1999) 937–941. https://doi.org/10.1002/(SICI)1521-4095(199908)11:11<937::AID-ADMA937>3.0.CO;2-9.

[11] F. Ahmed, B.S. Lalia, V. Kochkodan, N. Hilal, R. Hashaikeh, Electrically conductive polymeric membranes for fouling prevention and detection: A review, Desalination. 391 (2016) 1–15. https://doi.org/10.1016/j.desal.2016.01.030.

[12] M.A. Halali, C.-F. de Lannoy, The Effect of Cross-Linkers on the Permeability of Electrically Conductive Membranes, Ind. Eng. Chem. Res. 58 (2019) 3832–3844. https://doi.org/10.1021/acs.iecr.8b05691.

[13] H. Chen, M.B. Müller, K.J. Gilmore, G.G. Wallace, D. Li, Mechanically Strong, Electrically Conductive, and Biocompatible Graphene Paper, Adv. Mater. 20 (2008) 3557–3561. https://doi.org/10.1002/adma.200800757.

[14] H. Kim, Y. Miura, C.W. Macosko, Graphene/Polyurethane Nanocomposites for Improved Gas Barrier and Electrical Conductivity, Chem. Mater. 22 (2010) 3441–3450. https://doi.org/10.1021/cm100477v.

[15] W. Fu, X. Wang, J. Zheng, M. Liu, Z. Wang, Antifouling performance and mechanisms in an electrochemical ceramic membrane reactor for wastewater treatment, (2018). https://doi.org/10.1016/j.memsci.2018.10.077.

[16] P. Geng, G. Chen, Magnéli Ti4O7 modified ceramic membrane for electrically-assisted filtration with antifouling property, J. Memb. Sci. 498 (2016) 302–314. https://doi.org/10.1016/j.memsci.2015.07.055.

[17] W. Duan, A. Ronen, S. Walker, D. Jassby, Polyaniline-Coated Carbon Nanotube Ultrafiltration Membranes: Enhanced Anodic Stability for *In Situ* Cleaning and Electro-Oxidation Processes, ACS Appl. Mater. Interfaces. 8 (2016) 22574–22584. https://doi.org/10.1021/acsami.6b07196.

[18] Y. Gao, W. Li, W.C.L. Lay, H.G.L. Coster, A.G. Fane, C.Y. Tang, Characterization of forward osmosis membranes by electrochemical impedance spectroscopy, Desalination. 312 (2013) 45–51. https://doi.org/10.1016/j.desal.2012.03.006.

[19] J.S. Ho, L.N. Sim, R.D. Webster, B. Viswanath, H.G.L. Coster, A.G. Fane, Monitoring fouling behavior of reverse osmosis membranes using electrical impedance spectroscopy: A field trial study, Desalination. 407 (2017) 75–84. https://doi.org/10.1016/j.desal.2016.12.012.

[20] N. Zhang, M.A. Halali, C.F. de Lannoy, Detection of fouling on electrically conductive membranes by electrical impedance spectroscopy, Sep. Purif. Technol. 242 (2020) 116823. https://doi.org/10.1016/j.seppur.2020.116823.

[21] S.T. Sultana, J.T. Babauta, H. Beyenal, Electrochemical biofilm control: A review, Biofouling. 31 (2015) 745–758. https://doi.org/10.1080/08927014.2015.1105222.

[22] C. Piyadasa, H.F. Ridgway, T.R. Yeager, M.B. Stewart, C. Pelekani, S.R. Gray, J.D. Orbell, The application of electromagnetic fields to the control of the scaling and biofouling of reverse osmosis membranes - A review, Desalination. 418 (2017) 19–34. https://doi.org/10.1016/j.desal.2017.05.017.

[23] M.H.O. Rashid, S.F. Ralph, Carbon nanotube membranes: Synthesis, properties, and future filtration applications, Nanomaterials. 7 (2017). https://doi.org/10.3390/nano7050099.

[24] C. Trellu, B.P. Chaplin, C. Coetsier, R. Esmilaire, S. Cerneaux, C. Causserand, M. Cretin, Electro-oxidation of organic pollutants by reactive electrochemical membranes, Chemosphere. 208 (2018) 159–175. https://doi.org/10.1016/j.chemosphere.2018.05.026.

[25] C. Li, X. Guo, X. Wang, S. Fan, Q. Zhou, H. Shao, W. Hu, C. Li, L. Tong, R.R. Kumar, J. Huang, Membrane fouling mitigation by coupling applied electric field in membrane system: Configuration, mechanism and performance, Electrochim. Acta. 287 (2018) 124–134. https://doi.org/10.1016/j.electacta.2018.06.150.

[26] X. Zhu, D. Jassby, Electroactive Membranes for Water Treatment: Enhanced Treatment Functionalities, Energy Considerations, and Future Challenges, Acc. Chem. Res. 52 (2019) 1177–

1186. https://doi.org/10.1021/acs.accounts.8b00558.

[27] M. Sun, X. Wang, L.R. Winter, Y. Zhao, W. Ma, T. Hedtke, J.-H. Kim, M. Elimelech, Electrified Membranes for Water Treatment Applications, ACS ES&T Eng. 1 (2021) 725–752. https://doi.org/10.1021/acsestengg.1c00015.

[28] J. Mansouri, S. Harrisson, V. Chen, Strategies for controlling biofouling in membrane filtration systems: Challenges and opportunities, J. Mater. Chem. 20 (2010) 4567–4586. https://doi.org/10.1039/b926440j.

[29] I. Gall, M. Herzberg, Y. Oren, The effect of electric fields on bacterial attachment to conductive surfaces, Soft Matter. 9 (2013) 2443–2452. https://doi.org/10.1039/c2sm27270a.

[30] S. Pandit, S. Shanbhag, M. Mauter, Y. Oren, M. Herzberg, Influence of Electric Fields on Biofouling of Carbonaceous Electrodes, (2017). https://doi.org/10.1021/acs.est.6b06339.

[31] Y. Baek, H. Yoon, S. Shim, J. Choi, J. Yoon, Electroconductive Feed Spacer as a Tool for Biofouling Control in a Membrane System for Water Treatment, Environ. Sci. Technol. Lett. 1 (2014) 179–184. https://doi.org/10.1021/ez400206d.

[32] A. Ronen, W. Duan, I. Wheeldon, S. Walker, D. Jassby, Microbial Attachment Inhibition through Low-Voltage Electrochemical Reactions on Electrically Conducting Membranes, Environ. Sci. Technol. 49 (2015) 12741–12750. https://doi.org/10.1021/acs.est.5b01281.

[33] S.H. Hong, J. Jeong, S. Shim, H. Kang, S. Kwon, K.H. Ahn, J. Yoon, Effect of electric currents on bacterial detachment and inactivation, Biotechnol. Bioeng. 100 (2008) 379–386. https://doi.org/10.1002/bit.21760.

[34] A.K. Thakur, S.P. Singh, C. Thamaraiselvan, M. Nunes Kleinberg, C.J. Arnusch, Graphene oxide on laser-induced graphene filters for antifouling, electrically conductive ultrafiltration membranes, (2019). https://doi.org/10.1016/j.memsci.2019.117322.

[35] M.S. Rahaman, C.D. Vecitis, M. Elimelech, Electrochemical carbon-nanotube filter performance toward virus removal and inactivation in the presence of natural organic matter, Environ. Sci. Technol. 46 (2012) 1556–1564. https://doi.org/10.1021/es203607d.

[36] C.D. Vecitis, M.H. Schnoor, M.S. Rahaman, J.D. Schiffman, M. Elimelech, Electrochemical multiwalled carbon nanotube filter for viral and bacterial removal and inactivation, Environ. Sci. Technol. 45 (2011) 3672–3679. https://doi.org/10.1021/es2000062.

[37] A.K. Thakur, S.P. Singh, M.N. Kleinberg, A. Gupta, C.J. Arnusch, Laser-Induced Graphene−PVA Composites as Robust Electrically Conductive Water Treatment Membranes, (2019). https://doi.org/10.1021/acsami.9b00510.

[38] N. Mameda, H.J. Park, K.H. Choo, Membrane electro-oxidizer: A new hybrid membrane system with electrochemical oxidation for enhanced organics and fouling control, Water Res. 126 (2017) 40–49. https://doi.org/10.1016/j.watres.2017.09.009.

[39] C. Liu, X. Xie, W. Zhao, N. Liu, P.A. Maraccini, L.M. Sassoubre, A.B. Boehm, Y. Cui, Conducting Nanosponge Electroporation for Affordable and High-Efficiency Disinfection of Bacteria and Viruses in Water, (2013). https://doi.org/10.1021/nl402053z.

[40] L. Liu, F. Zhao, J. Liu, F. Yang, Preparation of highly conductive cathodic membrane with graphene (oxide)/PPy and the membrane antifouling property in filtrating yeast suspensions in EMBR, J. Memb. Sci. 437 (2013) 99–107. https://doi.org/10.1016/j.memsci.2013.02.045.

[41] S.P. Singh, Y. Li, J. Zhang, J.M. Tour, C.J. Arnusch, Sulfur-Doped Laser-Induced Porous Graphene

Derived from Polysulfone-Class Polymers and Membranes, (2017). https://doi.org/10.1021/acsnano.7b06263.

[42] B. Singh, F. Ejaz, T. Shah, N. Hilal, R. Hashaikeh, Electrically conductive membranes based on carbon nanostructures for self-cleaning of biofouling, DES. 360 (2015) 8–12. https://doi.org/10.1016/j.desal.2015.01.006.

[43] R. Hashaikeh, B.S. Lalia, V. Kochkodan, N. Hilal, A novel in situ membrane cleaning method using periodic electrolysis, J. Memb. Sci. 471 (2014) 149–154. https://doi.org/10.1016/J.MEMSCI.2014.08.017.

[44] D. Bell, R. Sengpiel, M. Wessling, Metallized hollow fiber membranes for electrochemical fouling control, J. Memb. Sci. 594 (2020) 117397. https://doi.org/10.1016/j.memsci.2019.117397.

[45] F.E. Ahmed, R. Hashaikeh, N. Hilal, Fouling control in reverse osmosis membranes through modification with conductive carbon nanostructures, Desalination. 470 (2019) 114118. https://doi.org/10.1016/j.desal.2019.114118.

[46] C.F. De Lannoy, D. Jassby, K. Gloe, A.D. Gordon, M.R. Wiesner, Aquatic biofouling prevention by electrically charged nanocomposite polymer thin film membranes, Environ. Sci. Technol. 47 (2013) 2760–2768. https://doi.org/10.1021/es3045168.

[47] S. Shim, S.H. Hong, Y. Tak, J. Yoon, Prevention of Pseudomonas aeruginosa adhesion by electric currents, Biofouling. 27 (2011) 217–224. https://doi.org/10.1080/08927014.2011.554831.

[48] C. Thamaraiselvan, A. Ronen, S. Lerman, M. Balaish, Y. Ein-Eli, C.G. Dosoretz, Low voltage electric potential as a driving force to hinder biofouling in self-supporting carbon nanotube membranes, Water Res. 129 (2018) 143–153. https://doi.org/10.1016/j.watres.2017.11.004.

[49] R.E. Perez-Roa, D.T. Tompkins, M. Paulose, C.A. Grimes, M.A. Anderson, D.R. Noguera, Effects of localised, low-voltage pulsed electric fields on the development and inhibition of Pseudomonas aeruginosa biofilms., Biofouling. 22 (2006) 383–90. https://doi.org/10.1080/08927010601053541.

[50] Y. Zhou, S. Maharubin, P. Tran, T. Reid, G.Z. Tan, Anti-biofilm AgNP-polyaniline-polysulfone composite membrane activated by low intensity direct/alternating current, Environ. Sci. Water Res. Technol. 4 (2018) 1511–1521. https://doi.org/10.1039/c8ew00259b.

[51] R. Narsetti, R.D. Curry, K.F. McDonald, T.E. Clevenger, L.M. Nichols, Microbial inactivation in water using pulsed electric fields and magnetic pulse compressor technology, IEEE Trans. Plasma Sci. 34 (2006) 1386–1393. https://doi.org/10.1109/TPS.2006.878386.

[52] S.M. Duda, J.E. Stout, Final Technical Report Biological Control in Cooling Water Systems Using Non--Chemical Treatment Devices Full--scale and pilot-- scale cooling towers, 2010.

[53] J.W. Costerton, B. Ellis, K. Lam, F. Johnson, A.E. Khoury, Mechanism of electrical enhancement of efficacy of antibiotics in killing biofilm bacteria, Antimicrob. Agents Chemother. 38 (1994) 2803–2809. https://doi.org/10.1128/AAC.38.12.2803.

[54] A. Esmaeili, E. Hashemi, Biotransformation of myrcene by Pseudomonas aeruginosa, Chem. Cent. J. 5 (2011). https://doi.org/10.1186/1752-153X-5-26.

[55] D.T. Schoen, A.P. Schoen, L. Hu, H.S. Kim, S.C. Heilshorn, Y. Cui, High speed water sterilization using one-dimensional nanostructures, Nano Lett. 10 (2010) 3628–3632. https://doi.org/10.1021/nl101944e.

[56] H. Vega-Mercado, U.R. Pothakamury, F.J. Chang, G. V. Barbosa-Cánovas, B.G. Swanson, Inactivation of Escherichia coli by combining pH, ionic strength and pulsed electric fields hurdles,

Food Res. Int. 29 (1996) 117–121. https://doi.org/10.1016/0963-9969(96)00015-4.

[57] Y. Yang, S. Qiao, R. Jin, J. Zhou, X. Quan, Novel Anaerobic Electrochemical Membrane Bioreactor with a CNTs Hollow Fiber Membrane Cathode to Mitigate Membrane Fouling and Enhance Energy Recovery, (2018). https://doi.org/10.1021/acs.est.8b05186.

[58] O. Istanbullu, J. Babauta, H. Duc Nguyen, H. Beyenal, Electrochemical biofilm control: mechanism of action, Biofouling. 28 (2012) 769–778. https://doi.org/10.1080/08927014.2012.707651.

[59] Y.K. Wang, W.W. Li, G.P. Sheng, B.J. Shi, H.Q. Yu, In-situ utilization of generated electricity in an electrochemical membrane bioreactor to mitigate membrane fouling, Water Res. 47 (2013) 5794–5800. https://doi.org/10.1016/j.watres.2013.06.058.

[60] L. Fu, S.-J. You, F. Yang, M. Gao, X. Fang, G. Zhang, Synthesis of hydrogen peroxide in microbial fuel cell, J. Chem. Technol. Biotechnol. 85 (2010) 715–719. https://doi.org/10.1002/jctb.2367.

[61] J.T. Babauta, H.D. Nguyen, O. Istanbullu, H. Beyenal, Microscale gradients of oxygen, hydrogen peroxide, and pH in freshwater cathodic biofilms, ChemSusChem. 6 (2013) 1252–1261. https://doi.org/10.1002/cssc.201300019.

[62] O. Istanbullu, J. Babauta, H. Duc Nguyen, H. Beyenal, Biofouling The Journal of Bioadhesion and Biofilm Research Electrochemical biofilm control: mechanism of action Electrochemical biofilm control: mechanism of action, (n.d.). https://doi.org/10.1080/08927014.2012.707651.

[63] C.T. Wang, W.L. Chou, Y.M. Kuo, F.L. Chang, Paired removal of color and COD from textile dyeing wastewater by simultaneous anodic and indirect cathodic oxidation, J. Hazard. Mater. 169 (2009) 16–22. https://doi.org/10.1016/j.jhazmat.2009.03.054.

[64] W. Fu, X. Wang, J. Zheng, M. Liu, Z. Wang, Antifouling performance and mechanisms in an electrochemical ceramic membrane reactor for wastewater treatment, J. Memb. Sci. 570–571 (2019) 355–361. https://doi.org/10.1016/j.memsci.2018.10.077.

[65] S. Shim, S. Hoon Hong, Y. Tak, J. Yoon, Biofouling The Journal of Bioadhesion and Biofilm Research Prevention of Pseudomonas aeruginosa adhesion by electric currents, (n.d.). https://doi.org/10.1080/08927014.2011.554831.

[66] A.J. Santiago, M.N.A. Ahmed, S.L. Wang, K. Damera, B. Wang, P.C. Tai, E.S. Gilbert, C.D. Derby, Inhibition and dispersal of Pseudomonas aeruginosa biofilms by combination treatment with escapin intermediate products and hydrogen peroxide, Antimicrob. Agents Chemother. 60 (2016) 5554–5562. https://doi.org/10.1128/AAC.02984-15.

[67] P.S. Stewart, F. Roe, J. Rayner, J.G. Elkins, Z. Lewandowski, U.A. Ochsner, D.J. Hassett, Effect of Catalase on Hydrogen Peroxide Penetration into Pseudomonas aeruginosa Biofilms, 2000. http://aem.asm.org/ (accessed June 24, 2020).

[68] J.G. Elkins, D.J. Hassett, P.S. Stewart, H.P. Schweizer, T.R. McDermott, Protective role of catalase in Pseudomonas aeruginosa biofilm resistance to hydrogen peroxide, Appl. Environ. Microbiol. 65 (1999) 4594–4600. https://doi.org/10.1128/aem.65.10.4594-4600.1999.

[69] Y. Liu, ab Juen Hon Dustin Lee, Q. Xia, Y. Ma, Y. Yu, L. Yue Lanry Yung, J. Xie, C. Nam Ong, C.D. Vecitis, Z. Zhou, A graphene-based electrochemical filter for water purification †, (2014). https://doi.org/10.1039/c4ta04006f.

[70] C.A. Martínez-Huitle, M.A. Rodrigo, I. Sirés, O. Scialdone, Single and Coupled Electrochemical Processes and Reactors for the Abatement of Organic Water Pollutants: A Critical Review, Chem. Rev. 115 (2015) 13362–13407. https://doi.org/10.1021/acs.chemrev.5b00361.

[71] J. Speight, LANGE'S HANDBOOK OF CHEMISTRY, 2017. https://www.accessengineeringlibrary.com/binary/mheaeworks/ea71143cd46bc712/7b87106e446793264e4b0625f45999c830e326b570e3044d32e4dddd9cf9e781/book-summary.pdf (accessed May 5, 2021).

[72] W.K. Liu, M.R.W. Brown, T.S.J. Elliott, Mechanisms of the bactericidal activity of low amperage electric current (DC), J. Antimicrob. Chemother. 39 (1997) 687–695. https://doi.org/10.1093/jac/39.6.687.

[73] R.E. Perez-Roa, D.T. Tompkins, M. Paulose, C.A. Grimes, M.A. Anderson, D.R. Noguera, Effects of localised, low-voltage pulsed electric fields on the development and inhibition of Pseudomonas aeruginosa biofilms, Biofouling. 22 (2006) 383–390. https://doi.org/10.1080/08927010601053541.

[74] H. Liu, A. Vajpayee, C.D. Vecitis, Bismuth-Doped Tin Oxide-Coated Carbon Nanotube Network: Improved Anode Stability and Efficiency for Flow-Through Organic Electrooxidation, (2013). https://doi.org/10.1021/am402621v.

[75] X. Fan, H. Zhao, X. Quan, Y. Liu, S. Chen, Nanocarbon-based membrane filtration integrated with electric field driving for effective membrane fouling mitigation, Water Res. 88 (2016) 285–292. https://doi.org/10.1016/j.watres.2015.10.043.

[76] Y. Liu, H. Liu, Z. Zhou, T. Wang, ‖ Choon, N. Ong, C.D. Vecitis, Degradation of the Common Aqueous Antibiotic Tetracycline using a Carbon Nanotube Electrochemical Filter, (2015). https://doi.org/10.1021/acs.est.5b00870.

[77] X. Fan, H. Zhao, Y. Liu, X. Quan, H. Yu, S. Chen, Enhanced Permeability, Selectivity, and Antifouling Ability of CNTs/ Al 2 O 3 Membrane under Electrochemical Assistance, Environ. Sci. Technol. 18 (2015) 24. https://doi.org/10.1021/es5039479.

[78] C. Trellu, C. Coetsier, J.C. Rouch, R. Esmilaire, M. Rivallin, M. Cretin, C. Causserand, Mineralization of organic pollutants by anodic oxidation using reactive electrochemical membrane synthesized from carbothermal reduction of TiO2, Water Res. 131 (2018) 310–319. https://doi.org/10.1016/j.watres.2017.12.070.

[79] A.R. Bakr, M.S. Rahaman, Electrochemical efficacy of a carboxylated multiwalled carbon nanotube filter for the removal of ibuprofen from aqueous solutions under acidic conditions, Chemosphere. 153 (2016) 508–520. https://doi.org/10.1016/j.chemosphere.2016.03.078.

[80] Z. Liu, M. Zhu, L. Zhao, C. Deng, J. Ma, Z. Wang, H. Liu, H. Wang, Aqueous tetracycline degradation by coal-based carbon electrocatalytic filtration membrane: Effect of nano antimony-doped tin dioxide coating, Chem. Eng. J. 314 (2017) 59–68. https://doi.org/10.1016/j.cej.2016.12.093.

[81] H. Liu, C.D. Vecitis, Reactive transport mechanism for organic oxidation during electrochemical filtration: Mass-transfer, physical adsorption, and electron-transfer, J. Phys. Chem. C. 116 (2012) 374–383. https://doi.org/10.1021/jp209390b.

[82] A.R. Bakr, M.S. Rahaman, Removal of bisphenol A by electrochemical carbon-nanotube filter: Influential factors and degradation pathway, Chemosphere. 185 (2017) 879–887. https://doi.org/10.1016/j.chemosphere.2017.07.082.

[83] Z. Liu, M. Zhu, Z. Wang, H. Wang, C. Deng, K. Li, Effective Degradation of Aqueous Tetracycline Using a Nano-TiO2/Carbon Electrocatalytic Membrane, Materials (Basel). 9 (2016) 364. https://doi.org/10.3390/ma9050364.

[84] G. Gao, C.D. Vecitis, Electrocatalysis aqueous phenol with carbon nanotubes networks as anodes: Electrodes passivation and regeneration and prevention, Electrochim. Acta. 98 (2013) 131–138.

https://doi.org/10.1016/j.electacta.2013.02.127.

[85] J. Li, Q. Liu, Y. Liu, J. Xie, Development of electro-active forward osmosis membranes to remove phenolic compounds and reject salts, Environ. Sci. Water Res. Technol. 3 (2017) 139–146. https://doi.org/10.1039/c6ew00275g.

[86] G. Gao, C.D. Vecitis, Doped Carbon Nanotube Networks for Electrochemical Filtration of Aqueous Phenol: Electrolyte Precipitation and Phenol Polymerization, (2012). https://doi.org/10.1021/am2017267.

[87] G. Gao, M. Pan, C.D. Vecitis, Effect of the oxidation approach on carbon nanotube surface functional groups and electrooxidative filtration performance †, (2015). https://doi.org/10.1039/c4ta07191c.

[88] P. Geng, G. Chen, Magnéli Ti 4 O 7 modified ceramic membrane for electrically-assisted filtration with antifouling property, (2015). https://doi.org/10.1016/j.memsci.2015.07.055.

[89] K. Wang, L. Xu, K. Li, L. Liu, Y. Zhang, J. Wang, Development of polyaniline conductive membrane for electrically enhanced membrane fouling mitigation, J. Memb. Sci. 570–571 (2019) 371–379. https://doi.org/10.1016/j.memsci.2018.10.050.

[90] Q. Zhang, C.D. Vecitis, Conductive CNT-PVDF membrane for capacitive organic fouling reduction, J. Memb. Sci. 459 (2014) 143–156. https://doi.org/10.1016/j.memsci.2014.02.017.

[91] W. Duan, A. Ronen, J.V. de Leon, A. Dudchenko, S. Yao, J. Corbala-Delgado, A. Yan, M. Matsumoto, D. Jassby, Treating anaerobic sequencing batch reactor effluent with electrically conducting ultrafiltration and nanofiltration membranes for fouling control, J. Memb. Sci. 504 (2016) 104–112. https://doi.org/10.1016/J.MEMSCI.2016.01.011.

[92] A. V. Dudchenko, J. Rolf, K. Russell, W. Duan, D. Jassby, Organic fouling inhibition on electrically conducting carbon nanotube-polyvinyl alcohol composite ultrafiltration membranes, J. Memb. Sci. 468 (2014) 1–10. https://doi.org/10.1016/j.memsci.2014.05.041.

[93] S. Wang, S. Liang, P. Liang, X. Zhang, J. Sun, S. Wu, X. Huang, In-situ combined dual-layer CNT/PVDF membrane for electrically-enhanced fouling resistance, J. Memb. Sci. 491 (2015) 37–44. https://doi.org/10.1016/j.memsci.2015.05.014.

[94] Z.H. Wu, H.B. Chen, Y.M. Dong, H.L. Mao, J.L. Sun, S.F. Chen, V.S.J. Craig, J. Hu, Cleaning using nanobubbles: Defouling by electrochemical generation of bubbles, J. Colloid Interface Sci. 328 (2008) 10–14. https://doi.org/10.1016/j.jcis.2008.08.064.

[95] X. Sun, J. Wu, Z. Chen, X. Su, B.J. Hinds, Fouling characteristics and electrochemical recovery of carbon nanotube membranes, Adv. Funct. Mater. 23 (2013) 1500–1506. https://doi.org/10.1002/adfm.201201265.

[96] M.A. Halali, M. Larocque, C.F. de Lannoy, Investigating the stability of electrically conductive membranes, J. Memb. Sci. 627 (2021) 119181. https://doi.org/10.1016/j.memsci.2021.119181.

[97] A. Karkooti, M. Rastgar, N. Nazemifard, M. Sadrzadeh, Graphene-based electro-conductive anti-fouling membranes for the treatment of oil sands produced water, (n.d.). https://doi.org/10.1016/j.scitotenv.2019.135365.

[98] H.M. Huotari, I.H. Huisman, G. Tra, È. Êrdh, Electrically enhanced cross¯ow membrane ®ltration of oily waste water using the membrane as a cathode, n.d.

[99] K.C. Ho, Y.H. Teow, A.W. Mohammad, Optimization of nanocomposite conductive membrane formulation and operating parameters for electrically-enhanced palm oil mill effluent filtration using response surface methodology, Process Saf. Environ. Prot. 126 (2019) 297–308.

https://doi.org/10.1016/j.psep.2019.03.019.

[100] W. Duan, A. Dudchenko, E. Mende, C. Flyer, X. Zhu, D. Jassby, Electrochemical mineral scale prevention and removal on electrically conducting carbon nanotube-polyamide reverse osmosis membranes † The electrochemical prevention and removal of CaSO 4 and CaCO 3 mineral scales on electrically, (2014). https://doi.org/10.1039/c3em00635b.

[101] C. Weidlich, K.M. Mangold, Electrochemically switchable polypyrrole coated membranes, in: Electrochim. Acta, 2011: pp. 3481–3484. https://doi.org/10.1016/j.electacta.2010.11.065.

[102] C.D. Vecitis, G. Gao, H. Liu, Electrochemical Carbon Nanotube Filter for Adsorption, Desorption, and Oxidation of Aqueous Dyes and Anions, J. Phys. Chem. C. 115 (2011) 3621–3629. https://doi.org/10.1021/jp111844j.

[103] L. Tang, A. Iddya, X. Zhu, A. V Dudchenko, W. Duan, C. Turchi, J. Vanneste, T.Y. Cath, D. Jassby, Enhanced Flux and Electrochemical Cleaning of Silicate Scaling on Carbon Nanotube-Coated Membrane Distillation Membranes Treating Geothermal Brines, (2017). https://doi.org/10.1021/acsami.7b12615.

[104] L. Liu, J. Liu, G. Bo, F. Yang, J. Crittenden, Y. Chen, Conductive and hydrophilic polypyrrole modified membrane cathodes and fouling reduction in MBR, J. Memb. Sci. 429 (2013) 252–258. https://doi.org/10.1016/j.memsci.2012.11.066.

[105] L. Liu, J. Liu, B. Gao, F. Yang, S. Chellam, Fouling reductions in a membrane bioreactor using an intermittent electric field and cathodic membrane modified by vapor phase polymerized pyrrole, J. Memb. Sci. 394–395 (2012) 202–208. https://doi.org/10.1016/j.memsci.2011.12.042.

[106] W. Duan, G. Chen, C. Chen, R. Sanghvi, A. Iddya, S. Walker, Electrochemical removal of hexavalent chromium using electrically conducting carbon nanotube / polymer composite ultra fi ltration membranes, J. Memb. Sci. 531 (2017) 160–171. https://doi.org/10.1016/j.memsci.2017.02.050.

[107] P. Gayen, J. Spataro, S. Avasarala, A.-M. Ali, J.J. Cerrato, B.P. Chaplin, Electrocatalytic Reduction of Nitrate Using Magneíi Phase TiO 2 Reactive Electrochemical Membranes Doped with Pd-Based Catalysts, (2018). https://doi.org/10.1021/acs.est.8b03038.

[108] D. Hou, A. Iddya, X. Chen, M. Wang, W. Zhang, Y. Ding, D. Jassby, Z.J. Ren, Nickel-Based Membrane Electrodes Enable High-Rate Electrochemical Ammonia Recovery, (2018). https://doi.org/10.1021/acs.est.8b01349.

[109] A. V Dudchenko, C. Chen, A. Cardenas, J. Rolf, D. Jassby, Frequency-dependent stability of CNT Joule heaters in ionizable media and desalination processes, Nat. Nanotechnol. |. 12 (2017). https://doi.org/10.1038/NNANO.2017.102.

[110] Y. Feng, L. Yang, J. Liu, B.E. Logan, Electrochemical technologies for wastewater treatment and resource reclamation, Environ. Sci. Water Res. Technol. 2 (2016) 800–831. https://doi.org/10.1039/c5ew00289c.

[111] S.H. Hong, J. Jeong, S. Shim, H. Kang, S. Kwon, K.H. Ahn, J. Yoon, Effect of electric currents on bacterial detachment and inactivation, Biotechnol. Bioeng. 100 (2008) 379–386. https://doi.org/10.1002/bit.21760.

[112] M. Čáp, L. Váchová, Z. Palková, Reactive oxygen species in the signaling and adaptation of multicellular microbial communities, Oxid. Med. Cell. Longev. 2012 (2012). https://doi.org/10.1155/2012/976753.

[113] R. Singh, Desalination and Water Treatment Analysis of energy usage at membrane water treatment plants, (2011). https://doi.org/10.5004/dwt.2011.1810.

Chapter 4

The Effect of Cross-Linkers on the Permeability of Electrically Conductive Membranes

4.1.Abstract

Microfiltration (MF) and Ultrafiltration (UF) electrically conductive membranes (ECMs) were fabricated by coating MF and UF polyethersulfone (PES) membranes, respectively, with a thin conductive film of cross-linked functionalized single and double-walled carbon nanotubes. The thin film was composed of a reacted network of carbon nanotubes, polyvinyl alcohol, and dicarboxylic cross-linkers. We analyzed the impact of cross-linker lengths, mass of CNTs, and cross-linking degree on the thin conductive film's electrical conductivity, pore size, porosity, surface hydrophilicity, and the resultant ECM transmembrane flux. It was found that conductive thin films containing longer cross-linkers increased transmembrane flux in MF and UF membranes by up to 187% and 254%, respectively, over control non-crosslinked membranes. Control MF and UF CNT membranes had average permeabilities of 1008 and 97 LMH/bar. Cross-linked membranes achieved an average permeability of 2901 and 344 LMH/bar, respectively. The bulk electrical conductivity was shown to be affected by both the presence of cross-linkers as well as the thickness of the thin film. Longer cross-linkers in MF and UF ECMs enhanced electrical conductivity by up to 61% and 440% as compared to control non-crosslinked MF and UF ECMs, respectively. Morphology of the membrane, wetting properties, surface roughness, and presence of covalent bonds were investigated using SEM, pendant-drop contact angle test, and AFM, respectively.

4.2. Introduction

Global population growth coupled to limited fresh water resources necessitate technologies to produce potable drinking water. Membranes have been shown to efficiently produce potable water from a wide variety of sources [2–8]. Membranes are also low cost, have a smaller footprint, and are flexible with respect to operating conditions [9,10]. Four categories of membranes are defined based on their pore size including microfiltration (MF), ultrafiltration (UF), nanofiltration (NF), and reverse osmosis (RO). Conventionally, separation across MF and UF membranes is based on size exclusion. It is well established that most particles in natural waters and wastewaters are electrically charged, including viruses, bacteria, and ions [11,12]. As such, a combination of size exclusion and electrical field generated repulsion may enhance membrane separations. Furthermore, electrochemically generated surface redox reactions have been shown to prevent the adsorption of common foulants to surfaces [13–17]. Electrically conductive membranes (ECMs) have been developed to enable enhanced membrane separation and antifouling properties. Their performance for water purification purposes has been investigated recently, showing improved membrane performance under high-fouling conditions [15,18–21]. The mechanisms by which ECMs prevent biofouling is investigated in [19,22,23]. The surfaces of most ECMs are thin composite coatings containing a conductive material such as carbon nanotubes (CNTs) [24,25], graphene [26,27], or graphite [28]. The first generation of ECMs consisted of CNTs deposited on a conventional membrane [24]. The underlying polymeric support governed rejection while the coating layer provided electrical conductivity. Surface properties and antifouling features of ECMs have been well studied in the literature.

Vecitis et al. [29] highlighted the anti-bacterial and anti-viral effect of anodic MWCNTs. They observed a 75% and 99.6% inactivation rate for viruses (MS2) and bacteria (E.Coli) after 30 s post-filtration under application of 2 and 3 V. In 2013, de Lannoy et al. [22] conducted research that revealed the superior antifouling performance of ECMs over conventional polymeric membranes. In their study, the ECMs consisted of CNTs embedded in a polyamide layer. The result revealed that a 45% decline in water flux

due to biofouling took 80 hr for an ECM while for a typical membrane it was about 22 hr. The flux recovery after back-flushing was also drastically increased for ECMs (92% and above). Recently, Duan et al. [30] carried out research on how a UF ECM composed of CNT-PVA was effective in eliminating hexavalent chromium from drinking water. They found that electrical repulsion, electrochemical reduction, and precipitation could contribute to the removal of toxic Cr(VI). They further evaluated the impact of operational (contact time, flux, and electric potential) and environmental (pH and salinity) conditions on the removal rate. Dudchenko et al. [14] presented a similar network (MWCNT-PVA) coated on polysulfone (PSf) as a viable candidate to reduce fouling of alginic acid (AA) under different potentials in an electro-filtration cell. The reduction in trans-membrane pressure decreased by 33% and 51% when a potential of 3 and 5 V was used, respectively, as compared to control experiments without an applied voltage. An interesting application of ECMs was brought forward by Duan et al. [31] where they coupled anaerobic sequencing batch reactors (aSBRs) to UF and NF ECMs. They illustrated that ECMs can be employed to reduce the degree of fouling and maintaining the high flux of the system. In their setup, degraded benzyl alcohol from the aSBR was rejected up to 90% through UF and NF ECM membranes. Duan et al. [32] successfully fabricated polyaniline-CNT UF ECMs with enhanced electrical conductivity, hydrophilicity, and stability under anodic conditions. The water flux recovery of the ECM was reported to be almost 100% under an applied potential of 3 V. In addition, a 95% degradation of methylene blue was observed through a single pass of anodically charged ECM. Hong et al. [23] investigated the effect of electric current on inactivation and detachment of bacteria. They claimed that cathodic current restricts the attachment of bacteria, while the anodic current has more contribution to the cell lysis rather than bacterial detachment. Hashaikeh et al. [33] presented the self-cleaning property of the ECMs through the evolution of non-destructive micro bubbles. They showed that electrolysis cleaning intervals of 30, 40, and 60 min during a 2 hr filtration process could successfully increase the flux by 63, 40, and 30 % for calcium carbonate and 15, 14, and 9 % for yeast suspension.

While much work has been devoted to the anti-fouling properties of these first generation ECMs, little attention has been paid to improving the material and membrane characteristics of ECMs. Generally, there is an inverse relationship between permeability and selectivity of a membrane, represented by permselectivity. ECMs have demonstrated potential in maintaining permselectivity through their unique antifouling properties. Fouling is one of the major challenges in membrane operation, reducing both flux and selectivity, but the pristine membrane characteristic must also be addressed for practical application. The promising results of ECMs have led to the current effort to enhance their flux, selectivity, and electrical conductivity, and improving their pore size distribution. Addressing the membrane characteristics is critical for eventual adoption of these membranes by industry. Currently, thin films in ECMs are randomly formed from CNTs with no order or uniform pore size.

CNTs are not dispersible in water due to their homo-aggregation and hydrophobicity. CNT aggregation in aqueous solutions can be prevented by functionalizing some of the carbon ring structures and/or by mixing CNT-slurries with compatible surfactants. Unbundled and well-dispersed CNTs are nevertheless curled. While they will uniformly coat a surface (e.g. using the pressure deposition technique), these coatings lack both order and orientation. Their high length to width aspect ratio hinders alignment. The resultant film is a random configuration of long curled CNTs. A thin film membrane composed of such a random structure has high pore polydispersity. Addressing this shortcoming of ECMs is critical for successful implementation of ECMs in industry. Hence, we investigated ECM material properties to increase the transmembrane flux, narrow the pore size distribution, and increase the electrical conductivity as compared to that reported in the literature.

In this paper, MF and UF ECMs have been fabricated by coating a membrane with a CNT- PVA-cross-linker network (Figure 4.1 (a)). We synthesized membranes with both multi-walled carbon nanotubes (MWCNT) and single walled/double walled carbon nanotubes (SW/DWCNT) solutions. We observed the stability over time of CNT suspensions made from MWCNTs and SW/DWCNTs. For SW/DWCNT suspensions,

there was no sign of sedimentation/aggregation after more than 2 months. The improved stability of SW/DWCNT formed membranes with substantially improved properties. As such, this paper only considers membranes formed from SW/DWCNTs. Control over pore size was achieved by introducing cross-linkers with different lengths. The cross-linkers used in this study were dicarboxylic acids with 4 and 8 carbons in their chains (succinic acid and suberic acid, respectively). PVA is a linear polymer and contains many hydroxyl groups along its backbone. These hydroxyl groups were cross-linked to carboxyl functionalized CNTs through an esterification reaction. Esterification reactions offer strong covalent bonds, crucial to the strength of the network. The cross-linked polymer-CNT network was cured into the polymeric support, providing stability to the dense CNT thin film. Dicarboxylic cross-linkers can further be cross-linked with PVA through a dehydrogenation reaction between hydroxyl-carboxyl groups [34,35]. It was hypothesized that integration of cross-linkers in the network can affect the compactness of the configuration as the cross-linkers act as spacers between CNTs. A similar network using only a single type of cross-linker (succinic acid) has previously been tested for UF membranes [24]. de Lannoy et al. [24] fabricated UF ECMs and investigated the effect of CNT concentration with respect to PVA in electrical conductivity, pure water flux, and PEO rejection, and water contact angle. PVA endows higher stability and hydrophilicity to the membrane, but at the sacrifice of lower electrical conductivity. In this study, they optimized the CNT-PVA trade-off and the optimal ratio of PVA to CNT was reported to be 10% (wt% CNT wrt PVA). In another study, Dlamini et al. [36] deposited a cross-linked PVA film on a PSf membrane and investigated the effect of crosslinking type and cross-linking degree in flux and rejection. The PVA was cross-linked with either aliphatic tricarboxylic acids or aromatic dicarboxylic acids. It was demonstrated that the crystallinity and pure water flux were correlated for cross-linked membranes.

Here, we demonstrated that integration of cross-linkers with different lengths in the network changes the compactness of the structure and directly affects pure water flux and electrical conductivity. In addition, complementary characterization tests were carried out

to investigate the morphology, thickness, presence of covalent bonds, and wetting properties of the membrane.

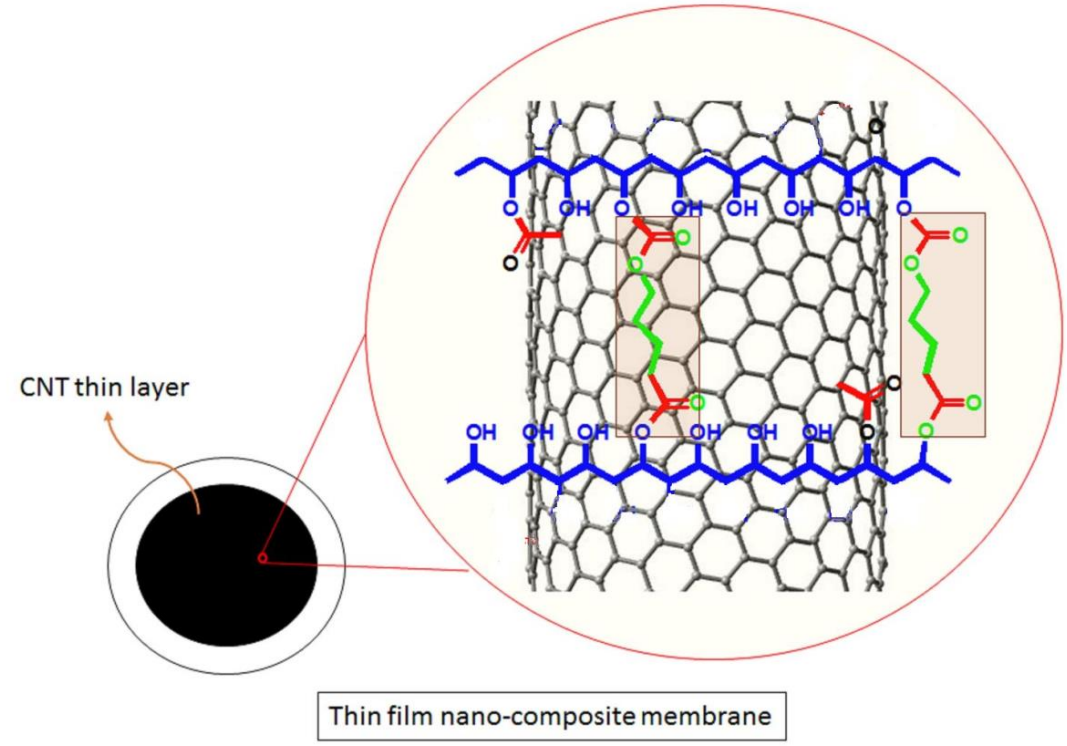

(a)

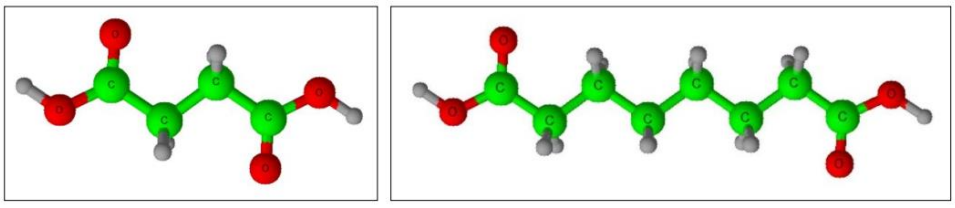

(b)

Figure 4.1. (a) the CNT network contains cross-linkers which help control the porosity of the network. (b) dicarboxylic acids of different lengths are used as cross-linkers.

4.3.Materials and methods

4.3.1. Materials

Carboxyl functionalized single walled and double walled carbon nanotubes (SW/DWCNT-COOH, outer diameter:1-4 nm, length: 5-30 μm, purity: >90w/%, functional content: 2.73 w/%) was purchased from Cheaptubes (USA). Sodium dodecyl sulfate (SDS) (MW: 288.38) and hydrochloric acid (38% w/w) were purchased from Anachemia (USA and Canada, respectively). Poly(vinyl alcohol) (PVA, MW:31000-50000, 98-99% hydrolyzed) was purchased from Aldrich chemistry (USA). Succinic acid (MW:118.9), and suberic acid (MW:174.20) were purchased from Alfa Aesar (India). UF and MF Polyethersulfone membranes (PES, diameter: 47 mm, pore size: 0.03 μm and 0.8 μm, respectively) were purchased from Sterlitech (USA). DI water used in the experiment is from an Arium system (resistivity: 0.047 μS/cm).

4.3.2. Membrane fabrication

A 0.75 mg/mL suspension of SW/DWCNT in DI water was prepared by stirring the suspension for 10 min (RPM 600, ambient temperature), then ultra-sonicated for 1 hr with a microtip (1/4" diameter) with a variable power but a constant intensity (40% of total intensity delivered) in intervals of 2s on and 2s off. A constant intensity was achieved by controlling the vibrational amplitude for the sonicator probe tip. This was set to 80 μm. By applying a constant amplitude in different experiments, the same intensity was delivered to CNT suspensions regardless of the sample volume, viscosity, or temperature. The samples were placed in an ice bath to avoid an excessive heat generation due to sonication. Simultaneously, 1.125 mg/mL solution of SDS in DI water was prepared in a separate beaker after stirring the solution for 30 min (RPM 600, ambient temperature). The CNT and SDS suspensions were mixed, stirred (15 min), and ultra-sonicated (2hr at the same amplitude and time intervals as above). The ratio of CNT to surfactant (SDS) was 1:1.5. A 500 mg/mL PVA solution was made after stirring the solution in a closed jar for 24 hr (RPM 800, 120°C). The PVA and CNT suspensions were mixed and ultra-sonicated for 2 hr (same amplitude and time intervals) (the ratio of CNT to PVA was always kept at 1:10). The cross-linker solutions were made separately in 50 ml of DI and added to the CNT-PVA suspension. The concentration of the cross-linker was adjusted in such a way that the cross-linking degree was either 10% or 20% [24]. After all components were well mixed,

hydrochloric acid was added to the suspension to catalyze the cross-linking reaction. 38% HCl was added to the suspension until a concentration of 2M is obtained. The solution was allowed to react for 24 hr. It should be noted that a well-dispersed solution is critical to forming a uniform coating of CNTs on the membrane. Representative solutions were left in a beaker for two months and no change in stability was observed, indicating highly stable suspensions.

Pristine membranes (PES) were kept in water for 48 hrs before use to ensure they were fully wetted. The nanocomposite thin film was made using the well-documented pressure filtration deposition method [24]. A wet membrane was placed in a glass flask and the final CNT suspension with a known mass of CNTs was filtered through the membrane (the ratio of CNT to PVA/cross-linkers is fixed in all solutions). Very low mass loadings do not provide desired electrical conductivity. High mass loadings are difficult to filter onto the membranes, produce non-uniform coatings, and reduce the membrane permeability significantly. Membranes were fabricated using a wide range of CNT mass loading (0.1-5 mg) and 1 and 3 mg CNTs were found to provide optimal conditions and were chosen for all subsequent experiments. Following CNT deposition, DI water was filtered through the membrane for 5 min at a vacuum pressure of 100 mbar to rinse any polymeric or acidic residuals from the surface. During the filtration process, clear bubbles were observed in the permeate solution. The bubbles are likely due to leaching of unbonded PVA chains and SDS. PVA is a long linear polymeric chain which is highly soluble in water. The radius of gyration, (the root mean square distance of the segments of the polymer from its center of mass), of the PVA used in these membranes is approximately 6 to 8 nm in water at 25 °C [37,38]. Therefore, unbonded PVA chains can pass through the pores of MF membranes (0.8 µm) as well as through those of the UF membranes (0.03 µm). Leaching of CNTs was found negligible during the filtration process (more information about leaching of CNT/PVA/SDS is presented in SI).

The rinsed thin film membrane was removed from the flask and cured in an oven for 1 hr at 100 °C. The membrane was cooled at room temperature, washed with DI water, and stored in DI water over night before use, characterization and further analysis. The

picture of a pristine PES and a CNT-PES thin film is illustrated in Figure 4.2(a). It should be noted that all membranes were made in triplicate to validate the reproducibility of the results. In this paper, “control” membranes are those composed of PES, CNT, and PVA, while “succinic acid” and “suberic acid” membranes are composed of PES, CNT, PVA, and the respective cross-linkers (succinic or suberic acid). The cross-linking degree was 20% unless otherwise mentioned.

4.3.3. Surface analysis

Scanning electron microscopy (SEM) and atomic force microscopy (AFM) were used to observe the thickness and morphology of the membranes. Membranes were completely dried prior to imaging. For the cross-sectional images, liquid nitrogen was used to crack the membranes without defecting the morphological structure. Hydrophilicity of the surface was calculated using a high speed contact angle instrument (OCA 35) and the angle was measured after dispensing 5 µL of DI water. This instrument is able to record a video of a water droplet from the time the droplet is dispensed through to the time that it spreads across the surface. The video was analyzed after each test and contact angles were measured once droplets achieved steady state (Figure 4.S4). There were three drops dispensed on each membrane and contact angle was reported as an average value. The conductivity of the membranes was measured using a four-point probe conductivity meter (Figure 4.2(b)). This instrument is able to measure the surface resistance of the thin layer by considering the resistance among different pairs of needles and the thickness of the thin film (Figure 4.S3). Membranes were completely dried using an oven (60 °C) and then cooled at room temperature for 1 hour prior to conductivity measurements. Surface potential is measured through two pairs of needles, which are attached to adjustable arms. During measurement, the needle contacts were placed in a square position with an equal distance from each other (Figure 4.2(b)). It was expected that for a uniform surface the resistivity between different pairs is within the same order of magnitude. Therefore, prior to determining surface conductivity, all the resistivity values between the pairs were closely monitored. Before use, we confirmed that the needles of the conductivity meter were made to touch only the CNT thin film of the membrane where the conductive properties are of

interest. Detailed information and formulae to calculate the conductivity of the nanolayer are provided in the SI.

Figure 4.2. (a) Pristine PES membrane (on the left) and electrically conductive membrane (on the right), (b) Four-point conductivity probe.

4.3.4. Pure water flux

The pure water permeance of the membranes was obtained by measurement of pure water flux in a dead-end stirred flow cell (Sterlitech stainless steel). The MF and UF membranes were compressed under high pressure 100 psi (6.9 bar) prior to the flux test for 60 min and 90 min, respectively. High pressure compression enables the porous polymer structure to achieve its steady-state structure and minimizes morphological changes during the flux test. For the flux test, pure water was filtered through the membrane and the volume of the permeate water was recorded every 10 seconds for one minute at a given pressure. The flux test was performed under pressures of 10, 20, 30, 40, 50, and 60 psi (0.69, 1.38, 2.07, 2.76, 3.45, and 4.14 bar). Each pure water flux test was conducted twice at each pressure and the average value was reported.

4.3.5. Selectivity test

We studied the separation properties of our CNT-modified UF membranes by conducting molecular weight cut off (MWCO) experiments. Solutions of 250 ppm

polyethylene oxide (PEO) containing different molecular weights were used as feed solutions. Feed was filtered onto the membranes under 10 psi (0.69 bar) and the permeate was collected and analyzed using a total organic content (TOC) analyzer to measure the rejection.

4.4.Results and discussion

4.4.1. Selectivity

During separation experiments using PEO solutions, we observed that in addition to PEO passing through the membrane, a portion of unbound polyvinyl alcohol (PVA) leached through the membrane as well. The permeate thus contained PVA as well as PEO, which confounded our MWCO measurements (more details can be found in SI). Due to this complication, we analyzed the rejection of nanocomposites formed on support membranes composed of CNTs without PVA. We synthesized nanocomposites containing 1 mg and 3 mg of CNT treated under the same conditions used to create the thin film composites that contained PVA. The CNT thin film composite membranes were exposed to the same fabrication conditions, i.e. exposure to strong acid and high heat, to study whether these conditions impacted their rejection. The pristine PES membranes were used untreated. We compared the rejection of these membranes and the results are shown in Figure 4.3. 1 mg and 3 mg CNT nanocomposites (without PVA) as well as support PES membranes rejected 0.6 MDa PEO to greater than 90%. The rejection of 0.3 MDa was also greater than 90% for 1 mg and 3 mg CNT nanocomposites while it dropped to 31% for PES support membrane. The greater rejection observed in CNT nanocomposites (either 1 mg or 3 mg) suggests formation of a denser network in the thin layer which leads to tighter surface pores. In addition, adsorption of PEO on CNTs likely leads to lower rejection as well [39].

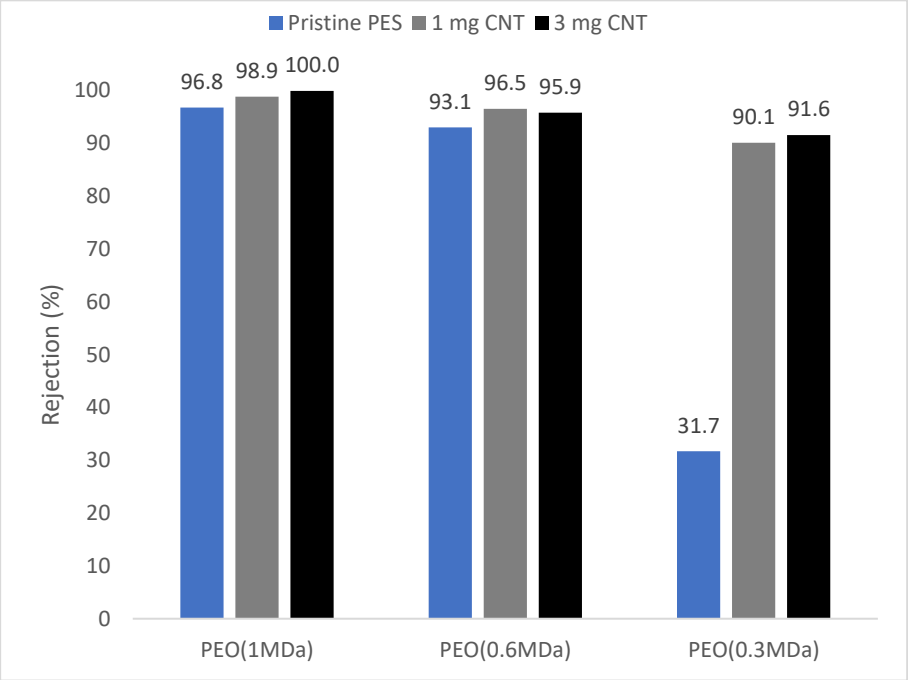

Figure 4.3. Rejection properties of pristine PES as well as 1 mg and 3 mg CNT UF membranes using 250 ppm PEO filtration test.

4.4.2. Chemical structure

In the catalyzed cross-linked CNT network, covalent bonds are formed between the CNTs, the PVA, and the cross-linkers. These covalent bonds chemically stabilize the CNT network. Ester bonds are formed between the carboxyl groups on either the cross-linkers or the CNTs and the hydroxyl groups on the PVA.

4.4.3. Thin film morphology

The conductive thin film thickness of the membranes impacts the bulk conductivity and the transmembrane permeability. Thin film thickness is measured from cross-sectional SEM. Bulk conductivity is inversely proportional to thin film thickness. In addition, water permeance of the membrane is inversely proportional to both the thickness of the polymer membrane active layer and that of the thin film [40–42]. A thicker conductive thin film may act as a pressure barrier in the filtration process leading to lower permeabilities. As such, a thinner surface layer is more desirable. Cross-sectional SEM images of MF and UF membranes are presented in Figure 4.4 and Figure 4.5, respectively. We hypothesized that

cross-linking would have an impact on thin film thickness as compared to CNT films formed without cross-linked PVA. Greater cross-linking was assumed to cause greater increases in thin film thickness, thus SEM measurements were only performed on membranes with 20% cross-linking degree. The thickness of the conductive thin film is an average value of three separate measurements along the film. For each measurement, Image J was used to quantify film thickness. The images compare the effect of CNT concentration (1 mg and 3 mg) and the effect of cross-linkers (control, succinic acid, and suberic acid) on the film thickness. Using a higher mass of CNTs increases the thickness of MF membranes by 296% (0.41 to 1.62 μm) and UF membranes by 47% (1.17 to 1.72 μm) on average. However, the presence of cross-linking molecules does not have a significant impact on thin film thickness. It should be noted that SEM images are presented to provide a comparison among different membranes and are not meant to be used for quantitative analysis due to the high variability associated with the thickness of the thin film. The pressure deposition technique used for the fabrication of membranes in this study inherently results in membranes with non-uniform thin film thicknesses.

A relatively low thickness (29.8% on average) was observed for MF membranes as compared to UF membranes. This is likely due to two factors. A greater resultant pressure is applied to CNT suspensions during the fabrication of MF membranes as compared to UF membranes. The vacuum pump used to pressure coat the membranes generates a vacuum pressure of 100 mbar. The difference between the atmospheric pressure (1 bar) and the vacuum drives the filtration process. Both membranes have the same nominal thickness, however, the smaller pores of UF membranes act as a greater pressure barrier as compared to MF membranes resulting in a lower pressure applied to CNT suspension. Further, it is hypothesized that a higher proportion of unbonded PVA and SDS chains passes through the large pores of the MF membranes during the fabrication process as mentioned above. Although the leaching of PVA and SDS is both possible, the leaching of PVA has a greater impact, since SDS is used in much lower concentration (1:1.5 wt% wrt to CNT) as compared to PVA (10:1 wt% wrt CNT). Furthermore, the molecular size of SDS is much smaller (1.5 nm) than that of PVA (6 – 8 nm) and has a minor effect on the membrane

thickness. Therefore, it is hypothesized that less PVA in the CNT thin film, as a result of transmembrane leaching, leads to a thinner film upon curing.

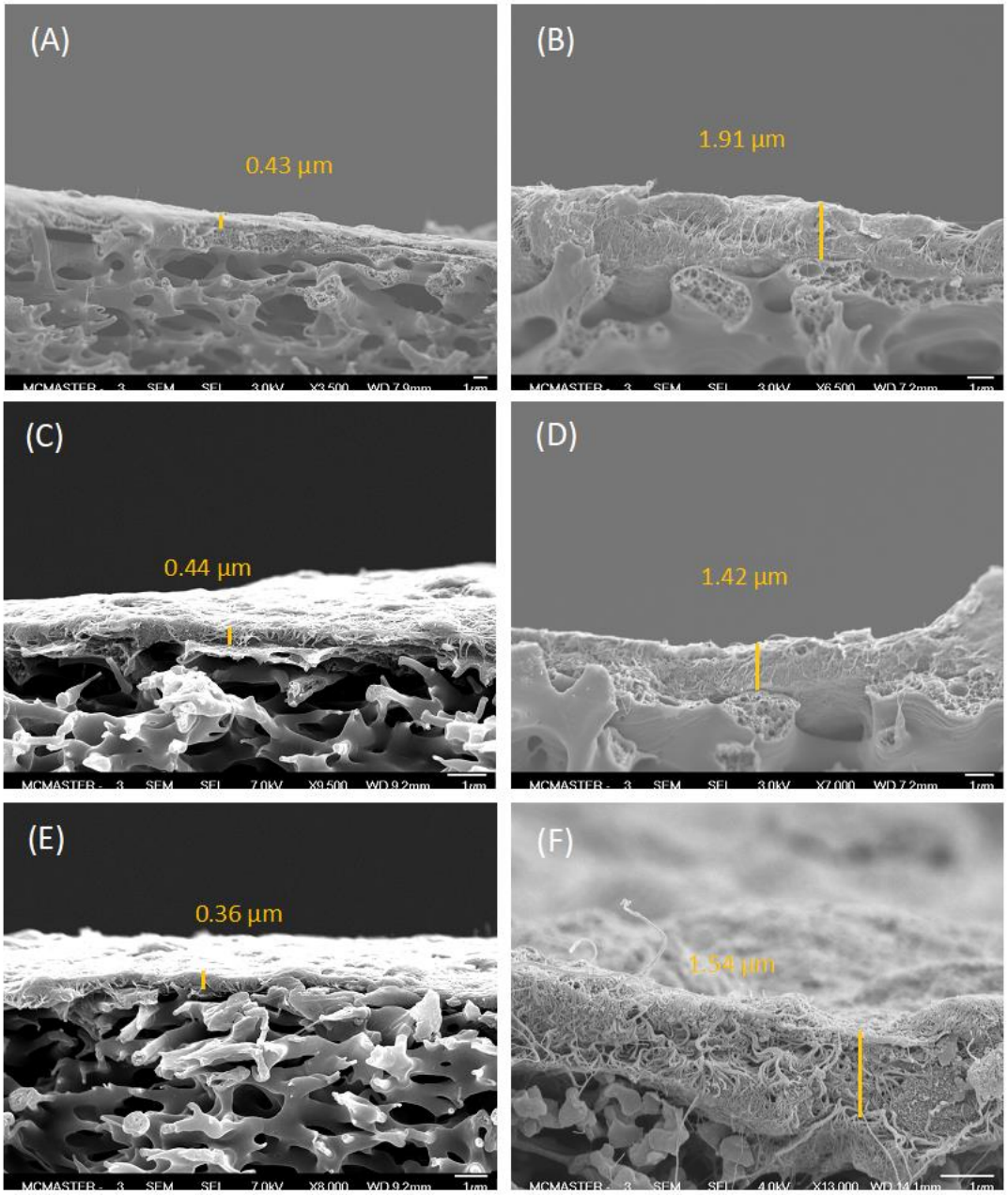

Figure 4.4. SEM images of MF membranes with CNT thin film made with 1 mg (left column) and 3 mg (right column). Top row (A), (B): control CNT thin films, Middle row (C), (D): succinic acid cross-linked CNT thin films (20% CL), Bottom row (E), (D): suberic acid cross-linked CNT thin films (20% CL).

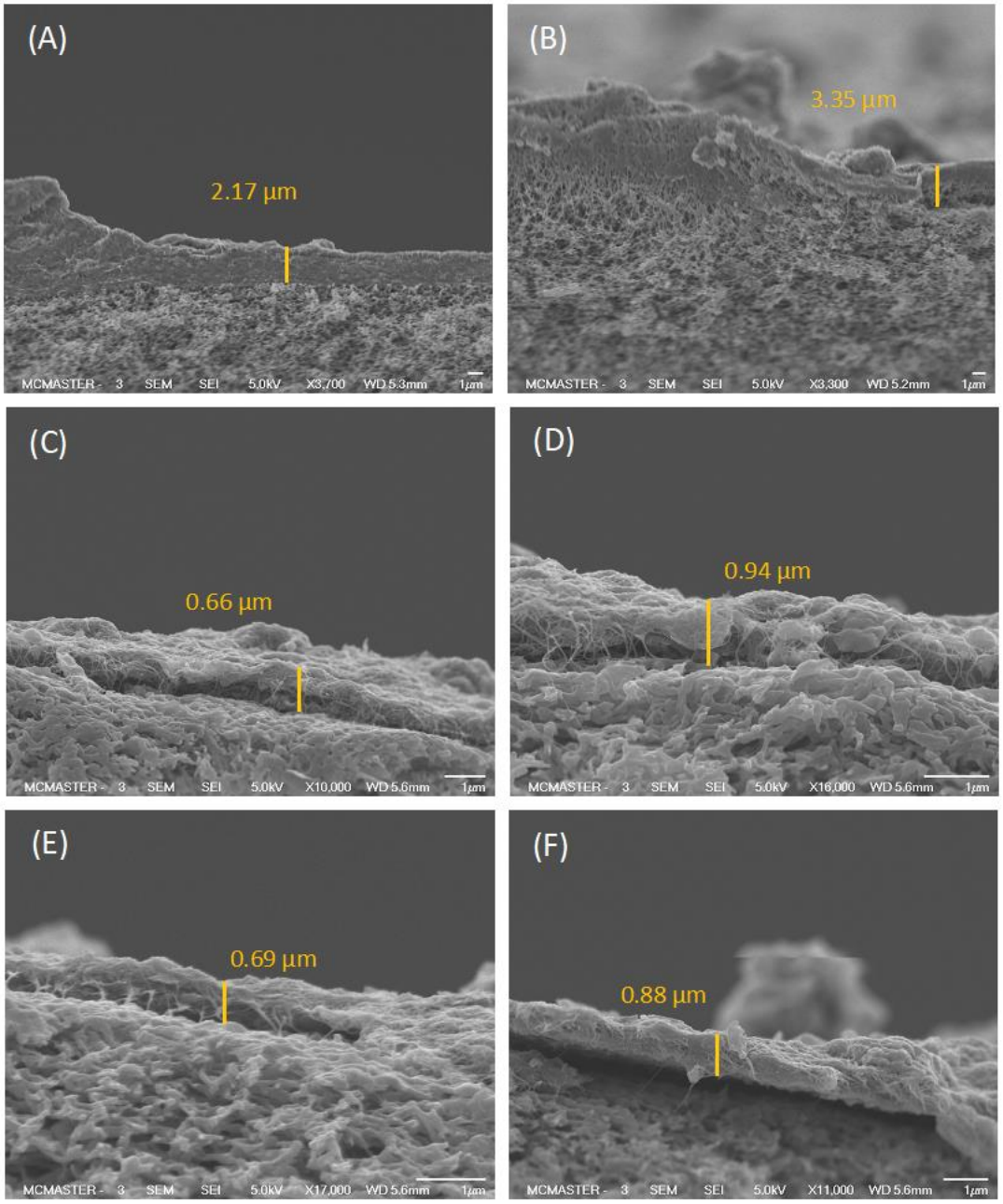

Figure 4.5. SEM images of UF membranes with CNT thin film made with 1 mg (left column) and 3 mg (right column). Top row (A), (B): control CNT thin films, Middle row (C), (D): succinic acid cross-linked CNT thin films (20% CL), Bottom row (E), (D): suberic acid cross-linked CNT thin films (20% CL).

4.4.4. Pure water permeance

Pure water flux tests were conducted to measure the effect of different cross-linkers on pure water permeance of the membrane. The results for MF and UF membranes are presented in Figure 4.6 (a), and (b), respectively. The pure water permeance of pristine MF and UF membranes is 15057 ± 4206 LMH/bar and 3045 ± 628 LMH/bar, respectively. Thin film CNT coatings greatly reduce the pure water permeance as compared to pristine MF and UF membranes.

Figure 4.6 indicates that for both types of membranes, the water permeance is increased by using a longer cross-linker in the network. In MF membranes, an average increase of 41% and 187% for succinic acid and suberic acid was observed with respect to the control membranes while for UF membrane, this increase was 84% and 254%, respectively. It is hypothesized that by reacting longer cross-linkers with the CNT-PVA network, the thin film becomes more porous which leads to lower membrane resistance towards the passage of water. Longer cross-linkers create more space between the random structure of the CNTs and PVA chains.

In addition to the impact of different length of cross-linkers, pure water flux tests were carried out for different degrees of cross-linking (10% and 20%) i.e. for different concentrations of cross-linkers in the CNT-PVA network. As can be seen in Figure 4.6, a higher degree of cross-linking leads to a higher flux for membrane thin films containing the same concentration of CNTs. This trend is valid for both the MF and UF membranes coated with the CNT thin film. This observation supports the above hypothesis that greater spacing between CNTs leads to higher water permeance. A higher degree of cross-linking is achieved by a higher concentration of cross-linkers in the network. It is hypothesized that the increased flux of membranes with a higher degree of cross-linking is a result of greater porosity throughout the CNT-PVA network. The presence of more cross-linkers expands the distance between PVA chains limiting PVA entanglement. Cross-linked PVA molecules, which are covalently bound to functionalized CNTs, increase the distance between CNTs and prevent CNT aggregation. This trend is generally observed across the series of 72 membranes synthesized, however, membrane thin films containing the shortest cross-linker, succinic acid, with the lowest cross-linking degree (10%), have fluxes that are

statistically similar to control membranes. This suggests that while cross-linkers form a more porous structure, their effect on pure water flux is more evident either for longer cross linkers (suberic acid) or a higher cross-linking degree (20%).

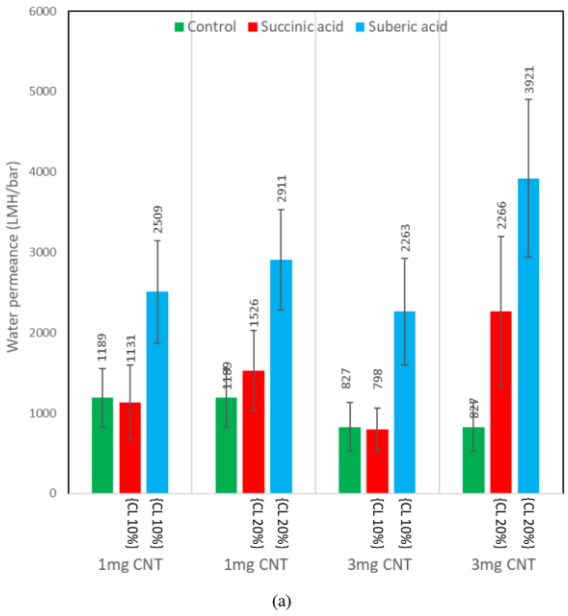

(a)

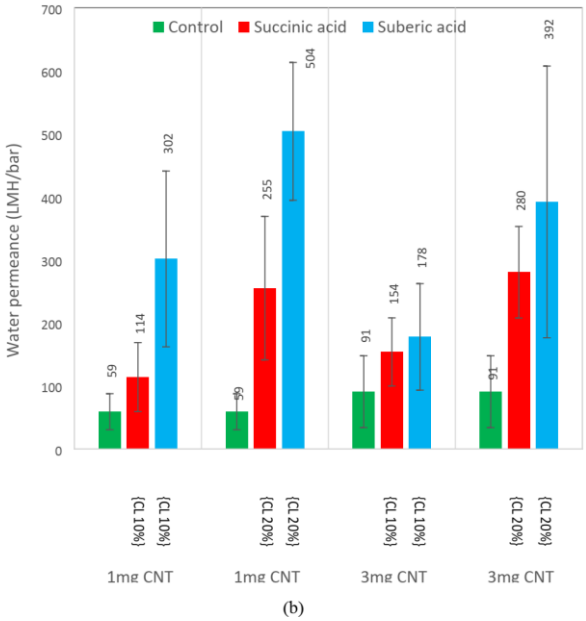

(b)

Figure 4.6. Pure water permeance of (a) MF and (b) UF membranes having different cross-linkers.

4.4.5. Conductivity

ECMs are designed to conduct charge across the surface or to hold electric potential on their surface. The interconnected CNT network enables the flow of charge. A minimum concentration of CNTs is needed to surpass the percolation threshold, but other factors impact electrical conductivity including the configuration and compactness of the CNT network, as well as the thickness of the thin-film. The electrical resistance of the surfaces was measured by using a four-point probe instrument linked with the Hall software. Detailed information about the instrument and conductivity measurement are provided in the SI.

Surface conductance shows the rate of charge transfer across the surface. Surface conductance is an important value for ECMs and can be used for studies related to inactivation of bacteria, oxidation of natural organic matter, charging of inorganic catalysts on the surface (iron, platinum, titanium), and indications of electrical potential difference in sensor applications. Figure 4.7 shows that there is no statistical difference between surface conductance of the MF and UF membranes for the same CNT mass and cross-linker type. Such an agreement is due to the same density of CNT in the conductive thin layer (same surface area and mass of CNT were used for each membrane).

Figure 4.7 shows that greater concentration of CNTs leads to greater surface conductance. By increasing the concentration of CNTs, a denser film is obtained with less free space. It is hypothesized that with more CNTs deposited on the membranes, they fill the gaps in the open spaces thereby increasing the compactness of the conductive network. This increased compactness lead to a higher conductance. Figure 4.7 reveals that longer cross-linking chains cause a greater surface conductance of the nanocomposite. Cross-linkers keep the CNTs well dispersed and non-aggregated and enable greater dispersibility of the CNTs within the nanocomposite, leading to a greater electrical percolation and a higher conductance [34,43–45].

The bulk conductivity of the CNT-network was calculated using the surface resistance obtained from the four-point probe conductivity measurements and the thickness of the thin film obtained from SEM images (Table 4.1). Bulk conductivity is a useful tool to examine the strength of the electric field which can be generated via ECMs under a given electrical current. Electric field generated by ECMs has previously been demonstrated to decrease fouling, which is hypothesized to occur either through electrostatic repulsion of charged particles in the feed or by increasing diffusive mobility of charged particles above the surface. Bulk conductivity depends on dispersability as well as density of the CNT network in the thin layer. Bulk conductivity depends on the thin layer thickness and surface resistance. The thin layer thickness and its associated uncertainty impact the bulk conductivity, and the error associated with the SEM measurements is propagated to that of the bulk conductivity.

The bulk conductivity results are shown in Figure 4.8. It can be seen that the bulk conductivity is related to the mass of the CNTs, the length of the cross-linkers, and the thickness of the conductive layer. In previous sections, we showed that MF membranes have a lower thickness than UF membranes. The same mass of CNT (per membrane surface area) was used for MF and UF membranes. A thinner conductive film therefore implies that the network is denser with less free space. In addition, the CNT networks is less covered by non-conductive polymers due to the higher leaching of PVA in MF membranes. In ECMs, the polymer endows stability to the network and prevents CNT aggregation. However, polymers reduce the conductivity of the network by wrapping, and thereby insulating, the conductive CNTs. It was expected that MF membranes would possess a higher bulk conductivity due to the thinner conductive film (higher density) and a more exposed CNT network (due to leaching of PVA). Figure 4.8 supports this hypothesis, indicating that MF membranes have higher bulk conductivity than UF membranes. The results are consistent for all membranes with the exception of succinic and suberic in a 3mg CNT network. This is most likely due to the high error and uncertainty associated with SEM images for measuring the thickness as was explained in section 4.4.3.

Table 4.1. Thickness of the membranes obtained from SEM images.

Membrane	CNT mass loading (mg)	Cross-linking density (%)	Cross-linker type	Thickness (µm)
MF	1	-	-	0.43
		20	succinic acid	0.44
			suberic acid	0.36
	3	-	-	1.91
		20	succinic acid	1.42
			suberic acid	1.54
UF	1	-	-	2.17
		20	succinic acid	0.66
			suberic acid	0.69
	3	-	-	3.35
		20	succinic acid	0.94
			suberic acid	0.88

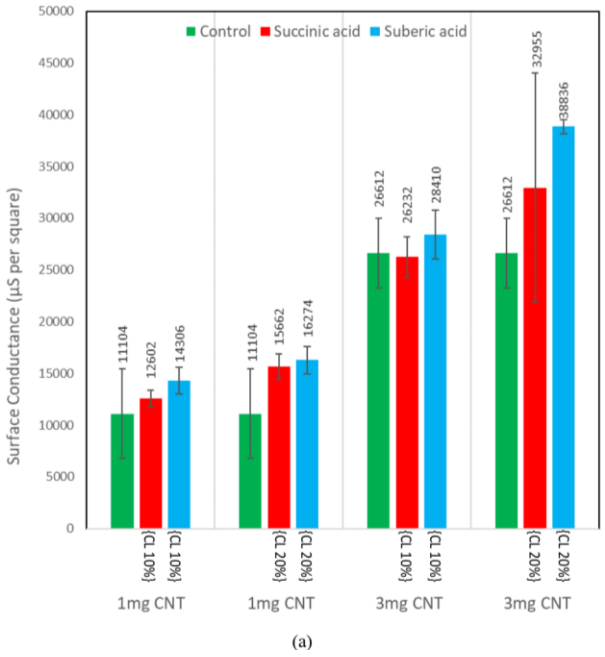

(a)

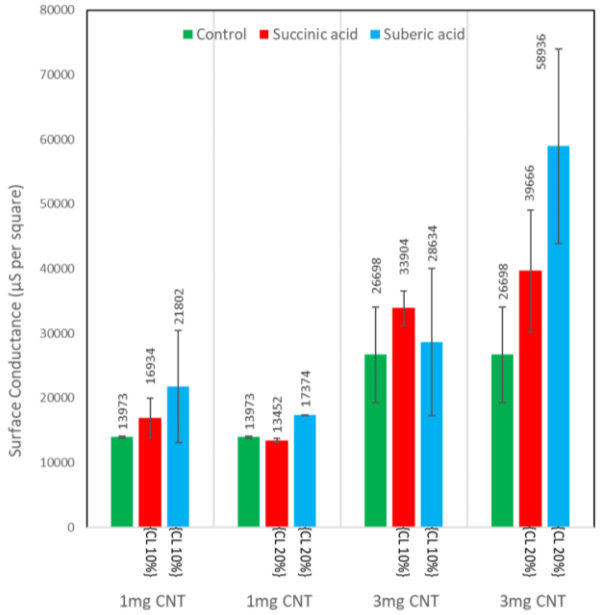

(b)

Figure 4.7. Effect of CNT mass, cross-linkers, and degree of functionalization on the surface conductance of the (a) MF and (b) UF thin film.

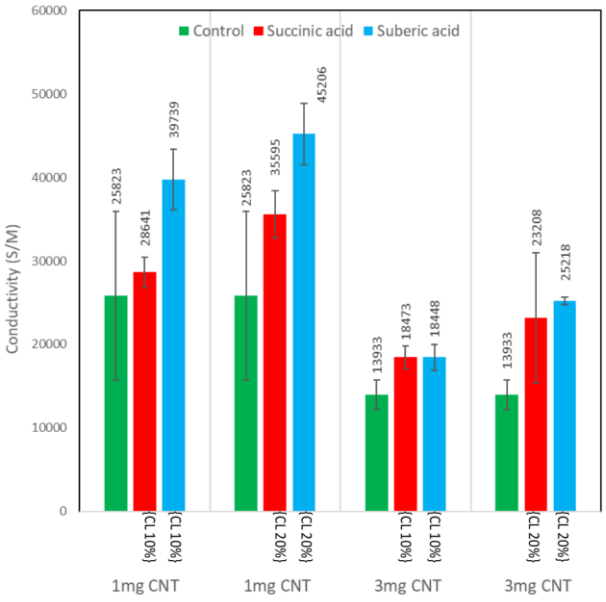

(a)

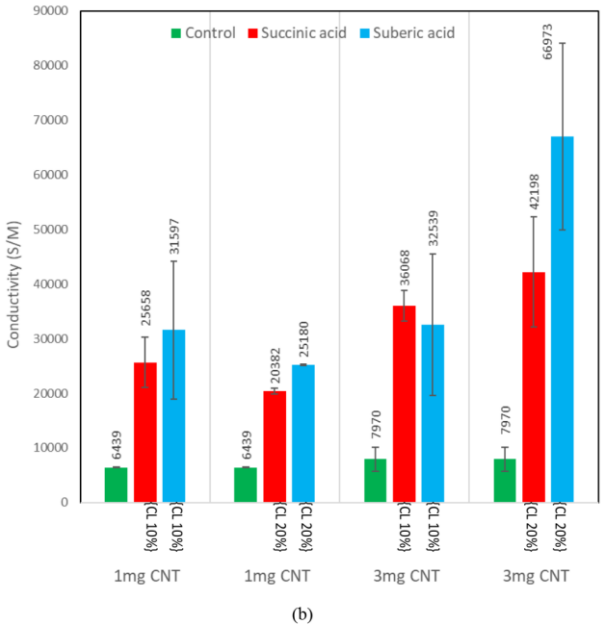

Figure 4.8. Effect of CNT mass, cross-linkers, and degree of functionalization on the bulk conductivity of the (a) MF and (b) UF thin film.

4.4.6. Surface hydrophilicity

Introducing a new chemistry to the surface of the membrane may alter other membrane properties including hydrophilicity and surface roughness. The presence of cross-linkers has been shown to have some impact on surface contact angle [46–49]. The wetting behaviour of the membrane is evaluated using an optical high-speed contact angle instrument. The contact angles were measured when droplets achieved steady state, i.e. as soon as the droplet came to rest on the surface without any further spreading. Further details are provided in the materials and methods. The results of the contact angle test for MF and UF membranes are presented in Figure 4.9 (a) and (b), respectively. The effect of CNT concentration, cross-linking length, and cross-linking degree on surface hydrophilicity was investigated. It is shown that CNT membranes have lower hydrophilicity as compared to PES membranes due to the presence of the hydrophobic CNTs in the network. With few exceptions, a general trend is observed revealing a higher contact angle for a higher mass of CNTs. However, cross-linking degree and cross-linker length were uncorrelated to the surface contact angle, indicating that PVA, not cross-linkers were responsible for the

hydrophilicity of the surfaces. The increase in water permeance observed for membranes which have longer cross-linkers in the network can be attributed to the spacing and arrangement of the CNT network. The results reveal that regardless of the type of cross-linkers or degree of cross-linking, these CNT-PVA electrically conductive membranes have sufficient hydrophilicity for water filtration purposes. Hydrophilic surfaces are generally desired for water treatment applications. It is generally accepted that membrane surfaces with contact angles of 80° or less are considered hydrophilic. The hydrophilicity of the membranes is generally below 70° and 80° for UF and MF membranes, respectively. The hydrophilicity of the ECMs is due to both presence of hydroxyl groups (of PVA) and carboxyl groups of CNTs. The comparatively higher contact angle for MF membranes over UF membranes can be attributed to the higher degree of leaching of unbonded PVA chains during the membrane fabrication process, as discussed in the materials and methods section. CNT thin film membranes on a UF PES support have less PVA leaching during membrane fabrication. As such, more PVA is retained within the CNT network leading to a lower contact angle.

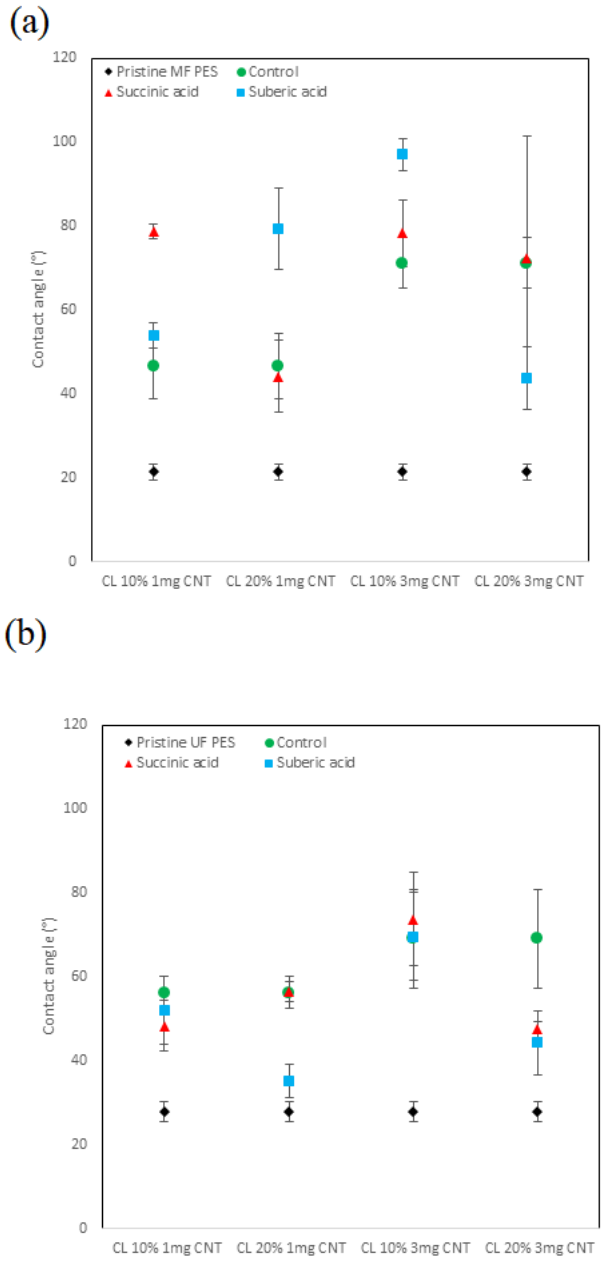

Figure 4.9. Contact angle test for (a) MF and (b) UF membranes with different CNT mass, cross-linkers, and degree of functionalization.

4.4.7. Surface roughness

The presence of cross-linkers within the CNT network may have an impact on membrane surface roughness. The impact of CNT concentration and cross-linkers on the

surface morphology was investigated using AFM. Suberic acid cross-linked membranes were compared to control CNT membranes to investigate the impact of cross-linkers on surface roughness. Longer cross-linkers were demonstrated to create looser CNT networks. We hypothesized that looser networks would be more irregular than denser networks. As such, we only evaluated the impact of suberic acid (the longer cross-linker) on surface roughness, in order to minimize the number of AFM experiments required. Figure 4.10 and Figure 4.11 show the results for MF and UF membranes, respectively. It is observed that all the membranes have a ridge-and-valley structure. This morphology is caused by the surface aggregation of CNTs during the deposition process [50–52]. The surface roughness did not significantly change with an increase in CNT concentration nor with the use of longer cross-linkers. More 2D images are given in the supplementary information.

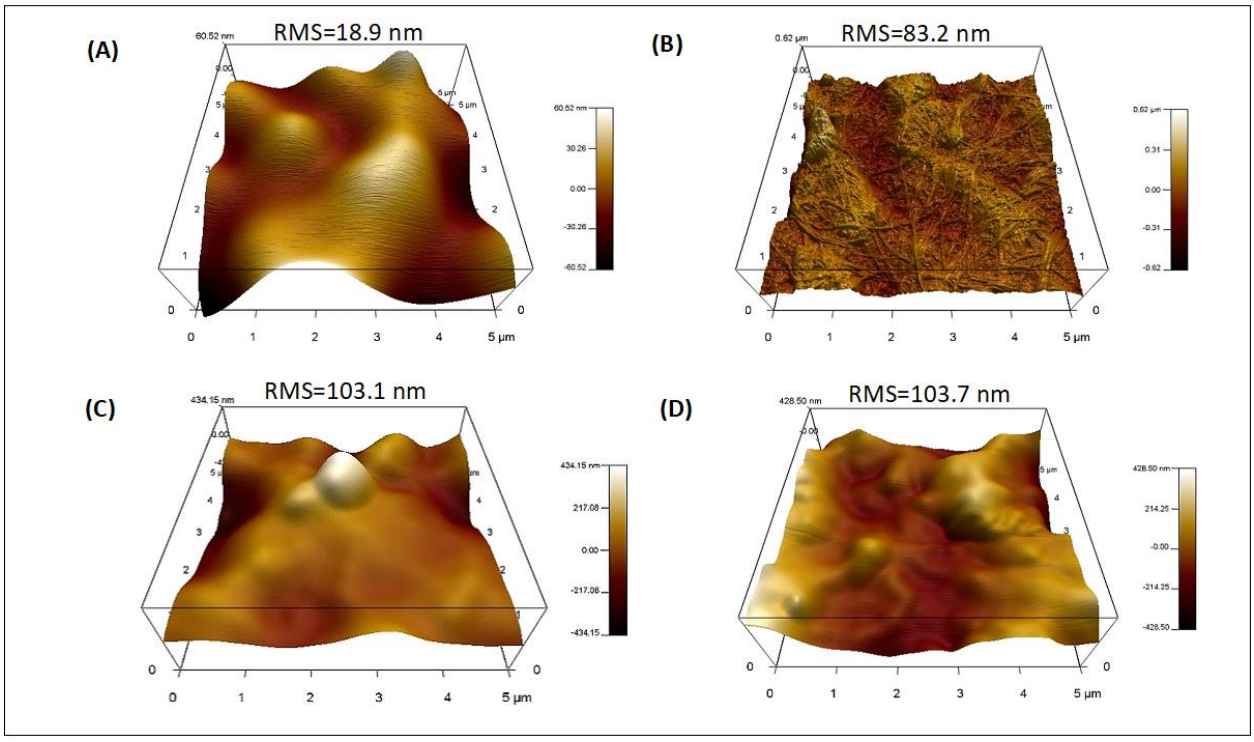

Figure 4.10. AFM images for MF membranes (A) Control 1mg, (B) Control 3mg, (C) Suberic acid 1mg, (D) Suberic acid 3 mg.

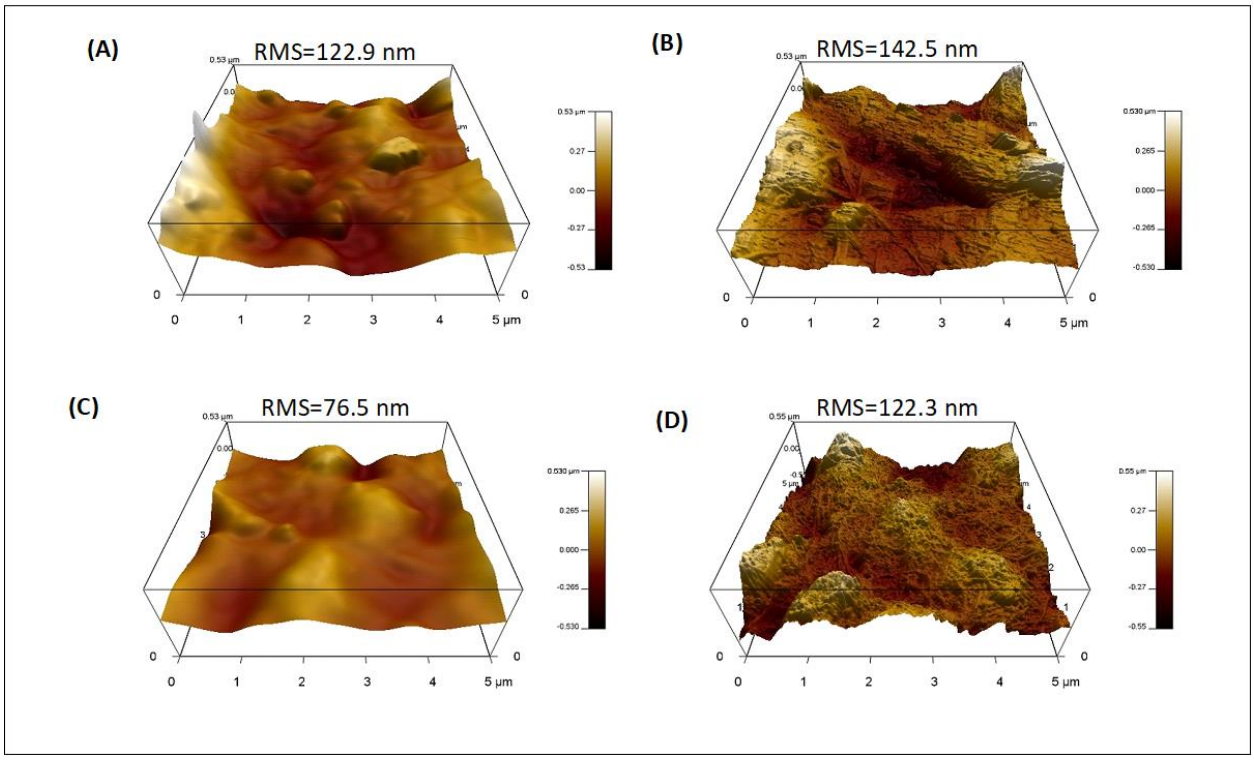

Figure 4.11. AFM images for UF membranes (A) Control 1mg, (B) Control 3mg, (C) Suberic acid 1mg, (D) Suberic acid 3 mg.

4.5.Conclusions

Advanced MF and UF electrically conductive membranes with a better control over pore structure were fabricated in this work. The ECMs consisted of an electrically conductive nanonetwork on top and a PES membrane as a support. Carboxyl functionalized SW/DW CNTs, PVA, and two cross-linkers with different lengths were used in the nanolayer. Strong covalent bonds between the carboxyl groups of cross-linkers or CNTs and the hydroxyl groups of PVA had the major contribution for the stability of the network. The effect of mass of CNT, cross-linking type, and cross-linking degree were investigated on membrane properties which include pure water flux, electrical conductivity, surface hydrophilicity, morphology, and surface roughness. The results revealed that integration of cross-linker with a higher length causes a higher pure water flux. It was attributed to the more open structure of networks with the presence of longer cross-linkers. The surface conductance of the nanolayer was shown to be greater either for surfaces with higher degree

of cross-liking or having longer cross-linkers. It was hypothesized that it is due to greater electrical percolation of the network as a result of a better CNT dispersibility. The MF membranes had relatively higher contact angle and lower thickness as compared to UF membranes which were likely due to the higher degree of leaching of unbonded PVA chains through the large pores of MF membranes during the fabrication process. Surface roughness images obtained from AFM showed no significant change for different networks (control, succinic acid, and suberic acid). It should be noted that this work mainly focused on the chemistry of the surface using cross-linkers. Selectivity as well as the antifouling properties of MF and UF ECMs will be investigated in future work.

4.6.Acknowledgments

This work was supported by Natural Sciences and Engineering Research Council of Canada (NSERC) discovery grant. The authors would like to acknowledge Canadian Centre for Electron Microscopy (CCEM), and Biointerfaces Institute (BI). In addition, we thank Christopher Butcher, Heera Marway, Alexander Sutherland, and Al-Asel Maizer for their generous help.

4.7.References

[1] M.A. Halali, C.-F. de Lannoy, The Effect of Cross-Linkers on the Permeability of Electrically Conductive Membranes, Ind. Eng. Chem. Res. 58 (2019) 3832–3844. https://doi.org/10.1021/acs.iecr.8b05691.

[2] M. Arora, R.C. Maheshwari, S.K. Jain, A. Gupta, Use of membrane technology for potable water production, Desalination. 170 (2004) 105–112. https://doi.org/10.1016/J.DESAL.2004.02.096.

[3] E. Brauns, Towards a worldwide sustainable and simultaneous large-scale production of renewable energy and potable water through salinity gradient power by combining reversed electrodialysis and solar power?, Desalination. 219 (2008) 312–323. https://doi.org/10.1016/J.DESAL.2007.04.056.

[4] K. Karakulski, M. Gryta, A. Morawski, Membrane processes used for potable water quality improvement, Desalination. 145 (2002) 315–319. https://doi.org/10.1016/S0011-9164(02)00429-0.

[5] M.S. Mohsen, J.O. Jaber, M.D. Afonso, Desalination of brackish water by nanofiltration and reverse osmosis, Desalination. 157 (2003) 167. https://doi.org/10.1016/S0011-9164(03)00397-7.

[6] M.P. del Pino, B. Durham, Wastewater reuse through dual-membrane processes: opportunities for sustainable water resources, Desalination. 124 (1999) 271–277. https://doi.org/10.1016/S0011-9164(99)00112-5.

[7] A.M. Comerton, R.C. Andrews, D.M. Bagley, Evaluation of an MBR–RO system to produce high quality reuse water: Microbial control, DBP formation and nitrate, Water Res. 39 (2005) 3982–3990. https://doi.org/10.1016/J.WATRES.2005.07.014.

[8] H. Al Abdulgader, V. Kochkodan, N. Hilal, Hybrid ion exchange – Pressure driven membrane processes in water treatment: A review, Sep. Purif. Technol. 116 (2013) 253–264. https://doi.org/10.1016/J.SEPPUR.2013.05.052.

[9] M.M. Pendergast, E.M.V. Hoek, A review of water treatment membrane nanotechnologies, Energy Environ. Sci. 4 (2011) 1946. https://doi.org/10.1039/c0ee00541j.

[10] G.M. Geise, H.-S. Lee, D.J. Miller, B.D. Freeman, J.E. McGrath, D.R. Paul, Water purification by membranes: The role of polymer science, J. Polym. Sci. Part B Polym. Phys. 48 (2010) 1685–1718. https://doi.org/10.1002/polb.22037.

[11] A. Matilainen, E.T. Gjessing, T. Lahtinen, L. Hed, A. Bhatnagar, M. Sillanpää, An overview of the methods used in the characterisation of natural organic matter (NOM) in relation to drinking water treatment, Chemosphere. 83 (2011) 1431–1442. https://doi.org/10.1016/J.CHEMOSPHERE.2011.01.018.

[12] Z. Yang, H. Yan, H. Yang, H. Li, A. Li, R. Cheng, Flocculation performance and mechanism of graphene oxide for removal of various contaminants from water, Water Res. 47 (2013) 3037–3046. https://doi.org/10.1016/J.WATRES.2013.03.027.

[13] B.S. Lalia, F.E. Ahmed, T. Shah, N. Hilal, R. Hashaikeh, Electrically conductive membranes based on carbon nanostructures for self-cleaning of biofouling, Desalination. 360 (2015) 8–12. https://doi.org/10.1016/J.DESAL.2015.01.006.

[14] A. V. Dudchenko, J. Rolf, K. Russell, W. Duan, D. Jassby, Organic fouling inhibition on electrically conducting carbon nanotube–polyvinyl alcohol composite ultrafiltration membranes, J. Memb. Sci. 468 (2014) 1–10. https://doi.org/10.1016/J.MEMSCI.2014.05.041.

[15] F. Ahmed, B.S. Lalia, V. Kochkodan, R. Hashaikeh, Electrically conductive polymeric membranes for fouling prevention and detection: A review, Desalination. 391 (2016) 1–15. https://doi.org/10.1016/J.DESAL.2016.01.030.

[16] H. Park, K.-H. Choo, H.-S. Park, J. Choi, M.R. Hoffmann, Electrochemical oxidation and microfiltration of municipal wastewater with simultaneous hydrogen production: Influence of organic and particulate matter, Chem. Eng. J. 215–216 (2013) 802–810. https://doi.org/10.1016/J.CEJ.2012.11.075.

[17] M. Dargahi, Z. Hosseinidoust, N. Tufenkji, S. Omanovic, Investigating electrochemical removal of bacterial biofilms from stainless steel substrates, Colloids Surfaces B Biointerfaces. 117 (2014) 152–157. https://doi.org/10.1016/J.COLSURFB.2014.02.021.

[18] A. Ronen, S.L. Walker, D. Jassby, Electroconductive and electroresponsive membranes for water treatment, Rev. Chem. Eng. 32 (2016) 533–550. https://doi.org/10.1515/revce-2015-0060.

[19] P. Formoso, E. Pantuso, G. De Filpo, F. Nicoletta, Electro-Conductive Membranes for Permeation Enhancement and Fouling Mitigation: A Short Review, Membranes (Basel). 7 (2017) 39. https://doi.org/10.3390/membranes7030039.

[20] I.-H. Loh, R.A. Moody, J.C. Huang, Electrically conductive membranes: Synthesis and applications, J. Memb. Sci. 50 (1990) 31–49. https://doi.org/10.1016/S0376-7388(00)80884-4.

[21] W. Hu, S. Chen, Z. Yang, L. Liu, H. Wang, Flexible Electrically Conductive Nanocomposite Membrane Based on Bacterial Cellulose and Polyaniline, J. Phys. Chem. B. 115 (2011) 8453–8457. https://doi.org/10.1021/jp204422v.

[22] C.F. De Lannoy, D. Jassby, K. Gloe, A.D. Gordon, M.R. Wiesner, Aquatic biofouling prevention by electrically charged nanocomposite polymer thin film membranes, Environ. Sci. Technol. 47 (2013)

2760–2768. https://doi.org/10.1021/es3045168.

[23] S.H. Hong, J. Jeong, S. Shim, H. Kang, S. Kwon, K.H. Ahn, J. Yoon, Effect of electric currents on bacterial detachment and inactivation, Biotechnol. Bioeng. 100 (2008) 379–386. https://doi.org/10.1002/bit.21760.

[24] C. de Lannoy, D. Jassby, D.D. Davis, M.R. Wiesner, A highly electrically conductive polymer–multiwalled carbon nanotube nanocomposite membrane, J. Memb. Sci. 415–416 (2012) 718–724. https://doi.org/10.1016/J.MEMSCI.2012.05.061.

[25] M.S.P. Shaffer, A.H. Windle, Fabrication and Characterization of Carbon Nanotube/Poly(vinyl alcohol) Composites, Adv. Mater. 11 (1999) 937–941. https://doi.org/10.1002/(SICI)1521-4095(199908)11:11<937::AID-ADMA937>3.0.CO;2-9.

[26] H. Chen, M.B. Müller, K.J. Gilmore, G.G. Wallace, D. Li, Mechanically Strong, Electrically Conductive, and Biocompatible Graphene Paper, Adv. Mater. 20 (2008) 3557–3561. https://doi.org/10.1002/adma.200800757.

[27] H. Kim, Y. Miura, C.W. Macosko, Graphene/Polyurethane Nanocomposites for Improved Gas Barrier and Electrical Conductivity, Chem. Mater. 22 (2010) 3441–3450. https://doi.org/10.1021/cm100477v.

[28] B.C.H. Steele, A. Heinzel, Materials for fuel-cell technologies, in: Mater. Sustain. Energy, Co-Published with Macmillan Publishers Ltd, UK, 2010: pp. 224–231. https://doi.org/10.1142/9789814317665_0031.

[29] C.D. Vecitis, M.H. Schnoor, M. Saifur Rahaman, J.D. Schiffman, M. Elimelech, Electrochemical Multiwalled Carbon Nanotube Filter for Viral and Bacterial Removal and Inactivation, Environ. Sci. Technol. 45 (2011) 3672–3679. https://doi.org/10.1021/es2000062.

[30] W. Duan, G. Chen, C. Chen, R. Sanghvi, A. Iddya, S. Walker, H. Liu, A. Ronen, D. Jassby, Electrochemical removal of hexavalent chromium using electrically conducting carbon nanotube/polymer composite ultrafiltration membranes, J. Memb. Sci. 531 (2017) 160–171. https://doi.org/10.1016/J.MEMSCI.2017.02.050.

[31] W. Duan, A. Ronen, J.V. de Leon, A. Dudchenko, S. Yao, J. Corbala-Delgado, A. Yan, M. Matsumoto, D. Jassby, Treating anaerobic sequencing batch reactor effluent with electrically conducting ultrafiltration and nanofiltration membranes for fouling control, J. Memb. Sci. 504 (2016) 104–112. https://doi.org/10.1016/J.MEMSCI.2016.01.011.

[32] W. Duan, A. Ronen, S. Walker, D. Jassby, Polyaniline-Coated Carbon Nanotube Ultrafiltration Membranes: Enhanced Anodic Stability for *In Situ* Cleaning and Electro-Oxidation Processes, ACS Appl. Mater. Interfaces. 8 (2016) 22574–22584. https://doi.org/10.1021/acsami.6b07196.

[33] R. Hashaikeh, B.S. Lalia, V. Kochkodan, N. Hilal, A novel in situ membrane cleaning method using periodic electrolysis, J. Memb. Sci. 471 (2014) 149–154. https://doi.org/10.1016/J.MEMSCI.2014.08.017.

[34] N.G. Sahoo, S. Rana, J.W. Cho, L. Li, S.H. Chan, Polymer nanocomposites based on functionalized carbon nanotubes, Prog. Polym. Sci. 35 (2010) 837–867. https://doi.org/10.1016/J.PROGPOLYMSCI.2010.03.002.

[35] A. Shameli, E. Ameri, Synthesis of cross-linked PVA membranes embedded with multi-wall carbon nanotubes and their application to esterification of acetic acid with methanol, Chem. Eng. J. 309 (2017) 381–396. https://doi.org/10.1016/J.CEJ.2016.10.039.

[36] D.S. Dlamini, J. Wang, A.K. Mishra, B.B. Mamba, E.M. V Hoek, Effect of Cross-Linking Agent

Chemistry and Coating Conditions on Physical, Chemical, and Separation Properties of PVA-Psf Composite Membranes, (n.d.). https://doi.org/10.1080/01496395.2013.813040.

[37] C. Wu, Handbook of size exclusion chromatography and related techniques: revised and expanded, 2003. https://books.google.ca/books?hl=en&lr=&id=BEc9qvSSxuoC&oi=fnd&pg=PR3&dq=Handbook+Of+Size+Exclusion+Chromatography+And+Related+Techniques:&ots=jU14YbhPxl&sig=TKkLhbf9ecJnInKLhWRJnATWnYo (accessed July 27, 2018).

[38] O. V. Khorolskyi, Effective Radii of Macromolecules in Dilute Polyvinyl Alcohol Solutions, Ukr. J. Phys. 63 (2018) 144. https://doi.org/10.15407/ujpe63.2.144.

[39] K.-J. Lee, H.-D. Park, The most densified vertically-aligned carbon nanotube membranes and their normalized water permeability and high pressure durability, J. Memb. Sci. 501 (2016) 144–151. https://doi.org/10.1016/J.MEMSCI.2015.12.009.

[40] J. Shen, H. Ruan, L. Wu, C. Gao, Preparation and characterization of PES–SiO2 organic–inorganic composite ultrafiltration membrane for raw water pretreatment, Chem. Eng. J. 168 (2011) 1272–1278. https://doi.org/10.1016/J.CEJ.2011.02.039.

[41] D.S. Wuu, W.C. Lo, C.C. Chiang, H.B. Lin, L.S. Chang, R.H. Horng, C.L. Huang, Y.J. Gao, Plasma-deposited silicon oxide barrier films on polyethersulfone substrates: temperature and thickness effects, Surf. Coatings Technol. 197 (2005) 253–259. https://doi.org/10.1016/J.SURFCOAT.2004.09.033.

[42] B.-W. Zhou, H.-Z. Zhang, Z.-L. Xu, Y.-J. Tang, Interfacial polymerization on PES hollow fiber membranes using mixed diamines for nanofiltration removal of salts containing oxyanions and ferric ions, Desalination. 394 (2016) 176–184. https://doi.org/10.1016/J.DESAL.2016.05.016.

[43] J.K.W. Sandler, J.E. Kirk, I.A. Kinloch, M.S.P. Shaffer, A.H. Windle, Ultra-low electrical percolation threshold in carbon-nanotube-epoxy composites, Polymer (Guildf). 44 (2003) 5893–5899. https://doi.org/10.1016/S0032-3861(03)00539-1.

[44] J. Li, P.C. Ma, W.S. Chow, C.K. To, B.Z. Tang, J.-K. Kim, Correlations between Percolation Threshold, Dispersion State, and Aspect Ratio of Carbon Nanotubes, Adv. Funct. Mater. 17 (2007) 3207–3215. https://doi.org/10.1002/adfm.200700065.

[45] Y.S. Song, J.R. Youn, Influence of dispersion states of carbon nanotubes on physical properties of epoxy nanocomposites, Carbon N. Y. 43 (2005) 1378–1385. https://doi.org/10.1016/J.CARBON.2005.01.007.

[46] F. Peng, Z. Jiang, E.M.V. Hoek, Tuning the molecular structure, separation performance and interfacial properties of poly(vinyl alcohol)–polysulfone interfacial composite membranes, J. Memb. Sci. 368 (2011) 26–33. https://doi.org/10.1016/J.MEMSCI.2010.10.056.

[47] J.-H. Kim, P.-K. Park, C.-H. Lee, H.-H. Kwon, Surface modification of nanofiltration membranes to improve the removal of organic micro-pollutants (EDCs and PhACs) in drinking water treatment: Graft polymerization and cross-linking followed by functional group substitution, J. Memb. Sci. 321 (2008) 190–198. https://doi.org/10.1016/j.memsci.2008.04.055.

[48] W.-S. Hung, C.-H. Tsou, M. De Guzman, Q.-F. An, Y.-L. Liu, Y.-M. Zhang, C.-C. Hu, K.-R. Lee, J.-Y. Lai, Cross-Linking with Diamine Monomers To Prepare Composite Graphene Oxide-Framework Membranes with Varying d-Spacing, (2014). https://doi.org/10.1021/cm5007873.

[49] C. Feng, J. Xu, M. Li, Y. Tang, C. Gao, Studies on a novel nanofiltration membrane prepared by cross-linking of polyethyleneimine on polyacrylonitrile substrate, J. Memb. Sci. 451 (2013) 103–110. https://doi.org/10.1016/j.memsci.2013.10.003.

[50] P.S. Goh, B.C. Ng, W.J. Lau, A.F. Ismail, Inorganic Nanomaterials in Polymeric Ultrafiltration Membranes for Water Treatment, Sep. Purif. Rev. 44 (2015) 216–249. https://doi.org/10.1080/15422119.2014.926274.

[51] Y. Takizawa, S. Inukai, T. Araki, R. Cruz-Silva, N. Uemura, A. Morelos-Gomez, J. Ortiz-Medina, S. Tejima, K. Takeuchi, T. Kawaguchi, T. Noguchi, T. Hayashi, M. Terrones, M. Endo, Antiorganic Fouling and Low-Protein Adhesion on Reverse-Osmosis Membranes Made of Carbon Nanotubes and Polyamide Nanocomposite, (2017). https://doi.org/10.1021/acsami.7b06420.

[52] A. Tiraferri, C.D. Vecitis, M. Elimelech, Covalent Binding of Single-Walled Carbon Nanotubes to Polyamide Membranes for Antimicrobial Surface Properties, ACS Appl. Mater. Interfaces. 3 (2011) 2869–2877. https://doi.org/10.1021/am200536p.

4.8.Supporting Information

S1. Scanning Electron Microscopy (SEM) images

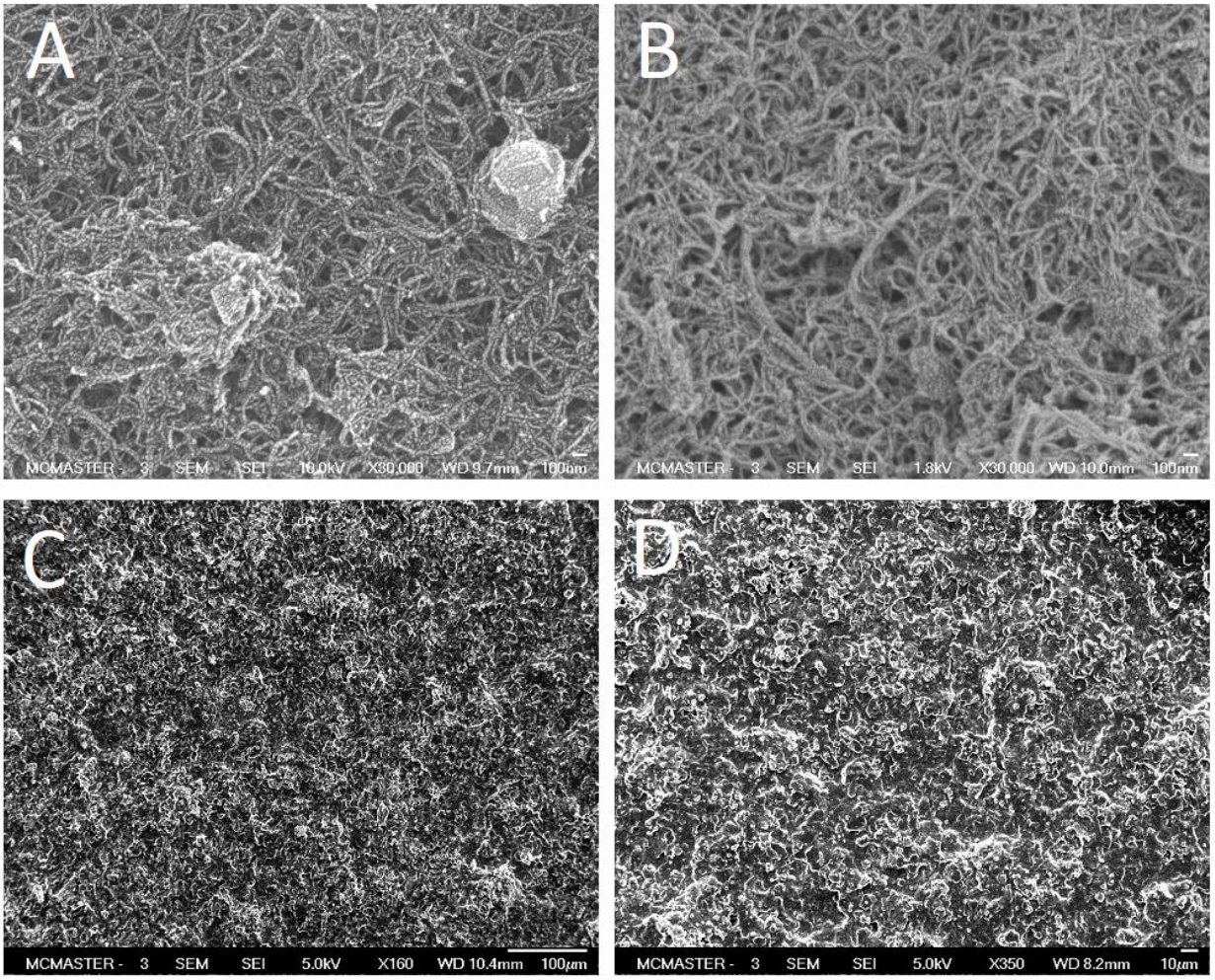

Figure 4.S1. Top view SEM images of A) MF 3 mg CNT, succinic acid, B) MF 3mg CNT, suberic.

S2. Investigating the leaching of CNT/PVA/SDS through MF and UF membranes during filtration process

We quantified the loss of CNT in UF and MF membranes using total organic carbon analyzer (TOC). We synthesized membranes from CNT suspensions contain 1 mg and 3mg CNTs without the presence of PVA and measured the leaching of CNTs through these membranes. The results reveal that CNT leaching through MF and UF membranes is almost negligible. The data is shown below:

Table 4.S1. Leaching results of CNT during membrane fabrication

Membrane	CNT mass loading (mg)	Mass of CNT leached (mg)	CNT leaching (%)
MF	1	1.9e-3	0.19
	3	8.1e-3	0.27
UF	1	1.4e-3	0.14
	3	3.0e-3	0.10

The leaching of PVA/SDS molecules during the membrane fabrication process using vacuum filtration was further analyzed in UF membranes having 3 mg CNT. CNT leaching was considered negligible in this test. The results reveal that a high portion of PVA/SDS molecules leach through pores of UF membranes during the vacuum filtration process.

Table 4.S2. Leaching results of PVA/SDS during membrane fabrication

Membrane	CNT mass loading (mg)	Mass of PVA/SDS in the feed (mg)	PVA/SDS leached (mg)	PVA/SDS leaching (%)
UF	3	34.5	18.96	54%

S3. MWCO experiment using 2 MDa PEO

During separation experiments using 250 ppm PEO solutions, it was observed that in addition to PEO passing through the membrane, a portion of unbound polyvinyl alcohol (PVA) leached through the membrane as well. The permeate thus contained PVA as well as PEO, which confounded our MWCO measurements. Due to the leaching of PVA, we conducted a preliminary study of the leaching of PVA to attempt to deconvolute PVA leaching from PEO rejection and quantify the selectivity of CNT-modified membranes. In this preliminary study, we determined that leaching of PVA may be due to many factors

including chemical stability of the dense layer, thickness of the dense layer, operating pressure, composition of the feed, and concentration of the foulant. To identify the cause of the PVA leaching, rejection tests were conducted on different membranes, either with or without PVA, under different conditions (Figure 4.S2). The results revealed that the fabrication conditions (strong acids and high heat) did not impact the support membrane's rejection of PEO. Further, it was demonstrated that pressurized water during pure water flux experiments did not cause leaching of PVA from the CNT thin films. When the feed solution contained 2 MDa PEO, a large amount of carbon was measured in the permeate by TOC analysis. Since the support membranes reject greater than 95% of 2MDa PEO, it was hypothesized that leached PVA was the source of the significant carbon content in the permeate during 2 MDa PEO rejection experiments.

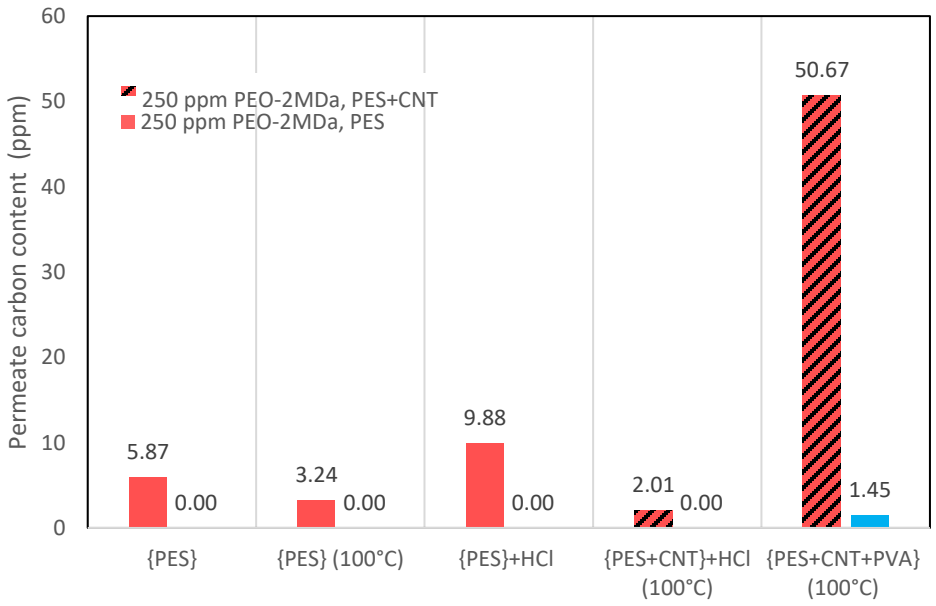

Figure 4.S2. TOC results of water and 250 ppm 2MDa PEO filtration.

S4. Electrical conductivity software

The conductivity of the membranes was measured using a four-point probe conductivity meter (Figure S2). This instrument is able to measure the bulk resistivity of the thin layer by considering the resistance among different pairs of needles and the thickness of the thin film. It is important to emphasize that the thickness of the membranes

was used to obtain the bulk conductivity, however, the error associated with SEM measurement was not quantified as this was not statistically relevant. Each error bar in figure 7 is attributed to measurements from three membranes with an identical network.

Sample calculation

For control MF 3 mg, from the sheet resistance measurements and SEM images we have:

$$Conductance = 26612\ microSiemens\ per\ square$$

$$Thickness = 1.91\ \mu m$$

Given the sheet resistivity formula, we can calculate electrical conductivity by inversing the equation as follows:

$$Resistivity\ (\Omega.m) = Resistance\left(\frac{\Omega}{sq}\right) \times thickness(m)$$

$$\rightarrow Conductivity\ \left(\frac{S}{m}\right) = \frac{conductance(S\ per\ square)}{thickness\ (m)}$$

$$\rightarrow Conductivity = 13933\ S/m$$

Accent HL5500 Hall System
Measured on 23/07/18 at 10:40 AM

SPECIMEN
Wafer ID:
Batch ID:
Material: Si
Description:
Thickness: 1.000 µm

MEASURING CONDITIONS
I-meas: 0.1 mA DC
Temperature: Error
Field: 0.323 Tesla

Targ.Vr: 20 mV

RESULTS SUMMARY

Rs:	52.01 ohm/sq	RHs:	m²/C	Ns:	/cm²
R :	0.005201 ohm-cm	Mob:	cm²/V-s	N :	/cm³

CONTACT CHECK

Pair	ohms
12	144
23	137
34	138
41	146
13	154
24	151

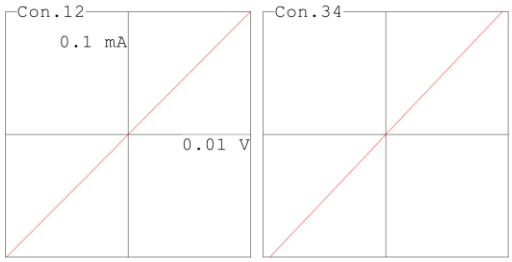

RESISTIVITY

Meas	+++	Vm	---	Sym	Factor	R-sheet
43	+1.151e-03	-1.113e-03		1.03	1.00	52.01
41	+1.185e-03	-1.140e-03		1.03	1.00	52.02
21	+1.148e-03	-1.117e-03		1.03	1.00	52.02
23	+1.176e-03	-1.150e-03		1.03	1.00	52.01

Figure 4.S3. (Top) Four-point conductivity probe, (bottom) Result sheet of Hall software.

S5. Contact angle

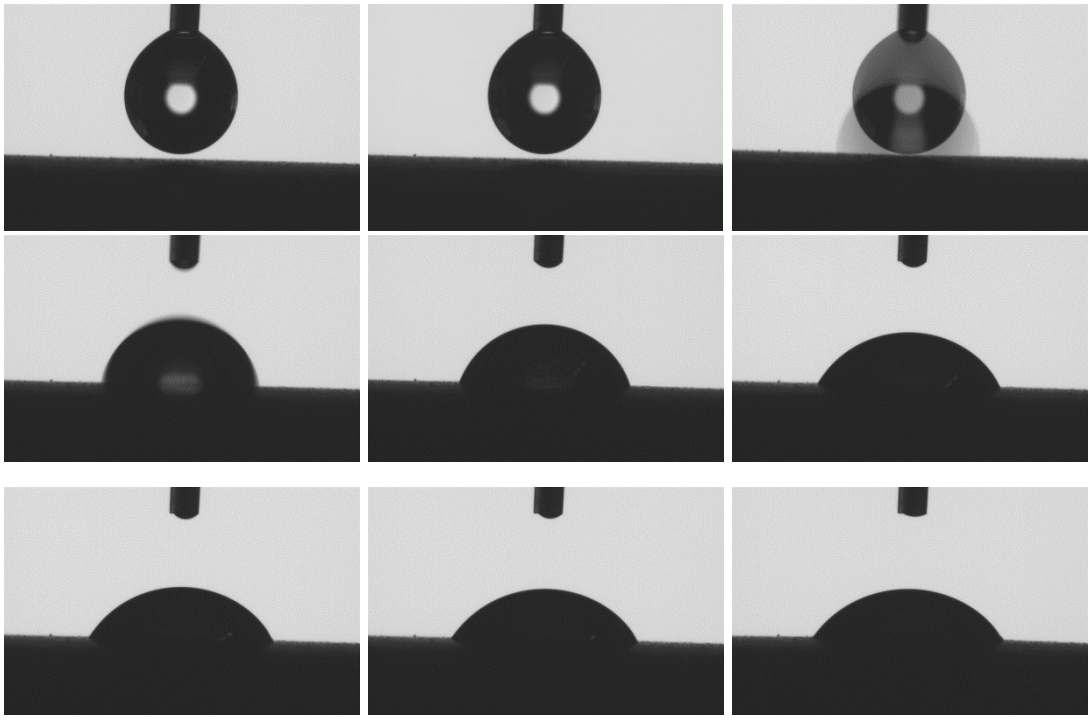

Figure 4.S4. Sequence of contact angle images from dispense time to steady state (Control 1mg CNT).

S6. Surface roughness

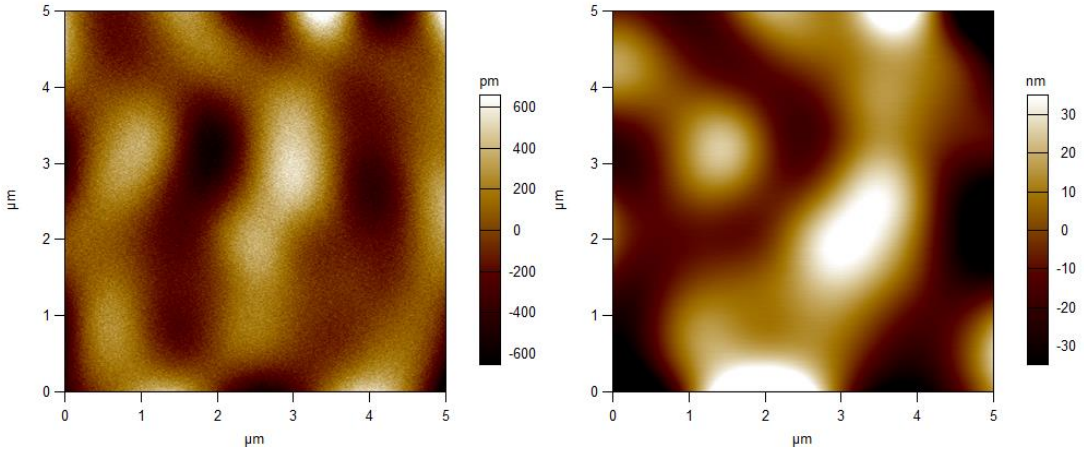

(a)

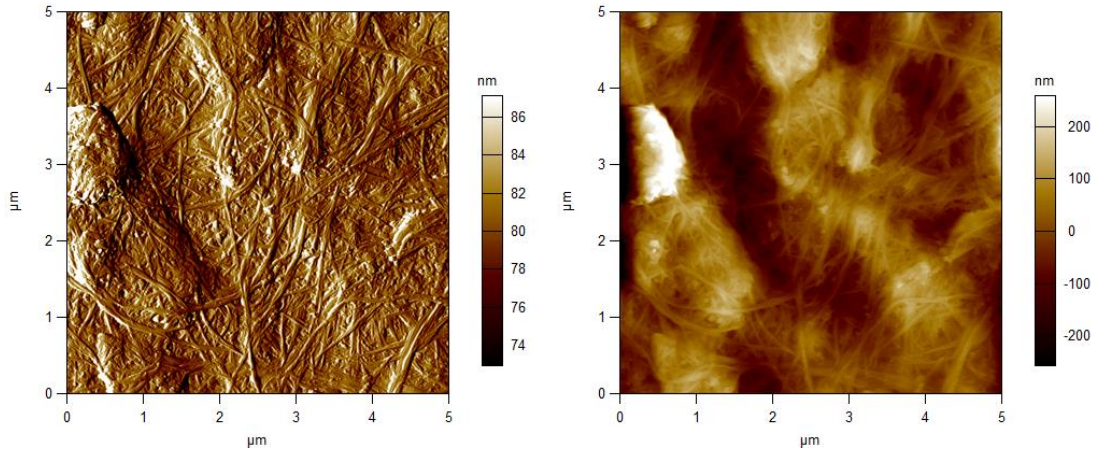
µm
nm
86
84
82
80
78
76
74
200
100
0
-100
-200

(b)

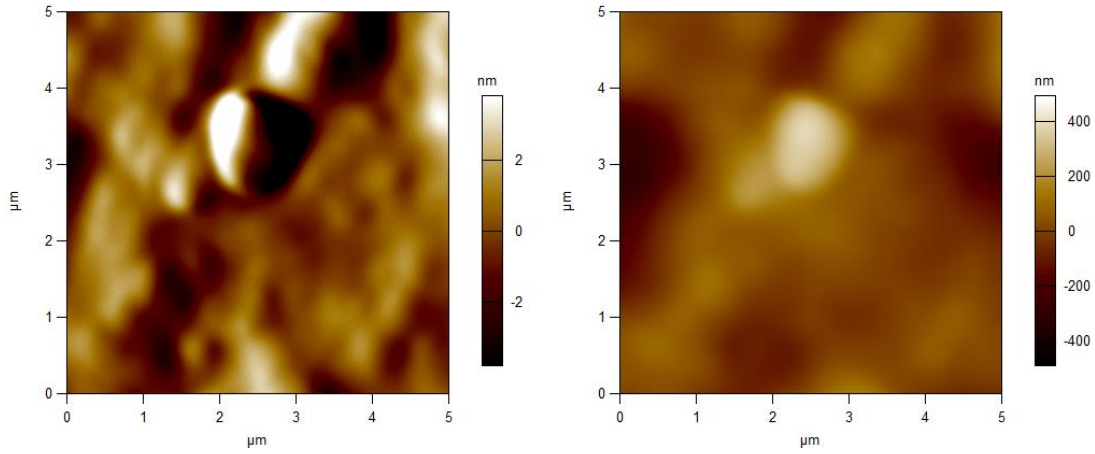
µm
nm
2
0
-2
400
200
0
-200
-400

(c)

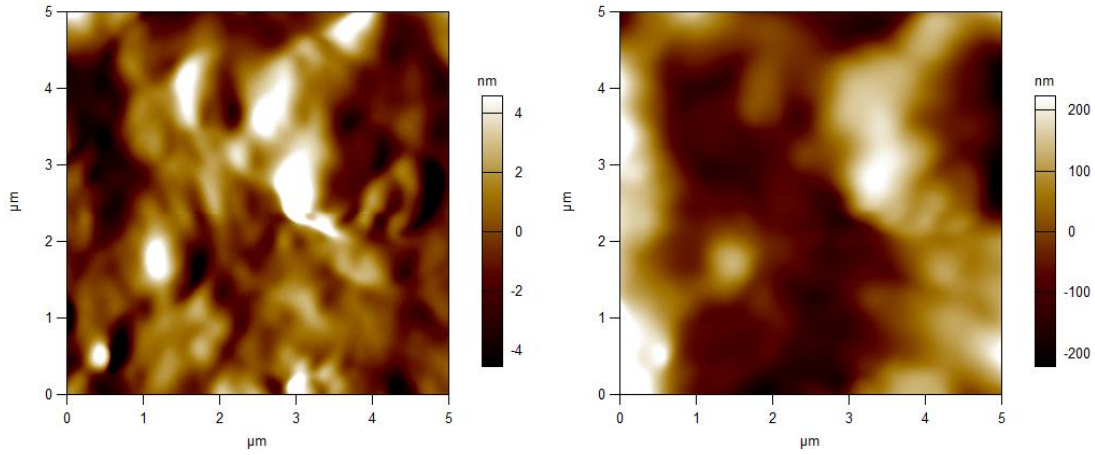
µm
nm
4
2
0
-2
-4
200
100
0
-100
-200

(d)

Figure 4.S5. AFM images for MF membranes where 2D images are on the left column and height mode is on the right column. (A) Control 1mg, (B) Control 3mg, (C) Suberic acid 1mg, (D) Suberic acid 3 mg.

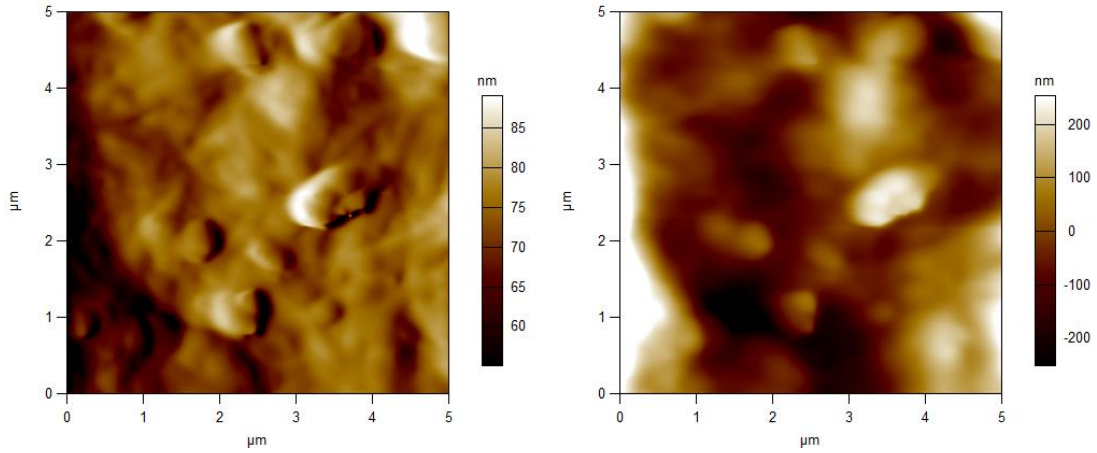

(a)

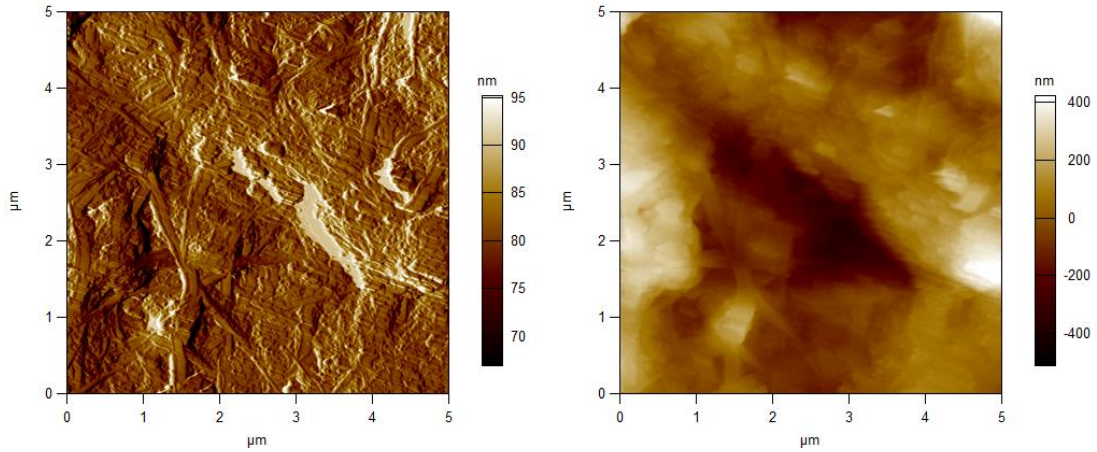

(b)

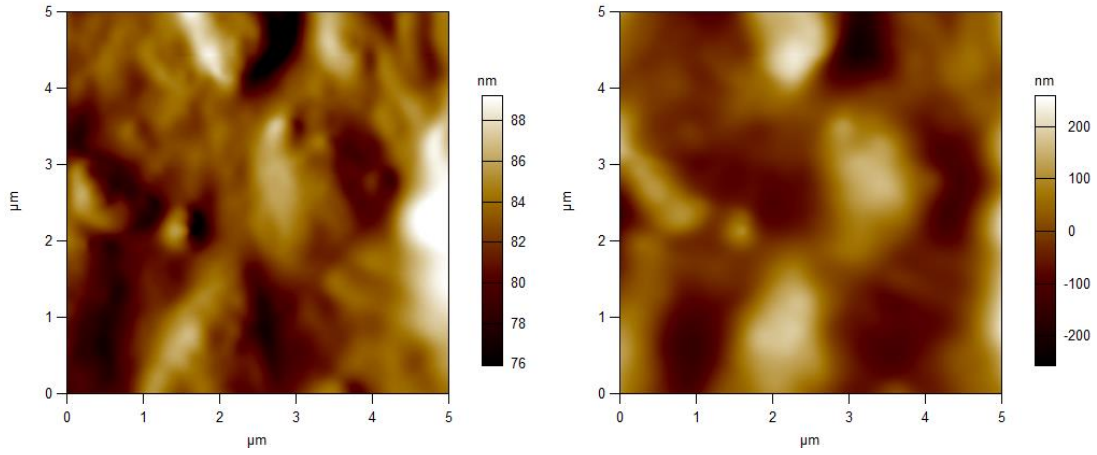

(c)

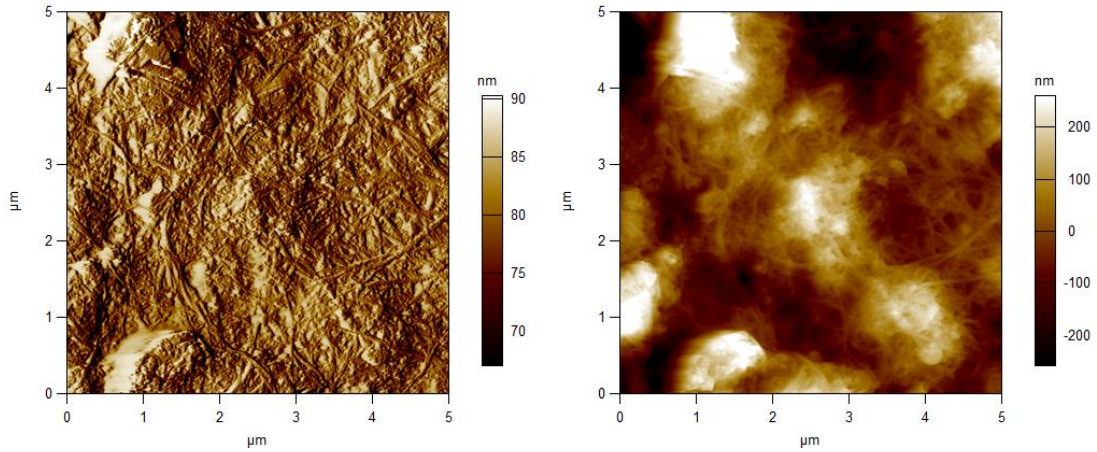

(d)

Figure 4.S6. AFM images for UF membranes where 2D images are on the left column and height mode is on the right column. (A) Control 1mg, (B) Control 3mg, (C) Suberic acid 1mg, (D) Suberic acid 3 mg.

Chapter 5

Investigating the Stability of Electrically Conductive Membranes

5.1.Abstract

Stability of electrically conductive membranes (ECM) is critical for expanding their application in separation-based technologies. In this work, ECMs were synthesized by coating polyethersulfone membranes with carbon nanotubes (CNT) crosslinked to polyvinyl alcohol (PVA) using two types of crosslinkers (succinic acid or glutaraldehyde). ECMs demonstrated a 21% reduction in flux over 4 hours under cathodic potential (2 V) in comparison to a 69% reduction in flux for control experiments when filtering a realistic bacterial suspension. Subsequently, the electrochemical, physical, and mechanical stability of the ECMs were explored using chronoamperometry and cyclic voltammetry, an evaluation of polymer leaching from membranes, and micro mechanical scratch testing, respectively. ECMs were shown to be unstable under anodic potentials (2-4 V) with the glutaraldehyde crosslinking demonstrating the highest electrochemical stability. PVA was shown to be a physically unstable crosslinking agent for CNTs under concentration polarization conditions. Instability was moderated by extending CP layers through thicker and less dense nanolayers. ECMs showed higher mechanical stability and resistance to surface damage, in particular when coated with glutaraldehyde. We quantified the relationship between ECM surface instability and their physical and electrochemical properties. In so doing, we provide guidance for making practical and scalable electrically conductive membranes.

Keywords: Membrane Stability; Fouling; Electrical conductivity; Concentration polarization; Electro-oxidation

5.2.Introduction

Fouling is one of the primary challenges limiting membranes' optimal performance. Fouling detrimentally impacts membrane performance causing a reduction in flux, an increase in the required transmembrane pressure, which lead to an increase in energy consumption, and a reduction in membrane longevity [2,3]. Membrane fouling mitigation is the focus of extensive research involving operating conditions, redox processes, and materials and interfaces [4–8].

Recently, electrically conductive membranes (ECMs) have demonstrated exceptional antifouling abilities [9–13]. Their antifouling mechanisms occur at the surface of the membrane, rather than in the feed solution as in the case of chemical antifoulants, thereby providing more direct and often more effective fouling mitigation. ECMs are membranes that contain an electrically conductive material surface, to which an externally applied electrical potential (positive or negative) is applied. The application of an electric potential to an ECM promotes various antifouling mechanisms at the membrane/water interface. These include electrostatic repulsion, electrochemically generated bubble scouring, direct redox surface reactions, or indirect radical-mediated reactions. The application of ECMs has gained increasing attention in research for mitigating fouling in water and wastewater treatment due to its in-situ application, low environmental impact, and presumed cost-effectiveness.

ECMs can be categorized as either organic (conductive polymer or graphitic material coatings) [14], inorganic (ceramic- or metallic-based coatings, e.g. RuO_2, TiO_2) [15,16], or hybrid (metal coatings embedded in or coated on polymeric material, e.g. ITO-PES) [17]. Ceramic-based ECMs offer better mechanical and chemical stability which allows for aggressive cleaning compared to polymeric membranes, however, challenging synthesis and high costs limit their future industrial adoption [15,16,18]. Organic ECMs are the most common form in the literature likely due to their mechanical flexibility, low cost, functionality, and tunable properties. The electrically conductive coating for organic ECMs is often a graphitic material such as carbon nanotubes (CNTs) [19,20], graphene [21,22], or graphite [23]. CNTs are the most widely used due to their high conductivity and

high surface area [14]. CNT-based conductive layers tend to be unstable and can leach into the solution or delaminate during manufacture and use [24–26]. Hence, a polymeric substance such as polyvinyl alcohol (PVA) is added to the nanolayer to (a) improve the adhesion between the CNTs and the supporting membrane [27], (b) increase the surface hydrophilicity [28], and (c) enable pore size tuning through controlled crosslinking reactions [29]. PVA bonds to CNTs via covalent bonds, electrostatic interactions, and Hydrogen-bonding [25,30,31]. Many studies have used CNT/PVA networks to demonstrate the application of ECMs [19,27,29,32–36].

Long term physical and chemical stability of membranes is critical for expanding their application into industrial separation technologies. In the current literature, research has focused on ECM antifouling performance, transmembrane flux, and separation properties. Little attention has been directed towards the post-fabrication stability and surface properties of ECMs. During separation and use, the surface properties of membranes can vary considerably from the initial properties as a result of surface instabilities [37]. Electrically conductive surfaces can be damaged or passivated by surface instabilities arising from pressure (high applied pressure, high concentration polarization), mechanical abrasion (contact with foulants under cross-flow velocities and possibly turbulent conditions, mechanical cleaning) [38], chemical reactions (chemical cleaning) [39], and electrochemical reactions (electro-oxidation) [40]. CNT-based ECMs have been found to be unstable under high anodic currents which degrade ECM conductivity and thereby compromise their antifouling performance [41–43]. Nanocomposite and nanoparticle stability under operating conditions (e.g. high applied pressures, mechanical forces, temperature differences, chemical attack) is an active area of investigation that has real-world ramifications from membranes to polymeric materials [40,44].

First, we demonstrated the antifouling abilities of our ECMs towards a realistic mixed bacterial culture in an aqueous feed. Subsequently, we investigated the 1) electrochemical, 2) physical, and 3) mechanical stability of microfiltration (MF) and ultrafiltration (UF) CNT/PVA-based ECMs, due to their widespread use in the literature. We investigated 1) the anodic oxidation of ECMs to determine their electrochemical

stability, 2) the physical stability of membranes stabilized with common crosslinking agents under various operating conditions such as transmembrane pressure, temperature, and foulant concentration, and 3) the mechanical stability of ECMs through micro scratch testing.

5.3.Materials and methods

5.3.1. Materials

Carboxyl functionalized single-walled/double-walled carbon nanotubes (SW/DWCNT-COOH, outer diameter: 1-4 nm, length: 5-30 µm, purity: >90w/%, functional content: 2.73 w/%) were purchased from Cheaptubes. Sodium dodecyl sulfate (SDS, Molecular weight (MW): 288.38) and hydrochloric acid (38%/) were purchased from Anachemia. Ethanol (85.6 %) and phosphate buffered saline (PBS, contains 137 mM sodium chloride, 2.7 mM potassium chloride, and 10 mM phosphate buffer) tablets were purchased from VWR. Glutaraldehyde (GA) solution (50.2 %, specific density: 1.127) and crystal violet were purchased Fisher Chemical. Yeast extract was purchased from Sigma-Aldrich. The poly(vinyl alcohol) (PVA, MW: 31,000-50,000, 98-99 % hydrolyzed) and poly(ethylene oxide) (PEO, 2 MDa) were purchased from Sigma-Aldrich. Succinic acid (MW: 118.9) was purchased from Alfa Aesar. Microfiltration (MF) and ultrafiltration (UF) Poly(ether sulfone) (PES, diameter: 47 mm, nominal pore size: 0.2 µm and 0.03 µm, respectively) membranes were purchased from Sterlitech. Deionized (DI) water was obtained from an Arium system (resistivity: 0.047 µS/cm).

5.3.2. Electrically conductive membrane preparation

The membrane fabrication method has been documented in our previous work [29]. In summary, a 7.5×10^{-4} w/% suspension of SWCNT/DWCNT in DI water was prepared by stirring the suspension for 10 min followed by ultra-sonicating (Qsonica, Q500, 500 Watts, 20 kHz) for 1 h with intervals of 2s on and 2s off. Simultaneously, 1.125×10^{-3} w/% solution of SDS in DI water was prepared separately after stirring the solution for 30 min. The CNT and SDS suspensions were mixed, stirred (15 min), and ultra-sonicated (2

h). SDS is used as a surfactant to make a well-dispersed CNT suspension. The ratio of CNT to surfactant (SDS) was kept at 1:1.5. A 0.5 w/% PVA solution was made after stirring the solution for 24 h (800 RPM, 120°C). The PVA and CNT suspensions were mixed and sonicated for 2 h (the ratio of CNT to PVA was kept at 1:10 unless otherwise mentioned). Succinic acid was added to the suspension as the crosslinker to achieve a crosslinking degree of 20%. After the suspension was well mixed, hydrochloric acid was added to a concentration of 2 M. The final suspension was allowed to react for 24 h. It should be noted that a well-dispersed solution is critical to forming a uniform coating of CNTs on the membrane.

The pristine PES membrane was kept in DI water for 24 h before use to ensure the surface was fully wetted. The wet membrane was placed in a filtration setup and the CNT suspension was filtered through a membrane to the target deposited mass. Following CNT deposition, DI water was filtered through the membrane for 5 min to rinse any polymeric or acidic residuals from the surface. The rinsed nanocomposite membrane was removed from the flask and cured in an oven for 1 h (100 °C). Following the curing step, membranes were cooled at ambient temperature and kept in DI water overnight for characterization and further analysis. To obtain a membrane with a thicker nanolayer, the following process was repeated up to three times before being cured in an oven: the CNT suspension (CNT/PVA/succinic acid) was vacuum filtered through the membrane, air dried, then washed with DI. The membrane was recovered and cured in oven at 100 °C for 1 h after.

Membranes fabricated with GA as the crosslinker followed a modified procedure. Following CNT/PVA vacuum deposition, the membranes were cured in an oven for 10 min at 100 °C followed by immersion in a 2.12 w/% solution of GA in DI water at 80 °C. The GA solution concentration was chosen following commonly reported values in literature, which theoretically yields a crosslinking degree of 93% when ECM contains 10 mg PVA and a crosslinking degree of 100% when ECM contains 5 mg PVA or less. Hydrochloric acid was added to the solution to a concentration of 0.1 M. After 1 h immersion in HCl solution, membranes were cured in an oven for 10 min at 100 °C.

5.3.3. Biosolution preparation and characterization

A multi-bacterial suspension was prepared by using 1 g of yeast extract in 100 ml of tap water for 24 h at 40 °C (RPM 100). Such an environment accelerates the growth of bacteria found in tap water as desired for the biofouling experiment [45]. The glass was covered in parafilm with a small gap for air to provide aerobic condition. The suspension was centrifuged three times each for 15 min (RPM 4500). After each interval, the supernatant was replaced with PBS solution and the suspension was well dispersed using a vortexer. The final suspension was mixed with PBS solution to yield an absorbance of 1 at a wavelength of 600 nm as measured by a UV–Vis Auto spectrophotometer (plate reader, SPARK 10M, Tecan Austria GmbH Inc.). The surface electrical charge of the particles in the suspension was measure by zeta potential analyzer (Zeta Plus, Brookhaven Instruments Corporation). Measurements were conducted for ten runs and the average value was reported.

5.3.4. Biofouling experiment

The anti-biofouling performance of the ECMs fabricated in this study was demonstrated via filtration of a bacteria enriched suspension cultivated from tap water. The biosuspension was pumped through the custom-designed cross-flow membrane filtration system. The schematic and the picture of the cross-flow cell are presented in Figure 5.1a and Figure 5.S1, respectively. More details about the cross-flow system is provided in the SI. The permeate was recycled to the feed reservoir to maintain a constant feed concentration. The pressure was kept constant at 10 psi (0.69 bar). The flow rate was 11.7 mL/s which provided a shear rate of 140.4 s^{-1}. The flow across the membrane was laminar with a Reynolds number of N_{Re} = 585 (more details are provided in the SI). In our setup, the flow-cell was fitted with electrodes to allow for an applied current to be supplied to the ECMs. The ECM was operated as a cathode and a graphite counter electrode was provided as an anode. Bacterial filtration cross-flow experiments were conducted for 4 h with flux and rejection recorded every hour. In experiments that were conducted to evaluate the application of electrical current on anti-biofouling performance of ECMs, an electrical

potential (2 V) was applied to the surface of the membrane by an external power generator operating in direct current (DC) mode.

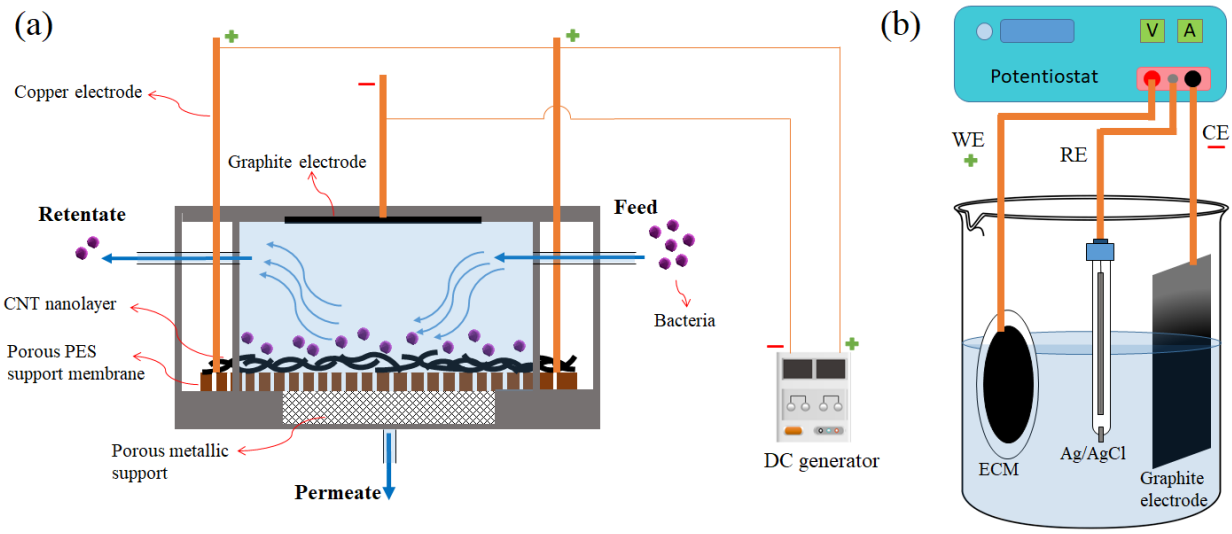

Figure 5.1. a) Schematic of the custom-designed cross-flow cell to assess ECM anti-biofouling performance b) Schematic of the batch electrochemical cell to check ECM anodic stability.

5.3.5. Surface analysis

Thickness of the nanolayer and morphology of ECMs were observed using scanning electron microscopy (SEM, JEOL JSM-7000F). SEM as well as crystal violet staining were used to assess the fouling intensity of the biofouled membranes. Details were provided in the supplementary information.

Fourier-transform infrared spectroscopy (FTIR, HYPERION 3000) was used to identify the chemical bonds at the surface. Hydrophilicity of the surface was calculated using a high-speed contact angle instrument (OCA 35). The contact angle was measured after dispensing 5 µL of DI water onto the membrane surface. Contact angles were measured once droplets achieved steady state. Three droplets were dispensed on each membrane and an average contact angle was reported.

Conductivity of the membranes was measured using a four-point probe conductivity meter. This instrument measures the bulk resistivity of the nanolayer given the resistance

among different pairs of needles and nanolayer thickness. Membranes were completely dried in an oven at 60 °C for 1 h, then cooled at room temperature for 1 h prior to conductivity measurements.

A micro scratch tester (Revetest scratch tester, Anton Paar) was used to measure the membrane surface mechanical strength. The membrane surface was scratched with a diamond-tipped conical indenter (radius: 100 µm) and a conical angle of 90°. The tip applied a normal force of 0.5 N. Scratch length and speed were 1 mm and 5 mm/min, respectively. Three scratches were performed on each surface to validate the reproducibility of the results. The penetration depth of the indenter over the scratch length was used as an indicator of the surface mechanical strength.

5.3.6. Electrochemical cell

A three-electrode electrochemical cell coupled to a Pontentiostat (Multi Autolab M204, Metrohm) was used to evaluate the anodic oxidation potential of the membranes through fixed potential chronoamperometry as well as cyclic voltammetry (CV) methods. Figure 5.1b and Figure 5.S2 present the schematic and the picture of the electrochemical cell, respectively. The ECM, graphite sheet, and an Ag/AgCl electrode (Metrohm, operating range: 0-80 °C) were used as the working electrode (WE, anode), counter electrode (CE), and reference electrode (RE), respectively. All electrodes were placed in an electrochemical cell containing PBS solution as the electrolyte. For the CV tests, 15 cycles at a scan rate of 0.1 mVs-1 were applied to each membrane, with a scan range of 0-3 V relative to the Ag/AgCl electrode. Fixed potential chronoamperometry tests were conducted by applying either 2 or 4 V (with respect to the reference electrode) to the membrane for 240 and 20 min, respectively.

5.3.7. Flux and rejection tests

Membrane permeability was measured with a custom-designed cross-flow cell (Figure 5.1a). UF membranes were compressed under pressure of 10 psi (0.69 bar) prior to the flux test for 1 h to reach their final morphological state. For the flux test, the biosuspension was filtered through the membrane with permeability being reported every

hour up to 4 h at 10 psi (0.69 bar). For each reported permeability value, three measurements were taken within 15 min (each 5 min) and the average value was reported. The rejection of the bacteria was calculated by reading the absorbance value of feed and collected permeate (at OD_{600}) every hour up to 4 h using a UV–Vis spectrophotometer. Permeability and rejection tests during the biofouling experiment were conducted for two identical membranes and the average value was reported. The PEO rejection test was conducted in a dead-end stirred flow cell (Sterlitech stainless steel) at 10 psi (0.69 bar) (unless otherwise mentioned), 100 RPM, and ambient temperature. The feed solution contained 250 ppm PEO in water (unless otherwise mentioned). The permeate was collected and analyzed using a total organic carbon analyzer (TOC, SHIMADZU). The rejection was calculated using the following Equation.

$$R = (1 - \frac{C_p}{C_f}) \times 100$$

Where R, C_p, and C_f represent rejection (%), the concentration of particles in the permeate, and the concentration of particles in the feed, respectively.

5.4.Results and discussion

The primary goal of the research was to evaluate the stability of electrically conductive membranes (ECMs). The stability of the surface coatings ensures consistent operational performance. We propose a suite of ECM stability measurements (electrochemical, physical, and mechanical) that should be applied to all ECMs to demonstrate their practical viability. In advance of these stability assessments, we validated our ECM anti-biofouling performance to confirm their practical application.

5.4.1. Anti-biofouling performance of ECMs

The anti-biofouling performance of the ECMs fabricated in this study was demonstrated by filtering a bacteria-enriched suspension cultivated from tap water. Both anodic and cathodic currents have been used for anti-biofouling purposes in the literature [41,46,47]. Anodic currents have been suggested to inactivate microorganisms through

direct and indirect oxidation (radical generation), and inhibit fouling through electrostatic repulsion force, oxygen gas generation, and pH changes while cathodic currents are thought to mitigate fouling through electrostatic repulsion, hydrogen peroxide generation, and hydrogen gas generation.

We demonstrated the anti-biofouling abilities of our synthesized ECMs using cathodic and anodic currents. The rejection and flux values of PES and CNT membranes during the bacterial filtration experiments are presented in Figure 5.2a. A sharp decrease in flux was observed for PES membranes while ECMs better maintained their flux, indicating promising anti-biofouling potential. The normalized 4 h flux was reduced by 21%, 42%, 46%, and 69% for ECMs with an applied cathodic potential, ECMs with an applied anodic potential, control ECMs without applied potential, and control PES membranes without applied potential, respectively (Figure 5.2b). All membranes showed excellent separation performance by retaining more than 91% of bacteria during the 4 h filtration.

SEM images were used to investigate the biofilm formation after the bacterial filtration experiments. As shown in Figure 5.3, bacteria formed thick, uniform biofilms on PES membranes after only 4 h of filtration. In contrast, ECMs with and without applied potentials showed significantly fewer bacteria on their surface, demonstrating better resistance toward biofilm formation. ECMs without applied potential are composed of CNT networks. CNT networks have an irregular porous structure which acts as a steric barrier toward deposition of bacteria on the surface. As a result, it is hypothesized that a less dense bacterial network is formed on the surface of the ECMs that is easily disrupted by the lateral shear force. CNTs also have inherent antibacterial properties that further contribute to ECM anti-biofouling performance [48,49].

Microbial cells found on ECMs charged with a 2 V applied anodic potentials demonstrated structural cellular damage as indicated by their deformed and irregular cellular shape (Figure 5.3). Cell lysis was mainly caused by oxidative stress either directly through electron transfer or indirectly through the generation of oxidative compounds. Free

radical generation induced by water splitting and the subsequent reactions at the anode are well documented in the literature and summarized as follows [50–52]:

$$2\,H_2O \rightarrow O_2(g) + 4H^+ + 4e^- \ (E° = 1.03V \text{ vs. } Ag/AgCl) \qquad \text{Reaction (1)}$$

$$OH^- + H^+ \rightarrow OH^\bullet \ (E° = 2.1 \text{ V vs. } Ag/AgCl) \qquad \text{Reaction (2)}$$

In addition, the sulfate and chloride ions present in the buffer solution can further contribute to radical generation as follows [50,52,53]:

$$SO_4{}^{2-} + H^+ \rightarrow SO_4{}^{\bullet-} \ (E° = 2.2 \text{ V vs. } Ag/AgCl) \qquad \text{Reaction (3)}$$

$$2Cl^- + H^+ \rightarrow 2Cl^\bullet (E° = 1.97 - 2.37 \text{ V vs. } Ag/AgCl) \qquad \text{Reaction (4)}$$

ECMs with a 2 V applied cathodic potential had the most anti-biofouling effect. Zeta potential of the bio-suspension used in this study was measured to be -16.06 ± 1.24 mV, hence the applied cathodic current on ECMs cause electrostatic repulsion of the negatively charged bacterial suspension. This has been previously demonstrated for pure bacterial cultures [54], while here we show the effect for mixed bacterial cultures enriched from tap water. Our main explanations for this anti-biofouling performance are as follows:

- A negatively charged surface limits attachment of negatively charged bacteria due to the strong electrostatic repulsive force.
- A charged irregular structure of CNTs on the surface reduces the CP due to electro-steric forces.
- Cathodic current results in the generation of hydrogen gas at the surface of the membrane. The shear force induced by generated bubbles can detach particles at the surface. [46].

  $$H_2O + 2e^- \rightarrow H_2(g) + 2OH^- \qquad \text{Reaction (5)}$$

- Cathodic current leads to the generation of reactive hydrogen peroxide which induced damage to bacterial cells and reduced cell viability [55,56]. However, concentrations of electro-generated hydrogen peroxide under the range of potentials applied (below or equal to 2 V) may only have a small contribution

to membrane self-cleaning performance [57,58]. Cathodic reduction of oxygen gas is shown as follows [56]:

$$O_2(g) + 2H^+ + 2e^- \rightarrow H_2O_2 \ (E° = 0.465 \text{ V vs. Ag/AgCl}) \qquad \text{Reaction (6)}$$

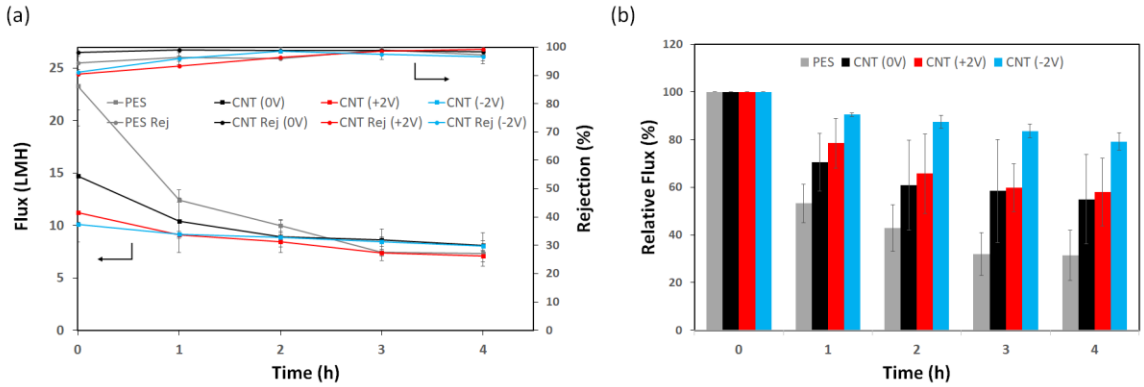

Figure 5.2. Membrane flux during a 4 h cross-flow filtration of the bacterial suspension. Gray: Control PES membrane with no applied potential, Black: Control CNT membrane (1 mg CNT) with no applied potential, Red: CNT membrane (1 mg CNT) used as an anode with an applied total cell potential of 2 V, Blue: CNT membrane (1 mg CNT) used as a cathode with an applied total cell potential of 2 V (a) rejection and actual measured flux, and (b) relative flux values. Error bars represent standard deviation for two membranes.

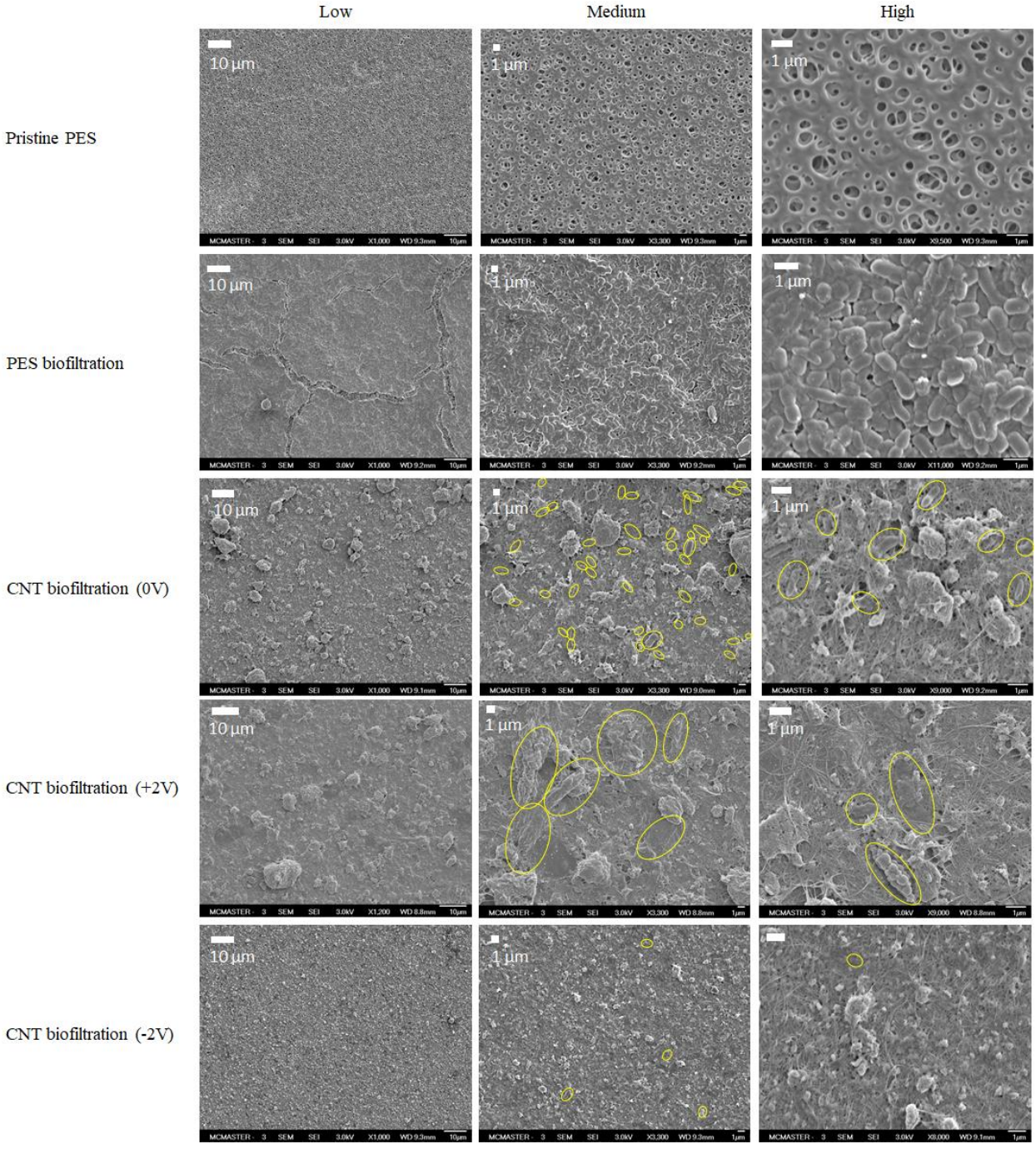

Figure 5.3. SEM images of the pristine PES membranes (first row), biofouled PES after 4 h (second row), biofouled ECM without applied potential after 4 h (third row), biofouled ECM after 4 h under an applied anodic potential of 2 V (fourth row), and biofouled ECM after 4 h under an applied cathodic potential of 2 V (fifth row). Left column: low magnification, middle column: medium magnification, and right column: high magnification of the membrane surfaces.

Biofouled membranes were further characterized by crystal violet staining to observe fouling intensity. Results are shown in Figure 5.S3a which are in good agreement with SEM images as they indicate the presence of bacteria after 4 h filtration. The findings in this section support previous work indicating that these ECMs have substantial in-situ anti-biofouling properties [9,10].

5.4.2. ECM stability

The physical, chemical, and mechanical stability of ECMs is crucial for their industrial adoption and implementation. ECM stability has not been systematically studied and it is unknown how ECM properties will change during operation. We hypothesized that their properties will differ considerably from their initially measured properties during use, thereby hindering their purported properties. We suggest that a comprehensive assessment of their operational stability is necessary to validate their industrial applicability. For example, ECMs may be subject to passivation, which would directly compromise the membrane performance (flux and separation properties), hinder their antifouling properties, shorten membrane life, and increase the system energy consumption. To analyze their passivation, we studied three forms of ECM stability: 1. Electrochemical stability – ECM electro-oxidation by the application of anodic current, 2. Physical stability – polymer leaching during separation of a model foulant, and 3. Mechanical stability – scratch resistance.

Electrochemical stability

CNT-based ECMs have the potential to reduce fouling when exposed to anodic, cathodic, or alternating currents (applied at either regular or irregular intervals). As discussed above, we have demonstrated anti-biofouling behavior at cathodic and anodic potentials. Alternating potentials (i.e. the use of both cathodic and anodic potentials) have been suggested to be particularly effective, suggesting that both anodic and cathodic potentials may be used in practice [58–60]. Many studies have focused on the impact of cathodic, anodic, and alternating potentials applied to ECMs on foulants, but have largely

ignored ECM electrochemical stability under these applied potentials. Herein we assess the stability of ECMs under cathodic and anodic potentials.

Cathodic stability of ECMs was evaluated using a high cathodic current (150 mA vs. Ag/AgCl reference electrode) applied to a membrane composed of CNT/PVA/SA for 20 min (Figure 5.S4). It was observed that the potential was maintained at (~ -2.8 V) over the electrochemical reaction interval indicating a stable cathodic surface. ECMs composed of CNTs were expected to be stable under reducing conditions [40].

Subsequently, the corrosion stability of ECMs was evaluated using anodic potentials (Figure 5.4). Anodic electro-oxidation was explored using fixed potential chronoamperometry as well as cyclic voltammetry (CV) methods. To the best of the authors' knowledge, the anodic oxidation of CNTs, CNTs and PVA crosslinked with succinic acid (CNT/PVA/SA), and CNTs and PVA crosslinked with glutaraldehyde (CNT/PVA/GA), has not been systematically studied. 4 V anodic potential was applied to ECMs to accelerate surface oxidation and demonstrate how different crosslinking chemistries impact ECM stability. 2 V anodic potential was applied to ECMs to represent common operating potentials as most studies operated above 1.2 V and near or above 2 V.

The current on ECMs decreased over time, as shown in Figure 5.4a, with an applied 4 V anodic potential. Over the course of the electrochemical reaction interval, the current dropped by 94%, 49%, and 14% for ECMs composed of CNTs alone, CNT/PVA/SA, and CNT/PVA/GA, respectively. ECMs crosslinked with GA showed the least oxidation-induced loss of conductivity. However, ECMs containing only CNTs and GA (without crosslinking) showed the same current drop (94%) as CNTs alone. Figure 5.4a presents the normalized current of the working electrode (ECM) over a span of 20 min with an applied potential of 4 V. Normalized currents were analyzed because variation in the steady-state current of ECMs depends on their initial conductivity, and material composition. The real current is presented in Figure 5.S5a. All ECM networks reached a steady oxidation state within 400 s, when a 4V anodic potential was applied.

CNTs have been found to be unstable under high anodic currents due to the degradation of the CNT structures [41–43]. In an electrochemical cell, electrons travel from cathode to anode, however, due to higher resistance of the media as compared to the electrode, they accumulate at the surface leading to the formation of an electric double layer (EDL). Once an EDL is fully developed with sufficient potential, electrons take part in electrochemical reactions including anodic electro-oxidation of the CNT nanolayer. The mechanism of CNT degradation has been studied elsewhere and is not the main focus of this study. Briefly, high surface hole generation due to harsh direct electron-transfer likely causes accelerated oxidation of CNTs. CNT corrosion damages the surface sp2 hybridization thereby decreasing the CNT conductivity critical for electrochemical applications. CNT degradation may also be caused by either the generation of free radicals (Reaction 1-4) at the CNT surface or by gas bubble-induced shear-forces generated from direct electron transfer at the CNT surface [50].

Oxidation of CNTs at anodic potentials above 1.2 V was expected due to the mechanisms explained above. The most unexpected observation, however, was the electro-oxidative stability of GA-cross-linked CNT-PVA ECMs (CNT/PVA/GA) in particular, and to a lesser extent the SA-cross-linked CNT-PVA (CNT/PVA/SA) ECMs. We hypothesize that PVA and GA work as sacrificial polymers that protect the CNTs against anodic oxidation. It has been shown that polymers embedded in a CNT-based conductive network are oxidized more readily as CNTs are electron receivers under the application of anodic current [61]. Therefore, we speculate that CNTs are anodically protected by the crosslinked polymeric coatings (PVA crosslinked with GA).

To support electrochemical current measurements, the surface conductivity of membranes was measured before and after ECMs were exposed to a 4V anodic potential (vs. Ag/AgCl reference electrode) for 20 min (Figure 5.4b). The decrease in the electrical conductivity of the membranes in response to the anodic potential was in good agreement with the drop in ECM current observed during the electrochemical test (with the exception of CNT/PVA/GA). The permanent drop in membrane electrical conductivity was 88%, 91%, 60%, and 60% for CNT, CNT/GA, CNT/PVA/SA, and CNT/PVA/GA, which was

consistent with 94%, 94%, 49%, and 14% decreases in measured current during the electrochemical tests, respectively. The permanent decrease in ECM conductivity explains the continuous drop in current throughout the electrochemical oxidation reactions.

While the optimal ECM electrical potential operating range is not known, ECMs are commonly evaluated in the literature in the range of 0.5-2 V. The critical anodic potential required for efficient antifouling performance has been frequently reported to be above 1 V [55,62,63]. The potential at which CNT oxidation occurs in real applications is debated in the literature ranging from 1.2 V up to 2.2 V (with respect to a Ag/AgCl reference electrode) [50,64,65].

A potential of 2 V was applied to the working electrode for a prolonged time (4 h) in order to evaluate the oxidative effect of commonly used potentials in comparison to more extreme potentials as evaluated above. The normalized and real current output over time are presented in Figure 5.4c and Figure 5.S5b, respectively. Under application of 2 V, ECMs were oxidized less severely and through different kinetic pathways than at 4 V. The time needed for ECMs to reach their steady-state oxidation was 5 times longer (~2000 s) under 2 V applied potential as compared with 4 V (400 s). However, oxidized ECMs had nearly identical steady-state currents at both 2 and 4 V (1-4 mA) (Figure 5.S5a and Figure 5.S5b). ECMs consisting of CNT/PVA/GA or CNT/PVA/SA showed higher anodic stability compared to CNT and CNT/GA ECMs consistent with the findings at 4 V applied potential. Interestingly, under 2 V applied potential, the current of the CNT/PVA/GA network steadily increased after ~1000 s surpassing its original conductivity after the 4 h duration.

At 2 V applied potentials, the lower CNT corrosion was expected because fewer side reactions occur that lead to the generation of detrimental free radicals ($OH^{\bullet}$ and $SO_4^{\bullet -}$). Further, the higher stability of ECMs crosslinked with SA or GA supports the hypothesis that PVA and GA can act as sacrificial polymers. We hypothesize that GA diffusion into the CNT/PVA network and subsequent crosslinking with PVA through acetylation reaction explains the higher conductivity of CNT/PVA/GA illustrated

in Figure 5.4c. Anodic surfaces generate high doses of protons which act as a catalyzer for acetylation reaction. PVA is well-blended with CNT molecules and has many hydroxyl groups branching from its backbone. The crosslinking reaction between hydroxyl groups of PVA and aldehyde groups of GA leads to stronger binding of CNTs and a subsequent higher conductivity. Figure 5.S6 shows FTIR spectra of each membrane after 2V applied potential, which suggests that acetylation reactions occurred between CNTs [66]. It was observed that the CNT/PVA/GA network had a higher relative intensity of carbonyl bonds as compared to CNT/GA. This relative difference was greater after electro-oxidation possibly due to the diffusion of GA into the CNT/PVA network.

Additional fixed potential chronoamperometry trials are presented in Figure 5.S7. The anodic CV results for 15 cycles under total anodic potentials of 0-3 V are presented in Figure 5.S8. Control CNT and CNT/GA membranes had a high current response for the first five cycles and became less conductive over time due to passivation. However, the CNT/PVA/GA network was more stable across all the cycles, represented by a lesser drop in conductivity due to anodic protection of GA and PVA. These findings are in close agreement with the fixed potential chronoamperometry results. Finally, there was little evidence that mechanical breakdown of CNTs occurred and this had minimal to no effect on the change in electrical conductivity (Figure 5.S9).

(a)

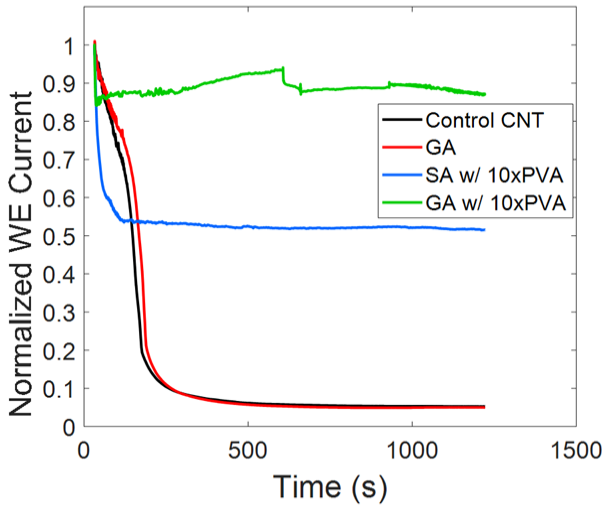
Normalized WE Current
Time (s)
Control CNT
GA
SA w/ 10xPVA
GA w/ 10xPVA

(b)

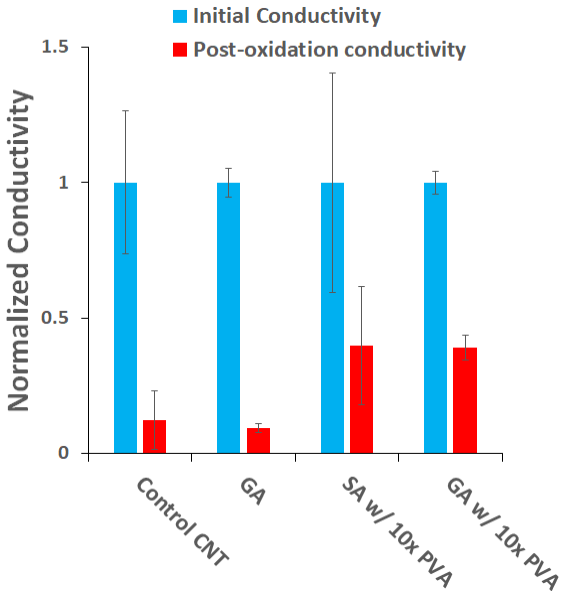
Initial Conductivity
Post-oxidation conductivity
Normalized Conductivity
Control CNT
GA
SA w/ 10x PVA
GA w/ 10x PVA

(c)

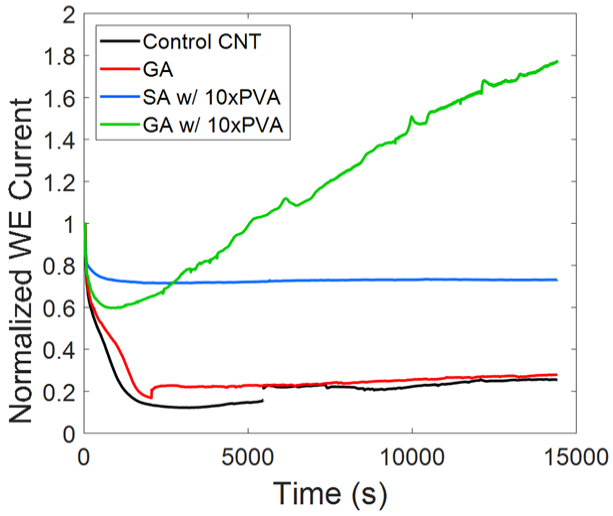
Normalized WE Current
Time (s)
Control CNT
GA
SA w/ 10xPVA
GA w/ 10xPVA

Figure 5.4. Electrochemical batch test for ECMs containing glutaraldehyde (GA), and a blend of polyvinyl alcohol (PVA) and either GA or succinic acid (SA). The ECM, graphite sheet, and an Ag/AgCl electrode were used as the working electrode (anode), counter electrode, and reference electrode, respectively. (a) Fixed potential chronoamperometry was applied to the conductive membrane with a total cell potential of 4 V (vs. Ag/AgCl reference electrode) for 20 min. (b) Normalized conductivity before and after a constant linear potential of 4V (vs. Ag/AgCl electrode) was applied to ECMs. (c) Fixed potential chronoamperometry was applied to the conductive membrane with a total cell potential of 2 V (vs. Ag/AgCl reference electrode) for 240 min. Error bars represent standard deviation for two membranes. All ECMs contained 1 mg CNT. "xPVA" shows the mass ratio of PVA to CNT. [PBS]= 137 mM sodium chloride, 2.7 mM potassium chloride, and 10 mM phosphate buffer.

Physical stability

ECMs are often composed of conductive materials (e.g. CNT), polymeric binders (e.g. PVA), and crosslinkers (e.g. GA and SA) coated on a support membrane (e.g. PES MF and UF membranes). The physical stability of the polymers within the ECM is important for their consistent separation and antifouling performance. Herein we studied the physical stability of ECMs composed of CNT/PVA/SA and CNT/PVA/GA with varying amounts of PVA.

SEM images of an ECM synthesized for the current study are presented in Figure 5.5, showing a typical nanolayer several micrometers thick. Polymers such as PVA are added to the conductive nanolayer to enhance surface hydrophilicity and nanolayer stability.

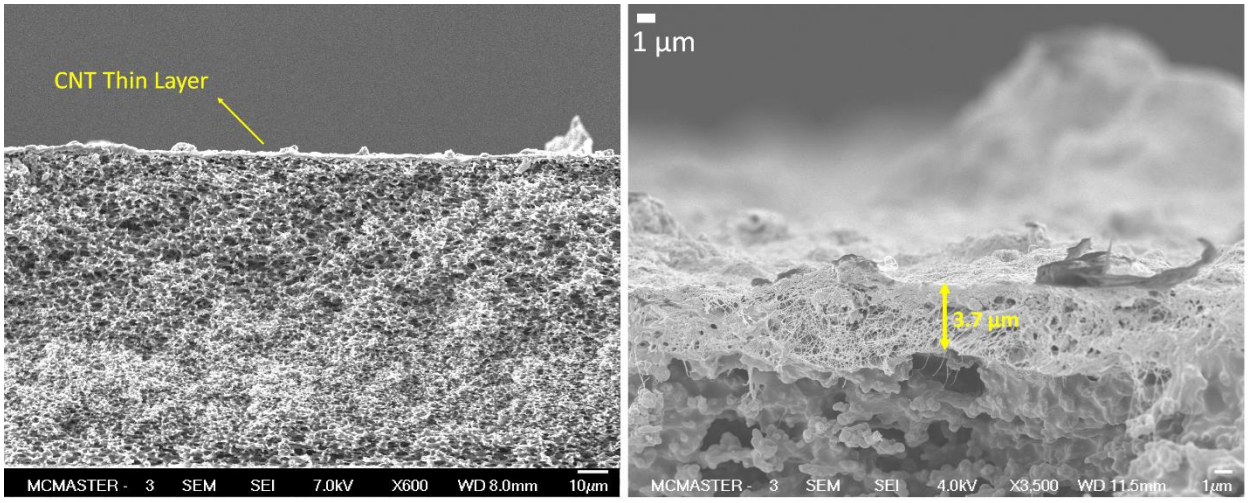

Figure 5.5. SEM images of UF electrically conductive membrane composed of CNT and PVA with a mass ratio of 1:10. Left: low magnification, right: high magnification.

A simple test was designed to evaluate if the content of the nanolayer is altered by filtration. This test involved filtering water and/or PEO suspensions of different concentrations through the membrane at various pressures and measuring the total organic carbon in the permeate. Figure 5.6 shows the measured permeate carbon content from the PEO rejection experiments. It should be noted that pristine UF PES membranes with a nominal pore size of 30 nm efficiently rejected 2 MDa PEO (>99.6 %) by size exclusion, and little to no organic carbon was measured in the permeate (Figure 5.S10). In Figure 5.6, ECMs (formed using these same UF PES membranes as supports) were found to have high permeate carbon content (24 - 85 ppm) for a range of PEO concentrations and applied pressures. These permeate concentrations are indicative of polymers leaching from the nanolayer.

The results shown in Figure 5.6a demonstrate that an increase in the PEO concentration from 50 to 250 ppm increased the leaching of polymers, as measured by permeate carbon content, by 41% on average. Furthermore, an increase in the transmembrane pressure from 10 psi to 100 psi (0.69 bar to 6.90 bar) for both PEO concentrations increased the permeate carbon content 80% on average. In contrast, filtering pure water at either 10 or 100 psi (0.69 to 6.90 bar), did not cause any significant permeate carbon content. We hypothesize that concentration polarization causes nanolayer

instability, based on the measured influence of PEO concentration and the lack of impact on leaching observed with pure water pressure.

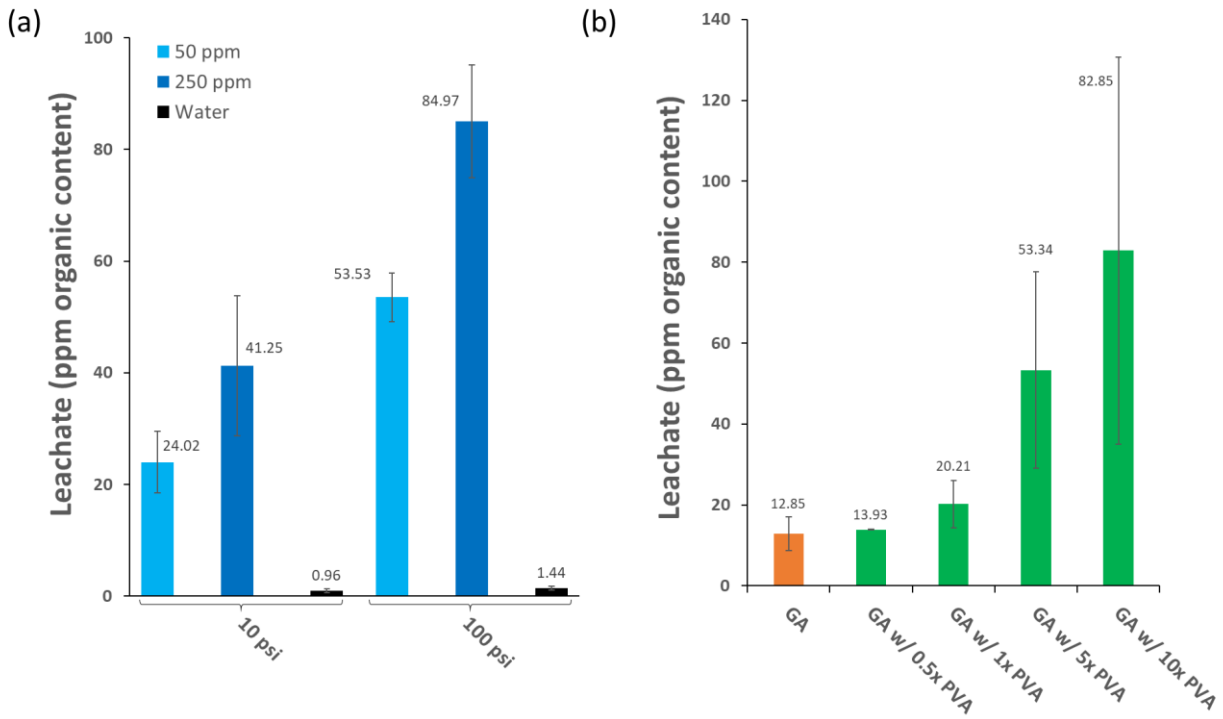

Figure 5.6. Carbon content in the collected permeate in the PEO (2 MDa) separation tests measured by a TOC analyzer. ECMs contained 1 mg CNT in the nanolayer. "N× PVA" shows the mass ratio of PVA to CNT where N is the multiplicative factor for mass. (a) Values were measured at PEO concentrations of either 50 or 250 ppm in water and at pressures of 10 psi or 100 psi (0.69 bar or 6.90 bar). PVA to CNT mass ratio was kept at 10:1. (b) CNT: PVA ratio was varied from 1:0.5 to 1:10 and the resultant leaching of PVA was measured. Concentration of GA solution was 2.12w% in all cases. GA and SA stand for glutaraldehyde and succinic acid used in the network. Error bars represent standard deviation for three membranes. Tests were conducted at 10 psi (0.69 bar).

The main reason for PVA leaching can be explained by the local pressure build-up induced by concentration polarization (CP) (Figure 5.S11). During a separation process, the foulant (PEO) accumulates on the surface, blocking pores and leading to local pressure increases. High local pressures cause leaching of unbonded PVA molecules. In comparison, during pure water flux experiments, in the absence of foulants no significant PVA leaching occurred at either pressure as there was no pore blockage and thus no local pressure build-up.

PVA interacts with CNTs through hydrogen-bonding and electrostatic interactions [25,30,31]. In addition, strong covalent ester bonds are formed upon crosslinking of the PVA and CNTs [29]. However, not all PVA chains are covalently bound to CNTs and loosely attached PVA molecules are unstable in the nanolayer. It is these unstable PVA molecules that are likely leached from the nanolayer.

ECMs have a separation barrier composed of a porous CNT network synthesized on pristine UF PES membranes. To control for the influence of ECM synthesis on rejection characteristics of the support UF PES membranes, UF PES membrane rejection experiments were conducted, controlling for each of the processing parameters (low pH ~3 and high temperatures 100 °C). These control experiments, (Figure 5.S10), demonstrate that processing parameters had little to no effect on UF PES rejection. Further, it should be noted that the CNTs had an average length of 10 – 30 um, and are thus unable to pass through the 30 nm pores of the UF membrane. CNTs do not enter the permeate and therefore do not contribute to the permeate carbon content.

ECM stability was assessed for membranes formed with different PVA concentrations using an alternative crosslinking agent, glutaraldehyde (GA), and approximately the same crosslinking degree at 10 psi (0.69 bar). These results are presented in Figure 5.6b. It was observed that nanolayers with more PVA content resulted in a higher degree of PVA leaching. While this correlation was clear, the greater PVA content leads to greater variability in the amount of PVA that leached. This is attributed to the high number of possible interactions between polymers and CNTs within the CNT-PVA-GA network.

It is known that extending the concentration polarization layer decreases the pressure on the membrane surface. We hypothesized that a thicker nanolayer would attenuate the local pressure build-up across the surface, based on our evidence that concentration polarization leads to nanolayer instability. To support this hypothesis, we synthesized CNT layers with increasing CNT mass loadings. Greater CNT mass loadings create thicker nanolayers in ECMs with identical chemical compositions as demonstrated

in our previous work [29]. Figure 5.7a shows that membranes with thicker CNT networks experience less PVA leaching.

Results in Figure 5.7a suggest that a thicker nanolayer may be able to extend the concentration polarization layer. A mechanistic diagram is presented in Figure 5.7b. During PEO filtration, PEO particles interact with the CNT structure. The impact of CNTs on physically limiting PVA leaching is presented in Figure 5.S12. It was observed that the presence of 1 mg CNT in the nanolayer can decrease PVA leaching from UF PES membranes by 86% on average. A thick nanolayer (~2 μm) moves the separation interface a few micrometers (1-2 μm) away from the surface. In this way, foulant particles become entangled within the nanolayer rather than forming a dense concentration polarization layer at the membrane surface [67]. The same explanation was used in other studies where membranes modified with a CNT layer were found more effective in controlling fouling [68–72].

These results show that CNT-based membranes synthesized with PVA are unstable at the early stages of a separation process under typical operating conditions. Such instabilities are likely to lead to changes in surface physicochemical properties such as surface conductivity and hydrophilicity. The impact of such leaching on surface properties is investigated in section 5.4.3 by measuring the surface properties of ECMs made with different mass ratios of PVA.

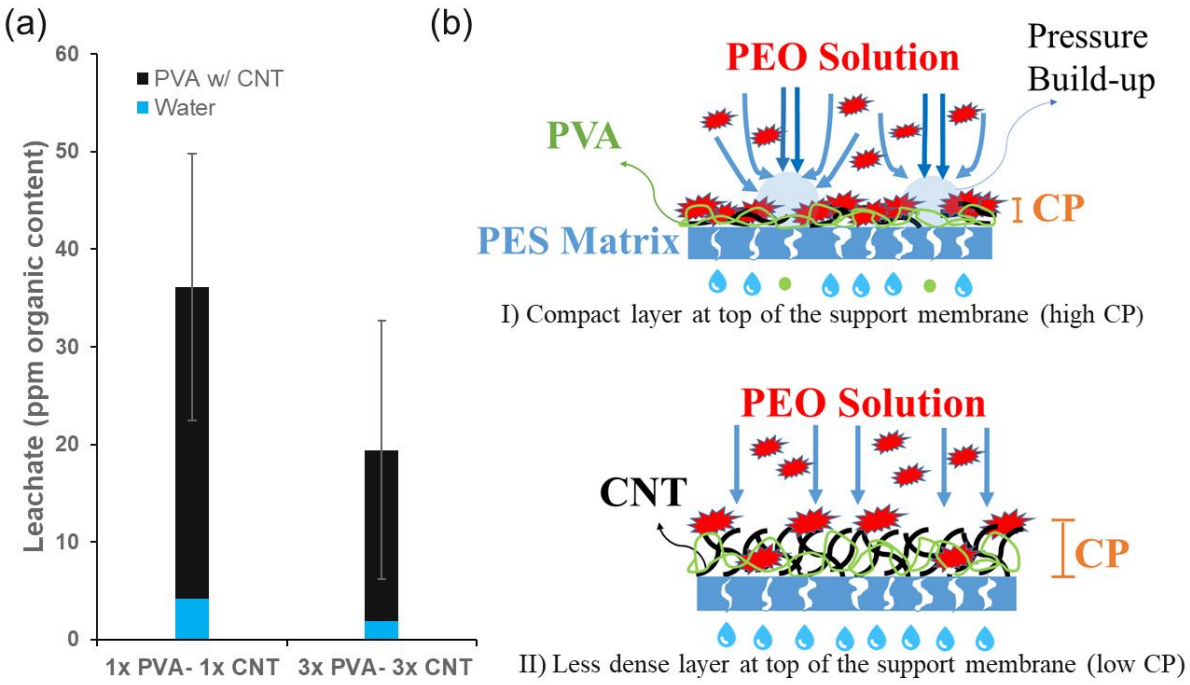

Figure 5.7. (a) The impact of CNT mass in the nanolayer on permeate carbon content. 1 mg or 3 mg CNT mass loadings were used in ECMs. PVA to CNT mass ratio was 10:1 in both cases. PEO (2 MDa) was used as the model foulant with a concentration of 250 ppm in water. Error bars represent standard deviation for three membranes. (b) Mechanistic diagram of the correlation between CNT thickness and concentration polarization. I) The thin nanolayer induces a more significant CP effect and subsequent local pressure increases, which causes PVA leaching. II) An increase in the nanolayer thickness reduces the effect of CP on surface pressure, which leads to less PVA leaching.

Mechanical stability

Mechanical stability is a concern for membranes modified with nanoparticles such as CNTs [68,73]. Membrane surfaces can be mechanically impacted during separation and cleaning. For example, long-term exposure of the membrane to lateral flow containing solid foulants may damage the surface via abrasion. Periodic backwashing may also cause mechanically unstable CNTs to detach from the ECM surface. Mechanical cleaning of membranes by adding scouring agents (granulate media particles) into the feed, may damage the membrane surface, compromise separation quality, and reduce the operational lifetime of the membrane [38,74–76]. It is therefore important to investigate the overall membrane mechanical stability of electrically conductive coatings.

ECM surface stability was evaluated using micro-scratch testing. The results of micro scratch tests on control CNT, CNT/PVA/SA, and CNT/PVA/GA networks are shown in Figure 5.8. ECMs showed a higher mechanical strength compared to pristine PES membranes. These results are consistent with those reported in the literature [27,31]. Scratch tests caused surface ruptures on pristine PES membranes which led to mechanical failure (Figure 5.S13 and Figure 5.S14). As presented in Figure 5.8, the most mechanically stable surfaces were CNT/PVA/GA, CNT/PVA/SA, and control CNT with an average final depth of penetration of 9.6 ± 1.17, 23.8 ± 0.23, and 28.6 ± 0.47 µm, respectively. We speculated that GA forms a rigid thin layer on top of the CNT nanolayer upon curing. The thin layer enhances the mechanical stability of the membrane and prevents surface rupture against applied forces.

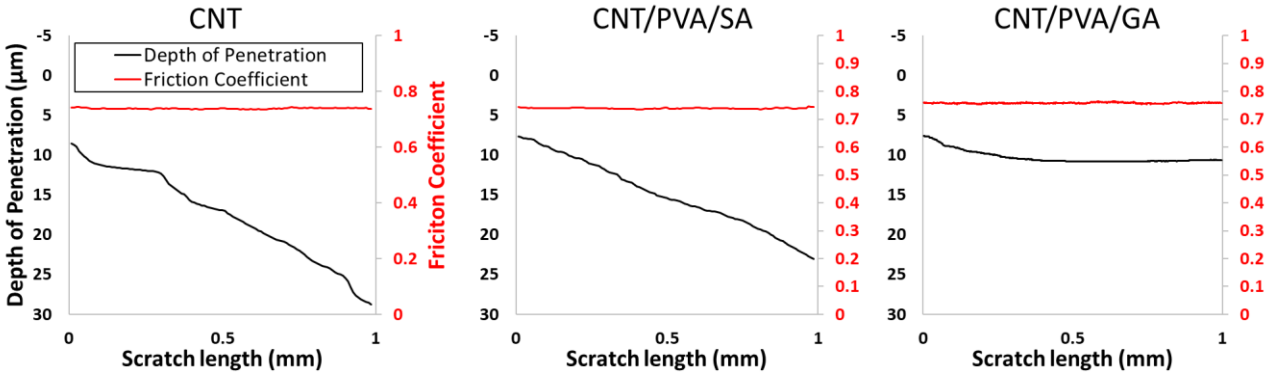

Figure 5.8. The Mechanical stability of ECMs containing different polymer binders, polyvinyl alcohol (PVA), succinic acid (SA), and glutaraldehyde (GA) measured in the micro-scratch tester. Nanolayer consists of (a) CNT, (b) CNT/PVA/SA, and (c) CNT/PVA/GA. The tip applied a normal force of 0.5 N with a scratch length of 5 mm and a scratch speed of 5 mm/min. All ECMs contained 1 mg CNT in the nanolayer. PVA to CNT mass ratio was kept at 10:1.

5.4.3. Surface hydrophilicity and surface conductivity of ECMs

Polymers, such as polyvinyl alcohol (PVA) are often added to the conductive nanolayers of ECMs to increase their hydrophilicity as well as to increase their mechanical stability. Findings in section 5.4.2. *Physical stability* revealed surface instabilities in such networks caused by leaching of PVA. As such, in a real application, changes in the PVA

content in the nanolayer can be correlated to changes in surface hydrophilicity, electrical conductivity, and stability of the nanolayer.

Surface hydrophilicity was measured at different PVA loadings, to demonstrate how PVA leaching would impact ECM surface properties. Figure 5.9a presents contact angles, as a measurement of the surface hydrophilicity, of ECMs made with different PVA loadings. All membranes contained 1 mg CNT in the nanolayer, and the PVA mass ratio with respect to CNTs varied from 0 to 10. Measured contact angle was observed to decrease from 104° to 60° with increasing PVA relative to the mass of CNTs. Such changes may have a significant impact on membrane performance. PVA has many hydroxyl groups along its backbone which increase the hydrophilicity of the surface by providing a higher surface interfacial energy with water. Hydrophilicity increased further with incorporation of GA in the nanolayer. The low contact angle with the presence of GA can be ascribed to the hydrophilic aldehyde groups of GA. In real applications, the ECM surface may lose PVA due to surface instabilities (leaching, mechanical abrasion, etc.), leading to an increase in ECM hydrophobicity over time. Greater ECM stability is important for limiting changes to ECM properties.

Surface electrical conductivity is critical to ensure ECMs can carry an electric charge across their surface. The surface electrical conductivity directly impacts their antifouling properties, including the electrostatic interactions of the membrane with foulants and their ability to generate gas bubbles or radical species at a given applied potential. Figure 5.9b presents the membrane surface electrical conductance as a function of PVA mass ratio. Surface conductance decreased with increased PVA content. This was due to the electrically resistant nature of PVA which we hypothesize was uniformly distributed throughout the CNT network. Interestingly, coating ECMs with GA does not significantly impact the electrical conductivity of the nanolayer. We speculate that the GA forms a very thin surface layer and has minimal impact on the bulk CNT electrical conductance.

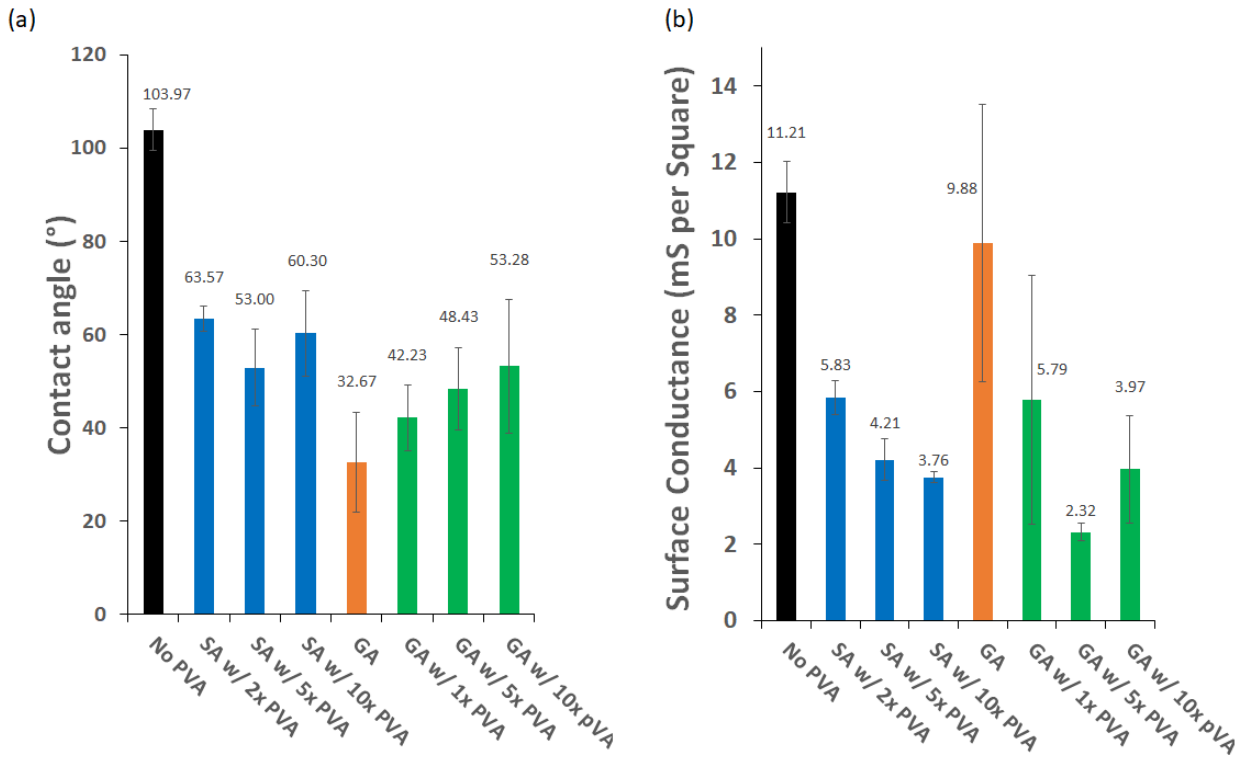

Figure 5.9. (a) Contact angle, and (b) Surface conductance of ECMs containing different polymer binders, polyvinyl alcohol (PVA), glutaraldehyde (GA), succinic acid (SA) and a blend of PVA and GA. All ECMs contained 1 mg CNT in the nanolayer. "xPVA" shows the mass ratio of PVA to CNT. The PVA: CNT mass ratio was changed from 0:1 to 10:1. Error bars represent the standard deviation of nine measurements (three samples each measured three times).

5.5.Conclusion

ECMs have shown promising antifouling potential that can be extended to a wide range of applications such as separation of bacteria, viruses, colloidal substances, and metals. The application of ECMs was investigated by filtration of a bacteria-enriched suspension cultivated from tap water. Cathodic ECMs had the highest performance with only 21% reduction in flux over 4 hours, demonstrating the antifouling abilities of these membranes. Stability of ECMs including their electrochemical, physical, and mechanical properties is essential for expanding their applications beyond lab-scale. ECMs were found to be cathodically stable, but anodically unstable under application of small voltages (2-4 V vs. Ag/AgCl reference electrode). The drop in their electrochemical conductance was

attributed to CNT oxidation under such potentials. CNT/PVA/GA networks were more resistant against anodic oxidation potentials likely because glutaraldehyde acted as a sacrificial polymer. ECMs made from CNT/PVA were found to be physically unstable during the filtration of PEO. The instabilities were attributed to local pressure build-up induced by concentration polarization, which lead to PVA leaching. PVA loss from ECMs during filtration lead to undesired changes in surface properties such as surface hydrophilicity and electrical conductivity. ECM mechanical stability of different networks containing CNTs alone, CNT/PVA/SA, or CNT/PVA/GA was comparable, however, the CNT/PVA/GA network was more stable likely due to the presence of a rigid GA layer at the surface. ECMs have become a highly researched topic recently due to their fouling mitigation potential, however, their surface instabilities necessitate the development of more stable membranes suitable for industrial adoption in real world applications.

5.6.References

[1] M.A. Halali, M. Larocque, C.F. de Lannoy, Investigating the stability of electrically conductive membranes, J. Memb. Sci. 627 (2021) 119181. https://doi.org/10.1016/j.memsci.2021.119181.

[2] H. Lin, W. Peng, M. Zhang, J. Chen, H. Hong, Y. Zhang, A review on anaerobic membrane bioreactors: Applications, membrane fouling and future perspectives, Desalination. 314 (2013) 169–188. https://doi.org/10.1016/j.desal.2013.01.019.

[3] A. Ruiz-García, N. Melián-Martel, I. Nuez, Short Review on Predicting Fouling in RO Desalination, Membranes (Basel). 7 (2017) 62. https://doi.org/10.3390/membranes7040062.

[4] W. Gao, H. Liang, J. Ma, M. Han, Z. lin Chen, Z. shuang Han, G. bai Li, Membrane fouling control in ultrafiltration technology for drinking water production: A review, Desalination. 272 (2011) 1–8. https://doi.org/10.1016/j.desal.2011.01.051.

[5] B.X. Thanh, N.P. Dan, N.T. Binh, Fouling mitigation in a submerged membrane bioreactor treating dyeing and textile wastewater, Desalin. Water Treat. 47 (2012) 150–156. https://doi.org/10.1080/19443994.2012.696799.

[6] E. Celik, H. Park, H. Choi, H. Choi, Carbon nanotube blended polyethersulfone membranes for fouling control in water treatment, Water Res. 45 (2011) 274–282. https://doi.org/10.1016/j.watres.2010.07.060.

[7] C. Thamaraiselvan, M. Noel, Membrane Processes for Dye Wastewater Treatment: Recent Progress in Fouling Control, Crit. Rev. Environ. Sci. Technol. 45 (2015) 1007–1040. https://doi.org/10.1080/10643389.2014.900242.

[8] J. Park, N. Yamashita, H. Tanaka, Membrane fouling control and enhanced removal of pharmaceuticals and personal care products by coagulation-MBR, Chemosphere. 197 (2018) 467–476. https://doi.org/10.1016/j.chemosphere.2018.01.063.

[9] F. Ahmed, B.S. Lalia, V. Kochkodan, R. Hashaikeh, Electrically conductive polymeric membranes

for fouling prevention and detection: A review, Desalination. 391 (2016) 1–15. https://doi.org/10.1016/J.DESAL.2016.01.030.

[10] A. Ronen, S.L. Walker, D. Jassby, Electroconductive and electroresponsive membranes for water treatment, Rev. Chem. Eng. 32 (2016) 533–550. https://doi.org/10.1515/revce-2015-0060.

[11] P. Formoso, E. Pantuso, G. De Filpo, F. Nicoletta, Electro-Conductive Membranes for Permeation Enhancement and Fouling Mitigation: A Short Review, Membranes (Basel). 7 (2017) 39. https://doi.org/10.3390/membranes7030039.

[12] I.-H. Loh, R.A. Moody, J.C. Huang, Electrically conductive membranes: Synthesis and applications, J. Memb. Sci. 50 (1990) 31–49. https://doi.org/10.1016/S0376-7388(00)80884-4.

[13] W. Hu, S. Chen, Z. Yang, L. Liu, H. Wang, Flexible electrically conductive nanocomposite membrane based on bacterial cellulose and polyaniline, J. Phys. Chem. B. 115 (2011) 8453–8457. https://doi.org/10.1021/jp204422v.

[14] F. Ahmed, B.S. Lalia, V. Kochkodan, N. Hilal, R. Hashaikeh, Electrically conductive polymeric membranes for fouling prevention and detection: A review, Desalination. 391 (2016) 1–15. https://doi.org/10.1016/j.desal.2016.01.030.

[15] W. Fu, X. Wang, J. Zheng, M. Liu, Z. Wang, Antifouling performance and mechanisms in an electrochemical ceramic membrane reactor for wastewater treatment, (2018). https://doi.org/10.1016/j.memsci.2018.10.077.

[16] P. Geng, G. Chen, Magnéli Ti4O7 modified ceramic membrane for electrically-assisted filtration with antifouling property, J. Memb. Sci. 498 (2016) 302–314. https://doi.org/10.1016/j.memsci.2015.07.055.

[17] B. Khorshidi, J. Hajinasiri, G. Ma, S. Bhattacharjee, M. Sadrzadeh, Thermally resistant and electrically conductive PES/ITO nanocomposite membrane, J. Memb. Sci. 500 (2016) 151–160. https://doi.org/10.1016/j.memsci.2015.11.015.

[18] M.T. Alresheedi, B. Barbeau, O.D. Basu, Comparisons of NOM fouling and cleaning of ceramic and polymeric membranes during water treatment, Sep. Purif. Technol. 209 (2019) 452–460. https://doi.org/10.1016/j.seppur.2018.07.070.

[19] C. de Lannoy, D. Jassby, D.D. Davis, M.R. Wiesner, A highly electrically conductive polymer–multiwalled carbon nanotube nanocomposite membrane, J. Memb. Sci. 415–416 (2012) 718–724. https://doi.org/10.1016/J.MEMSCI.2012.05.061.

[20] M.S.P. Shaffer, A.H. Windle, Fabrication and Characterization of Carbon Nanotube/Poly(vinyl alcohol) Composites, Adv. Mater. 11 (1999) 937–941. https://doi.org/10.1002/(SICI)1521-4095(199908)11:11<937::AID-ADMA937>3.0.CO;2-9.

[21] H. Chen, M.B. Müller, K.J. Gilmore, G.G. Wallace, D. Li, Mechanically Strong, Electrically Conductive, and Biocompatible Graphene Paper, Adv. Mater. 20 (2008) 3557–3561. https://doi.org/10.1002/adma.200800757.

[22] H. Kim, Y. Miura, C.W. Macosko, Graphene/Polyurethane Nanocomposites for Improved Gas Barrier and Electrical Conductivity, Chem. Mater. 22 (2010) 3441–3450. https://doi.org/10.1021/cm100477v.

[23] B.C.H. Steele, A. Heinzel, Materials for fuel-cell technologies, in: Mater. Sustain. Energy, Co-Published with Macmillan Publishers Ltd, UK, 2010: pp. 224–231. https://doi.org/10.1142/9789814317665_0031.

[24] X. Zhu, D. Jassby, Electroactive Membranes for Water Treatment: Enhanced Treatment Functionalities, Energy Considerations, and Future Challenges, Acc. Chem. Res. 52 (2019) 1177–1186. https://doi.org/10.1021/acs.accounts.8b00558.

[25] F. Pan, Y. Li, Y. Song, M. Wang, Y. Zhang, H. Yang, H. Wang, Z. Jiang, Graphene oxide membranes with fixed interlayer distance via dual crosslinkers for efficient liquid molecular separations, J. Memb. Sci. 595 (2020) 117486. https://doi.org/10.1016/j.memsci.2019.117486.

[26] G. Gao, Q. Zhang, C.D. Vecitis, CNT-PVDF composite flow-through electrode for single-pass sequential reduction-oxidation †, (2014). https://doi.org/10.1039/c3ta14080f.

[27] F.E. Ahmed, R. Hashaikeh, N. Hilal, Fouling control in reverse osmosis membranes through modification with conductive carbon nanostructures, Desalination. 470 (2019) 114118. https://doi.org/10.1016/j.desal.2019.114118.

[28] Y. Liu, Y. Su, J. Cao, J. Guan, R. Zhang, M. He, L. Fan, Q. Zhang, Z. Jiang, Antifouling, high-flux oil/water separation carbon nanotube membranes by polymer-mediated surface charging and hydrophilization, J. Memb. Sci. 542 (2017) 254–263. https://doi.org/10.1016/j.memsci.2017.08.018.

[29] M.A. Halali, C.-F. de Lannoy, The Effect of Cross-Linkers on the Permeability of Electrically Conductive Membranes, Ind. Eng. Chem. Res. 58 (2019) 3832–3844. https://doi.org/10.1021/acs.iecr.8b05691.

[30] A. Shameli, E. Ameri, Synthesis of cross-linked PVA membranes embedded with multi-wall carbon nanotubes and their application to esterification of acetic acid with methanol, Chem. Eng. J. 309 (2017) 381–396. https://doi.org/10.1016/J.CEJ.2016.10.039.

[31] H. Bang, M. Gopiraman, B. Kim, S. Kim, I. Kim, Colloids and Surfaces A : Physicochemical and Engineering Aspects Effects of pH on electrospun PVA / acid-treated MWNT composite nanofibers, Colloids Surfaces A Physicochem. Eng. Asp. 409 (2012) 112–117. https://doi.org/10.1016/j.colsurfa.2012.05.046.

[32] W. Duan, G. Chen, C. Chen, R. Sanghvi, A. Iddya, S. Walker, H. Liu, A. Ronen, D. Jassby, Electrochemical removal of hexavalent chromium using electrically conducting carbon nanotube/polymer composite ultrafiltration membranes, J. Memb. Sci. 531 (2017) 160–171. https://doi.org/10.1016/J.MEMSCI.2017.02.050.

[33] A. V Dudchenko, J. Rolf, K. Russell, W. Duan, D. Jassby, Organic fouling inhibition on electrically conducting carbon nanotube – polyvinyl alcohol composite ultra fi ltration membranes, J. Memb. Sci. 468 (2014) 1–10. https://doi.org/10.1016/j.memsci.2014.05.041.

[34] W. Duan, A. Ronen, J.V. de Leon, A. Dudchenko, S. Yao, J. Corbala-Delgado, A. Yan, M. Matsumoto, D. Jassby, Treating anaerobic sequencing batch reactor effluent with electrically conducting ultrafiltration and nanofiltration membranes for fouling control, J. Memb. Sci. 504 (2016) 104–112. https://doi.org/10.1016/J.MEMSCI.2016.01.011.

[35] A. Ronen, W. Duan, I. Wheeldon, S. Walker, D. Jassby, Microbial Attachment Inhibition through Low-Voltage Electrochemical Reactions on Electrically Conducting Membranes, (2015). https://doi.org/10.1021/acs.est.5b01281.

[36] L. Tang, A. Iddya, X. Zhu, A. V Dudchenko, W. Duan, C. Turchi, J. Vanneste, T.Y. Cath, D. Jassby, Enhanced Flux and Electrochemical Cleaning of Silicate Scaling on Carbon Nanotube-Coated Membrane Distillation Membranes Treating Geothermal Brines, (2017). https://doi.org/10.1021/acsami.7b12615.

[37] A.L. McGaughey, R.D. Gustafson, A.E. Childress, Effect of long-term operation on membrane surface characteristics and performance in membrane distillation, J. Memb. Sci. 543 (2017) 143–150.

https://doi.org/10.1016/j.memsci.2017.08.040.

[38] B. Siembida, P. Cornel, S. Krause, B. Zimmermann, Effect of mechanical cleaning with granular material on the permeability of submerged membranes in the MBR process, Water Res. 44 (2010) 4037–4046. https://doi.org/10.1016/j.watres.2010.05.016.

[39] J. Mansouri, S. Harrisson, V. Chen, Strategies for controlling biofouling in membrane filtration systems: Challenges and opportunities, J. Mater. Chem. 20 (2010) 4567–4586. https://doi.org/10.1039/b926440j.

[40] W. Duan, A. Ronen, S. Walker, D. Jassby, Polyaniline-Coated Carbon Nanotube Ultrafiltration Membranes: Enhanced Anodic Stability for In Situ Cleaning and Electro-Oxidation Processes, (2016). https://doi.org/10.1021/acsami.6b07196.

[41] C.D. Vecitis, M.H. Schnoor, M. Saifur Rahaman, J.D. Schiffman, M. Elimelech, Electrochemical Multiwalled Carbon Nanotube Filter for Viral and Bacterial Removal and Inactivation, Environ. Sci. Technol. 45 (2011) 3672–3679. https://doi.org/10.1021/es2000062.

[42] M. Tominaga, Y. Yatsugi, N. Watanabe, Oxidative corrosion potential vs. pH diagram for single-walled carbon nanotubes, RSC Adv. 4 (2014) 27224–27227. https://doi.org/10.1039/c4ra02875a.

[43] S. Ohmori, T. Saito, Electrochemical durability of single-wall carbon nanotube electrode against anodic oxidation in water, Carbon N. Y. 50 (2012) 4932–4938. https://doi.org/10.1016/j.carbon.2012.06.023.

[44] Y. Wen, J. Yuan, X. Ma, S. Wang, Y. Liu, Polymeric nanocomposite membranes for water treatment: a review, 17 (2019) 1539–1551. https://doi.org/10.1007/s10311-019-00895-9.

[45] M. Osborne, A. Aryasomayajula, A. Shakeri, P.R. Selvaganapathy, T.F. Didar, Suppression of Biofouling on a Permeable Membrane for Dissolved Oxygen Sensing Using a Lubricant-Infused Coating, ACS Sensors. 4 (2019) 687–693. https://doi.org/10.1021/acssensors.8b01541.

[46] B.S. Lalia, F.E. Ahmed, T. Shah, N. Hilal, R. Hashaikeh, Electrically conductive membranes based on carbon nanostructures for self-cleaning of biofouling, Desalination. 360 (2015) 8–12. https://doi.org/10.1016/J.DESAL.2015.01.006.

[47] M.S. Rahaman, C.D. Vecitis, M. Elimelech, Electrochemical carbon-nanotube filter performance toward virus removal and inactivation in the presence of natural organic matter, Environ. Sci. Technol. 46 (2012) 1556–1564. https://doi.org/10.1021/es203607d.

[48] S.M. Dizaj, A. Mennati, S. Jafari, K. Khezri, K. Adibkia, Antimicrobial activity of carbon-based nanoparticles, Adv. Pharm. Bull. 5 (2015) 19–23. https://doi.org/10.5681/apb.2015.003.

[49] J. Venkatesan, R. Jayakumar, A. Mohandas, I. Bhatnagar, S.-K. Kim, Antimicrobial Activity of Chitosan-Carbon Nanotube Hydrogels, Materials (Basel). 7 (2014) 3946–3955. https://doi.org/10.3390/ma7053946.

[50] H. Liu, A. Vajpayee, C.D. Vecitis, Bismuth-Doped Tin Oxide-Coated Carbon Nanotube Network: Improved Anode Stability and Efficiency for Flow-Through Organic Electrooxidation, (2013). https://doi.org/10.1021/am402621v.

[51] S.G. Bratsch, Standard Electrode Potentials and Temperature Coefficients in Water at 298.15 K, J. Phys. Chem. Ref. Data. 18 (1989) 1807. https://doi.org/10.1063/1.555839.

[52] P. Wardman, Reduction Potentials of One-Electron Couples Involving Free Radicals in Aqueous Solution, J. Phys. Chem. Ref. Data. 18 (1989) 1637. https://doi.org/10.1063/1.555843.

[53] Y. Baek, H. Yoon, S. Shim, J. Choi, J. Yoon, Electroconductive Feed Spacer as a Tool for Biofouling

Control in a Membrane System for Water Treatment, Environ. Sci. Technol. Lett. 1 (2014) 179–184. https://doi.org/10.1021/ez400206d.

[54] O. Istanbullu, J. Babauta, H. Duc Nguyen, H. Beyenal, Electrochemical biofilm control: mechanism of action, Biofouling. 28 (2012) 769–778. https://doi.org/10.1080/08927014.2012.707651.

[55] A. Ronen, W. Duan, I. Wheeldon, S. Walker, D. Jassby, Microbial Attachment Inhibition through Low-Voltage Electrochemical Reactions on Electrically Conducting Membranes, Environ. Sci. Technol. 49 (2015) 12741–12750. https://doi.org/10.1021/acs.est.5b01281.

[56] Y. Liu, ab Juen Hon Dustin Lee, Q. Xia, Y. Ma, Y. Yu, L. Yue Lanry Yung, J. Xie, C. Nam Ong, C.D. Vecitis, Z. Zhou, A graphene-based electrochemical filter for water purification †, (2014). https://doi.org/10.1039/c4ta04006f.

[57] S. Pandit, S. Shanbhag, M. Mauter, Y. Oren, M. Herzberg, Influence of Electric Fields on Biofouling of Carbonaceous Electrodes, (2017). https://doi.org/10.1021/acs.est.6b06339.

[58] S.H. Hong, J. Jeong, S. Shim, H. Kang, S. Kwon, K.H. Ahn, J. Yoon, Effect of electric currents on bacterial detachment and inactivation, Biotechnol. Bioeng. 100 (2008) 379–386. https://doi.org/10.1002/bit.21760.

[59] M.S. Rahaman, C.D. Vecitis, M. Elimelech, Electrochemical carbon-nanotube filter performance toward virus removal and inactivation in the presence of natural organic matter, Environ. Sci. Technol. 46 (2012) 1556–1564. https://doi.org/10.1021/es203607d.

[60] C.D. Vecitis, M.H. Schnoor, M.S. Rahaman, J.D. Schiffman, M. Elimelech, Electrochemical multiwalled carbon nanotube filter for viral and bacterial removal and inactivation, Environ. Sci. Technol. 45 (2011) 3672–3679. https://doi.org/10.1021/es2000062.

[61] G. Wu, L. Li, J.H. Li, B.Q. Xu, Methanol electrooxidation on Pt particles dispersed into PANI/SWNT composite films, J. Power Sources. 155 (2006) 118–127. https://doi.org/10.1016/j.jpowsour.2005.04.035.

[62] C.D. Vecitis, G. Gao, H. Liu, Electrochemical Carbon Nanotube Filter for Adsorption, Desorption, and Oxidation of Aqueous Dyes and Anions, J. Phys. Chem. C. 115 (2011) 3621–3629. https://doi.org/10.1021/jp111844j.

[63] H. Liu, C.D. Vecitis, Reactive transport mechanism for organic oxidation during electrochemical filtration: Mass-transfer, physical adsorption, and electron-transfer, J. Phys. Chem. C. 116 (2012) 374–383. https://doi.org/10.1021/jp209390b.

[64] D. Wei, Y. Liu, L. Cao, H. Zhang, L. Huang, G. Yu, H. Kajiura, Y. Li, Selective Electrochemical Etching of Single-Walled Carbon Nanotubes, Adv. Funct. Mater. 19 (2009) 3618–3624. https://doi.org/10.1002/adfm.200900924.

[65] X. Lu, C. Zhao, Highly efficient and robust oxygen evolution catalysts achieved by anchoring nanocrystalline cobalt oxides onto mildly oxidized multiwalled carbon nanotubes, J. Mater. Chem. A. 1 (2013) 12053–12059. https://doi.org/10.1039/c3ta12912h.

[66] H.S. Mansur, C.M. Sadahira, A.N. Souza, A.A.P. Mansur, FTIR spectroscopy characterization of poly (vinyl alcohol) hydrogel with different hydrolysis degree and chemically crosslinked with glutaraldehyde, Mater. Sci. Eng. C. 28 (2008) 539–548. https://doi.org/10.1016/j.msec.2007.10.088.

[67] Y. Zhang, Y. Chen, L. Hou, F. Guo, J. Liu, S. Qiu, Y. Xu, ¨ U Wang, Y. Zhao, Pine-branch-like TiO 2 nanofibrous membrane for high efficiency strong corrosive emulsion separation †, (2017). https://doi.org/10.1039/c7ta00833c.

[68] G.S. Ajmani, D. Goodwin, K. Marsh, D.H. Fairbrother, K.J. Schwab, J.G. Jacangelo, H. Huang, Modification of low pressure membranes with carbon nanotube layers for fouling control, Water Res. 46 (2012) 5645–5654. https://doi.org/10.1016/j.watres.2012.07.059.

[69] J. Guo, J.-H. Liu, L.-Y. Wang, H. Liu, Modification of ultrafiltration membranes with carbon nanotube buckypaper for fouling alleviation, n.d.

[70] L. Bai, H. Liang, J. Crittenden, F. Qu, A. Ding, J. Ma, X. Du, S. Guo, G. Li, Surface modification of UF membranes with functionalized MWCNTs to control membrane fouling by NOM fractions, J. Memb. Sci. 492 (2015) 400–411. https://doi.org/10.1016/j.memsci.2015.06.006.

[71] A. Khalid, A.A. Al-juhani, O.C. Al-hamouz, T. Laoui, Z. Khan, M. Ali, Preparation and properties of nanocomposite polysulfone / multi-walled carbon nanotubes membranes for desalination, DES. 367 (2015) 134–144. https://doi.org/10.1016/j.desal.2015.04.001.

[72] J. Shi, T. Wu, K. Teng, W. Wang, M. Shan, Z. Xu, H. Lv, H. Deng, Simultaneous electrospinning and spraying toward branch-like nanofibrous membranes functionalised with carboxylated MWCNTs for dye removal, Mater. Lett. 166 (2016) 26–29. https://doi.org/10.1016/j.matlet.2015.12.024.

[73] J. Kim, B. Van Der Bruggen, The use of nanoparticles in polymeric and ceramic membrane structures: Review of manufacturing procedures and performance improvement for water treatment, Environ. Pollut. 158 (2010) 2335–2349. https://doi.org/10.1016/j.envpol.2010.03.024.

[74] M. Aslam, A. Charfi, G. Lesage, M. Heran, J. Kim, Membrane bioreactors for wastewater treatment: A review of mechanical cleaning by scouring agents to control membrane fouling, Chem. Eng. J. 307 (2017) 897–913. https://doi.org/10.1016/j.cej.2016.08.144.

[75] D. Kwon, H. Chang, H. Seo, J. Kim, Fouling behavior and system performance in membrane bioreactor introduced by granular media as a mechanical cleaning effect on membranes, Desalin. Water Treat. 57 (2016) 9018–9026. https://doi.org/10.1080/19443994.2015.1049404.

[76] B. Siembida-Lösch, Physical Cleaning, in: Encycl. Membr., Springer Berlin Heidelberg, Berlin, Heidelberg, 2015: pp. 1–4. https://doi.org/10.1007/978-3-642-40872-4_1976-1.

[77] H. Liu, A. Vajpayee, C.D. Vecitis, Bismuth-doped tin oxide-coated carbon nanotube network: Improved anode stability and efficiency for flow-through organic electrooxidation, ACS Appl. Mater. Interfaces. 5 (2013) 10054–10066. https://doi.org/10.1021/am402621v.

5.7.Supplementary Information

Materials and Method

SEM and crystal violet staining

Biofouled membranes were fixed with GA and thoroughly dried prior to the SEM imaging. GA fixation was conducted by staining membranes with 4% v/v GA in DI water. Stained membranes were kept in the fridge for 1 h followed by dehydration at three stages (3 min each) using 50, 80, 96 % ethanol, respectively. Membranes were air-dried overnight before imaging. Biofouled membranes were rinsed with DI water prior to being stained by crystal violet (0.05 w/v%) at room temperature for 20 min. After staining, membranes were rinsed with DI water, air-dried overnight and stained with acetic acid (30%) for 20 min to extract the unabsorbed crystal violet. The exchanged solution on membranes was collected and the absorbance value was recorded at 590 nm. Prior to acetic acid wash, surface pictures of the membranes were also captured under ambient and ultraviolet (UV) light (365 nm wavelength, UV flood curing system, Cure Zone 2, Con-Trol-Cure Inc.).

Cross-flow system design

The infeed chamber will be 17 mm square. The counter electrode (graphite) was cut and glued to the base of the chamber and a wire attached in the center using conductive epoxy. Fittings for the inlet and outlet tubes will be 1/8 npt. The design “sandwiches” the membrane with two square O-rings with an OD of 24 mm. Two stainless steel rods are placed inside the flow cell to touch the surface of the membrane between two O-rings. Three threaded studs with wing nuts will be used to clamp the cell. A square grid pattern made of stainless steel at the base of the cell bottom supports the membrane. The Auto-CAD drawings as well as the flow cell are presented in Figure 5.S1.

(a)

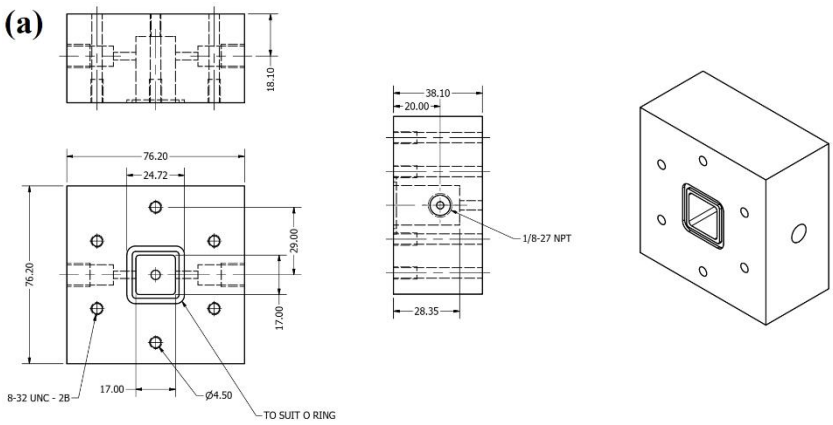

Top Cell

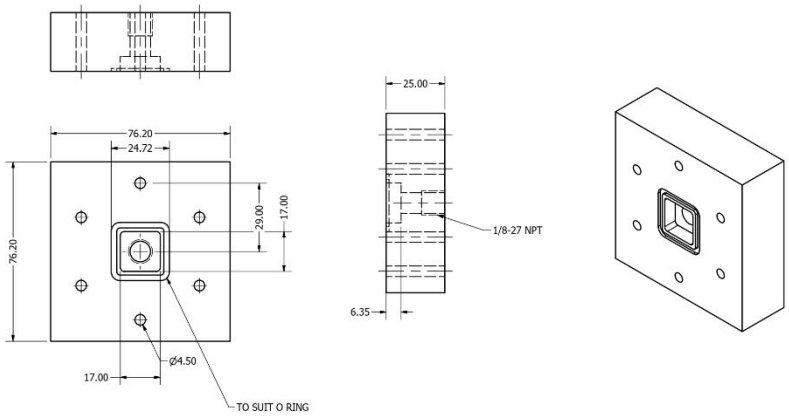

Bottom Cell

(b)

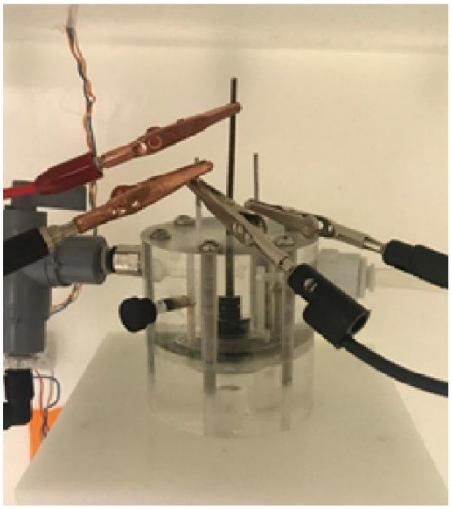

Figure 5.S1. (a) Auto-CAD drawings of the cross-flow system, (b) Custom-made cross-flow cell for biofouling experiments.

Flow regime in the flow-through cell

Reynolds number (N_{Re}) was calculated using the formulation below:

$$N_{Re} = \frac{\rho v H}{\mu} = \frac{4\rho Q}{\pi \mu H}$$

where ρ is the density of the feed, μ is the dynamic viscosity, H is the height of the crossflow channel, and Q is the flow rate.

A sample calculation is provided to determine the Reynolds number in the flow-cell.

$$N_{Re} = \frac{1\left(^{gr}/_{cm^3}\right)\times 11.7(^{cm}/_{s})\times 0.5(cm)}{0.01(^{cm^2}/_{s})} = 585$$

Shear rate (γ) can be calculated using equation below:

$$\gamma = \frac{3Q}{2W(\frac{H}{2})^2}$$

where is the thickness of the flow channel (2 cm), and the shear rate was calculated to be 140.4 1/s.

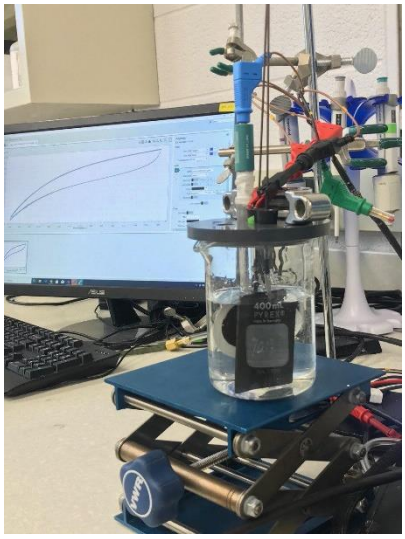

Figure 5.S2. Electrochemical Cell. ECM, Ag/AgCl electrode, and graphite were used as anode, reference electrode, and cathode, respectively. The electrolyte used was 10 mM PBS.

Anti-biofouling performance of ECMs

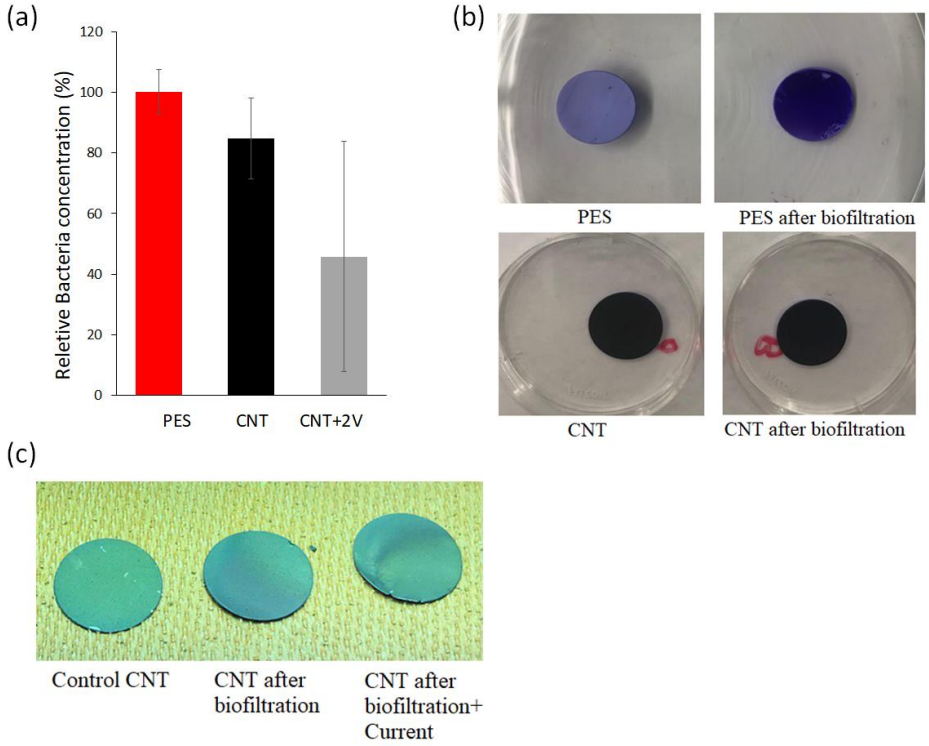

Figure 5.S3. Crystal violet-stained membranes after filter bacteria for 4 h. (a) Relative bacteria concentrations on the surface of membranes as measured by crystal violet staining

Red: control PES membrane with no applied potential, Black: Control CNT membrane (1 mg CNT mass loading) with no applied potential, Gray: CNT membrane (1 mg CNT) used as a cathode with 2V applied potential. Error bars represent the standard deviation for two membranes. Images under (b) ambient light, and (c) UV light at a wavelength of 365 nm.

Electrochemical Stability

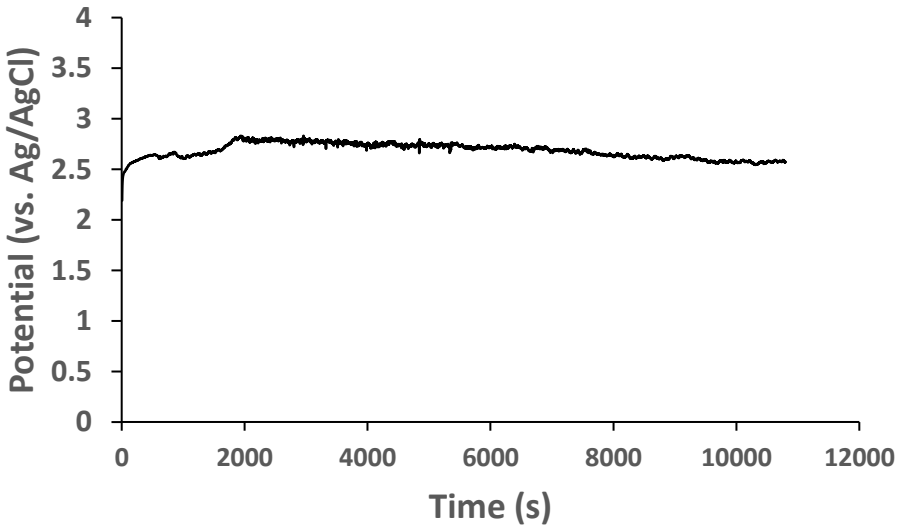

Figure 5.S4. Potential of the cathode in response to a 150 mA current (vs. Ag/AgCl reference electrode) applied to the electrode composed of CNT/PVA/SA for 3 hr.

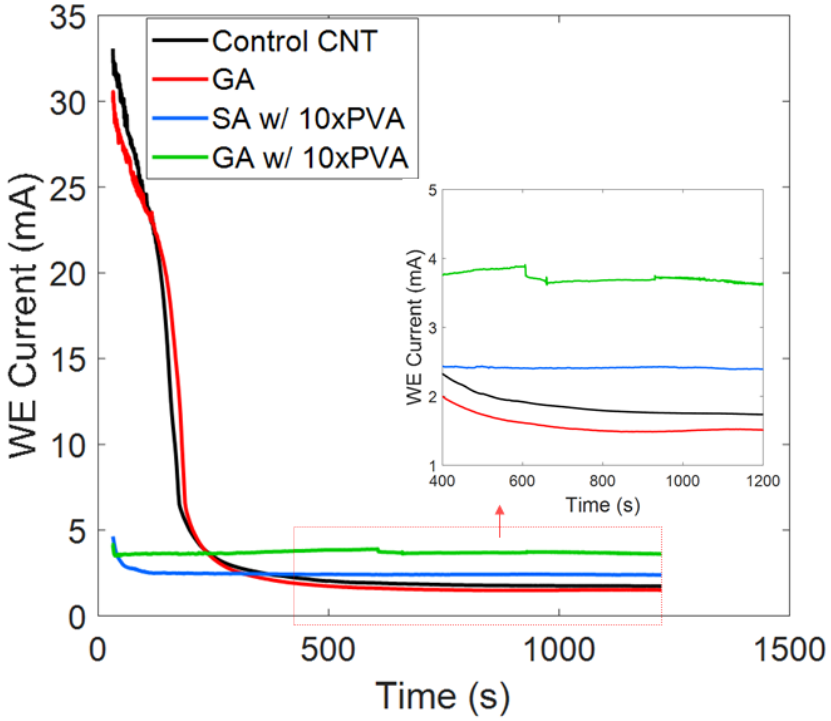
Control CNT
GA
SA w/ 10xPVA
GA w/ 10xPVA
WE Current (mA)
Time (s)
0
5
10
15
20
25
30
35
0
500
1000
1500
WE Current (mA)
Time (s)
1
2
3
4
5
400
600
800
1000
1200

(a)

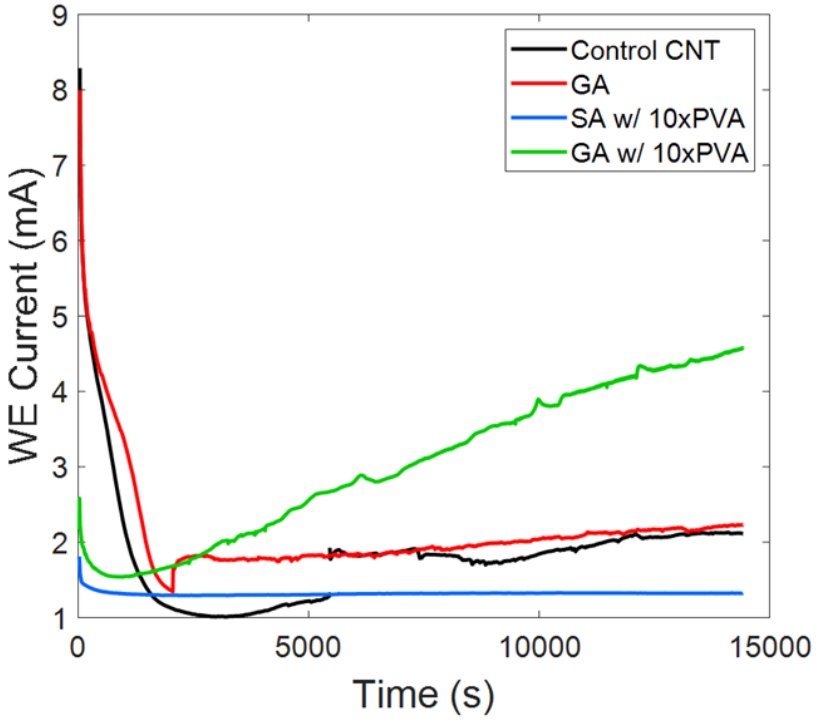
Control CNT
GA
SA w/ 10xPVA
GA w/ 10xPVA
WE Current (mA)
Time (s)
1
2
3
4
5
6
7
8
9
0
5000
10000
15000

(b)

Figure 5.S5. Electrochemical batch test for ECMs containing glutaraldehyde (GA), and a blend of polyvinyl alcohol (PVA) and either GA or succinic acid (SA). The ECM, graphite sheet, and an Ag/AgCl electrode were used as the working electrode (anode), counter electrode, and reference electrode, respectively. Fixed potential chronoamperometry was applied to the conductive membrane (a) with a total cell potential of 4 V (vs. Ag/AgCl reference electrode) for 20 min. (b) with a total cell potential of 2 V (vs. Ag/AgCl reference electrode) for 240 min. All ECMs contained 1 mg CNT. "xPVA" shows the mass ratio of PVA to CNT. [PBS]= 137 mM sodium chloride, 2.7 mM potassium chloride, and 10 mM phosphate buffer.

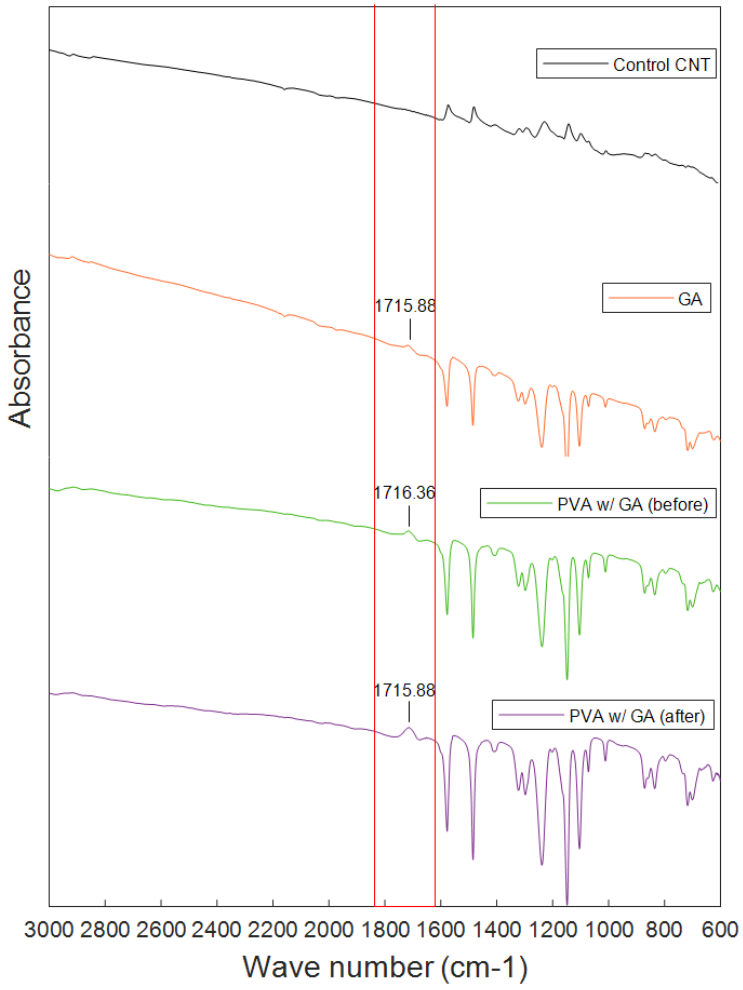

Figure 5.S6. Fourier-transform infrared (FTIR) spectroscopy reflecting the presence of carbonyl bonds.

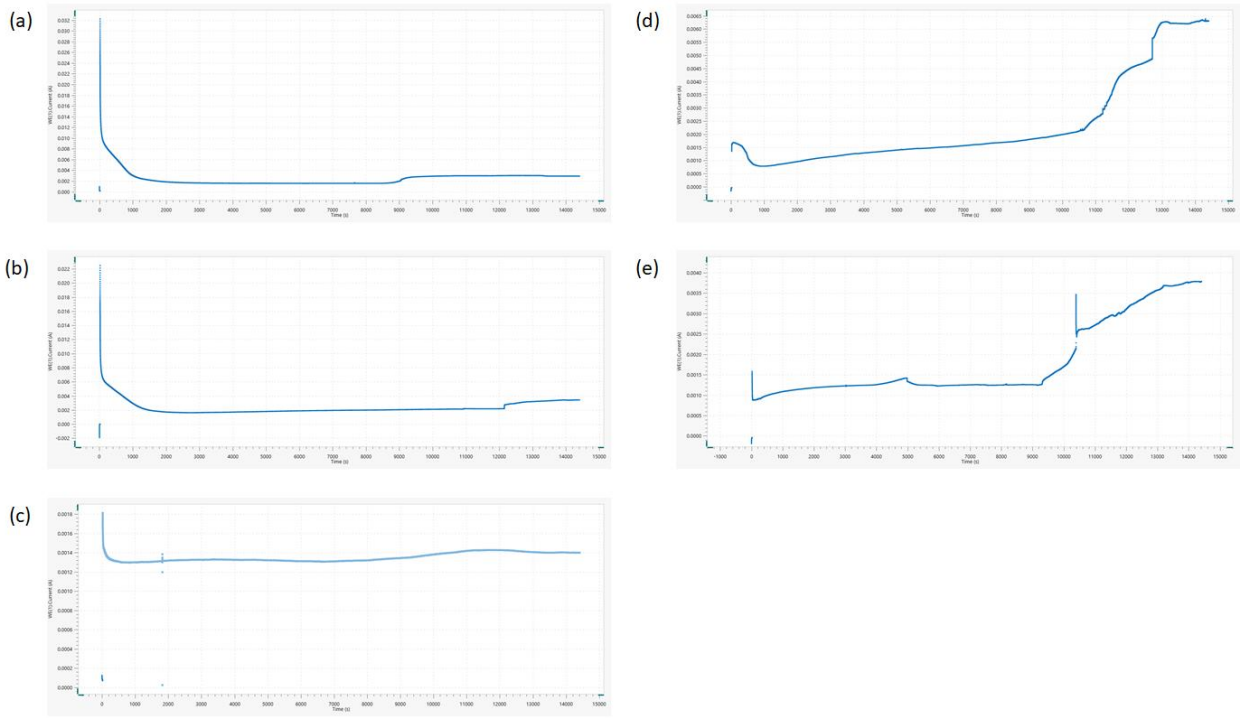

Figure 5.S7. Fixed potential chronoamperometry for membranes with different chemistries. Trials were conducted for each network as follows: (a) Control CNT, (b) CNT/GA, (c) CNT /10x PVA /SA (1:10), (d)-(e) CNT/PVA/GA. ECM, graphite sheet, and an Ag/AgCl electrode were used as the working electrode (anode), counter electrode, and reference electrode, respectively. The total cell potential was 2 V. All ECMs contain 1 mg CNT.

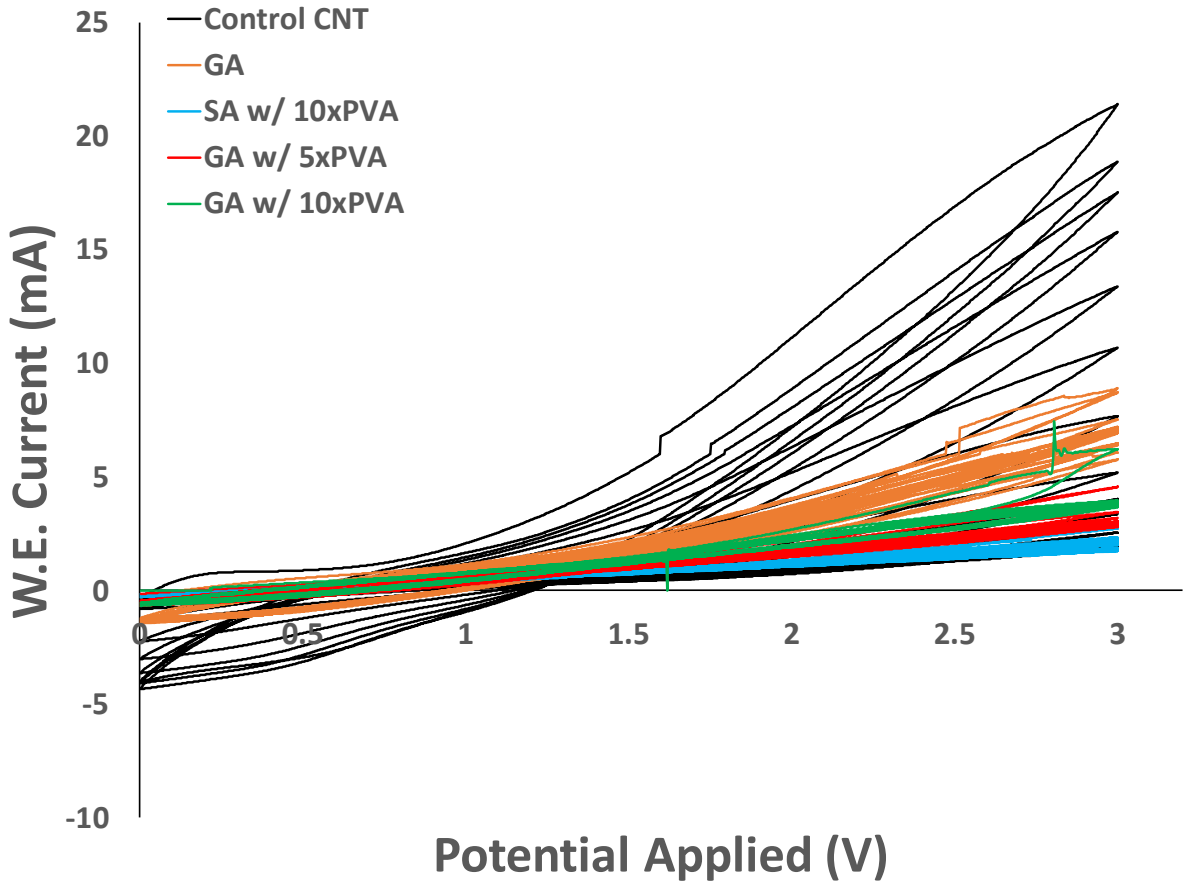

Figure 5.S8. Cyclic voltammetry for conductive membranes with different chemistries. ECMs contain 1 mg CNT mass loading. The conductive ECM, graphite sheet, and an Ag/AgCl electrode were used as the working electrode (anode), counter electrode, and reference electrode, respectively. The scan range was 0-3 V at a scan rate of 0.1 mVs^{-1}.

The mechanical breakdown of CNT-CNT networks reduces the network electrical conductivity by limiting the electrical percolation [77]. CNT leaching into the solution as a result of mechanical breakdown can be quantified by monitoring the carbon content in the solution. Therefore, mechanical breakdown of conductive networks was determined by measuring the amount of carbon in the electrolyte after the more sever anodic oxidation (4 V) using total organic carbon (TOC) analysis (Figure 5.S9). Mechanical breakdown of ECMs was found to be insignificant and occur equally for all surface chemistries.

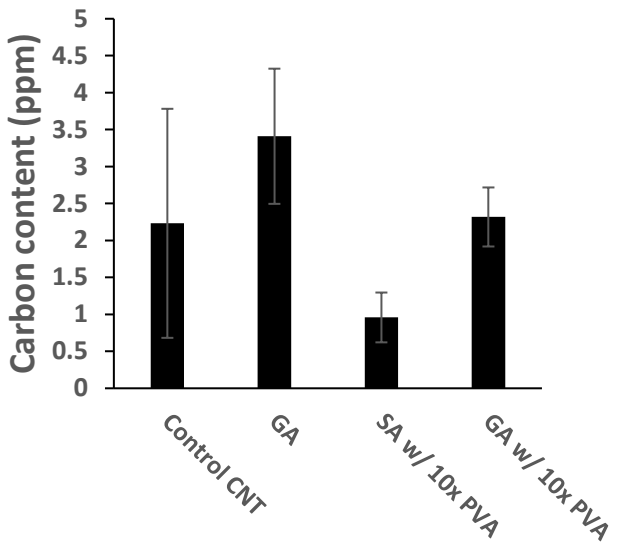

Figure 5.S9. Measurements of carbon content in the 200 mL electrochemical cell electrolyte after a constant linear potential of 4V (vs. Ag/AgCl electrode) was applied to ECMs containing different polymer binders, polyvinyl alcohol (PVA), glutaraldehyde (GA), and succinic acid (SA) for 20 min. The ECM, graphite sheet, and an Ag/AgCl electrode were used as the working electrode (anode), counter electrode, and reference electrode, respectively.

Physical Stability

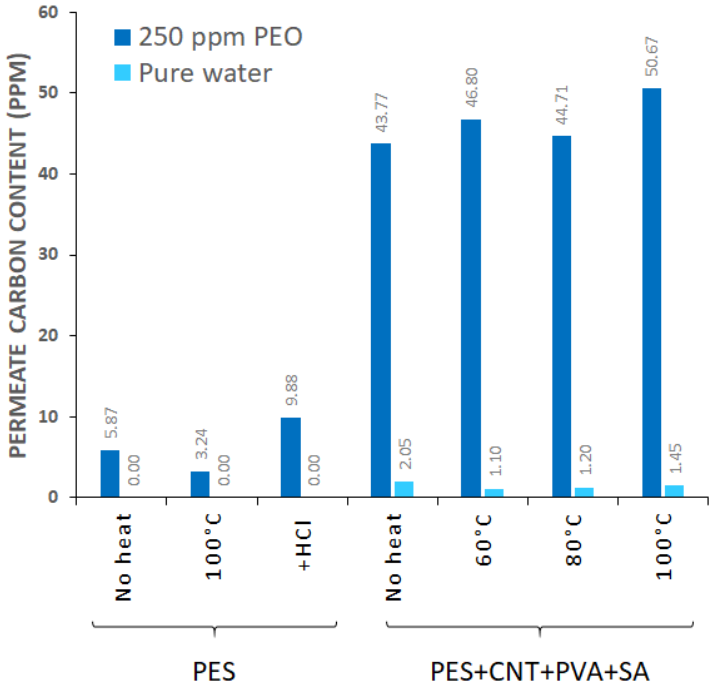

Figure 5.S10. The carbon content for the collected permeate in the PEO separation tests, measured by a TOC analyzer. PEO (2 MDa) was used as the model foulant at a feed concentration of 250 ppm in water. ECMs contained 1 mg CNT in the nanolayer.

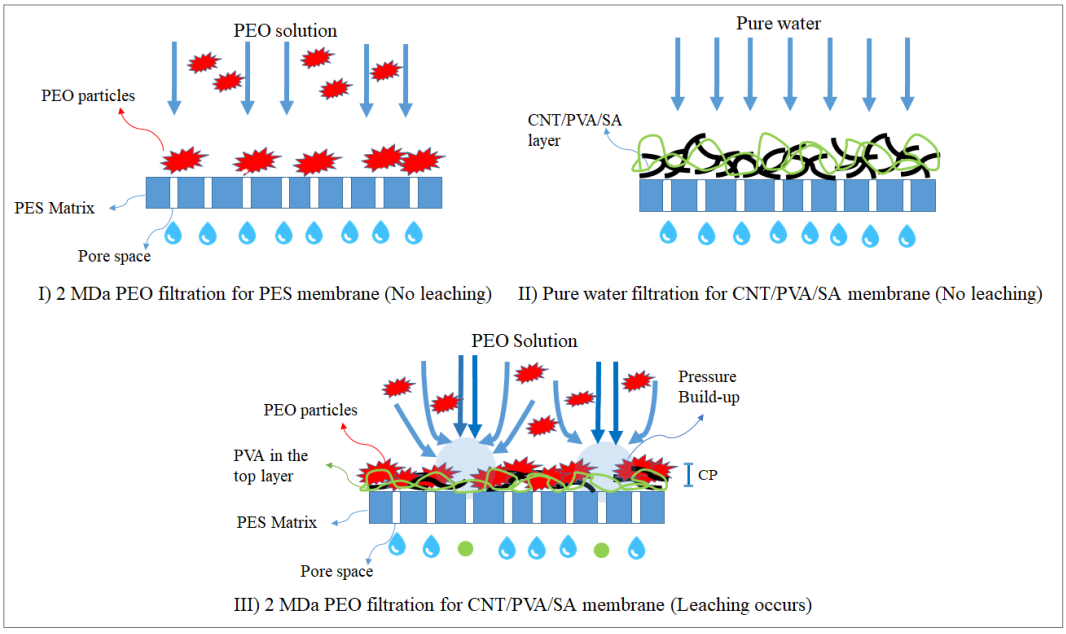

Figure 5.S11. High degree of carbon content found in the permeate during the PEO rejection test can be solely ascribed to PVA leaching.

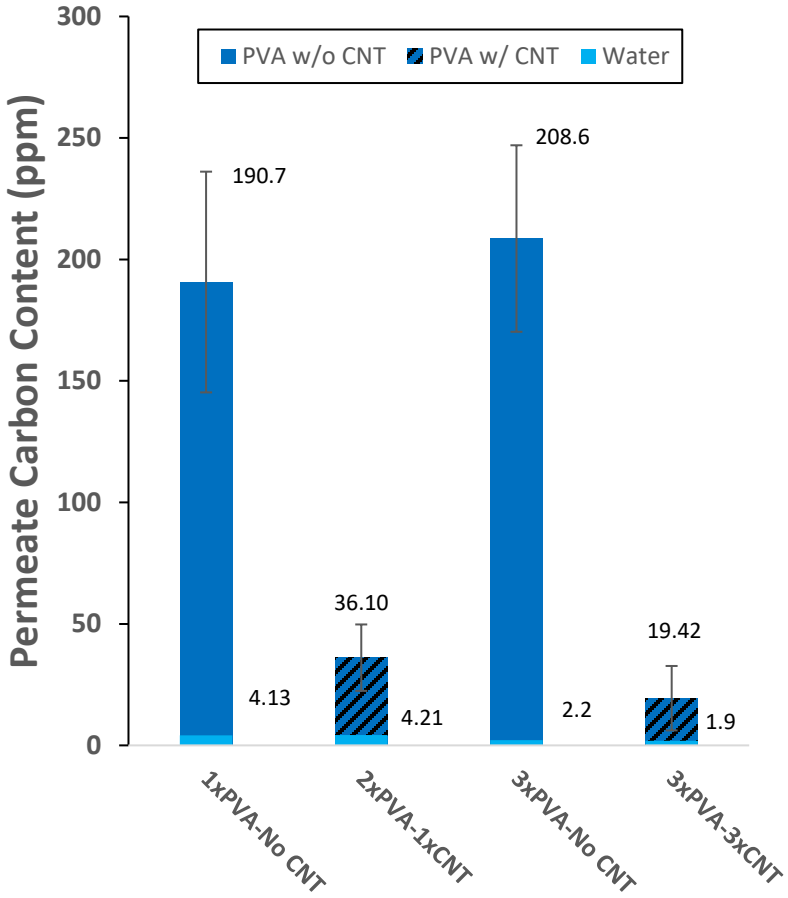

Figure 5.S12. The impact of CNT incorporation in the nanolayer on TOC results. 1 mg or 3 mg CNT mass loadings were used in ECMs. PEO (2 MDa) was used as the model foulant with a concentration of 250 ppm in water. Error bars represent the standard deviation for three membranes.

Mechanical Stability

(I)

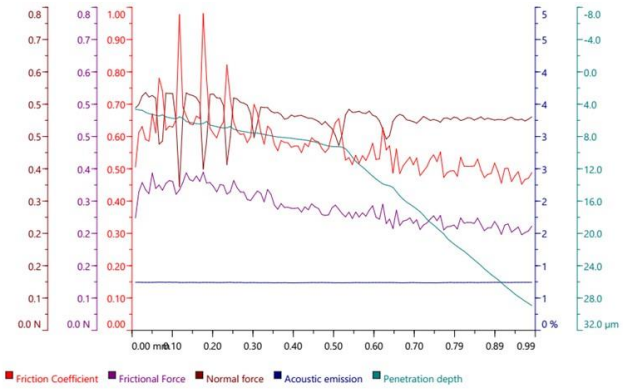
Friction Coefficient
Frictional Force
Normal force
Acoustic emission
Penetration depth

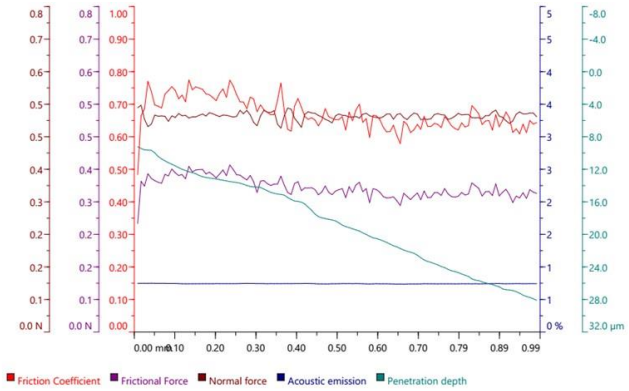
Friction Coefficient
Frictional Force
Normal force
Acoustic emission
Penetration depth

(II)

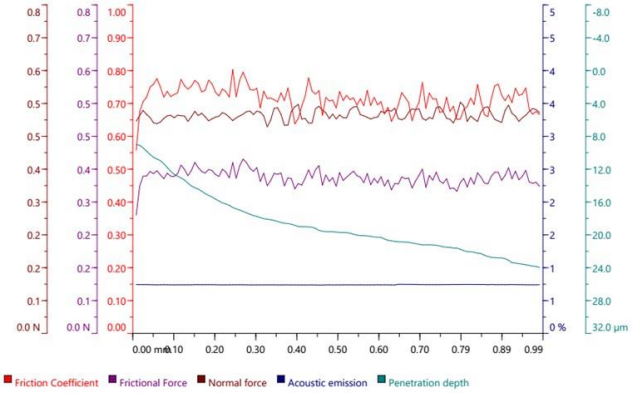
Friction Coefficient
Frictional Force
Normal force
Acoustic emission
Penetration depth

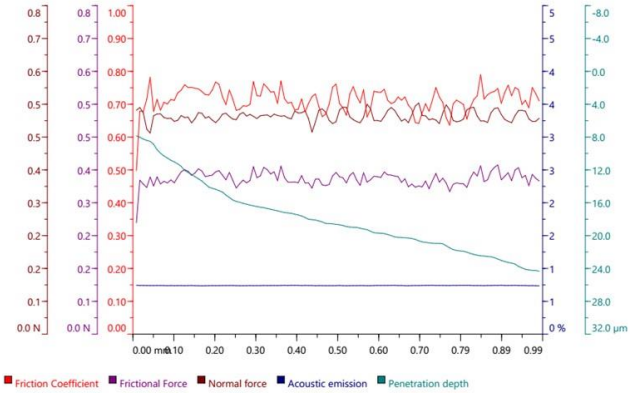
Friction Coefficient
Frictional Force
Normal force
Acoustic emission
Penetration depth

(III)

(IV)

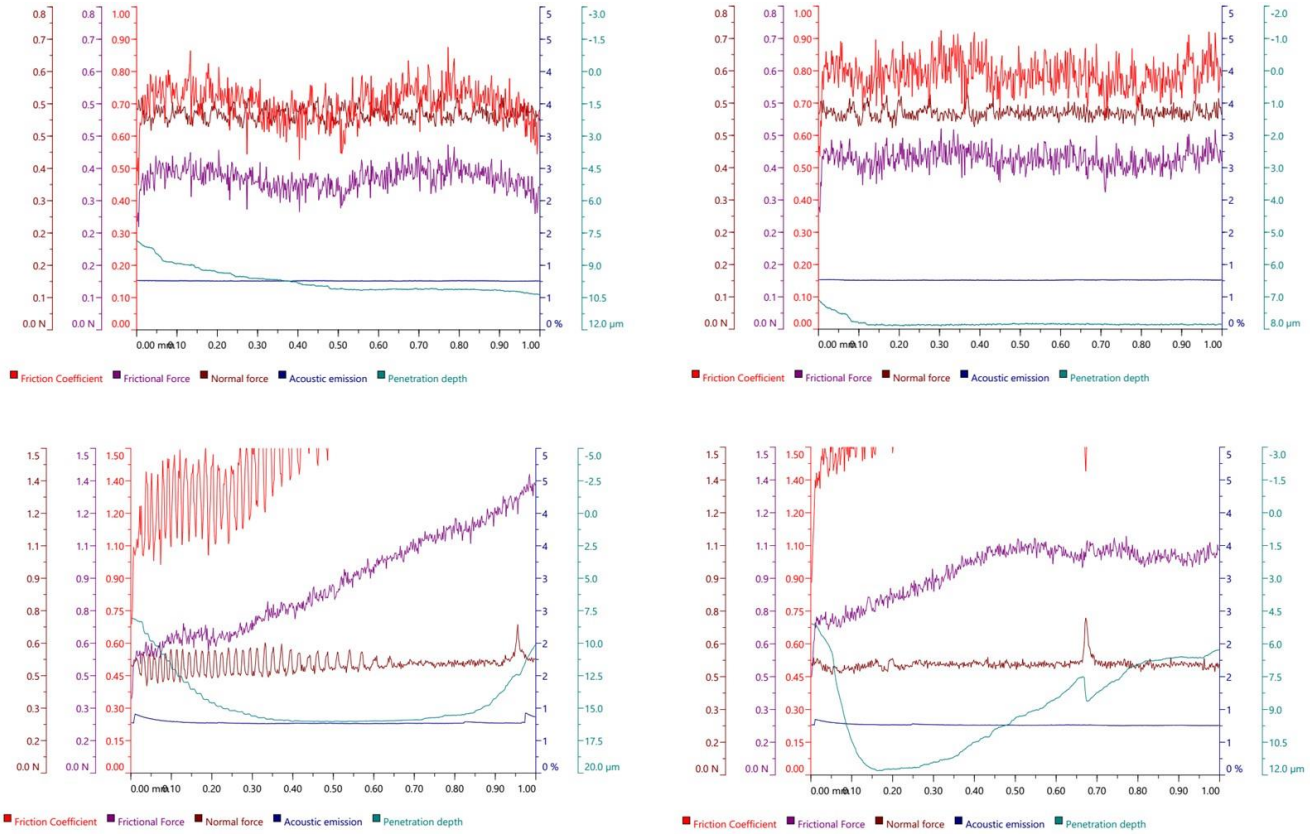

Figure 5.S13. The mechanical stability of membranes with different chemistries measured by micro-scratch testing. Two trials for each nanolayer network were conducted as follows: (I) CNT, (II) CNT/PVA/SA, (III) CNT/GA, and (IV) Pristine PES. The tip applied a normal force of 0.5 N and the scratch length and scratch speed were 1 mm and 5 mm/min, respectively.

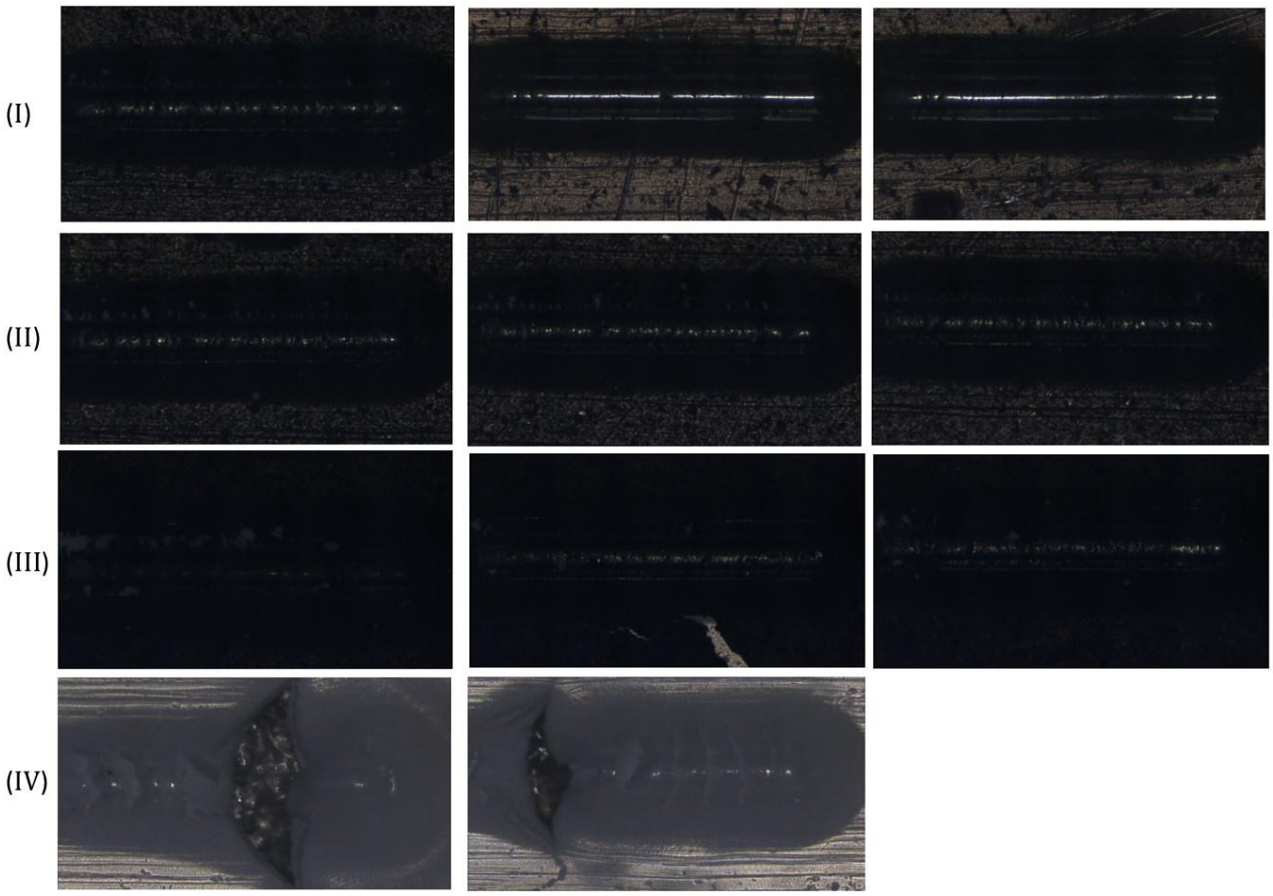

Figure 5.S14. Surface images of membranes after the micro-scratch test. Trials for each nanolayer network were conducted as follows: (I) CNT, (II) CNT/PVA/SA, (III) CNT/GA, and (IV) Pristine PES. The tip applied a normal force of 0.5 N and the scratch length and scratch speed were 5 mm and 5 mm/min, respectively.

Supplementary Information II

Stability assessment of electrically conductive membranes

Submitted to Elsevier MethodsX

Abstract

The surface properties of electrically conductive membranes (ECMs) govern their advanced abilities. During operation, these properties may differ considerably from their initially measured properties. Depending on their operating conditions, ECMs may undergo various degrees of passivation. ECM passivation can detrimentally impact their real time performance, causing large deviations from expected behaviour based on their initially measured properties. Quantifying these changes will enable consistent performance comparisons across the active and electrically conductive membrane research field. As such, consistent methods must be established to quantify ECM membrane properties. In this work, we proposed three standardized methods to assess the electrochemical, chemical, and physical stability of such membrane coatings: 1) electrochemical oxidation, 2) surface scratch testing, and 3) pressurized leaching. ECMs were synthesized by the most common approach – coating support UF and/or MF polyethersulfone (PES) membranes with carbon nanotubes (CNT) cross-linked with polyvinyl alcohol (PVA) and two types of cross-linkers (either succinic acid (SA) or glutaraldehyde (GA)). We then evaluated these ECMs based on the three standardized methods: 1) We evaluated electrochemical stability as a function of electro-oxidation induced by applying anodic potentials. 2) We measured the scratch resistance to quantify the surface mechanical stability. 3) We measured physical stability by quantifying the leaching of PVA during separation of a model foulant (polyethylene oxide (PEO)). Our methods can be extended to all types of electrically conductive membranes including microfiltration, ultrafiltration, nanofiltration, and reverse osmosis ECMs. We propose that these fundamental measurements are critical to assessing the viability of ECMs for industrial MF, UF, NF, and RO application.

Keywords: Electrically conductive membranes, material stability, scratch testing, electrochemical oxidation, polyvinyl alcohol, carbon nanotubes

Method details

Membranes are the technology of choice for water and wastewater treatment due to their selectivity, smaller footprint, and lower cost. Recently, electrically conductive membranes (ECMs) have gained great attention for their potential to improve the antifouling performance of membranes [1–5]. The first generation of ECMs are commonly made of CNT/PVA networks cross-linked with a cross-linking agent such as dicarboxylic acid or dialdehyde. These membranes can carry an externally applied electrical charge across their surface. The application of an electric potential to an ECM promotes various antifouling mechanisms at the membrane/water interface [1,3,6–8]. ECMs are synthesized with specific surface properties such as pore size, surface hydrophilicity, and surface conductivity to target different antifouling applications. The in-situ properties of membranes during the operation, however, may differ significantly with their initial properties. Membranes may be subjected to passivation leading to alterations in their surface properties [9]. Membrane passivation would hinder their antifouling performance, damage their integrity, and increase the system energy consumption. For instance, the surface conductivity of ECMs allows for charge mobility across a surface, which in turn promotes antifouling mechanisms at the surface. Hence, the loss in conductivity would directly compromise the antifouling performance of such membranes. It is difficult to monitor the real time passivation of surfaces, and the in-situ membrane properties are often assumed to be unchanged from their initially measured properties. To date, the common characterization tests carried out after fabrication of membranes have failed to take into account the operational impacts given that significant changes occur at the surface. The challenges of real time measurements (either direct or indirect) necessitates proper assessment of surface properties before use.

There are three main types of stability associated with ECMs studied in this work. Electrochemical stability, mechanical stability, and physical stability. We propose that these three methods should form the basis for all ECM assessments. Their importance and method of testing are described here:

Electrochemical Stability: ECMs are exposed to anodic, cathodic, alternating, or block currents (distinguished from alternating currents as anodic and cathodic currents applied sequentially at irregular intervals) depending on the foulant type and their application. Anodic current can permanently oxidize CNT-membranes [10–12]. CNT-corrosion decreases the surface conductivity critical for their antifouling performance. Many studies reported the optimum potential required to promote interfacial mechanisms such as electrostatic repulsion, biofoulant inactivation, organic oxidation, or hydrogen peroxide generation [13–17]. The current density correlated to reported optimized potentials, however, is significantly different from the real current density applied to the surface over the membrane's operational window. The real current density is often ignored due to lack of real time measurements and often overestimated. In this report, a method is proposed to assess the anodic stability of CNT-based membranes using a three-electrode electrochemical cell.

Mechanical Stability: Cross-flow is the most common configuration in membrane-based systems regardless of the membrane type (MF, UF, NF, or RO) or membranes shape (flat sheet, hollow fiber, or spiral-wound). In such systems, membranes are constantly exposed to shear forces induced by tangential flow containing solid particles. In addition, cleaning procedures such as mechanical cleaning can damage the membrane surface. It is expected that surface damage induced by fouling, aging, scaling, or mechanical cleaning alter the surface properties of electrically conductive membranes [18–22]. Therefore, it is important to assess the mechanical stability of membranes used in separation-based systems. Mechanical stability of membranes is less explored as compared to other surface properties such as hydrophilicity, surface charge, and surface roughness. We proposed the scratch test using a diamond tip to quantify the surface mechanical stability of membranes where the impact of surface chemistries is distinguishable.

Physical Stability: CNT-based membranes are composed of CNTs, organic polymers, and binders. The polymers and cross-linkers are added to take advantage of their hydrophilicity, stability, and film-forming ability. Polymers (PVA) and cross-linkers are attached via covalent bond, electrostatic interactions, and H-bonding [23–25], however, a

portion of PVA is loosely bound to the network and leaches under certain operating conditions which results in changes in surface properties. A model foulant (PEO) separation test was proposed to quantify the network instabilities under different operating conditions.

It is worthy to note that although the interplay between all types of stability is not fully understood, the stability assessment methods discussed in this paper allow us to compare membranes with different chemistries from mechanical, electrochemical, and physical perspectives. The described methods are focused on MF and UF membranes, however, they can easily be extended to NF and RO membranes as well.

Materials and procedures

ECMs used in this study are synthesized following the same method published in our other work [26]. In short, pristine UF PES membranes were coated with CNT/PVA network cross-linked with either succinic acid (SA) or glutaraldehyde (GA). Unless otherwise mentioned, all ECMs contain 1 mg CNT and the CNT: PVA ratio was kept at 1:10 in all the membranes.

Electrochemical stability

A three-electrode electrochemical cell (Figure 5.S2) coupled to a pontentiostat (Multi Autolab M204, Metrohm) was used to quantify the anodic oxidation state of the membranes through fixed potential chronoamperometry as well as cyclic voltammetry methods. In order to be able to record currents higher than 10 mA in response to high applied potentials, a booster (1A Metrohm) was coupled to the pontentiostat. The CNT-based membrane, graphite sheet, and an Ag/AgCl electrode (Metrohm, operating range: 0-80 °C) were used as the working electrode (anode), counter electrode (cathode), and reference electrode, respectively. All electrodes were placed in an electrochemical cell containing phosphate buffered saline (PBS, purchased from VWR) solution as the electrolyte. PBS solution contains 137 mM sodium chloride, 2.7 mM potassium chloride, and 10 mM phosphate buffer. The batch was stirred constantly at an rpm of 200. A couple of supplementary tests were carried out to gain a better understating of the stability and CNT degradation mechanisms involved. The tests are described as follows:

Fixed potential chronoamperometry

Anodic potential can oxidize CNT surfaces leading to current drops in the surface. Fixed potential chronoamperometry can provide useful insights on oxidation state of membranes over time. As such, it reveals the magnitude and duration of the current that can be applied on the surface before it undergoes severe oxidation. In addition, the real current densities reported from this test can be used for closer predictions of antifouling mechanisms promoted by current density such as electrostatic repulsion force, gas generation, and radical generation. Fixed potential chronoamperometry tests were carried out by applying either 2 or 4 V (with respect to the Ag/AgCl reference electrode) to the membrane for 240 and 20 min, respectively. The efficient potential range for antifouling performance of ECMs is reported to be 0-2 V. In addition, there are different oxidizing mechanisms responsible for corrosion of CNTs such as mechanical breakdown, oxidation of CNT, and radical generation. A number of oxidation mechanisms are activated at potentials above 2 V [27–29]. This explains why 2 and 4 V were chosen as our testing anodic potentials to explore the oxidation process. The time periods were chosen because the currents were shown to reach steady state over the test window. Hence, surfaces are expected to have minor oxidation changes over extended periods. Further, anodic current is applied often in different current types (direct or alternating current) or with different current duty ratios (ratio of pulsing time over one cycle). Therefore, the duration of the test represents a longer current window than would occur in normal operating conditions.

Cyclic voltammetry

Cyclic voltammetry (CV) is a complementary test to fixed potential chronoamperometry. In this test, anodic potentials were applied to ECMs at a certain scan rate and for a number of cycles. It is expected that the current drops over each cycle until it reaches a final oxidation state. The rate of current drop over each cycle features the anodic stability. CV test is an informative test as it exposes the membrane to a wide range of potentials that can induce different oxidizing mechanism. For the CV test, 15 cycles at a

scan rate of 0.1 mVs-1 were applied to each membrane, with a scan range of 0-3 V relative to the Ag/AgCl electrode.

Four-point conductivity meter

The conductive nanolayer in ECMs consists of a connected porous CNT network. Corrosion of CNTs leads to lower total conductivity of the network. As a result, it is expected that the decrease in ECM surface conductivity will lead to a decrease in their electrochemical conductivity. Therefore, the surface conductivity of membranes was measured before and after anodic oxidation at 4 V (with respect to the Ag/AgCl reference electrode) for 20 min. The surface conductivity was measured using a four-point probe conductivity meter. Before the test, membranes were fully dried at 60 °C using an oven and cooled at ambient temperature. This instrument is equipped with two pairs of sharp needles attached to adjustable arms. The needles need to be placed correctly on the conductive surface (to only contact the conductive layer). The probe applies a potential to the surface and calculates the sheet resistance by considering the resistance between different pairs of the needles. Before reporting the sheet resistance, the correct position of the needles should be confirmed by monitoring the resistance values between different pairs. The needles are in a square configuration. Assuming a uniform distribution of CNTs across the surface, the resistance between the pairs of needles is expected to be on the same order magnitude. Any significant difference in the resistance between pairs of needles indicates that the needle probes have not contacted the surface properly.

Total organic carbon analyzer

Mechanical breakdown of CNT structures as a result of passivation is expected to increase the organic carbon content in the electrochemical batch. The generation of hydrogen/oxygen gas during application of cathodic/anodic currents leads to formation of micro-bubbles. Micro-bubbles may get trapped inside the CNT network, and the subsequent increase in the size of these bubbles may cause mechanical breakdown of the CNT structures. Therefore, the organic carbon content of the batch was measured before and after electro-oxidation at 4 V (with respect to the Ag/AgCl reference electrode) for 20

min using a total organic carbon analyzer (TOC, SHIMADZU). The data obtained from this method can indicate the extent to which electrical currents applied to the CNTs contribute to the mechanical breakdown of CNTs, which in turn leads to electrochemical instability.

Fourier-transform infrared spectroscopy (FTIR)

Fourier-transform infrared spectroscopy (FTIR) is used to monitor the oxidation state of chemical structures. As it was mentioned earlier, functionalized CNT, PVA, and cross-linkers are bound in an ECM network through covalent bonds, electrostatic interactions, and H-bonding. The intensity of C-O, C=O, and O-H bonds associated with such components is expected to change over the oxidation period. As a result, FTIR allows us to identify the changes in their chemical bonds.

Micro scratch tester

Scratch test can be used to assess the mechanical stability of the materials. Scratch test can be carried out on three different scales: macro, micro, and nano. In this study, a micro scratch tester manufactured by Anton Paar (Revetest scratch tester) was used. The specifications of this device are shown in Table 6.1. Scratch test consists of three steps: 1. Pre-scan – The physical state and topography of the surface is monitored before applying any force, 2. Scratch – The surface is scratched using predefined settings such as scratch path, speed, and type, and 3. Post-scan – to the physical state and topography of the surface is monitored after scratching and damaging the surface. It should be noted that pre-scan and post-scan should be carried out under the lowest pressure possible to minimize any additional damage to the surface beyond that caused by the scratch-test. We defined the correct scratch settings based on instructions of the manufacturer for polymeric coatings as well as performing different scratch trials prior to the real scratch test. These settings include the scratch type (constant, progressive, or incremental), scratch length, scratch speed, applied normal load, indenter type, indenter shape (Spherical, Berkovich, and Vickers), indenter radius, and indenter angle. The manufacturer recommends a scratch test with a Rockwell diamond indenter to evaluate the resistance of polymeric or ceramic

materials. The critical load (loads at which material failure occurs), scratch length, and scratch speed must be defined by the user depending on the type of the material. The settings used in our study for each of the parameters in Table 6.1 are provided in Table 6.2. These settings have been identified as optimal for membrane surfaces in this study. The micro scratch tester reports parameters such as depth of penetration, normal force, tangential force, acoustic emission, and friction coefficient. Acoustic emission is used to monitor the material failures including cracks and voids across the network in non-destructive testing [30]. Friction coefficient is the ratio of tangential force over normal force and is mostly μ <1. A rupture in surface would lead to friction coefficients μ >1. Depth of penetration of the indenter over the scratch length was used as an indication of the mechanical stability. Three scratches should be performed on each surface to validate the reproducibility of the results.

Table 1. Specifications of the micro scratch tester (Anton Paar)

Parameter	**Value**
Maximum Normal load	100 N
Normal load resolution	0.1 mN
Maximum friction load	100 N
Friction force resolution	0.1 mN
Maximum strength length	70 mm
Scratch speed	0.4-600 mm/min
Maximum depth	1000 μm
Depth resolution	0.5 nm

Table 2. Micro scratch settings used

Settings	**Value**
Indenter characteristics	
Type	Rockwell
Shape	Spherical
Material	Diamond
Radius	200 μm
Tip angle	90 °
Serial number	AJ-259
Scratch characteristics	
Type	Constant

Normal load	0.5 N
Scratch length	1 mm
Scratch speed	5 mm/min

Model foulant separation test

The coatings in electrically conductive membranes (ECMs) contain nanoparticles and polymers. Loosely bound molecules may leach from such coatings leading to surface instabilities. Surface passivation induced by leaching of molecules may cause alterations in surface properties, therefore, it is important to quantify the chemical stability of ECMs. To this end, we recommend to challenge the surface with model foulants in a separation process. A filtration process allows for model foulants to accumulates at the surface leading to formation of concentration polarization (CP) layer. Pressures locally builds up at the CP layer which in turn, can dislodge chemically unstable molecules. Leached molecules should be quantified in the permeate side to evaluate the physical stability of the nanolayer. Our suggestion is to use the polyethylene oxide (PEO) as the model foulant. PEO is commonly used to identify the molecular weight cut off (MWCO) of the membranes. The MWCO of a membrane is defined based on the size of PEO particles where membranes shows >90% rejection. However, in our pressured stability test PEO is used for a different approach. As such, we should choose a PEO particle size that gets effectively rejected from the membrane (>99.5%). Therefore, it is expected that PEO particles only accumulate as the surface, form a strong CP layer, and challenge the loosely bound molecules. We conducted a polyethylene oxide (PEO) separation test to evaluate the physical stability of the nanolayer with the experimental conditions provided in Table 6.3. The carbon content in the permeate was quantified using a total organic carbon analyzer (TOC, SHIMADZU). Pristine polyether sulfone (PES) membranes efficiently reject 2 MDa polyethylene oxide (PEO) particles. Under the assumption of a robust stable nanolayer, ECMs are expected to have an equal or higher rejection performance as compared to pristine PES membranes due to the presence of the extra separation barrier on top of the support membrane (porous CNT network). On the other hand, if the nanolayer is assumed unstable, the carbon content in

the permeate may be found higher as compared to pristine PES membranes due to leaching of loosely bound polymeric components. Pursuing with the second assumption, the degree of instability can be correlated to the magnitude of leaching. Leaching from the ECM can be quantified by measuring the change in the organic carbon content in the permeate. The organic carbon content in the permeate, however, is composed of both PEO that passed through the membrane as well as polymer that leached from the ECM. Therefore, a series of control separation tests should be performed to deconvolute the sources of carbon content in the permeate as follows:

- Separation test on pristine PES membrane: This test provides an average value for permeated PEO particles through PES membranes.
- Separation test on PES membrane exposed to harsh conditions such as high temperature and acidic solutions: ECMs were exposed to these parameters during the fabrication process and this test shows if such parameters contribute to rejection performance of membranes.
- Pure water flux on PES membranes and ECMs: This is a negative control test to make sure pure water does not cause any physical instability.
- Separation test on membranes with different conductive networks: Network composed of CNT, CNT/PVA, and CNT/PVA/cross-linker should be tested under the same experimental conditions. The separation result of each network with consideration of other networks would provide the leaching of each component individually.

In our example, the main factor responsible for leaching of loosely bound polymeric particles is the local pressure build-up induced by concentration polarization. As the UF membrane retains organic particles, the concentration of rejected ions increases at the surface of the membrane. As a result of concentration polarization, PEO particles partially cover the surface and leave fewer pathways for water. Therefore, the pressure locally builds-up in the remaining pore leads to leaching of unstable polymers (PVA). In order to quantify the degree of leaching, the physical instability should be tested at different

operating pressures, different feed concertation, and at thicknesses of the nanolayer as provided in Table 6.3.

Table 3. Operating conditions of the separation test

Parameter	**Value**
Membrane Nominal pore size	30 nm
Model foulant	Polyethylene oxide
Foulant size	2 MDa
Feed concentration	50-250 ppm
Transmembrane pressure	10-100 psi
CNT mass loading in nanolayer	1-3 mg

Method validation

Anodic oxidation

Figure 1 shows the results of cyclic voltammetry applied on an ECM containing 1 mg CNT, 5 mg PVA, and glutaraldehyde (GA) as the cross-linker. The conductivity of the membrane decreases over 15 cycles, as shown in Figure 1. The drop in conductivity is greater in the first 5 cycles indicating a fast oxidation rate while it is lesser in the next 10 cycles indicating steady state oxidation. These results can be correlated to findings in Figure 2 where fixed potential chronoamperometry was applied. In Figure 2, the conductivity of an ECM with the same chemistry as in Figure 1, follows the same trend in oxidative change. Initial fast corrosion leads to a steady state plateau. This method is used to quantify the electrochemical stability of variously synthesized ECMs. As such, a comparison among different ECMs is provided in Figure 2. Membranes containing CNT/10xPVA/GA showed higher final conductivity regardless of their lower initial conductivity. Detailed experiments as well as the results of surface conductivity, mechanical conductivity, and chemical bonding state of membranes with different networks are provided in the original manuscript. ECM conductivity measurements before and after surface oxidation (not shown here) revealed that the ECM surface conductivity was lower for all ECMs after oxidation, supporting the results from chronoamperometry. The mechanical breakdown of CNT structures was quantified using a total organic carbon

analyzer and found to be insignificant. FTIR analysis was conducted to monitor the presence of chemical bond formation in response to a current applied to the ECMs. The presence of C=O bonds increased during electrochemical oxidation. We hypothesize that this increase in C=O bond formation is a result of acetylation reactions between the cross-linker (GA) and PVA.

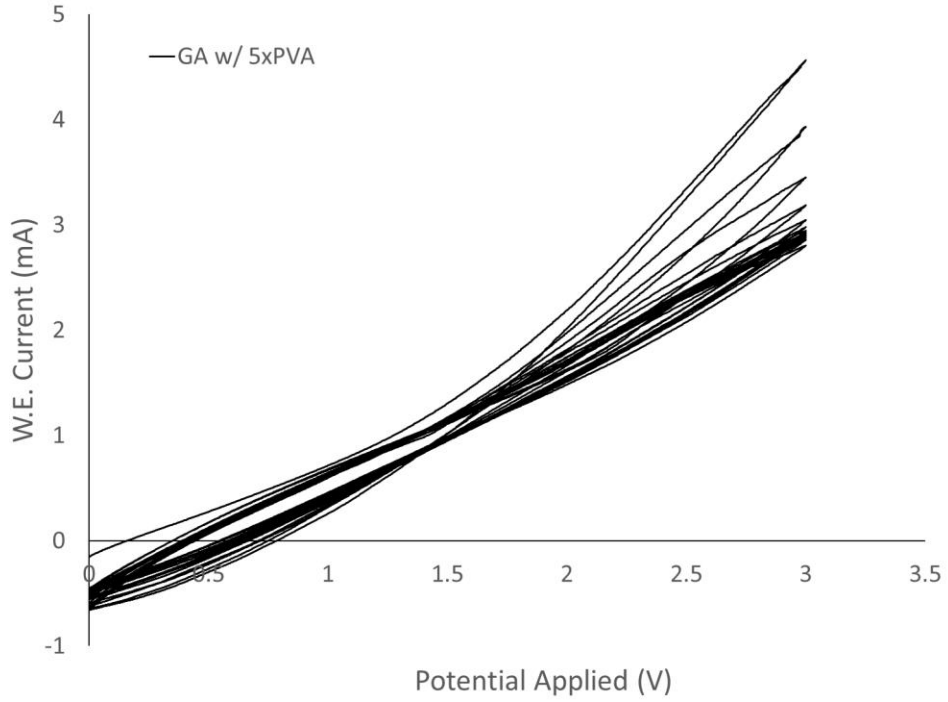

Figure 1. Cyclic voltammetry. ECM contains 1 mg CNT mass loading. The conductive ECM, graphite sheet, and an Ag/AgCl electrode were used as the working electrode (anode), counter electrode, and reference electrode, respectively. The scan range was 0-3 V at a scan rate of 0.1 mVs^{-1}.

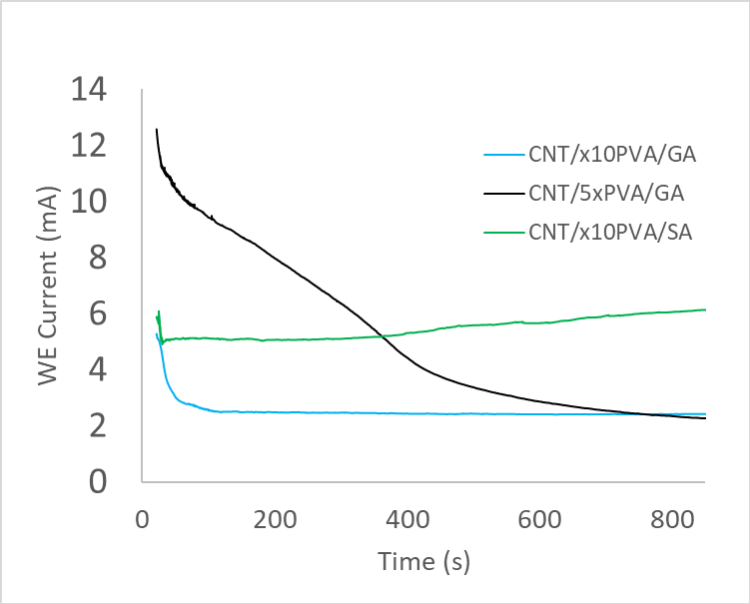

Figure 2. Fixed potential chronoamperometry for membranes with different chemistries containing CNT, PVA, and cross-linkers. Trials were conducted for each network as follows. ECM, graphite sheet, and an Ag/AgCl electrode were used as the working electrode (anode), counter electrode, and reference electrode, respectively. The total cell potential was 4 V. All ECMs contain 1 mg CNT.

Scratch test

The results of the micro scratch test on an electrically conductive membrane with the correct settings is presented in Figure 3a. As indicated, the depth of penetration increased over the scratch length which shows the degree of instability. Membrane rupture leads to data that cannot be quantifiably analyzed, thus it is important to identify the critical operational settings to avoid this outcome by running different control tests. The settings include indenter radius, applied normal force, scratch length, and scratch speed. Thus, membranes were purposefully ruptured to demonstrate this outcome, i.e. failed scratch tests. An example of a failed test is presented in Figure 3b. More results of failed tests can be found in the supplementary information.

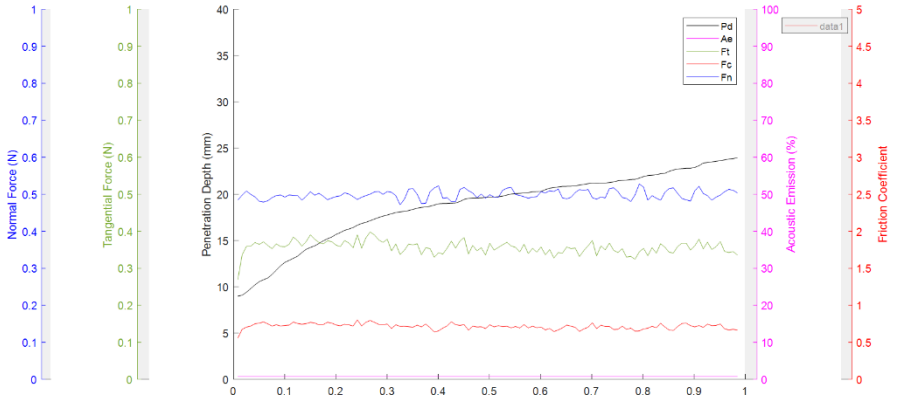

(a)

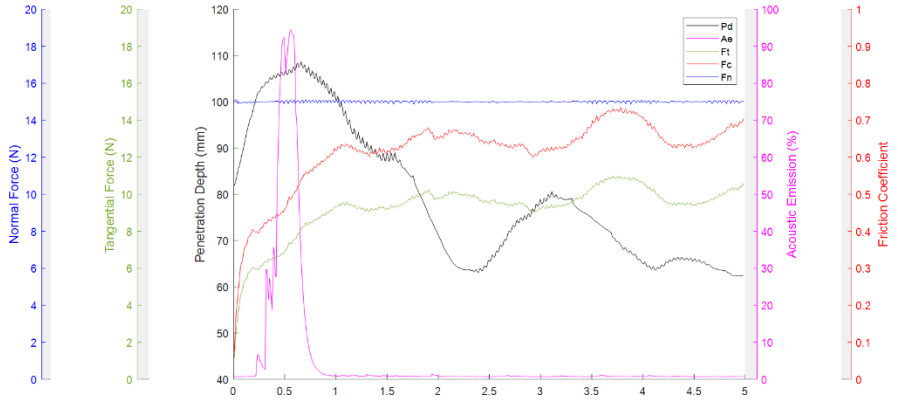

(b)

Figure 3. The mechanical stability of an ECM measured in the micro-scratch test with different input settings. The settings are as follows: (A) The tip of radius 200 μm applied a normal force of 0.5 N and the scratch length and scratch speed were 1 mm and 5 mm/min, and (B) The tip of radius 100 μm applied a normal force of 15 N and the scratch length and scratch speed were 5 mm and 5 mm/min.

Rejection test

The results were discussed in detail in the Chapter 5. As explained in the Methods section, a series of control tests were conducted to assess the stability of the nanolayer followed by deconvolution of leaching sources as follows:

- 2 MDa PEO separation test on pristine PES membrane: Negligible carbon content in the permeate side
- 2 MDa PEO separation test on PES membrane exposed to harsh conditions such as high temperature and acidic solutions: Negligible carbon content in the permeate side
- Pure water flux on PES membranes and ECMs: Negligible carbon content in the permeate side
- 2 MDa PEO separation test on ECMs containing PVA: High carbon content observed in the permeate side

In short, UF PES membranes fully rejected 2 MDa PEO particles (99.6%). However, the permeate carbon content was found higher in ECMs where they had an extra barrier (nanolayer) on top of support PES membrane. These findings led us to speculate that the nanolayer is physically unstable and the PVA leaches through the membrane during PEO separation test. It should be noted that pure water flux did not lead to increase in the permeate carbon content. As a result, we hypothesize that local pressure build-up induced by concentration polarization is the responsible factor for leaching of PVA. PEO separation tests under either a higher PEO concentration (250 ppm compared to 50 ppm) and a higher transmembrane pressure (TMP, 100 psi compared to 10 psi) were conducted to confirm our hypothesis. It was observed that either a higher feed concentration or a higher TMP leads to a higher pressure build-up and a higher leaching degree, correspondingly. To alleviate the local pressure build-up, thicker CNT layers (containing three times higher CNT mass loading) were synthesized which could potentially extend the concentration polarization layer. The results revealed that membranes with thicker nanolayers resulted in less leaching (by 50%) due to an extended concentration polarization layer.

Acknowledgments

This work was supported and funded by Natural Sciences and Engineering Research Council of Canada (NSERC). We are especially thankful for the facilities and assistance of the McMaster Manufacturing Research Institute (MMRI) and McMaster Biointerfaces Institute (BI).

References

[1] F. Ahmed, B.S. Lalia, V. Kochkodan, R. Hashaikeh, Electrically conductive polymeric membranes for fouling prevention and detection: A review, Desalination. 391 (2016) 1–15. https://doi.org/10.1016/J.DESAL.2016.01.030.

[2] A. Ronen, S.L. Walker, D. Jassby, Electroconductive and electroresponsive membranes for water treatment, Rev. Chem. Eng. 32 (2016) 533–550. https://doi.org/10.1515/revce-2015-0060.

[3] P. Formoso, E. Pantuso, G. De Filpo, F. Nicoletta, Electro-Conductive Membranes for Permeation Enhancement and Fouling Mitigation: A Short Review, Membranes (Basel). 7 (2017) 39. https://doi.org/10.3390/membranes7030039.

[4] I.-H. Loh, R.A. Moody, J.C. Huang, Electrically conductive membranes: Synthesis and applications, J. Memb. Sci. 50 (1990) 31–49. https://doi.org/10.1016/S0376-7388(00)80884-4.

[5] W. Hu, S. Chen, Z. Yang, L. Liu, H. Wang, Flexible electrically conductive nanocomposite membrane based on bacterial cellulose and polyaniline, J. Phys. Chem. B. 115 (2011) 8453–8457. https://doi.org/10.1021/jp204422v.

[6] C.F. De Lannoy, D. Jassby, K. Gloe, A.D. Gordon, M.R. Wiesner, Aquatic biofouling prevention by electrically charged nanocomposite polymer thin film membranes, Environ. Sci. Technol. 47 (2013) 2760–2768. https://doi.org/10.1021/es3045168.

[7] S.H. Hong, J. Jeong, S. Shim, H. Kang, S. Kwon, K.H. Ahn, J. Yoon, Effect of electric currents on bacterial detachment and inactivation, Biotechnol. Bioeng. 100 (2008) 379–386. https://doi.org/10.1002/bit.21760.

[8] H. Särkkä, M. Vepsäläinen, M. Sillanpää, Natural organic matter (NOM) removal by electrochemical methods - A review, J. Electroanal. Chem. 755 (2015) 100–108. https://doi.org/10.1016/j.jelechem.2015.07.029.

[9] A.L. McGaughey, R.D. Gustafson, A.E. Childress, Effect of long-term operation on membrane surface characteristics and performance in membrane distillation, J. Memb. Sci. 543 (2017) 143–150. https://doi.org/10.1016/j.memsci.2017.08.040.

[10] C.D. Vecitis, M.H. Schnoor, M. Saifur Rahaman, J.D. Schiffman, M. Elimelech, Electrochemical Multiwalled Carbon Nanotube Filter for Viral and Bacterial Removal and Inactivation, Environ. Sci. Technol. 45 (2011) 3672–3679. https://doi.org/10.1021/es2000062.

[11] M. Tominaga, Y. Yatsugi, N. Watanabe, Oxidative corrosion potential vs. pH diagram for single-walled carbon nanotubes, RSC Adv. 4 (2014) 27224–27227. https://doi.org/10.1039/c4ra02875a.

[12] S. Ohmori, T. Saito, Electrochemical durability of single-wall carbon nanotube electrode against anodic oxidation in water, Carbon N. Y. 50 (2012) 4932–4938. https://doi.org/10.1016/j.carbon.2012.06.023.

[13] E.L. Sandvik, B.R. Mcleod, A.E. Parker, P.S. Stewart, Direct Electric Current Treatment under Physiologic Saline Conditions Kills Staphylococcus epidermidis Biofilms via Electrolytic Generation of Hypochlorous Acid, PLoS One. 8 (2013) 55118. https://doi.org/10.1371/journal.pone.0055118.

[14] A.R. Khataee, M. Safarpour, M. Zarei, S. Aber, generation of H2O2 using immobilized carbon nanotubes on graphite Electrochemicalelectrode fed with air: Investigation of operational parameters, J. Electroanal. Chem. 659 (2011) 63–68. https://doi.org/10.1016/j.jelechem.2011.05.002.

[15] T.H.R. Niepa, J.L. Gilbert, D. Ren, Controlling Pseudomonas aeruginosa persister cells by weak electrochemical currents and synergistic effects with tobramycin, Biomaterials. 33 (2012) 7356–

7365. https://doi.org/10.1016/j.biomaterials.2012.06.092.

[16] S. Pandit, S. Shanbhag, M. Mauter, Y. Oren, M. Herzberg, Influence of Electric Fields on Biofouling of Carbonaceous Electrodes, (2017). https://doi.org/10.1021/acs.est.6b06339.

[17] A. Ronen, W. Duan, I. Wheeldon, S. Walker, D. Jassby, Microbial Attachment Inhibition through Low-Voltage Electrochemical Reactions on Electrically Conducting Membranes, Environ. Sci. Technol. 49 (2015) 12741–12750. https://doi.org/10.1021/acs.est.5b01281.

[18] J. Kim, B. Van Der Bruggen, The use of nanoparticles in polymeric and ceramic membrane structures: Review of manufacturing procedures and performance improvement for water treatment, Environ. Pollut. 158 (2010) 2335–2349. https://doi.org/10.1016/j.envpol.2010.03.024.

[19] G.S. Ajmani, D. Goodwin, K. Marsh, D.H. Fairbrother, K.J. Schwab, J.G. Jacangelo, H. Huang, Modification of low pressure membranes with carbon nanotube layers for fouling control, Water Res. 46 (2012) 5645–5654. https://doi.org/10.1016/j.watres.2012.07.059.

[20] M.L. Pype, B.C. Donose, L. Martí, D. Patureau, N. Wery, W. Gernjak, Virus removal and integrity in aged RO membranes, Water Res. 90 (2016) 167–175. https://doi.org/10.1016/j.watres.2015.12.023.

[21] B.C. Donose, S. Sukumar, M. Pidou, Y. Poussade, J. Keller, W. Gernjak, Effect of pH on the ageing of reverse osmosis membranes upon exposure to hypochlorite, Desalination. 309 (2013) 97–105. https://doi.org/10.1016/j.desal.2012.09.027.

[22] H. Hagihara, K. Ito, N. Oshima, A. Yabuuchi, H. Suda, H. Yanagishita, Depth profiling of the free-volume holes in cellulose triacetate hollow-fiber membranes for reverse osmosis by means of variable-energy positron annihilation lifetime spectroscopy, Desalination. 344 (2014) 86–89. https://doi.org/10.1016/j.desal.2014.03.015.

[23] F. Pan, Y. Li, Y. Song, M. Wang, Y. Zhang, H. Yang, H. Wang, Z. Jiang, Graphene oxide membranes with fixed interlayer distance via dual crosslinkers for efficient liquid molecular separations, J. Memb. Sci. 595 (2020) 117486. https://doi.org/10.1016/j.memsci.2019.117486.

[24] A. Shameli, E. Ameri, Synthesis of cross-linked PVA membranes embedded with multi-wall carbon nanotubes and their application to esterification of acetic acid with methanol, Chem. Eng. J. 309 (2017) 381–396. https://doi.org/10.1016/J.CEJ.2016.10.039.

[25] H. Bang, M. Gopiraman, B. Kim, S. Kim, I. Kim, Colloids and Surfaces A : Physicochemical and Engineering Aspects Effects of pH on electrospun PVA / acid-treated MWNT composite nanofibers, Colloids Surfaces A Physicochem. Eng. Asp. 409 (2012) 112–117. https://doi.org/10.1016/j.colsurfa.2012.05.046.

[26] M.A. Halali, C.-F. de Lannoy, The Effect of Cross-Linkers on the Permeability of Electrically Conductive Membranes, Ind. Eng. Chem. Res. 58 (2019) 3832–3844. https://doi.org/10.1021/acs.iecr.8b05691.

[27] Y. Baek, H. Yoon, S. Shim, J. Choi, J. Yoon, Electroconductive Feed Spacer as a Tool for Biofouling Control in a Membrane System for Water Treatment, Environ. Sci. Technol. Lett. 1 (2014) 179–184. https://doi.org/10.1021/ez400206d.

[28] H. Liu, A. Vajpayee, C.D. Vecitis, Bismuth-Doped Tin Oxide-Coated Carbon Nanotube Network: Improved Anode Stability and Efficiency for Flow-Through Organic Electrooxidation, (2013). https://doi.org/10.1021/am402621v.

[29] S.G. Bratsch, Standard Electrode Potentials and Temperature Coefficients in Water at 298.15 K, J. Phys. Chem. Ref. Data. 18 (1989) 1807. https://doi.org/10.1063/1.555839.

[30] R. Piotrkowski, ACOUSTIC EMISSION TECHNIQUE TO ASSESS MICROFRACTURES OF METALIC COATINGS WITH SCRATCH-TESTS, n.d. https://www.researchgate.net/publication/237710525 (accessed April 11, 2020).

Supplementary Information

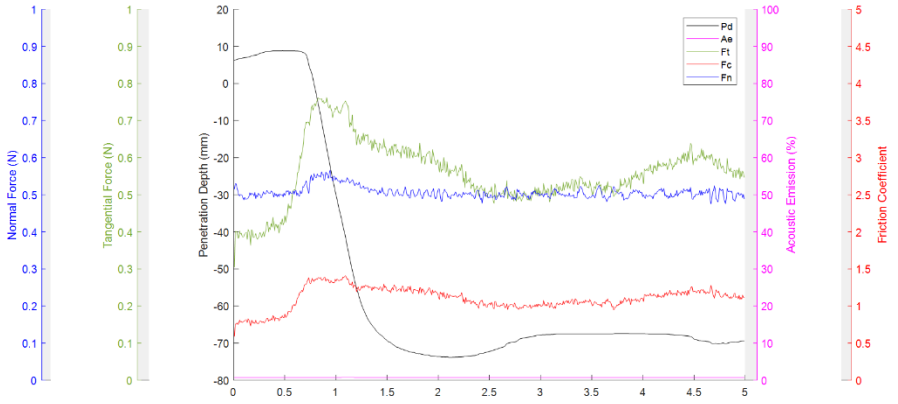

(a)

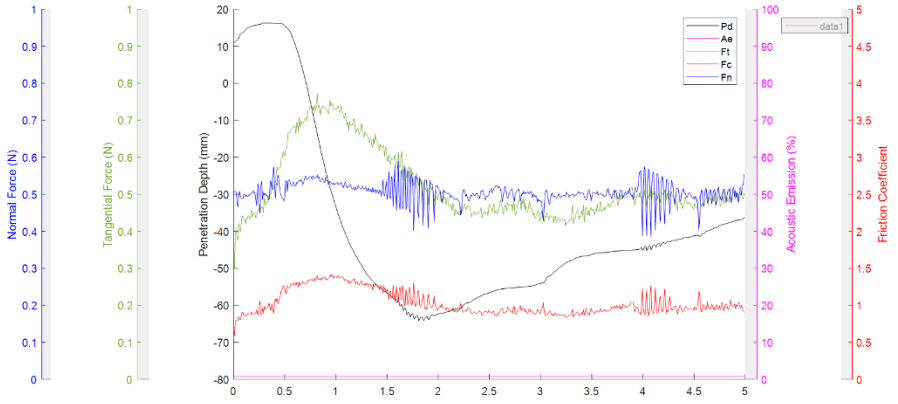

(b)

Figure S1. The mechanical stability of an ECM measured in the micro-scratch test with different input settings. The settings are as follows: (A) The tip of radius 100 µm applied a normal force of 0.5 N and the scratch length and scratch speed were 5 mm and 5 mm/min, and (B) The tip of radius 200 µm applied a normal force of 0.5 N and the scratch length and scratch speed were 5 mm and 5 mm/min, respectively.

Chapter 6

Quantifying the impact of Electrically Conductive Membrane Generated Hydrogen Peroxide and Extreme pH on the viability of Escherichia Coli Biofilms

Submitted to Environmental Science and Technology

6.1.Abstract

Electrically conductive membranes (ECMs) can induce antifouling mechanisms at their surface under certain applied electrical currents. Identifying these mechanisms is critical to enhancing ECMs' self-cleaning performance. We quantified the impact of electrochemically-induced acidic conditions, alkaline conditions, and H_2O_2 concentration on model bacteria, *Escherichia Coli*. To this end, we first quantified the electrochemical potential of CNT-based ECMs to generate stressors such as protons, hydroxyl ions, and H_2O_2, under a range of applied electrical currents (± 0 – 150 mA, 0 – 2.7 V). Next, these chemical stressors with identical magnitude to that generated at ECM surfaces were imposed on *E. Coli* cells and biofilms. In the flow-through electrically conductive membrane systems, biofilm viability using LIVE/DEAD staining indicated biofilm viability of 39 ± 9.9 %, 38 ± 4.7 %, 45 ± 5.0 %, 34 ± 3.1 %, and 75 ± 4.9 % after separate exposure to pH 3.5, anodic potential (2V), pH 11, cathodic potential (2V), and H_2O_2 concentration (188 μM). Electrical current-induced pH change at the membrane surface was shown to be more effective in reducing bacterial viability than H_2O_2 generation, and more efficient than bulk pH changes. This study identified anti-biofouling mechanisms of ECMs and provides guidance for determining the current patterns that maximize their antifouling effects.

Keywords: Electrically conductive membranes; Fouling; Water treatment; Wastewater treatment; Electrochemical reactions; Reactive membranes; Responsive membranes

6.2.Introduction

Electrically conductive membranes (ECMs) have demonstrated promising self-cleaning capabilities to control fouling , the major limitation of traditional separation processes [1–3]. An applied charge to ECMs' surfaces promotes antifouling mechanisms at the membrane-water interface. These antifouling mechanisms include electrostatic repulsion of like-charged contaminates [4], electrochemical [5] and electrocatalytic [6] reactions, and enhanced electrophoretic mobility of foulant particles [7]. Often applied as coatings to conventional polymeric membranes, ECMs:

(a) controllably target foulants at their point of adhesion at the membrane/water interface. This makes them more effective than traditional bulk solution cleaning, which often do not penetrate to the membrane surface. This also makes them more efficient than bulk cleaning methods which alter the entire bulk feed solution rather than the local surface environment.
(b) use electrons, "clean reagents", as anti-fouling mediators, making the process chemical free and easy to operate. This reduces the handling and storage costs of acids, bases, or other biocides and reduces the volume of chemical waste.
(c) can tailor their antifouling mechanisms by varying the applied electrical properties (polarity, magnitude, frequency). Therefore, the antifouling strategy can be tailored to match the foulant type.

Over the past decade, many research article have explored ECM materials and anti-fouling applications;[1–3,8]; however, the underlying anti-fouling mechanisms have not been explored to the same extent. Understanding the details of how different surface polarizations promote antifouling mechanisms will enable efficient application. The present study aims to systematically quantify the antibiofouling mechanisms of direct current applied to ECMs on model bacteria, *Escherichia Coli* (*E. Coli*). The biocidal mechanisms include extreme acidic and alkaline conditions, and hydrogen peroxide (H_2O_2) generation.

Extreme pH conditions (both high [9] and low [10]) mitigate the growth of pH-sensitive microorganisms [10,11], and can lead to biochemical modifications of cells' DNA and ATP [12], alter enzyme activities, and promote reduction-oxidation reactions inside the cell [13]. Electric fields have been shown to increase the inactivation efficiency of extreme pH [14]. Electrical fields can increase pore sizes of cell membranes, which increases the flux of protons or hydroxyl ions into the cell [14,15]. Fundamental details about the relation between pH and inactivation mechanism can be found elsewhere [15,16].

Hydrogen peroxide (H_2O_2) is used in environmental applications as a biocide as well as to enhance bioremediation. H_2O_2 is often used as an oxidizing biocide through the production of free oxygen radicals [17,18], which cause oxidative stress on biological compounds, targeting their cell physicochemical properties such as cell adhesion, leading to cell detachment and apoptosis [17,18]. In the presence of electrical fields, cells are less selective and more susceptible to the surrounding stimuli, enhancing the destructive impact of hydrogen peroxide [19]. However, H_2O_2 can also be used to enhance bacterial growth by supplying additional oxygen to aqueous systems, for example in the bioremediation of aquifers [20].

In our study, we quantified the CNT-based ECM's (CNT-ECM) electrochemical anti-biofouling mechanisms (generation of protons, hydroxyl ions, and H_2O_2) at their surface, under a range of applied electrical currents (± 0 – 150 mA (± 0 – 2.69 V)). We grew *E. Coli* on the surface of ECMs, and then compared how *E. Coli* viability was impacted by each of these products, electrochemically-generated from the ECM surface compared to added in the bulk at identical conditions. The results of batch and flow-through membrane experiments illuminated the impacts of electrochemically generated extreme local pH and H_2O_2 on E. *Coli*.

6.3.Materials and methods

6.3.1. Chemical and solutions

Carboxyl functionalized carbon nanotubes (CNT-COOH) were purchased from Cheaptubes. Ethanol and phosphate buffered saline (PBS) tablets were procured from VWR. Glutaraldehyde (GA) was purchased from Fisher Chemical. Sodium dodecyl sulfate (SDS) and hydrochloric acid were supplied by Anachemia. Poly(vinyl alcohol) (PVA) was purchased from Sigma Aldrich. Microfiltration Poly(ether sulfone) (PES) were ordered from Sterlitech. Deionized (DI) water was produced in the lab from Sartotius system. More details are found in Table S1.

6.3.2. CNT characterization

CNTs were characterized using scanning electron microscopy (SEM, JEOL JSM-7000F), transmission electron microscopy (TEM, Talos 200X), X-ray photoelectron spectroscopy (XPS, PHI Quantera II Scanning XPS Microprobe), energy-dispersive X-ray spectroscopy (EDS, Oxford Instruments X-Max^n 50 mm^2 detector), and thermogravimetric analysis (TGA, Mettler Toledo TGA/DSC 3+). Details of experimental conditions are provided in the SI and the results of TEM, SEM, XPS, EDS, and TGA are presented in Figure 6.S8 (a), Figure 6.S8 (b), Figure 6.S9, Figure 6.S10, and Figure 6.S11, respectively.

6.3.3. Membrane fabrication

The membrane fabrication method has been documented in our previous work [21,22]. In summary, a well-dispersed suspension of SWCNT/DWCNT/PVA/SDS in DI water was vacuum filtered through an MF PES membrane Following CNT deposition, the membranes were immersed in a 2.12 w/% solution of GA in DI water at 80 °C, immersed in 0.1 M HCl for 1 h, and cured in an oven for 10 min at 100 °C.

6.3.4. Electrochemical cell

The schematic and the picture of the electrochemical cell are presented in Figure 6.1a and Figure 6.S1, respectively. Five electrodes included the CNT-ECM as the working electrode (WE), graphite sheet as the counter electrode (CE), Ag/AgCl electrode (Metrohm, operating range: 0-80 °C) as the reference electrode (RE), dissolved oxygen (DO) sensor, and a benchtop pH meter. CNT-ECM, graphite sheet, and reference electrode were coupled

to a Pontentiostat (Multi Autolab M204, Metrohm). All measurements were collected simultaneously. Fixed potential chronoamperometry was used to measured electrochemically induced pH change, H_2O_2, and DO at a wide range of currents (± 20 – 150 mA (± 0 – 2.69 V) with respect to the reference electrode) for 180 min.

(a)

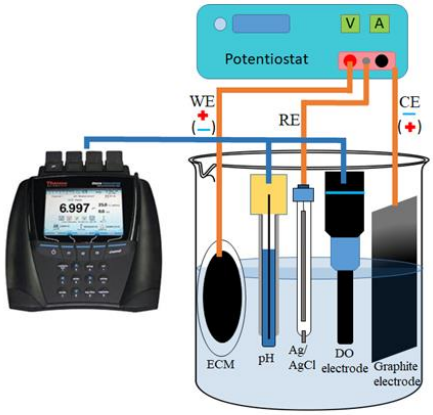

(b)

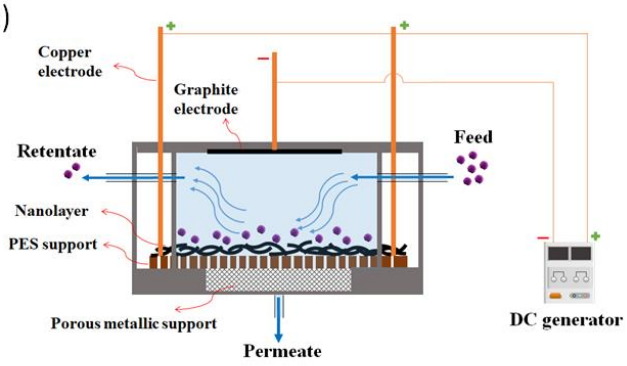

(c)

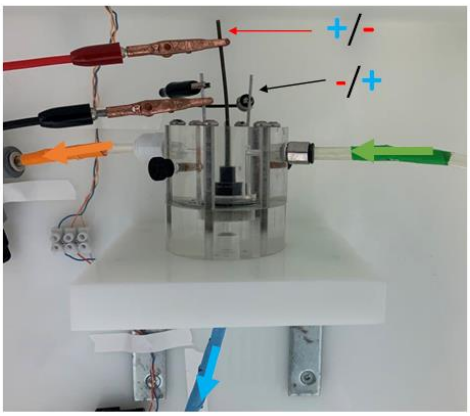

Figure 6.1. (a) Schematic of the electrochemical batch cell. Electrochemical flow-through cell: (b) Schematic, (c) Picture; green, orange, and blue colors represent feed, retentate, and permeate lines.

6.3.5. Hydrogen peroxide measurement

Hydrogen peroxide (H_2O_2) concentration in the batch test was measured using an Amplex red Hydrogen Peroxide/Peroxidase Assay Kit (Molecular Probes), with H_2O_2 as low as 50 nM. H_2O_2 concentration were measured in PBS buffer at different time steps (0, 1, 5, 10, 20, 30, 40, 50, 60, 80, 100, 120, 150, 180 min). Following probe protocols, equal volumes of sample and probe were mixed, excited at 520 ± 10 nm, fluorescence detected at 595 ± 35 nm, and quantified in comparison to a calibration curve (Figure 6.S2).

6.3.6. pH and zeta potential measurements

A universal pH indicator (HYDRION) affixed to a syringe was used to measure the pH close to the ECM surface. The pH paper was analyzed 1 min and 5 min after electrolysis to check for pH value. All readings were done in triplicate. Details of the zeta potential are found in the SI.

6.3.7. *E. Coli* suspension, treatment, and characterization

E. Coli wild-type strain, K12, was harvested in a tryptic soy broth (TSB) media. Details of bacterial growth, treatment, and characterization are found in the SI. In sum, bacteria were grown in a shaking incubator at 37 °C and 225 RPM for 20 h then diluted to 7×10^8 CFU/mL. The concentration of *E. Coli* cells (viable cells) was enumerated every hour up to 3 h by total plate count and fluorescence spectroscopy methods. In fluorescence spectroscopy, the viability of bacterial cells was measured using LIVE/DEAD® bacLight bacterial viability kit. This kit utilizes two nucleic acid strains, SYTO® 9 green-fluorescent, and propidium iodide (PI) red-fluorescent. Strained green bacteria represent the viable (live) bacteria, while stained red cells represent damaged (dead) bacteria. Samples were exited with $OD_{485 \pm 20}$, emission wavelengths were measured at 535 ± 25 nm and 635 ± 35 nm to label the green (live) and red (dead) cells, respectively, and compared to a calibration curve (Figure 6.S4) for quantification.

6.3.8. Biofilm formation and treatment in a flow cell

In our setup (Figure 6.1 (b) and Figure 6.S5), the feed was dosed with freshly harvested *E. Coli* suspension to reach a final concentration of 7×10^8 CFU/mL. Bio-suspension was filtered through the membrane for 18 h under a constant pressure of 10 psi (0.69 bar). The rejection of the bacteria was calculated by recording the absorbance value of feed and collected permeate (at OD_{600}) over the filtration period. A calibration curve was generated (Figure 6.S6) and the rejection was calculated using the following equation:

$$Rej. = \left(1 - {C_p}/{C_f}\right) \times 100$$

where C_p and C_f represent the concentration of bacteria in the permeate and feed, respectively.

Biofilms were then treated with different antifouling stressors such as low pH (3.5), high pH (11), and H_2O_2 (188 µM) either in-situ or externally for 3 h. We used HCl and NaOH to adjust the pH externally. To provide identical in-situ oxidation conditions, open circuit potential (OCP), constant potentials of +2 V, and constant potential of -2 V between working (CNT-ECM) and counter electrode (graphite sheet) were applied to ECMs for 3 h by an external power generator operating in direct current (DC) mode. More details are found in the SI.

6.3.9. Biofilm characterization

The morphology of biofilm was observed using scanning electron microscopy (SEM, JEOL JSM-7000F). The biofilm was stained with LIVE/DEAD® bacLight bacterial viability kit (3 µL SYTO® 9 strain and 3 µL PI strain) and analyzed using confocal laser scanning microscopy (CLSM). Live cells, dead cells, and the viability ratio of biofilm were quantified using ImageJ software, determining the relative abundance of red and green pixels in the digital image. Therefore, the percentage of green pixels and red pixels were assumed as the ratio of live cells and dead cells, respectively. More details are found in the SI.

6.4.Results and discussion

The electrochemical properties of CNT-based electrically conductive membranes (ECMs), such as their ability to generate H_2O_2, protons, and hydroxyl ions, were quantified under application of electrical current. The oxidative properties of the ECMs were then used to inactivate mature *E. Coli* in a batch test.

In a flow-through system, HCl, NaOH, or H_2O_2 were added to bulk solutions containing fully developed *E. Coli* biofilms in amounts that produced identical conditions of pH or H_2O_2 levels generated from ECMs, and compared with ECMs operated as cathode or anode membranes. In each case, cell viability analyses were supported by confocal laser scanning microscopy (CLSM) and scanning electron microscopy (SEM) imaging.

6.4.1. Electrochemical characteristics of the CNT-based electrode

Surface hydrogen peroxide production

Carbonaceous materials such as CNT and graphite are capable of producing hydrogen peroxide (H_2O_2) in-situ under the application of current. We used cyclic voltammetry and fixed current chronoamperometry to identify the current range suitable for H_2O_2 generation from the ECMs. As shown in Figure 6.2 (a), the onset of H_2O_2 production was observed at -19 – -25 mA when the current decreased to a plateau state.

We quantified the concentration of electrochemically-generated H_2O_2 by applying a wide range of electrical currents; -20 mA, -50 mA, -100 mA, and -150 mA, which corresponded to 1.66 V, 2.09 V, 2.45 V, and 2.69 V. The steady state H_2O_2 concentrations were calculated at each current, (Figure 6.2 (b)), and the maximum H_2O_2 concentration of 31.19 μM was measured at 50 mA, with higher applied currents producing less H_2O_2. Steady state H_2O_2 production occurred within 30 minutes as supported by our H_2O_2 concentration calculations, shown in Figure 6.S12. In contrast, the maximum theoretical concentration of H_2O_2 at 50 mA was calculated to be 188 μM (eq S4). The concentration of H_2O_2 measured at the bulk might be different from the local concentration of H_2O_2 at

the surface as H_2O_2 is surface-induced, its transport to the bulk is diffusion limited, and H_2O_2 can decompose (eq. S2 and eq. S3) over time.

The dominant H_2O_2 production pathway is the $2e^-$ oxygen reduction reaction of oxygen at cathodic surfaces and occurs over a wide range of potentials from 65 mV to 1000 mV in different acidic and alkaline conditions [20,23,24].

$$O_2(g) + 2H^+ + 2e^- \rightarrow H_2O_2 \quad (1)$$

At higher current, $4e^-$ reduction of oxygen occurs, which produces water instead of H_2O_2. At low current (-20 mA (1.66 V)), H_2O_2 was produced but did not saturate the ECM surface and at a higher current (-50 mA (2.09 V)), more H_2O_2 was produced (Figure 6.2 (a), Zone I). Dissolved oxygen diffusion to the surface is the rate-limiting step for H_2O_2 production in this current range [25]. At higher currents above 50 mA (Figure 6.2 (a), zone II), H_2O_2 generation reduced because (a) the $4e^-$ reduction reaction dominated converting oxygen to water and (b) oxygen was depleted at the surface (more details are found in the Section S2 of the SI).

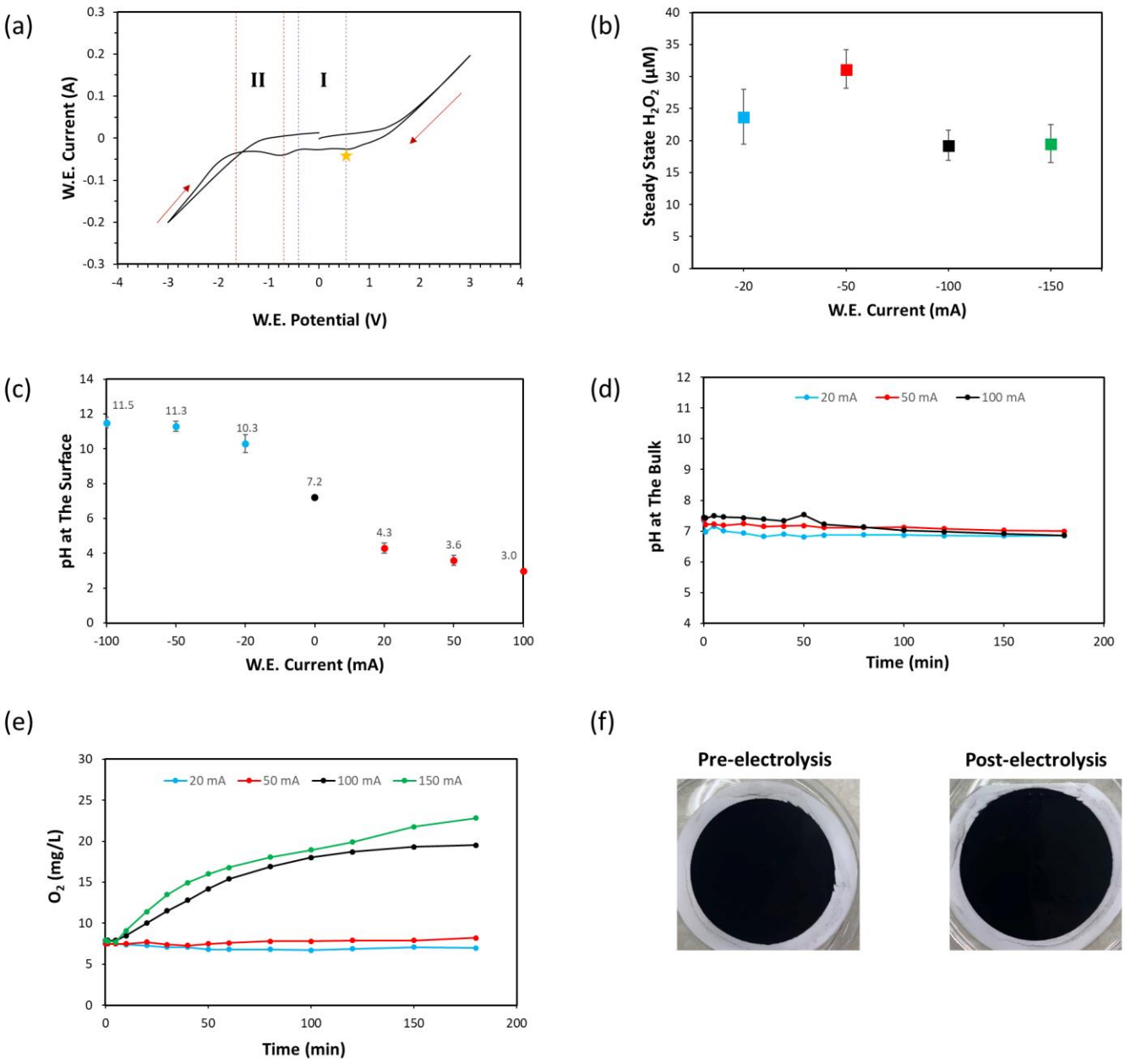

Figure 6.2. (a) Cyclic voltammetry for CNT-ECM. The conductive ECM, graphite sheet, and an Ag/AgCl electrode were used as the working electrode, counter electrode, and reference electrode, respectively. The scan range was -3 V to +3 V at a scan rate of 0.1 mVs-1. Red arrows show applied current direction and the star indicates the onset of hydrogen peroxide generation , (b) Steady state H2O2 measured at the bulk of the electrochemical cell under different applied negative currents (20 – 150 mA, 1.66 – 2.69 V) over 180 min, Blue, red, black, and green colors represent 20 mA, 50 mA, 100 mA, and

150 mA, respectively, (c) Steady state pH measured at the surface of the CNT-ECM under different applied electrical currents (± 20 – 100 mA, 1.66 – 2.45 V), (d) pH measured at the bulk of the electrochemical cell under different applied negative currents (20 – 100 mA, 1.66 – 2.45 V) over 180 min, (e) Dissolved oxygen measured in the bulk of the electrochemical cell under different applied negative currents (20 – 150 mA, 1.66 – 2.69 V) over 180 min, (f) CNT-ECM before and after electrolysis working as a cathode under 150 mA (2.69 V) for 180 min. ECMs contain 1 mg CNT. Error bars represent the standard deviation for three data points.

Surface pH change

Electrically conductive surfaces are able to alter the local pH in-situ. We polarized the ECMs at a wide range of electrical currents (-100 – 100 mA, -2.45 – 2.21 V) and measured the change in surface pH (Figure 6.2 (c)), which ranged from 11.5 to 3.0, representing a change of over 4 orders of magnitude in hydroxyl and proton concentrations, respectively. Electrochemical water splitting promoted by surface polarization encourages reactions primarily responsible for pH changes. Under cathodic polarization, water is directly reduced to hydroxyl ions and hydrogen gas (eq 2), while under anodic polarization, water is oxidized to protons and oxygen gas (eq 3).

$$2H_2O + 2e^- \rightarrow 2OH^- + H_2 \quad (2)$$

$$2H_2O \rightarrow O_2 + 4H^+ + 4e^- \quad (3)$$

The variations in the system bulk pH were monitored over 3 h under the application of different electrical currents and was shown to be stable (Figure 6.2 (d) and Figure 6.S15). Evidently local changes were not sufficient to produce bulk pH changes, and anode and cathode reactions tend to neutralize in the bulk.

Other surface properties of CNT-based ECM

The concentration of DO under application of cathodic currents (-20 mA – -150 mA, 1.66 – 2.69 V) is shown in Figure 6.2 (e). Findings indicate that at lower currents (-20 mA (1.66 V) and 50 mA (2.09) V)), the DO concentration in the solution remains stable over 3 h of electrolysis, while at higher currents (100 mA (2.45 V) and 150 mA (2.69 V)) the concentration of oxygen increases likely due to generation of excess oxygen micro-

bubbles at the anode. The DO concentration is expected to be substantially lower at the ECM surface, where oxygen is quickly consumed in surface redox reactions (eq 1 and eq S1) in contrast to the bulk electrolyte [25].

The potential of the working electrode was monitored under the application of fixed current chronoamperometry over 3 h (Figure 6.S16). Cathodic surfaces demonstrated electrochemical stability over 3 h of electrolysis, supported by their observed physical stability, as shown in Figure 6.2 (f).

6.4.2. *E. Coli* cell viability in batch

Harsh physical and chemical environmental conditions challenge the survival of many microorganisms [26,27]. As such, strong external stimuli, including acidic and alkaline solutions, as well as high concentrations of hydrogen peroxide (H_2O_2) may limit/stop the growth of bacteria [9–11]. We assessed the cell viability of *E. Coli* as model bacteria under exposure to acidic (pH 3, pH 4, and pH 5) and alkaline solutions (pH 10, pH 11, and pH 12), and H_2O_2 (0 – 188 μM) at concentrations that matched those generated from CNT-ECMs under applied potentials in Section 3.1.

Cell culturability using plate counting method

The results of cell culturability in the batch test using the plate counting method are presented in Figure 6.3 and Figure 6.S18. The plate counting method reveals if cells are culturable under nutrient conditions after exposure to different stressors. Cell culturability as a property of a community of bacteria has been validated elsewhere [28]. Findings suggest that acidic environments (pH 3 – 5) have a more substantial biocidal impact on *E. Coli* as compared to alkaline conditions (pH 10 – 12). The culturability of *E. Coli* cells was reduced by 56%, 47%, and 36% at pH 3, pH 4, and pH 5 on average, respectively, while their culturability decreased by 18%, 26%, and 27% at pH 10, pH 11, and pH 12 on average, respectively. Biostatic and biocidal activities of acidic solutions on *E. Coli* have been reported in other research studies [10]. Inactivation of biological cells in acidic conditions is caused by proton influx to the cell and protonation of weak organic acids on the cell

membrane causing damage to DNA and ATP within the cell [12,14,29,30], and modification to enzyme activities [13]. Alkaline solutions have also been reported to cause bacterial inactivation [9,11,31]. Exposure of bacteria to extreme alkaline media destroys the cell membrane and damages the structural integrity of peptidoglycan layer. Accordingly, leakage of cell components, solubilization of proteins, or saponification of lipids promote alkaline pH hemostasis [32,33]. The inactivation of bacteria is not correlated to the type of cation or anion associated with base or acid [10,31].

H_2O_2 exposure had less of an impact on *E. Coli* culturability than extreme pH exposure as shown in Figure 6.3, demonstrating that H_2O_2 has little added impact to pH. Findings in Figure 6.3 suggest that H_2O_2 has minimal biocidal impact in acidic conditions, while in extreme alkaline conditions of pH 12 there was moderate decrease in culturability; concentrations of 33 μM and 188 μM caused 17% and 31% more inactivation as compared to control experiment without H_2O_2. H_2O_2 causes oxidative stress on microorganisms, through radical oxygen species generation, which damages cell components such as DNA, proteins, and lipids, in turn leading to mutagenesis and cell death [34]. The self-decomposition of H_2O_2 has been reported in the literature [20], however, the decomposition rate is expected to be insignificant under the temperature (25 °C) and relatively short reaction time (3 h) used in our study [20].

The low biocidal impact of H_2O_2 on *E. Coli* can be explained by intrinsic regulatory responses of biological cells to the externally-induced oxidative stress. Exposure of *E. Coli* to H_2O_2 triggers the expression of genes that encode DNA repair enzymes, in turn protecting cell from oxidative stress [34]. In addition, two critical genes in *E. Coli*, *soxRS* and *oxyR*, regulate the expression of H_2O_2 scavenging proteins [34]. Other defensive mechanisms of *E. Coli* in response to H_2O_2 have been discussed elsewhere [35–37]. Interestingly, low dosages of H_2O_2 (μM) have been shown more lethal to *E. Coli* as compared to higher dosages (mM), which may be related either to exposure time or to the activation of cells' defense mechanism at higher H_2O_2 concentration gradients [36,37].

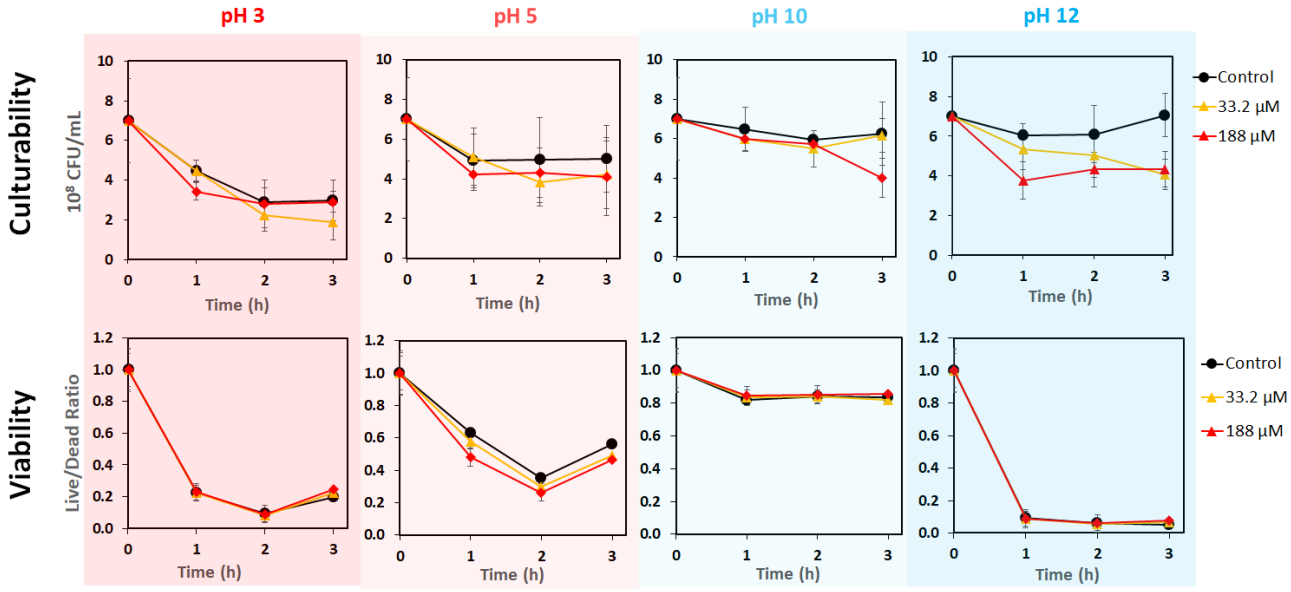

Figure 6.3. (Top row) Cell culturability of E. Coli after exposure to different pH values (3, 5, 10, and 12) and different H2O2concentrations (0, 33.2, and 188 µM). Error bars represent the standard deviation for four data points. (Bottom row) Cell viability of E. Coli using LIVE/DEAD staining method after exposure to different pH values (3, 5, 10, and 12) and different H2O2 concentrations (0, 33.2 and 188 µM). Error bars represent standard deviation for six data points.

Cell viability using LIVE/DEAD staining method

Bacterial viability was assessed by the established LIVE/DEAD staining of nucleic acids, in which 'dead' cells indicated cellular damage sufficient for the penetration of propidium iodide (PI), a red-fluorescent dye (670 Da). The viability of *E. Coli* cells dropped by 81%, 58%, and 54% at pH 3, pH 4, and pH 5 on average, respectively, while the viability dropped by 25%, 87%, and 98% at pH 10, pH 11, and pH 12 on average, respectively (Figure 6.3). A comparison between Section 3.2.1. and Section 3.2.2 indicates that the percentage of dead bacteria measured in the plate counting method is smaller than the inactivated percentage quantified by the LIVE/DEAD staining method. This suggests that bacteria with damaged membranes can repair themselves and continue to grow within the nutrient-rich environment of agar plates, as observed in other studies [38]. It is clear that H_2O_2 had only a minor damaging effect on bacterial membranes, while H_2O_2 showed a

slightly higher impact on the culturability of bacteria, likely due to its oxidative impact on DNA and ATP. Overall, the impact of H_2O_2 on bacterial viability and cellular integrity was insignificant compared to that of extreme pH.

6.4.3. *E. Coli* cell and biofilm integrity on flow-through membranes

CNT-ECMs were used as membranes to induce antibiofouling mechanisms (H_2O_2, low pH, high pH) on established *E. Coli* biofilms. In-situ, antifouling mechanisms were either generated electrochemically at the ECM surface, or through modifications of the feed solution using identical oxidative conditions as determined above. The main goal was to evaluate the impact of electrically-induced low-pH, high-pH, and H_2O_2 on *mature* biofilms. Therefore, long filtration periods (18 h) on UF membranes with rejection efficiency higher than 90% (Figure 6.S19) allowed for formation of mature and thick biofilms (Figure 6.S7).

Individual bacteria and young biofilms are more susceptible to the impacts of electrical currents as compared with mature biofilms. For example, electric fields can electrostatically repel charged bacteria, create suboxic surface conditions that suppress biofilm development, and reduce the ability of young biofilms to express extracellular polymeric substances (EPS) [19], which makes them more susceptible to cell lysis and cellular inactivation. In this study, mature biofilms were established on membranes prior to electrochemical exposure to identify biofilm inactivation mechanisms separate from the effects on cells and the early stages of biofilm development.

Viability of biofilm under no stimuli

All biofilms were recovered and characterized through CLSM and SEM as indicated in Figure 6.4 and Figure 6.5, respectively The viability of the control biofilm (no stimuli) is presented in Figure 6.4 (a) and their quantification using ImageJ in Figure 6.4 (b). As shown, almost the entire biofilm on the membrane was found viable (89 ± 4.4 %) after 21 h of filtration. The minor reduction in cellular viability (~10%) can be attributed to the prolonged starvation of bacteria in a non-nutrient condition (PBS buffer) [39]. SEM

images further support the viability of the biofilm in the control condition as the bacteria maintained their regular shape and formed a thick biofilm.

Impact of H_2O_2 on biofilm viability

Biofilms were exposed to H_2O_2 at a bulk concentration of 188 μM, equal to the maximum theoretical H_2O_2 concentration that CNT-ECMs could generate under cathodic potentials (2 V), (details, Section 3.1). As shown in Figure 6.4, the viability of *E. Coli* biofilms under H_2O_2 exposure was 75 ± 4.9 %, 14% lower than controls. SEM images show a thick and uniform biofilm after exposure to H_2O_2 (Figure 6.5). The research literature contains contradictory reports of both successful H_2O_2- bacterial inactivation [17,40–44] and ineffectiveness [19,23,45–47]. Discrepancies among research studies on H_2O_2 inactivation on membrane biofouling may stem from differences in operating conditions (pH, flow rate, operational window (exposure time)), flow configuration (crossflow, flow-through), biofilm condition (maturity, thickness), and local measurement uncertainties. These parameters effect the local oxygen level, and thus the growth of the bacteria in the biofilm. Therefore, bulk H_2O_2 concentration alone cannot be relied upon to demonstrate the biocidal impact of its oxidative stress on biofilms. In general, H_2O_2 can be sensed by the bacteria in extremely low concentrations (<1 μM) regulating their cellular pathways. For instance, it has been shown that exposure of *E. Coli* to low dosages of H_2O_2 influences the expression of 39 genes related to cellular respiration, energy metabolisms, and adhesion properties [40,48,49]. In our study, the impact of hydrogen peroxide was found to be insignificant due to the maturity of the film and short window of exposure (3 h).

Impact of high pH on biofilm viability

The viability of biofilms under harsh alkaline conditions was evaluated by adjusting the feed pH to 11 using NaOH. Quantitative analysis on CLSM images indicates biofilm viability of 45 ± 5.0 %. Research evidence has demonstrated the susceptibility of microorganisms to alkaline conditions [9,11,31]. Although, the bacteria seem to maintain their shape under externally-induced alkaline conditions (Figure 6.5).

E. Coli biofilms were grown on ECMs during filtration of bacterial solutions and subsequently H_2O_2 and alkaline conditions were electrochemically-generated at the membrane surface in-situ under cathodic polarization. Cathodic potential equal to 2 V is able to generate a high local pH (11.3) and a maximum theoretical concentration of 188 µM, as discussed previously. The findings in Figure 6.4 indicate biofilm viability of $34 \pm 3.1\,\%$, suggesting biofilm inactivation by synergistic impacts of H_2O_2 and high pH triggered by cathodic polarization. The non-viable ratio under cathodic current was statistically higher than that obtained with extreme pH dosed into the bulk feed solution, and substantially higher (by ~41%) than the non-viable ratios observed from exposure to high H_2O_2 concentration. The deformation of bacterial morphology under cathodic stress is presented by SEM images (Figure 6.5).

Generation of endogenous reactive oxygen species (ROS) under application of electrical current can further contribute to bacterial inactivation in addition to the deleterious impacts of high local pH and H_2O_2 [50]. Generation of excess ROS has been reported at potentials above 0.3 V [19].

Impact of low pH on biofilm viability

Biofilms were also challenged with low pH conditions (pH 3.5) by externally dosing the feed with HCl during membrane filtration of bacterial solutions. The CLSM and quantitative analysis revealed biofilm viability of $39 \pm 9.9\,\%$. A comparison between *E. Coli* culturability in the batch ($44 \pm 3.5\,\%$) and flow-through system ($39 \pm 9.9\,\%$) indicate a similar response of *E. Coli* to acid treatment in batch and flow-through systems. SEM images further demonstrated the oxidation of bacteria under acidic conditions. As shown in Figure 6.5, bacterial cells experienced deformation and shape irregularities under external harsh acidic conditions. The impacts of low-pH environments on microorganisms were explained in Section 3.2.

Identical low-pH conditions were introduced to the biofilms under anodic polarization. As suggested in Section 3.1, potentials equal to 2.09 V (50 mA) can shift the local pH down to as low as 3.6. After exposing the biofilm to 2 V anodic potential, $38 \pm$

4.7 % of the biofilm was found live (Figure 6.4 (b)), statistically similar to the viable ratio that was measured under bulk solution acid treatment. Several methods of bacterial inactivation are available to anodic surfaces. The generation of extreme low-pH conditions has been discussed above. In addition anodic currents can inactivate microorganisms via oxidation through direct electron transfer [51]. The abundance of chloride ions in proximity to the anodic surface could generate reactive chlorine species (~22 mM chlorate) [52], well-known biocides [53]. Therefore, the anodic current was expected to result in more inactivation as compared to acid treatment due to synergistic effects of low-pH, direct electron transfer, and radical transfer. Despite the strong inactivation, we assume that the applied surface current decreased over the course of the filtration experiment due to CNT-ECM oxidative instability under anodic potentials. This led to lower surface activity over time, including a gradually increasing pH above 3.6 and less direct oxidation. The oxidation state of similar ECMs under anodic current has been shown in our previous manuscript [38]. The in-depth mechanism of bacterial inactivation under anodic current is out of the scope of this study but in sum, anodic currents (700 – 740 mA) [19,54] can oxidize coenzyme A (CoA), a vital enzyme for bacterial respiration [55] and cell viability [19].

SEM images (Figure 6.5) show that anodic current led to deformation and irregularity of the bacterial cells. The deformation process begins with small pores appearing on the cell wall (red square in Figure 6.5). Electrically-induced pores evolve into advanced cellular deformation (Figure 6.S20 (b)).

(a)

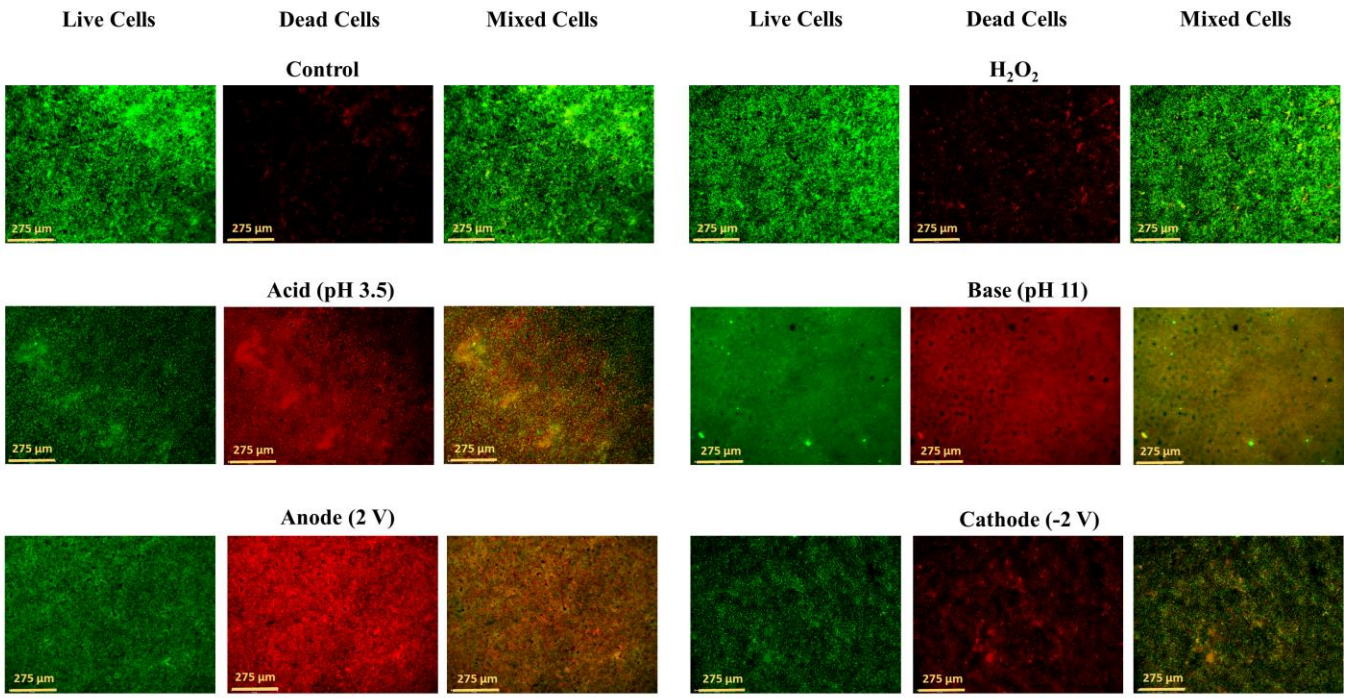
Live Cells
Dead Cells
Mixed Cells
Live Cells
Dead Cells
Mixed Cells
Control
H_2O_2
Acid (pH 3.5)
Base (pH 11)
Anode (2 V)
Cathode (-2 V)
275 µm

(b)

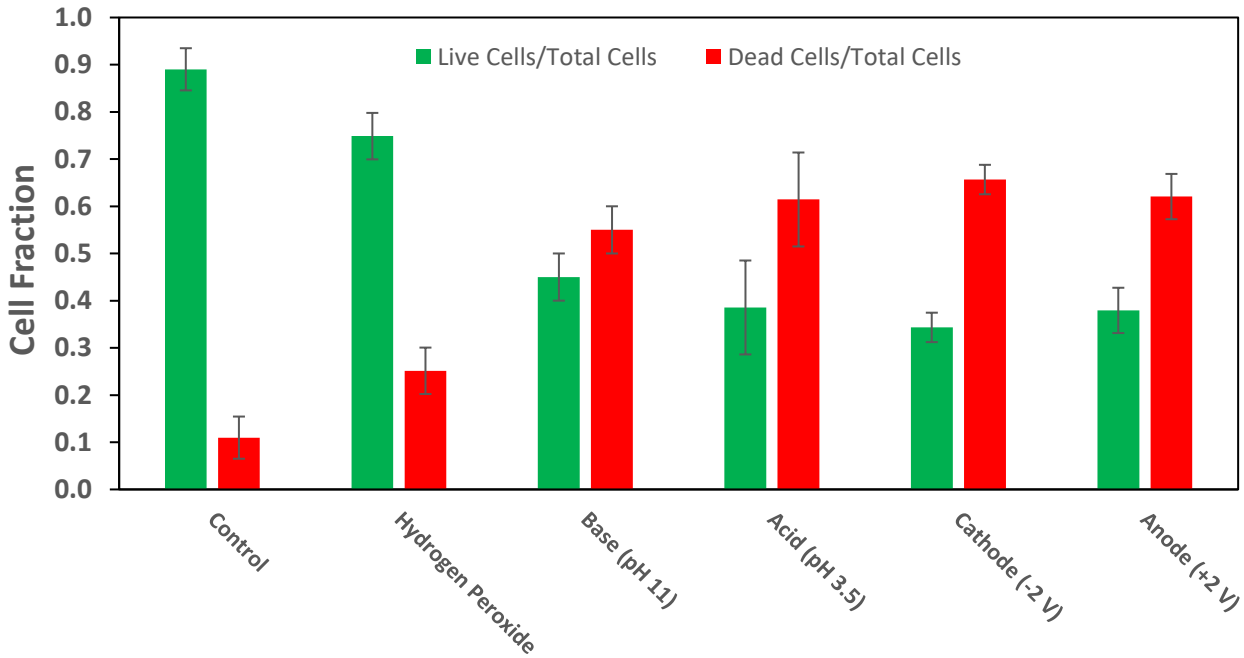
Live Cells/Total Cells
Dead Cells/Total Cells
Cell Fraction
1.0
0.9
0.8
0.7
0.6
0.5
0.4
0.3
0.2
0.1
0.0
Control
Hydrogen Peroxide
Base (pH 11)
Acid (pH 3.5)
Cathode (-2 V)
Anode (+2 V)

Figure 6.4. (a) Confocal laser scanning microscopy images, and (b) Quantitative cell count analysis of Treated E. Coli biofilms under different stimuli including the following conditions: control, H2O2 (188 µM), NaOH (pH 11), HCl (pH 3.5), cathodic potential (2 V), and anodic potential (2 V). Error bars represent the standard deviation for four samples.

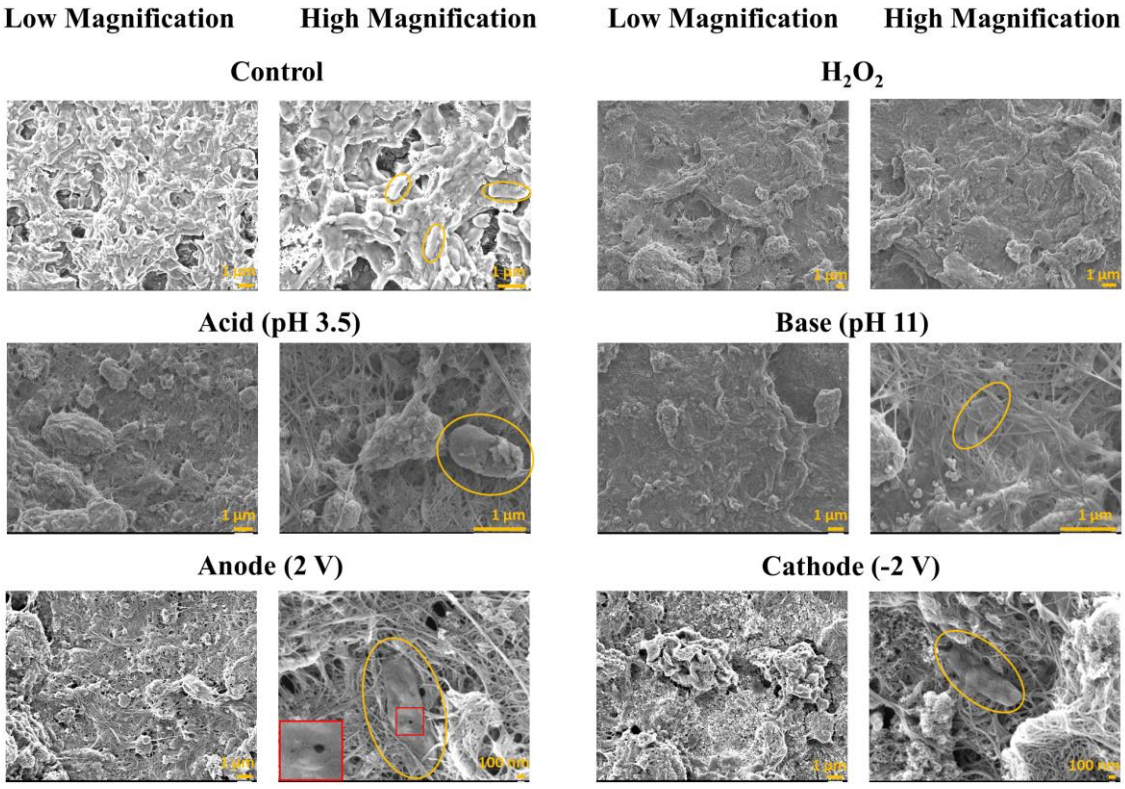

Figure 6.5. Scanning electron microscopy images of treated E. Coli biofilm under different stimuli including control condition, H2O2 (188 µM), low pH (3.5), high pH (11), anodic potential (2 V), and cathodic potential (2 V). Yellow ovals highlight representative bacteria at the surface.

6.5. Outlook

Conventional antibiofouling methods use bulk chemical dosing to treat biofilms and other foulants, while ECMs generate their own oxidizing agents to inactivate bacteria, and target foulants at their point of adhesion. Researchers using ECMs for anti-fouling studies use a variety of applied current patterns to achieve anti-fouling results, but little research has been done to identify the mechanisms involved and thereby the optimally efficient current patterns to use. This is critical to reduce energy consumption, optimally target specific foulants, and minimize oxidative membrane damage.

Here, we investigated individual electrochemically generated products that could impact mature biofilms (low pH, high pH, and H_2O_2) and demonstrated that cathodic and anodic potentials applied to ECMs were more effective in treating biofilms and inactivating bacteria than adjusting bulk solution pH to pH values measured at ECM surfaces. One of the significant hurdles in adopting ECMs in established separation processes is their additional material cost, manufacturing complications, module design, and their electrical energy consumption. ECMs have been made from carbonaceous nanomaterial [22], metals [56], metal oxides [57], and conductive polymers [58]. Carbonaceous nanomaterials account for 60% of the total ECMs reported in the literature. Our cost analysis based on the CNT-ECMs used in this study indicate that coating a porous UF polymeric support (PES) with functionalized multi-walled CNTs to a surface coating thickness of 1 μm would cost \$2.88/m^2, equal to 0.4% in total material cost. Manufacturing methods are currently only appropriate for lab-scale development, although recent hollow fiber coating techniques by our lab [59] and others [60] indicate some promise for scalable techniques. Module designs have been proposed but are still lacking.

The specific energy consumption (SEC, kWh/m^3) can be calculated using the following equation:

$$SEC = \frac{UIt}{V}$$

Where U is the electrical potential applied (V), I is the current across the membrane (A), t is the operation time (h), and V is the filtration volume (m^3). The additional energy consumption for a typical UF ECMs is about 0.01-0.0015 kWh/m^3 (see Table S3 for more details). This additional energy consumption by the ECM is equal to 5%, 2%, 2%, and 0.2% of the total energy demand for a pressurized MF/UF system, immersed MBR, standard reverse osmosis system (with feed TSS<1000 ppm), and seawater desalination system, respectively.

It should be noted that traditional separation processes require large doses of chemicals (~30 L/m^3) [61,62], biocides, oxidants, and antiscalants to mitigate fouling,

while ECMs minimize the need for such large chemical consumptions by offering antifouling performance and self-cleaning surfaces. Hence, it is anticipated that ECMs will reduce the costs associated with chemical purchasing, transportation, handling and safety [63]. In addition, using electrical current only during intermittent cleaning periods has shown promise in permeate recovery, which can drastically reduce the energy consumption.

6.6.Acknowledgements

The authors acknowledge funding from Natural Sciences and Engineering Research Council of Canada-Collaborative Research and Development (NSERC-CRD), NSERC Discovery, Pall Water and Trojan Technologies. The authors would like to acknowledge Canadian Centre for Electron Microscopy (CCEM) and Biointerfaces Institute (BI). We would like to thank Arndt Nottrott (Pall Water), Erick Cornfoot (Pall Water), and Dr. Siva Sarathy (Trojan Technologies) for their generous help and support.

6.7.References

[1] F. Ahmed, B.S. Lalia, V. Kochkodan, R. Hashaikeh, Electrically conductive polymeric membranes for fouling prevention and detection: A review, Desalination. 391 (2016) 1–15. https://doi.org/10.1016/J.DESAL.2016.01.030.

[2] A. Ronen, S.L. Walker, D. Jassby, Electroconductive and electroresponsive membranes for water treatment, Rev. Chem. Eng. 32 (2016) 533–550. https://doi.org/10.1515/revce-2015-0060.

[3] P. Formoso, E. Pantuso, G. De Filpo, F. Nicoletta, Electro-Conductive Membranes for Permeation Enhancement and Fouling Mitigation: A Short Review, Membranes (Basel). 7 (2017) 39. https://doi.org/10.3390/membranes7030039.

[4] C. Thamaraiselvan, A. Ronen, S. Lerman, M. Balaish, Y. Ein-Eli, C.G. Dosoretz, Low voltage electric potential as a driving force to hinder biofouling in self-supporting carbon nanotube membranes, Water Res. 129 (2018) 143–153. https://doi.org/10.1016/j.watres.2017.11.004.

[5] P. Held, An Introduction to Reactive Oxygen Species Measurement of ROS in Cells, 2015. www.biotek.com (accessed July 22, 2020).

[6] A.J. Sutherland, M.X. Ruiz-Caldas, C.F. de Lannoy, Electro-catalytic microfiltration membranes electrochemically degrade azo dyes in solution, J. Memb. Sci. 611 (2020) 118335. https://doi.org/10.1016/j.memsci.2020.118335.

[7] A.T. Poortinga, J. Smit, H.C. van der Mei, H.J. Busscher, Electric field induced desorption of bacteria from a conditioning film covered substratum, Biotechnol. Bioeng. 76 (2001) 395–399. https://doi.org/10.1002/bit.10129.

[8] W. Hu, S. Chen, Z. Yang, L. Liu, H. Wang, Flexible electrically conductive nanocomposite membrane based on bacterial cellulose and polyaniline, J. Phys. Chem. B. 115 (2011) 8453–8457.

https://doi.org/10.1021/jp204422v.

[9] R.E. Speece, The pH tolerance of anaerobic digestion, 1971. https://www.researchgate.net/publication/308396454 (accessed June 30, 2020).

[10] R.S. Tanner, S.A. James, Rapid bactericidal effect of low pH against Pseudomonas aeruginosa, 1992. https://doi.org/10.1007/BF01569771.

[11] M. Kästner, M. Breuer-Jammali, B. Mahro, Impact of inoculation protocols, salinity, and pH on the degradation of polycyclic aromatic hydrocarbons (PAHs) and survival of PAH-degrading bacteria introduced into soil, Appl. Environ. Microbiol. 64 (1998) 359–362. https://doi.org/10.1128/aem.64.1.359-362.1998.

[12] P.M. Wiggins, Cellular functions of a cell in a metastable equilibrium state, J. Theor. Biol. 52 (1975) 99–111. https://doi.org/10.1016/0022-5193(75)90042-9.

[13] S.E. Gilliland, M.L. Speck, Mechanism of the Bactericidal Action Produced by Electrohydraulic Shock, Appl. Environ. Microbiol. 15 (1967).

[14] R.A.H. Timmermans, M.N. Nierop Groot, A.L. Nederhoff, M.A.J.S. van Boekel, A.M. Matser, H.C. Mastwijk, Pulsed electric field processing of different fruit juices: Impact of pH and temperature on inactivation of spoilage and pathogenic micro-organisms, Int. J. Food Microbiol. 173 (2014) 105–111. https://doi.org/10.1016/j.ijfoodmicro.2013.12.022.

[15] D. García, N. Gómez, J. Raso, R. Pagán, Bacterial resistance after pulsed electric fields depending on the treatment medium pH, Innov. Food Sci. Emerg. Technol. 6 (2005) 388–395. https://doi.org/10.1016/j.ifset.2005.04.003.

[16] G. Saldaña, E. Puértolas, S. Condón, I. Álvarez, J. Raso, Modeling inactivation kinetics and occurrence of sublethal injury of a pulsed electric field-resistant strain of Escherichia coli and Salmonella Typhimurium in media of different pH, Innov. Food Sci. Emerg. Technol. 11 (2010) 290–298. https://doi.org/10.1016/j.ifset.2010.01.003.

[17] A. Hegde, G. Bhat, S. Mallya, Effect of exposure to hydrogen peroxide on the virulence of Escherichia coli, (2008).

[18] A. Mai-Prochnow, P. Lucas-Elio, S. Egan, T. Thomas, J.S. Webb, A. Sanchez-Amat, S. Kjelleberg, Hydrogen peroxide linked to lysine oxidase activity facilitates biofilm differentiation and dispersal in several gram-negative bacteria, J. Bacteriol. 190 (2008) 5493–5501. https://doi.org/10.1128/JB.00549-08.

[19] S. Pandit, S. Shanbhag, M. Mauter, Y. Oren, M. Herzberg, Influence of Electric Fields on Biofouling of Carbonaceous Electrodes, (2017). https://doi.org/10.1021/acs.est.6b06339.

[20] Z. Qiang, J.H. Chang, C.P. Huang, Electrochemical generation of hydrogen peroxide from dissolved oxygen in acidic solutions, Water Res. 36 (2002) 85–94. https://doi.org/10.1016/S0043-1354(01)00235-4.

[21] M.A. Halali, C.-F. de Lannoy, The Effect of Cross-Linkers on the Permeability of Electrically Conductive Membranes, Ind. Eng. Chem. Res. 58 (2019) 3832–3844. https://doi.org/10.1021/acs.iecr.8b05691.

[22] M.A. Halali, M. Larocque, C.F. de Lannoy, Investigating the stability of electrically conductive membranes, J. Memb. Sci. 627 (2021) 119181. https://doi.org/10.1016/j.memsci.2021.119181.

[23] O. Istanbullu, J. Babauta, H. Duc Nguyen, H. Beyenal, Electrochemical biofilm control: mechanism of action, Biofouling. 28 (2012) 769–778. https://doi.org/10.1080/08927014.2012.707651.

[24] G. Gao, Q. Zhang, Z. Hao, C.D. Vecitis, Carbon nanotube membrane stack for flow-through sequential regenerative electro-Fenton, Environ. Sci. Technol. 49 (2015) 2375–2383. https://doi.org/10.1021/es505679e.

[25] J.T. Babauta, H.D. Nguyen, O. Istanbullu, H. Beyenal, Microscale gradients of oxygen, hydrogen peroxide, and pH in freshwater cathodic biofilms, ChemSusChem. 6 (2013) 1252–1261. https://doi.org/10.1002/cssc.201300019.

[26] A. Sharma, Y. Kawarabayasi, T. Satyanarayana, Acidophilic bacteria and archaea: Acid stable biocatalysts and their potential applications, Extremophiles. 16 (2012) 1–19. https://doi.org/10.1007/s00792-011-0402-3.

[27] H. Vega-Mercado, U.R. Pothakamury, F.J. Chang, G. V. Barbosa-Cánovas, B.G. Swanson, Inactivation of Escherichia coli by combining pH, ionic strength and pulsed electric fields hurdles, Food Res. Int. 29 (1996) 117–121. https://doi.org/10.1016/0963-9969(96)00015-4.

[28] M.R. Barer, C.R. Harwood, Bacterial viability and culturability, Adv. Microb. Physiol. 41 (1999) 93–137. https://doi.org/10.1016/s0065-2911(08)60166-6.

[29] H. Vega-Mercado, U.R. Pothakamury, F.J. Chang, G. V. Barbosa-Cánovas, B.G. Swanson, Inactivation of Escherichia coli by combining pH, ionic strength and pulsed electric fields hurdles, Food Res. Int. 29 (1996) 117–121. https://doi.org/10.1016/0963-9969(96)00015-4.

[30] K. Dołowy, Uniform hypothesis of cell behaviour-movement, contact inhibition of movement, adhesion, chemotaaris, phagocytosis, pinocytosis, division, contact inhibition of division, fusion, J. Theor. Biol. 52 (1975) 83–97. https://doi.org/10.1016/0022-5193(75)90041-7.

[31] N.M. Parhad, N.U. Rao, Effect of pH on Survival of Escherichia coli, 1974.

[32] E. Padan, E. Bibi, M. Ito, T.A. Krulwich, Alkaline pH homeostasis in bacteria: New insights, Biochim. Biophys. Acta - Biomembr. 1717 (2005) 67–88. https://doi.org/10.1016/j.bbamem.2005.09.010.

[33] M. Sharma, L.R. Beuchat, Sensitivity of Escherichia coli O157:H7 to Commercially Available Alkaline Cleaners and Subsequent Resistance to Heat and Sanitizers, Appl. Environ. Microbiol. 70 (2004) 1795–1803. https://doi.org/10.1128/AEM.70.3.1795-1803.2004.

[34] N.R. Asad, L.M.B.O. Asad, C.E.B. de Almeida, I. Felzenszwalb, J.B. Cabral-Neto, A.C. Leitão, Several pathways of hydrogen peroxide action that damage the E. coli genome, Genet. Mol. Biol. 27 (2004) 291–303. https://doi.org/10.1590/S1415-47572004000200026.

[35] C. Jiménez-Sánchez, J. Lozano-Sánchez, A. Segura-Carretero, A. Fernández-Gutiérrez, C. Jim Enez-S Anchez, J. Us Lozano-S Anchez, A. Fern Andez-Guti Errez, Critical Reviews in Food Science and Nutrition Alternatives to conventional thermal treatments in fruit-juice processing. Part 1: Techniques and applications Alternatives to conventional thermal treatments in fruit-juice processing. Part 1: Techniques and, (2017). https://doi.org/10.1080/10408398.2013.867828.

[36] L. Uhl, S. Dukan, Hydrogen peroxide induced cell death: The major defences relative roles and consequences in E. coli, PLoS One. 11 (2016) 159706. https://doi.org/10.1371/journal.pone.0159706.

[37] N.R. Asad, L.M.B.O. Asad, A.B. Silva, I. Felzenszwalb, A.C. Leitão, Hydrogen peroxide effects in Escherichia coli cells, Acta Biochim. Pol. 45 (1998) 677–690.

https://doi.org/10.18388/abp.1998_4261.

[38] C. Liu, X. Xie, W. Zhao, N. Liu, P.A. Maraccini, L.M. Sassoubre, A.B. Boehm, Y. Cui, Conducting Nanosponge Electroporation for Affordable and High-Efficiency Disinfection of Bacteria and Viruses in Water, (2013). https://doi.org/10.1021/nl402053z.

[39] R.S. Tanner, S.A. James, Rapid bactericidal effect of low pH againstPseudomonas aeruginosa, J. Ind. Microbiol. 10 (1992) 229–232. https://doi.org/10.1007/BF01569771.

[40] A. Mai-Prochnow, P. Lucas-Elio, S. Egan, T. Thomas, J.S. Webb, A. Sanchez-Amat, S. Kjelleberg, Hydrogen peroxide linked to lysine oxidase activity facilitates biofilm differentiation and dispersal in several gram-negative bacteria, J. Bacteriol. 190 (2008) 5493–5501. https://doi.org/10.1128/JB.00549-08.

[41] K. Hori, S. Matsumoto, Bacterial adhesion: From mechanism to control, Biochem. Eng. J. 48 (2010) 424–434. https://doi.org/10.1016/j.bej.2009.11.014.

[42] Q. Zhang, J. Nghiem, G.J. Silverberg, C.D. Vecitis, Semiquantitative performance and mechanism evaluation of carbon nanomaterials as cathode coatings for microbial fouling reduction, Appl. Environ. Microbiol. 81 (2015) 4744–4755. https://doi.org/10.1128/AEM.00582-15.

[43] G. Brandi, P. Sestili, M.A. Pedrini, L. Salvaggio, F. Cattabeni, O. Cantoni, The effect of temperature or anoxia on Escherichia coli killing induced by hydrogen peroxide, Mutat. Res. Lett. 190 (1987) 237–240. https://doi.org/10.1016/0165-7992(87)90002-9.

[44] J. Nakamura, E.R. Purvis, J.A. Swenberg, Micromolar concentrations of hydrogen peroxide induce oxidative DNA lesions more efficiently than millimolar concentrations in mammalian cells, Nucleic Acids Res. 31 (2003) 1790–1795. https://doi.org/10.1093/nar/gkg263.

[45] J.G. Elkins, D.J. Hassett, P.S. Stewart, H.P. Schweizer, T.R. McDermott, Protective role of catalase in Pseudomonas aeruginosa biofilm resistance to hydrogen peroxide, Appl. Environ. Microbiol. 65 (1999) 4594–4600. https://doi.org/10.1128/aem.65.10.4594-4600.1999.

[46] P.S. Stewart, F. Roe, J. Rayner, J.G. Elkins, Z. Lewandowski, U.A. Ochsner, D.J. Hassett, Effect of catalase on hydrogen peroxide penetration into Pseudomonas aeruginosa biofilms, Appl. Environ. Microbiol. 66 (2000) 836–838. https://doi.org/10.1128/AEM.66.2.836-838.2000.

[47] V.A. Plyuta, J. V. Andreenko, A.E. Kuznetsov, I.A. Khmel', Formation of Pseudomonas aeruginosa PAO1 biofilms in the presence of hydrogen peroxide. the effect of the aiiA gene, Mol. Genet. Microbiol. Virol. 28 (2013) 141–146. https://doi.org/10.3103/S089141681304006X.

[48] N. Barraud, D.J. Hassett, S.H. Hwang, S.A. Rice, S. Kjelleberg, J.S. Webb, Involvement of nitric oxide in biofilm dispersal of Pseudomonas aeruginosa, J. Bacteriol. 188 (2006) 7344–7353. https://doi.org/10.1128/JB.00779-06.

[49] X.S. Zhang, R. García-Contreras, T.K. Wood, YcfR (BhsA) influences Escherichia coli biofilm formation through stress response and surface hydrophobicity, J. Bacteriol. 189 (2007) 3051–3062. https://doi.org/10.1128/JB.01832-06.

[50] E. Cabiscol Català, J. Tamarit Sumalla, J. Ros Salvador, Oxidative stress in bacteria and protein damage by reactive oxygen species, Springer-Verlag Ibérica, 2000. https://repositori.udl.cat/handle/10459.1/56751 (accessed February 11, 2021).

[51] J. Jeong, J.Y. Kim, M. Cho, W. Choi, J. Yoon, Inactivation of Escherichia coli in the electrochemical disinfection process using a Pt anode, Chemosphere. 67 (2007) 652–659.

https://doi.org/10.1016/j.chemosphere.2006.11.035.

[52] W. Wu, Z.H. Huang, T.T. Lim, A comparative study on electrochemical oxidation of bisphenol A by boron-doped diamond anode and modified SnO2-Sb anodes: Influencing parameters and reaction pathways, J. Environ. Chem. Eng. 4 (2016) 2807–2815. https://doi.org/10.1016/j.jece.2016.05.034.

[53] E.L. Sandvik, B.R. Mcleod, A.E. Parker, P.S. Stewart, Direct Electric Current Treatment under Physiologic Saline Conditions Kills Staphylococcus epidermidis Biofilms via Electrolytic Generation of Hypochlorous Acid, PLoS One. 8 (2013) 55118. https://doi.org/10.1371/journal.pone.0055118.

[54] A. Ronen, W. Duan, I. Wheeldon, S. Walker, D. Jassby, Microbial Attachment Inhibition through Low-Voltage Electrochemical Reactions on Electrically Conducting Membranes, (2015). https://doi.org/10.1021/acs.est.5b01281.

[55] T. Matsunaga, Y. Namba, T. Nakajima, 751-Electrochemical sterilization of microbial cells, Bioelectrochemistry Bioenerg. 13 (1984) 393–400. https://doi.org/10.1016/0302-4598(84)87040-3.

[56] N. Zhang, M.A. Halali, C.F. de Lannoy, Detection of fouling on electrically conductive membranes by electrical impedance spectroscopy, Sep. Purif. Technol. 242 (2020) 116823. https://doi.org/10.1016/j.seppur.2020.116823.

[57] A.M. Zaky, B.P. Chaplin, Porous substoichiometric TiO2 anodes as reactive electrochemical membranes for water treatment, Environ. Sci. Technol. 47 (2013) 6554–6563. https://doi.org/10.1021/es401287e.

[58] L. Liu, J. Liu, G. Bo, F. Yang, J. Crittenden, Y. Chen, Conductive and hydrophilic polypyrrole modified membrane cathodes and fouling reduction in MBR, (2012). https://doi.org/10.1016/j.memsci.2012.11.066.

[59] M.J. Larocque, D.R. Latulippe, C.F. de Lannoy, Formation of electrically conductive hollow fiber membranes via crossflow deposition of carbon nanotubes – Addressing the conductivity/permeability trade-off, J. Memb. Sci. 620 (2021) 118859. https://doi.org/10.1016/j.memsci.2020.118859.

[60] D. Bell, R. Sengpiel, M. Wessling, Metallized hollow fiber membranes for electrochemical fouling control, J. Memb. Sci. 594 (2020) 117397. https://doi.org/10.1016/j.memsci.2019.117397.

[61] P.M. Doran, Unit Operations, in: Bioprocess Eng. Princ., Elsevier, 2013: pp. 445–595. https://doi.org/10.1016/B978-0-12-220851-5.00011-3.

[62] Y.C. Woo, J.J. Lee, L.D. Tijing, H.K. Shon, M. Yao, H.S. Kim, Characteristics of membrane fouling by consecutive chemical cleaning in pressurized ultrafiltration as pre-treatment of seawater desalination, Desalination. 369 (2015) 51–61. https://doi.org/10.1016/j.desal.2015.04.030.

[63] R. Singh, Desalination and Water Treatment Analysis of energy usage at membrane water treatment plants, (2011). https://doi.org/10.5004/dwt.2011.1810.

[64] M. Zhou, Z. Diwu, N. Panchuk-Voloshina, R.P. Haugland, A stable nonfluorescent derivative of resorufin for the fluorometric determination of trace hydrogen peroxide: Applications in detecting the activity of phagocyte NADPH oxidase and other oxidases, Anal. Biochem. 253 (1997) 162–168. https://doi.org/10.1006/abio.1997.2391.

[65] M. Gündoan-Paul, S.S. Çelebi, H. Özyörük, A. Yldz, Amperometric enzyme electrode for organic peroxides determination prepared from horseradish peroxidase immobilized in poly(vinylferrocenium) film, Biosens. Bioelectron. 17 (2002) 875–881. https://doi.org/10.1016/S0956-5663(02)00072-6.

[66] L. Boulos, M. Prévost, B. Barbeau, J. Coallier, R. Desjardins, LIVE/DEAD(®) BacLight(TM): Application of a new rapid staining method for direct enumeration of viable and total bacteria in drinking water, J. Microbiol. Methods. 37 (1999) 77–86. https://doi.org/10.1016/S0167-7012(99)00048-2.

[67] A.R. Bakr, M.S. Rahaman, Electrochemical efficacy of a carboxylated multiwalled carbon nanotube filter for the removal of ibuprofen from aqueous solutions under acidic conditions, Chemosphere. 153 (2016) 508–520. https://doi.org/10.1016/j.chemosphere.2016.03.078.

[68] O. Istanbullu, J. Babauta, H. Duc Nguyen, H. Beyenal, Biofouling The Journal of Bioadhesion and Biofilm Research Electrochemical biofilm control: mechanism of action Electrochemical biofilm control: mechanism of action, (n.d.). https://doi.org/10.1080/08927014.2012.707651.

[69] W.D. Nicoll, A.F. Smith, Stability of Dilute Alkaline Solutions of Hydrogen Peroxide, Ind. Eng. Chem. 47 (1955) 2548–2554. https://doi.org/10.1021/ie50552a051.

[70] M.R. Singh, Y. Kwon, Y. Lum, J.W. Ager, A.T. Bell, Hydrolysis of Electrolyte Cations Enhances the Electrochemical Reduction of CO2 over Ag and Cu, J. Am. Chem. Soc. 138 (2016) 13006–13012. https://doi.org/10.1021/jacs.6b07612.

6.8.Supplementary Information

MATERIALS AND METHODS

Chemical and Solutions

Table 6.S1. Information on materials, their properties, and suppliers.

Material/Solution	Properties	Supplier
Carboxyl functionalized single-walled/double-walled carbon nanotubes (SW/DWCNT-COOH)	Inner diameter: 1-4 nm Length: 5-30 µm Purity: >90 w/% Functional content: 2.73 w/%	Cheaptubes
Ethanol	85.6 %	VWR
Phosphate buffered saline (PBS) tablet	137 mM sodium chloride 2.7 mM potassium chloride 10 mM phosphate buffer	VWR
Glutaraldehyde (GA) solution	50.2 % Specific density: 1.127	Fisher Chemical
Sodium dodecyl sulfate (SDS)	Molecular weight (MW): 288.38	Anachemia
Hydrochloric acid	(38%)	Anachemia
The poly(vinyl alcohol) (PVA)	MW: 31,000-50,000 98-99 % hydrolyzed	Sigma-Aldrich
Poly(ether sulfone) (PES membrane	Microfiltration (MF) Diameter: 47 mm Nominal pore size: 0.2 µm	Sterlitech

Deionized (DI)	Arium system Resistivity: 0.047 µS/cm	Sartotius

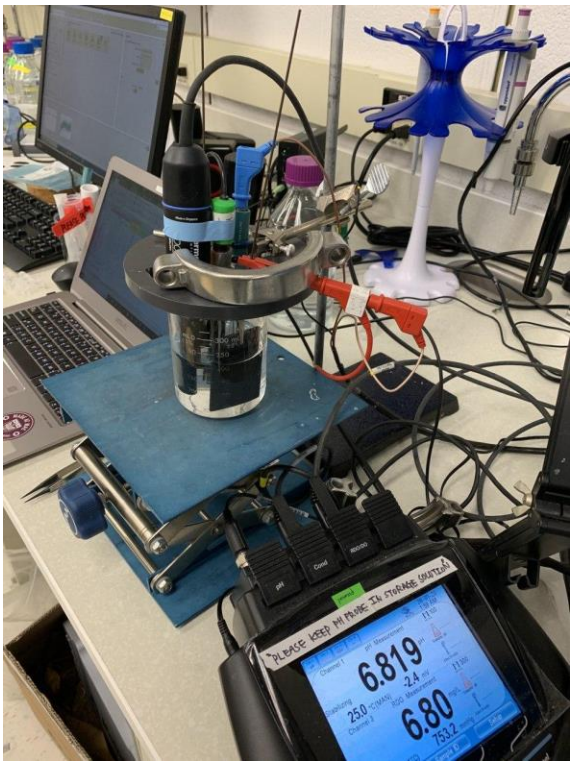

Figure 6.S1. Picture of the electrochemical batch cell.

CNT characterization

Scanning electron microscopy (SEM, JEOL JSM-7000F) and transmission electron microscopy (TEM, Talos 200X) were carried out to demonstrate the morphology and thickness of CNT. Elemental analysis on CNTs were performed using X-ray photoelectron spectroscopy (XPS, PHI Quantera II Scanning XPS Microprobe) and energy-dispersive X-ray spectroscopy (EDS, Oxford Instruments X-Max^n 50 mm^2 detector). XPS analysis were carried out at three different points of the samples considering the random structure of CNT powder. At each point, survey spectrum (0.0-1100.0 eV), C1s (284.8-291.3 eV), O1s (531.3-535.7 eV) scans were carried out. Data were further analyzed using CasaXPS software and ratios of integrated peak areas for each element were used to calculate the surficial CNT elemental ratios. For EDS, AZtec EDS/EBSD software was used for post-

processing as well as simultaneous acquisition of elemental data. In addition, thermogravimetric analysis (TGA, Mettler Toledo TGA/DSC 3+) was performed to verify the thermal stability of CNT structures. As such, samples were heated from room temperature to 1000.0 °C at 0.0 °C/min under air atmosphere with flowrate of 30.0 mL/min.

Hydrogen peroxide measurement

To quantify the concentration of electrochemically-generation H_2O_2 at CNT-based ECM (CNT-ECM), we polarized the CNT surface at a wide range of direct cathodic currents (-20 mA to -150 mA) and used a highly sensitive assay kit, Amplex Red, able to detect H_2O_2 at concentrations as low as 50 nM. Amplex red assay kit is widely used in the literature and functions through a reaction between the main reagent (10-acetyl-3,7-dihydroxyphenoxazine) and H_2O_2 (with 1:1 stoichiometry) in the presence of horseradish peroxidase (HRP) to produce red-fluorescent resorufin, which is detectable by UV-Vis spectrometer.[64] The reaction between H_2O_2 and HRP might not be specific to H_2O_2 in the presence of organic peroxide.[65] However, since no background organic compounds were used in our study, the reported values can be solely attributed to the presence of H_2O_2.

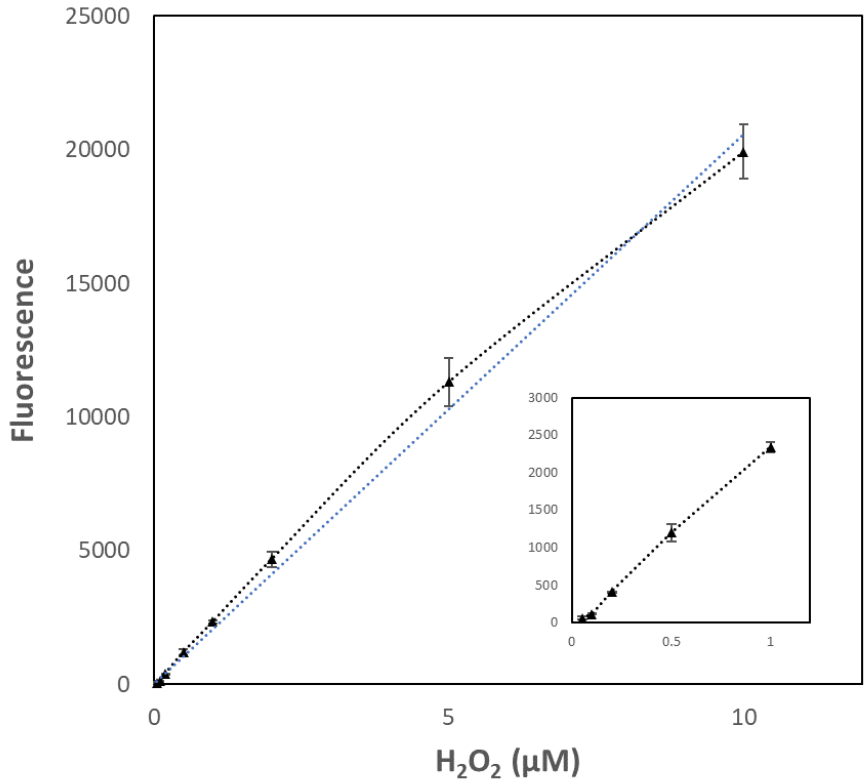

Figure 6.S2. Detection of H_2O_2 using the Amplex® Red Hydrogen Peroxide/Peroxidase Assay Kit. The inset shows the sensitivity of the assay at very low levels of H_2O_2. Background fluorescence, determined for a no-H_2O_2 control reaction, has been subtracted from each value. The best linear model fit on data is Y=2059 X with an R^2 value of 0.9966, where Y is fluorescence and X is hydrogen peroxide concentration (µM). Error bars represent the standard deviation for three data points.

Zeta potential measurements

The surface electrical charge of the *E. Coli* particles in PBS buffer with a concentration of 7×10^8 CFU/mL was measure by a zeta potential analyzer (Zeta Plus, Brookhaven Instruments Corporation) at different pH values (pH 4, pH 7, pH 11). Measurements were carried out for two batches and in ten runs for each batch, and the average value was reported in Figure 6.S3. The results are consistent with what reported in literature.[54]

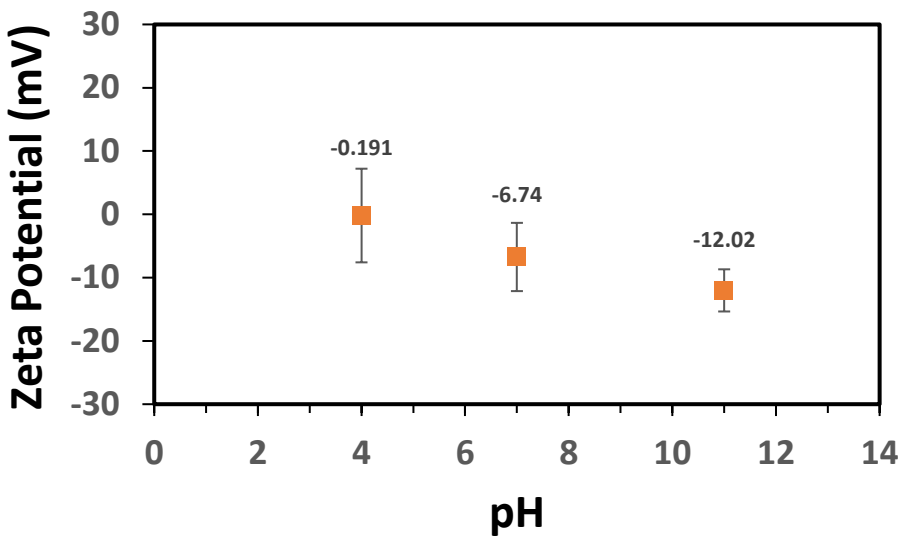

Figure 6.S3. The zeta potential of *E. Coli* suspension at different pH values (4, 7, and 11). Error bars represent the standard deviation for three data points.

E. Coli Suspension, treatment, and characterization

E. Coli was harvested in a tryptic soy broth (TSB) media. In sum, bacteria were grown in a shaking incubator at 37 °C and 225 RPM for 20 h then diluted to 7×10^8 CFU/mL. The concentration of *E. Coli* cells (viable cells) was enumerated every hour up to 3 h by total plate count and fluorescence spectroscopy methods. In plate counting, samples (10 µL) were taken from the batch, serially diluted (5-8 times) and cultured on tryptic soy agar (TSA) plates at 27 °C for 18 h.

Using fluorescence spectroscopy, we followed a recommended procedure by Molecular Probes. a LIVE/DEAD *bac*Light bacterial viability kit was used in which two-color fluorescence nucleic acids, SYTO® 9 green-fluorescent and propidium iodide (PI) red-fluorescent were used to label live and dead cells, respectively. SYTO® 9 labels the intact bacteria while PI (a relatively large molecule, ~670 Da) can only penetrate into the cell and bind to the cellular DNA if the bacteria is damaged.[66] In short, 100 µL of a solution containing SYTO 9 dye (3.34 mM) and Propidium iodide (PI, 20 mM) with the mixing ratio of 1:1 was mixed with 100 µL of bacterial suspension in a 96-well flat-bottom microplate. Samples were prepared in triplicate, and suspensions in each well were mixed

thoroughly by pipetting up and down several times. The plate was incubated in a dark room for 15 min prior to fluorescence spectroscopy. Samples were exited with $OD_{485 \pm 20}$, emission wavelengths were measured at 535 ± 25 nm and 635 ± 35 nm to label the green (live) and red (dead) cells, respectively, and compared to a calibration curve (Figure 6.S4) for quantification.

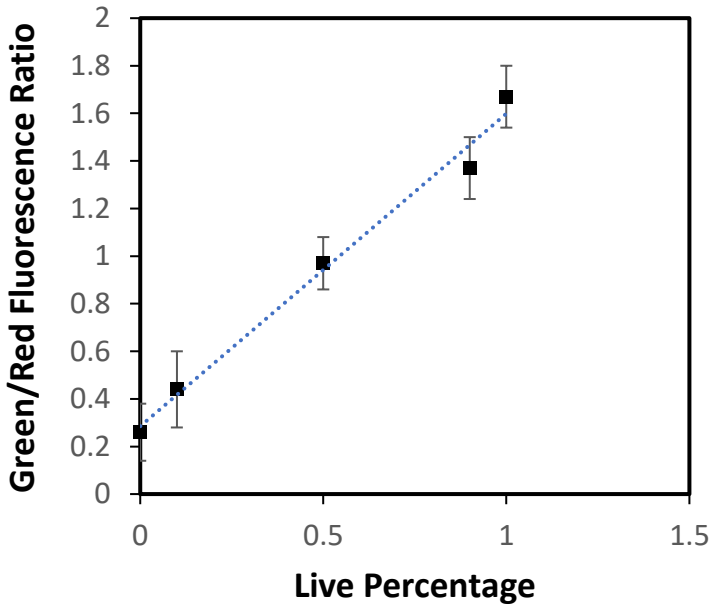

Figure 6.S4. Relative viability of *Escherichia Coli* in fluorescence microplate reader. Live and Dead suspensions were mixed with ratios of 100:0, 90:10, 50:50, 10:90, and 0:100. Green fluorescence was acquired by cell excitation and emission of 485 ± 20 nm and 535 ± 25 nm, respectively. Red fluorescence was acquired by cell excitation and emission 485 ± 20 nm and 635 ± 35 nm, respectively. Green/Red fluorescence ratio was calculated for each proportion of live:dead *Escherichia Coli* suspension. The best linear model fit on data is Y=1.32 X + 0.28 with an R^2 value of 0.9884, where Y is Green/Red fluorescence ratio and X is live percentage of *Escherichia Coli* suspension. Error bars represent the standard deviation for six data points.

Biofilm Formation and treatment in a flow cell

Prior to the start of the experiment, the flow-through system (Figure 6.S5) was sanitized with 70% ethanol for 30 min and thoroughly rinsed with sterile distilled water for 1 h. Membranes were first conditioned for 1 h with PBS buffer solution under identical operating conditions (10 psi (0.69 bar), ambient temperature). Following membrane

compaction, the feed was dosed with freshly harvested *E. Coli* suspension (harvested as previously described in last section) to reach a final concentration of 7×10^8 CFU/mL. Bio-suspension was filtered through the membrane for 18 h to form a uniform and thick biofilm (Figure 6.S6). The pressure was kept constant at 10 psi (0.69 bar). The flow rate was 11.7 mL/s which provided a shear rate of 140.4 s^{-1}. The flow across the membrane was laminar with a Reynolds number of N_{Re} = 585.

Next, biofilms were treated with different antifouling stressors such as low pH, high pH, and H_2O_2 either in-situ or externally for 3 h. To induce external acidic and alkaline conditions, the pH of the feed was adjusted to 3.5 and 11 using HCl and NaOH, respectively. External oxidation stress by H_2O_2 was provided by directly dosing the feed with H_2O_2 to a final concentration of 188 μM. Identical oxidation conditions were provided in-situ through the application of electrical potential to the surface of the CNT-ECM. In our setup, the flow-cell was fitted with electrodes to allow for an externally applied current to be supplied to CNT-ECMs. The CNT-ECM was acted as a working electrode, and a graphite counter electrode was provided as a counter electrode. Treated fouled membranes were recovered and processed for further analysis.

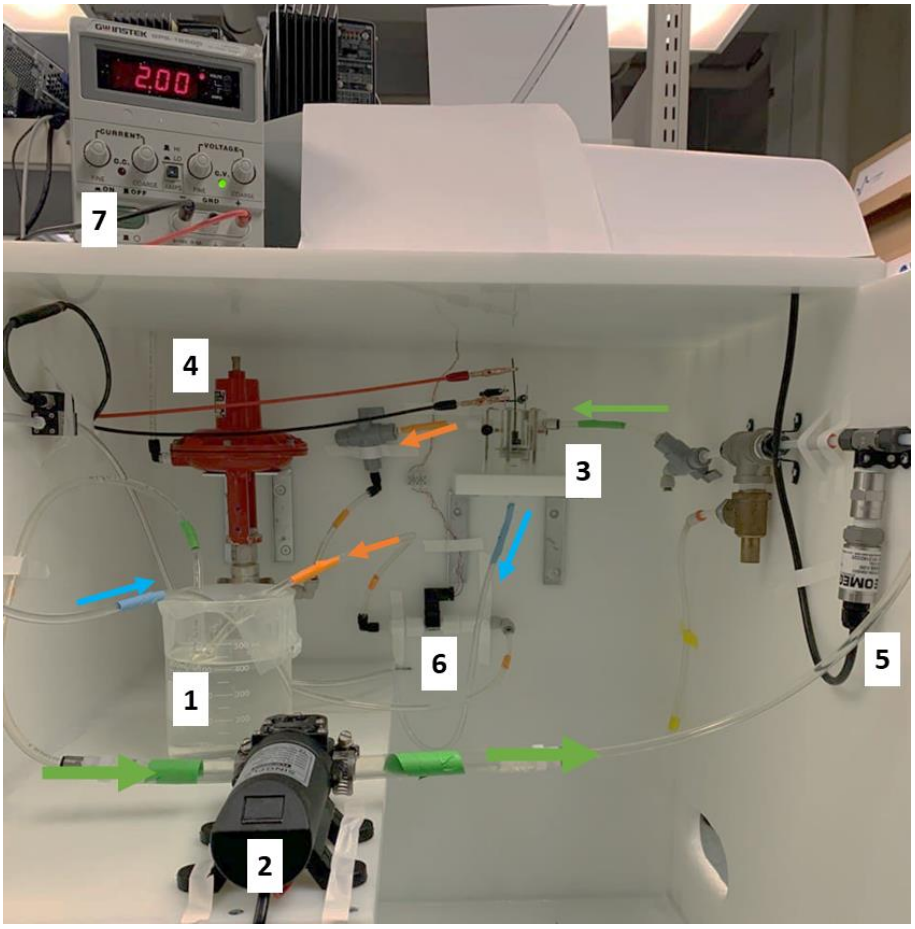

Figure 6.S5. Picture of the low-pressure flow-through system. 1: Reservoir, 2: Pump, 3: Flow cell, 4: Air regulator, 5: Pressure sensor, 6: Flow sensor, 7: DC power generator. Green, orange, and blue colors represent feed, retentate, and permeate lines.

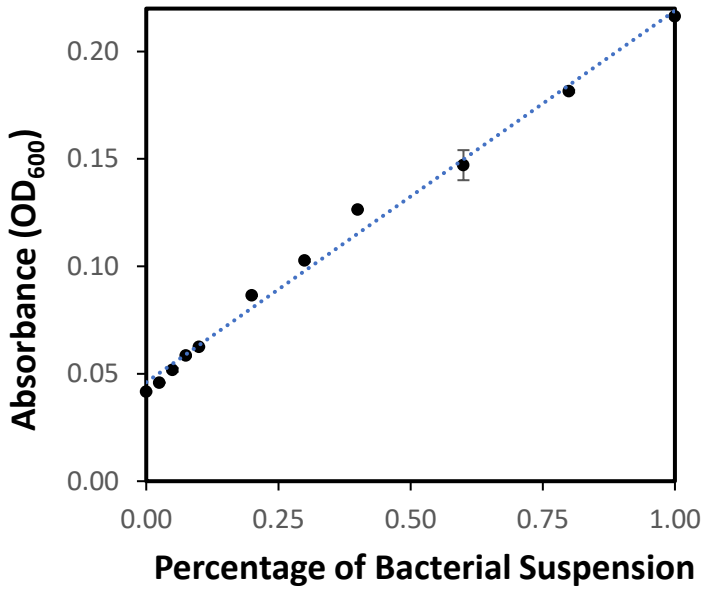

Figure 6.S6. Absorbance values of bacterial enriched suspension at different dilution ratios with PBS buffer. Biosuspension had initial concentration of 7×10^8 CFU/mL and mixtures were prepared with biosuspension: PBS ratios of 1:0, 0.8:0.2, 0.6:0.4, 0.4:0.6, 0.3:0.7, 0.2:0.8, 0.1:0.9, 0.075:0.925, 0.05:0.95, 0.025:0.975, and 0:1. The best linear model fit on data is Y=0.1729 X + 0.046 with an R^2 value of 0.9928, where Y is absorbance at OD_{600} and X is percentage of bacterial enriched suspension. Error bars represent the standard deviation for three data points.

Figure 6.S7. Picture of the biofouled membrane after 18 h filtration of *E. Coli* suspension with a concentration of 1×10^7 CFU/mL.

Biofilm characterization

The morphology of biofilm was observed using scanning electron microscopy (SEM, JEOL JSM-7000F). Biofouled membranes were fixed with GA and thoroughly dried prior to the SEM imaging. GA fixation was conducted by staining membranes with 4% v/v GA

in DI water. Stained membranes were kept in the fridge for 1 h followed by dehydration at three stages (3 min each) using 50, 80, 96 % ethanol, respectively. Membranes were air-dried overnight before imaging.

The viability of bacterial cells was measured using LIVE/DEAD® *bac*Light bacterial viability kit. This kit utilizes two nucleic acid strains, SYTO® 9 green-fluorescent, and propidium iodide (PI) red-fluorescent. The SYTO® 9 strains label all the cells in a population, including intact and damaged membranes, while PI strain only tags damaged bacteria with destructed membranes so PI can diffuse into and react with cellular DNA.[66] As such, penetration of PI into cells reduces the SYTO® 9 fluorescent when both dyes are present. Therefore, strained green bacteria represent the viable (live) bacteria, while stained red cells represent damaged (dead) bacteria.

The staining protocol was carried out as follows: 3 µL SYTO® 9 strain and 3 µL PI strain were dispersed in DI water using vortex mixing. Then, a few droplets of the mixture were used to stain the biofilm. The stained membrane was kept in a dark room at room temperature (20 °C) for 30 min, allowing the staining reactions to compete. Next, the membranes were rinsed gently with DI water to avoid unreacted residuals on the surface and placed on a glass microscope slide, ready for confocal laser scanning microscopy (CLSM). CLSM was equipped with krypton–argon laser (488 nm) and two He–Ne lasers (543 and 633 nm). Four images were taken randomly on each surface (with an area of 1 mm^2). Live cells, dead cells, and the viability ratio of biofilm were quantified using ImageJ software, determining the relative abundance of red and green pixels in the digital image. Therefore, the percentage of green pixels and red pixels were assumed as the ratio of live cells and dead cells, respectively.

1. RESULTS AND DISCUSSION

CNT Characterization

TEM and SEM images are shown in Figure 6.S8a and Figure 6.S8b, respectively. As indicated in Figure 6.S8a, CNTs have outer and inner diameters of 20 nm and 4 nm, respectively.

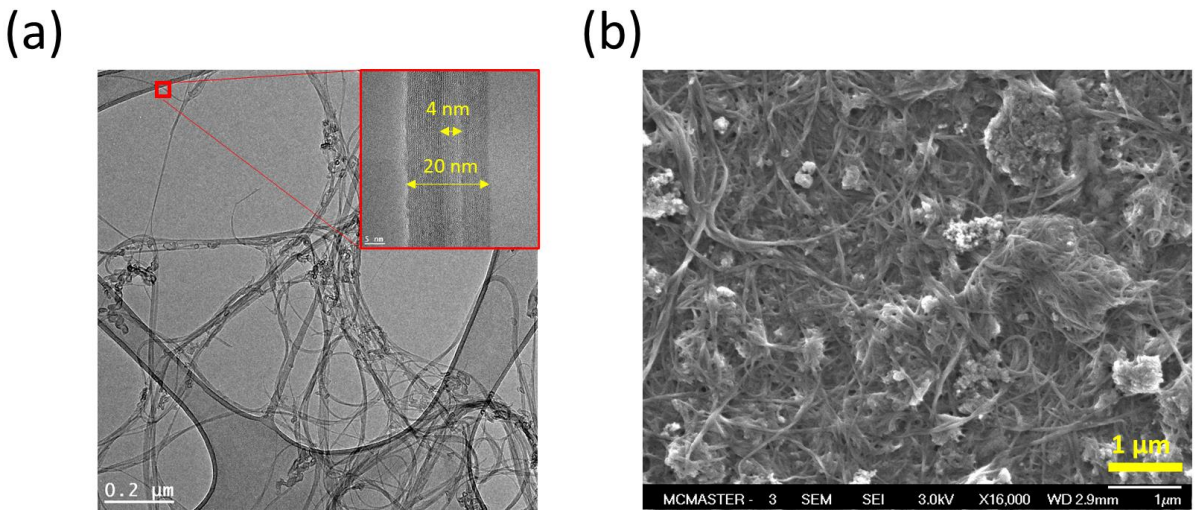

Figure 6.S8. (a) Transmission electron microscopy (TEM) of carbon nanotubes, (b) Scanning electron microscopy (SEM) of CNT-ECM.

XPS analysis reveals high percentage of C and O elements, with 94.74% and 5.26% on average, respectively (Figure 6.S9). N and S elements were not detected (or their concentration could be lower than XPS detection limit, i.e., 0.1%). The elemental concentrations were presented in Table S2. The XPS spectra with peak fittings for C1s and O1s are shown in Figure 6.S9b.

EDS results are presented in Figure 6.S10. As indicated, two main elements are C and O with recorded weight percent of 94.1% and 4.5%, respectively. Map analysis shows the uniform distribution of carbon and oxygen at the surface.

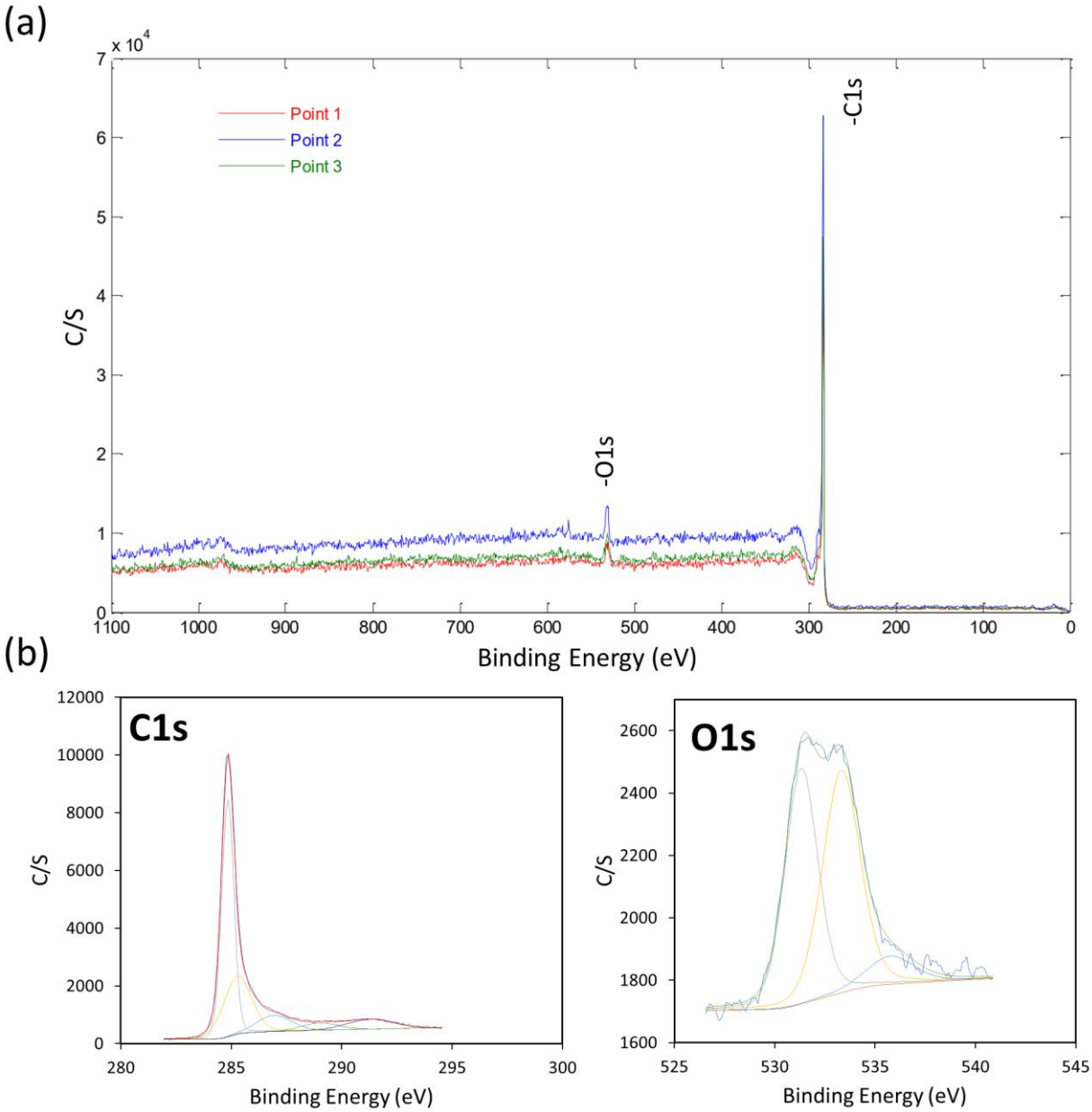

Figure 6.S9. XPS scans of carboxylated CNTs. (a) Survey spectrum (0.0-1100.0 eV), (b) C1s (284.8-291.3 eV) and O1s (531.3-535.7 eV) scans.

Table 6.S2. The proportions of elements in XPS spectra of CNTs.

CNT	C	O
Point 1	94.60	5.4
Point 2	95.17	4.82
Point 3	94.44	5.54
Average	94.74	5.26

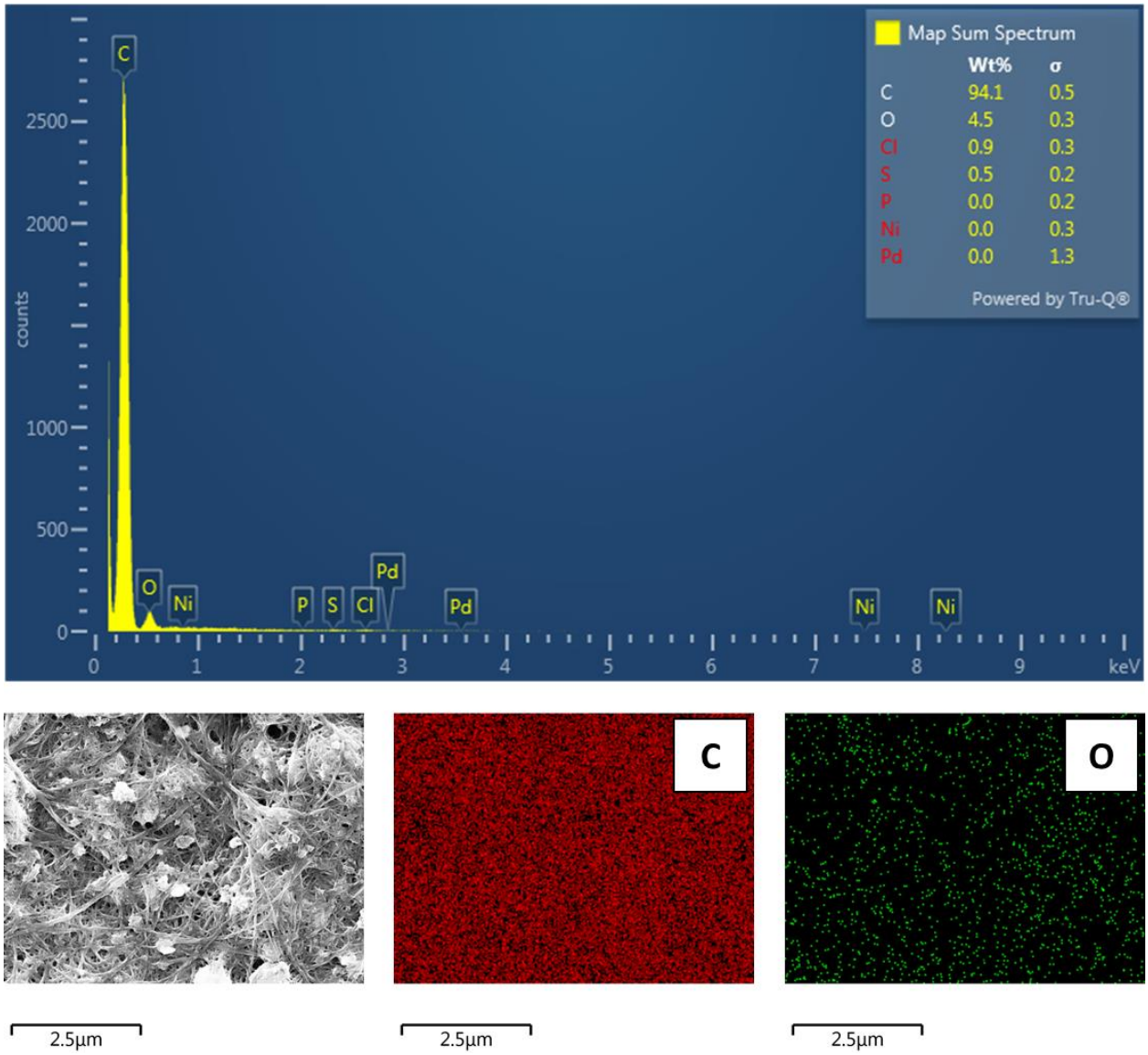

Figure 6.S10. EDS analysis on carbon nanotubes. (Top) Map sum spectrum, (bottom) Electron image, carbon map, and oxygen map.

TGA analysis are presented in Figure 6.S11. TGA burn temperature indicated CNT instability at the range of 450-700 °C which is consistent with what reported in literature [67].

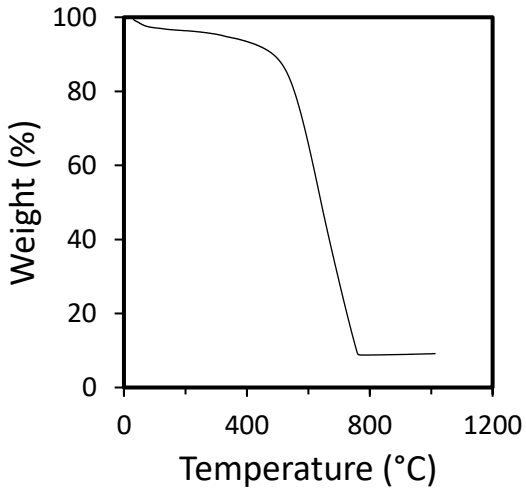

Figure 6.S11. Thermal analysis curve of carboxylated CNTs.

Surface hydrogen peroxide production

Carbonaceous materials such as CNT and graphite are capable of producing hydrogen peroxide (H_2O_2) in-situ under the application of current. We quantified the amount of hydrogen peroxide generated from carbon nanotube-based ECMs applying - 20 mA to -150 mA current. The dominant H_2O_2 production pathway is the $2e^-$ oxygen reduction reaction of oxygen at cathodic surfaces (eq 1). There are other side reactions co-occurring at the cathode, such as $4e^-$ reduction of oxygen to water (known as $4e^-$ pathway), reduction of H_2O_2 to water, and further reduction of H_2O_2 to $HO_2^{\bullet}$ as follows:

$$O_2(g) + 4H^+ + 4e^- \rightarrow 2H_2O \quad (S1)$$

$$H_2O_2 + 2H^+ + 2e^- \rightarrow 2H_2O \quad (S2)$$

$$H_2O_2 \rightarrow HO_2^{\bullet} + H^+ + e^- \quad (S3)$$

We used cyclic voltammetry and fixed current chronoamperometry to identify the current range suitable for H_2O_2 generation from the ECMs (Figure 6.2). The real values for each current are presented in Figure 6.S12. As demonstrated, H_2O_2 concentration reaches a steady state within ~30 min from the start of the experiment. The steady state condition can be explained by (a) a constant dissolved oxygen concentration is maintained in the boundary layer resulted from a balance between ORRs, oxygen diffusion, and system convention, (b) H_2O_2 is simultaneously generated (eq 1), decomposed (eq S2 and eq S3),

and diffused to the bulk (due to concentration imbalance) [20,68], and (c) the presence of calcium and magnesium ions is suggested to stabilize the H_2O_2 concentration [69].

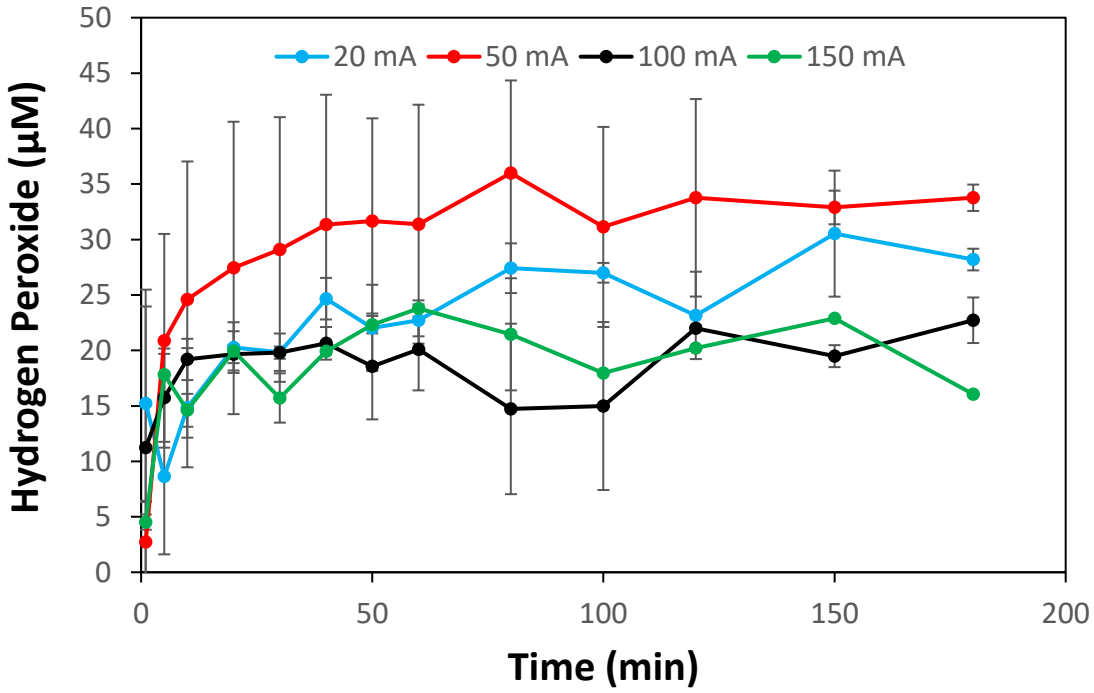

Figure 6.S12. Measured hydrogen peroxide concentration at the bulk of the electrochemical cell under different applied currents (20-150 mA) over 180 min. Error bars represent the standard deviation for three data points.

The maximum concentration of hydrogen peroxide with respect to current efficiency

We calculated the maximum concentration of hydrogen peroxide (HP) that can be theoretically generated.[19] The maximum concentration was estimated using eq S4 with considering a 100% Faradic current efficiency (η) for HP production during the fixed current chronoamperometry.

$$C_{Local\ HP} = \frac{\eta \int_0^t Idt}{nFV100} \quad \text{(S4)}$$

where C_{HP} denotes the molar concentration of HP at the surface (M), n is the number of electrons mediated in the eq 1, F is the Faraday constant (96500 $Cmol^{-1}$), V is the solution volume (L), i and t represent the applied current (A), time (s), respectively. Current efficiency is the ratio of the current used for HP production over the total current transferred through the circuit over electrolysis time. The current efficiency of 100% means if all the

applied current was spent on HP generation. With that, the maximum HP that can be theoretically generated by the cathode under application of 50 mA is 188 µM. While in actual experimental measurements using Amplex® Red assay kit, a maximum HP concentration of 31.19 µM was detected.

Theoretical calculation of the hydrogen peroxide thermodynamically

The theoretical concentration of hydrogen peroxide at the surface was calculated based on stoichiometry in eq 1, and the results are compared with the real measured values in Figure 6.S13. As demonstrated, up to 20 min from the start of the experiment, the theoretical concentrations follow the experimental values before they start to deviate. Hydrogen peroxide concentration directly corresponds to available oxygen at the surface. The dissolved oxygen (DO) at the cathode approaches zero immediately after the start of electrolysis. Therefore, the limiting parameter in eq 1 is the diffusion of DO into the boundary layer rather than the electron transfer at the cathode. Thus, the influx of DO to the surface needs to be calculated using Fick's first law (eq S5) to estimate the HP concentration in eq 1.

$$J = -D\frac{\partial C}{\partial \delta} \tag{S5}$$

Where J is the diffusion flux (mol.m^{-2}.s), D is the diffusion coefficient of oxygen (m^2/s). C denotes the concentration of DO (mol/m^3), and δ represents the length of the boundary layer (m).

D is assumed to be equal to 2×10^{-9} m^2/s. C was measured with the DO sensor and was found to be equal to 2×10^{-4} M, and δ can be solved by combining eq S6 and eq S7. Eq S6 expresses the limiting current under a steady state condition for macroscopic electrodes and solved for k_m, while eq S7 solves for δ by using calculated mass transfer coefficient and diffusion coefficient as follows:

$$I_L = k_m n F A_e C \tag{S6}$$

$$\delta = \frac{D}{k_m} \tag{S7}$$

where k_m is the mass transfer coefficient (m.s^{-1}) I_L is the limiting current (A) estimated in Figure 2a, n represents the stoichiometric number of electrons transferred in eq 1, F is the

Faraday's constant (96490 $Cmol^{-1}$), and A_e is the effective surface area of the CNT electrode (m^2). As such, the thickness of the diffusion layer is calculated to be approximately 31 µm. Therefore, the theoretical concentrations of HP were estimated by following eq 1. As findings suggest in Figure 6.S13, the theoretical concentration is in good agreement with the measured concentration up to ~ 20 min. Beyond that, the values start to deviate, likely due to: (a) instant consumption of excessive HP by eq S2 and eq S3, (b) depletion of oxygen at the surface, and (c) diffusion of generated HP to the bulk. In addition, the theoretical values do not account for the convection induced by system stirring and bubble generation, the competitive reduction reactions at the cathode, and the anodic reactions happening at the anode. For instance, excessive proton generation by eq 3 indirectly negates eq 1 based on *Le Chatelier's principle*.

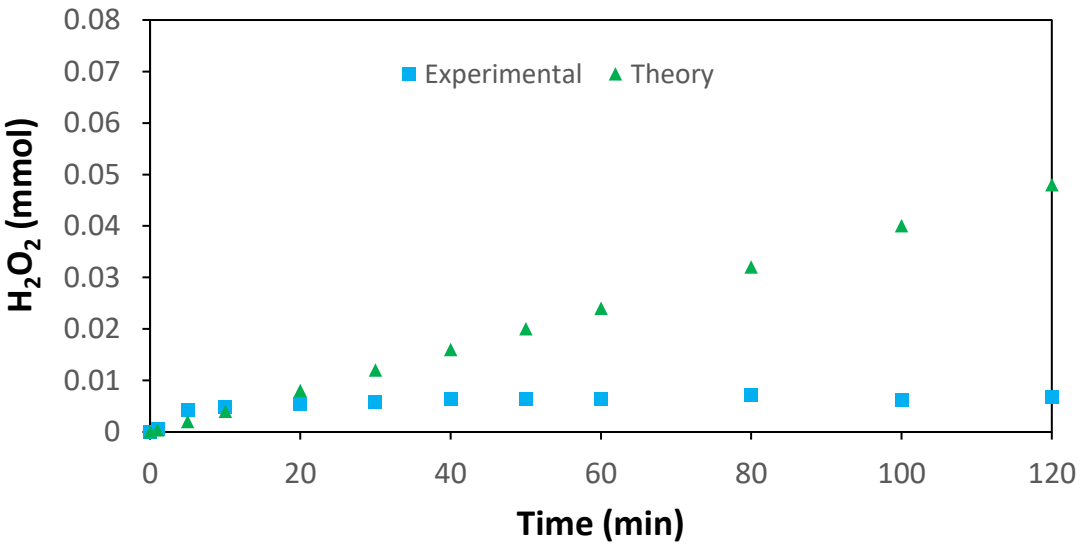

Figure 6.S13. Measured and theoretical molar mass of generated hydrogen peroxide at the bulk of the electrochemical cell under applied electrical current equal to 50 mA over time.

Current efficiency of CNT-ECMs for generation of hydrogen peroxide

We calculated the current efficiency at each current to determine the best condition for H_2O_2 production with respect to H_2O_2 concentration and electrical current consumption. The current efficiency (η) is the ratio of the electricity consumed by the CNT-ECM to

produce H_2O_2 over the total electricity passed through the circuit during the electrolysis period, which can be calculated using eq S8.

$$\eta = \frac{nFC_{HP}V}{\int_0^t Idt} \times 100 \quad \text{(S8)}$$

where n is the number of electrons mediated in the eq 1, F is the Faraday constant (96490 $Cmol^{-1}$), V is the solution volume (L), C_{HP} denotes the molar concentration of H_2O_2 (M), I is the applied current (A) and t is time (s). The current efficiencies were found to be 26.2%, 16.4%, 4.2%, and 2.8% at 20 mA, 50 mA, 100 mA, and 150 mA, respectively. The results indicate that 20 mA is the optimum current to generate H_2O_2 although the highest concentration was observed at 50 mA.

Hydrogen peroxide generation: A comparison between CNT and graphite

For comparison purposes, the H_2O_2 generation properties of CNT-based ECM and graphite electrode were quantified under 50 mA and identical conditions, with the results indicating a steady state H_2O_2 concentration of 37.3 μM and 21.9 μM for CNT-ECM and graphite electrode, respectively (Figure 6.S14). In addition, the current efficiency of electrodes was calculated to be 16.4% and 9.7% for CNT and graphite, respectively. Higher H_2O_2 concentration and current efficiency of CNT-ECM can be ascribed to its high specific surface area and presence of mesopores, in turn providing greater available surface area for oxygen reduction.

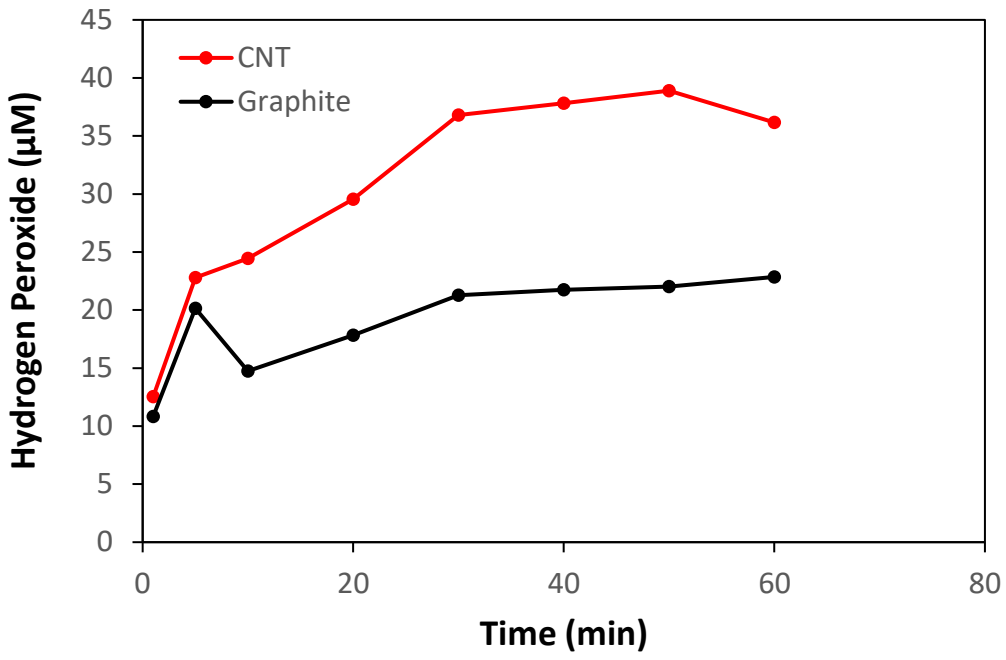

Figure 6.S14. The measured hydrogen peroxide concentration at the bulk of the electrochemical cell at 50 mA over 180 min. Red and black lines represent hydrogen peroxide concentration for CNT and graphite electrodes, respectively.

pH Changes in bulk

As it is shown, the pH in the buffer zone is nearly stable over time. Stable pH can be explained as the low local pH of the anode cancels out the high local pH of the cathode.[70] In addition, generation of CO_2 due to graphite oxidation allows for a carbonate buffer environment. Carbonaceous material can be readily oxidated at the anode following eq 8.[35] Also, the presence of Ca ions can further buffer the solution.[70]

$$C + 2H_2O \rightarrow CO_2 + 4H^+ + 4e^- \quad \text{(S9)}$$

At 150 mA, high rates of bubble gas generation were observed at the surface of either cathode or anode electrodes which may skew the pH readings at this current (Figure 6.S15).

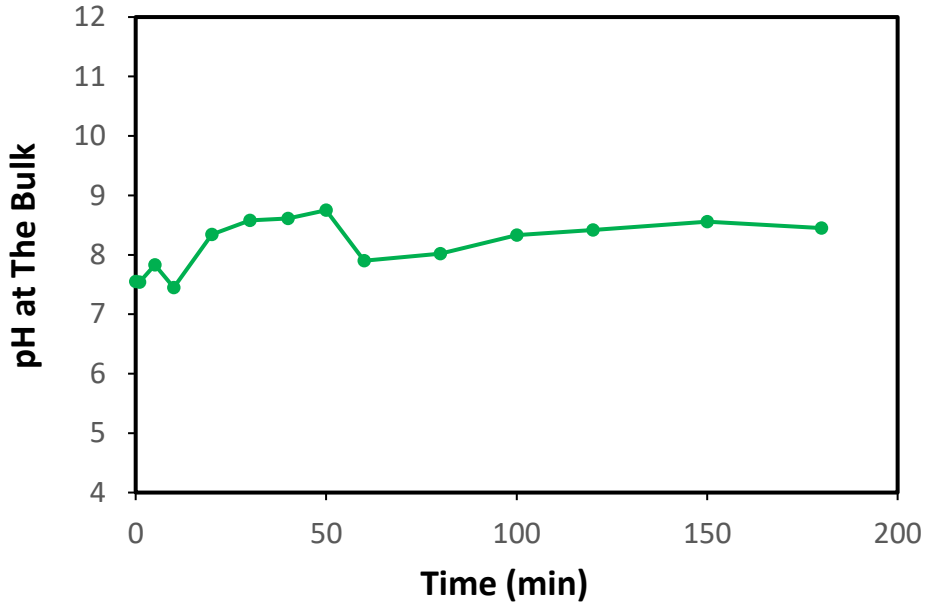

Figure 6.S15. pH measured at the bulk of the electrochemical cell under different applied current equal to -150 mA over 180 min.

Surface electrical properties of CNT-based ECM

The potential of the working electrode was monitored under the application of fixed current chronoamperometry over 3 h and the results are shown in Figure 6.S16. Findings in Figure 6.S16 allow us to match the potential of the working electrode (CNT-ECM) with the corresponding currents applied to them. For instance, the highest H_2O_2 concentration was observed at -50 mA, which corresponds to the potential of 2 V. In addition, electrical current can lead to CNT degradation by damaging the CNT surface sp^2 hybridization thereby decreasing the CNT conductivity.[22] Therefore, higher potential is needed to maintain the current at a damaged surface with reduced conductivity. Cathodic surfaces demonstrated stable electrochemical stability supported by their stable potential over 3 h of electrolysis. CNT-based ECMs are susceptible to anodic oxidation, which results in increases in the reading potential over time; however, the cathodic potential was shown to have a minor effect on surface stability. The physical stability of the surface is further verified by their physical status after electrolysis, as shown in Figure 6.2F. In contrast, identical surfaces experienced severe oxidation under anodic current (Figure 6.S17).

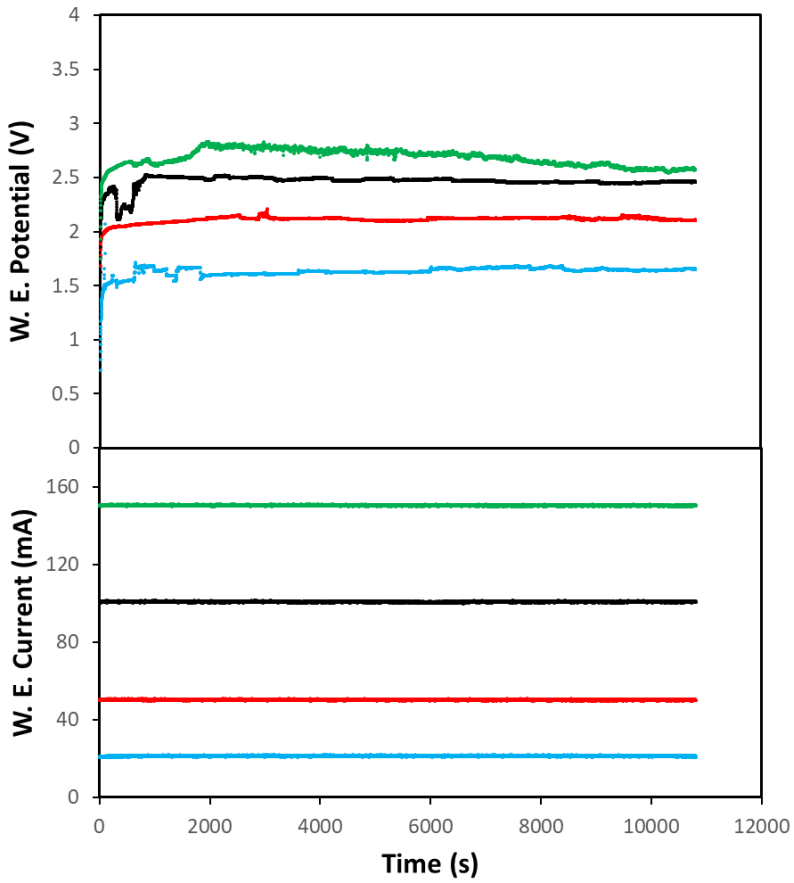

Figure 6.S16. Measured electrical potential of the working electrode (CNT-ECM) under different applied currents (20-150 mA) over 180 min, and (c) CNT-ECM before and after electrolysis working as a cathode under 150 mA for 180 min. Blue, red, black, and green colors represent 20 mA, 50 mA, 100 mA, and 150 mA, respectively.

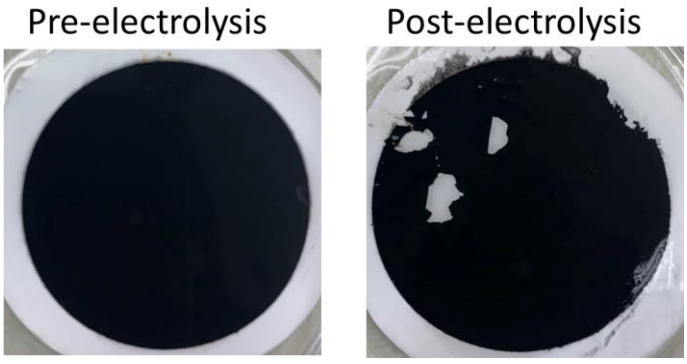

Figure 6.S17. CNT membrane before and after electrolysis acting as a working electrode (anode) under 150 mA for 180 min.

E. Coli cell viability in batch

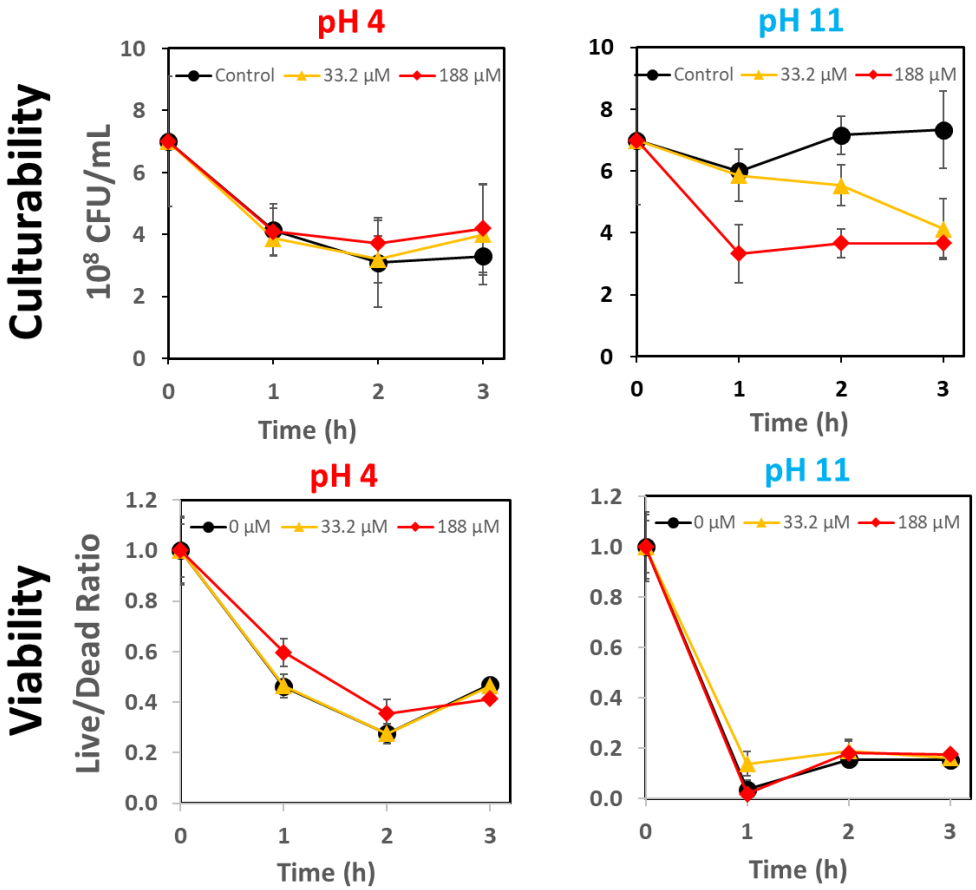

Figure 6.S18. Top row: Cell culturability of *E. Coli* after exposure to different pH values (4, 11) and different H_2O_2 concentrations (0, 33.2, and 188 µM). Error bars represent the standard deviation for four data points. Bottom row: Cell viability of *E. Coli* using LIVE/DEAD staining method after exposure to different pH values (4, 11) and different H_2O_2 concentrations (0, 33.2 and 188 µM). Error bars represent standard deviation for six data points.

E. Coli rejection in flow-through cell

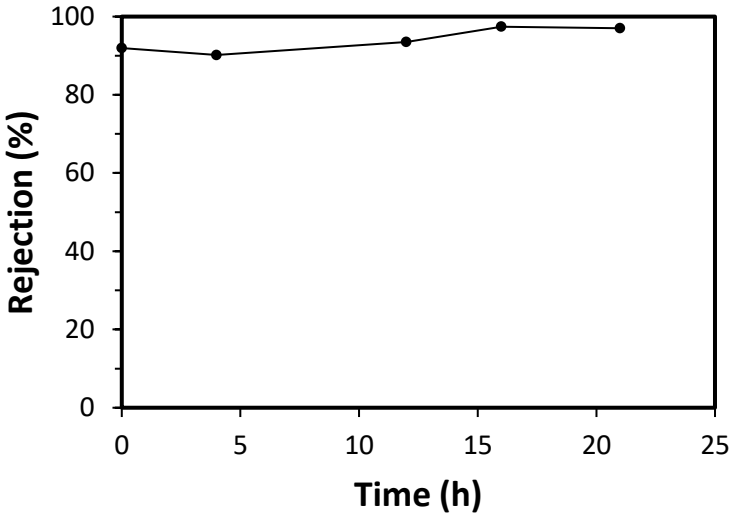

Figure 6.S19. CNT-ECM rejection over 21 h filtration of *E. Coli* suspension in flow-through cell. Biosuspension had initial concentration of 1×10^7 CFU/mL.

***E. Coli* cell and biofilm integrity on flow-through membranes**

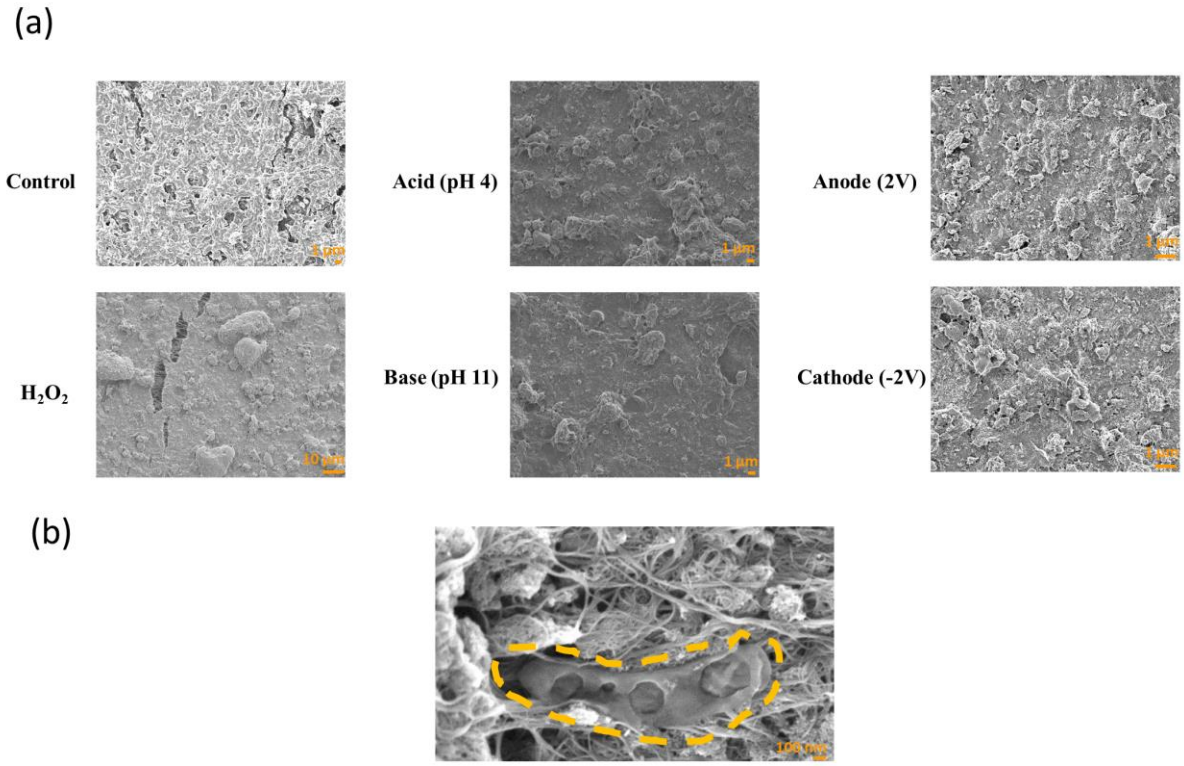

Figure 6.S20. (a) Scanning electron microscopy images of treated *E. Coli* biofilm with the magnification of x3000. In the top row, biofilms are treated with no stimulus, anodic potential (2 V), and low pH (4), respectively, and in the bottom row, the biofilms are treated with hydrogen peroxide (188 μM), cathodic potential (2 V), and high pH (11), respectively, (b) advanced stage of cellular deformation induced by anodic oxidation.

Table 6.S3. Information of UF membrane process for calculating specific energy consumptions.

Material/Solution	**Membrane Type**	**Membrane Area (m^2)**	**Flux (LMH)**	**Potential (V)**	**Current (mA)**	**Time (h)**
CNT-PES	UF	0.003	15	1-2	20-100	3

Chapter 7

Conclusions and Recommendations

7.1.Key findings and contributions

Membrane processes are the technology of choice in separation and purification technology. Many studies have consistently sought to improve the performance and sustainability of membranes. To this end, electrically conductive membranes (ECMs) have been introduced to tackle the limitations of conventional membrane technologies. ECMs can control and mitigate fouling by using electrical potential externally applied to their surfaces. ECMs, owing to their conductive surface, can distribute the charge across the surface that in turn induce antifouling and self-cleaning mechanisms at the membrane/solvent interface. Their unique electrochemical and electrocatalytic properties have made them viable options for water and wastewater treatment and stimulated new applications in water decontamination and disinfection areas. However, application of ECMs is still relatively new, and their optimized disinfecting, antifouling, and self-cleaning potential has not been fully explored. Optimized and cost-effective application of ECMs necessitates understanding the underlying mechanisms, linking the mechanism to the application of membranes, and advancing the chemical properties and stability of conductive surfaces. To this end, this study focused on understanding, exploring, and improving the application of electrically conductive membranes (ECMs) in water and wastewater treatment processes. The key findings and contribution of this work are further elaborated as follows:

In Chapter 2, we comprehensively discussed electrically-induced antifouling and disinfecting mechanisms with respect to surface polarization. ECMs have responsive surface that offers various electrochemical properties with respect to the current externally applied to their surface. The mechanisms are exclusive to the current pattern. Although identifying the mechanisms is critical to target foulants and contaminants across electro-separation interfaces, no work has comprehensively studied them with respect to current pattern. We showed how different polarizations (anodic, cathodic) and different current types (direct, alternating) can promote various mechanisms. Some of the mechanisms contribute to antifouling and self-cleaning performance of ECMs, while some are more effective in disinfecting and decontaminating water in electrically-assisted separation

processes. Common cathodic mechanisms include electrostatic repulsion with negatively charged particles, hydrogen gas generation, and electrically-induced alkaline pH. In contrast, dominant mechanisms under anodic polarization include direct oxidation by electron transfer, indirect oxidation through ROS, electrostatic repulsion with positively charged particles, and electrically-promoted acidic pH. Alternating potentials are advantageous as they offer a combination of cathodic and anodic mechanisms and reduce the destructive impact of anodic-corrosion, particularly on carbonaceous material. However, tuning the current frequency is pivotal in AC applications. Depending on the application of ECMs, high frequencies eliminate antifouling mechanisms that usually result from direct anodic or cathodic currents such as gas generation, radical generation, or extreme pH induction.

We then demonstrated how such mechanisms have been incorporated in ECM-based separation and purification technologies over the past few decades. We discussed the application of ECMs for four major fouling categories: biofouling, organic fouling, oil wetting, and mineral scaling, focusing on surface polarization. In biofouling, anodic current has been often suggested to inactivate microorganisms, while cathodic current was suggested for advanced repulsion with negatively charged biological compounds. Application of ECMs for organic filtration processes have followed two primary goals: (a) offering an antifouling surface and (b) removal of emerging organic compounds. The antifouling performance of ECMs mainly was relied on electrostatic repulsion with commonly negatively charged particles and enhanced bubble generation under cathodic current. In contrast, anodic currents were suggested to remove emerging compounds due to their excellent oxidation potential. In oil separation processes, the application of anodic and cathodic currents at high potentials (> 10 V) was reported due to promoting electro-wetting mechanism. Last but not least, the current pattern in ion and colloidal separation processes was often chosen with respect to ions' charge. It is important to note that the presented patterns describe the central body of articles, while application of other current types can be found within each fouling category.

In Chapter 4, we explored the surface properties of ECMs. We synthesized common ECMs consisting of a CNT thin layer deposited on a PES support. In the thin layer, carboxyl functionalized CNTs were covalently bonded with PVA molecules. PVA was added to the structure due to its excellent film-forming properties and inherent hydrophilicity. In addition, two linear dicarboxylic acids (succinic acid and suberic acid) were used to crosslink the CNT-PVA structure. We thoroughly characterized the membranes and investigated the impact of CNT mass loading, crosslinking type, and crosslinking degree on transmembrane flux, electrical conductivity, hydrophilicity, and surface roughness. Our results indicated that crosslinking length could impact pure water flux and electrical conductivity while was uncorrelated to surface hydrophilicity and morphology.

Although characterization tests in our work provided us with physicochemical properties of the surface, such properties are valid at lab-scale and before harsh electrochemical conditions challenge ECMs. Research evidence has shown that membranes are susceptible to passivation, which drastically changes their initial surface properties. For example, carbon-based ECMs are subjected to electro-corrosion under anodic current leading to drops in their surface conductivity. Therefore, we proposed straightforward and practical methodologies to detect and quantify the electrochemical, physical, and mechanical stability of ECMs. We used a common UF ECM fabricated from CNT-PVA network to demonstrate the practicality of our methods. Our findings revealed that ECMs were stable under cathodic polarization but anodically unstable under the application of small voltages (2–4 V vs. Ag/AgCl reference electrode). In addition, ECMs made were found to be physically unstable when challenged by PEO particles. ECMs showed to be more stable in the mechanical test than uncoated PES membranes due to their protective thin layer.

Although we used a model CNT-based UF ECM, our methods can readily be extended to other membrane materials (ceramics, conductive polymers) and separation categories (MF, NF, RO). The findings in Chapter 5 offer a systematic approach to evaluate the stability of ECMs. It is expected that our methods provide guidance to making more

stable ECMs and act as a roadmap for industrial applicability. The anti-biofouling performance of ECMs was also demonstrated by filtering a suspension enriched from mixed-bacterial cultures. Our results indicated excellent antifouling and self-cleaning properties of ECMs under application of current.

In this work, we acknowledged the importance of understanding antifouling mechanisms to facilitate the optimized performance of ECMs. Therefore, we pursued this goal by investigating the viability of model foulant *E. Coli* under electrically-induced antifouling mechanisms in batch systems and when membranes wer operated in flow-through configuration. The mechanisms of interest were electrically-generated protons (acidic pH), hydroxyl ions (alkaline pH), and H_2O_2. Control experiments such as filtration under open circuit, anodic potential, and cathodic potential were conducted to rule out the contribution of other mechanisms such as direct electron transfer, radical generation, and bubble gas generation. Our results indicated a significant biofilm's inactivation rate under acidic conditions (pH <5), alkaline conditions (pH >9), and electrical potential (± 2 V). This study provides insight on how to match antifouling mechanisms to the foulant type. Once primary antifouling mechanisms are identified for an application, the corresponding current pattern can be applied to maximize the efficiency of ECMs.

7.2.Future work and recommendations

This study recommends advances in a variety of research topics. The most important directions that should be perused are described as follows:

- The major body of articles on ECMs has been carried out in well-controlled experimental conditions. While ECMs have shown excellent antifouling properties against various fouling types separately, treatment of the real wastewater is expected to be more complex. Natural wastewater contains various contaminants (ions, NOM, microorganisms) with different physicochemical properties that complicate the electrochemical treatment processes. Therefore, future research is needed to challenge ECMs with natural wastewater to demonstrate their industrial viability. To this end, the

application of alternating current (AC) can be considered for treating complex wastewater. The combined effects of anodic and cathodic currents can be used to advance antifouling performance of ECMs by offering a wider variety of mechanisms. However, the frequency in AC mode should be carefully tuned to match the response time of antifouling mechanisms. Antifouling mechanisms result from electron transfer, ion diffusion, and electrochemical reactions with different response times. Therefore, high frequencies can eliminate the occurrence of some mechanisms with high response time (indirect oxidation, gas generation).

- It is unlikely that ECMs can target all foulants filtering a real wastewater. Therefore, this study recommends identifying and targeting troublesome foulants to enhance the separation efficiency. For example, internal fouling (pore blockage) was shown to be the primary source of irreversible fouling and permanent permeate flux reduction. Therefore, minimizing internal fouling should be considered to enhance the long-term viability and productivity of membranes.
- The stability of conductive electrodes is of great importance in electrochemical processes which is directly related to membrane performance and energy consumption. ECMs should be able to withstand harsh electro-corrosive conditions under application under anodic potential. In addition, conductive surfaces in composite membranes should be resistant against leaching (release of polymeric substances or nanoparticles) as well as delamination under extreme physical (mechanical cleaning, abrasion) and chemical conditions (extreme acidic or basic pH). In addition, when ECMs operate as cathode, the counter electrode should withstand anodic passivation. The common materials for counter electrodes are graphite, titanium, or steel. Titanium and steel are more resistant than graphite, while their higher cost limits their application. This study

recommends considering the stability of ECMs before their deployment in real applications.

- Low-pressure membranes are ineffective in rejecting emerging contaminants (pharmaceuticals) or some naturally occurring toxic elements (arsenic). Rejection of small substances requires deployment of energy-intense high-pressure separation processes (NF, RO). The combination of conventional separation processes with electrocatalytic properties of ECMs has presented the promise to effectively remove contaminants using low-pressure systems. To this end, doping ECMs with metals (such as Fe, Cu, Ti, Zn, Ag, or Ni) has been proposed to enhance the electrocatalytic performance of ECMs. In addition, these metals can enhance the hydrophilicity, electrical conductivity, and antimicrobial properties of the surface (Ag, Cu).
- In electrofiltration applications, ECMs operate as working electrode while a counter electrode is placed either in the feed or permeate side. Accommodating the counter electrode in currently available membrane modules (e.g., spiral wound) has been a complicating factor toward the commercialization of ECMs. Therefore, advances in module configuration are critical to ease the technology transport from laboratory to the industry.

Cleaning procedures should be planned with respect to foulant properties and operating conditions. In biological solutions, research studies have suggested an early application of the electrical potential to maximize ECMs' efficiency in filtration processes when biofilms are more susceptible to oxidative stresses [1]. For example, research evidence has indicated that H_2O_2 can mitigate monolayer cell coverage from growing into a mature film [1]. It should be noted that in chapter 6, formation of a thick biofilm was allowed for research purposes to negate the impact of electrostatic repulsive force on charged bacteria. In addition, some studies have demonstrated the successful application of electrical field during cleaning procedures such as back-flush. Application of current during

shorter intervals can make the process less energy-intense while protecting the material from electro-corrosion.

Development of membrane material with high conductivity is essential to reduce the overall energy consumption. In this line, research has been directed to application of ceramic membranes or doped carbonaceous material. Doping carbonaceous material has also been suggested to enhance the conductivity and uniform distribution of charge across the surface [2]. Development of conductive and stable material facilitates application of ECM in sensors. ECMs can be coupled to electrochemical impedance spectroscopy (EIS) to detect and monitor fouling at the early stages of filtration [3]. It is anticipated that advances in EIS lead to the intelligent and responsive application of ECMs.

Last but not least, electrically-induced mechanisms originate from the membrane surface and impact the foulant at the interface. In contrast, mechanisms induced by chemical cleaning (biocides, pH adjustment) take place in the bulk and impact the foulant from the feed side. Chapter 6 showed the impact of extreme pHs either promoted from the conductive surface (i.e., using electrical potential) or bulk adjustment (i.e., dosing chemicals externally) on a thick biofilm. Therefore, it is interesting to validate the direction of inactivation by 3D confocal laser scanning microscopy.

7.3.References

[1] O. Istanbullu, J. Babauta, H. Duc Nguyen, H. Beyenal, Electrochemical biofilm control: mechanism of action, Biofouling. 28 (2012) 769–778. https://doi.org/10.1080/08927014.2012.707651.

[2] D. Hou, A. Iddya, X. Chen, M. Wang, W. Zhang, Y. Ding, D. Jassby, Z.J. Ren, Nickel-Based Membrane Electrodes Enable High-Rate Electrochemical Ammonia Recovery, Environ. Sci. Technol. 52 (2018) 8930–8938. https://doi.org/10.1021/acs.est.8b01349.

[3] N. Zhang, M.A. Halali, C.F. de Lannoy, Detection of fouling on electrically conductive membranes by electrical impedance spectroscopy, Sep. Purif. Technol. 242 (2020) 116823. https://doi.org/10.1016/j.seppur.2020.116823.